

2014

# Synthesis, Characterization, and Evaluation of Novel BODIPY Dyes With Theranostic Applications

Jaime Suzanne Hayes

*Louisiana State University and Agricultural and Mechanical College, [jaimegibbs@outlook.com](mailto:jaimegibbs@outlook.com)*

Follow this and additional works at: [https://digitalcommons.lsu.edu/gradschool\\_dissertations](https://digitalcommons.lsu.edu/gradschool_dissertations)



Part of the [Chemistry Commons](#)

---

## Recommended Citation

Hayes, Jaime Suzanne, "Synthesis, Characterization, and Evaluation of Novel BODIPY Dyes With Theranostic Applications" (2014). *LSU Doctoral Dissertations*. 291.

[https://digitalcommons.lsu.edu/gradschool\\_dissertations/291](https://digitalcommons.lsu.edu/gradschool_dissertations/291)

This Dissertation is brought to you for free and open access by the Graduate School at LSU Digital Commons. It has been accepted for inclusion in LSU Doctoral Dissertations by an authorized graduate school editor of LSU Digital Commons. For more information, please contact [gradetd@lsu.edu](mailto:gradetd@lsu.edu).

SYNTHESIS, CHARACTERIZATION, AND EVALUATION OF NOVEL BODIPY DYES  
WITH THERANOSTIC APPLICATIONS

A Dissertation

Submitted to the Graduate Faculty of the  
Louisiana State University and  
Agricultural and Mechanical College  
in partial fulfillment of the  
requirements for the degree of  
Doctor of Philosophy

in

The Department of Chemistry

by

Jaime Suzanne Hayes  
B.S., St. Andrews Presbyterian College, 2010  
August 2014

To my extraordinary family, my parents Tom M. Hayes and Teri B. Hayes and my sister Kelly R. Hayes, for their undying love and encouragement to fulfill my dreams, and to my loving husband, David J. Gibbs, for his unquestionable love, patience, and support on this journey we have all shared.

## ACKNOWLEDGEMENTS

The intellectual journey I have taken from the infancy of my doctoral studies to the completion of this dissertation was not accomplished on my lonesome. This work could not have been completed without the innumerable supporters who have guided me along the way and to whom I offer unbounding appreciation.

My most heartfelt appreciation is owed to my revered doctoral mentor, Dr. M. Graça H. Vicente. With her unwavering guidance, she molded me into an intellectual who can stand on her own two feet from a young scientist without a clue of what being a researcher meant. Her acceptance into her research group, faith in my abilities, and encouragement from the very beginning gave me confidence in my intellectual capacity and the courage to take on each new challenge she placed before me. Each day she met me with her enthusiasm to share her wealth of knowledge, creativity, and passion for her research and that same enthusiasm has been instilled in me. Thank you, Graça for dedicating your time and energy in making me a stronger intellectual, a better writer, and for simply helping to mold me into the woman I am today. I will forever admire you for your determination in expanding your knowledge and the knowledge of your students, and for showing women in the sciences that we can have it all. My words of thanks will never be truly sufficient to express to you my undying gratitude.

A most gracious thank you is owed to my doctoral committee members, Dr. Carol M. Taylor, Dr. George G. Stanley, and Dr. Kevin M. Smith, for serving on my advisory committee and for supporting my intellectual development over the course of my doctoral studies. I would also like to thank Dr. Jong H. Ham from the Department of Plant Pathology and Crop Physiology for sharing his precious time serving as my external examiner.

I would like to express my gratitude to the Department of Chemistry at Louisiana State University, especially to those faculty and staff who played a direct role in growing my intellect and understanding. To Dr. Frank R. Fronczek and his colleagues, Dr. Gregory T. McCandless and Dr. Svetlana Pakhomova, for their crystallographic expertise, Ms. Zehua Zhou for *in vitro* cellular investigations, the late Dr. W. Dale Treleaven and Dr. Thomas Weldgheorghis for their NMR training and expertise, and Ms. Connie David for her mass spectrometry efforts, I express my thanks for your time and support in helping to complete the story of my work.

Thank you to my collaborators, Dr. Petia Bobadova-Parvanova, Assistant Professor of Chemistry at Rockhurst University, Kansas City, MO, and Michael Cottom, Chemistry major, Rockhurst University, for sharing their computational chemistry expertise in completing computational calculations on some *meso*-aryl and thienyl BODIPYs discussed in Chapter 2.

To the talented group of scientists in the Vicente and Smith research groups, I thank you for your friendship, insight, and support as we embarked on this journey to knowledge together. Thank you Dr. Alecia M. McCall, Dr. Krystal R. Fontenot, Dr. Javoris V. Hollingsworth, Dr. R. G. Waruna Jinadasa, Dr. Moses I. Ihachi, Dr. Benson G. Ongarora, Dr. Haijun Wang, Tyrslai Williams, Qianli Meng, Ning Zhao, Elizabeth Okoth, and Alex Nguyen for their insightful suggestions and camaraderie, all of which exponentially enriched my experience. A special thank you is due to Dr. Edith K. Amuhaya and Dr. N. V. S. Dinesh K. Bhupathiraju for their patience and technical assistance in the early days. My sincerest appreciation goes out to Larry T. Robins, Russell Ledet, and Logan E. Leblanc, my undergraduate mentees, for your assistance in completing the work detailed in the forthcoming pages, your friendship, and for educating me on being an effective and intuitive mentor. You have taught me invaluable life skills that I will never forget. I am forever indebted to my friends and colleagues with whom I began and shared this

incredible journey with, for their companionship, encouragement, criticism, advice, and for always keeping in view the light at the end of the tunnel.

There are not enough words in me to express how grateful I am to my wonderful parents, my amazing sister, and my exceptional husband. To my parents and sister, your infinite love and support for me while I pursued my intellectual goals has given me the courage and ambition to expand my knowledge to the fullest. Thank you for showing me the light in the darkest parts of this journey and for celebrating my achievements with the greatest of gusto. To my husband, David, your daily encouragement and belief in me gave me the strength to carry on to the next day despite innumerable challenges and frustrations. Thank you for letting me pursue my goals, regardless of where it took us. Your unwavering commitment to me, to us, and this journey we embarked upon together means more to me than you will ever know. Thank you all for being my teachers, my cheerleaders, my role models, and my steadfast rocks. This triumph is only a small part of the woman you have made me to be.

Thank you to all of the amazing people with whom I have shared this adventure. Without your out-pouring of support, encouragement, and friendship, this dissertation could not have been achieved.

## TABLE OF CONTENTS

ACKNOWLEDGEMENTS .....	iii
GLOSSARY OF ABBREVIATIONS .....	viii
ABSTRACT .....	xi
CHAPTER 1: INTRODUCTION .....	1
1.1 Structure of BODIPY <sup>®</sup> Dyes .....	1
1.2 Synthetic Methodologies .....	6
1.3 Derivatization of the BODIPY Platform .....	12
1.4 Applications of BODIPY Dyes .....	21
1.5 Research Outlook .....	33
1.6 References .....	34
CHAPTER 2: SYNTHESIS, SPECTROSCOPIC STUDIES, COMPUTATIONAL MODELING AND IN VITRO EVALUATION OF A SERIES OF <i>MESO</i> -ARYL-BODIPYS <sup>[a]</sup> .....	46
2.1 Introduction .....	46
2.2 Results and Discussion .....	55
2.3 Conclusions .....	86
2.4 Experimental .....	87
2.5 References .....	102
CHAPTER 3: SYNTHESIS, SPECTROSCOPIC, AND IN VITRO EVALUATION OF NEAR- IR DIIDO-BODIPYS WITH MULTI-MODE IMAGING AND PDT APPLICATIONS .....	109
3.1 Introduction .....	109
3.2 Results and Discussion .....	112
3.3 Conclusions .....	147
3.4 Experimental .....	149
3.5 References .....	163
CHAPTER 4: SYNTHESIS, SPECTROSCOPIC, AND IN VITRO EVALUATION OF NEAR- IR BODIPYS WITH MULTI-MODE IMAGING APPLICATIONS .....	169
4.1 Introduction .....	169
4.2 Results and Discussion .....	174
4.3 Conclusions .....	191
4.4 Experimental .....	191
4.5 References .....	198
CHAPTER 5: SYNTHESIS, SPECTROSCOPIC, AND IN VITRO EVALUATION OF CARBORANYL-BODIPY DYES AS BNCT ANTI-CANCER AGENTS .....	201
5.1 Introduction .....	201
5.2 Results and Discussion .....	210

5.3 Conclusions .....	236
5.4 Experimental .....	237
5.5 References .....	248
APPENDIX .....	254
A. NMR SPECTRA OF COMPOUNDS FOUND IN CHAPTER 2 .....	254
B. NMR SPECTRA OF COMPOUNDS FOUND IN CHAPTER 3 .....	276
C. NMR SPECTRA OF COMPOUNDS FOUND IN CHAPTER 4 .....	287
D. COPYRIGHT RELEASES .....	292
VITA .....	294

## GLOSSARY OF ABBREVIATIONS

$^1\text{H}$	Proton NMR
$^{13}\text{C}$	Carbon-13 NMR
$^{11}\text{B}$	Boron-11 NMR
$\delta$	Chemical shift
$\epsilon$	Extinction coefficient
$\lambda_{\text{max}}$	Maximum wavelength
BBB	Blood Brain Barrier
BNCT	Boron Neutron Capture Therapy
BODIPY	Boron Dipyrromethene
$\text{CDCl}_3$	Deuterated Chloroform
d	Doublet
DBU	1,8-Diazabicyclo[5.4.0]-undec-7-ene
DCM	Dichloromethane
DDQ	2, 3-dichloro-5, 6-dicyano- <i>p</i> -benzoquinone
DMSO	Dimethyl Sulfoxide
ESI-MS	Electrospray Ionization Mass Spectrometry
Et	Ethyl
EtOAc	Ethyl acetate
FRET	Fluorescence Resonance Energy Transfer
GBM	Glioblastoma multiforme
h	Hours
HOMO	Highest Occupied Molecular Orbital
Hz	Hertz
ICT	Internal Charge Transfer
ICS	Intersystem Crossing

IR	Infra Red
J	Coupling constant
LUMO	Lowest Occupied Molecular Orbital
M	Molarity
m/z	Mass to charge ratio
MALDI-TOF MS	Matrix Assisted Laser Desorption/Ionization Time of Flight Mass Spectrometry
Me	Methyl
mg	Milligram
MHz	Mega Hertz
min	Minutes
mL	Milliliter
MO	Molecular Orbitals
MS	Mass Spectrometry
nBuLi	n-Butyl Lithium
nm	Nanometer
NMR	Nuclear Magnetic Resonance
PEG	Polyethylene glycol
PET	Photoinduced Electron Transfer
PET	Positron Emission Tomography
Ph	Phenyl
ppm	Parts per million
RT	Room temperature
s	Singlet
SPECT	Single Photon Emission Computed Tomography
t	Triplet
TFA	Trifluoroacetic Acid

THF	Tetrahydrofuran
TLC	Thin Layer Chromatography
TMS	Trimethylsilane
UV	Ultra violet
UV-Vis	Ultra violet-visible

## ABSTRACT

Boron dipyrromethene (BODIPY) dyes, have garnered much attention in recent decades due to their enticing photophysical properties and their bioimaging applicability. Despite the progression of this field, the development of BODIPY based anti-cancer agents and radioimaging dyes has seen little progress. The utilization of fluorescent BODIPYs as photosensitizers for photodynamic therapy, and as boron delivery agents for boron neutron capture therapy offers promise as theranostic agents. Additionally, BODIPY derivatives that absorb and emit in the near-IR regions of the electromagnetic spectrum and bear radioisotopes suitable for radioimaging techniques are of great interest.

**Chapter 1** is a concise overview of the fundamental concepts of the BODIPY fluorophores. The synthetic routes, post-synthetic modification strategies, and several biological applications of BODIPYs are introduced and will be elaborated upon in subsequent chapters.

**Chapter 2** describes the synthesis, characterization, computational modeling and *in vitro* biological investigations of a series of *meso*-aryl tetramethyl BODIPYs and their diiodo derivatives as photodynamic therapy photosensitizers. Variances in the *meso*-substituent of BODIPY were found to influence the phototoxicity of diiodo-BODIPYs, with some possessing phototoxicity while others were non-toxic. The photophysical properties of these compounds were also explored computationally in collaboration with Dr. Petia Bobadova-Parvanova of Rockhurst University.

**Chapter 3** reports on the synthesis of several near-IR styrylated diiodo-BODIPYs prepared via the Knoevenagel reaction strategy from one of the most phototoxic BODIPYs described in

Chapter 2. The effects of the number and type of styryl substituents on their photophysical properties and *in vitro* photodynamic activities are discussed.

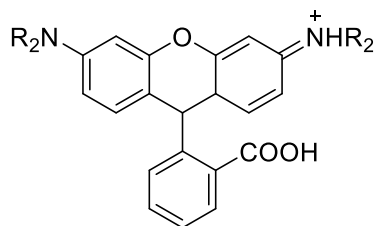
**Chapter 4** explores the synthesis, photophysical, and *in vitro* biological properties of near-IR styryl BODIPYs with applications in near-IR fluorescence, PET, and SPECT imaging. The exploration of radiolabelling highly functionalized long wavelength BODIPYs is detailed herein.

**Chapter 5** conveys an effective method towards the preparation of carborane-appended BODIPYs for boron neutron capture therapy. The use of highly efficient palladium-catalyzed Suzuki coupling yielded two carboranyl-BODIPYs of varying optical properties in good yield. The photophysical properties and blood brain permeability of these novel-carboranyl BODIPYs was reported.

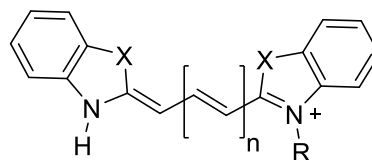
## CHAPTER 1: INTRODUCTION

### 1.1 Structure of BODIPY® Dyes

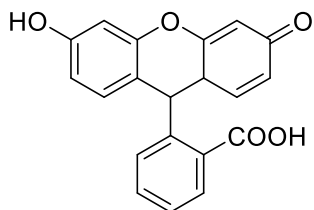
Modern medicine continues to advance without bound, especially with the development of new technologies and novel techniques for bioimaging and disease therapies, and with such progression comes the need for new fluorophores capable of being excited and emitting in the red to near-infrared (IR) region of the visible spectrum.<sup>1</sup> The optimal “biological window” of 600 – 850 nm allows for minimal interference from endogenous chromophores, such as heme, and optimal light penetration through tissues with reduced light scattering and diminished damage to the tissues being imaged.<sup>2-5</sup> These fluorophores can no longer possess a single use, and the demand for dual purpose theranostic agents is on the rise. Although numerous nonradioactive fluorophores, including rhodamines, cyanines and fluorescein (Figure 1.1), are on the market for facile modification and use, the difluoro - boraindacene family of dyes has garnered much attention for their seemingly unlimited versatility.



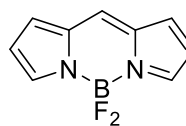
**Rhodamine platform**



**Cyanine platform**



**Fluorescein platform**



**BODIPY platform**

Figure 1.1: Generic structure of common fluorophores including BODIPY.

Boron dipyrromethene (4,4-difluoro-4-bora-3a,4a-diaza-s-indacene, hereafter referred to as BODIPY), is formed from the complexation of a dipyrromethene ligand with a disubstituted boron moiety, typically in the form of  $\text{BF}_2$ , achieved using boron trifluoride diethyl etherate.<sup>6-8</sup> The dipyrromethene ligand is formed from the linking of the  $\alpha$ -position of two pyrroles via a methine bridge. Complexation of the dipyrromethene ligand with the  $\text{BF}_2$  unit forms a rigid tricyclic system and prevents *cis/trans* isomerization of the dipyrromethene, allowing for the conjugation of  $\pi$ -electrons along the carbon-nitrogen backbone which leads to unusually high fluorescence quantum yields.<sup>9</sup> The BODIPY fluorophore, once complexed with  $\text{BF}_2$  can be compared to a “constrained” cross-conjugated cyanine dye possessing fixed planarity of the fluorophore’s conjugated  $\pi$ -system.<sup>10</sup> The resultant zwitterionic species possesses an overall neutral charge.

Several approaches have been accepted in the systematic naming the BODIPY core. The first utilizes the similarity in BODIPY’s structure to that of s-indacene, it’s all-carbon tricyclic analog (Figure 1.2).<sup>6</sup> Following this identification system, the 3- and 5- carbons are referred to as alpha and the 1, 2, 6 and 7 are denoted as beta, parallel to that of pyrrole.<sup>11</sup> The C-8 position is referred to as the *meso*-position, following the accepted labeling of porphyrinic systems.<sup>7</sup>

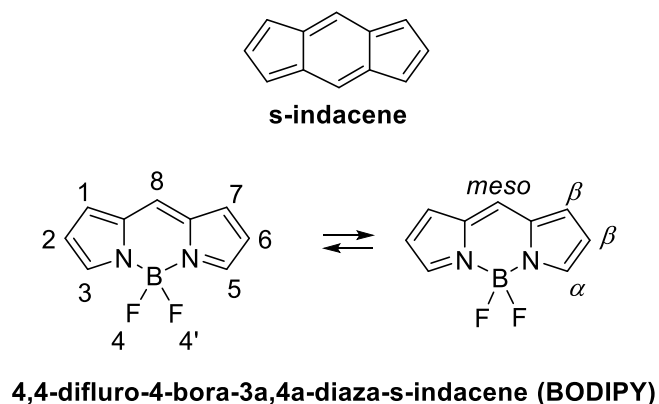


Figure 1.2: Naming and numbering of BODIPY based on s-indacene.

Analysis of single crystalline BODIPY chromophores units identifies a three-ring fused framework, as shown in Figure 1.3, exhibiting strong  $\pi$ -electron delocalization across the nine carbons and two nitrogens making up the central six-membered ring and the two flanking five-membered pyrrolic rings.<sup>12</sup> This  $\pi$ -conjugation is disrupted by the B-N bonds, indicating the  $\text{BF}_2$  moiety plays very little to no role in the system's extended  $\pi$ -delocalization. The mean bond length between  $\text{N}_1\text{-C}_3$  depicts double bond character, whereas the  $\text{N}_1\text{-C}_4$  indicates single bond character. The central boron atom displays a distorted tetrahedron  $\text{BF}_2\text{N}_2$  configuration as noted by the  $\text{N}_1\text{-B}_1\text{-N}_2$  and  $\text{F}_1\text{-B}_1\text{-F}_2$  bond angles.<sup>13</sup> The BODIPY fluorophore is isoelectronic with heptamine cyanine possessing  $12\pi$  electrons delocalized over eleven atoms, rather than the monomethine cyanine dye with  $6\pi$  electrons equally distributed over five atoms the BODIPY more closely resembles.<sup>14</sup>

The monoclinic unit cell of the BODIPY fluorophore consists of four molecules stacked head-to-tail, an arrangement that aids in optimizing  $\pi$ - $\pi$  interactions between adjacent hydrophobic BODIPY molecules and countering the variability of the fluorine atoms' dipole moments.<sup>15</sup> The slight polarization of the heteroatoms generates electronically diverse reaction sites of the BODIPY carbon core, favoring both nucleophilic and electrophilic reactions. Such electronic diversity across a single molecular structure opens the door for countless structural modifications on the core.<sup>16</sup>

Known affectionately as “porphyrin's little sister,” these fluorescent molecules bear outstanding optical properties compared to traditional fluorophores such as rhodamines and fluorescein.<sup>6</sup> Like porphyrins, BODIPY and its derivatives absorb strongly visible region, have relatively sharp emission peaks, possess high fluorescence quantum yields, and high molar absorption coefficients (in the range of 40,000 to 80,000  $\text{M}^{-1} \text{cm}^{-1}$ ), and have relatively small

Stokes' shift (around 10 nm).<sup>6,9</sup> Other favorable properties of BODIPY as imaging agents include negligible triplet-state formation of non-halogenated BODIPYs (due to a slow rate of intersystem crossing (ca.  $10^6$  s<sup>-1</sup>)), resistance toward self-aggregation, and fluorescence lifetimes in the nanosecond range.<sup>1</sup> Additionally, most BODIPY dyes exhibit thermal and photostability in solid and solution phases, are highly soluble in most organic solvents, and are insensitive to solvent polarity and pH.<sup>7, 17, 18</sup>

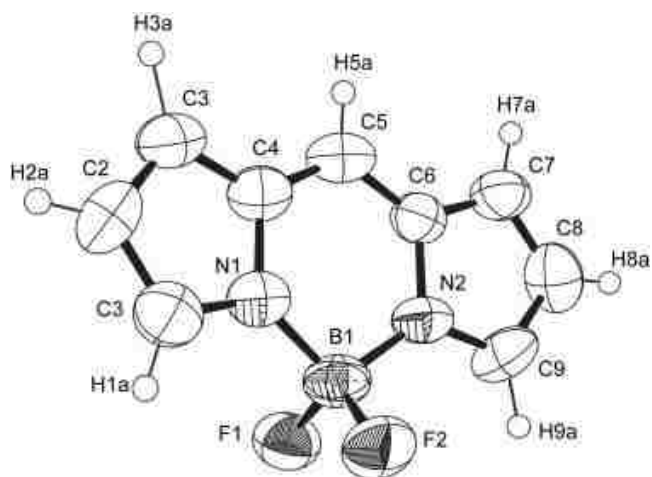


Figure 1.3: The crystal structure of unsubstituted BODIPY elucidated by X-ray analysis with atoms labelled and 50% probability displacement ellipsoids.<sup>19</sup>

The BODIPY absorption profile shows a strong, narrow absorption band in the visible region signifying the  $S_0$ - $S_1$  ( $\pi$ - $\pi^*$ ) transition with a shoulder of high energy around 480 nm assigned to the 0 - 1 vibrational translation. A broad, much weaker band around 350 nm denotes the  $S_0$ - $S_2$  ( $\pi$ - $\pi^*$ ) transition.<sup>20</sup> Upon excitation to either the  $S_1$  or  $S_2$  states, an equally narrow emission band of mirror image to the absorption spectra is observed from the  $S_1$  state. Most BODIPYs emit at wavelengths less than 600 nm, routinely providing yellow to green emissions (500 nm – 590 nm).<sup>6, 21</sup> Unsubstituted BODIPY typically absorbs near 500 nm and emits around

510 nm. Small Stokes' shifts are routinely seen and indicate a modest change in the core structure following  $S_0$ - $S_1$  transition and vibrational relaxation.<sup>22</sup>

Addition of functionality at any position of the aromatic core alters the photochemical profile to varying degrees, dependent upon the groups added. The BODIPY core can be easily modified to bear desired functionalities at the  $\alpha$ -,  $\beta$ -, and *meso*- positions as well as through substitution of the fluorines. As seen in Figure 1.4, the addition of functional groups to the BODIPY core can have varying effects dependent upon the placement and symmetry of the substituent.<sup>23, 24</sup> Symmetrical BODIPYs **1** and **3** appear to produce more red-shifted absorptions compared to either equally substituted asymmetric counterpart. However, greater substitution of the BODIPY core does not necessarily produce a larger bathochromic shift, as depicted upon the comparison of the penta-substituted BODIPY **4** to the tetra-substituted BODIPY **3**.

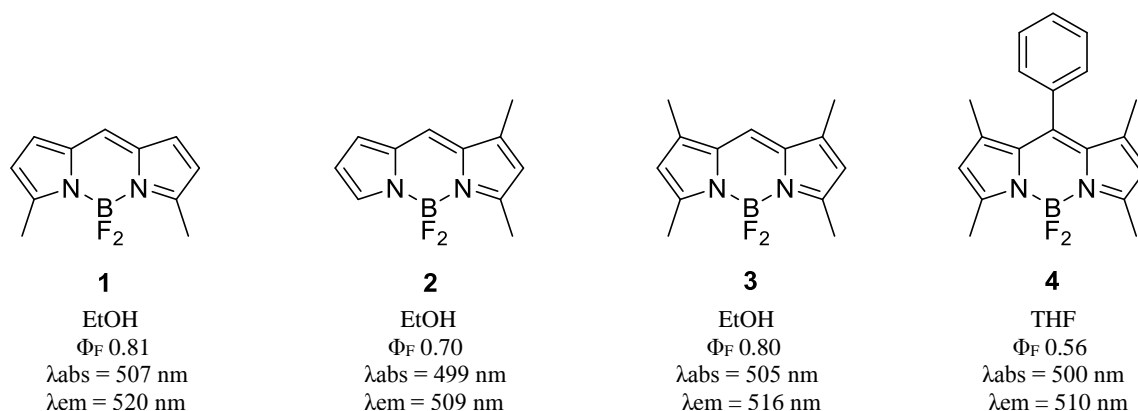


Figure 1.4: The effect of substituents on the absorption wavelength of simple BODIPYs.<sup>23, 24</sup>

Red to NIR shifts are typically achieved through facile modification to the BODIPY core, extending the degree of  $\pi$ -delocalization. In addition, the emissive behavior of BODIPY fluorophores are greatly influenced by steric and electronic interactions of substituents. Rotation

or rigidity of pendant components, as well as their electron-donating or withdrawing effects on the conjugated core greatly influences both the brightness and absorptive and emissive properties of BODIPY.<sup>25</sup>

Increasing development of facile synthetic modifications had led to an outpouring of research dedicated to functionally diverse BODIPY dyes. Many of the techniques used in modification of the spectroscopic characteristics and functional properties of these versatile fluorophores to develop multi - purpose fluorescent probes will be discussed within the pages of this dissertation.

## **1.2 Synthetic Methodologies**

The first BODIPY was synthesized by Treibs and Kreuzer in 1968 by accident through the combining of 2,4-dimethylpyrrole and acetic anhydride in the presence of  $\text{BF}_3 \cdot \text{OEt}_2$ , and was initially developed for use as tunable laser dyes.<sup>26</sup> Immediately following its discovery, little work was done on this photo-stable substitute for fluorescein.<sup>6</sup> It was not until the late 1980s that the potential of BODIPY in many areas, especially in cellular imaging, was recognized. Work on BODIPYs boomed in the mid-1990 and has increased significantly since. Despite their initial lack of interest, study of these compounds has led to exuberant research interest in recent decades in many different applications which take advantage of their readily amended optical profiles yielding numerous patents and review articles.<sup>1, 6, 7, 9, 22</sup> Extensive research surrounding the reactivity of the BODIPY core has produced methodologies for synthesizing amphiphilic and longer-wavelength absorbing and emitting fluorophores for a plethora of applications including as fluorescent labels for biomolecules and cellular imaging, light-emitting devices, drug delivery

agents, photosensitizers, fluorescent switches, chemosensors, energy transfer cassettes, and solar cells.

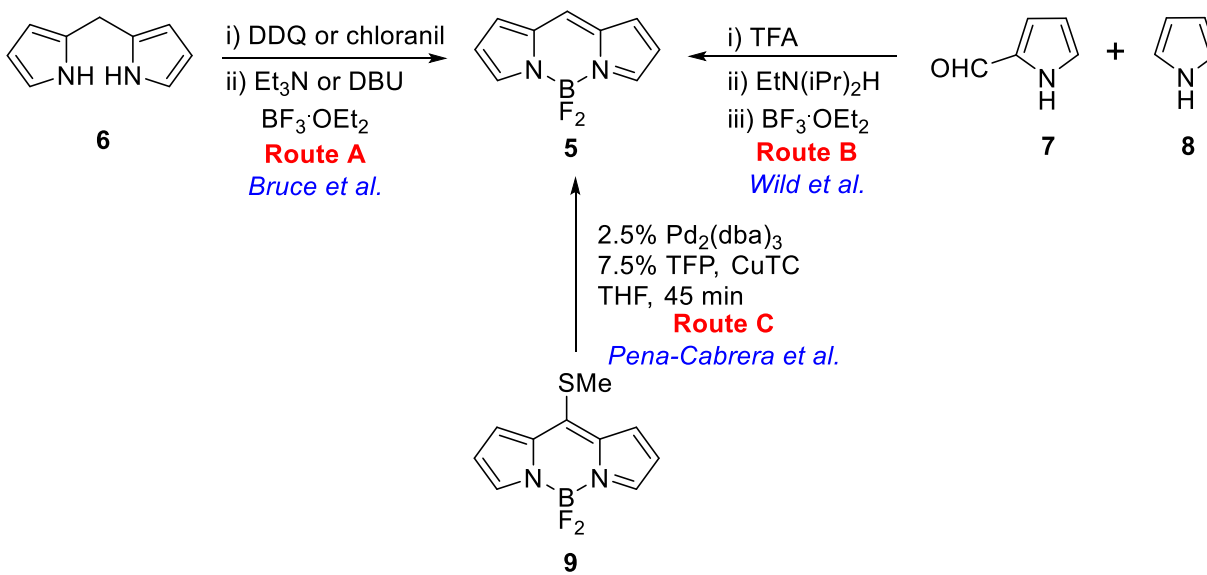
### 1.2.1 Synthesis of the BODIPY Core

Various methodologies derived from the well-known chemistry of pyrroles and dipyrromethanes have been utilized in the synthesis of these fluorophores. Incorporation of readily available pyrroles with highly electrophilic carbonyl compounds yields a variety of dipyrromethene ligands. Complexation with  $\text{BF}_2$  in the presence of a non-nucleophilic base, typically a secondary or tertiary amine, affords the BODIPY fluorophore in moderate, yet reproducible yields.

Although literature boasts countless reports on the ease of synthesizing highly substituted BODIPY cores, the synthesis of the unsubstituted parent fluorophore remained a challenge. The highly unstable dipyrromethene precursor made producing the “naked” core in appreciable yields difficult. Not until recently, through the simultaneous work of three independent research groups, was a route to producing this compound established. The first synthetic route was reported by Bruce and co-workers (Scheme 1.1, Route A),<sup>19</sup> in which the highly reactive precursor dipyrromethane **6** was oxidized to the dipyrromethene. To control side reactions, the DDQ oxidation was carried out at  $-78^\circ\text{C}$  under inert conditions followed by subsequent *in situ* complexation with  $\text{BF}_3\cdot\text{OEt}_2$  with the aid of DBU to form the target compound in 5-10% yield. The parent BODIPY was characterized by  $^1\text{H}$ -,  $^{13}\text{C}$ -,  $^{11}\text{B}$ -, and  $^{19}\text{F}$ -NMR and single crystal X-ray analysis.

Applying a classic one-pot synthetic approach of combining pyrrole-2-carbaldehyde **7** and pyrrole **8** in the presence of an acid catalyst followed by complexation of  $\text{BF}_2$  in the presence of a

base, Wild and co-workers<sup>16</sup> were able to synthesize the desired BODIPY **5** in 8% yield (Route B). Extensive column chromatography was employed in order to produce product of pure quality. The resultant BODIPY displayed the characteristic green fluorescence with a maximum absorbance wavelength of 503 nm and a fluorescence maximum wavelength of 512 nm. Over the course of experimentation it was noted that BODIPY exhibits high photostability ( $\tau = 7.2$  ns) but readily decomposes above 50°C, as a result of lacking substitution.



Scheme 1.1: Synthesis of the unsubstituted BODIPY **5**.

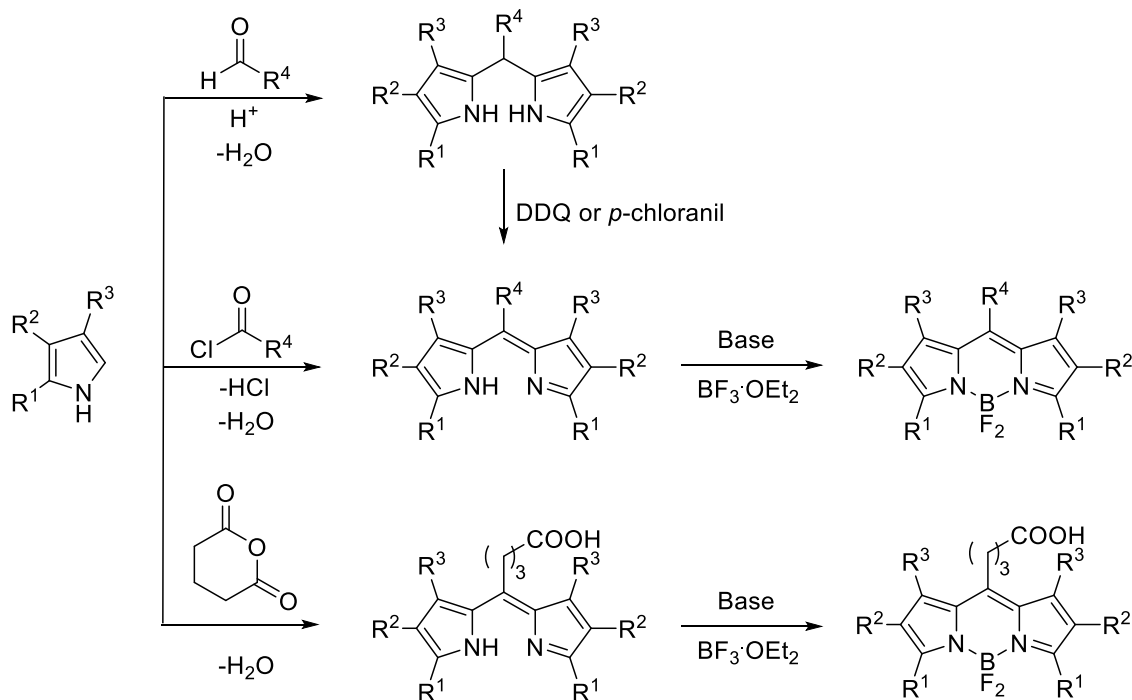
The most efficient route was penned by Pena-Cabrera and co-workers (Route C),<sup>15</sup> producing the target parent BODIPY in an impressive 98% yield. The mild reaction between 8-thiomethyl BODIPY **9** and trimethylsilane with the aid of a stoichiometric amount of copper(I) thienyl-2-carboxylate (CuTc) and a catalytic amount of palladium in THF stirred at 55°C for 45 minutes, afforded the desired BODIPY **5** which exhibits quantum yields up to 94% in both polar and non-polar solvents.

### 1.2.2 Synthesis of Symmetric BODIPY Dyes

Syntheses of 8- or *meso*- substituted BODIPYs are found most frequently in literature and involve preparation of the dipyrromethene ligand by acid-catalyzed condensation of two pyrroles with an acid chloride, anhydride, or aryl-aldehyde. Reaction with an aldehyde affords the dipyrromethane rather than the dipyrromethene and must be subsequently oxidized to generate the desired conjugated bipyrrrolic system. In order to avoid forming pyrrolic chains longer than two units, the starting pyrrole must have only one  $\alpha$ -position available for reaction.<sup>27</sup> Once formed, the dipyrromethene ligand can be complexed to form the BODIPY by reacting with  $\text{BF}_2\text{OEt}_2$  in the presence of a tertiary amine. Substituted BODIPYs, especially at the *meso*-position, show greater stability than their *meso*-unsubstituted counterparts. As described, this two/three step-one pot reaction has become standard practice for synthesizing *meso*-substituted BODIPYs. These relatively mild reaction conditions allow for the formation of BODIPYs bearing a large range of functional groups. With such diversity of functional groups tolerated by this synthetic method, the functionalized *meso*-substituent has served as a point of embellishment to build larger, specific function fluorophores for a variety of purposes, most extensively for use as bioimaging labels.<sup>28</sup>

Most common syntheses of symmetrical BODIPYs involve condensation of an aryl-aldehyde with two equivalents of an  $\alpha$ -free pyrrole. An oxidation step is required to transform the dipyrromethane to a dipyrromethene unit before further complexation with  $\text{BF}_2$ . The use of oxidizing agents such as DDQ (2,3-dichloro-5,6-dicyano-*p*-benzoquinone) and *p*-chloranil are common. However, use of such agents creates byproducts which must be separated by tedious chromatography. This method produces a symmetric structure bearing the aryl moiety at the *meso*-position, Scheme 1.2.

Another common method of synthesizing symmetrical BODIPYs, also shown in Scheme 1.2, involves the condensation of an acid chloride with two units of an  $\alpha$ -free pyrrole. Unlike the synthesis involving aryl-aldehydes, there is no need for an oxidation step in forming dipyrromethene from the dipyrromethane, often resulting in larger yields with less purification required.



Scheme 1.2: General procedure for the synthesis of symmetrical BODIPY via condensation of two pyrrole units with an activated carbonyl.

Despite the addition of an aromatic substituent to an extended  $\pi$ -system, an aryl-moiety at the *meso*-position typically lies almost perpendicular to the BODIPY core, thus practically eliminating conjugation.<sup>6, 7, 13, 29</sup> Due to the opposite orientation of the *meso*-substituent and the BODIPY core, the aryl-group participates little in electron conjugation which prevents it from having any significant effect on altering the absorption and emission wavelengths of the

fluorophore. Substituents at the 1,7-positions of the core prevent free rotation of the *meso*-group which reduces energy lost from excited states by non-radiative decay.<sup>7</sup> *Ortho*-substituents on a phenyl ring located at the *meso*-position also prevent free rotation which increases the brightness of fluorescence. Although the *meso*-group often has little effect on the photophysical properties of BODIPY, variations in the *meso*-position yield structurally and functionally unique compounds. This also allows for selective groups to be introduced without affecting the optical properties of the dye. Such variations allow for these compounds to be used in many applications across many fields, from medicinal chemistry to materials chemistry to imaging and energy transfer.

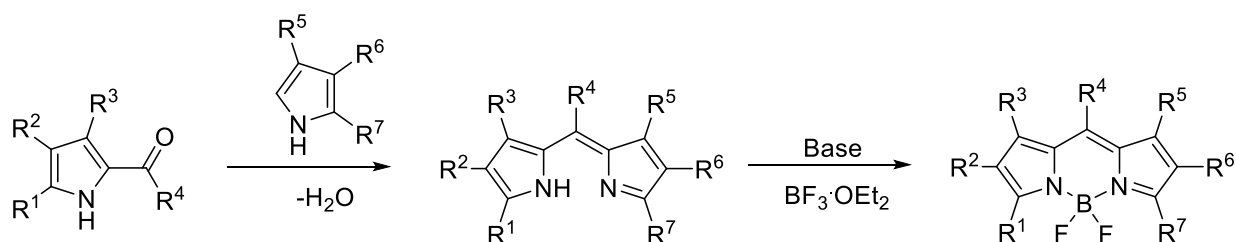
Acid anhydrides can also be used in synthesizing symmetrical BODIPYs. The use of the anhydride produces a free carboxylic acid which may be utilized in labeling biological molecules such as proteins, DNA, and lipids.<sup>17, 30</sup>

Symmetric BODIPYs lacking a *meso*-substituent are obtained from condensation between a carbonyl-bearing pyrrole and an  $\alpha$ -free pyrrole of equal substitution. An acid catalyst, typically *p*-toluenesulfonic acid or Montmorillonite clay, is required to generate the pyrrole carbonyl cation which condenses with a second  $\alpha$ -free pyrrole to form a dipyrromethene that is complexed by BF<sub>2</sub>.<sup>31, 32</sup> In a modified approach reported more recently by Wu and Burgess,<sup>33</sup> pyrrole-2-carbaldehyde self-condenses in the presence of phosphorous oxychloride, via a dipyrromethenium cation and dichlorophosphate anion which readily complexes with BF<sub>2</sub>. This new method produces the desired *meso*-free BODIPY in much higher yields than the conventional approach.

### 1.2.3 Synthesis of Unsymmetrical BODIPY Dyes

Unsymmetrical BODIPYs can be formed from the acid-catalyzed condensation of a carbonyl-containing pyrrole and a dissimilar  $\alpha$ -free pyrrole in similar protocol to that of acid

chloride condensation, Scheme 1.3.<sup>34</sup> The condensation of a 2-carbonyl-pyrrole with an  $\alpha$ -free pyrrole under catalytically acidic conditions typically affords the desired BODIPY in high yields when electron-rich pyrroles are used. When electron-deficient pyrroles are employed, self-condensation of pyrrole-2-carboxaldehyde are favored resulting in higher yields of the undesired symmetric BODIPY.



Scheme 1.3: Common procedure for the synthesis of asymmetric BODIPY from carbonyl-substituted pyrrole.

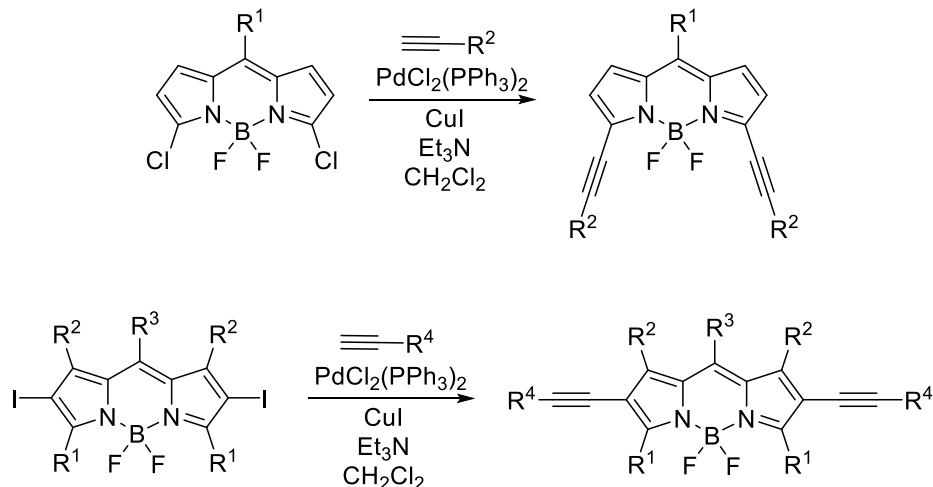
The resultant dipyrromethene is usually isolated in its salt form, which readily reacts with  $\text{BF}_3\cdot\text{OEt}_2$  in the presence of a tertiary amine to afford the desired BODIPY. This method allows for the formation of BODIPYs bearing different functional moieties on the left and right hemispheres facilitating further functionalization and bioconjugation.

### 1.3 Derivatization of the BODIPY Platform

In addition to their outstanding photophysical properties, these intrinsically electron-rich compounds are relatively easy to synthesize and derivatize due to their variable reactivity to numerous reaction types. Functionality may be added to nearly every position of the formed BODIPY core, as well as, being incorporated via commercially and synthetically accessible substituted pyrroles in their initial synthesis. The absorption and fluorescence properties of

BODIPY are highly influenced by the extent of electron delocalization around the core and also through conjugated substituents, and as such, may be tuned to have particular photophysical characteristics. However, there is still a lack of strategy for incorporation of function groups that allow for facile conjugation to biomolecules.

Many research groups, including Vicente,<sup>29, 35, 36</sup> Burgess,<sup>37</sup> Ziesse,<sup>8</sup> Boens and Dehaen,<sup>1, 38</sup> Nagano,<sup>39</sup> Akkaya,<sup>40</sup> O'Shea,<sup>41</sup> Rurack and Daub,<sup>42</sup> and Carreira<sup>43</sup> are intensively exploring strategies for modifying the optoelectronic properties as well as the function of these dyes, including i) electrophilic substitutions at the 2,6-positions, ii) addition of functionalized styryl groups at the 3,5-positions via electrophilic methyl groups, iii) nucleophilic substitution at the 3,5-positions, iv) Palladium-mediated cross couplings with halo-derivatives, v) replacement of the *meso*-carbon with nitrogen, vi) fusion of aromatic rings to the pyrrolic units, vii) replacement of pyrrole with isoindole or indole derivatives and viii) nucleophilic substitution of fluorine at the boron center. Halogens typically located at the 2, 3, 5 and 6 positions are capable of undergoing metal-mediated cross-couplings. Examples of Suzuki,<sup>44-46</sup> Sonagashira (Scheme 1.4),<sup>36, 44, 47</sup> Heck<sup>48</sup>, and Stille<sup>49</sup> couplings can be found in literature.



Scheme 1.4: Sonagashira couplings of halogenated BODIPYs.

### 1.3.1 Modification at the C8-Position

Functionalization at the C-8 position or *meso*-position occurs most readily compared to substitution at the pyrrolic positions. Functionality at this position is incorporated during the synthesis of the dipyrromethane via acid-catalyzed condensation of pyrrole with a specifically substituted aryl-aldehyde or acyl-chloride.<sup>50</sup> This point of variability remains the most utilized for its versatility in incorporating utility groups such as ion capture ligands,<sup>1, 6, 51</sup> donor-acceptor groups,<sup>52-54</sup> chiral auxiliaries,<sup>55, 56</sup> water solubilizing groups,<sup>5, 18</sup> and biomolecules<sup>57</sup> for applications as pH probes, chemosensors, light-harvesting devices and biological labels (Figure 1.5, structures **10** to **13**).

The effect of electron-rich or electron-deficient groups at the *meso*-position has been studied extensively by Boens and co-workers.<sup>1, 38, 58</sup> Notably, the *meso*-substituent of aryl- or alkyl-type has very little effect on the optoelectronic properties of the BODIPY. Since this group favors orienting itself orthogonally to the BODIPY core, it does not extend the electron conjugation of the system. Although conjugation is unaffected by this group, the compound's fluorescence efficiency is impacted by the free rotation of the *meso*-substituent. Incorporation of substituents at the 1,7-positions of the core sterically impedes this rotation and increases the fluorescence quantum yield.

Exchange of the *meso*-carbon for nitrogen generates an analogous class of compounds referred to as aza-BODIPYs (Figures 1.5, structures **14** and **15**, and Figure 1.6). Despite the predecessor dipyrromethane having been in chemical existence for some time, the synthesis and use of aza-BODIPYs has only recently garnered attention. Like BODIPY, aza-BODIPY has high molar extinction coefficients and moderate fluorescence quantum yields (*ca.* 0.20 - 0.40).

Incorporation of the lone pair on the nitrogen greatly influences the HOMO-LUMO energy gap through stabilization.<sup>6</sup> This enhanced stability creates a red-shift in the absorption and emission profiles into the 650 - 850 nm range.<sup>59</sup> Aza-BODIPYs can be synthesized from nitroso-bearing pyrroles, via Michael addition products from chalcones and formamide, and from cyanide Michael addition products and ammonia.<sup>60,61,62</sup> This class of BODIPY has found use as photosensitizers,<sup>49, 63</sup> near-IR emitting chemosensors and imaging probes,<sup>43, 64-66</sup> and as fluorescent labels.<sup>67, 68</sup>

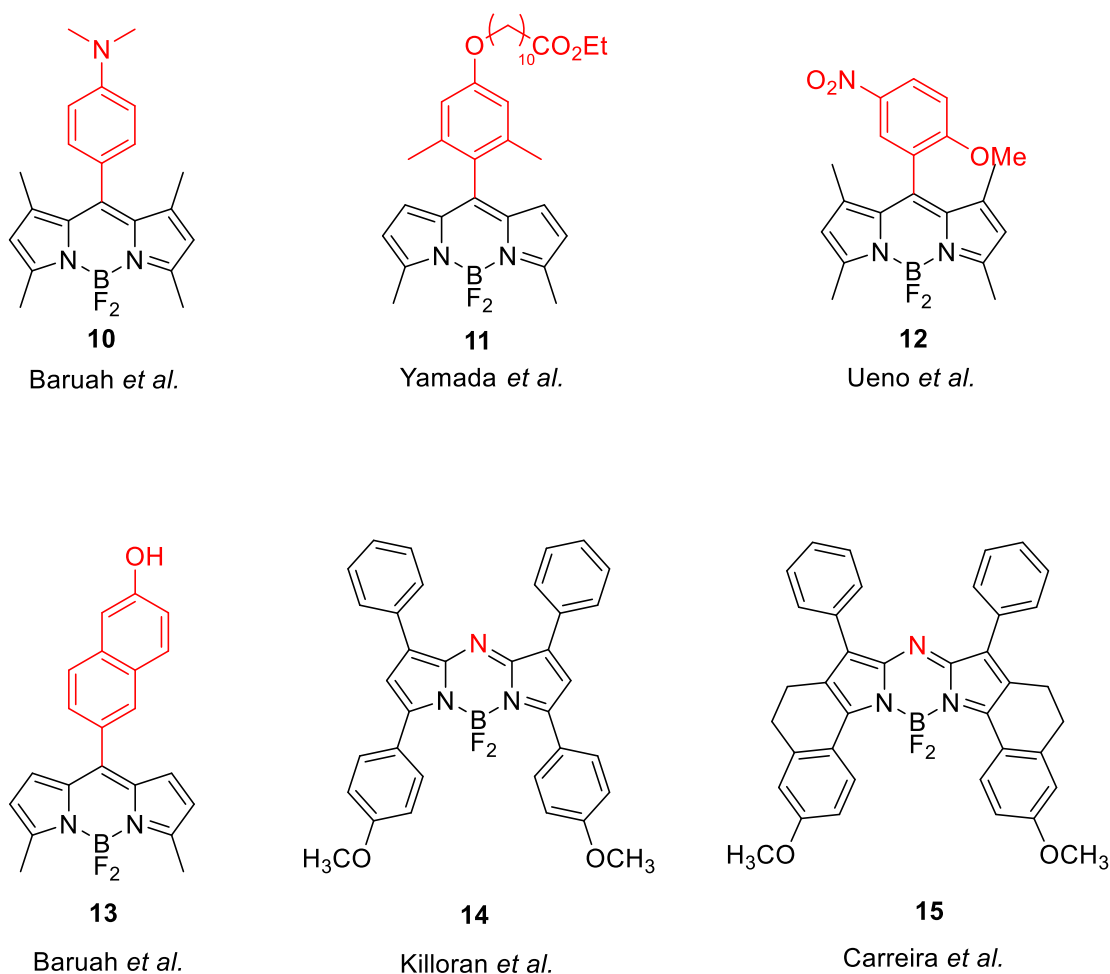


Figure 1.5: Chemical structures of various *meso*-substituted BODIPYs from literature: **10**,<sup>58</sup> **11**,<sup>69</sup> **12**,<sup>70</sup> **13**,<sup>58</sup> **14**,<sup>71</sup> and **15**.<sup>43</sup>

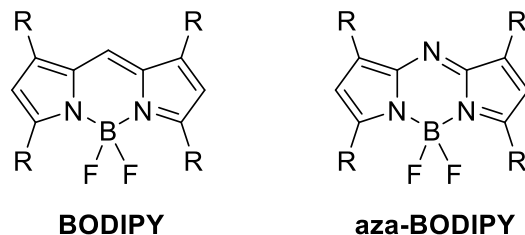


Figure 1.6: Structure comparison of BODIPY and aza-BODIPY dyes.

### 1.3.2 Functionalization of the 1, 3, 5, 7-Positions

Due to the electron density concentrated within the nine carbons and two nitrogens of the BODIPY core, methyls located at the 1, 3, 5, and 7-positions are strongly nucleophilic, with the 3,5-methyls bearing the most nucleophilic behavior, and can be easily deprotonated under mild basic conditions. Most commonly, the *in situ* deprotonated anionic methene is added to an electron-rich aromatic aldehyde by way of a Knoevenagel condensation to generate a styryl group (Figure 1.7, **16**, **17**).<sup>72-74</sup> Although the tetra-styryl BODIPY has been synthesized by activation and subsequent condensation of the 1, 3, 5, and 7-methyls,<sup>75</sup> extension of  $\pi$ -conjugation and addition of functionality is most frequently accomplished through the 3,5-methyls. Addition of conjugation at the 3,5-positions generally produces a greater bathochromic shift (*ca.* 50 - 100 nm) than adding conjugation through the 2,6-positions, displaying the greatest shift when all four methyls have converted to styryl groups.

Conjugation with highly decorated aryl-aldehydes offers a convenient approach for adding pendent functionalities that is easily controllable through simple modification to reaction conditions. Extension of the  $\pi$ -system, typically through the 1, 3, 5, and 7-positions effects the absorption and emission profile of the BODIPY system most drastically, although addition at the 2,6-positions does have an effect as well. Incorporation of electron-donating groups immediately adjacent to the core creates a red-shift in the absorption and emission maxima.<sup>7</sup>

Furthermore, good leaving groups, such as chlorines or iodines occupying the 3,5-positions allows electron-deficient BODIPYs to undergo nucleophilic substitution reactions (as shown by structure **18**). Various nucleophiles, including carbon, nitrogen, oxygen, and sulfur, have been used to add functionality or to extend conjugation and red-shift the emission profile of the BODIPY.<sup>17</sup> The presence of halogens at the 3,5-positions also allows the use of palladium-mediated couplings for the incorporation of ethynyl, ethenyl, and aryl-substituents for use in long wavelength BODIPY-based (**19**) fluorescent biosensing material and biolabels.

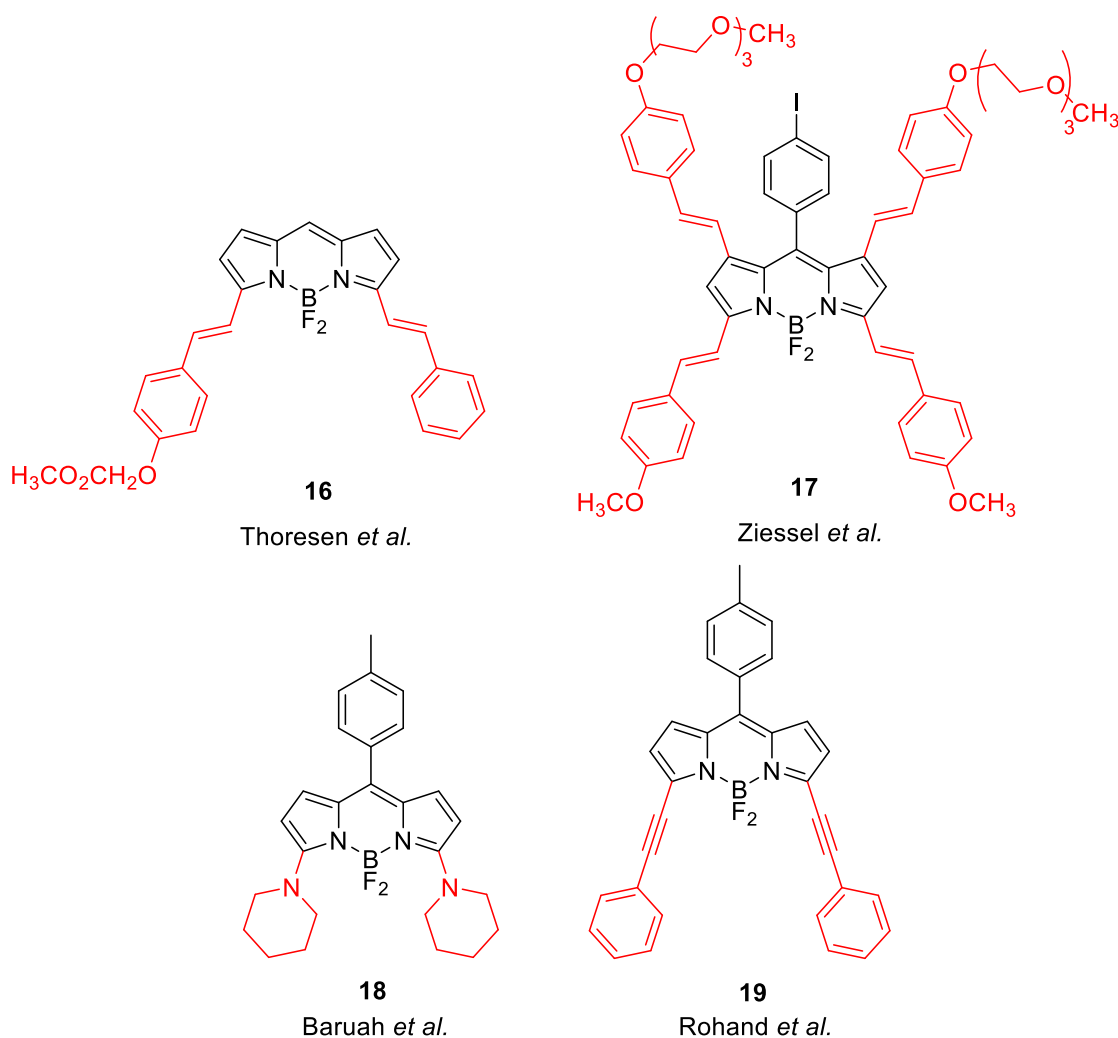


Figure 1.7: Chemical structures of 1,3,5,7-modified BODIPY dyes: **16**,<sup>76</sup> **17**,<sup>75</sup> **18**,<sup>77</sup> **19**.<sup>78</sup>

### 1.3.3 Functionalization of the 2, 6-Positions

Electronic mapping study of resonance structures of the BODIPY core show that the 2 and 6-positions bear the least positive charge and are the least electrophilic, Figure 1.8. As such, they readily undergo electrophilic aromatic substitution reactions.

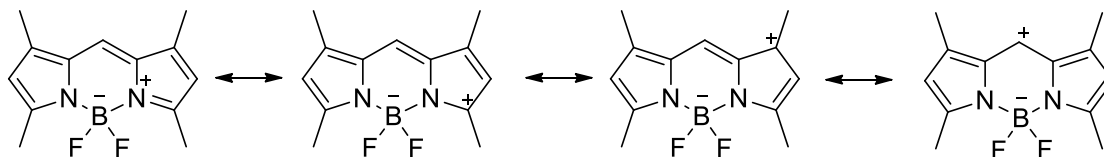


Figure 1.8: Resonance delocalization of positive charge over the BODIPY core.

Despite there only being a few electrophilic substitution reactions reported, including halogenation (Br, Cl and I),<sup>39</sup> nitration (via nitric acid),<sup>79</sup> sulfonation (by way of chlorosulfonic acid, Figure 1.9, **20**),<sup>17, 80, 81</sup> and most recently formylation,<sup>50</sup> they have been extensively employed. The use of sulfonate groups to improve-water solubility of the typically lipophilic core without impacting the BODIPY's optical properties is seen frequently in literature reports of BODIPYs with biological purposes.

The introduction of halogens, usually Br or I, at these positions causes a bathochromic shift in the absorption and emission spectra and fluorescence quenching in comparison to the parent dye. This can be attributed to an heavy atom effect.<sup>7</sup> Subsequent reaction occurs readily at these positions while leaving the BF<sub>2</sub> chelate intact. This type of modification is usually used as a precursor to palladium-catalyzed couplings, including Suzuki,<sup>82</sup> Stille,<sup>78</sup> Sonagashira (e.g. **21**),<sup>83</sup> and Heck couplings.<sup>84</sup>

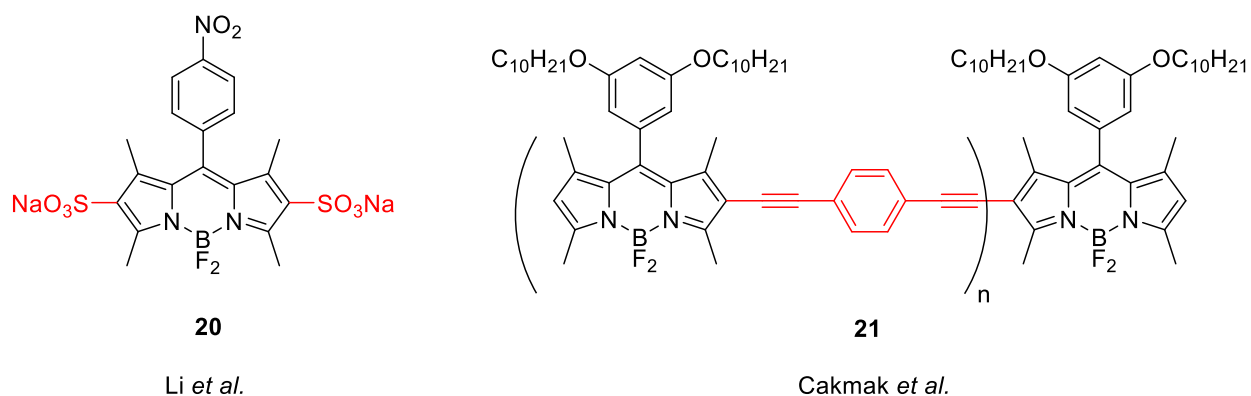


Figure 1.9: Chemical structures of 2,6-functionalized BODIPYs from literature: **20**,<sup>30</sup> **21**.<sup>85</sup>

### 1.3.4 Boron Center

To date, few attempts have been made to substitute the fluorines of the boron difluoride chelate. Functionalization at this position has become an increasingly more popular target and more manuscripts are being published to that effect. Incorporation of alkyl groups,<sup>86</sup> large aryl groups,<sup>87</sup> ethynyl groups and ethynyl aryl moieties,<sup>8, 21, 88-91</sup> and alkoxy groups<sup>92</sup> can be found in literature (Figure 1.10, structures **22-24**). Replacement of the fluorines by carbon, ethynyl, and oxygen nucleophiles has led to a family of photostable, highly luminescent redox-active *C*-BODIPYs, *E*-BODIPYs, and *O*-BODIPYs, respectively.<sup>7</sup> Modification of the boron chelate has shown to enhance the stability and Stokes' shift of the fluorophore. Substitution of fluorine requires the use of organometallic compounds, typically an organolithium or Grignard complex, in order to be accomplished.

The grafting of large light-harvesting units onto the core through the boron chelate has been explored for use as rapid energy transfer cassettes by way of through-space energy transfer from the donor to the core acceptor that is facilitated by significant overlap of the donor's emission spectra with the absorption spectra of the acceptor. Much like the *meso*-substituent, attachments through the boron center do not affect the photophysical properties of the fluorophore. These novel

donor-acceptor systems have found possible uses as molecular dyads, energy transfer cassettes, electroluminescent devices, photovoltaic and supramolecular assemblies.<sup>87, 89, 93</sup>

### 1.3.5 Ring Fusion

In order to shift the absorption and emission profiles of BODIPY into the far red to near-IR regions, an extended electron delocalization pathway is needed. As seen frequently in literature, this can be accomplished through the addition of styryl and thienyl groups, as already discussed.<sup>46</sup> Another way to achieve extended conjugation is through the fusion of benzene rings directly to the pyrrolic units.<sup>94-96</sup>

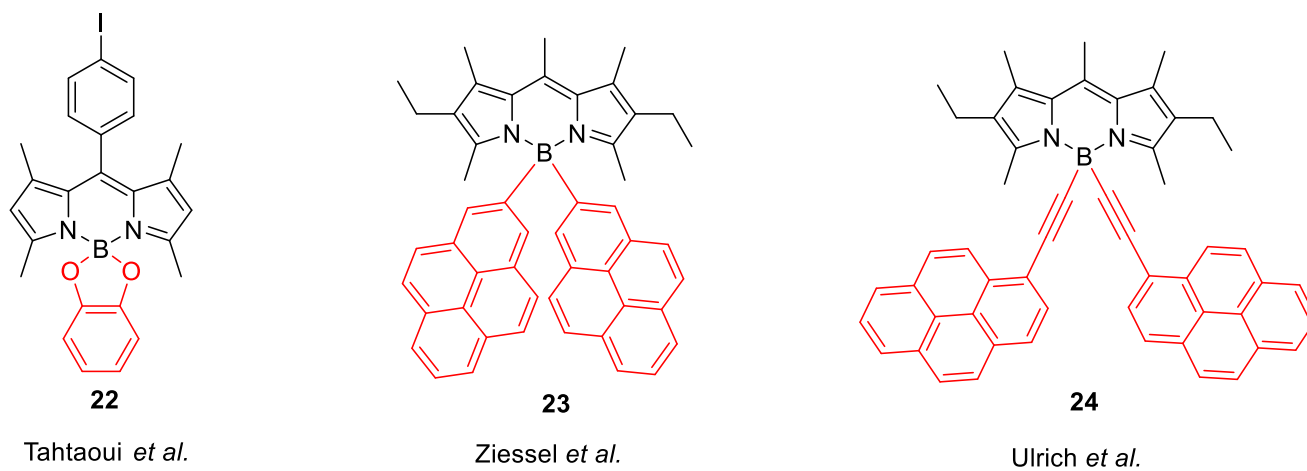


Figure 1.10: Chemical structures of F-substituted BODIPYs from literature: **22**,<sup>97</sup> **23**,<sup>8</sup> **24**.<sup>88</sup>

Red and near-IR emitting dyes have become a valuable target for biological imaging. Fusion of aromatic rings onto the BODIPY core has been recently utilized in achieving dyes with longer wavelengths. Strategies involving the use of aryl-fused pyrroles, 2-acetyl phenols,<sup>91</sup> and retro Diels-Alder syntheses of norbornane-derived pyrroles<sup>12, 98</sup> have allowed for the formation of

these  $\pi$ -extensive systems, Figure 1.11, **25** to **27**. Incorporation of various benzene and substituted benzene,<sup>91</sup> indole and isoindole,<sup>99, 100</sup> and larger aromatic systems<sup>101</sup> fused to the BODIPY core has allowed for the development of red-shifted, brighter emitting fluorophores compared to their unconstrained analogs.

All of these various ways of modifying the BODIPY core increase the versatility of these dyes immensely. Simple modifications allow for these compounds to be tailored to particular wavelengths or functions. The possible uses for these readily synthesized and functionalized small molecules are endless.

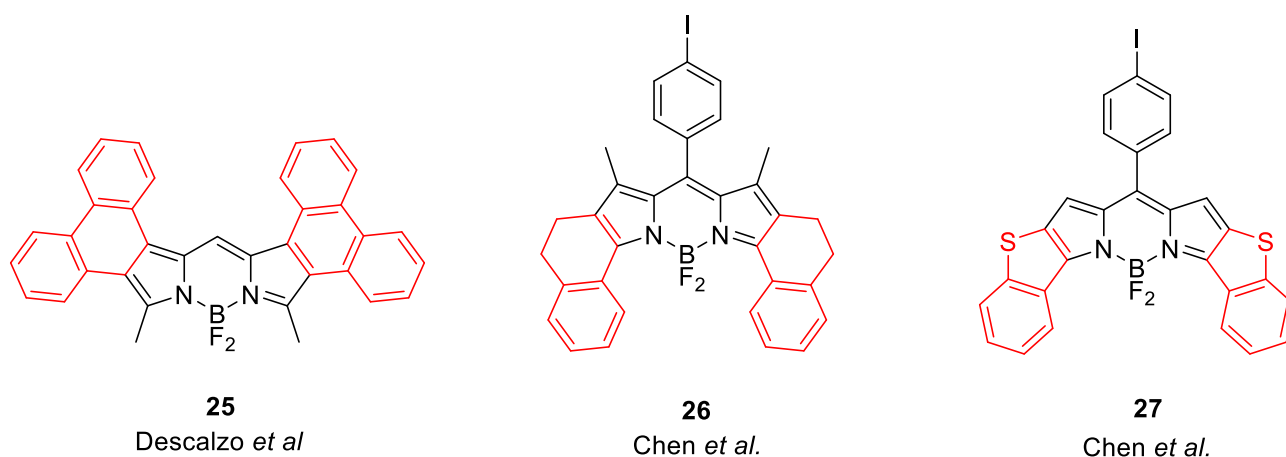


Figure 1.11: Chemical structures of aromatic-fused BODIPYs from literature: **25**,<sup>101</sup> **26**,<sup>102</sup> **27**.<sup>102</sup>

#### 1.4 Applications of BODIPY Dyes

Most commonly, these fluorophores are used as tunable laser dyes,<sup>45</sup> in biological labeling and imaging,<sup>30, 36</sup> and as electroluminescent devices.<sup>53</sup> Other current uses include donor-acceptor systems (energy transfer cassettes),<sup>54, 89, 93, 103</sup> fluorescent chemosensors,<sup>29, 47, 100</sup> electron transfer reagents,<sup>72</sup> light-emitting and ion signaling devices,<sup>1</sup> and photodynamic therapy (PDT) agents.<sup>104,</sup>

Fluorescence microscopy has become an ever more valuable tool for imaging in living cells. In addition to providing high sensitivity and specificity, microscopy yields good spatial and temporal sampling ability, instruments are simple to operate, and the technique is minimally invasive to cells.<sup>1</sup> Because light can traverse biological tissues, microscopy imaging makes it possible to visualize location and concentration of analytes contained within all parts of a living cell. BODIPYs have been used in bioimaging in many ways.

### 1.4.1 Biological Applications

In the biological realm, fluorescent dyes have demonstrated to be essential for use as reporting molecules for various intracellular analytes (metal ions and protons) and biomolecules including peptides, proteins, enzymes, nucleic acids, and lipid membranes. Particularly, fluorescent organic dyes have been employed as non-radioactive ligand as biomarkers in *in vivo* imaging and for biological processes.<sup>80</sup> The advancement of bioanalytical and optical imaging techniques in recent years has created a need for dyes that fluoresce in the red and near-IR region of the visible spectrum. Advancements in DNA sequencing, nucleic acid detection, gel electrophoresis, *in vivo* imaging, vasculature mapping and tissue perfusion have driven such a demand.<sup>106</sup>

Working in the red/near-IR region has many advantages. Imaging in the 600- 900 nm region of the electromagnetic spectrum improves light penetration and helps to eliminate much of the light scattering caused by endogenous chromophores found within biological tissues. Chromophores such as lipids, hemoglobin, some amino acid side chains, and other chemicals present in living tissues absorb and scatter short wavelength visible light, drastically limiting its penetration depth to only a few millimeters, as displayed in Figure 1.12. By utilizing longer

wavelength absorbing and emitting fluorophores, the large amount of background noise caused by this tissue auto-fluorescence which obscures the detection and quantification of biological signals is mostly eliminated.<sup>9, 36</sup> Advantageously, the absorption coefficient for near-IR light in tissues is much lower than shorter wavelength visible light which sanctions deeper penetration up to several centimeters.<sup>4</sup>

In addition to greater penetration depth, light scattering is greatly reduced in the near-IR region due to the inverse fourth power of the wavelength proportionality to the scattering intensity. The result is a low signal to noise ratio of the near-IR radiation which corresponds to highly sensitive signal detection. Furthermore, employing long wavelength light shows low interference from Raman scattering and reduced sample degradation. Because of these advantages, the 600 - 900 nm region of the electromagnetic spectrum has been deemed the “biological window.” With such imaging advantages paired with the availability of low-cost long wavelength lasers and red/near-IR detectors, an influx of research has surrounded the design, synthesis, and evaluation of novel red/near-IR fluorescent probes for a multitude of applications.

An ideal near-IR fluorescent dye should possess a number of desirable characteristics including high molar absorption coefficients, high fluorescence quantum yields, photo- and chemo-stability, good solubility in aqueous media, resistance toward self-aggregation, and facile synthetic and functionalization routes allowing for the construction and modification of fluorescent probes and indicators.<sup>1</sup>

The development of near-IR fluorescent organic dyes with greater photostability and fluorescence maxima based on porphyrin, phthalocyanine, cyanine, fluorescein, squaraine, and BODIPY platforms has made significant progress in recent decades (Table 1.1). Although strides have been made in this field, current dyes are not without limitations. Low fluorescence quantum

yields, limited solubility in aqueous media, and poor photo- and/or chemo-stability are some of the drawbacks of current fluorophores.

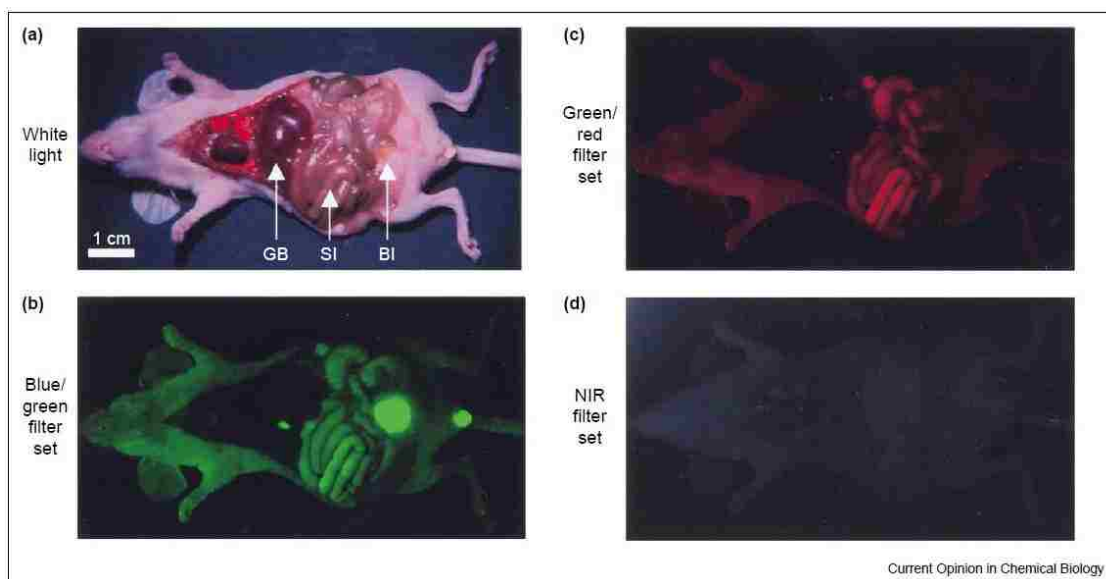


Figure 1.12: Tissue autofluorescence in the mouse using various excitation/emission filters. a) no filter; b) blue/green filter; c) green/red filter; d) near-IR filter. GB: gall bladder, SI: small intestine, BI: bladder. Reprinted with permission from [107] Copyright (2002) Elsevier.

Currently, cyanine-based dyes form the largest group of long wavelength fluorophores for biological imaging purposes. However, only indocyanine green (ICG:cardiogreen) is FDA and EMA approved for medicinal near-IR imaging and has been used for many years as a non-toxic, minimal side effect angiographic contrast agent. Regrettably, ICG has a low quantum yield (0.3% in water and 1.2% in blood) like most cyanine-derived dyes, and lacks any pendent functionality for biomolecule conjugation.<sup>108</sup> A newer, improved near-IR fluorescent imaging agent of greater promise, IRDye<sup>®</sup>800CW, has undergone extensive study. This dye bears a reactive N-hydroxysuccinimide or maleimide group which allows it to be attached to targeting

biomolecules.<sup>109</sup> Although this dye has been investigated in pre-clinical trials, it has yet to undergo clinical testing.

With so many dyes currently on the market with countless shortcomings, there has been a drive to develop a new class of readily modifiable near-IR dyes for various biological applications. The BODIPY-family of fluorophores has caught much interest as small, fluorescent molecules with potential applications as stains, indicators, and labels. Potently fluorescent BODIPYs inherently possess many of the desired characteristics of near-IR dyes such as strong, narrow spectral bandwidths (for multicolor imaging), high molar absorption coefficients ( $\log \epsilon_{\max} < 8.8$ ), solvent polarity ineffectualness, and small Stokes' shifts. Compared with positively charged rhodamines and cyanines, BODIPYs have an overall neutral charge and are relatively nonpolar.<sup>110</sup> With the lack of a charge on the BODIPY platform, the affinity for targeted analytes or receptors is enhanced. BODIPY has found many application in the biological imaging realm particularly as cellular stains, fluorescent analyte indicators for protons and metal ions, as labels for various biomolecules, and as enzymatic activity monitors.

#### **1.4.1.1 Cellular Stains**

Under the lens of a microscope, most biological samples, especially cells, appear relatively transparent. The most highly studied parts of the cell, the internal organelles, are so transparent that they are difficult to see even under the lens of a high powered microscope. Cellular stains are valuable tools for the visualization of the cell and its organelles. Organelle specific stains allow for microscopic imaging which provides greater understanding of cell morphology and function. Small, neutral dyes, such as BODIPYs, have gained favor as cellular stains for the ability to

permeate cell membranes and be retained within the cell depending on their designed reactivity and inherent hydrophobic nature.

Table 1.1: Various commercially available NIR dyes for bimolecular conjugation.

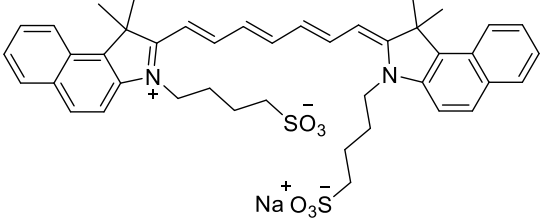
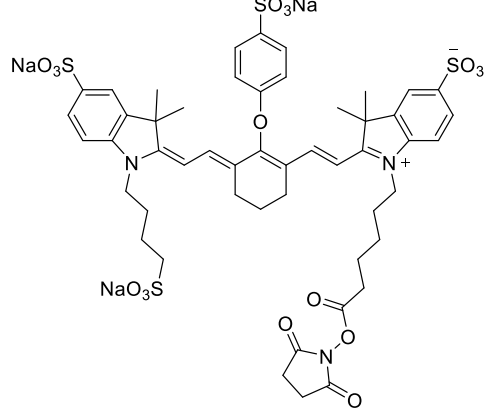
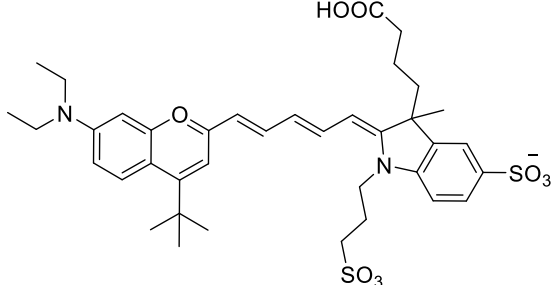
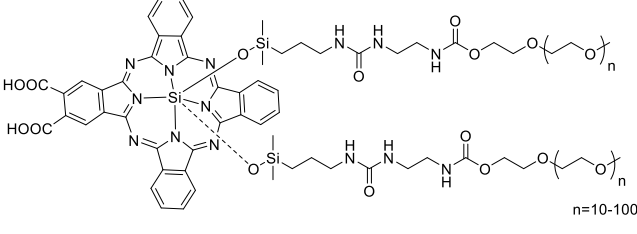
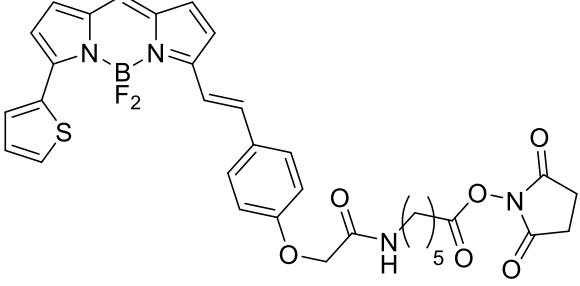
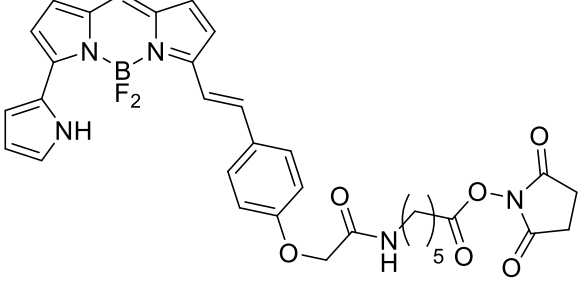
Dye Name (Manufacturer)	Chemical Structure	Absorption Maximum (nm)	Emission Maximum (nm)
ICG (Sigma Aldrich)		800	810
IRDye <sup>®</sup> 800CW NHS ester (LI-COR Biosciences)		774	789
Dye 783 NHS ester (Dyomics GmbH.)		783	800
La Jolla Blue (Hyperion Inc.)		680	700

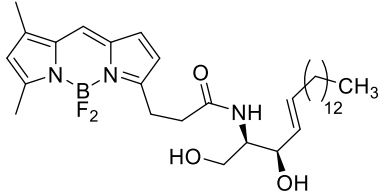
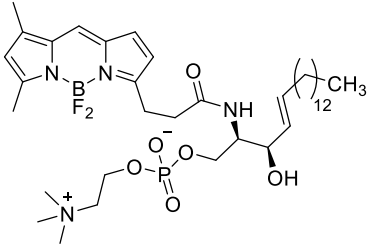
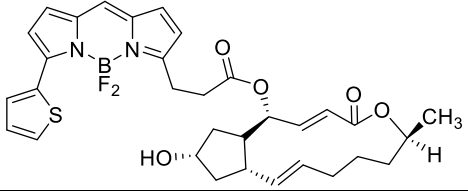
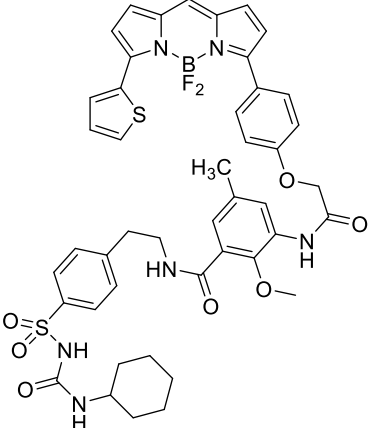
Table 1.1: (continued)

Dye Name (Manufacturer)	Chemical Structure	Absorption Maximum (nm)	Emission Maximum (nm)
BODIPY 630/650-X Succinimidyl ester (Life Technologies Inc.)		625	640
BODIPY 650/665-X Succinimidyl ester (Life Technologies Inc.)		646	664

A number of cell-permeable BODIPY dyes, either conjugated to a biomolecule or designed as a target-specific reactive fluorophore, have found use both *in vitro* and *in vivo* intracellular imaging. The dyes utilized for imaging the organelles of greatest interest to cellular function, the Golgi apparatus, endoplasmic reticulum, mitochondria, lysosomes and nuclei, are designed in such a way that their optoelectronic properties are not altered once in the cellular and subcellular environments.<sup>37</sup> Some of the best known commercially available for visualizing the endoplasmic reticulum and Golgi apparatus are the red fluorescent BODIPY TR-glibenclamide and BODIPY TR-ceramide, respectively, manufactured by Life Technologies, Inc, Table 1.2. As one of the largest commercial producers of BODIPYs and holding several patents on BODIPY fluorophores, Life Technologies, Inc, also produces numerous yellow or green-fluorescent BODIPY conjugates

for live cell or fixed cell imaging and for flow cytometry including BODIPY FL-ceramide, BODIPY FL-C<sub>5</sub>-sphingomyelin, and BODIPY-brefeldin A conjugates. Low molecular weight neutral BODIPY dye conjugates are found to permeate living cells better than their charged conjugate counterparts. Staining of cells and their organelles using low concentrations of BODIPY fluorophores has shown to lack any toxic effects on the cells.<sup>106</sup>

Table 1.2: Commercially available BODIPY-based cellular stains from Life Technologies Inc.

Dye Name	Chemical Structure	Absorption Max (nm)	Emission Max (nm)
BODIPY FL-ceramide		505	520
BODIPY FL-C <sub>5</sub> -sphingomyelin		505	520
BODIPY-brefeldin A		558	568
BODIPY TR-glibenclamide		587	615

### 1.4.1.2 Environmental Indicators

Intracellular pH and metal ions have great impact on cellular function including numerous biological processes and disorders. The need for selective and sensitive fluorescent chemosensors has amplified and has led to extensive research interest over the recent decade. The design of many fluorescent sensors are based on one of two models; 1) fluorophore-spacer-receptor systems, or 2) intrinsic fluorescent probes, in which the receptor is a part of the  $\pi$ -electron system of the fluorophore and affects the absorption/emission profile.

Photoinduced electron transfer (PET) and internal charge transfer (ICT) processes are the fundamental principles fueling the fluorophore-spacer-receptor systems. Alterations in either the fluorescence intensity or wavelength correspond to the binding of an analyte, either a proton or a metal, to the active site of the sensor. In both PET and ICT systems, the absence of an analyte in the binding site quenches the fluorescence due to PET or ICT in the excited state.<sup>111</sup>

ICT sensors display a significant emission spectra shift and a moderate increase in fluorescence intensity when the analyte is bound. An analyte bound to a PET sensor, on the other hand, inhibits the PET which increases emission intensity without causing a shift in the optical spectra. Due to the greater sensitivity of fluorescence, interaction with an analyte is usually measured by the easily monitored “off/on” or less common “on/off” fluorescence switching.<sup>55</sup>

BODIPY chemosensors have shown to have high potential for colorimetric and fluorometric assays.<sup>112, 113</sup> Several reports of fluorescent BODIPY-based sensors have been published for the detection of metal cations and anions, protons, pH, and reactive-oxygen species.<sup>1</sup> The sensing and imaging of pH,<sup>114</sup>  $K^+$ ,<sup>77</sup>  $Ni^{2+}$ ,<sup>115</sup>  $Cu^{2+}$ ,<sup>29</sup>  $Zn^{2+}$ ,<sup>116</sup>  $Hg^{2+}$ ,<sup>117</sup> and other metal ions in living cells (Figure 1.13, **28-30**) is crucial for monitoring important cellular processes. The detection of protons, sodium, calcium, potassium, and transition metal ions using crown ethers,<sup>77</sup>

<sup>118</sup> cryptand, <sup>119</sup> podand, <sup>120</sup> 2,2'-dipyridyl, <sup>121, 122</sup> calixarene<sup>123</sup> and p-(N,N-dialkyl)aniline<sup>42</sup>-based PET sensors, respectively dominate the literature.

### 1.4.1.3 Biological Labels

A growing demand for the visualization and investigation of function of proteins, enzymes, and other biomolecules in living cells has brought BODIPYs to the forefront of labelling biomolecules with fluorescent markers. Due to their outstanding photophysical properties and low cellular toxicities,<sup>36</sup> BODIPYs have become one of the most promising candidates for fluorescent labels and probes. Their small molecular size allows for BODIPYs to be attached to biomolecules without significantly influencing the biological function.

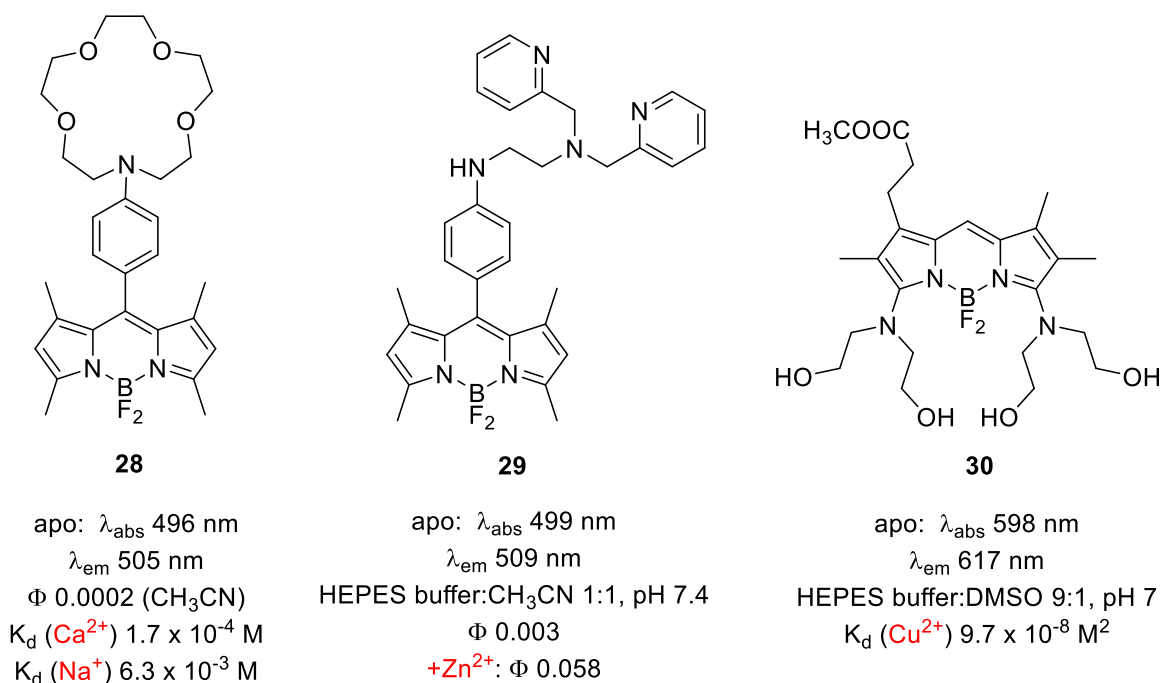


Figure 1.13: BODIPY based fluorescent indicators<sup>1</sup> for Ca<sup>2+</sup>, Na<sup>+</sup>, Cu<sup>2+</sup>, and Zn<sup>2+</sup>.

To date, several reports describe BODIPY-based fluorescent labels to target specific biological compounds such as DNA, RNA, lipids, amino acids, nucleotides, polystyrene microspheres, dextran, and proteins.<sup>111, 124-127</sup> To accomplish such conjugations, BODIPY probes are functionalized with reactive pendent groups such as carboxylic acids, sulphonic acids, polyethylene glycol moieties, polysaccharides, and oligonucleotides.<sup>5</sup> Various proteins including  $\beta$ -amyloid plaques,<sup>128, 129</sup> A $\beta$ 1-42 soluble oligomers,<sup>130</sup> and neurofibrillary tangles (NFTs) tau proteins<sup>131</sup> have been visualized via ligand-targeted BODIPYs.

BODIPYs have also found employment in various analytical techniques due to their high peak intensity which make them among the most readily detectable fluorophores. Oligonucleotide conjugates of BODIPY have been used in gel electrophoresis and DNA sequencing since the small fluorophore induces minimal effect on DNA fragment mobility during electrophoresis.<sup>110</sup>

In addition to be attached to DNA and proteins extracellularly, many fluorescent BODIPY probes are being engaged in live cell labeling of biomolecules. There are a few reports in literature in which BODIPY-based imaging probes have shown promise for both single and two photon microscopic imaging of living tissue.<sup>132</sup> Raymer and colleagues<sup>57</sup> reported a BODIPY-labeled derivative of Soraphen A capable of binding to acetyl-CoA carboxylase (ACC) providing the ability to identify ACC inhibitors that bind to the Soraphen A site (Figure 1.14, **31** and **32**). In another report by Wolfbeis and co-workers,<sup>133</sup> biomolecules such as sugars, amino acids, and nucleotides could be labeled *in vivo* using copper-free and copper-mediated click chemistry. BODIPY-based clickable fluorophores were designed for the labeling of azide modified surface glycans of Chinese hamster ovary (CHO) cells.

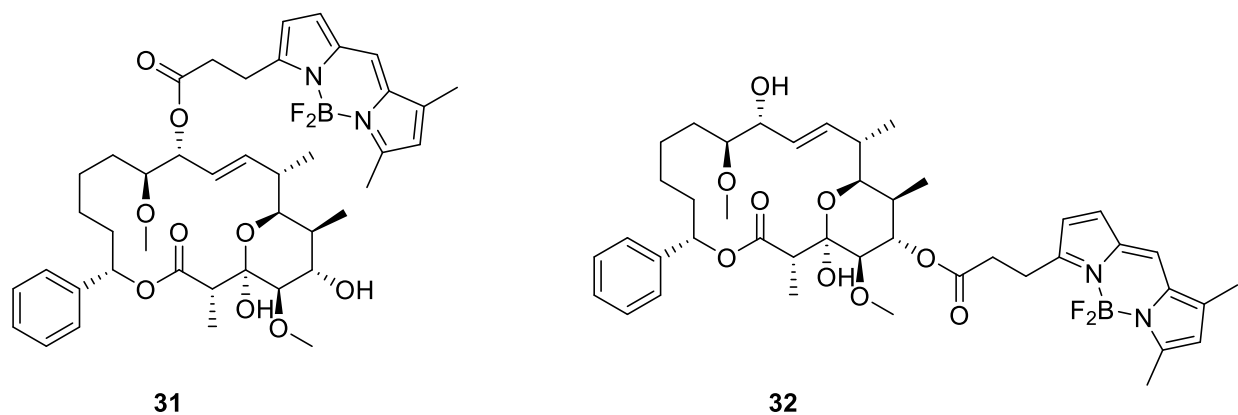


Figure 1.14: BODIPY-labeled Soraphen derivatives.<sup>57</sup>

#### 1.4.1.4 Enzyme Substrates

Fluorescent tags are often employed in assessing enzyme activity through the measurement of fluorescence change when a fluorophore is conjugated to a substrate and when the fluorophore is cleaved by the enzyme. BODIPYs have been linked to fatty acids, triglycerides, phospholipids, glycolipids, cholesterol, and a number of other biological substrates for fluorometric assays for measuring enzymatic activities of proteases, phospholipases, chloramphenicol acetyltransferases, amylase, and other enzymes.<sup>7, 28, 134-140</sup> Many of the homogeneous fluorometric assays for proteases which utilize BODIPY fluorophore are based on Fluorescence Resonance Energy Transfer (FRET).<sup>141, 142</sup> The BODIPY is conjugated to a protease substrate which yields a non-fluorescent reporter moiety due to the “self-quenching” phenomenon. Once the protease enzyme hydrolyses the conjugate into smaller fragments, fluorescence is restored due to a disruption of intramolecular FRET quenching. The fluorescence restoration can be quantified to correlate with enzyme activity. This simple off/on measure of fluorescence in relation of enzymatic cleavage has formed the basis of both simple and continuum assays for numerous proteases.

In 1997, Jones and co-workers<sup>141</sup> reported a pair of BODIPY-casein conjugates for the assay of protease activity. Using a BODIPY whose fluorescence was heavily quenched when conjugated with casein, they reported a direct correlation in fluorescence restoration with enzyme activity as the fluorophore was cleaved from the substrate. Due to the lack of effect of solvent polarity and pH on the fluorescence of BODIPY, these fluorophores have produced greater assay sensitivity, and surpass the highly used fluorescein as an enzyme activity monitor, whose fluorescence has shown to be greatly affected by the solvent in which it is contained. Just over a decade later, Saba and co-workers<sup>143</sup> reported a BODIPY-labeled sphingosine-1-phosphate lyase (SPL) substrate capable of effectively measuring SPL activity in tissues and cells. This new  $\omega$ -labeled BODIPY-sphingosine-1-phosphate lyase (**BODIPY-S1P**, Figure 1.15, structure **33**) replaced the standard radioactive SPL assay which employed the photolabile and toxic, polar 7-nitro-benz-2-oxa-1,3-diazole (**NBD-S1P**, **34**) fluorophore.

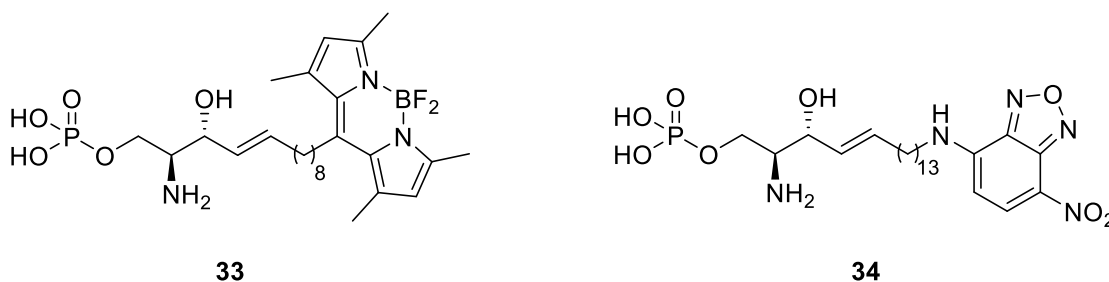


Figure 1.15: Sphingosine labeled **BODIPY-S1P** and **NBD-S1P**.<sup>143</sup>

## 1.5 Research Outlook

Despite the innumerable reports of BODIPY synthetic methodologies and derivatizations, little has been accomplished in exploring the capacity that BODIPYs hold for therapeutic purposes, as near-IR probes, and for positron emission tomography (PET) and single photon emission

computed tomography (SPECT) for *in vivo* imaging. Most of the available long-wavelength BODIPY dyes and bioconjugates emit at close to 600 nm and few water-soluble BODIPYs suitable for *in vivo* imaging have been reported in literature. Knowing these shortcomings, the synthesis, characterization, and *in vitro* evaluations of novel BODIPY dyes as dual purpose bioimaging and therapeutic agents will be discussed in the subsequent Chapters of this dissertation.

## 1.6 References

1. Boens, N.; Leen, V.; Dehaen, W., Fluorescent indicators based on BODIPY. *Chem. Soc. Rev.* **2012**, *41*, 8212-8212.
2. Escobedo, J. O.; Rusin, O.; Lim, S.; Strongin, R. M., NIR dyes for bioimaging applications. *Current Opinion in Chemical Biology* **2010**, *14*, 64-70.
3. Ntziachristos, V.; Bremer, C.; Weissleder, R., Fluorescence imaging with near-infrared light: new technological advances that enable *in vivo* molecular imaging. *European Radiology* **2003**, *13*, 195-208.
4. Amiot, C. L.; Xu, S.; Liang, S.; Pan, L.; Zhao, J. X., Near-infrared fluorescent materials for sensing of biological targets. *Sensors* **2008**, *8*, 3082-3105.
5. Niu, S. L.; Massif, C.; Ulrich, G.; Ziessel, R.; Renard, P.-Y.; Romieu, A., Water-solubilisation and bio-conjugation of a red-emitting BODIPY marker. *Organic & Biomolecular Chemistry* **2011**, *9*, 66-69.
6. Ulrich, G.; Ziessel, R.; Harriman, A., The chemistry of fluorescent bodipy dyes: Versatility unsurpassed. *Angewandte Chemie-International Edition* **2008**, *47*, 1184-1201.
7. Loudet, A.; Burgess, K., BODIPY Dyes and Their Derivatives: Syntheses and Spectroscopic Properties. *Chemical Reviews* **2007**, *107*, 4891-4932.
8. Ziessel, R.; Ulrich, G.; Harriman, A., The chemistry of Bodipy: a new El Dorado for fluorescence tools. *New Journal of Chemistry* **2007**, *31*, 496-501.
9. Descalzo, A. B.; Xu, H. J.; Shen, Z.; Rurack, K., Red/near-infrared boron-dipyrromethene dyes as strongly emitting fluorophores. In *Fluorescence Methods and Applications: Spectroscopy, Imaging, and Probes*, Wolfbeis, O. S., Ed.2008; Vol. 1130, pp 164-171.
10. Wang, Y.-W.; Descalzo, A. B.; Shen, Z.; You, X.-Z.; Rurack, K., Dihydronaphthalene-Fused Boron-Dipyrromethene (BODIPY) Dyes: Insight into the Electronic and Conformational Tuning Modes of BODIPY Fluorophores. *Chemistry-A European Journal* **2012**, *18*, 7306-7309.

11. Harreus, A. L., Pyrrole. In *Ullmann's Encyclopedia of Industrial Chemistry*, Wiley-VCH Verlag GmbH & Co. KGaA2000.
12. Shen, Z.; Rohr, H.; Rurack, K.; Uno, H.; Spieles, M.; Schulz, B.; Reck, G.; Ono, N., Boron-diindomethene (BDI) dyes and their tetrahydrobicyclo precursors - en route to a new class of highly emissive fluorophores for the red spectral range. *Chemistry-A European Journal* **2004**, *10*, 4853-4871.
13. Zheng, Q. D.; Xu, G. X.; Prasad, P. N., Conformationally restricted dipyrromethene boron difluoride (BODIPY) dyes: Highly fluorescent, multicolored probes for cellular imaging. *Chemistry-A European Journal* **2008**, *14*, 5812-5819.
14. Qin, W. W.; Baruah, M.; De Borggraeve, W. M.; Boens, N., Photophysical properties of an on/off fluorescent pH indicator excitable with visible light based on a borondipyrromethene-linked phenol. *Journal of Photochemistry & Photobiology A-Chemistry* **2006**, *183*, 190-197.
15. Arroyo, I. J.; Hu, R.; Merino, G.; Tang, B. Z.; Pena-Cabrera, E., The Smallest and One of the Brightest. Efficient Preparation and Optical Description of the Parent Borondipyrromethene System. *Journal of Organic Chemistry* **2009**, *74*, 5719-5722.
16. Schmitt, A.; Hinkeldey, B.; Wild, M.; Jung, G., Synthesis of the Core Compound of the BODIPY Dye Class: 4,4'-Difluoro-4-bora-(3a,4a)-diazas-indacene. *Journal of Fluorescence* **2009**, *19*, 755-758.
17. Li, L.; Nguyen, B.; Burgess, K., Functionalization of the 4,4-difluoro-4-bora-3a, 4a-diazas-indacene (BODIPY) core. *Bioorganic & Medicinal Chemistry Letters* **2008**, *18*, 3112-3116.
18. Thivierge, C.; Bandichhor, R.; Burgess, K., Spectral dispersion and water solubilization of BODIPY dyes via palladium-catalyzed C-H functionalization. *Organic Letters* **2007**, *9*, 2135-2138.
19. Tram, K.; Yan, H.; Jenkins, H. A.; Vassiliev, S.; Brucec, D., The synthesis and crystal structure of unsubstituted 4,4-difluoro-4-bora-3a, 4a-diazas-indacene (BODIPY). *Dyes and Pigments* **2009**, *82*, 392-395.
20. Meng, G.; Velayudham, S.; Smith, A.; Luck, R.; Liu, H. Y., Color Tuning of Polyfluorene Emission with BODIPY Monomers. *Macromolecules* **2009**, *42*, 1995-2001.
21. Bonardi, L.; Ulrich, G.; Ziessel, R., Tailoring the properties of boron-dipyrromethene dyes with acetylenic functions at the 2,6,8 and 4-B substitution positions *Organic Letters* **2008**, *10*, 2183-2186.
22. Benniston, A. C.; Copley, G., Lighting the way ahead with boron dipyrromethene (Bodipy) dyes. *Physical Chemistry Chemical Physics* **2009**, *11*, 4124-4131.

23. Wael, E. V. d.; Pardoën, J. A.; Koevering, J. A. v.; Lugtenburg, J.; Pyrromethene-BF<sub>2</sub> complexes (4,4'-difluoro-4-bora-3a,4a-diaza-s-indacenes). Synthesis and luminescence properties. *Recueil des Travaux Chimiques des Pays-Bas* **1977**, *96*, 306-309.
24. Bandichhor, R.; Thivierge, C.; Bhuvanesh, N. S. P.; Burgess, K., 4,4-difluoro-1,3,5,7-tetramethyl-4-bora-3a,4a-diaza-s-indacene. *Acta Crystallographica Section E-Structure Reports Online* **2006**, *62*, O4310-O4311.
25. Hu, R.; Lager, E.; Aguilar-Aguilar, A.; Liu, J.; Lam, J. W. Y.; Sung, H. H. Y.; Williams, I. D.; Zhong, Y.; Wong, K. S.; Pena-Cabrera, E.; Tang, B. Z., Twisted Intramolecular Charge Transfer and Aggregation-Induced Emission of BODIPY Derivatives. *Journal of Physical Chemistry C* **2009**, *113*, 15845-15853.
26. Treibs, A.; Kreuzer, F.-H., Difluorboryl-Komplexe von Di- und Tripyrrylmethenen. *Justus Liebigs Annalen der Chemie* **1968**, *718*, 208-223.
27. Goud, T. V.; Tutar, A.; Biellmann, J.-F., Synthesis of 8-heteroatom-substituted 4,4-difluoro-4-bora-3a, 4a-diaza-s-indacene dyes (BODIPY). *Tetrahedron* **2006**, *62*, 5084-5091.
28. Wood, T. E.; Thompson, A., Advances in the chemistry of dipyrins and their complexes. *Chemistry Reviews* **2007**, *107*, 1831-1861.
29. Jiao, L. J.; Li, J. L.; Zhang, S. Z.; Wei, C.; Hao, E. H.; Vicente, M. G. H., A selective fluorescent sensor for imaging Cu<sup>2+</sup> in living cells. *New Journal of Chemistry* **2009**, *33*, 1888-1893.
30. Li, L.; Han, J.; Nguyen, B.; Burgess, K., Syntheses and spectral properties of functionalized, water-soluble BODIPY derivatives. *Journal of Organic Chemistry* **2008**, *73*, 1963-1970.
31. Jackson, A. H.; Pandey, R. K.; Rao, K. R. N.; Roberts, E., Reactions on Solid Supports 2: A Convenient Method for Synthesis of Pyrromethanes Using a Montmorillonite Clay as Catalyst. *Tetrahedron Letters* **1985**, *26*, 793-796.
32. Bari, S. E.; Iturraspe, J.; Frydman, B., Synthesis of Biliverdins with Stable Extended Conformations. *Tetrahedron* **1995**, *51*, 2255-2266.
33. Wu, L.; Burgess, K., A new synthesis of symmetric boraindacene (BODIPY) dyes. *Chemical Communications* **2008**, 4933-4935.
34. Sobenina, L. N.; Vasil'tsov, A. M.; Petrova, O. V.; Petrushenko, K. B.; Ushakov, I. A.; Clavier, G.; Meallet-Renault, R.; Mikhaleva, A. I.; Trofimov, B. A., General Route to Symmetric and Asymmetric meso-CF<sub>3</sub>-3(5)-Aryl(hetaryl)- and 3,5-Diaryl(dihetaryl)-BODIPY Dyes. *Organic Letters* **2011**, *13*, 2524-2527.

35. Uppal, T.; Hu, X. K.; Fronczek, F. R.; Maschek, S.; Bobadova-Parvanova, P.; Vicente, M. G. H., Synthesis, Computational Modeling, and Properties of Benzo-Appended BODIPYs. *Chemistry-A European Journal* **2012**, *18*, 3893-3905.
36. Jiao, L. J.; Yu, C. J.; Uppal, T.; Liu, M. M.; Li, Y.; Zhou, Y. Y.; Hao, E. H.; Hu, X. K.; Vicente, M. G. H., Long wavelength red fluorescent dyes from 3,5-diiodo-BODIPYs. *Organic & Biomedical Chemistry* **2010**, *8*, 2517-2519.
37. Loudet, A.; Ueno, Y.; Wu, L.; Jose, J.; Barhoumi, R.; Burghardt, R.; Burgess, K., Organelle-selective energy transfer: A fluorescent indicator of intracellular environment. *Bioorganic & Medicinal Chemistry Letters* **2011**, *21*, 1849-1851.
38. Baruah, M.; Qin, W. W.; Flors, C.; Hofkens, J.; Vallee, R. A. L.; Beljonne, D.; Van der Auweraer, M.; De Borggraeve, W. M.; Boens, N., Solvent and pH dependent fluorescent properties of a dimethylaminostyryl borondipyrromethene dye in solution. *Journal of Physical Chemistry A* **2006**, *110*, 5998-6009.
39. Yogo, T.; Urano, Y.; Ishitsuka, Y.; Maniwa, F.; Nagano, T., Highly efficient and photostable photosensitizer based on BODIPY chromophore. *Journal of the American Chemical Society* **2005**, *127*, 12162-12163.
40. Atilgan, S.; Ekmekci, Z.; Dogan, A. L.; Guc, D.; Akkaya, E. U., Water soluble distyryl-boradiazaindacenes as efficient photosensitizers for photodynamic therapy. *Chemical Communications* **2006**, 4398-4400.
41. Murtagh, J.; Frimannsson, D. O.; O'Shea, D. F., Azide Conjugatable and pH Responsive Near-Infrared Fluorescent Imaging Probes. *Organic Letters* **2009**, *11*, 5386-5389.
42. Rurack, K.; Kollmannsberger, M.; Daub, J., Molecular switching in the near infrared (NIR) with a functionalized boron - Dipyrromethene dye. *Angewandte Chemie-International Edition* **2001**, *40*, 385-387.
43. Zhao, W. L.; Carreira, E. M., Conformationally restricted aza-bodipy: A highly fluorescent, stable, near-infrared-absorbing dye. *Angewandte Chemie-International Edition*. **2005**, *44*, 1677-1679.
44. Leen, V., Braeken, E., Luckermans, K., Jackers, C., Van der Auweraer, M., Boens, N., and Dahaen, W., A versatile, modular synthesis of monofunctionalized BODIPY dyes. *Chemical Communications* **2009**, 4515-4517.
45. Ortiz, M. J., Garcia-Moreno, I., Agarrabeitia, A. R., Duran-Sampedro, G., Costela, A., Sastre, R., Arbeloa, F. L., Prieto, J. B., and Arbeloa, I. L., Red-edge-wavelength finely-tunable laser action from new BODIPY dyes. *Physical Chemistry Chemical Physics* **2010**, *12*, 7804-7811.
46. Rihn, S.; Retailleau, P.; Bugsaliewicz, N.; De Nicola, A.; Ziessel, R., Versatile synthetic methods for the engineering of thiophene-substituted Bodipy dyes. *Tetrahedron Letters* **2009**, *50*, 7008-7013.

47. Rao, M. R.; Mobin, S. M.; Ravikanth, M., Boron-dipyrromethene based specific chemodosimeter for fluoride ion. *Tetrahedron* **2010**, *66*, 1728-1734.
48. Rihn, S.; Retailleau, P.; De Nicola, A.; Ulrich, G.; Ziessel, R., Synthetic Routes to Fluorescent Dyes Exhibiting Large Stokes Shifts. *Journal of Organic Chemistry* **2012**, *77*, 8851-8863.
49. Gresser, R.; Hartmann, H.; Wrackmeyer, M.; Leo, K.; Riede, M., Synthesis of thiophene-substituted aza-BODIPYs and their optical and electrochemical properties. *Tetrahedron* **2011**, *67*, 7148-7155.
50. Jiao, L. J.; Yu, C. J.; Li, J. L.; Wang, Z. Y.; Wu, M.; Hao, E. H., beta-Formyl-BODIPYs from the Vilsmeier-Haack Reaction. *Journal of Organic Chemistry* **2009**, *74*, 7525-7528.
51. Ulrich, G.; Ziessel, R., Convenient and efficient synthesis of functionalized oligopyridine ligands bearing accessory pyrromethene-BF<sub>2</sub> fluorophores. *Journal of Organic Chemistry* **2004**, *69*, 2070-2083.
52. Zrig, S.; Remy, P.; Andrioletti, B.; Rose, E.; Asselberghs, I.; Clays, K., Engineering tuneable light-harvesting systems with oligothiophene donors and mono- or bis-bodipy acceptors. *Journal of Organic Chemistry* **2008**, *73*, 1563-1566.
53. Ziessel, R.; Bonardi, L.; Ulrich, G., Boron dipyrromethene dyes: a rational avenue for sensing and light emitting devices. *Dalton Transactions* **2006**, 2913-2918.
54. Wu, L.; Loudet, A.; Barhoumi, R.; Burghardt, R. C.; Burgess, K., Fluorescent Cassettes for Monitoring Three-Component Interactions in Vitro and in Living Cells. *Journal of the American Chemical Society* **2009**, *131*, 9156-9157.
55. Moczar, I.; Huszthy, P.; Maidics, Z.; Kadar, M.; Toth, K., Synthesis and optical characterization of novel enantiopure BODIPY linked azacrown ethers as potential fluorescent chemosensors. *Tetrahedron* **2009**, *65*, 8250-8258.
56. Gossauer, A.; Nydegger, F.; Kiss, T.; Sleziak, R.; Stoeckli-Evans, H., Synthesis, chiroptical properties, and solid-state structure determination of two new chiral dipyrroin difluoroboryl chelates. *Journal of the American Chemical Society* **2004**, *126*, 1772-1780.
57. Raymer, B.; Kavana, M.; Price, A.; Wang, B.; Corcoran, L.; Kulathila, R.; Groarke, J.; Mann, T., Synthesis and characterization of a BODIPY-labeled derivative of Soraphen A that binds to acetyl-CoA carboxylase. *Bioorganic & Medicinal Chemistry Letters* **2009**, *19*, 2804-2807.
58. Baruah, M.; Qin, W. W.; Basaric, N.; De Borggraeve, W. M.; Boens, N., BODIPY-based hydroxyaryl derivatives as fluorescent pH probes. *Journal of Organic Chemistry* **2005**, *70*, 4152-4157.
59. McDonnell, S. O.; O'Shea, D. F., Near-infrared sensing properties of dimethylamino-substituted BF<sub>2</sub>-azadipyrromethenes. *Organic Letters* **2006**, *8*, 3493-3496.

60. Rogers, M. A. T., 2,4-diarylpyrroles Part I Synthesis of 2,4-diarylpyrroles and 2,2',4,4'-tetra-arylazadipyromethines. *Journal of the Chemical Society* **1943**, 590-596.
61. Davies, W. H.; Rogers, M. A. T., 2,4-diarylpyrroles part IV The formation of acylated 5-amino-2,4-di-phenylpyrroles from beta-benzoyl-alpha-phenylpropionitrile and some notes on the Leuckart reaction. *Journal of the Chemical Society* **1944**, 126-131.
62. Knott, E. B., Beta-Cyclopropionitriles.2. Conversion Into Bis-(5-Cyclopyrrole)Azamethin Salts. *Journal of the Chemical Society* **1947**, 1196-1201.
63. Adarsh, N.; Avirah, R. R.; Ramaiah, D., Tuning Photosensitized Singlet Oxygen Generation Efficiency of Novel Aza-BODIPY Dyes. *Organic Letters* **2010**, *12*, 5720-5723.
64. Li, Y.; Dolphin, D.; Patrick, B. O., Synthesis of a BF<sub>2</sub> complex of indol-2-yl-isoindol-1-ylidene-amine: a fully conjugated azadipyromethene. *Tetrahedron Letters* **2010**, *51*, 811-814.
65. Loudet, A., Bandichhor, R., Burgess, K., Palma, A., McDonnell, S. O., Hall, M. J., O'Shea, D. F., B,O-chelated azadipyromethenes as near-IR probes. *Organic Letters* **2008**, *10*, 4771-4774.
66. Loudet, A., Bandichhor, R., Wu, L., Burgess, K., Functionalized BF<sub>2</sub> chelated azadipyromethene dyes. *Tetrahedron* **2008**, *64*, 3642-3654.
67. Palma, A.; Tasiar, M.; Frimannsson, D. O.; Vu, T. T.; Meallet-Renault, R.; O'Shea, D. F., New On-Bead Near-Infrared Fluorophores and Fluorescent Sensor Constructs. *Organic Letters* **2009**, *11*, 3638-3641.
68. Yoshii, R.; Nagai, A.; Chujo, Y., Highly Near-Infrared Photoluminescence from Aza-Borondipyromethene-Based Conjugated Polymers. *Journal of Polymer Science Part a-Polymer Chemistry* **2010**, *48*, 5348-5356.
69. Yamada, K.; Toyota, T.; Takakura, K.; Ishimaru, M.; Sugawara, T., Preparation of BODIPY probes for multicolor fluorescence imaging studies of membrane dynamics. *New Journal of Chemistry* **2001**, *25*, 667-669.
70. Ueno, T.; Urano, Y.; Kojima, H.; Nagano, T., Mechanism-based molecular design of highly selective fluorescence probes for nitrate stress. *Journal of the American Chemical Society* **2006**, *128*, 10640-10641.
71. Killoran, J.; O'Shea, D. F., Impact of a conformationally restricted receptor on the BF<sub>2</sub> chelated azadipyromethene fluorosensing platform. *Chemical Communications* **2006**, 1503-1505.
72. Dost, Z.; Atilgan, S.; Akkaya, E. U., Distyryl-boradiazaindacenes: facile synthesis of novel near IR emitting fluorophores. *Tetrahedron* **2006**, *62*, 8484-8488.

73. Galangau, O.; Dumas-Verdes, C.; Méallet-Renault, R.; Clavier, G., Rational design of visible and NIR distyryl-BODIPY dyes from a novel fluorinated platform *Organic & Biomolecular Chemistry* **2010**, *8*, 4546-4553.
74. Zhu, S. L.; Zhang, J. T.; Vegesna, G.; Luo, F. T.; Green, S. A.; Liu, H. Y., Highly Water-Soluble Neutral BODIPY Dyes with Controllable Fluorescence Quantum Yields. *Organic Letters* **2011**, *13*, 438-441.
75. Bura, T.; Retailleau, P.; Ulrich, G.; Ziessel, R., Highly Substituted Bodipy Dyes with Spectroscopic Features Sensitive to the Environment. *Journal of Organic Chemistry* **2011**, *76*, 1109-1117.
76. Thoresen, L. H.; Kim, H. J.; Welch, M. B.; Burghart, A.; Burgess, K., Synthesis of 3,5-diaryl-4,4-difluoro-4-bora-3a,4a-diaza-s-indacene (BODIPY (R)) dyes. *Synlett* **1998**, 1276-+.
77. Baruah, M.; Qin, W. W.; Vallee, R. A. L.; Beljonne, D.; Rohand, T.; Dehaen, W.; Boens, N., A highly potassium-selective ratiometric fluorescent indicator based on BODIPY azacrown ether excitable with visible light. *Organic Letters* **2005**, *7*, 4377-4380.
78. Rohand, T.; Qin, W.; Boens, N.; Dehaen, W., Palladium-catalyzed coupling reactions for the functionalization of BODIPY dyes with fluorescence spanning the visible spectrum. *European Journal of Organic Chemistry* **2006**, 4658-4663.
79. Pavlopoulos, T. G.; Boyer, J. H.; Shah, M.; Thangaraj, K.; Soong, M. L., Laser Action From 2,6,8-Position Trisubstituted 1,3,5,7-Tetramethylpyrromethene-BF<sub>2</sub> Complexes. *Applied Optics* **1990**, *29*, 3885-3886.
80. Niu, S. L.; Ulrich, G.; Ziessel, R.; Kiss, A.; Renard, P.-Y.; Romieu, A., Water-Soluble BODIPY Derivatives. *Organic Letters* **2009**, *11*, 2049-2052.
81. Worries, H. J.; Koek, J. H.; Lodder, G.; Lugtenburg, J.; Fokkens, R.; Driessen, O.; Mohn, G. R., A Novel Water-Soluble Fluorescent-Probe - Synthesis, Luminescence and Biological Properties of the Sodium-Salt of the 4-Sulfonato-3,3',5,5'-Tetramethyl-2,2'-Pyrromethen-1,1'-BF<sub>2</sub> Complex. *Recueil Des Travaux Chimiques Des Pays-Bas-Journal of the Royal Netherlands Chemical Society* **1985**, *104*, 288-291.
82. Zhai, J.; Pan, T.; Zhu, J.; Xu, Y.; Chen, J.; Xie, Y.; Qin, Y., Boronic Acid Functionalized Boron Dipyrromethene Fluorescent Probes: Preparation, Characterization, and Saccharides Sensing Applications. *Analytical Chemistry* **2012**, *84*, 10214-10220.
83. Goeb, S.; Ziessel, R., Synthesis of novel tetrachromophoric cascade-type Bodipy dyes. *Tetrahedron Letters* **2008**, *49*, 2569-2574.
84. Chen, J.; Mizumura, M.; Shinokubo, H.; Osuka, A., Functionalization of Boron Dipyrin (BODIPY) Dyes through Iridium and Rhodium Catalysis: A Complementary Approach to alpha- and beta-Substituted BODIPYs. *Chemistry-A European Journal* **2009**, *15*, 5942-5949.

85. Cakmak, Y.; Akkaya, E. U., Phenylethynyl-BODIPY Oligomers: Bright Dyes and Fluorescent Building Blocks. *Organic Letters* **2009**, *11*, 85-88.
86. Kee, H. L.; Kirmaier, C.; Yu, L. H.; Thamyongkit, P.; Youngblood, W. J.; Calder, M. E.; Ramos, L.; Noll, B. C.; Bocian, D. F.; Scheidt, W. R.; Birge, R. R.; Lindsey, J. S.; Holten, D., Structural control of the photodynamics of boron-dipyrrin complexes. *Journal of Physical Chemistry B* **2005**, *109*, 20433-20443.
87. Goze, C.; Ulrich, G.; Mallon, L. J.; Allen, B. D.; Harriman, A.; Ziessel, R., Synthesis and photophysical properties of borondipyrrromethene dyes bearing aryl substituents at the boron center. *Journal of the American Chemical Society* **2006**, *128*, 10231-10239.
88. Ulrich, G.; Goze, C.; Guardigli, M.; Roda, A.; Ziessel, R., Pyrromethene dialkynyl borane complexes for "cascatelle" energy transfer and protein labeling. *Angewandte Chemie-International Edition* **2005**, *44*, 3694-3698.
89. Harriman, A., Izzet, G., and Ziessel, R., Rapid Energy Transfer in Cascade-Type Bodipy Dyes. *Journal of the American Chemical Society* **2006**, *128*, 10868-10875.
90. Ziessel, R.; Goze, C.; Ulrich, G., Design and synthesis of alkyne-substituted boron in dipyrromethene frameworks. *Synthesis-Stuttgart* **2007**, 936-949.
91. Ulrich, G.; Goeb, S.; De Nicola, A.; Retailleau, P.; Ziessel, R., Chemistry at Boron: Synthesis and Properties of Red to Near-IR Fluorescent Dyes Based on Boron-Substituted Diisoindolomethene Frameworks. *Journal of Organic Chemistry* **2011**, *76*, 4489-4505.
92. Gabe, Y.; Ueno, T.; Urano, Y.; Kojima, H.; Nagano, T., Tuneable design strategy for fluorescence probes based on 4-substituted BODIPY chromophore: improvement of highly sensitive fluorescence probe for nitric oxide. *Analytical and Bioanalytical Chemistry* **2006**, *386*, 621-626.
93. Goze, C.; Ulrich, G.; Ziessel, R., Tetrahedral Boron Chemistry for the Preparation of Highly Efficient "Cascatelle" Devices. *Journal of Organic Chemistry* **2007**, *72*, 313-322.
94. Nagai, A.; Chujo, Y., Aromatic Ring-Fused BODIPY-Based Conjugated Polymers Exhibiting Narrow Near-Infrared Emission Bands. *Macromolecules* **2010**, *43*, 193-200.
95. Nakamura, M.; Tahara, H.; Takahashi, K.; Nagata, T.; Uoyama, H.; Kuzuhara, D.; Mori, S.; Okujima, T.; Yamadad, H.; Uno, H., pi-Fused bis-BODIPY as a candidate for NIR dyes. *Organic & Biomolecular Chemistry* **2012**, *10*, 6840-6849.
96. Okujima, T.; Tomimori, Y.; Nakamura, J.; Yamada, H.; Uno, H.; Ono, N., Synthesis of pi-expanded BODIPYs and their fluorescent properties in the visible-near-infrared region. *Tetrahedron* **2010**, *66*, 6895-6900.
97. Tahtaoui, C.; Thomas, C.; Rohmer, F.; Klotz, P.; Duportail, G.; Mely, Y.; Bonnet, D.; Hibert, M., Convenient method to access new 4,4-dialkoxy- and 4,4-diaryloxy-diaza-s-

- indacene dyes: Synthesis and spectroscopic evaluation. *Journal of Organic Chemistry* **2007**, *72*, 269-272.
98. Wada, M.; Ito, S.; Uno, H.; Murashima, T.; Ono, N.; Urano, T.; Urano, Y., Synthesis and optical properties of a new class of pyrromethene-BF<sub>2</sub> complexes fused with rigid bicyclo rings and benzo derivatives. *Tetrahedron Letters* **2001**, *42*, 6711-6713.
  99. Ni, Y. Z., Wangdong; Huang, Kuo-Wei; Wu, Jishan, Benzene-fused BODIPYs: synthesis and the impact of fusion mode. *Chemistry Communications* **2013**, *49*, 1217-1219.
  100. Zhao, C. C.; Zhou, Y.; Lin, Q. N.; Zhu, L. Y.; Feng, P.; Zhang, Y. L.; Cao, J. A., Development of an Indole-Based Boron-Dipyrromethene Fluorescent Probe for Benzenethiols. *Journal of Physical Chemistry B* **2011**, *115*, 642-647.
  101. Descalzo, A. B.; Xu, H. J.; Xue, Z. L.; Hoffmann, K.; Shen, Z.; Weller, M. G.; You, X. Z.; Rurack, K., Phenanthrene-fused boron-dipyrromethenes as bright long-wavelength fluorophores. *Organic Letters* **2008**, *10*, 1581-1584.
  102. Chen, J.; Burghart, A.; Derecskei-Kovacs, A.; Burgess, K., 4,4-difluoro-4-bora-3a,4a-diaza-s-indacene (BODIPY) dyes modified for extended conjugation and restricted bond rotations. *Journal of Organic Chemistry* **2000**, *65*, 2900-2906.
  103. Benstead, M.; Mehl, G. H.; Boyle, R. W., 4,4'-Difluoro-4-bora-3a,4a-diaza-s-indacenes (BODIPYs) as components of novel light active materials. *Tetrahedron* **2011**, *67*, 3573-3601.
  104. Lim, S. H., Thivierge, C., Nowak-Sliwinska, P., Han, J., van den Bergh, H., Wagnières, G., Burgess, K., and Lee, H. B., In Vitro and In Vivo Photocytotoxicity of Boron Dipyrromethene Derivatives for Photodynamic Therapy. *Journal of Medicinal Chemistry* **2010**, *53*, 2865-2874.
  105. Erbas, S.; Gorgulu, A.; Kocakusakogullari, M.; Akkaya, E. U., Non-covalent functionalized SWNTs as delivery agents for novel Bodipy-based potential PDT sensitizers. *Chemical Communications* **2009**, 4956-4958.
  106. Haugland, R. P., *The Handbook A Guide to Fluorescent Probes and Labeling Technologies*. Tenth ed.: United States of America, 2005.
  107. Frangioni, J. V., In vivo near-infrared fluorescence imaging. *Current Opinion in Chemical Biology* **2003**, *7*, 626-634.
  108. Marshall, M. V.; Draney, D.; Sevick-Muraca, E. M.; Olive, D. M., Single-Dose Intravenous Toxicity Study of IRDye 800CW in Sprague-Dawley Rats. *Molecular Imaging and Biology* **2010**, *12*, 583-594.
  109. Cohen, R.; Vugts, D. J.; Stigter-van Walsum, M.; Visser, G. W. M.; van Dongen, G. A. M. S., Inert coupling of IRDye800CW and zirconium-89 to monoclonal antibodies for single- or dual-mode fluorescence and PET imaging. *Nature Protocols* **2013**, *8*, 1010-1018.

110. Goncalves, M. S. T., Fluorescent labeling of biomolecules with organic probes. *Chemistry Reviews* **2009**, *109*, 190-212.
111. Kalai, T.; Hideg, K., Synthesis of new, BODIPY-based sensors and labels. *Tetrahedron* **2006**, *62*, 10352-10360.
112. Yin, S.; Leen, V.; Van Snick, S.; Boens, N.; Dehaen, W., A highly sensitive, selective, colorimetric and near-infrared fluorescent turn-on chemosensor for Cu<sup>2+</sup> based on BODIPY. *Chemical Communications* **2010**, *46*, 6329-6331.
113. Hudnall, T. W.; Gabbai, F. P., A BODIPY boronium cation for the sensing of fluoride ions. *Chemical Communications* **2008**, 4596-4597.
114. Ziessel, R.; Ulrich, G.; Harriman, A.; Alamiry, M. A. H.; Stewart, B.; Retailleau, P., Solid-State Gas Sensors Developed from Functional Difluoroboradiazaindacene Dyes. *Chemistry-A European Journal* **2009**, *15*, 1359-1369.
115. Dodani, S. C.; He, Q.; Chang, C. J., A Turn-On Fluorescent Sensor for Detecting Nickel in Living Cells. *Journal of the American Chemical Society* **2009**, *131*, 18020-18021.
116. Wu, Y. K.; Peng, X. J.; Guo, B. C.; Fan, J. L.; Zhang, Z. C.; Wang, J. Y.; Cui, A. J.; Gao, Y. L., Boron dipyrromethene fluorophore based fluorescence sensor for the selective imaging of Zn(II) in living cells. *Organic & Biomolecular Chemistry* **2005**, *3*, 1387-1392.
117. Coskun, A.; Akkaya, E. U., Ion sensing coupled to resonance energy transfer: A highly selective and sensitive ratiometric fluorescent chemosensor for Ag(I) by a modular approach. *Journal of the American Chemical Society* **2005**, *127*, 10464-10465.
118. Yamada, K.; Nomura, Y.; Citterio, D.; Iwasawa, N.; Suzuki, K., Highly sodium-selective fluoroionophore based on conformational restriction of oligoethyleneglycol-bridged biaryl boron-dipyrromethene. *Journal of American Chemical Society* **2005**, *127*, 6956-6957.
119. De Silva, A. P.; Gunaratne, H. Q. N.; Sandanayake, K., A New Benzo-Annelated Cryptand and a Derivative with Alkali Cation-Sensitive Fluorescence. *Tetrahedron Letters* **1990**, *31*, 5193-5196.
120. Arunkumar, E.; Ajayaghosh, A., Proton controlled intramolecular photoinduced electron transfer (PET) in podand linked squaraine-aniline dyads. *Chemical Communications* **2005**, 599-601.
121. Turfan, B.; Akkaya, E. U., Modulation of boradiazaindacene emission by cation-mediated oxidative PET. *Organic Letters* **2002**, *4*, 2857-2859.
122. Ziessel, R.; Bonardi, L.; Retailleau, P.; Ulrich, G., Isocyanate-, isothiocyanate-, urea-, and thiourea-substituted boron dipyrromethene dyes as fluorescent probes. *Journal of Organic Chemistry* **2006**, *71*, 3093-3102.

123. Kim, S. K.; Lee, S. H.; Lee, J. Y.; Lee, J. Y.; Bartsch, R. A.; Kim, J. S., An excimer-based, binuclear, on-off switchable calix 4 crown chemosensor. *Journal of the American Chemical Society* **2004**, *126*, 16499-16506.
124. Karolin, J.; Johansson, L. B. A.; Strandberg, L.; Ny, T., Fluorescence and Absorption Spectroscopic Properties of Dipyrrometheneboron Difluoride (BODIPY) Derivatives In Liquids, Lipid-Membranes, and Proteins. *Journal of the American Chemical Society* **1994**, *116*, 7801-7806.
125. Ehrenschwender, T.; Wagenknecht, H. A., 4,4-Difluoro-4-bora-3a,4a-diaza-s-indacene as a Bright Fluorescent Label for DNA. *Journal of Organic Chemistry* **2011**, *76*, 2301-2304.
126. Giessler, K.; Griesser, H.; Goehringer, D.; Sabirov, T.; Richert, C., Synthesis of 3'-BODIPY-Labeled Active Esters of Nucleotides and a Chemical Primer Extension Assay on Beads. *European Journal of Organic Chemistry* **2010**, 3611-3620.
127. Namkung, W.; Padmawar, P.; Mills, A. D.; Verkman, A. S., Cell-based fluorescence screen for K(+) channels and transporters using an extracellular triazacryptand-based K(+) sensor. *Journal of the American Chemical Society* **2008**, *130*, 7794-7796.
128. Parhi, A. K.; Kung, M.-P.; Ploessl, K.; Kung, H. F., Synthesis of fluorescent probes based on stilbenes and diphenylacetylenes targeting beta-amyloid plaques. *Tetrahedron Letters* **2008**, *49*, 3395-3399.
129. Ono, M.; Ishikawa, M.; Kimura, H.; Hayashi, S.; Matsumura, K.; Watanabe, H.; Shimizu, Y.; Cheng, Y.; Cui, M.; Kawashima, H.; Saji, H., Development of dual functional SPECT/fluorescent probes for imaging cerebral beta-amyloid plaques. *Bioorganic & Medicinal Chemistry Letters* **2010**, *20*, 3885-3888.
130. Smith, N. W.; Alonso, A.; Brown, C. M.; Dzyuba, S. V., Triazole-containing BODIPY dyes as novel fluorescent probes for soluble oligomers of amyloid A beta 1-42 peptide. *Biochemical and Biophysical Research Communications* **2010**, *391*, 1455-1458.
131. Ojida, A.; Sakamoto, T.; Inoue, M.-a.; Fujishima, S.-h.; Lippens, G.; Hamachi, I., Fluorescent BODIPY-Based Zn(II) Complex as a Molecular Probe for Selective Detection of Neurofibrillary Tangles in the Brains of Alzheimer's Disease Patients. *Journal of the American Chemical Society* **2009**, *131*, 6543-6548.
132. Zhang, D. K.; Wang, Y. C.; Xiao, Y.; Qian, S. X.; Qian, X. H., Long-wavelength boradiazaindacene derivatives with two-photon absorption activity and strong emission: versatile candidates for biological imaging applications. *Tetrahedron* **2009**, *65*, 8099-8103.
133. Kele, P.; Li, X.; Link, M.; Nagy, K.; Herner, A.; Lorincz, K.; Beni, S.; Wolfbeis, O. S., Clickable fluorophores for biological labeling-with or without copper. *Organic & Biomolecular Chemistry* **2009**, *7*, 3486-3490.

134. Peters, C.; Billich, A.; Ghobrial, M.; Hoegenauer, K.; Ullrich, T.; Nussbaumer, P., Synthesis of borondipyrromethene (BODIPY)-labeled sphingosine derivatives by cross-metathesis reaction. *Journal of Organic Chemistry* **2007**, *72*, 1842-1845.
135. Li, Z. B.; Lin, T. P.; Liu, S. L.; Huang, C. W.; Hudnall, T. W.; Gabbai, F. P.; Conti, P. S., Rapid aqueous F-18 -labeling of a bodipy dye for positron emission tomography/fluorescence dual modality imaging. *Chemical Communications* **2011**, *47*, 9324-9326.
136. Li, Z. G.; Mintzer, E.; Bittman, R., First synthesis of free cholesterol - BODIPY conjugates. *Journal of Organic Chemistry* **2006**, *71*, 1718-1721.
137. Marks, D. L.; Bittman, R.; Pagano, R. E., Use of Bodipy-labeled sphingolipid and cholesterol analogs to examine membrane microdomains in cells. *Histochemistry and Cell Biology* **2008**, *130*, 819-832.
138. Holtta-Vuori, M.; Uronen, R.-L.; Repakova, J.; Salonen, E.; Vattulainen, I.; Panula, P.; Li, Z.; Bittman, R.; Ikonen, E., BODIPY-Cholesterol: A New Tool to Visualize Sterol Trafficking in Living Cells and Organisms. *Traffic* **2008**, *9*, 1839-1849.
139. Burgdorf, C.; Prey, A.; Richardt, G.; Kurz, T., A HPLC-fluorescence detection method for determination of phosphatidic acid phosphohydrolase activity: Application in human myocardium. *Analytical Biochemistry* **2008**, *374*, 291-297.
140. Darroch, P. I.; Dagan, A.; Granot, T.; He, X. X.; Gatt, S.; Schuchman, E. H., A lipid analogue that inhibits sphingomyelin hydrolysis and synthesis, increases ceramide, and leads to cell death. *Journal of Lipid Research* **2005**, *46*, 2315-2324.
141. Jones, L. J.; Upson, R. H.; Haugland, R. P.; PanchukVoloshina, N.; Zhou, M. J.; Haugland, R. P., Quenched BODIPY dye-labeled casein substrates for the assay of protease activity by direct fluorescence measurement. *Analytical Biochemistry* **1997**, *251*, 144-152.
142. Olsen, M. J.; Stephens, D.; Griffiths, D.; Daugherty, P.; Georgiou, G.; Iverson, B. L., Function-based isolation of novel enzymes from a large library. *Nature Biotechnology* **2000**, *18*, 1071-1074.
143. Bandhuvula, P.; Li, Z.; Bittman, R.; Saba, J. D., Sphingosine 1-phosphate lyase enzyme assay using a BODIPY-labeled substrate. *Biochemical and Biophysical Research Communications* **2009**, *380*, 366-370.

## CHAPTER 2: SYNTHESIS, SPECTROSCOPIC STUDIES, COMPUTATIONAL MODELING AND IN VITRO EVALUATION OF A SERIES OF *MESO*-ARYL-BODIPYS <sup>[a]</sup>

### 2.1 Introduction

*Meso*-aryl substituted BODIPYs riddle the literature for their ease in synthesis and readily generated diversity due to the multitude of aromatic aldehydes available both commercially and via facile syntheses.<sup>1-3</sup> Benefits surrounding the ability to modify and functionalize the *meso*-substituent without effecting the photophysical properties of the BODIPY core make it highly favorable for conjugation to biomolecules and other targeting groups. *Meso*-aromatic groups have also been employed to influence the hydrophilicity and targeting ability of BODIPY since BODIPY is inherently lipophilic.<sup>4</sup>

The addition of halogens at every pyrrolic position of the BODIPY platform has been explored for their effect on the optical properties of the fluorophore as well as for their ability to facilitate aromatic substitution and palladium-catalyzed cross coupling reactions.<sup>5-7, 8, 9</sup> The addition of heavy atoms to the BODIPY core has the potential to generate effective photosensitizers for photodynamic therapy (PDT) via enhanced intersystem crossing from the singlet to the triplet excited state. This conversion controls the production of singlet oxygen, the main cytotoxic species produced in PDT, due to spin-orbit coupling by the “heavy atom effect”.<sup>7, 10, 11, 13, 14</sup> Furthermore, the absorption and emission profiles of halogenated BODIPYs are also expected to be red-shifted compared with their non-halogenated analogs. Halogens can be readily installed via a variety of methods, most commonly through the N-halo-succinimide (NBS, NCS, and NIS) halogenation of starting pyrroles, dipyrromethenes, and unsubstituted BODIPYs.<sup>12-14</sup>

---

[a] This Chapter originally appeared as Gibbs, J. H., Robins, L. T., Zhou, Z., Bobadova-Parvanova, P., Cottam, M., McCandless, G. T., Fronczek, F. R., Vicente, M. G. H., Spectroscopic, computational modeling and cytotoxicity studies of a series of *meso*-phenyl and *meso*-thienyl-BODIPYs. *Bioorganic & Medicinal Chemistry* **2013**, *21*, 5770-5781. Reprinted with permission from [1] Copyright (2013) Elsevier.

BODIPYs bearing halogens at the 1, 3, 5, and 7-positions have shown fluorescence enhancement<sup>7</sup> compared to the 2,6-halo BODIPYs and undergo nucleophilic aromatic substitution reactions with a multitude of nucleophiles and palladium-catalyzed Suzuki, Stille, Sonagashira, and Heck couplings.<sup>2, 15</sup> In contrast, halogenation at the 2,6-positions is typically utilized to induce intersystem crossing (ISC) and effect spectral changes, as well as for preliminary platforms for subsequent palladium-mediated couplings.<sup>10</sup>

BODIPY is highly favored for its fundamental properties and applications in various disciplines, but has recently emerged as a non-porphyrin photosensitizer for PDT.<sup>10</sup> Banfi and co-workers,<sup>4</sup> note that heavy atomic halogens, Br and I, when located at the 2,6-positions of the BODIPY induce not only a red-shift in the photophysical spectra, but also display inhibited fluorescence caused by enhanced ISC from the singlet excited state to the triplet state due to heavy atom effect. The heavy atom effect is defined by large, electron rich atoms, such as halogens, exerting influence over the rates of ISC. ISC in BODIPY has been shown to progress faster for iodine compared to bromine due to its larger spin-orbit coupling.<sup>16</sup> Halogens enhance ISC without exerting much change on the electronic structure of BODIPY and yield photosensitizers that can undergo the necessary singlet excited state to triplet excited state conversion by way of relatively large spin orbit coupling constants of high nuclear charge atoms.<sup>17</sup>

### **2.1.1 Photodynamic Therapy**

PDT is an effective and FDA approved treatment for lung, esophageal, and cutaneous cancers, age related macular degeneration, and Barrett's esophagus.<sup>18</sup> PDT is a relatively non-invasive process that combines three independently non-toxic components, a photosensitizer (PS), light, and systemic or intracellular oxygen, in a manner that transfers energy from light

to the photosensitizer. The triplet state PS subsequently interacts with molecular oxygen to generate reactive oxygen species, including singlet oxygen, that induce cell apoptosis and necrosis.<sup>19, 20</sup> Treatment is initiated by administration of the photosensitizer either through intravenous injection or topical application for dermal treatments. After a latent period in which the photosensitizer is allowed to selectively accumulate within tumor cells, usually 24 - 96 hours depending on the photosensitizer and cancer type, the tumor is selectively irradiated with light of a specified wavelength in order to effectively excite the photosensitizer, Figure 2.1.

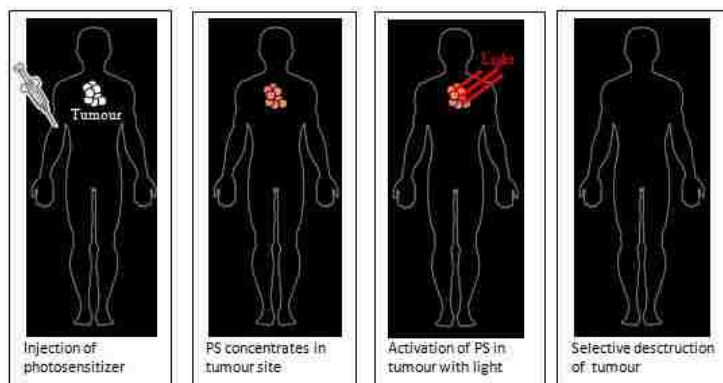


Figure 2.1: General overview of photodynamic therapy.<sup>21</sup>

Following activation of the photosensitizer by light, typically achieved by a laser source, the photosensitizer is excited from the ground state ( $^1\text{PS}$ ) to the short-lived excited singlet state ( $^1\text{PS}^*$ ),<sup>19</sup> Figure 2.2. From this singlet state, energy is released via fluorescence which allows for the clinical photodetection of the photosensitizer *in vivo*. The short-lived singlet state may undergo intersystem crossing by way of an electron spin conversion to the longer-lived triplet excited state. It is this triplet excited state that has the capacity to interact with various components intracellularly to generate reactive oxygen species that lead to cell death. More specifically, the photosensitizer

can generate reactive oxygen species of two types.<sup>18</sup> Type I reactive oxygen species are produced indirectly through the transfer of protons or electrons from the photosensitizer to substrates within the cell to form radicals which then go on to interact with oxygen to produce toxic oxygenated species. On the other hand, the photosensitizer can directly transfer its excitation energy to triplet oxygen, the most abundant and stable form of oxygen, which reacts to form singlet oxygen (Type II), the most damaging of oxygen species. ISC of the singlet excited state to the triplet excited state of the photosensitizer allows ground state triplet oxygen to overcome spin forbidden triplet state to singlet state transformation.<sup>17</sup> The triplet state photosensitizer and triplet oxygen are coupled to return the photosensitizer to the ground state and send oxygen to the reactive singlet state in an overall spin-allowed fashion. Both Type I and Type II oxygen species are formed simultaneously. The ratio in which each is produced depends upon the photosensitizer, the concentration of systemic and intracellular oxygen, and, for Type I species, the binding affinity of the photosensitizer to the substrate.

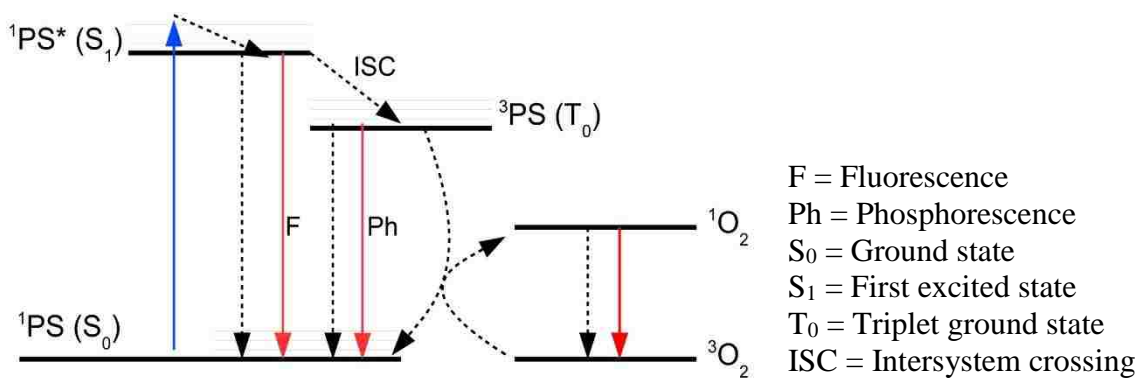


Figure 2.2: Jablonski diagram of singlet oxygen generation caused by energy transfer from an excited photosensitizer.<sup>22</sup>

PDT efficacy depends upon several factors including the type of photosensitizer, the

drug concentration and its intracellular localization, the light dose, and the dose rate. The greatest factor determining how well PDT works is the concentration of oxygen surrounding the photosensitizer. Without oxygen, the photosensitizer would simply lose its excitation energy via non-radiative decay pathways, *ie.* fluorescence and phosphorescence.

Singlet oxygen is a highly reactive species with a very short half-life ( $< 0.04 \mu\text{s}$ ). As a result, it can only diffuse  $0.01 - 0.02 \mu\text{m}$ , therefore, only cells that are immediately adjacent to the location of the photosensitizer will be affected. Localization of the photosensitizer as close to the targeted tumor cell is therefore essential for treatment to be efficacious.

Due to its limited treatment scope, PDT can only be utilized as a local treatment of small size cancers and is not suited for systemic treatments of metastatic wide-spread cancers. PDT mediates tumor destruction in three ways: (1) reactive oxygen species directly kill cancer cells; (2) through damage to the tumor's vasculature thus cutting off its nutrient source; and (3) by eliciting an immune response to attack PDT-induced damaged tissues.<sup>19</sup>

PDT has many advantages over the most commonly utilized cancer treatment methods. PDT is typically completed as an outpatient therapy and requires a short (1 - 4 days) dwell period between injection with the photosensitizer and light treatment. Radiation therapy, on the other hand, requires approximately six to seven weeks of treatment to irradiate the tumor. Chemotherapy is extensively time intensive with treatments being administered for hours at a time over months. Although surgery is typically the quickest treatment method, the amount of time needed for healing can be prolonged. Clinical studies have shown PDT to be a more cost-effective method of treatment and provides an increased life-expectancy.

Most PDT agents absorb between 630 nm and 680 nm. The therapeutic wavelength of light needed to excite these photosensitizers produces a narrow limit of light penetration.

Since light treatment must be focused, normal healthy tissues around and below the tumor are spared, which allows for faster rebuilding of damaged tissues without scarring. Although some ulceration at the treatment site typically occurs following irradiation, the long term damage to normal tissues is minimal, unlike the extensive damage caused to healthy tissues by radiation and chemotherapy.

### **2.1.2 Photosensitizers**

To date, four clinically approved photosensitizers are available to treat a variety of cancer types across the globe. In the U.S., two porphyrin-based macrocycles and a porphyrin precursor (Figure 2.3) have been FDA-approved for use as photosensitizers and several other porphyrinoids are under investigation for the PDT treatment of various neoplastic and non-malignant conditions in dermatology, ophthalmology, and cardiology.<sup>23,24</sup> Current PDT agents fall short in their ability to treat a broad range of cancer types, with one of the greatest drawbacks being their effective depths of treatment penetration. Photofrin® (porfimer sodium, registered trademark of Pinnacle Biologics, Inc.) is a first generation photosensitizer and was approved in 1993 for the treatment of esophageal and lung cancers.<sup>18</sup> Photofrin was the first photosensitizer to be approved for PDT and is still the most widely used PDT agent. Although Photofrin is used as an effective PDT agent, it suffers several inadequacies. Photofrin exists as a mixture of mono, di, and oligomers and the therapeutic composition is difficult to replicate.<sup>25</sup> Despite having an absorption near the desired therapeutic window (650 – 800 nm), its weak absorption at 630 nm causes a need for greater light doses of 100 – 200 J/cm<sup>2</sup> for tumor control. Furthermore, Photofrin has a long retention time within the body leading to skin sensitivity lasting four to twelve weeks.

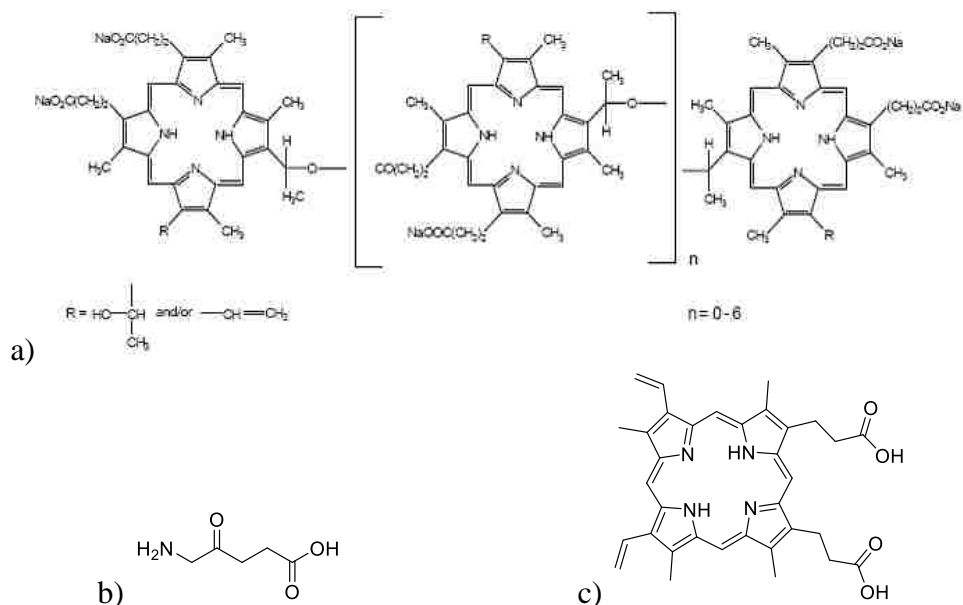


Figure 2.3: Molecular structures of FDA approved photosensitizers: a) Photofrin,<sup>26</sup> b) ALA, and c) protoporphyrin IX.

ALA, or 5-aminolevulinic acid, a second generation photosensitizer, was approved in 1999 for the treatment of cutaneous cancer lesions, oral, and digestive cancers.<sup>18</sup> Although ALA has no photosensitizing abilities itself, it is a natural precursor of heme and forms protoporphyrin IX *in vivo* which has shown to possess photosensitizing properties. ALA has several advantages over Photofrin including a more rapid clearance from the body (one to two days of photosensitivity). However, ALA is strongly hydrophilic and is not readily internalized by cells. As such, the methyl ester of ALA has been synthesized and studied and has shown to have better uptake thus increasing its effectiveness.

Highly effectual “ideal” photosensitizers must possess a unique set of characteristics including preferential accumulation in target tissue, a triplet state of adequate energy ( $E_T \geq 95 \text{ kJ mol}^{-1}$ ) for efficient energy transfer, high quantum yields of the triplet state ( $\Phi_T > 0.4$ ), long triplet

state lifetimes ( $\tau_T = 1 \mu\text{s}$ ), high photostability, high absorption coefficients at the therapeutic excitation window (650 nm - 800 nm), and low dark but high phototoxicity.<sup>19, 20</sup>

### 2.1.3 Radioiodine Imaging

The use of isotopically and radioactively labeled heavy atoms, such as  $^{123}\text{I}$ ,  $^{124}\text{I}$ , and  $^{131}\text{I}$ , can allow iodinated BODIPYs to be utilized in various bioimaging applications. Radioactive isotopically labeled iodine has been effectively used in single photon emission computed tomography (SPECT) and positron emission tomography (PET) imaging studies.<sup>27, 28</sup> Iodine-120 and  $^{124}\text{I}$  ( $t_{1/2} = 81$  minutes and 4.18 days, respectively) are the only radioisopes of iodine to possess favorable PET qualities.<sup>29</sup> However, because of their low positron emission abundance, high positron energies, and lengthy synthetic protocol, radioiodine isotopes have yet to be adopted for widespread application in habitual PET imaging. Conversely,  $^{123}\text{I}$  and  $^{131}\text{I}$  ( $t_{1/2} = 13.2$  hours and 8.05 days, respectively) have been significantly employed as SPECT radiotracers for long term *in vitro* studies and radioimmunoassays. Iodine-123 nuclei have been successfully used in nuclear medicine including blood flow, myocardial, and thyroid scintigraphy and for uptake measurements in tumors.<sup>30</sup> The use of radioactively labeled iodine has gained popularity in bioimaging for its longer half-life (*ca.* 13 h) compared with other commonly used radio agents, including fluorine.<sup>31</sup> Numerous SPECT radiotracers have gained FDA approval and are frequently utilized in clinical diagnostics for a large portion of patients in need of imaging. SPECT imaging is favorable for imaging endogenous peptides and antibodies, and, provides a means for measuring the slow kinetic processes of these ligands facilitated by the relatively long half-life of the most common isotopes utilized.

In order to be suitable for radioimaging compounds must possess specific targeting abilities. Incorporation of targeting moieties, as seen with DHEA, cholesterol, and cyclooctyne-BODIPY conjugates,<sup>32-34</sup> can be easily accomplished by amending the BODIPY scaffold, via the starting pyrroles or through post-synthetic modifications. With such targeting capabilities incorporated, radioiodine-labeled BODIPYs have the potential for use in SPECT and PET.

As of yet, no radioiodine-labelled BODIPYs have been published for use as SPECT radiotracers. An ideal radiopharmaceutical should possess characteristics to provide detectable diagnostic particles with minimal biological effect to the cells or tissues. Radiopharmaceuticals should have a relatively short half-life, maintaining radioactivity for only the necessary length of time needed to complete the diagnostic study, produce suitable radionucleotide emissions of desired energy, have high target to normal tissue ratio, possess a high target uptake, efficiently clear from blood and non-target tissue while lingering in target tissues for effective image contrast, and be inexpensive and relatively easy to produce.

#### **2.1.4 Research Prospective**

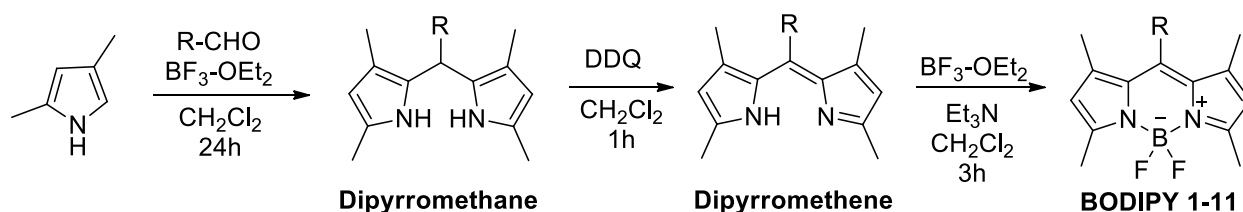
In order to broaden the effective scope of PDT, development of photosensitizers capable of treating a range of cancer types in various states of the disease must be explored. This chapter details the synthesis of a series of eleven photo-stable *meso*-aryl-BODIPYs from 2,4-dimethylpyrrole and various aryl aldehydes. Furthermore, iodination at the 2,6-positions yielded the corresponding diiodo-BODIPY derivatives with high yield and selectivity. These 3,5-dimethyl substituted BODIPYs can undergo Knoevenagel condensation reactions with aldehydes to give mono- and di-styryl functionalized long wavelength absorbing BODIPY dyes, within the biological window suitable for PDT.<sup>35-37</sup> BODIPY-based dyes can be synthesized with extended

$\pi$ -systems for excitation within the therapeutic window, however their high phototoxicity/low dark toxicity requirement and the structural features that optimize tumor cell uptake and cytotoxicity remain poorly understood. In this study the effects of the *meso*-aryl substituents on the spectroscopic and cytotoxic properties of a series of eleven BODIPYs and their 2,6-diiodo derivatives were investigated.

## 2.2 Results and Discussion

### 2.2.1 Syntheses

Although functionalization can be achieved at nearly every position of the BODIPY core, incorporation of various aryl aldehydes via condensation with two pyrroles affords the simplest and most direct route to add functionality and diversity to this group of fluorophores. Following the classic three-step, one-pot strategy often employed in BODIPY synthesis eleven *meso*-aryl BODIPYs (**1 - 11**) were synthesized from commercially obtained 2,4-dimethylpyrrole and one of eleven different aryl aldehydes (Scheme 2.1).<sup>38</sup>



Scheme 2.1: Synthesis of BODIPYs **1 - 11** from 2,4-dimethylpyrrole and an aryl aldehyde.

The synthesis of *meso*-aryl BODIPYs began with condensation of two pyrrole units with an aryl aldehyde in dichloromethane. An acid catalyst, either TFA or  $\text{BF}_3\cdot\text{OEt}_2$ , is required to promote the condensation through protonation or chelation to the carbonyl oxygen, thus enhancing

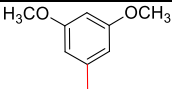
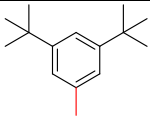
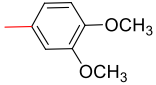
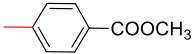
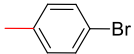
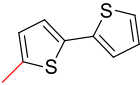
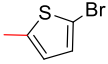
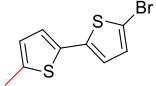
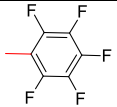
the partial positive charge on the carbonyl carbon and ensuring nucleophilic attack by pyrrole. In all syntheses reported herein,  $\text{BF}_3 \cdot \text{OEt}_2$  facilitated this conversion to the desired dipyrromethanes. After stirring under inert argon conditions for 48 hours, the resultant dipyrromethanes were subsequently oxidized using 2,3-dichloro-5,6-dicyano-*p*-benzoquinone (DDQ) to afford the more stable dipyrromethenes. Once formed, the dipyrromethenes were first deprotonated under basic conditions using  $\text{Et}_3\text{N}$  before being exposed to excess  $\text{BF}_3 \cdot \text{OEt}_2$  to deliver the  $\text{BF}_2$ -complexed BODIPY structures. Following aqueous work-up, extraction with dichloromethane, and removal of any remnant water with  $\text{Na}_2\text{SO}_4$ , the BODIPYs were purified by silica gel column chromatography using a 30:70 mixture of DCM and petroleum ether as eluent. Recrystallization afforded the target compounds as red-orange, bright red, or deep red crystals in 18 to 58% yields, shown in Table 2.1.

All aldehydes used in these syntheses were acquired commercially with the exception 5'-bromo-[2,2'-bithiophen]-5-carbaldehyde, compound **12**, used in the synthesis of BODIPY **10**. Bromo-bithiophene **12** was prepared through facile bromination of [2,2'-bithiophen]-5-carbaldehyde in one step using bromine and sodium bicarbonate to obtain a yellow solid in 64% yield, Scheme 2.2.<sup>39</sup>



Scheme 2.2: Synthesis of **12** from [2,2'-bithiophen]-5-carbaldehyde.

Table 2.1: R-group identification and corresponding percent yields of BODIPYs **1** - **11**.

<b>BODIPY</b>	<b>R</b>	<b>% Yield</b>
<b>1</b>		22
<b>2</b>		58
<b>3</b>		23
<b>4</b>		25
<b>5</b>		23
<b>6</b>		19
<b>7</b>		20
<b>8</b>		20
<b>9</b>		18
<b>10</b>		30
<b>11</b>		52

With several pyrrole options available from both commercial producers and relatively straightforward synthetic routes, choosing one for the syntheses detailed herein required some

strategy. Therefore, 2,4-dimethylpyrrole (also known as Knorr pyrrole) was selected for its potential to offer multiple reactive points for later modification. The methyl groups of the pyrroles resided at the 1,3,5, and 7-positions of the BODIPY core are quite acidic in nature, particularly the 3,5-dimethyls, allowing for facile extension of  $\pi$ -conjugation via use of the well-developed Knoevenagel condensation with aryl aldehydes in order to develop near-IR bioimaging dyes. In addition to bearing acidic properties, the 1,7-dimethyls enhance steric hindrance of *meso*-aryl group, limiting its rotational ability which increases the BODIPY's fluorescence quantum yield. Finally, the 2,6-positions were left unoccupied to easily add functionality, by way of halogens, nitro or sulfonate groups, and to potentially extend conjugation via subsequent metal-mediated couplings.

The 2,6-positions of the BODIPY core can behave rather nucleophilically. By resonance, these positions bear the least positive charge of the potentially reactive sites of the nine-carbon, two-nitrogen core. As such, they readily undergo electrophilic substitution, most commonly seen in literature with the incorporation of halogens,<sup>11</sup> nitro,<sup>40</sup> or sulfonate groups.<sup>41</sup>

With this knowledge in hand, BODIPYs **1** - **11** underwent iodination in the presence of iodine and iodic acid in 1:1 ethanol/dichloromethane heated to 60 °C for 2 hours to yield red crystalline diiodo-BODIPYs **1a** - **11a** in 65-94% yield after column chromatography using DCM for elution (Table 2.2).<sup>7, 10</sup>

Synthesis and evaluation of a series of *meso*-aryl BODIPYs and diiodo-*meso*-aryl BODIPYs allowed for the investigation of the effect halogenation had on the photophysical and cytotoxic properties, while at the same time exploring how the nature of the *meso*-aryl groups influences intracellular localization of the BODIPYs. Previous work has shown that substitution, especially *meso*-substitution with an aryl moiety, increase the photostability of the BODIPY

core.<sup>42, 43</sup> Additionally, halogenation at the 2,6-positions is reported to create a bathochromic shift in the absorption and emission profiles of the BODIPY, as well as enhances intersystem crossing from the singlet excited state to the triplet state due to the heavy atom effect, and consequently induces phototoxicity through the production of singlet oxygen *in vitro* and *in vivo*.<sup>7, 10, 11</sup> However, if halogenation is carried out at the 3,5-positions or at the BODIPY *meso*-phenyl or *meso*-thienyl substituents there is little to no significant effect the cytotoxicity of the compounds.

Table 2.2: Percent yields of diiodo BODIPYs **1a** - **11a**.

<b>BODIPY</b>	<b>% Yield</b>
<b>1a</b>	91
<b>2a</b>	84
<b>3a</b>	93
<b>4a</b>	94
<b>5a</b>	86
<b>6a</b>	71
<b>7a</b>	79
<b>8a</b>	84
<b>9a</b>	91
<b>10a</b>	65
<b>11a</b>	90

All BODIPYs were characterized by  $^1\text{H}$ - and  $^{13}\text{C}$ -NMR, HRMS and, in the case of **3**, **7**, **1a**, **2a**, and **9a**, by X-ray crystallography. Analysis of the NMR spectra shows the anticipated 2-fold symmetry of the BODIPY. Single peaks for the 2,6-hydrogens, the 1,7- and 3,5-dimethyl groups observed on the  $^1\text{H}$ -NMR spectra and the occurrence of signals for only half of the BODIPY core's carbons in  $^{13}\text{C}$ -NMR specify a plane of symmetry extending through the boron and carbon-8. The observed upfield shift of the 1,7-dimethyls (at approximately 1.6 ppm) compared with the 3,5-dimethyls (at approximately 2.5 ppm) is likely caused by shielding incurred by the *meso*-aryl groups. The departure of the 2,6-hydrogens (at  $\sim$  6.0 ppm) in the  $^1\text{H}$ -NMR spectra indicated complete iodination; additional evidence was provided by the shift from 120 to 85 ppm of the carbon atoms bearing these hydrogens in  $^{13}\text{C}$ -NMR.

### 2.2.2 X-ray Crystal Structure Determinations

Confirmation of the absolute configuration of several of the BODIPYs were obtained from analysis of X-ray crystal structures. Single crystals of four BODIPYS, two  $\beta$ -free and two di-iodo, suitable for X-ray analyses were recrystallized from dichloromethane, acetone, or chloroform-*d* and their molecular structures are shown in Figure 2.4. X-ray analyses reveal the expected approximate two-fold symmetry of all five compounds, with two conformers of BODIPYs **7** and **9a** being elucidated (only one of each is shown in Figure 2.4). The refinement details and cell parameters are reported in the experimental details Section 2.4.3.

The occurrence of two conformers suggests that the *meso*-thienyl group has greater rotational freedom compared with the phenyl substituent located at the same position. The nine-carbon two-nitrogen BODIPY core shows high rigidity resulting in planarity that allows for strong  $\pi$ -electron delocalization between the adjacent pyrrole rings. However, no  $\pi$ -electron

delocalization is seen between the *meso*-aryl substituent and the core, due to their orthogonal orientation to one another in the molecule's most relaxed form. This positioning reduces the steric strain on the *meso*-aryl group caused by the 1,7-dimethyl groups.<sup>44</sup> The boron displays nearly tetrahedral geometry with the two fluorines also lying perpendicular to the BODIPY core.

In comparison to previously reported boron-dipyrromethene compounds, the BODIPY cores of **1a**, **3**, **7** and **9a** adopt expected bond lengths, planarity, and orthogonal dihedral angles of the F atoms relative to the C<sub>9</sub>N<sub>2</sub>B (excluding peripheral H atoms and substituents) aromatic framework.<sup>45, 46</sup> The dihedral angles of the *meso*-substituents are also nearly 90° out-of-plane of the BODIPY core in the four crystal structures (**1a** 88.01(5)°; **3** 78.60(4)°; **7** two partially occupied orientations: 82.8(2)° and 84.19(11)°; **9a** two independent molecules 82.83(3)° and 89.54(2)°). Intermolecular halogen-halogen bonding exist in the iodinated BODIPYs **1a** (F...I 3.108(2) Å) and in **9a** (F...Br 2.903(1) and 2.971(1) Å; I...Br 3.598(1) and 3.717(1) Å). Intramolecular hydrogen bonding (C—H 0.98 Å, H...F 2.51 Å, C...F 3.1982(16) Å, C—H...F 127°) between the F atoms with an H atom of a methyl group (on the BODIPY core's  $\alpha$ -carbon site) is present in BODIPY **3**.

For BODIPY **7**, the average structure contains two partially occupied orientations. The orientations can be modeled using static (positional) disorder with a refined occupancy ratio of 0.824(2):0.176(2) for two of the thiophene atoms (S and one of the C atoms). In Figure 2.4, only one of the two orientations is shown. The crystal structure of BODIPY **3** has been previously reported in literature and Cambridge Structural Database (CCDC 712038) based on room temperature measurements.<sup>47</sup> Other close matches can be found for two other crystal structures (**1a** and **7**) determined in this study. These close matches (CCDC 812643 and 856179) have been characterized by others and are extensions of **1a** (with a *meso*-mesityl group, instead of a phenyl) and **7** (with additional quinolin-2-yl on the thiophene's other  $\alpha$ -carbon atom).<sup>48, 49</sup>

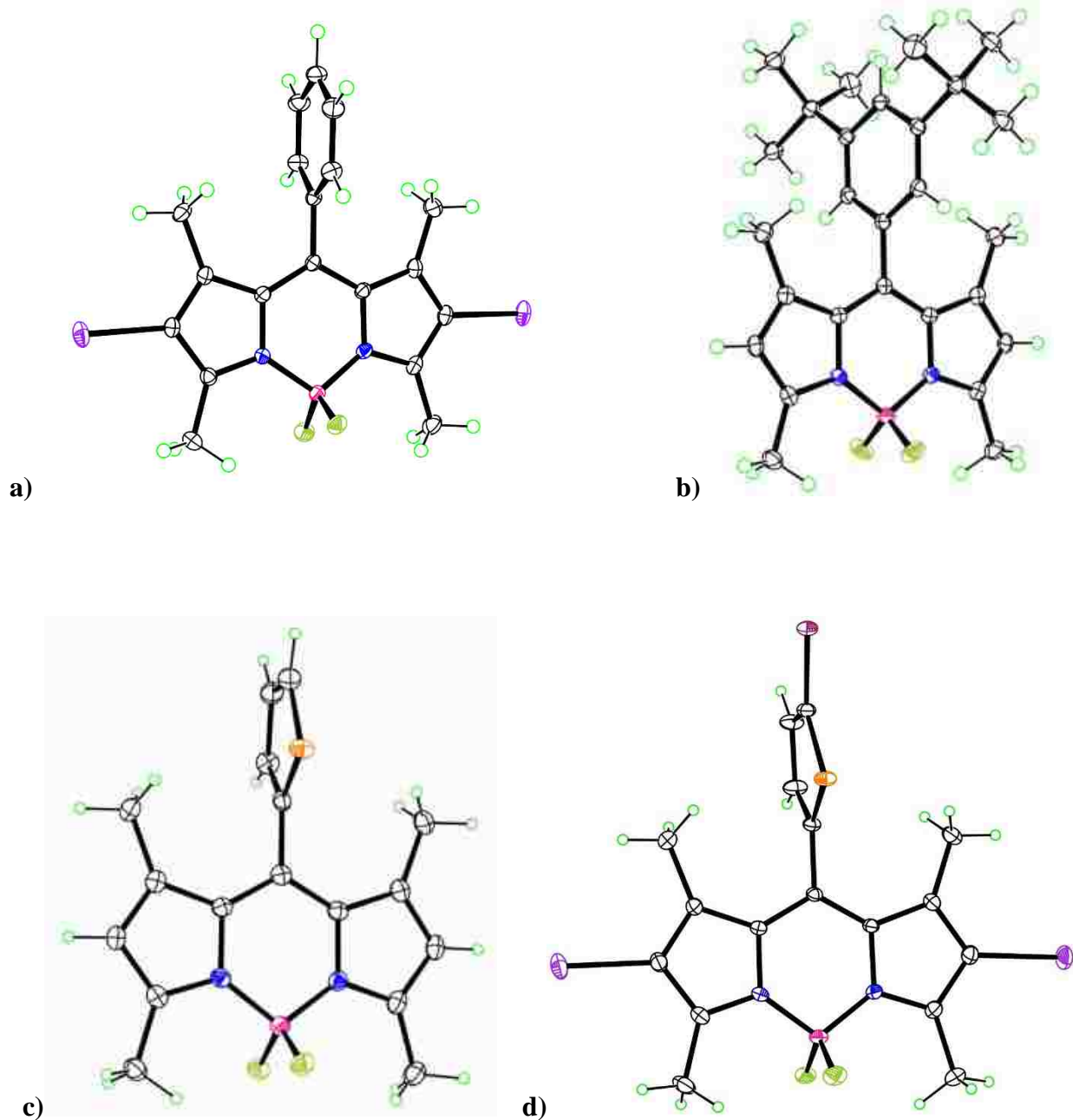


Figure 2.4: Molecular structures of BODIPYs **1a** (a), **3** (b), **7** (c), and **9a** (d) from X-ray crystal structure determinations. Ellipsoids are drawn at the 50% probability level.

### 2.2.3 Spectroscopic Investigations

The spectroscopic properties of BODIPYs **1 - 11** and **1a - 11a** were evaluated in dichloromethane and tetrahydrofuran, and the results obtained are summarized in Table 2.3 and

also shown in Figures 2.5 - 2.10. Little to no solvent effect was observed for these two solvents in the absorption and emission maxima wavelengths. Such lack of influence by the polarity of the solvent indicates that the permanent dipole moments of the BODIPYs do not change between the ground state and the excited state.<sup>50</sup> The synthesized  $\beta$ -free, *meso*-aryl BODIPYs display absorptions between 499 nm and 517 nm and emission bands between 507 nm and 530 nm (Table 2.3). BODIPYs **1 - 11** show typical fluorescence of a simple alkyl substituted BODIPY in the green/yellow spectral region with fluorescence quantum yields in the range of 0.03 – 1.0. The *meso*-thienyl- and pentafluorophenyl BODIPYs exhibited the largest red-shifted profiles and the lowest quantum yields of this series of compounds due to the presence of the sulfur and five fluorines, respectively, which impact the conjugation of the BODIPY  $\pi$ -system.

Incorporation of iodines onto the BODIPY core, as in compounds **1a - 11a**, causes a shift in the absorption and emission profiles to longer wavelengths, into the orange/red spectral region, and decrease the fluorescence quantum yields, as previously observed (Table 2.4).<sup>7, 10, 11</sup> The trend observed in the  $\beta$ -free BODIPYs is also seen in their diiodo analogs with absorption and emission profiles becoming more red-shifted with the incorporation of thienyl- and pentafluorophenyl-groups.

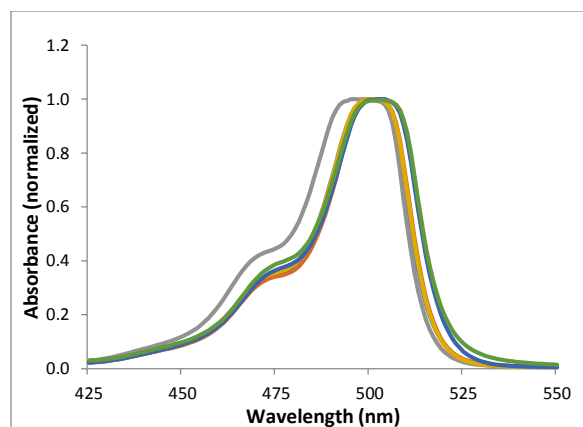
All compounds displayed high extinction coefficients, in the order of 23,000 to 118,000  $M^{-1} cm^{-1}$  (log  $\epsilon$  values between 4.34 and 5.07), and Stokes' shifts in the range 5 - 20 nm. BODIPYs **7 - 11** and **7a - 11a**, bearing *meso*-thienyl and pentafluorophenyl substituents, displayed greater red-shifted absorptions and emissions (by 13 - 41 nm) compared with the other *meso*-phenyl BODIPYs **1 - 6** and **1a - 6a**. The electron-withdrawing effects of the sulfur and the five fluorine atoms on the *meso*-substituent of BODIPYs **7 - 11** and **7a - 11a** tend to stabilize the lowest unoccupied molecular orbital (LUMO) via delocalization of the electron density.<sup>51</sup> This causes a

decrease in the energy of the LUMO, decreasing the HOMO (highest occupied molecular orbital)

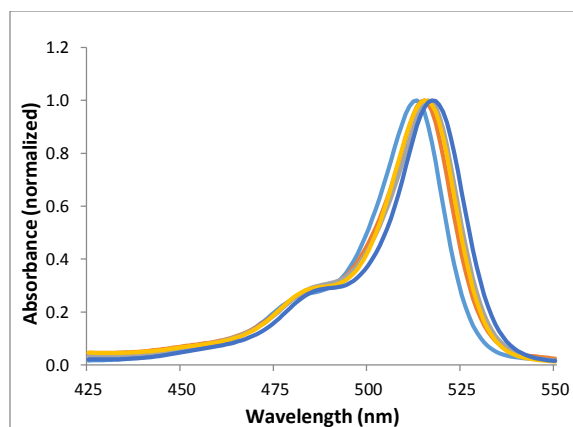
- LUMO gap, and therefore increasing the absorbance and emission maxima wavelengths.

Table 2.3: Absorption and emission spectral properties of *meso*-aryl BODIPYs **1** – **11** in DCM and THF (in parentheses) at room temperature.

BODIPY	$\Phi_f$	Absorption $\lambda_{\max}$ (nm)	Emission $\lambda_{\max}$ (nm)	Stokes' shift (nm)	log $\epsilon$
<b>1</b>	0.63 (0.79)	501 (501)	511 (509)	10 (8)	4.98 (4.84)
<b>2</b>	1.00 (0.99)	502 (501)	510 (510)	8 (9)	4.78 (4.86)
<b>3</b>	0.97 (0.73)	499 (499)	507 (507)	8 (8)	4.66 (4.60)
<b>4</b>	0.94 (0.93)	501 (501)	510 (509)	9 (8)	4.90 (4.92)
<b>5</b>	0.56 (0.43)	503 (502)	513 (512)	10 (10)	4.80 (4.81)
<b>6</b>	0.84 (0.53)	503 (502)	513 (511)	10 (9)	4.84 (4.90)
<b>7</b>	0.11 (0.09)	513 (513)	520 (520)	7 (7)	4.73 (4.84)
<b>8</b>	0.03 (0.04)	515 (515)	523 (520)	8 (5)	4.34 (4.57)
<b>9</b>	0.12 (0.10)	516 (516)	524 (524)	8 (8)	5.07 (4.89)
<b>10</b>	0.06 (0.06)	516 (515)	522 (524)	6 (9)	4.66 (4.76)
<b>11</b>	0.91 (1.00)	517 (516)	530 (528)	13 (12)	4.57 (4.77)

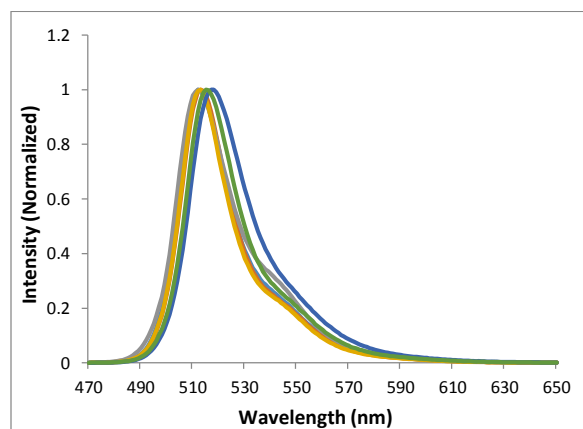


(a)

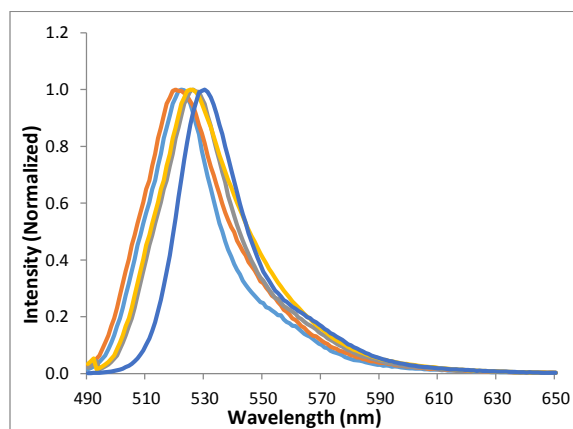


(b)

Figure 2.5: Normalized absorbance spectra of BODIPYs **1 - 6** (a) and **7 - 11** (b) in dichloromethane. (a) BODIPYs **1** (dark blue), **2** (red), **3** (green), **4** (purple), **5** (light blue), **6** (orange). (b) BODIPYs **7** (dark blue), **8** (red), **9** (green), **10** (purple), **11** (light blue).

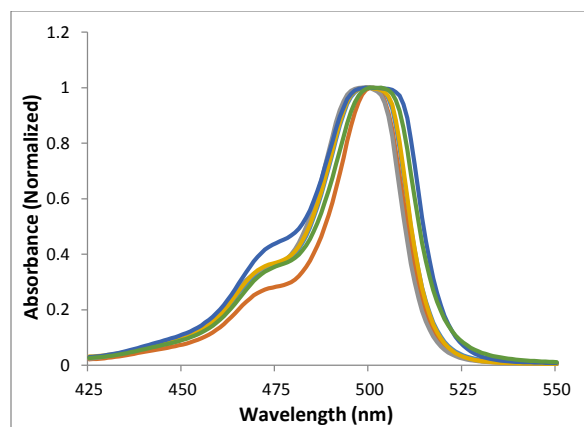


(a)

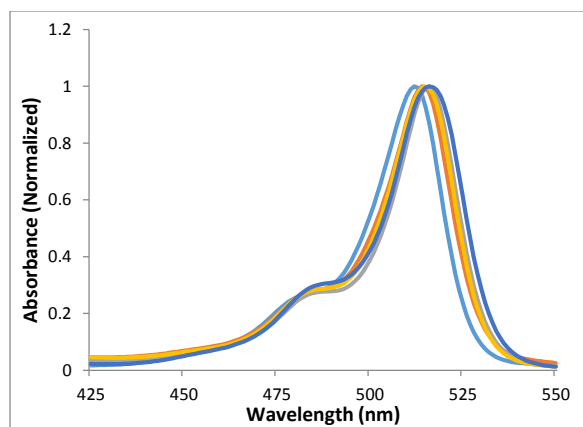


(b)

Figure 2.6: Normalized emission spectra of BODIPYs **1 - 6** (a) and **7 - 11** (b) in dichloromethane. (a) BODIPYs **1** (dark blue), **2** (red), **3** (green), **4** (purple), **5** (light blue), **6** (orange). (b) BODIPYs **7** (dark blue), **8** (red), **9** (green), **10** (purple), **11** (light blue).

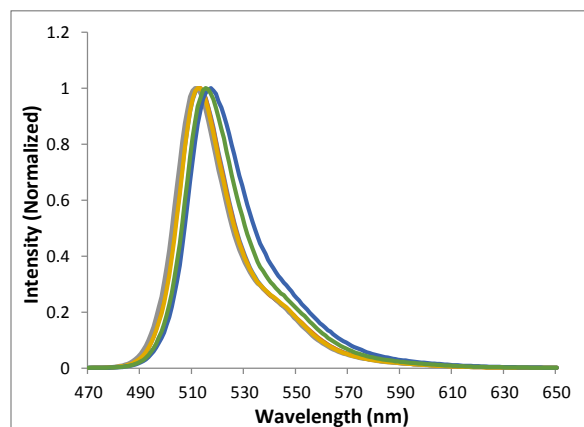


(a)

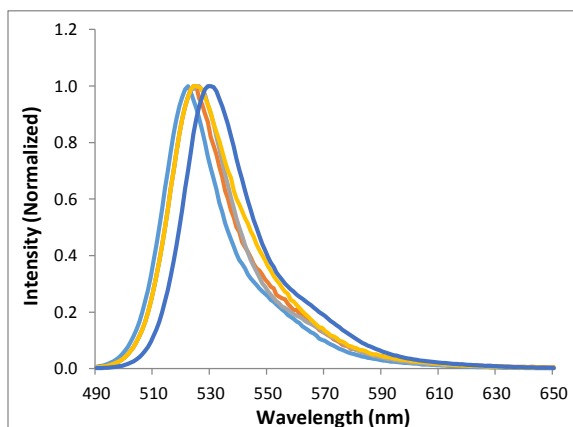


(b)

Figure 2.7: Normalized absorbance spectra of BODIPYs **1 - 6** (a) and **7 - 11** (b) in tetrahydrofuran. (a) BODIPYs **1** (dark blue), **2** (red), **3** (green), **4** (purple), **5** (light blue), **6** (orange). (b) BODIPYs **7** (dark blue), **8** (red), **9** (green), **10** (purple), **11** (light blue).



(a)



(b)

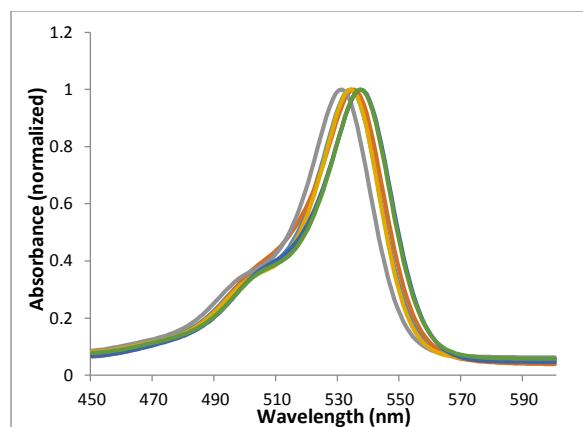
Figure 2.8: Normalized emission spectra of BODIPYs **1 - 6** (a) and **7 - 11** (b) in tetrahydrofuran. (a) BODIPYs **1** (dark blue), **2** (red), **3** (green), **4** (purple), **5** (light blue), **6** (orange). (b) BODIPYs **7** (dark blue), **8** (red), **9** (green), **10** (purple), **11** (light blue).

It was also observed that the fluorescence quantum yields for the *meso*-phenyl BODIPYs **1 - 6** and **11** ( $0.4 < \Phi_F < 1.0$ ) were greater than for the *meso*-thienyl BODIPYs **7 - 10** ( $0.04 < \Phi_F < 0.12$ ). Due to the smaller size of the *meso*-group, the thienyl substituent has greater freedom of

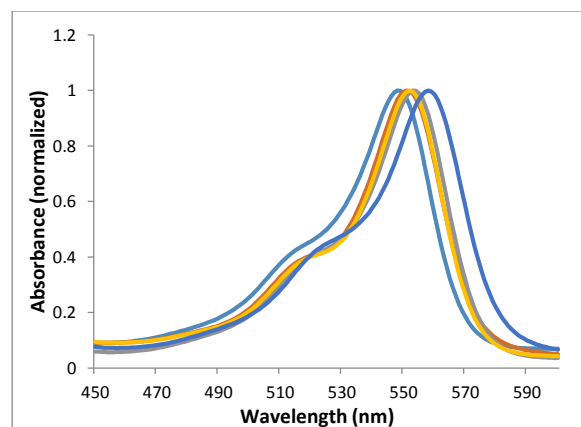
rotation, which increases the amount of energy lost to non-radiative decay. This spinning motion increases the energy of the system which, in turn, decreases the number of photons that become excited and relax via fluorescence. Negligible effects were caused by the change of solvent. Nevertheless, these results suggest that the *meso*-phenyl BODIPYs with appropriate functionalization may serve as significantly brighter fluorophores in aqueous media than the *meso*-thienyl derivatives. Furthermore, incorporating a longer chain group in the *meso*-position increases the degree of rotational freedom, which also decreases the fluorescence quantum yield as indicated by the results obtained for BODIPYs **7** ( $\Phi_F = 0.09 - 0.11$ ) and **8** ( $\Phi_F = 0.03 - 0.04$ ).

Table 2.4: Absorption and emission spectral properties of 2, 6-diiodo-BODIPYs **1a** - **11a** in DCM and THF (in parentheses) at room temperature.

<b>BODIPY</b>	<b><math>\Phi_f</math></b>	<b>Absorption <math>\lambda_{\max}</math> (nm)</b>	<b>Emission <math>\lambda_{\max}</math> (nm)</b>	<b>Stokes' shift (nm)</b>	<b>log <math>\epsilon</math></b>
<b>1a</b>	0.05 (0.04)	534 (533)	550 (546)	16 (13)	4.97 (4.92)
<b>2a</b>	0.07 (0.05)	535 (534)	549 (547)	14 (13)	4.89 (4.94)
<b>3a</b>	0.06 (0.04)	531 (531)	546 (546)	15 (15)	4.84 (4.83)
<b>4a</b>	0.05 (0.04)	534 (532)	546 (546)	12 (14)	4.96 (4.88)
<b>5a</b>	0.05 (0.04)	537 (536)	554 (555)	17 (19)	4.82 (4.77)
<b>6a</b>	0.04 (0.03)	537 (536)	554 (553)	17 (17)	4.81 (4.84)
<b>7a</b>	0.04 (0.03)	548 (548)	561 (561)	13 (13)	4.37 (4.68)
<b>8a</b>	0.01 (0.01)	551 (550)	565 (566)	14 (16)	4.59 (4.60)
<b>9a</b>	0.03 (0.02)	553 (553)	570 (571)	17 (18)	5.07 (5.05)
<b>10a</b>	0.01 (0.01)	552 (551)	569 (571)	17 (20)	4.87 (4.81)
<b>11a</b>	0.04 (0.03)	558 (557)	576 (571)	18 (19)	4.80 (4.76)

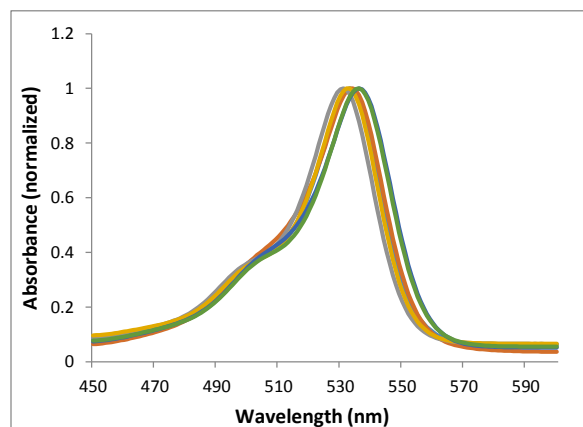


(a)

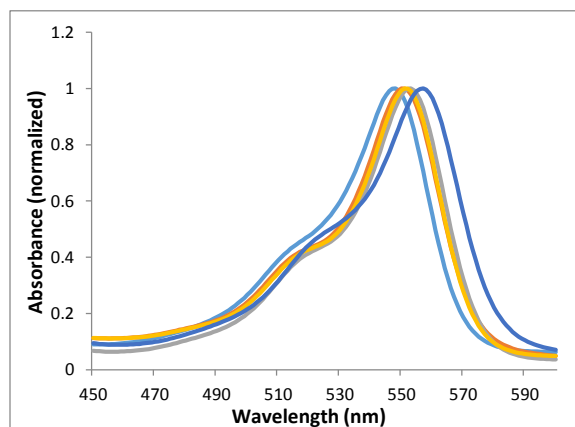


(b)

Figure 2.9: Normalized absorbance spectra of BODIPYs **1a** - **6a** (a) and **7a** - **11a** (b) in dichloromethane. (a) BODIPYs **1a** (dark blue), **2a** (red), **3a** (green), **4a** (purple), **5a** (light blue), **6a** (orange). (b) BODIPYs **7a** (dark blue), **8a** (red), **9a** (green), **10a** (purple), **11a** (light blue).



(a)



(b)

Figure 2.10: Normalized absorption spectra of BODIPYs **1a** - **6a** (a) and **7a** - **11a** (b) in tetrahydrofuran. (a) BODIPYs **1a** (dark blue), **2a** (red), **3a** (green), **4a** (purple), **5a** (light blue), **6a** (orange). (b) BODIPYs **7a** (dark blue), **8a** (red), **9a** (green), **10a** (purple), **11a** (light blue).

Addition of bromine onto the *meso*-thienyl group has only a slight effect on the fluorescence quantum yield, as observed for BODIPYs **7** ( $\Phi_F = 0.11$ ) and **9** ( $\Phi_F = 0.12$ ) in dichloromethane. This result suggests that addition of heavy atoms, such as bromine, onto the

*meso*-substituent has little effect on the fluorescence quantum yield, while incorporation of iodines at the 2,6-positions of the BODIPY core, and of *meso*-thienyl groups, significantly decrease the fluorescence quantum yields. With the exception of the fluorines on the *meso*-pentafluorophenyl-BODIPY **11**, the quantum yields significantly declined with halogenation at the 2,6-positions (**1a** - **11a**,  $0.01 < \Phi_F < 0.07$ ).

#### 2.2.4 Computational Analysis

Computational modeling was accomplished to confirm the symmetric nature of the BODIPYs previously shown by NMR and X-ray. No symmetry constraints were initially used in the calculations and the initial geometries were not symmetric, however, the optimized geometries of BODIPYs are nearly symmetric (e.g.  $C_2$  for BODIPY **3** and  $C_s$  for BODIPY **7**). The BODIPY core and *meso*-substituent form angles between  $89.9^\circ$  and  $90.1^\circ$ , elucidating perpendicular geometry.

The effect of the orthogonal relationship on the HOMO - LUMO gap energy of all BODIPYs and the *meso*-group rotational barrier of BODIPYs **1** - **11** were examined computationally (details of the theoretical level are given the Experimental section). The calculated HOMO - LUMO gaps are listed in Table 2.5, along with the HOMO and LUMO energies. Indeed, it was observed that the LUMO decreases gradually for BODIPYs **5** - **11** in agreement with the observed spectral properties. However, this is not the sole effect determining the gap. In addition to LUMO lowering, the HOMO varies substantially. Therefore, the combination of the HOMO and LUMO effects determine the observed trend. In general, the computational models predict that the BODIPYs will be grouped into four groups: BODIPYs **1** - **6** with gaps around 3.0 eV,

BODIPYs **7 - 11** and **1a - 6a** with gaps around 2.9 eV, and BODIPY **7a - 11a** with significantly lower gap of 2.7 eV (see Figure 2.11).

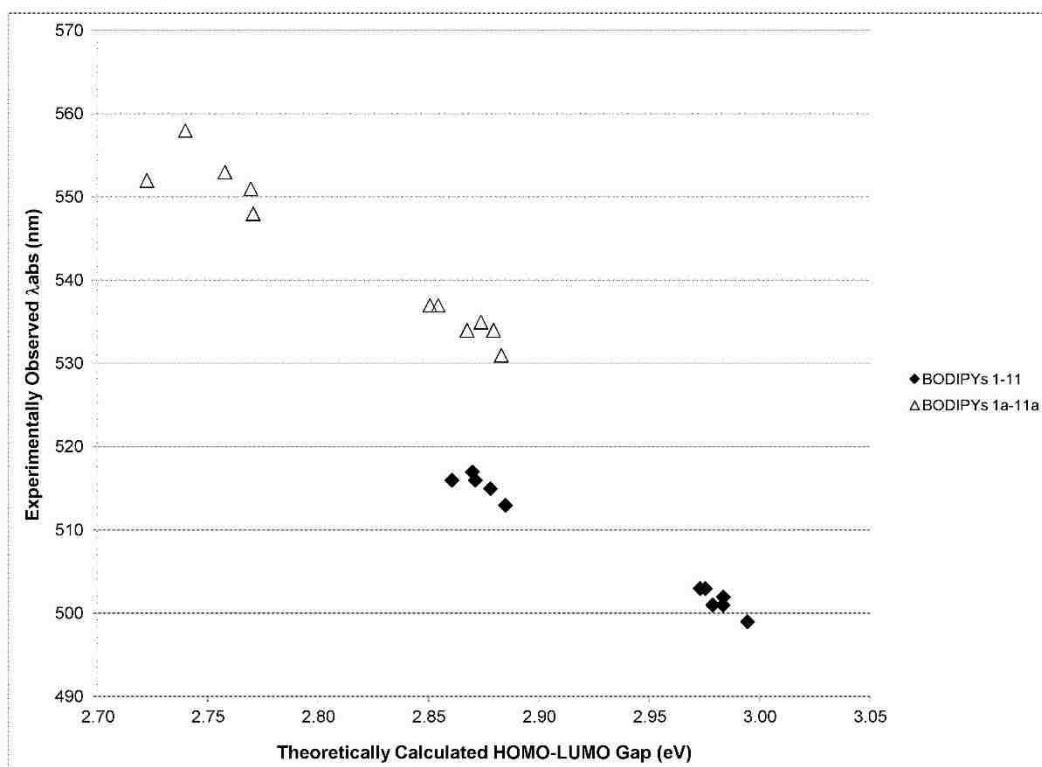


Figure 2.11: Experimentally observed absorption wavelengths versus the theoretically calculated HOMO - LUMO gap.

This theoretical prediction is in exceptional agreement with the experimentally determined red-shifts of the *meso*-thienyl-BODIPYs **7 - 10** and **7a - 10a** and the *meso*-pentafluorophenyl-BODIPY **11** and **11a**. In general, the diiodo substitution at the 2,6-positions lowers both the HOMO and LUMO, with a slightly greater effect on the LUMO. Overall, a slight lowering of the HOMO-LUMO gap is observed with all diiodo BODIPYs, which agrees well with the experimentally observed red-shifts when compared with their β-free analogs.

Table 2.5: Theoretically calculated energies of HOMO (a.u.), LUMO (a.u.), HOMO - LUMO gap,  $E_g$  (eV), and *meso*-group rotational barrier,  $\Delta E_{\text{rot}}$  (kcal/mol) in vacuum and in dichloromethane (in parentheses), for BODIPYs **1 - 11** and **1a - 11a**.

<b>BODIPY</b>	<b>HOMO</b>	<b>LUMO</b>	$E_g$	$\Delta E_{\text{rot}}$
<b>1</b>	-0.2072	-0.0976	2.98	20.3 (19.7)
<b>2</b>	-0.2028	-0.0931	2.98	21.0 (20.6)
<b>3</b>	-0.2048	-0.0948	2.99	21.7 (21.2)
<b>4</b>	-0.2068	-0.0973	2.98	24.2 (18.6)
<b>5</b>	-0.2107	-0.1013	2.98	20.5 (20.2)
<b>6</b>	-0.2112	-0.1020	2.97	25.3 (25.0)
<b>7</b>	-0.2090	-0.1030	2.88	15.3 (14.4)
<b>8</b>	-0.2093	-0.1035	2.88	13.6 (12.5)
<b>9</b>	-0.2124	-0.1073	2.86	15.8 (15.2)
<b>10</b>	-0.2113	-0.1058	2.87	14.1 (13.3)
<b>11</b>	-0.2189	-0.1134	2.87	33.0 (33.0)
<b>1a</b>	-0.2159	-0.1106	2.87	–
<b>2a</b>	-0.2117	-0.1061	2.87	–
<b>3a</b>	-0.2136	-0.1076	2.88	–
<b>4a</b>	-0.2152	-0.1094	2.88	–
<b>5a</b>	-0.2188	-0.1139	2.85	–
<b>6a</b>	-0.2195	-0.1147	2.85	–
<b>7a</b>	-0.2175	-0.1157	2.77	–
<b>8a</b>	-0.2173	-0.1155	2.77	–
<b>9a</b>	-0.2204	-0.1190	2.76	–
<b>10a</b>	-0.2222	-0.1222	2.72	–
<b>11a</b>	-0.2260	-0.1253	2.74	–

The rotational freedom of the *meso*-substituent in vacuum and in dichloromethane was studied computationally at the B3LYP/6-31+G (d, p) level for BODIPYs **1** - **11**. The rotational energy barriers of the *meso*-aryl group are recorded in the last column of Table 2.5. For most compounds, there is a clear correlation between the rotational barrier and the fluorescence quantum yield (Figure 2.12).

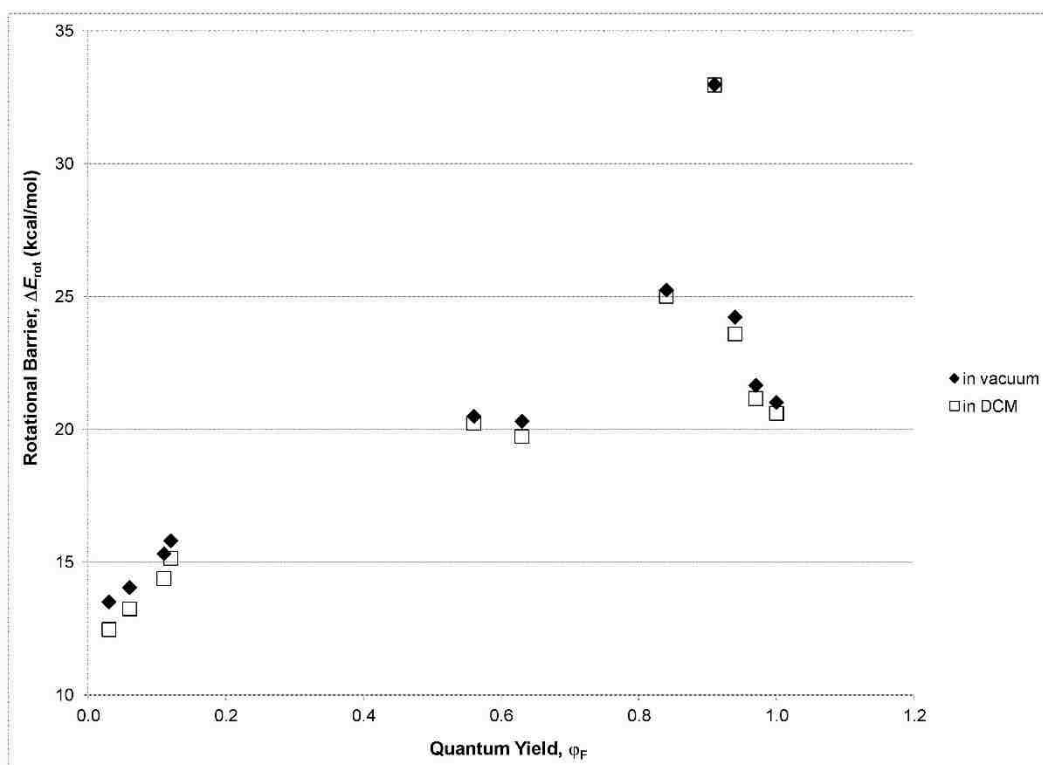


Figure 2.12: Theoretically calculated *meso*-aryl group rotational barrier (in vacuum and in dichloromethane) versus the experimentally observed quantum yield.

The *meso*-thienyl group in BODIPYs **7** - **10** can readily rotate, as noted with a barrier of only 14 - 16 kcal/mol, which explains the decline in quantum yield observed for this series of compounds. Heavy atom substitution of the BODIPY core does not have significant effect on the rotational barrier, in agreement with the negligible changes observed in the quantum yield. Taking

the solvent into account slightly lowers the rotational barriers but the effect is small and the tendency remains very similar.

BODIPYs **1** and **5** demonstrate intermediate rotational barriers and intermediate fluorescence quantum yields. As observed experimentally, possessing a *meso*-phenyl group with substituents at the *meta*-position (OCH<sub>3</sub> or tBu, **2** and **3**, respectively) hinders the group's rotation and results in significantly higher quantum yields, compared with substituents at the *para*-position (**5** and **6**). BODIPYs **2**, **3**, **4**, and **6** experience rotational barriers of 20 - 24 kcal/mol, which is comparable to the kinetic energy at room temperature. The C<sub>6</sub>F<sub>5</sub>-substituted BODIPY **11** deviates from the relationship to the highest extent probably due to the strong electron-withdrawing character of the present fluorines. Still, it displays the highest rotational barrier and a large fluorescence quantum yield.

## 2.2.5 *In vitro* Studies

**2.2.5.1 Time-Dependent Cellular Uptake.** The results acquired from time-dependent cellular uptake of BODIPYs **5**, **7**, **8**, **10**, **1a**, **2a**, **4a**, **6a**, and **10a** at a 10 μM concentration in human HEp2 cells, obtained over a 24 hour period, are shown in Figure 2.17. Significant differences were seen with alteration of the *meso*-aryl group and with the incorporation of iodines. With the exception of BODIPY **10a**, the diiodo-BODIPYs were internalized less effectively than the β-free BODIPYs. Amongst the β-free BODIPYs, those bearing a *meso*-thienyl group (**7**, **8**, and **10**) accumulated only slightly less than their *meso*-phenyl counterpart **5**. By possessing groups that enhance the polar hydrophilicity of the molecule, the sulfur in the thiophene rings and the methyl ester on **5**, the BODIPYs have greater affinity for hydrogen bonding, and bearing

partial charges enhances the ability of these BODIPYs to interact with the cellular membrane thus attributing to greater uptake.

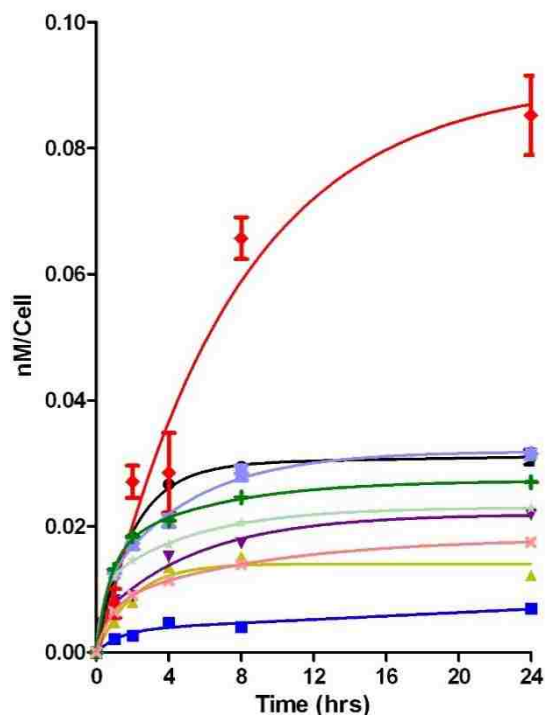


Figure 2.17: Time-dependent uptake of *meso*-aryl-BODIPYs **1a** (black), **2a** (blue), **4a** (yellow), **5** (light purple), **6a** (purple), **7** (light green), **8** (dark green), **10** (pink) and **10a** (red) at 10  $\mu$ M by human HEp2 cells

On the other hand, the diiodo-BODIPYs did not follow any specific trend in their internalization. BODIPY **10a** showed remarkably higher cellular uptake than any other BODIPY tested. Incorporation of iodines onto the scaffold of BODIPY **10** significantly enhanced the uptake of this compound, with four times more compound be internalized by cells. This result was rather interesting since similar diiodo-BODIPYs as well as *meso*-thienyl BODIPYs were difficult to solubilize in aqueous media and required prolonged sonification to dissolve. Nevertheless, this remarkably high cellular uptake may attribute to the high dark and

phototoxicity observed for BODIPY **10a**. Likewise, BODIPYs **2a** and **4a** were the least accumulated within HEp2 cells, presumably due to a noticeable decrease in solubility of diiodo-BODIPYs in aqueous media. However, they were also highly phototoxic, which might be due to their binding to certain protein lipophilic sites.<sup>52</sup>

**2.2.5.2 Cytotoxicity.** The *in vitro* cytotoxicity of a select group of  $\beta$ -free BODIPYs (**5**, **7**, **8** and **10**) and of all 2,6-diiodo-BODIPYs were investigated in human HEp2 cells using the Cell Titer Blue assay, the results of which are summarized in Table 2.6. The cells were exposed to increasing concentration of BODIPY up to 400  $\mu\text{M}$ . For phototoxicity studies, the cells containing internalized BODIPY were irradiated with 1.5  $\text{J}/\text{cm}^2$  of broad spectrum light. Working stock solutions were prepared by dissolving an adequate amount of BODIPY in 96% DMSO and 4% Cremophor. The dose-dependent survival curves are shown in Figures 2.13 - 2.16 and the toxicity results are summarized in Table 2.6. Results are expressed as  $\text{IC}_{50}$  values, the concentration of dye (in  $\mu\text{M}$ ) necessary to kill 50% of the cells. All but one BODIPY (**10a**,  $\text{IC}_{50} = 8 \mu\text{M}$ ) were found to be non-toxic in the dark, with determined  $\text{IC}_{50}$  values above 400  $\mu\text{M}$ . Upon exposure to a low light dose (1.5  $\text{J}/\text{cm}^2$ ) all of the  $\beta$ -free BODIPYs investigated showed low cytotoxicity ( $\text{IC}_{50} > 80 \mu\text{M}$ ) in agreement with previous investigations.<sup>10,43</sup> Among the 2,6-diiodo-BODIPYs, **1a**, **2a**, **4a**, **6a**, **7a** and **10a** showed  $\text{IC}_{50}$  values between 3.5 and 28  $\mu\text{M}$ , while all others showed  $\text{IC}_{50} > 200 \mu\text{M}$ .

This is a surprising result, since the 2,6-diiodo-BODIPYs previously investigated are reported to have high phototoxicity,<sup>10, 11</sup> attributed to the “heavy atom effect,” and clearly shows the effect of the *meso*-aryl groups. In particular, BODIPYs **2a**, **4a** and **10a** bearing *meso*-dimethoxyphenyl or bromo-bithienyl substituents show the highest phototoxicity ( $\text{IC}_{50} = 3.5 -$

7.5  $\mu\text{M}$  at 1.5  $\text{J}/\text{cm}^2$ ); among these, BODIPYs **2a** and **4a** are the most promising for PDT applications due to their high dark/phototoxicity ratio ( $> 50$ ).

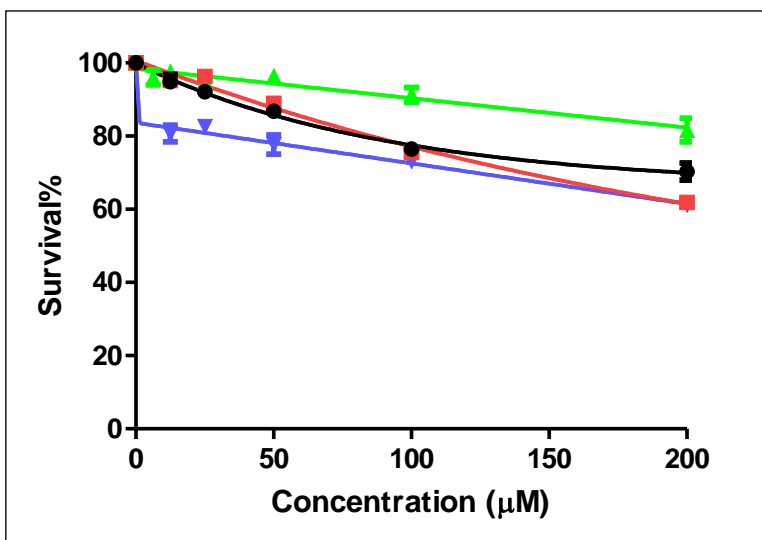


Figure 2.13: Dark toxicity of compounds, **5** (black), **7** (red), **8** (green), and **10** (blue) toward HEp2 cells using the Cell Titer Blue assay.

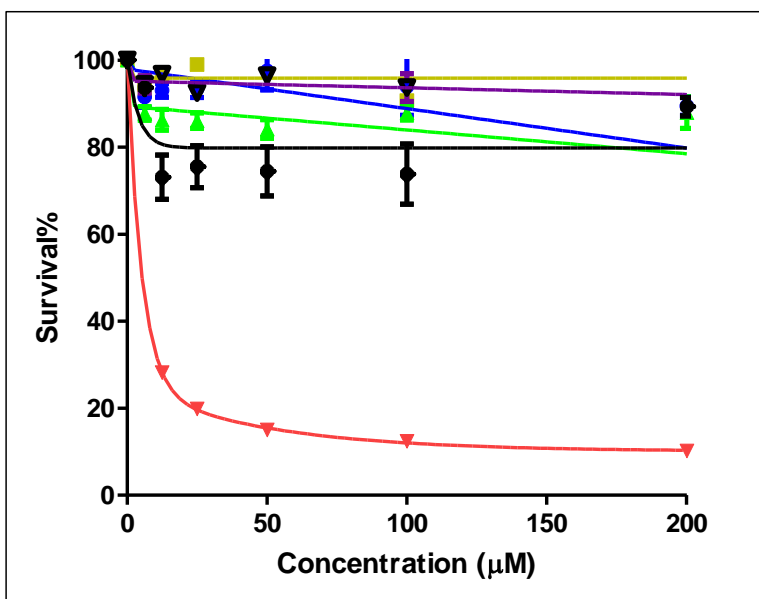


Figure 2.14: Dark toxicity of compounds, **1a** (black), **2a** (blue), **4a** (yellow), **6a** (purple), **7a** (green) and **10a** (red) toward HEp2 cells using the Cell Titer Blue assay.

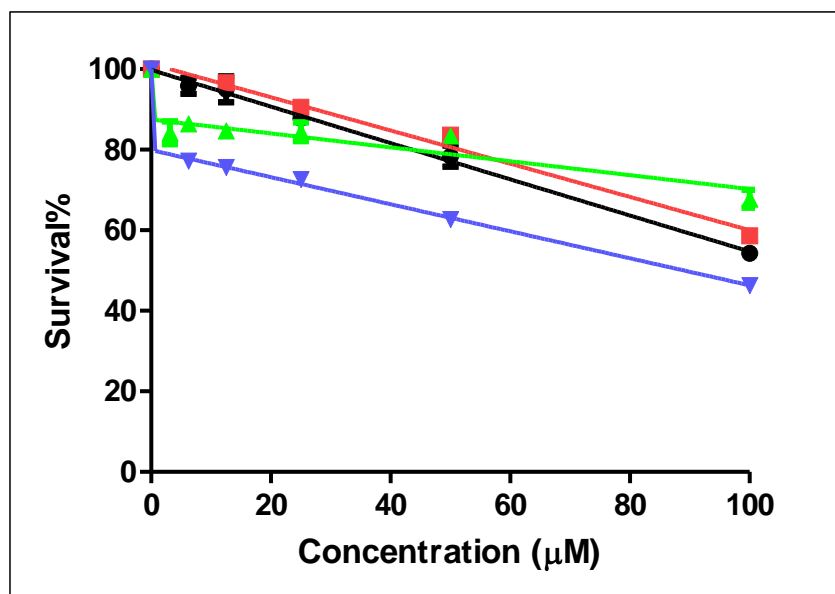


Figure 2.15: Phototoxicity of compounds, **5** (black), **7** (red), **8** (green), and **10** (blue) after exposure to 1 J/cm<sup>2</sup> light dose toward HEp2 cells using the Cell Titer Blue assay.

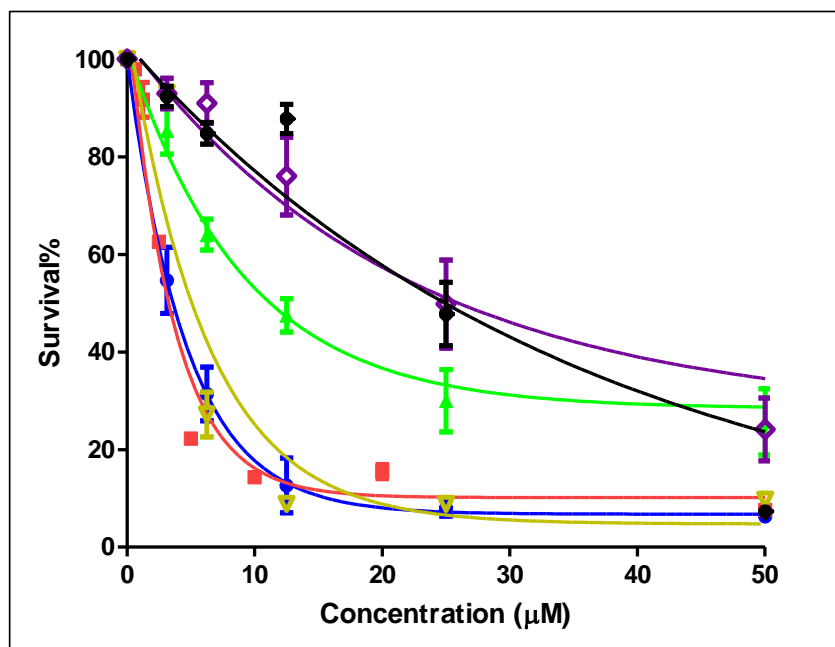


Figure 2.16: Phototoxicity of compounds, **1a** (black), **2a** (blue), **4a** (yellow), **6a** (purple), **7a** (green) and **10a** (red) toward HEp2 cells using the Cell Titer Blue assay after exposure to 1 J/cm<sup>2</sup> light dose.

Table 2.6: Dark, phototoxicity (at 1.5 J/cm<sup>2</sup> light dose), and comparative singlet oxygen quantum yields (relative to methylene blue) of selected BODIPYs toward HEp2 cells using the Cell Titer Blue assay.

<b>BODIPY</b>	<b>Dark toxicity IC<sub>50</sub> (μM)</b>	<b>Phototoxicity IC<sub>50</sub> (μM)</b>	<b>Φ<sub>Δ</sub></b>
<b>5</b>	> 400	>100	0.18
<b>7</b>	>300	>100	0.10
<b>8</b>	>400	>100	0.29
<b>10</b>	>300	82	0.38
<b>1a</b>	> 400	27	0.76
<b>2a</b>	>400	4	0.40
<b>3a</b>	>400	>200	0.32
<b>4a</b>	>400	7.5	0.38
<b>5a</b>	>400	>200	0.27
<b>6a</b>	>400	28	0.31
<b>7a</b>	>400	14	0.02
<b>8a</b>	>400	>200	0.27
<b>9a</b>	>400	>200	0.10
<b>10a</b>	8	3.5	0.34
<b>11a</b>	>400	>200	0.19

BODIPY **10a**'s inherently high phototoxicity is likely attributed to its substantial dark-toxicity, and can be eliminated as a potential PDT or bioimaging agent. On the other hand, BODIPYs **3a**, **5a**, **8a**, **9a** and **11a** showed no dark/photo cytotoxicities and could therefore find application as radioiodine-labeled imaging agents for SPECT and PET, provided they are deemed to possess specific cellular targeting attributes not yet investigated.

**2.2.5.3 Intracellular Localization.** The preferential sites of BODIPYs **5**, **7**, **8**, **10**, and **1a - 11a** localization within cells were evaluated by fluorescence microscopy upon exposure of HEp2 cells to 10  $\mu$ M concentration of BODIPY for 6 hours, Figures 2.18 – 2.22. Overlay experiments were carried out using organelle specific fluorescent trackers, LysoSensor Green (lysosomes), MitoTracker Green (mitochondria), ER Tracker Blue/white (endoplasmic reticulum), and BODIPY FL C5 Ceramide (Golgi). Fluorescence patterns for cells containing tracker and cells containing localized BODIPYs **5**, **7**, **8**, **10**, and **10a** are shown in Figures 2.18 - 2.22 and the results are summarized in Table 2.7. These results show preferential localization of the  $\beta$ -free BODIPYs primarily in the mitochondria and endoplasmic reticulum. The diiodo-BODIPY **10a** showed preference for internalization within the lysosomes and Golgi.

Preliminary results (not shown) reveal that all the phototoxic BODIPYs (**1a**, **2a**, **4a**, **6a**, **7a** and **10a**) localized subcellularly partly within mitochondria, the cell “power house”.<sup>53</sup> In particular, the role played by mitochondria in apoptosis, the process of programmed cell death, makes these cellular organelles highly desirable targets for PDT.<sup>54</sup> These results are in agreement with a previous study<sup>10</sup> that shows preferential localization of a *meso*-propionate-2,6-diiodo-BODIPY in the mitochondria of HSC-2 cells.

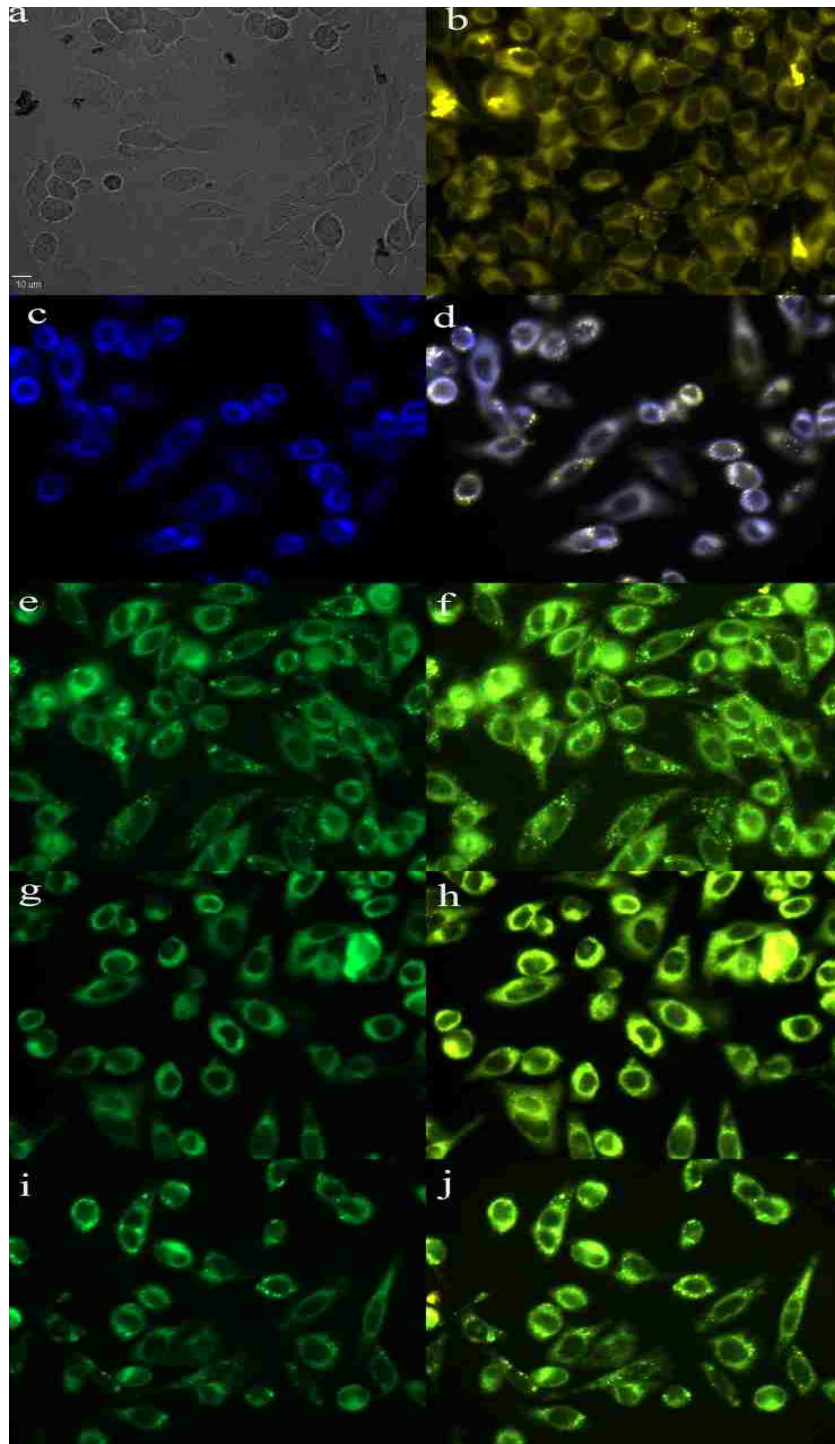


Figure 2.18: Subcellular localization of BODIPY 5 in HEp2 cells at 10  $\mu$ M for 6 h. a) Phase contrast, b) overlay of the BODIPY fluorescence and phase contrast, c) ER tracker blue/white fluorescence, e) MitoTracker green fluorescence, g) BODIPY Ceramide, i) Lyso-Sensor green fluorescence, and d), f), h), and j) overlays of organelle tracers with the BODIPY fluorescence. Scale bar: 10  $\mu$ m.

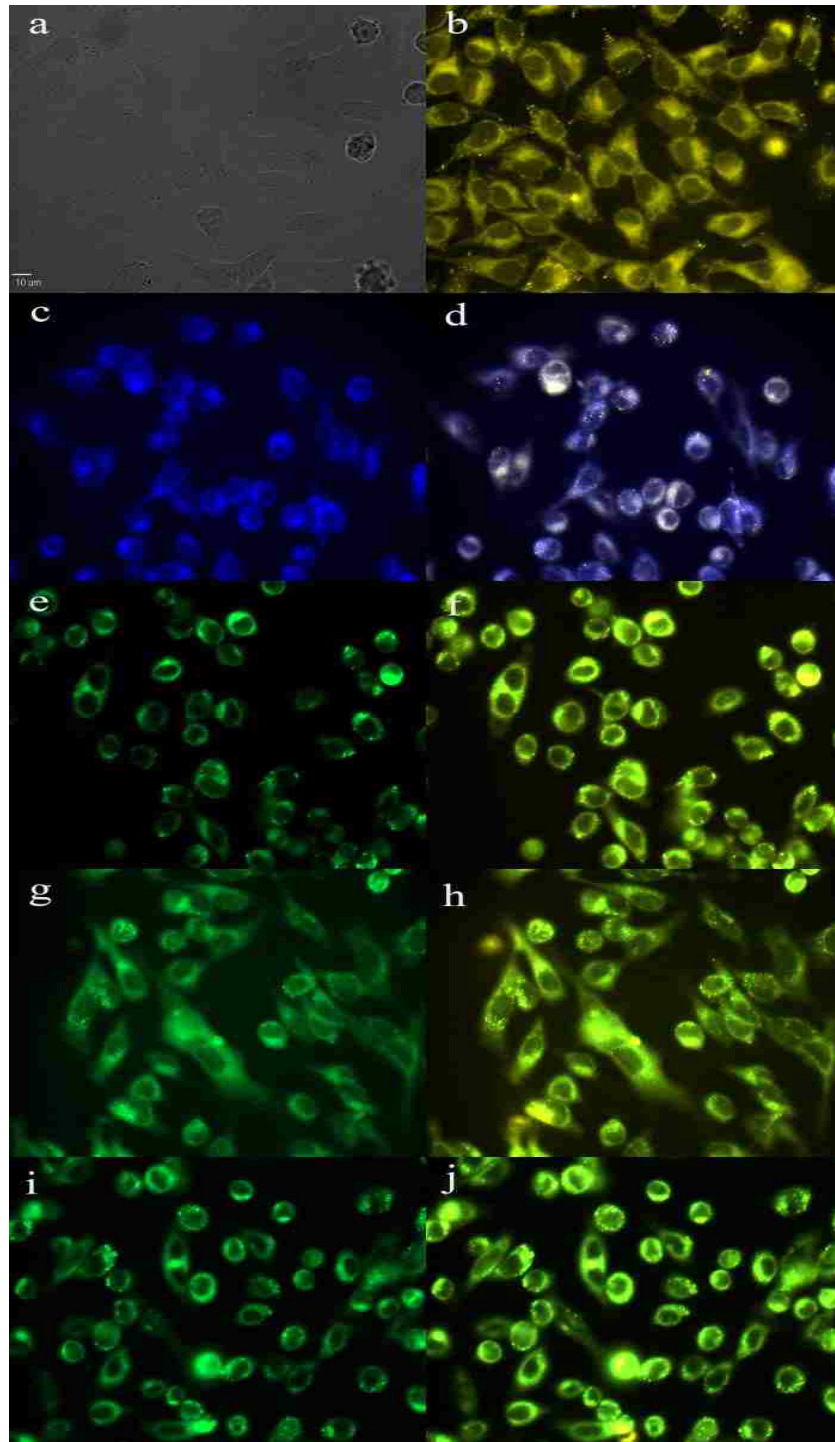


Figure 2.19: Subcellular localization of BODIPY 7 in HEp2 cells at 10  $\mu$ M for 6 h. a) Phase contrast, b) overlay of the BODIPY fluorescence and phase contrast, c) ER tracker blue/white fluorescence, e) MitoTracker green fluorescence, g) BODIPY Ceramide, i) Lyso-Sensor green fluorescence, and d), f), h), and j) overlays of organelle tracers with the BODIPY fluorescence. Scale bar: 10  $\mu$ m.

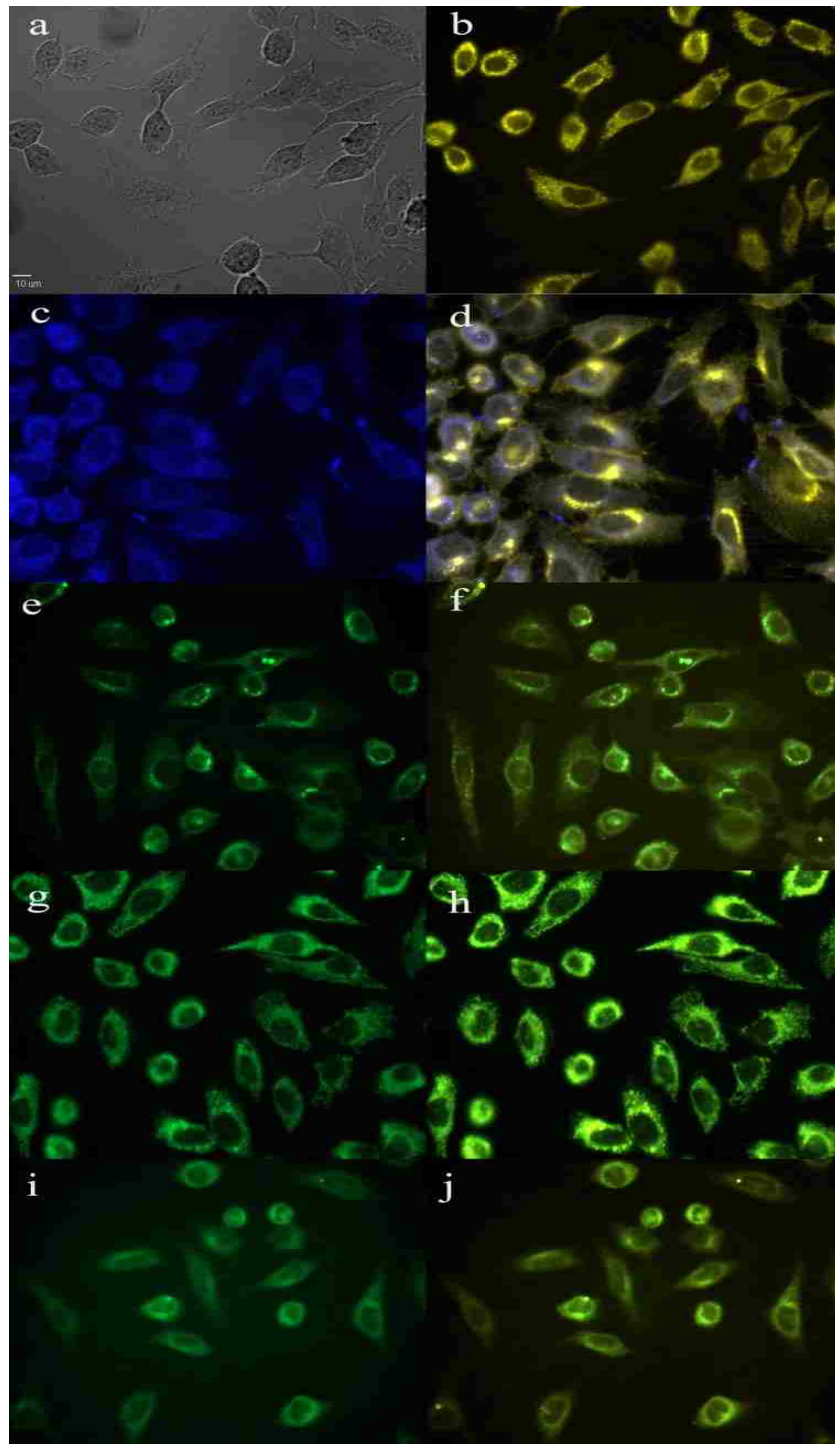


Figure 2.20: Subcellular localization of BODIPY **8** in HEp2 cells at 10  $\mu$ M for 6 h. a) Phase contrast, b) overlay of the BODIPY fluorescence and phase contrast, c) ER tracker blue/white fluorescence, e) MitoTracker green fluorescence, g) BODIPY Ceramide, i) Lyso-Sensor green fluorescence, and d), f), h), and j) overlays of organelle tracers with the BODIPY fluorescence. Scale bar: 10  $\mu$ m.

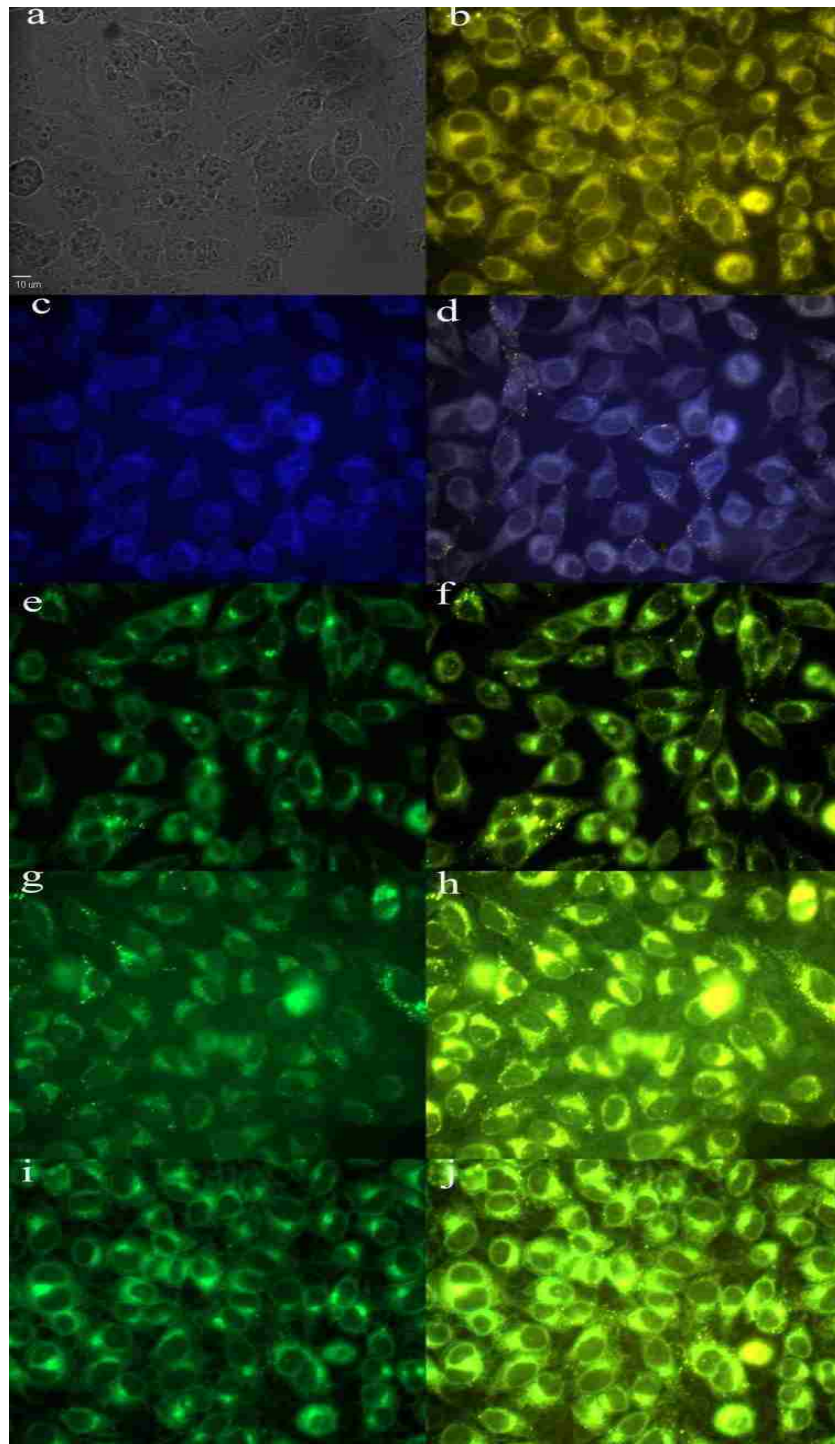


Figure 2.21: Subcellular localization of BODIPY **10** in HEp2 cells at 10  $\mu$ M for 6 h. a) Phase contrast, b) overlay of the BODIPY fluorescence and phase contrast, c) ER tracker blue/white fluorescence, e) MitoTracker green fluorescence, g) BODIPY Ceramide, i) Lyso-Sensor green fluorescence, and d), f), h), and j) overlays of organelle tracers with the BODIPY fluorescence. Scale bar: 10  $\mu$ m.

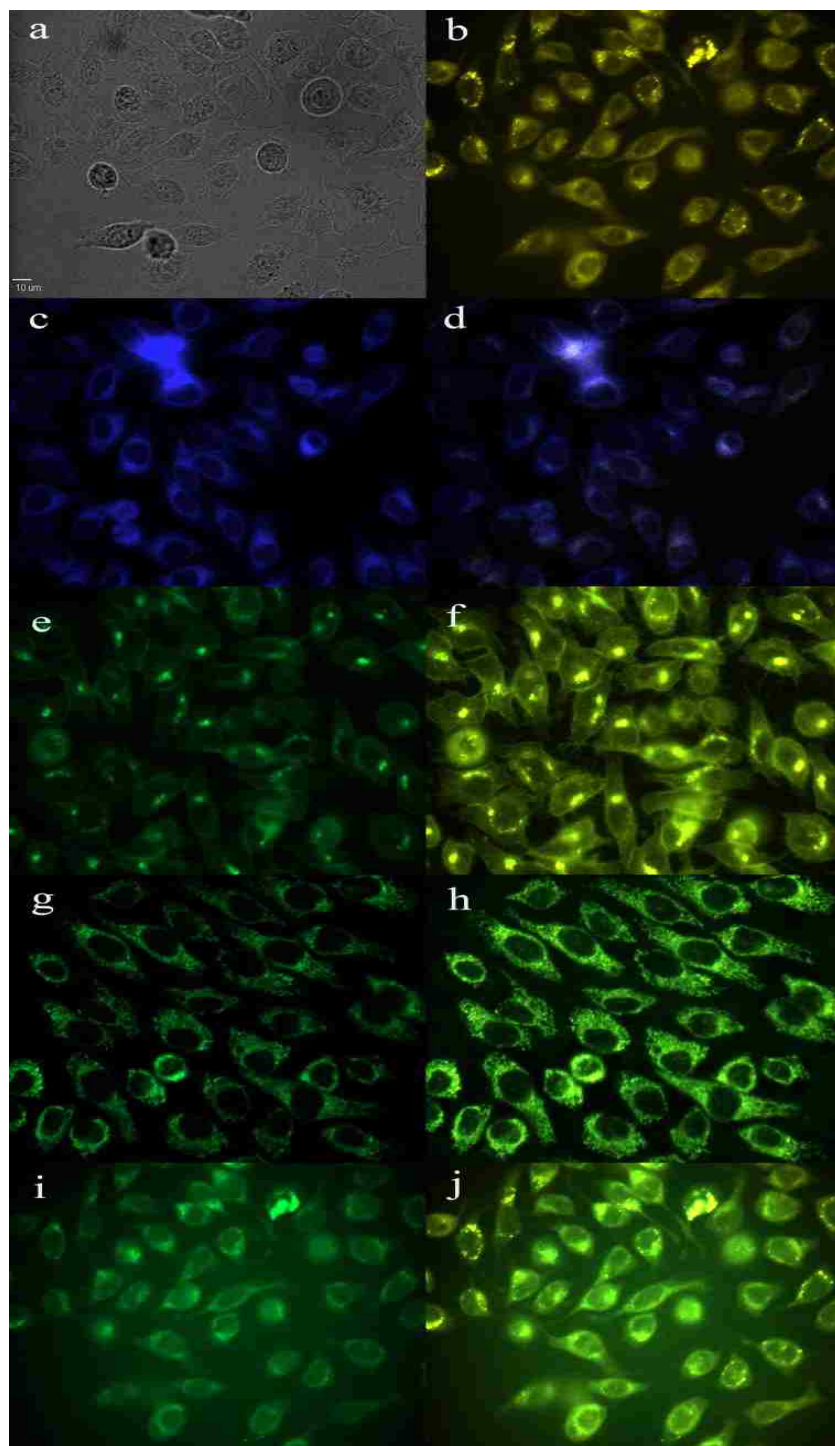


Figure 2.22: Subcellular localization of BODIPY **10a** in HEp2 cells at 10  $\mu\text{M}$  for 6 h. a) Phase contrast, b) overlay of the BODIPY fluorescence and phase contrast, c) ER tracker blue/white fluorescence, e) MitoTracker green fluorescence, g) BODIPY Ceramide, i) Lyso-Sensor green fluorescence, and d), f), h), and j) overlays of organelle tracers with the BODIPY fluorescence. Scale bar: 10  $\mu\text{m}$ .

Table 2.7: Major (++) and Minor (+) Subcellular Sites of Localization for BODIPYs **5**, **7**, **8**, **10**, and **10a** in HEp2 Cells.

Compound	Lysosomes	ER	Golgi	Mitochondria
<b>5</b>	+	++	+	++
<b>7</b>	+	+	+	++
<b>8</b>	+	++	+	+
<b>10</b>	++	++	+	++
<b>10a</b>	++	+	++	+

### 2.2.6 Singlet Oxygen Generation Studies

The singlet oxygen quantum yields were determined for compounds **5**, **7**, **8**, **10**, and **1a** - **11a** by measuring the change in absorbance of a known singlet oxygen acceptor, 1,3-diphenylisobenzofuran (DPBF), in the presence of photosensitizer produced singlet oxygen.<sup>10, 55</sup> The change in the 410 nm absorbance of DPBF (at an initial concentration of 50  $\mu$ M in DMSO) was measured in 15 minute intervals over the course of an hour. The photosensitizer and DPBF were subjected to a long-pass filtered light source of > 500 nm to effectively excite the photosensitizer and to minimize the photobleaching of DPBF, which would have caused an underestimation of the singlet oxygen generation rate. Each photosensitizer was referenced to an equivalent concentration of methylene blue ( $\Phi_{\Delta} = 0.52$ ).

Singlet oxygen quantum yields ranged from 0.1 to 0.76 (shown in Table 2.6), and generally correlated with the *in vitro* toxicity of the photosensitizer. BODIPYs **2a** and **4a**, which showed high phototoxicity values, also revealed to be moderate singlet oxygen generators ( $\Phi_{\Delta} = 0.40$  and 0.38, respectively). Along with their key subcellular localization, such generation leads them to possess highly effective photosensitizer qualities. BODIPY **1a** proved to be a good singlet oxygen

generator ( $\Phi_{\Delta} = 0.76$ ),<sup>56</sup> however, due to its lipophilic nature, low cellular uptake likely prevents it from being an effective agent. In comparison, **10a**, which possessed both high dark and phototoxicity, is a less effective singlet oxygen generator ( $\Phi_{\Delta} = 0.34$ ). Its greater cellular uptake and potential effect of the thienyl-*meso* substituent may play a larger role in its toxicity.

## 2.3 Conclusions

A series of eleven photo-stable *meso*-aryl-BODIPYs, bearing both *meso*-phenyl and *meso*-thienyl groups, were synthesized and iodinated at the 2,6-positions to investigate the effect of the iodine atoms and the nature of the *meso*-aryl group on their photophysical properties and cytotoxicity. BODIPYs bearing *meso*-thienyl and *meso*-pentafluorophenyl substituents, showed the largest red-shifted absorptions and emissions due to their lower HOMO - LUMO gap, as determined computationally. The 2,6-diiodo-BODIPYs showed lower HOMO and LUMO energies compared with the corresponding non-iodinated derivatives. Furthermore, *meso*-thienyl BODIPYs showed drastically reduced fluorescence quantum yields due to the greater freedom of rotation of the small thienyl group. Addition of bromine onto the *meso*-substituent had only a slight effect on the rotational barrier and the fluorescence quantum yields.

Studies in human HEP2 cells revealed that all BODIPYs with exception of **10a** were non-toxic in the dark ( $IC_{50} > 400 \mu M$ ). Upon light treatment ( $1.5 J/cm^2$ ) the  $\beta$ -free BODIPYs showed low cytotoxicity ( $IC_{50} > 80 \mu M$ ) and five of the 2,6-diiodo BODIPYs (**3a**, **5a**, **8a**, **9a** and **11a**) showed no phototoxicity up to  $200 \mu M$ . On the other hand, six of the 2,6-diiodo-BODIPYs (**1a**, **2a**, **4a**, **6a**, **7a** and **10a**) showed  $IC_{50} = 3.5 - 28 \mu M$  at  $1.5 J/cm^2$ , demonstrating the significant effect of both the 2,6-diiodo and the *meso*-aryl groups on the cytotoxic

properties of BODIPYs. BODIPYs **2a** and **4a** had the highest dark/phototoxicity ratio (> 50) and are the most promising for PDT. The high dark and phototoxicity observed for BODIPY **10a** is probably due to its very high cellular uptake, and preferential accumulation within the cell mitochondria. The non-toxic diiodo-BODIPYs may find purpose as radio-iodine imaging agents with appropriate amendments to install radioactive isotope of iodine. BODIPYs **2a** and **4a** that showed favorable qualities as PDT agents would better serve said purpose with a bathochromic shift of the BODIPY's absorption and emission wavelengths into the near-IR, as will be explored in the following Chapter.

## **2.4 Experimental**

### **2.4.1 General Information**

All reagents and solvents were purchased from either Sigma Aldrich or Alfa Aesar as reagent grade and used without further purification. Reactions were monitored by TLC using 0.2 mm silica with UV indicator (UV254). Column chromatography was performed using Sorbent Technologies 60Å silica gel (230 - 400 mesh). All <sup>1</sup>H NMR and <sup>13</sup>C NMR spectra were obtained using a Bruker DPX-400, AV-400, or DPX-250 spectrometer (400 MHz or 250 MHz for <sup>1</sup>H, 100 MHz for <sup>13</sup>C) in deuterated chloroform as solvent with trimethylsilane as an internal indicator. Chemical shifts ( $\delta$ ) are reported in ppm with CDCl<sub>3</sub> (<sup>1</sup>H: 7.27 ppm; <sup>13</sup>C: 77.16 ppm) used as reference. Coupling constants (*J*) are reported in Hertz (Hz). High resolution electrospray ionization (ESI) and matrix assisted laser desorption/ionization (MALDI) mass spectra were obtained using an Agilent Technologies 6210 ESI-TOF Mass Spectrometer or a Bruker UltrafleXtreme MALDI-TOF/TOF. Melting points were determined using a MEL-TEMP

electrothermal instrument. 5'-Bromo-[2,2'-bithiophen]-5-carbaldehyde was synthesized in 64% yield as previously reported.<sup>39</sup>

## 2.4.2 Syntheses

### General Procedure for Synthesis of BODIPYs 1-11

In an oven dried flask, 2, 4-dimethylpyrrole (1 g, 10.5 mmol) and the corresponding aryl aldehyde (5.0 mmol) were dissolved in dry dichloromethane (DCM, 300 mL). Boron trifluoride diethyl etherate (BF<sub>3</sub>·OEt<sub>2</sub>, 0.15 mL) was added drop-wise and the mixture was stirred at room temperature under nitrogen atmosphere for 48 hours (until TLC revealed disappearance of the aldehyde). 2,3-Dichloro-5,6-dicyano-*p*-benzoquinone (DDQ, 1.2 g, 5.1 mmol) in DCM (5 mL) was added to the solution and stirred for 1 hour. Triethylamine (3.8 g, 37.5 mmol) was then added to the mixture and stirred for 30 minutes followed by the introduction of BF<sub>3</sub>·OEt<sub>2</sub> (6.2 mL, 50 mmol) in DCM (10 mL) and stirred for 3 hours. The mixture was poured into water and the organic layer was extracted with DCM. The organic layer was passed through a bed of anhydrous Na<sub>2</sub>SO<sub>4</sub> and the solvent was evaporated under reduced pressure. The resulting residue was purified by silica gel flash chromatography using 30% dichloromethane in petroleum ether to yield the desired BODIPY.

**BODIPY 1:** Obtained as a red solid (0.35 g) in 22% yield, mp: 168-169 °C; <sup>1</sup>H-NMR (400 MHz, CDCl<sub>3</sub>) δ 7.49-7.48 (dd, *J* = 5.2, 1.4, 3H), 7.30-7.27 (dd, *J* = 7.2 and 2.2, 2H), 5.98 (s, 2H), 2.56 (s, 6H), 1.38 (s, 6H); <sup>13</sup>C-NMR (100 MHz, CDCl<sub>3</sub>) δ 155.83, 143.56, 142.14, 135.40, 131.84, 129.53, 129.34, 128.35, 121.60, 14.98, 14.73; HRMS (ESI-TOF) *m/z* 325.1709 [M+H]<sup>+</sup>, calculated for C<sub>19</sub>H<sub>20</sub>BF<sub>2</sub>N<sub>2</sub>: 325.1688. The NMR data is in agreement with that previously reported.<sup>57</sup>

**BODIPY 2:** Obtained as a red-orange solid (1.11 g) in 58% yield, mp = 162 °C (decomposes); <sup>1</sup>H-NMR (400 MHz, CDCl<sub>3</sub>) δ 6.55-6.54 (t, *J* = 2.0, 2H), 6.46-6.45 (d, *J* = 2.0), 5.99 (s, 2H), 3.80 (s, 6H), 2.56 (s, 6H), 1.55 (s, 6H); <sup>13</sup>C-NMR (100 MHz, CDCl<sub>3</sub>) δ 161.59, 155.46, 143.10, 141.33, 136.57, 131.06, 121.08, 105.90, 100.92, 55.52, 14.54, 14.17; HRMS (ESI-TOF) *m/z* 385.1894 [M+H]<sup>+</sup>, calculated for C<sub>21</sub>H<sub>24</sub>BF<sub>2</sub>N<sub>2</sub>O<sub>2</sub>: 385.1899. The NMR data is in agreement with that previously reported.<sup>58</sup>

**BODIPY 3:** Obtained as a red-orange solid (0.51 g) in 23% yield, mp = 115 °C (decomposes); <sup>1</sup>H-NMR (400 MHz, CDCl<sub>3</sub>) δ 7.48-7.47 (t, *J* = 1.8, 1H), 7.13-7.12 (d, *J* = 1.3, 2H), 5.98 (s, 2H), 2.56 (s, 6H), 1.36 (s, 6H), 1.32 (s, 18H); <sup>13</sup>C-NMR (100 MHz, CDCl<sub>3</sub>) δ 155.08, 151.96, 143.25, 143.17, 133.97, 131.52, 122.08, 121.82, 120.99, 35.08, 31.40, 14.56, 14.12; HRMS (ESI-TOF) *m/z* 437.2977 [M+H]<sup>+</sup>, calculated for C<sub>27</sub>H<sub>36</sub>BF<sub>2</sub>N<sub>2</sub>: 437.2940. The NMR data is in agreement with that previously reported.<sup>47</sup>

**BODIPY 4:** Obtained a bright red solid (0.48 g) in 25% yield, mp = 182-183 °C. <sup>1</sup>H-NMR (400 MHz, CDCl<sub>3</sub>) δ 6.98-6.96 (d, *J* = 7.8, 1H), 6.83-6.80 (dd, *J* = 8.7 and 1.5, 2H), 6.79-6.78 (d, *J* = 1.5, 1H), 5.98 (s, 2H), 3.94 (s, 3H), 3.84 (s, 3H), 2.54 (s, 6H), 1.47 (s, 6H); <sup>13</sup>C-NMR (100 MHz, CDCl<sub>3</sub>) δ 155.38, 149.79, 149.50, 143.16, 141.58, 131.72, 127.13, 121.11, 120.42, 111.52, 111.07, 56.11, 55.91, 14.57, 14.45; HRMS (ESI-TOF) *m/z* 385.1893 [M+H]<sup>+</sup>, calculated for C<sub>21</sub>H<sub>24</sub>BF<sub>2</sub>N<sub>2</sub>O<sub>2</sub>: 385.1899. The NMR data is in agreement with that previously reported.<sup>59</sup>

**BODIPY 5:** Obtained a bright red solid (0.44 g) in 23% yield, mp = 181-182 °C; <sup>1</sup>H-NMR (400 MHz, CDCl<sub>3</sub>) δ 8.19 (d, *J* = 7.9, 2H), 7.42-7.40 (d, *J* = 7.9, 2H), 5.99 (s, 2H), 3.97 (s, 3H), 2.56 (s, 6H), 1.35 (s, 6H); <sup>13</sup>C-NMR (100MHz, CDCl<sub>3</sub>) δ 166.47, 156.00, 142.88, 140.21, 139.95, 130.80, 130.37, 128.39, 121.48, 52.40, 14.62, 14.51; HRMS (ESI-TOF) *m/z* 383.1746 [M+H]<sup>+</sup>, calculated for C<sub>21</sub>H<sub>22</sub>BF<sub>2</sub>N<sub>2</sub>O<sub>2</sub>: 383.1742. The NMR data is in agreement with that previously reported.<sup>60</sup>

**BODIPY 6:** Obtained as a red solid (0.38 g) in 19% yield, mp = 172-173 °C; <sup>1</sup>H-NMR (400 MHz, CDCl<sub>3</sub>) δ 7.66-7.64 (d, *J* = 8.2, 2H), 7.19-7.17 (d, *J* = 8.2, 2H), 5.99 (s, 2H), 2.55 (s, 6H), 1.41 (s, 6H); <sup>13</sup>C-NMR (100 MHz, CDCl<sub>3</sub>) δ 155.91, 142.92, 140.03, 133.96, 132.45, 131.19, 129.84, 123.27, 121.47, 14.65, 14.61; HRMS (ESI-TOF) *m/z* 403.0780 [M+H]<sup>+</sup>, calculated for C<sub>19</sub>H<sub>19</sub>BBBrF<sub>2</sub>N<sub>2</sub>: 403.0793. The NMR data is in agreement with that previously reported.<sup>61</sup>

**BODIPY 7:** Obtained a red solid (0.33 g) in 20% yield, mp = 190-191 °C; <sup>1</sup>H-NMR (400 MHz, CDCl<sub>3</sub>) δ 7.51-7.50 (d, *J* = 5.0, 1H), 7.15-7.12 (t, *J* = 4.4, 1H), 6.99-6.98 (d, *J* = 3.2, 1H), 6.00 (s, 2H), 2.55 (s, 6H), 1.58 (s, 6H); <sup>13</sup>C-NMR (100 MHz, CDCl<sub>3</sub>) δ 156.07, 143.50, 134.63, 134.00, 132.40, 127.81, 127.61, 127.41, 121.50, 14.65, 13.55; HRMS (ESI-TOF) *m/z* 331.1306 [M+H]<sup>+</sup>, calculated for C<sub>17</sub>H<sub>18</sub>BF<sub>2</sub>N<sub>2</sub>S: 331.1252. The NMR data is in agreement with that previously reported.<sup>62</sup>

**BODIPY 8:** Obtained a dark red solid (0.42 g) in 20% yield, mp = 157 °C (decomposes); <sup>1</sup>H-NMR (400 MHz, CDCl<sub>3</sub>) δ 7.23-7.22 (d, *J* = 3.5, 1H), 7.22-7.21 (d, *J* = 3.5, 1H), 7.21-7.20 (d, *J* = 3.5, 1H), 7.06-7.04 (dd, *J* = 4.9 and 3.7, 1H), 6.90-6.89 (d, *J* = 3.5, 1H), 6.02 (s, 2H), 2.56 (s, 6H), 1.75

(s, 6H);  $^{13}\text{C}$ -NMR (100 MHz,  $\text{CDCl}_3$ )  $\delta$  156.28, 143.44, 133.14, 128.65, 127.98, 125.02, 124.33, 123.73, 121.58, 14.66, 13.95; HRMS (ESI-TOF)  $m/z$  413.1116  $[\text{M}+\text{H}]^+$ , calculated for  $\text{C}_{21}\text{H}_{20}\text{BF}_2\text{N}_2\text{S}$ : 413.1129.

**BODIPY 9:** Obtained a dark red solid (0.37 g) in 18% yield, mp = 167-168 °C;  $^1\text{H}$ -NMR (400 MHz,  $\text{CDCl}_3$ )  $\delta$  7.10-7.09 (d,  $J$  = 3.5, 1H), 6.77-6.76 (d,  $J$  = 3.9, 1H), 6.01 (s, 2H), 2.54 (s, 6H), 1.69 (s, 6H);  $^{13}\text{C}$ -NMR (100MHz,  $\text{CDCl}_3$ )  $\delta$  156.57, 143.34, 136.32, 132.11, 130.36, 128.43, 121.75, 113.83, 14.65, 13.87; HRMS (ESI-TOF)  $m/z$  409.0315  $[\text{M}+\text{H}]^+$ , Calculated for  $\text{C}_{17}\text{H}_{17}\text{BBrF}_2\text{N}_2\text{S}$ : 409.0357.

**BODIPY 10:** Obtained as a dark red solid (0.74 g) from 5'-bromo-[2,2'-bithiophen]-5-carbaldehyde<sup>39</sup> (1.3658 g) in 30% yield, mp = 205 °C (decomposes);  $^1\text{H}$ -NMR (400 MHz,  $\text{CDCl}_3$ )  $\delta$  7.14-7.13 (d,  $J$  = 3.5, 1H), 7.01-7.00 (d,  $J$  = 3.5, 1H), 6.97-6.96 (d,  $J$  = 3.9, 1H), 6.90-6.89 (d,  $J$  = 3.9, 1H), 6.03 (s, 2H), 2.56 (s, 6H), 1.73 (s, 6H);  $^{13}\text{C}$ -NMR (100 MHz,  $\text{CDCl}_3$ )  $\delta$  156.42, 143.36, 135.64, 133.70, 132.29, 130.75, 128.76, 124.41, 123.96, 121.64, 111.80, 14.67, 13.93; HRMS (ESI-TOF, negative ion)  $m/z$  489.0089  $[\text{M}+\text{H}]^+$ , calculated for  $\text{C}_{21}\text{H}_{17}\text{BBrF}_2\text{N}_2\text{S}_2$ : 489.0078.

**BODIPY 11:** Obtained as a red solid (0.38 g) from pentafluorobenzaldehyde (0.39 g, 2 mmol) in 52% yield, mp = 109 °C (decomposes);  $^1\text{H}$ -NMR (400 MHz,  $\text{CDCl}_3$ )  $\delta$  6.06 (s, 2H), 2.57 (s, 6H), 1.62 (s, 6H);  $^{13}\text{C}$ -NMR (100 MHz,  $\text{CDCl}_3$ )  $\delta$  157.78, 145.26, 142.77, 141.50, 139.44, 137.10, 130.99, 122.73, 122.26, 14.76, 13.57; HRMS (ESI-TOF)  $m/z$  415.1337  $[\text{M}+\text{H}]^+$ , calculated for  $\text{C}_{19}\text{H}_{15}\text{BF}_7\text{N}_2$ : 415.1216. The NMR data is in agreement with that previously reported.<sup>63</sup>

## General Procedure for Iodination of BODIPYs 1-11

Iodic acid (2 equiv.) was dissolved in a minimal amount of water and added drop-wise to a solution of the BODIPY (1 equiv.) and iodine (2.5 equiv.) in a solution of 50:50 ethanol/DCM (~ 35  $\mu$ M solution). The resulting mixture was stirred at 60 °C for 2 hours. After cooling, the solvent was evaporated under vacuum and the resulting residue was purified by silica gel column chromatography using 50:50 hexanes/DCM for elution.

**BODIPY 1a:** Obtained as a red solid (0.16 g) in 91% yield from **1** (0.1 g, 0.31 mmol), iodic acid (0.11 g, 0.62 mmol), iodine (0.10 g, 0.77 mmol), mp = 204-206 °C;  $^1\text{H-NMR}$  (400 MHz,  $\text{CDCl}_3$ )  $\delta$  7.53-7.51 (dd,  $J$  = 5.2, 1.4, 3H), 7.27-7.24 (dd,  $J$  = 7.2 and 2.2, 2H), 2.65 (s, 6H), 1.39 (s, 6H);  $^{13}\text{C-NMR}$  (100 MHz,  $\text{CDCl}_3$ )  $\delta$  156.78, 145.37, 141.38, 134.74, 131.30, 129.54, 129.47, 127.79, 85.65, 16.95, 16.04; HRMS (ESI-TOF)  $m/z$  575.9461  $[\text{M}]^+$ , calculated for  $\text{C}_{19}\text{H}_{17}\text{BF}_2\text{I}_2\text{N}_2$ : 575.9543. The NMR data is in agreement with that previously reported.<sup>64</sup>

**BODIPY 2a:** Obtained as a red solid (0.28 g) in 84% yield from **2** (0.2 g, 0.52 mmol), iodic acid (0.18 g, 1.0 mmol), iodine (0.17 g, 1.3 mmol), mp = 192-193 °C;  $^1\text{H-NMR}$  (400 MHz,  $\text{CDCl}_3$ )  $\delta$  6.60-6.59 (t,  $J$  = 2.0, 2H), 6.42-6.41 (d,  $J$  = 2.0, 1H), 3.81 (s, 6H), 2.65 (s, 6H), 1.57 (s, 6H);  $^{13}\text{C-NMR}$  (100 MHz,  $\text{CDCl}_3$ )  $\delta$  161.94, 156.84, 149.46, 145.42, 136.31, 131.12, 105.77, 101.45, 85.58, 55.65, 16.88, 16.06; HRMS (ESI-TOF)  $m/z$  636.9810  $[\text{M}+\text{H}]^+$ , calculated for  $\text{C}_{21}\text{H}_{21}\text{BF}_2\text{I}_2\text{N}_2\text{O}_2$ : 636.9832.

**BODIPY 3a:** Obtained as a red solid (0.37 g) in 93% yield from **3** (0.25 g, 0.57 mmol), iodic acid (0.2 g, 1.15 mmol) and iodine (0.18 g, 1.43 mmol);  $^1\text{H-NMR}$  (400 MHz,  $\text{CDCl}_3$ )  $\delta$  7.54-7.53 (t,  $J$

= 1.8, 1H), 7.08-7.07 (d,  $J = 1.3$ , 2H), 2.66 (s, 6H), 1.37 (s, 6H), 1.33 (s, 18H);  $^{13}\text{C}$ -NMR (100MHz,  $\text{CDCl}_3$ )  $\delta$  156.40, 152.48, 145.35, 142.94, 133.76, 131.39, 122.46, 121.87, 85.45, 35.15, 31.40, 16.69, 15.99; HRMS (ESI-TOF)  $m/z$  688.0730  $[\text{M}]^+$ , calculated for  $\text{C}_{27}\text{H}_{33}\text{BF}_2\text{I}_2\text{N}_2$ : 688.0794.

**BODIPY 4a:** Obtained as a red solid (0.39 g) in 94% yield from **4** (0.25 g, 0.65 mmol), iodic acid (0.23 g, 1.3 mmol), iodine (0.21 g, 1.62 mmol), mp = 215-217 °C;  $^1\text{H}$ -NMR (400 MHz,  $\text{CDCl}_3$ )  $\delta$  7.02-7.01 (d,  $J = 7.8$ , 1H), 6.82-6.78 (dd,  $J = 8.7$ , 1.5, 2H), 6.75-6.74 (d,  $J = 1.5$ ), 3.98 (s, 3H), 3.87 (s, 3H), 2.65 (s, 6H), 1.49 (s, 6H);  $^{13}\text{C}$ -NMR (100 MHz,  $\text{CDCl}_3$ )  $\delta$  156.70, 150.10, 149.97, 145.37, 141.28, 131.62, 126.78, 120.33, 111.76, 111.81, 85.58, 56.18, 56.01, 17.07, 16.01; HRMS (ESI-TOF)  $m/z$  635.9840  $[\text{M}]^+$ , calculated for  $\text{C}_{21}\text{H}_{21}\text{BF}_2\text{I}_2\text{N}_2\text{O}_2$ : 635.9754. The NMR data is in agreement with that previously reported.<sup>65</sup>

**BODIPY 5a:** Obtained as a red solid (0.36 g) in 86% yield from **5** (0.25 g, 0.65 mmol), iodic acid (0.23 g, 1.31 mmol), iodine (0.21 g, 1.64 mmol), mp = 215 °C (decomposes);  $^1\text{H}$ -NMR (400 MHz,  $\text{CDCl}_3$ )  $\delta$  8.24-8.20 (d,  $J = 7.9$ , 2H), 7.40-7.37 (d,  $J = 7.9$ , 2H), 3.99 (s, 3H), 2.65 (s, 6H), 1.37 (s, 6H);  $^{13}\text{C}$ -NMR (100 MHz,  $\text{CDCl}_3$ )  $\delta$  166.24, 157.34, 145.07, 139.81, 139.46, 131.34, 130.81, 130.66, 128.24, 86.04, 52.53, 17.14, 16.12; HRMS (ESI-TOF)  $m/z$  634.9663  $[\text{M}+\text{H}]^+$ , calculated for  $\text{C}_{21}\text{H}_{20}\text{BF}_2\text{I}_2\text{N}_2\text{O}_2$ : 634.9676. The NMR data is in agreement with that previously reported.<sup>16</sup>

**BODIPY 6a:** Obtained as a red solid (0.44 g) in 71% yield from **6** (0.25 g, 0.62 mmol), iodic acid (0.22 g, 1.24 mmol), iodine (0.2 g, 1.55 mmol), mp = 232 °C (decomposes);  $^1\text{H}$ -NMR (400 MHz,  $\text{CDCl}_3$ )  $\delta$  7.71-7.68 (d,  $J = 8.2$ , 2H), 7.18-7.14 (d,  $J = 8.2$ , 2H), 2.65 (s, 6H), 1.44 (s, 6H);  $^{13}\text{C}$ -

NMR (100 MHz, CDCl<sub>3</sub>)  $\delta$  157.27, 145.13, 139.64, 133.69, 132.80, 131.08, 129.66, 123.91, 85.99, 17.28, 16.09; HRMS (ESI-TOF)  $m/z$  653.8638 [M]<sup>+</sup>, calculated for C<sub>19</sub>H<sub>16</sub>BBrF<sub>2</sub>I<sub>2</sub>N<sub>2</sub>: 653.8648.

**BODIPY 7a:** Obtained as a red solid (0.6 g) in 79% yield from **7** (0.25 g, 0.76 mmol), iodic acid (0.27 g, 1.51 mmol), iodine (0.24 g, 1.9 mmol), mp = 186-187 °C; <sup>1</sup>H-NMR (400 MHz, CDCl<sub>3</sub>)  $\delta$  7.57-7.56 (d,  $J$  = 5.0, 1H), 7.19-7.17 (t,  $J$  = 4.4, 1H), 7.00-6.99 (d,  $J$  = 3.2, 1H), 2.65 (s, 6H), 1.59 (s, 6H); <sup>13</sup>C-NMR (100MHz, CDCl<sub>3</sub>)  $\delta$  157.35, 145.65, 134.34, 133.75, 132.25, 128.20, 128.14, 127.97, 86.17, 16.27, 16.11; HRMS (ESI-TOF)  $m/z$  582.9173 [M+H]<sup>+</sup>, calculated for C<sub>17</sub>H<sub>16</sub>BF<sub>2</sub>I<sub>2</sub>N<sub>2</sub>S: 582.9185.

**BODIPY 8a:** Obtained as a red solid (0.51 g) in 84% yield from **8** (0.25 g, 0.61 mmol), iodic acid (0.21 g, 1.21 mmol), iodine (0.19 g, 1.52 mmol), mp = 195-196 °C; <sup>1</sup>H-NMR (400 MHz, CDCl<sub>3</sub>)  $\delta$  7.25-7.23 (t,  $J$  = 3.3, 1H), 7.21-7.20 (d,  $J$  = 3.9, 1H), 7.18-7.17 (d,  $J$  = 3.4, 1H), 6.91-6.89 (dd,  $J$  = 5.1 and 4.2, 2H), 2.66 (s, 6H), 1.74 (s, 6H); <sup>13</sup>C-NMR (100MHz, CDCl<sub>3</sub>)  $\delta$  157.67, 145.50, 141.83, 139.22, 137.88, 133.23, 129.13, 129.04, 128.09, 125.95, 125.41, 124.67, 86.28, 16.69, 16.14; HRMS (ESI-TOF)  $m/z$  663.8988 [M+H]<sup>+</sup>, calculated for C<sub>21</sub>H<sub>17</sub>BF<sub>2</sub>I<sub>1</sub>N<sub>2</sub>S<sub>2</sub>: 663.8984.

**BODIPY 9a:** Obtained as a red solid (0.07 g) in 91% yield from **9** (0.05 g, 0.12 mmol), iodic acid (0.04 g, 0.24 mmol), iodine (0.04 g, 0.31 mmol), mp = 212 °C (decomposes); <sup>1</sup>H-NMR (400 MHz, CDCl<sub>3</sub>)  $\delta$  7.15-7.14 (d,  $J$  = 3.4, 1H), 6.79-6.78 (d,  $J$  = 3.9, 1H), 2.65 (s, 6H), 1.71 (s, 6H); <sup>13</sup>C-NMR (100MHz, CDCl<sub>3</sub>)  $\delta$  158.18, 145.48, 136.18, 132.63, 130.65, 128.79, 114.84, 86.05, 16.63, 16.15; HRMS (ESI-TOF)  $m/z$  660.8246 [M+H]<sup>+</sup>, calculated for C<sub>17</sub>H<sub>15</sub>BBrF<sub>2</sub>I<sub>2</sub>N<sub>2</sub>S: 660.8290.

**BODIPY 10a:** Obtained as a red solid (0.25 g) in 65% yield from **10** (0.25 g, 0.51 mmol), iodic acid (0.18 g, 1.02 mmol), iodine (0.16 g, 1.27 mmol), mp = 198 °C (decomposes); <sup>1</sup>H-NMR (400 MHz, CDCl<sub>3</sub>) δ 7.17-7.16 (d, *J* = 3.5, 1H), 7.03-7.02 (d, *J* = 3.9, 1H), 6.99-6.98 (d, *J* = 3.9, 1H), 6.90-6.89 (d, *J* = 3.5, 1H), 2.65 (s, 6H), 1.74 (s, 6H); <sup>13</sup>C-NMR (100 MHz, CDCl<sub>3</sub>) δ 157.68, 145.50, 139.38, 137.40, 133.20, 132.42, 132.16, 130.85, 129.13, 124.75, 124.14, 112.25, 86.32, 16.68, 16.15; MS (MALDI-TOF) *m/z* 741.8490 [M+H]<sup>+</sup>, calculated for C<sub>21</sub>H<sub>16</sub>BBrF<sub>2</sub>I<sub>2</sub>N<sub>2</sub>S<sub>2</sub>: 741.8089.

**BODIPY 11a:** Obtained as a red solid (0.07 g) in 90% yield from **11** (0.05 g, 0.12 mmol), iodic acid (0.04 g, 0.24 mmol), iodine (0.04 g, 0.3 mmol), mp = 198 °C (decomposes); <sup>1</sup>H-NMR (400 MHz, CDCl<sub>3</sub>) δ 2.68 (s, 6H), 1.65 (s, 6H); <sup>13</sup>C-NMR (100 MHz, CDCl<sub>3</sub>) δ 159.13, 145.11, 143.74, 142.70, 139.65, 137.07, 130.89, 122.46, 87.05, 16.31, 16.20; HRMS (ESI-TOF) *m/z* 666.9130 [M+H]<sup>+</sup>, calculated for C<sub>19</sub>H<sub>13</sub>BF<sub>7</sub>I<sub>2</sub>N<sub>2</sub>: 666.9150.

### 2.4.3 X-ray Determined Molecular Structures

The crystal structures of BODIPYs **3**, **7**, **1a** and **9a** were determined at low temperature using MoK $\alpha$  radiation on a Nonius KappaCCD (**1a**) diffractometer, CuK $\alpha$  radiation on a Bruker Kappa Apex-II (**3**), or CuK $\alpha$  (**7**) or MoK $\alpha$  (**9a**) radiation on a Bruker Kappa Apex-II DUO diffractometer. For **7**, the thiophene substituent was disordered into two orientations with 0.824(2)/0.176(2) occupancies, and for **9a**, there were two independent molecules in the asymmetric unit.

*Crystal data for 1a:* C<sub>19</sub>H<sub>17</sub>BF<sub>2</sub>I<sub>2</sub>N<sub>2</sub>, M = 575.96, monoclinic space group P2<sub>1</sub>/c, a = 11.4673 (15), b = 12.9564 (15), c = 17.3920 (15) Å,  $\beta$  = 130.446 (4)°, U = 1966.5 (4) Å<sup>3</sup>, T = 95 K, Z = 4. A

total of 16872 reflections were measured ( $R_{\text{int}} = 0.032$ ).  $R = 0.031$  for 6345 data points with  $I > 2\sigma$  (I) of 8604 unique data points and 239 refined parameters.

*Crystal data for 3:*  $C_{27}H_{35}BF_2N_2$ ,  $M = 436.38$ , monoclinic space group  $P2_1/c$ ,  $a = 6.6395$  (8),  $b = 12.1074$  (14),  $c = 15.139$  (2) Å,  $\beta = 101.284$  (10)°,  $U = 1193.5$  (3) Å<sup>3</sup>,  $T = 90$  K. A total of 9239 reflections were measured ( $R_{\text{int}} = 0.042$ ).  $R = 0.036$  for 1887 data points with  $I > 2\sigma$  (I) of 2097 unique data points and 153 refined parameters.

*Crystal data for 7:*  $C_{17}H_{17}BF_2N_2S$ ,  $M = 330.20$ , monoclinic space group  $P2_1/c$ ,  $a = 6.6059$  (3),  $b = 18.5456$  (9),  $c = 12.7397$  (6) Å,  $\beta = 92.791$ (2)°,  $U = 1558.89$  (13) Å<sup>3</sup>,  $T = 90$  K,  $Z = 4$ . A total of 14155 reflections were measured ( $R_{\text{int}} = 0.035$ ).  $R = 0.034$  for 2762 data points with  $I > 2\sigma$  (I) of 2797 unique data points and 220 refined parameters.

*Crystal data for 9a:*  $C_{17}H_{14}BBBrF_2I_2N_2S$ ,  $M = 660.88$ , monoclinic space group  $P2_1/c$ ,  $a = 21.871$  (2),  $b = 9.8112$  (10),  $c = 19.478$  (2) Å,  $\beta = 107.585$  (5)°,  $U = 3984.3$  (7) Å<sup>3</sup>,  $T = 100$  K,  $Z = 8$ . A total of 162,698 reflections were measured ( $R_{\text{int}} = 0.052$ ).  $R = 0.029$  for 19,684 data points with  $I > 2\sigma$  (I) of 26,346 unique data points and 477 refined parameters.

#### 2.4.4 Steady-state Absorption and Fluorescence Spectroscopy

The spectral properties of compounds **1-11** and **1a-11a** were investigated using solutions prepared by dissolving an adequate amount of crystalline compound in either dichloromethane or tetrahydrofuran. Stock solutions of concentrations ranging from  $1.5 \times 10^{-5}$  to  $5 \times 10^{-5}$  M were prepared and diluted to suitable concentrations for collection of absorbance and emission spectra.

Absorption spectra were acquired using a PerkinElmer Lambda 35 UV/VIS Spectrometer. Measurements obtained for calculating the optical density,  $\epsilon$ , were taken from prepared solutions

with concentrations between  $7.5 \times 10^{-6}$  and  $2.5 \times 10^{-5}$  M. These solutions provided absorption  $\lambda_{\max}$  between 0.5 and 1.0.

Emission measurements were chronicled on a PTI QuantaMaster4/2006SE spectrofluorometer with the slit width set at 2 nm. Rhodamine 6G was used as a standard in calculating the fluorescence quantum yields ( $\Phi_F = 0.95$  in ethanol). Fluorescence spectra were determined by subsequent dilution of solutions to between  $1.5 \times 10^{-6}$  and  $8 \times 10^{-6}$  M to achieve an optical density between 0.04 and 0.06 at the excitation wavelength, in order to minimize intermolecular reabsorption and inner-filter effects.<sup>66</sup> Fluorescence emissions were recorded for all samples, including the standard, after excitation at 480 nm.

The fluorescent quantum yields ( $\Phi_{exp}$ ) were calculated using the following equation:<sup>67</sup>

$$\Phi_{exp} = \Phi_{ref} \frac{F_x [A_{std}] n^2}{F_{std} [A_x] n_{std}^2}$$

$\Phi_{ref}$  is the fluorescent quantum yield of the standard,  $F_x$  is the area under the sample's emission peak,  $F_{std}$  is the area under the standard's emission peak,  $A_{std}$  is the optical density at which the standard was excited,  $A_x$  is the optical density at which the sample was excited,  $n$  is the refractive index of the sample's solvent, and  $n_{std}$  is the refractive index of the standard's solvent.

All measurements, both absorbance and emission, were acquired within 4 hours of solution preparation at room temperature (23 - 25 °C), using non-degassed samples and a 10 mm quartz spectrophotometric cuvette.

## 2.4.5 Computational Modeling

Electronic structure calculations of BODIPYs **1-11** and **1a-11a** were carried out using the hybrid Becke's Three Parameter DFT Functional.<sup>68,69</sup> All atoms except iodine were modeled using the 6-31+G(d,p) basis sets. For BODIPY's **1a-11a** the iodine atoms were treated using the Stevens-Basch-Krauss (SBK)<sup>70-72</sup> relativistic effective core potentials and the standard CEP-31G basis set. All structures were optimized without symmetry constraints. The Highest Occupied Molecular Orbital (HOMO) and the Lowest Unoccupied Molecular Orbital (LUMO) were rigorously determined without any further approximations. Potential energy surface minima were confirmed with frequency calculations. Rotational energy barriers were determined by performing relaxed scans of the potential energy surface. All calculations were performed using the Gaussian 09 program package.<sup>73</sup>

## 2.4.6 Cell Studies

The human HEP2 cells used in this study were purchased from ATCC (derived from HeLa, cervical cancer, contamination). The HEP2 cells were maintained in a 50:50 mixture of DMEM:AMEM (Invitrogen) supplemented with 10% FBS (Invitrogen) and 1% antibiotic (Penicillin-streptomycin) and 5% CO<sub>2</sub> at 37 °C. A 32 mM BODIPY stock solution was prepared by dissolving the compound in 96% DMSO and 4% Cremophor EL (a nonionic emulsifier). A 2 mL of a 400 μM BODIPY solution containing 1.94% DMSO and 0.05% Cremophor EL was prepared by adding 15 μL DMSO, 1 μL Cremophor EL, and 25 μL of the 32 mM stock solution into 1960 μL medium. The final solution was sonicated to aid in BODIPY solubilization.

**2.4.6.1 Time-Dependent Cellular Uptake.** The HEp2 cells were plated at 15,000 cells per well in a Costar 96-well plate (BD biosciences) and grown overnight. The 10  $\mu\text{M}$  BODIPY solution was prepared by diluting 400  $\mu\text{M}$  stock solution with medium containing 5% FBS and 1% antibiotic. The cells were treated by adding 100  $\mu\text{L}$ /well of the 10  $\mu\text{M}$  BODIPY solution at time periods of 0, 1, 2, 4, 8, and 24 hours. The loading medium was removed at the end of the treatments. The cells were washed with 1X PBS, and solubilized by adding 0.25% Triton X-100 in 1X PBS. BODIPY standard curves at 10  $\mu\text{M}$ , 5  $\mu\text{M}$ , 2.5  $\mu\text{M}$ , 1.25  $\mu\text{M}$ , 0.625  $\mu\text{M}$  and 0.3125  $\mu\text{M}$  concentrations were obtained by diluting 20 mM BODIPY solution with 0.25% Triton X-100 in 1X PBS. A cell standard curve was prepared using 10,000, 20,000, 40,000, 60,000, 80,000, and 100,000 cells per well. The cells were quantified using the CyQuant Cell Proliferation Assay (Life Technologies). The compound and cell number were determined using a FluoStar Optima micro-plate reader (BMG LRBTEH), with wavelengths 355/520 nm and 570/615 nm. Cellular uptake was expressed in terms of nM compound per cell.

**2.4.6.2 Dark Cytotoxicity.** The HEp2 cells were placed in a 96-well plate as above, with BODIPY concentrations of 400, 200, 100, 50, 25, 12.5, and 0  $\mu\text{M}$ , five repetitions for each concentration, and then incubated at 37  $^{\circ}\text{C}$ . After 24 hour incubation, the compound was removed by washing the cells with 1X PBS and replaced with media containing 20% Cell Titer Blue. The cells were incubated for an additional 4 hours at 37  $^{\circ}\text{C}$ . The viable cells were measured using fluorescence at 570/615 nm using a FluoStar Optima micro-plate reader. The dark toxicity was expressed in terms of the percentage of viable cells.

**2.4.6.3 Phototoxicity.** The concentrations of 200, 100, 50, 25, 12.5, 6.25, 3.125 and 0  $\mu\text{M}$  were used for the phototoxicity experiments. The HEp2 cells were placed in 96-well plates as described above, and treated with compound for 24 hours at 37 °C. After the 24 hour treatment, the loading media was removed. The cells were washed with media, and then refilled with fresh media. The cells were placed on ice and exposed to 610 nm LP filter light from a 100 W halogen lamp filtered through a 610 nm long pass filter (Chroma) for 20 minutes. An inverted plate lid filled with cold water to a depth of 5 mm acted as an IR filter. The total light dose was approximately 1.5 J/cm<sup>2</sup>. After exposure to light, the cells were returned back to the incubator for 24 hours. After 24 hour incubation, the medium was removed and replaced with medium containing 20% of Cell Titer Blue. The cells were incubated for an additional 4 hours. The viable cells were measured by fluorescence at 570/615 nm using a FluoStar Optima micro-plate reader. The phototoxicity was expressed in terms of the percentage of viable cells.

**2.4.6.4 Microscopy.** HEp2 cells were plated in a 6-well plate and allowed to grow overnight. The cells were then exposed to 10  $\mu\text{M}$  of the compound at 37 °C for more than 6 hours before adding the organelle tracer (Invitrogen). The working concentrations of organelle tracers were as following: LysoSensor Green 50 nM, MitoTracker Green 250 nM, ER Tracker Blue/white 100 nM, and BODIPY FL C5 Ceramide 50 nM. The organelle tracers were diluted in growing medium and the cells were incubated concurrently with the compound and the tracer for 30 minutes. After adding the tracer for 30 minutes, the loading medium is removed and cells were washed with 1X PBS three times. Images were acquired using a Leica DMRXA2 microscope with a water immersion objective and a YFP filter cube (Chroma Technologies).

### 2.4.7 Comparative Singlet Oxygen Quantum Yield Measurements

To each well of a 6-well plate was added 2 mL containing 50  $\mu\text{M}$  of 1, 3-diphenylisobenzofuran (DPBF) and 5  $\mu\text{M}$  of photosensitizers in DMSO. The plate was irradiated using a 71 W filtered light source of  $>500$  nm with a Schott glass 500 nm long-pass yellow filter for 1 hour. At 15 minute increments, 200  $\mu\text{L}$  aliquots were removed from each of the six wells and the absorbance was measured at 410 nm. The rate of singlet oxygen generation was determined by the decrease in absorbance of DPBF over time. Control solutions of DPBF-DMSO (negative control) and DPBF-methylene blue-DMSO (reference standard) were irradiated under the previous mentioned conditions. Singlet oxygen quantum yields were determined using the following equation:

$$\Phi_{\Delta(U)} = \Phi_{\Delta(Std)} \times \frac{S_U}{S_{Std}}$$

$\Phi_{\Delta(U)}$  is the singlet oxygen quantum yield of the sample,  $\Phi_{\Delta(Std)}$  is the singlet oxygen quantum yield of the standard (methylene blue, 0.52),  $S_U$  is the slope of the plot of absorbance versus time of the sample, and  $S_{Std}$  is the slope of the plot of absorbance versus time of the standard.

### 2.4.8. Octanol-water partition coefficients

The partition coefficients ( $\log P$ ) were measured at room temperature by 1 mg of BODIPY in 4 mL 1-octanol in a volumetric tube followed by addition of 4 mL of water. After vortexing for 5 min, the phases were allowed to separate.<sup>74</sup> An aliquot of 1 mL from each layer was removed and the absorbance was read on a Varian Cary 50 Bio UV/VIS spectrophotometer with 10 mm path length quartz cuvette.

## 2.5 References

1. Gibbs, J. H.; Robins, L. T.; Zhou, Z.; Bobadova-Parvanova, P.; Cottam, M.; McCandless, G. T.; Fronczek, F. R.; Vicente, M. G. H., Spectroscopic, computational modeling and cytotoxicity of a series of meso-phenyl and meso-thienyl-BODIPYs. *Bioorganic and Medicinal Chemistry* **2013**, *21*, 5770-5781.
2. Loudet, A.; Burgess, K., BODIPY dyes and their derivatives: Syntheses and spectroscopic properties. *Chemical Reviews* **2007**, *107*, 4891-4932.
3. Ziessel, R.; Ulrich, G.; Harriman, A., The chemistry of Bodipy: a new El Dorado for fluorescence tools. *New Journal of Chemistry* **2007**, *31*, 496-501.
4. Banfi, S.; Nasini, G.; Zaza, S.; Caruso, E., Synthesis and photo-physical properties of a series of BODIPY dyes. *Tetrahedron* **2013**, *69*, 4845-4856.
5. Jiao, L. J.; Li, J. L.; Zhang, S. Z.; Wei, C.; Hao, E. H.; Vicente, M. G. H., A selective fluorescent sensor for imaging Cu<sup>2+</sup> in living cells. *New Journal of Chemistry* **2009**, *33*, 1888-1893.
6. Jiao, L. J.; Yu, C. J.; Uppal, T.; Liu, M. M.; Li, Y.; Zhou, Y. Y.; Hao, E. H.; Hu, X. K.; Vicente, M. G. H., Long wavelength red fluorescent dyes from 3,5-diiodo-BODIPYs. *Organic & Biomolecular Chemistry* **2010**, *8*, 2517-2519.
7. Ortiz, M. J.; Agarrabeitia, A. R.; Duran-Sampedro, G.; Prieto, J. B.; Lopez, T. A.; Massad, W. A.; Montejano, H. A.; Garcia, N. A.; Arbeloa, I. L., Synthesis and functionalization of new polyhalogenated BODIPY dyes. Study of their photophysical properties and singlet oxygen generation. *Tetrahedron* **2012**, *68*, 1153-1162.
8. Awuah, S. G.; You, Y., Boron dipyrromethene (BODIPY)-based photosensitizers for photodynamic therapy. *RSC Advances* **2012**, *2*, 11169-11183.
9. Kamkaew, A.; Lim, S. H.; Lee, H. B.; Kiew, L. V.; Chung, L. Y.; Burgess, K., BODIPY dyes in photodynamic therapy. *Chemistry Society Review* **2013**, *42*, 77-88.
10. Lim, S. H.; Thivierge, C.; Nowak-Sliwinska, P.; Han, J. Y.; van den Bergh, H.; Wagnieres, G.; Burgess, K.; Lee, H. B., In Vitro and In Vivo Photocytotoxicity of Boron Dipyrromethene Derivatives for Photodynamic Therapy. *Journal of Medicinal Chemistry* **2010**, *53*, 2865-2874.
11. Yogo, T.; Urano, Y.; Ishitsuka, Y.; Maniwa, F.; Nagano, T., Highly efficient and photostable photosensitizer based on BODIPY chromophore. *Journal of the American Chemical Society* **2005**, *127*, 12162-12163.
12. Duran-Sampedro, G.; Agarrabeitia, A. R.; Garcia-Moreno, I.; Costela, A.; Banuelos, J.; Arbeloa, T.; Lopez Arbeloa, I.; Luis Chiara, J.; Ortiz, M. J., Chlorinated BODIPYs:

- Surprisingly Efficient and Highly Photostable Laser Dyes. *European Journal of Organic Chemistry* **2012**, 6335-6350.
13. Leen, V.; Leemans, T.; Boens, N.; Dehaen, W., 2-and 3-Monohalogenated BODIPY Dyes and Their Functionalized Analogues: Synthesis and Spectroscopy. *European Journal of Organic Chemistry* **2011**, 4386-4396.
  14. Leen, V.; Miscoria, D.; Yin, S.; Filarowski, A.; Ngongo, J. M.; Van der Auweraer, M.; Boens, N.; Dehaen, W., 1,7-Disubstituted Boron Dipyrromethene (BODIPY) Dyes: Synthesis and Spectroscopic Properties. *Journal of Organic Chemistry* **2011**, 76, 8168-8176.
  15. Ulrich, G.; Ziesel, R.; Harriman, A., The chemistry of fluorescent bodipy dyes: Versatility unsurpassed. *Angewandte Chemie-International Edition* **2008**, 47, 1184-1201.
  16. Sabatini, R. P.; McCormick, T. M.; Lazarides, T.; Wilson, K. C.; Eisenberg, R.; McCamant, D. W., Intersystem Crossing in Halogenated Bodipy Chromophores Used for Solar Hydrogen Production. *Journal of Physical Chemistry Letters* **2011**, 2, 223-227.
  17. Duman, S.; Cakmak, Y.; Kolemen, S.; Akkaya, E. U.; Dede, Y., Heavy Atom Free Singlet Oxygen Generation: Doubly Substituted Configurations Dominate S-1 States of Bis-BODIPYs. *Journal of Organic Chemistry* **2012**, 77, 4516-4527.
  18. Triesscheijn, M.; Baas, P.; Schellens, J. H. M.; Stewart, F. A., Photodynamic therapy in oncology. *Oncologist* **2006**, 11, 1034-1044.
  19. Dolmans, D. E. J. G. J.; Fukumura, D.; Jain, R. K., Photodynamic therapy for cancer. *Nature Reviews Cancer* **2003**, 3, 380-387.
  20. Dougherty, T. J.; Gomer, C. J.; Henderson, B. W.; Jori, G.; Kessel, D.; Korbely, M.; Moan, J.; Peng, Q., Photodynamic therapy. *Journal of the National Cancer Institute* **1998**, 90, 889-905.
  21. Medicinal Chemistry. <http://www.tcd.ie/IMM/medicinal-chemistry/>
  22. Singlet Oxygen Detection and Photodynamic Therapy. <http://kchf-45.karlov.mff.cuni.cz/~jakub/dept/SingletOxygen.htm>
  23. Brown, S. B.; Brown, E. A.; Walker, I., The present and future role of photodynamic therapy in cancer treatment. *Lancet Oncology* **2004**, 5, 497-508.
  24. Huang, Z., A review of progress in clinical photodynamic therapy. *Technology in Cancer Research & Treatment* **2005**, 4, 283-293.
  25. Kadish, K. M. S., K. M.; Guillard, R., *Handbook of Porphyrin Science: with Applications to Chemistry, Physics, Materials Science, Engineering, Biology and Medicine*. World Scientific Publishing Co. Pte. Ltd.2010; Vol. 4.

26. Photofrin. <http://www.photofrin.com/>
27. Darwish, A.; Blacker, M.; Janzen, N.; Rathmann, S. M.; Czorny, S.; Hillier, S. M.; Joyal, J. L.; Babich, J. W.; Valliant, J. F., Triazole Appending Agent (TAAG): A New Synthon for Preparing Iodine-Based Molecular Imaging and Radiotherapy Agents. *ACS Medicinal Chemistry Letters* **2012**, *3*, 313-316.
28. Pandey, S. K.; Pan, S.; Kant, R.; Kuruvilla, S. A.; Pan, M. L.; Mukherjee, J., Synthesis and evaluation of 3-I-123-iodo-5- 2-(S)-3-pyrrolinylmethoxy -pyridine (niodene) as a potential nicotinic alpha 4 beta 2 receptor imaging agent. *Bioorganic & Medicinal Chemistry Letters* **2012**, *22*, 7610-7614.
29. Khalil, M. M. E., *Basic Sciences of Nuclear Medicine*. Springer-Verlag: Berlin Heidelberg, 2011.
30. Tanaka, M.; Uehara, S.; Kojima, A.; Matsumoto, M., Monte Carlo simulation of energy spectra for I-123 imaging. *Physics in Medicine & Biology* **2007**, *52*, 4409-4425.
31. Agdeppa, E. D.; Spilker, M. E., A Review of Imaging Agent Development. *AAPS Journal* **2009**, *11*, 286-299.
32. Beatty, K. E.; Szychowski, J.; Fisk, J. D.; Tirrell, D. A., A BODIPY-Cyclooctyne for Protein Imaging in Live Cells. *ChemBioChem* **2011**, *12*, 2137-2139.
33. Lemcke, S.; Honnscheidt, C.; Waschatko, G.; Bopp, A.; Lutjohann, D.; Bertram, N.; Gehrig-Burger, K., DHEA-Bodipy-A functional fluorescent DHEA analog for live cell imaging. *Molecular & Cellular Endocrinology* **2010**, *314*, 31-40.
34. Lund, F. W.; Lomholt, M. A.; Solanko, L. M.; Bittman, R.; Wustner, D., Two-photon time-lapse microscopy of BODIPY-cholesterol reveals anomalous sterol diffusion in chinese hamster ovary cells. *BMC Biophysics* **2012**, *5*, 15.
35. Atilgan, S.; Ekmekci, Z.; Dogan, A. L.; Guc, D.; Akkaya, E. U., Water soluble distyryl-boradiazaindacenes as efficient photosensitizers for photodynamic therapy. *Chemical Communications* **2006**, 4398-4400.
36. He, H.; Lo, P. C.; Yeung, S. L.; Fong, W. P.; Ng, D. K. P., Preparation of unsymmetrical distyryl BODIPY derivatives and effects of the styryl substituents on their in vitro photodynamic properties. *Chemical Communications* **2011**, *47*, 4748-4750.
37. Uppal, T.; Bhupathiraju, N.; Vicente, M. G. H., Synthesis and cellular properties of Near-IR BODIPY-PEG and carbohydrate conjugates. *Tetrahedron* **2013**, *69*, 4687-4693.
38. Meng, G.; Velayudham, S.; Smith, A.; Luck, R.; Liu, H. Y., Color Tuning of Polyfluorene Emission with BODIPY Monomers. *Macromolecules* **2009**, *42*, 1995-2001.

39. Yang, F.; Xu, X. L.; Gong, Y. H.; Qiu, W. W.; Sun, Z. R.; Zhou, J. W.; Audebert, P.; Tang, J., Synthesis and nonlinear optical absorption properties of two new conjugated ferrocene-bridge-pyridinium compounds. *Tetrahedron* **2007**, *63*, 9188-9194.
40. Pavlopoulos, T. G.; Boyer, J. H.; Sathyamoorthi, G., Laser action from a 2,6,8-position trisubstituted 1,3,5,7-tetramethylpyrromethene-BF<sub>2</sub> complex: part 3. *Applied Optics* **1998**, *37*, 7797-7800.
41. Niu, S. L.; Ulrich, G.; Ziessel, R.; Kiss, A.; Renard, P.-Y.; Romieu, A., Water-Soluble BODIPY Derivatives. *Organic Letters* **2009**, *11*, 2049-2052.
42. Mula, S.; Ray, A. K.; Banerjee, M.; Chaudhuri, T.; Dasgupta, K.; Chattopadhyay, S., Design and development of a new pyrromethene dye with improved photostability and lasing efficiency: Theoretical rationalization of photophysical and photochemical properties. *Journal of Organic Chemistry* **2008**, *73*, 2146-2154.
43. Uppal, T.; Hu, X. K.; Fronczek, F. R.; Maschek, S.; Bobadova-Parvanova, P.; Vicente, M. G. H., Synthesis, Computational Modeling, and Properties of Benzo-Appended BODIPYs. *Chemistry-A European Journal* **2012**, *18*, 3893-3905.
44. Rihn, S.; Retailleau, P.; Bugsaliewicz, N.; De Nicola, A.; Ziessel, R., Versatile synthetic methods for the engineering of thiophene-substituted Bodipy dyes. *Tetrahedron Letters* **2009**, *50*, 7008-7013.
45. Shen, Z.; Rohr, H.; Rurack, K.; Uno, H.; Spieles, M.; Schulz, B.; Reck, G.; Ono, N., Boron-diindomethene (BDI) dyes and their tetrahydrobicyclo precursors - en route to a new class of highly emissive fluorophores for the red spectral range. *Chemistry-A European Journal* **2004**, *10*, 4853-4871.
46. Zheng, Q. D.; Xu, G. X.; Prasad, P. N., Conformationally restricted dipyrromethene boron difluoride (BODIPY) dyes: Highly fluorescent, multicolored probes for cellular imaging. *Chemistry-A European Journal* **2008**, *14*, 5812-5819.
47. Ozdemir, T.; Atilgan, S.; Kutuk, I.; Yildirim, L. T.; Tulek, A.; Bayindir, M.; Akkaya, E. U., Solid-State Emissive BODIPY Dyes with Bulky Substituents As Spacers. *Organic Letters* **2009**, *11*, 2105-2107.
48. Fu, L.; Jiang, F. L.; Fortin, D.; Harvey, P. D.; Liu, Y., A reaction-based chromogenic and fluorescent chemodosimeter for fluoride anions. *Chemical Communications* **2011**, *47*, 5503-5505.
49. Qu, X. Y.; Liu, Q.; Ji, X. N.; Chen, H. C.; Zhou, Z. K.; Shen, Z., Enhancing the Stokes' shift of BODIPY dyes via through-bond energy transfer and its application for Fe<sup>3+</sup>-detection in live cell imaging. *Chemical Communications* **2012**, *48*, 4600-4602.
50. Benniston, A. C.; Copley, G., Lighting the way ahead with boron dipyrromethene (Bodipy) dyes. *Physical Chemistry Chemical Physics* **2009**, *11*, 4124-4131.

51. Kim, K.; Jo, C.; Easwaramoorthi, S.; Sung, J.; Kim, D. H.; Churchill, D. G., Crystallographic, Photophysical, NMR Spectroscopic and Reactivity Manifestations of the "8-Heteroaryl Effect" in 4,4-Difluoro-8-(C<sub>4</sub>H<sub>3</sub>X)-4-bora-3a,4a-diaza-s-indacene (X=O, S, Se) (BODIPY) Systems. *Inorganic Chemistry* **2010**, *49*, 4881-4894.
52. Yogo, T.; Urano, Y.; Mizushima, A.; Sunahara, H.; Inoue, T.; Hirose, K.; Iino, M.; Kikuchi, K.; Nagano, T., Selective photo inactivation of protein function through environment-sensitive switching of singlet oxygen generation by photosensitizer. *Proceedings from the National Academy of Science U. S. A.* **2008**, *105*, 28-32.
53. Weissig, V., Targeted drug delivery to mammalian mitochondria in living cells. *Expert Opinions in Drug Delivery* **2005**, *2*, 89-102.
54. Kessel, D.; Luo, Y., Mitochondrial photodamage and PDT-induced apoptosis. *Journal of Photochemical & Photobiology B-Biology* **1998**, *42*, 89-95.
55. Kochevar, I. E.; Redmond, R. W., Photosensitized production of singlet oxygen. *Methods Enzymology* **2000**, *319*, 20-28.
56. Huang, L.; Zhao, J. Z.; Guo, S.; Zhang, C. S.; Ma, J., Bodipy Derivatives as Organic Triplet Photosensitizers for Aerobic Photoorganocatalytic Oxidative Coupling of Amines and Photooxidation of Dihydroxynaphthalenes. *Journal of Organic Chemistry* **2013**, *78*, 5627-5637.
57. Kollmannsberger, M.; Rurack, K.; Resch-Genger, U.; Daub, J., Ultrafast charge transfer in amino-substituted boron dipyrromethene dyes and its inhibition by cation complexation: A new design concept for highly sensitive fluorescent probes. *Journal of Physical Chemistry A* **1998**, *102*, 10211-10220.
58. Jiao, L. J.; Yu, C. J.; Li, J. L.; Wang, Z. Y.; Wu, M.; Hao, E. H.,  $\beta$ -Formyl-BODIPYs from the Vilsmeier-Haack Reaction. *Journal of Organic Chemistry* **2009**, *74*, 7525-7528.
59. Wang, J. G.; Hou, Y. J.; Li, C.; Zhang, B. W.; Wang, X. S., Selectivity tune of fluoride ion sensing for phenolic OH-containing BODIPY dyes. *Sensors & Actuator B-Chemistry* **2011**, *157*, 586-593.
60. Qin, W. W.; Baruah, M.; De Borggraeve, W. M.; Boens, N., Photophysical properties of an on/off fluorescent pH indicator excitable with visible light based on a borondipyrromethene-linked phenol. *Journal of Photochemistry Photobiology A-Chemistry* **2006**, *183*, 190-197.
61. Zhang, X. L.; Xiao, Y.; Qian, X. H., Highly efficient energy transfer in the light harvesting system composed of three kinds of boron-dipyrromethene derivatives. *Organic Letters* **2008**, *10*, 29-32.
62. Jun, T.; Kim, K.; Lee, K. M.; Benniston, A. C.; Churchill, D. G., Meso-thienyl and furyl rotor effects in BF<sub>2</sub>-chelated dipyrin dyes: solution spectroscopic studies and X-ray

- structural packing analysis of isomer and congener effects. *Journal of Coordination Chemistry* **2012**, *65*, 4299-4314.
63. Alamiry, M. A. H.; Benniston, A. C.; Hagon, J.; Winstanley, T. P. L.; Lemmetyinen, H.; Tkachenko, N. V., The fluorine effect: photophysical properties of borondipyrromethene (bodipy) dyes appended at the meso position with fluorinated aryl groups. *RSC Advances* **2012**, *2*, 4944-4950.
  64. Zhang, D. K.; Wang, Y. C.; Xiao, Y.; Qian, S. X.; Qian, X. H., Long-wavelength boradiazaindacene derivatives with two-photon absorption activity and strong emission: versatile candidates for biological imaging applications. *Tetrahedron* **2009**, *65*, 8099-8103.
  65. Ye, J. H.; Hu, Z. J.; Wang, Y. X.; Zhang, W. C.; Zhang, Y., A new practical and highly efficient iodination of BODIPY derivatives with hypervalent iodine reagent. *Tetrahedron Letters* **2012**, *53*, 6858-6860.
  66. Mathai, S.; Smith, T. A.; Ghiggino, K. P., Singlet oxygen quantum yields of potential porphyrin-based photosensitisers for photodynamic therapy. *Photochemistry & Photobiology Science* **2007**, *6*, 995-1002.
  67. Didier, P.; Ulrich, G.; Mely, Y.; Ziessel, R., Improved push-pull-push E-Bodipy fluorophores for two-photon cell-imaging. *Organic & Biomolecular Chemistry* **2009**, *7*, 3639-3642.
  68. Becke, A. D., Density-Functional Thermochemistry III. The Role of Exact Exchange. *Journal of Chemical Physics* **1993**, *98*, 5648-5652.
  69. Lee, C. T.; Yang, W. T.; Parr, R. G., Development of the Colle-Salvetti Correlation-Energy Formula into a Functional of the Electron-Density *Physics Reviews B* **1988**, *37*, 785-789.
  70. Cundari, T. R.; Stevens, W. J., Effective Core Potential Methods for the Lanthanides. *Journal of Chemical Physics* **1993**, *98*, 5555-5565.
  71. Stevens, W. J.; Basch, H.; Krauss, M., Compact Effective Potentials and Efficient Shared-Exponent Basis-Sets for the 1st-Row and 2nd-Row Atoms. *Journal of Chemical Physics* **1984**, *81*, 6026-6033.
  72. Stevens, W. J.; Krauss, M.; Basch, H.; Jasien, P. G., Relativistic Compact Effective Potentials and Efficient Shared-Exponent Basis-Sets for the 3rd-Row, 4th-Row, and 5th-Row Atoms. *Canadian Journal of Chemistry.-Revue Canadienne de Chimie* **1992**, *70*, 612-630.
  73. Frisch, M. J. T., G. W.; Schlegel, H. B.; Robb, M. A.; Cheeseman, J. R.; Scalmani, G.; Barone, V.; Mennucci, B.; Petersson, G. A.; Nakatsuji, H.; Caricato, M.; Li, X.; Hratchian, H. P.; Izmaylov, A. F.; Bloino, J.; Zheng, G.; Sonnenberg, J. L.; Hada, M.; Ehara, M.; Toyota, K.; Fukuda, R.; Hasegawa, J.; Ishida, M.; Nakajima, T.; Honda, Y.; Kitao, O.; Nakai, H.; Vreven, T.; Montgomery, J. A.; Peralta, J. E.; Ogliaro, F.; Bearpark, M.; Heyd, J. J.; Brothers, E.; Kudin, K. N.; Staroverov, V. N.; Kobayashi, R.; Normand, J.;

Raghavachari, K.; Rendell, N.; Burant, J. C.; Iyengar, S. S.; Tomasi, J.; Cossi, M.; Rega, N.; Millam, J. M.; Klene, N.; Knox, J. E.; Cross, J. B.; Bakken, V.; Adamo, C.; Jaramillo, J.; Gomperts, R.; Stratmann, R. E.; Yazyev, O.; Austin, A. J.; Cammi, R.; Pomelli, C.; Ochterski, J. W.; Martin, R. L.; Morokuma, K.; Zakrzewski, V. G.; Voth, G. A.; Salvador, P.; Dannenberg, J. J.; Dapprich, S.; Daniels, A. D.; Farkas, O.; Foresman, J. B.; Ortiz, J. B.; Cioslowski, J.; Fox, D. J. *Gaussian, Inc.*, Gaussian, Inc.: Wallingford, CT, 2009.

74. Sangster, J., Octanol-Water Partition Coefficients of Simple Organic Compounds. *Journal of Physical and Chemical Reference Data* **1989**, *18*, 1111-1229.

## CHAPTER 3: SYNTHESIS, SPECTROSCOPIC, AND IN VITRO EVALUATION OF NEAR-IR DIIDO-BODIPYS WITH MULTI-MODE IMAGING AND PDT APPLICATIONS

### 3.1 Introduction

Recent advances in the field of oncology have provided many new treatment methods that provide valuable improvements over traditional therapies. The development of targeted therapies has allowed for more precise treatment of various cancers by limiting treatment to specified and targeted tissues. The combination of targeting moieties with innovative treatment methods creates cancer therapy options that have the potential to be less physically damaging to patients while still remaining effective. As such, anti-cancer agents that have both fluorescent and therapeutic properties are highly valuable and underappreciated.

The exploration of BODIPY (difluoro boron dipyrromethene)-based bioimaging agents has blossomed as an active area of research in recent decades, producing a multitude of fluorescent dyes with a variety of purposes including use as labels for biomolecules such as DNA, peptides, and lipids,<sup>1-4</sup> as well as for applications as enzyme substrate fluorescent tags,<sup>5,6</sup> as environmental indicators (pH and ion sensors),<sup>7-10</sup> and as cellular stains.<sup>11</sup> Despite their extensive investigation and applicability, only a few studies have been published detailing the photophysical and biological properties on near-IR BODIPYs for applications as PDT photosensitizers and as radioimaging agents, particularly for PET and SPECT.

PDT is an under-utilized effective and FDA approved treatment for several forms of cancer and age related macular degeneration. PDT is a tri-modal cancer treatment therapy combining a photosensitizer, light, and cellular oxygen to generate cytotoxic oxygen species, including singlet oxygen in particular, that induce apoptosis and necrosis.<sup>12, 13</sup> PDT has many benefits including limited long-term side effects, relatively short treatment times, the option of multiple treatments

to be administered, and is non-invasive due to its limited area of exposure.<sup>14-16</sup> Effective photosensitizers must possess properties favoring singlet oxygen generation including high quantum yields of photosensitizer triplet state ( $\Phi_T > 0.4$ ), long lifetimes of the triplet state ( $\tau_T = 1 \mu\text{s}$ ), and must possess adequate energy ( $E_T \geq 95 \text{ kJ mol}^{-1}$ ) for efficient energy transfer to triplet oxygen. In addition, target cell selectivity over normal cells, low dark toxicity, high photostability, and high absorption coefficients in the near-infrared fluorescence imaging range 630 nm-800 nm are highly sought after. Utilizing fluorophores that absorb and emit in this “ideal biological window” allows for the use of valuable long wavelength light sources which provide more effective imaging through the reduction of autofluorescence of intracellular chromophores, decreased light scattering, and deeper tissue penetration, all while maintaining low photo-damage to cells.<sup>17, 18</sup>

Current PDT agents fall short in their ability to treat a broad range of cancer types, most notably as a result of their limited effective depths of treatment penetration. Photofrin® (registered trademark of Pinnacle Biologics, Inc.) and Visudyne® (registered trademark of Novartis AG) are PDT agents that have been FDA approved for the treatment of esophageal, digestive tract, genitourinary tract, and lung cancer, and age related macular degeneration, respectively. Although effective, both drugs have drawbacks that limit their utilization. The more commonly prescribed Photofrin® is delivered as a mixture of isomers, displayed a diminished absorption at the clinically prescribed excitation wavelength, and showed prolonged retention in the body, which is accompanied by patient photosensitivity for several weeks following treatment.<sup>19</sup> In order to broaden the effective scope of PDT, development of photosensitizers with increased extinction coefficient within the therapeutic window, high phototoxicity, and solubility in biological media capable of treating a range of cancer types in various states of the disease must be explored.

BODIPY dyes have recently been shown to have potential as effective PDT photosensitizers.<sup>20, 21</sup> Their remarkable photophysical properties, including high extinction coefficients, high fluorescence quantum yields, strong absorption profiles and bright emissions, as well as their known ability to permeate cells make them suitable for exploration as PDT agents.<sup>22, 23</sup> Recent studies have shown that some BODIPYs bearing heavy atoms, such as iodine or bromine, possess cytotoxic properties when exposed to light while others remain non-toxic.<sup>24-26</sup> It is believed that the additional effects of the “spin-orbit couplings” of heavy atoms helps to enhance intersystem crossing from the excited singlet to the triplet state desired for producing singlet oxygen.<sup>27-29</sup> As several reports have shown, incorporation of iodines at the 2,6-positions leads to enhanced intersystem crossing, whereas addition of at the 3,5-positions promotes fluorescence.<sup>30</sup>

On the other hand, the discovery of non-toxic halogenated BODIPYs, specifically those bearing iodines and fluorines, have the potential to serve as radioactive bioimaging agents for PET and SPECT, in addition to fluorescence imaging, with the incorporation of radioisotopes of iodine and fluorine. Nuclear imaging allows for the translation of the pathophysiological status of the tissues being imaged without interference. PET and SPECT are non-invasive 3D nuclear imaging techniques that allow for the mapping of a radiotracer’s uptake *in vivo*.<sup>28</sup> PET most commonly utilizes <sup>18</sup>F labeled radiopharmaceuticals ( $t_{1/2} = 109$  minutes) and a <sup>18</sup>F-labelled glucose derivative has shown to have great success in clinical imaging. Only a handful of reports have been published detailing the synthesis and evaluation of <sup>18</sup>F-bearing BODIPYs for PET/fluorescence dual modality imaging.<sup>31-33</sup>

An ideal radiopharmaceutical should possess characteristics such to provide detectable diagnostic particles with minimal biological effect to the cells or tissues. Radiopharmaceuticals should have a relatively short half-life, maintaining radioactivity for only the necessary length of

time needed to complete the diagnostic study, produce suitable radionucleotide emissions of desired energy, have high target to normal tissue ratio, possess a high target uptake, efficiently clear from blood and non-target tissue while lingering in target tissues for effective image contrast, and be inexpensive and relatively easy to produce.

We have recently discovered that 8-(3,5-dimethoxyphenyl)-2,6-diiodo-1,3,5,7-tetramethyl-BODIPY (**1**) was readily taken up by HEp2 cells and induced phototoxic properties while remaining non-toxic in the dark ( $IC_{50} = 4 \mu\text{M}$  at  $1.5 \text{ J/cm}^2$ ).<sup>24</sup> The less than ideal absorption and emission wavelengths (535 nm and 549 nm, respectively) prevented this compound from being considered as a PDT agent. Subsequent work to extend the conjugation of the BODIPY-scaffold and induce a bathochromic shift via a Knoevenagel condensation of the 3, 5-dimethyls with indolyl, phenyl, thienyl, and pyrrolyl-aldehydes is explored herein. The photophysical and biological properties of these near-IR compounds has also been evaluated.

## 3.2 Results and Discussion

### 3.2.1 Syntheses

In the previous Chapter, the synthesis of phototoxic BODIPY **1** (BODIPY **2a** in Chapter 2) via condensation of 2,4-dimethylpyrrole with 3,5-dimethoxybenzaldehyde, followed by oxidation, boron complexation, and iodination using iodic acid, in 33% overall yield (4 steps), was detailed.<sup>24</sup> Compound **1** was found to possess favorable qualities as a PDT agent, with sufficient internal cellular uptake and a high dark:phototoxicity ratio (> 100). The major drawbacks of this compound were the inability to differentiate the compound from the organelle trackers under the fluorescence microscope and the compound's low solubility in aqueous media. An increase in the compound's absorption and emission maxima ( $\lambda_{\text{max}} = 535$  and  $549$  nm, respectively, in

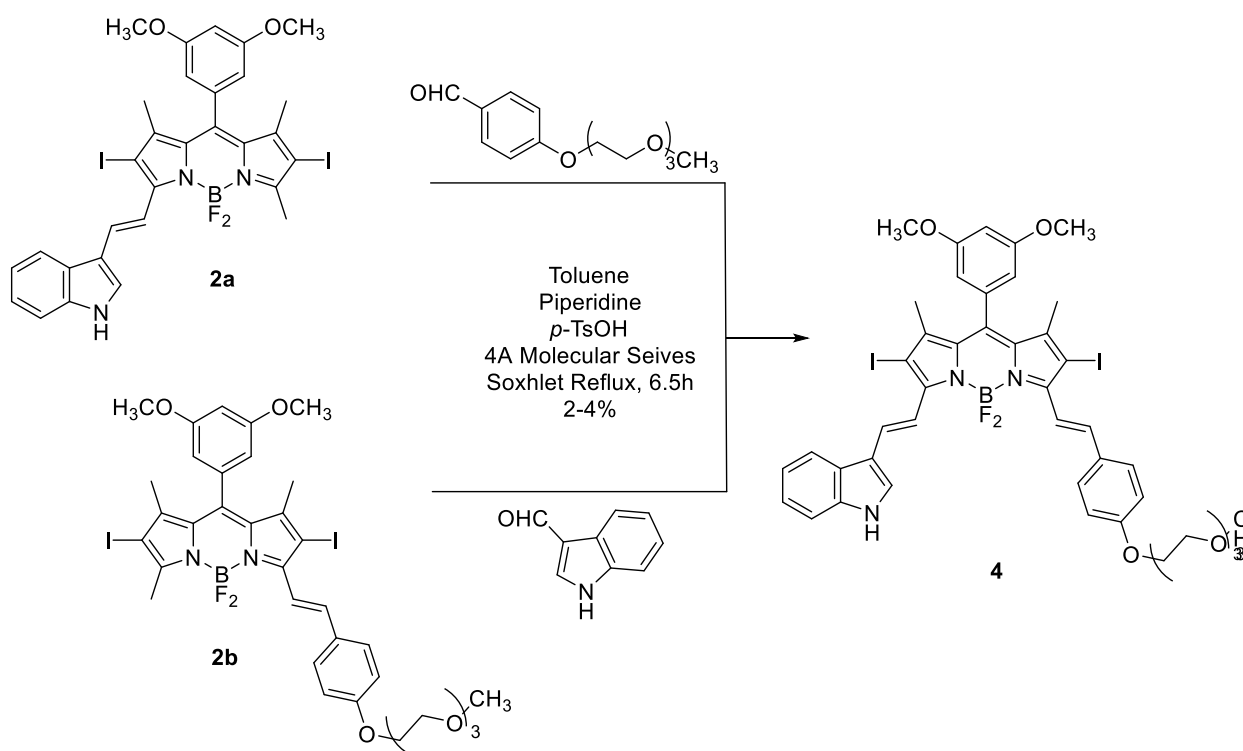


Microwave-assisted syntheses and functionalizations of BODIPYs have been previously investigated<sup>34-36</sup> and applied to Knoevenagel condensations.<sup>37</sup> Heating under microwave irradiation allows for shorter reaction times, producing high yields and low decomposition of products, and recently has been utilized to functionalize BODIPY with aliphatic chains,<sup>35</sup> and in the synthesis of an aza-dipyrin.<sup>36</sup> It was noted that over the course of experimentation that concentration played a significant role in yields with a 20 $\mu$ M solution being ideal. Upon completion, the mixture was quenched with water. The aqueous layer was extracted with DCM and the combined organic layers were dried over Na<sub>2</sub>SO<sub>4</sub>. The solvent was removed under vacuum and the styryl-BODIPYs were purified by silica gel column chromatography to yield blue solid mono-styryl-BODIPYs and green solid di-styryl-BODIPYs.

Several attempts were made to synthesize the unsymmetrical mixed di-styryl BODIPY **4** by condensing the mono-styryl **2a** with tri(ethyleneglycol)benzaldehyde **8** or mono-styryl **2b** with indole-3-carboxaldehyde, Scheme 3.2. Despite modifying reaction conditions, including the number of aldehyde equivalents used, temperature, microwave radiation versus bench-top heating/reflux, and the use of a Soxhlet extractor filled with calcium chloride to remove water from the refluxing toluene, BODIPY **4** could never be produced in greater than 4% yield and reproducibility was challenging. As such, BODIPY **4** could not be characterized by NMR but was identified by ESI-HRMS with *m/z* corresponding to [M+Na]<sup>+</sup> found at 1036.1300.

The aryl groups chosen to extend the  $\pi$ -conjugation of BODIPY **1**, a triethylene glycol or a heteroatom aromatic group, were selected for their ability to increase the styryl-BODIPY solubility in aqueous media and enhance cellular permeability.<sup>32</sup> Initially, indole-3-carbaldehyde was utilized with the intent of extending  $\pi$ -conjugation and increasing the wavelengths of absorption and emission of the styryl-BODIPY, and to enhance cellular uptake and biological

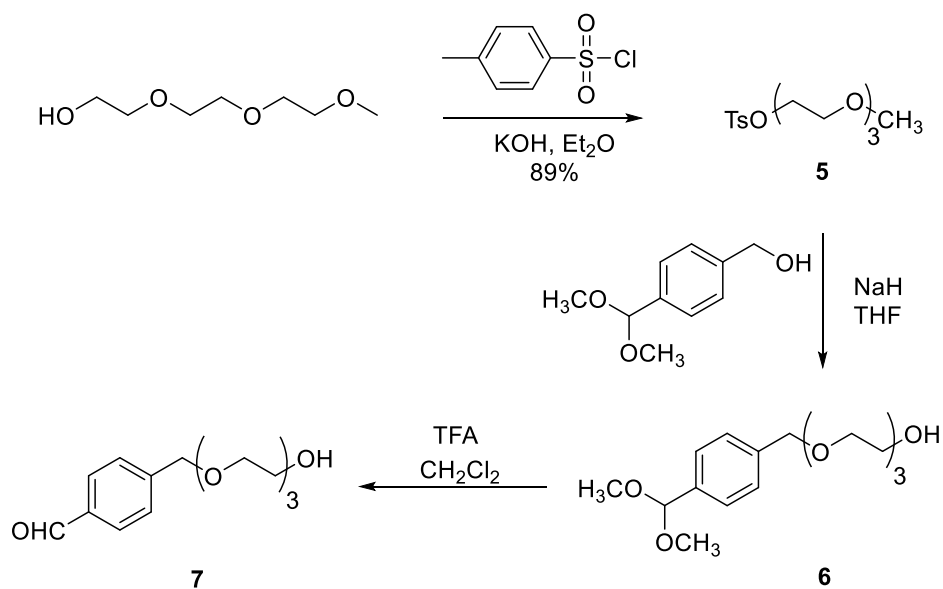
efficacy of the diiodo-BODIPY due to its resemblance to the naturally occurring amino acid tryptophan, a key component in the structure of many enzymes and proteins, and a precursor to the necessary biomolecules serotonin, melatonin, and niacin.<sup>38</sup> We have also recently reported the synthesis and cytotoxicity properties of near-IR mono- and di-indolylstyryl-BODIPYs<sup>34</sup>, that showed high uptake by HEP2 cells with no detectable cytotoxicity in the absence or presence of light). This offered a direct comparison for the efficacy of iodination of BODIPYs **2a** and **3a** for their PDT applicability.



Scheme 3.2: Synthesis of **4** from **2a** and **2b**.

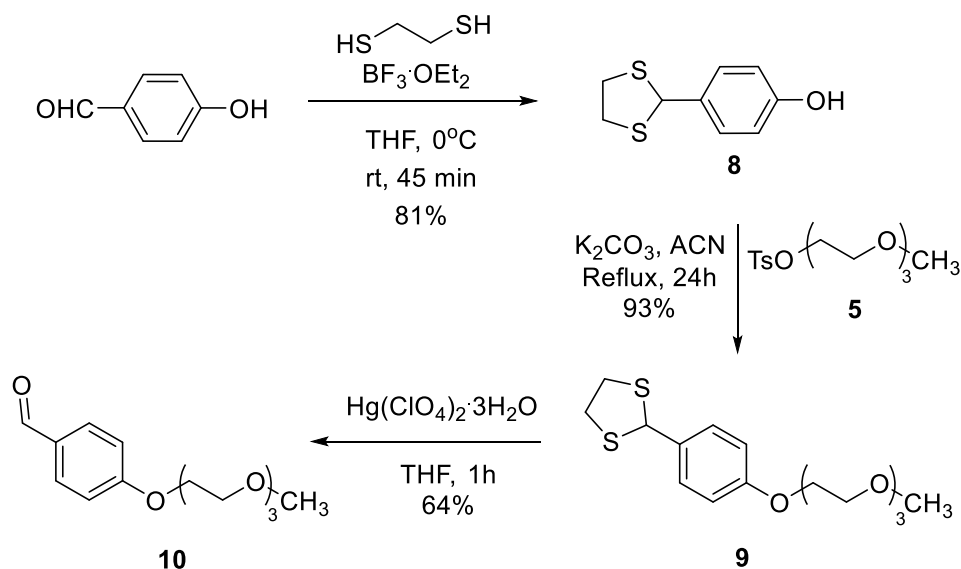
Choosing an appropriate route for the synthesis of the water solubilizing tri(ethylene glycol)benzaldehyde proved challenging. Because BODIPY **1** is relatively water insoluble, incorporating polyethylene glycol (PEG) groups onto the fluorophore would enhance

delivery to target tissues by increasing water solubility, cell permeability, and serum life.<sup>39</sup> Creating our desired PEG group had its own challenges. Our synthesis began with the simple conversion of the terminal hydroxyl group of tri(ethyleneglycol)monomethyl ether into a sufficient leaving group, in this case a tosylate group was chosen, Scheme 3.3. The terminal hydroxyl group of commercially available tri(ethyleneglycol)monomethyl ether was converted into a tosylate group by treating the ether with KOH and *p*-toluenesulfonyl chloride giving compound **5**.<sup>40</sup> Addition of compound **5** to commercially available 4-(hydroxymethyl)benzaldehyde dimethyl acetal using NaH in THF at room temperature readily yielded compound **6** in quantitative yield.<sup>41</sup> At this point, separation of the starting materials and product was feasible. Deacetalization proved to be more challenging. Compound **6** was treated with excess TFA to convert the acetal into the desired aldehyde **7**.<sup>42</sup> However, complete conversion from the acetal to the aldehyde was never achieved, despite numerous attempts under extended reaction times. Furthermore, separation of the starting material **6**, from the aldehyde product **7** proved unmanageable.



Scheme 3.3: Attempted synthesis of aldehyde **7**.

At this point, the decision was made to employ a different protecting group in hopes of easier purification and complete conversion to the desired aldehyde. The thiolane protecting group proved to be an ample choice. Synthesis of the PEG-moiety was carried out in 3 steps from 4-hydroxybenzaldehyde using the previously synthesized tosyl-tri(ethyleneglycol)monomethyl ether **5**, Scheme 3.4. The thiolane group was readily added to 4-hydroxybenzaldehyde in the presence of  $\text{BF}_3 \cdot \text{OEt}_2$  in THF to produce compound **8** as a yellow solid in 81% yield.<sup>43</sup> Compound **5** from the previous synthesis was employed and readily added to compound **8** using  $\text{K}_2\text{CO}_3$  in refluxing ACN to yield compound **9** in 93% as a light brown oil.<sup>44</sup> Removal of the thiolane group using mercury perchlorate in THF afforded aldehyde **10** as a colorless oil in 64% yield.<sup>45</sup>



Scheme 3.4: Synthesis of tri(ethyleneglycol)benzaldehyde **10**.

It was noted over the course of experimentation that prolonged reflux led to significant decomposition of both starting materials, BODIPY **1** in particular, and products; BODIPYs **2a** and **3a** quickly decomposed (< 24 h) when left in solution or in crystalline form under ambient light, Figure 3.1 a/b, c/d, and Figure 3.2 a/b. For this reason, 5-nitroindole-3-carboxaldehyde was

prepared according to the literature from 5-nitroindole using POCl<sub>3</sub>,<sup>46</sup> and was condensed with **1** by stirring in toluene at 60°C in the presence of *p*-TsOH and piperidine for 6.5 hours to yield 15% of the mono-nitroindolylstyryl product **2c** and 22% of the di-nitroindolylstyryl BODIPY **3c** after careful column chromatography.

Incorporation of the electron-withdrawing nitro group on the indole-3-carboxaldehyde was hoped to enhance the stability of BODIPYs **2c** and **3c** relative to **2a** and **3a**. As expected, the addition of the nitro group did enhance the stability of the BODIPYs to an extent, Figure 3.1 g/h and Figure 3.2 e/f, however, significant decomposition was still observed with time for the indolylstyryl-BODIPYs **2a/3a** and **2c/3c**. <sup>1</sup>H-NMR investigations of **2c** and **3c** in DMSO-d<sub>6</sub> upon exposure to ambient light for up to 12 days were also conducted, Figure 3.3. Both compounds maintained stability up to 1 day, however decomposition was observed after that with new aromatic peaks becoming present over time, particularly for the di-substituted BODIPY **3c**. The integration of the NMR signals corresponding to the nitroindolylstyryl group of BODIPY **3c** detected at 9.1 (NH), 8.8, 8.4, 8.2, 7.8, 7.7, and 7.5 significantly decreased by day 12, while signals corresponding to what appears to be nitroindolyl derivatives were noted as time progressed.

With only two of the six synthesized BODIPY possessing significant stability, the decision was made to explore other heteroatom aromatic aldehydes. The commercially available thiophene-2-carboxaldehyde and the previously synthesized by the Vicente/Smith research group 5-methylester-2,4-dimethyl-pyrrol-3-carboxaldehyde were condensed with BODIPY **1** in the presence of piperidine and *p*-TsOH. The mono- and di-thienylstyryl BODIPYs **2d** and **3d** were acquired after refluxing in toluene for 4 hours, in 19% and 25% yields, respectively. Over the course of experimentation and condition optimization, it was noted that the greater reactivity of the thiophene-2-carbaldehyde favored greater production of the di-styryl product over the mono

and careful monitoring of the reaction was required in order to return mono-styryl BODIPY **2d** in sufficient yield.

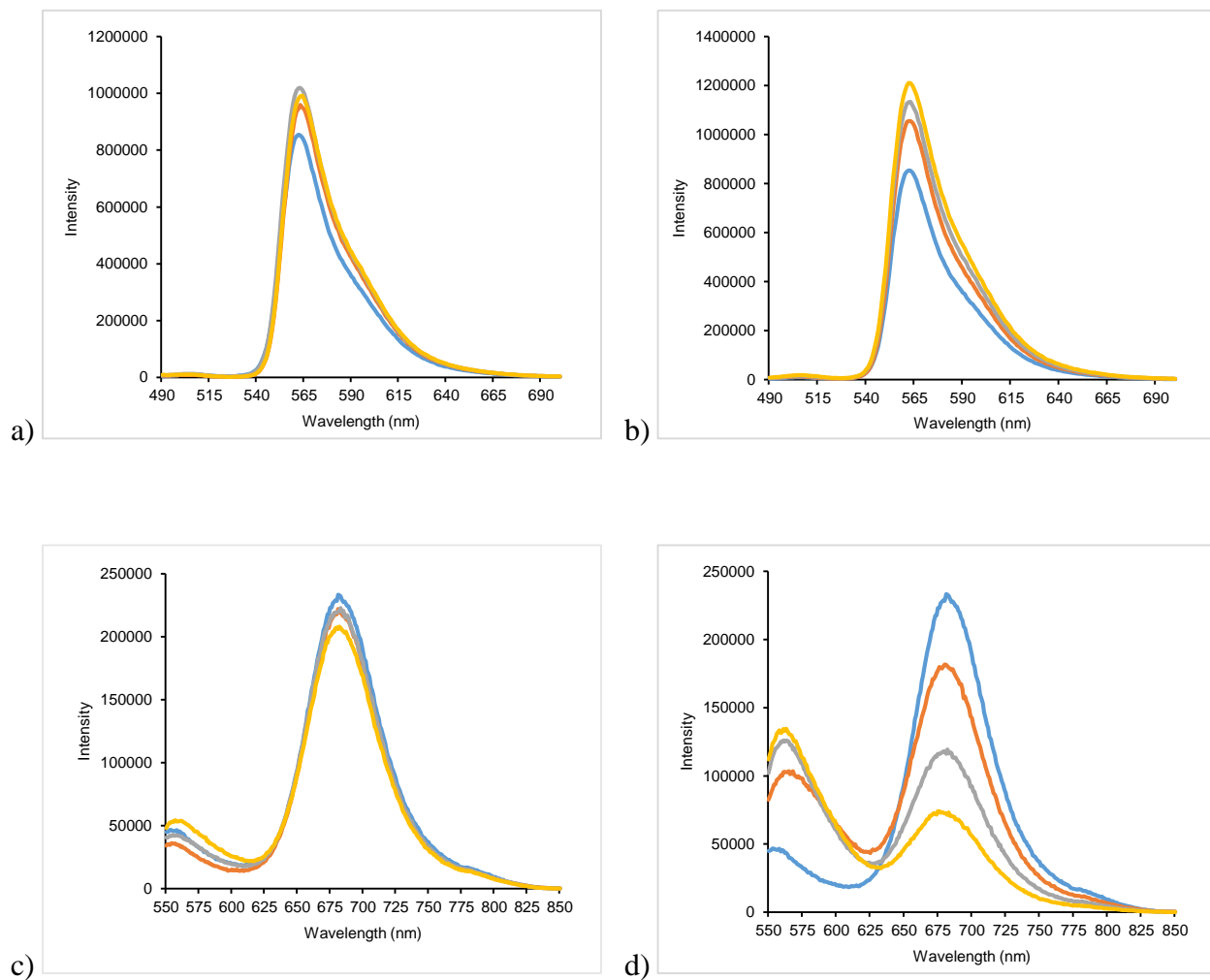
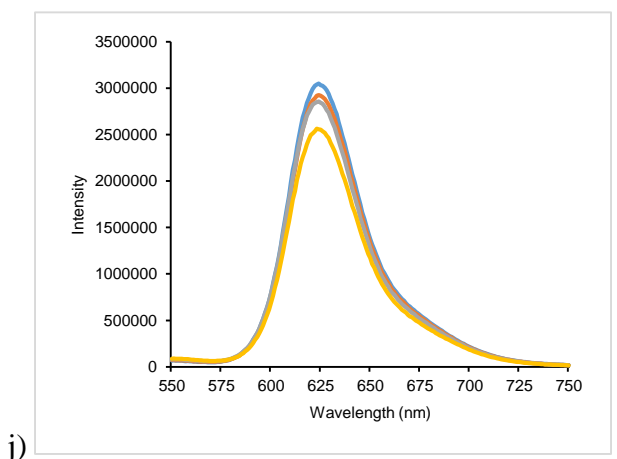
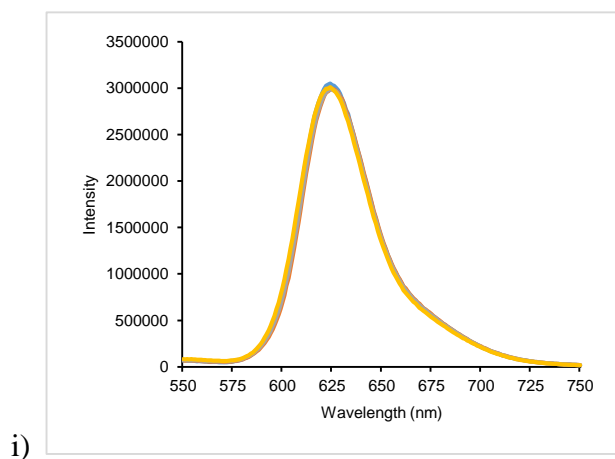
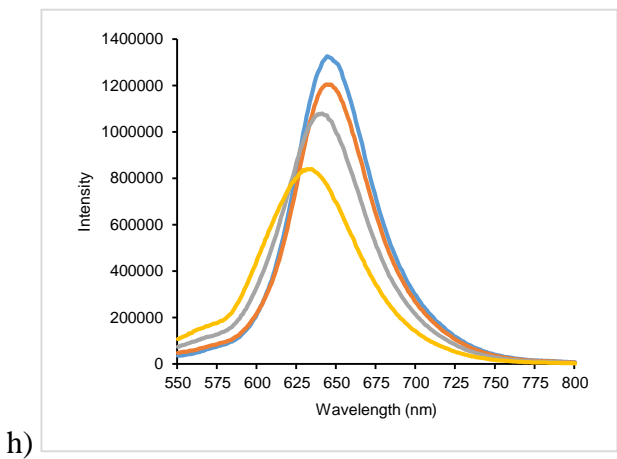
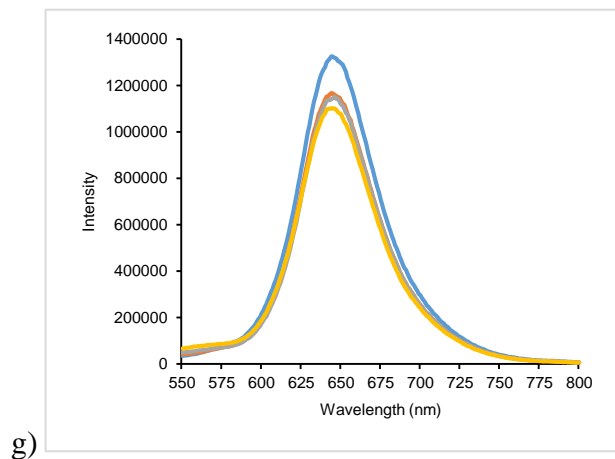
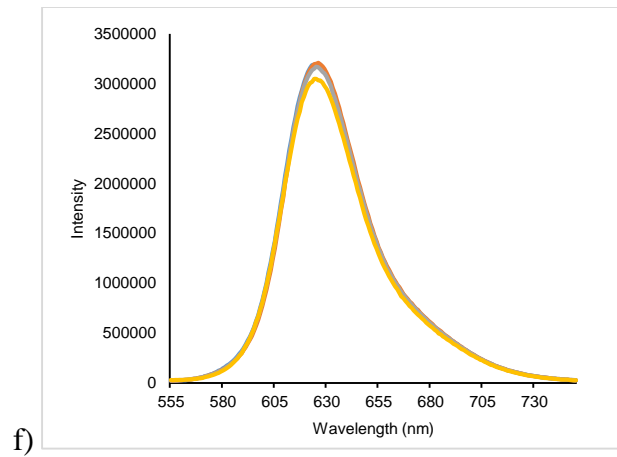
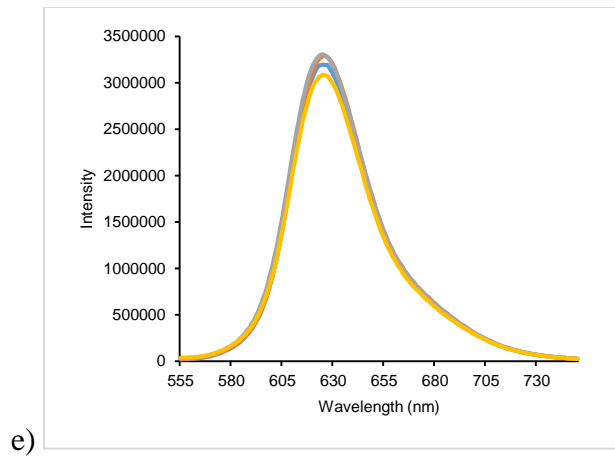
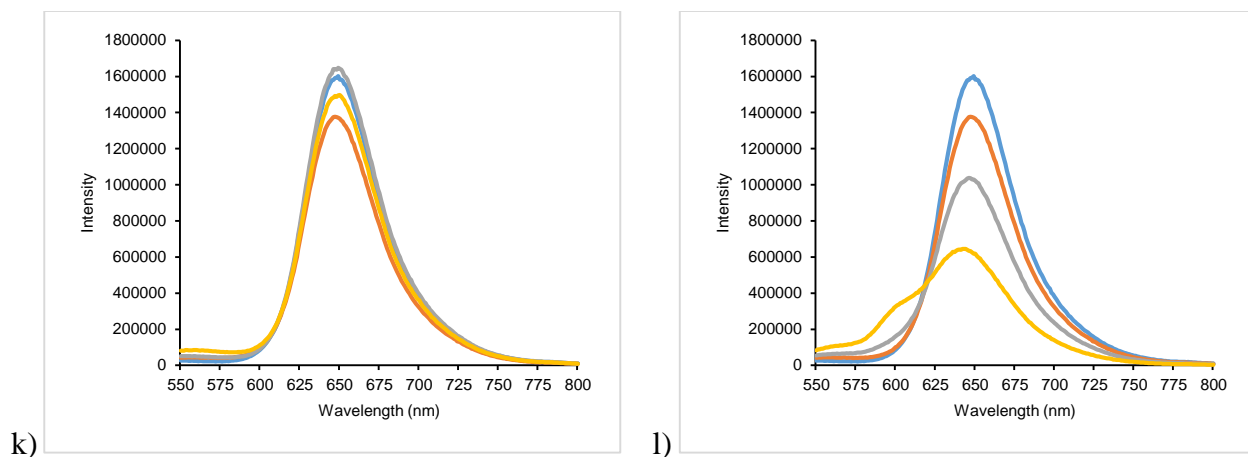


Figure 3.1. Time-dependent fluorescence spectra of 25 mM solutions of BODIPYs **1** (a: dark, b: light), **2a** (c: dark, d: light), **2b** (e: dark, f: light), **2c** (g: dark, h: light), **2d** (i: dark, j: light), **2e** (k: dark, l: light) in DMSO at 0 min (blue), 4 hours (orange), 10 hours (grey), and 24 hours (yellow) after solution preparation at room temperature. Compounds were tested in the absence of light and after exposure to ambient light. The excitation wavelengths for BODIPYs were **1** (480 nm), **2a**, **2c**, **2d**, and **2e** (540 nm), **2b** (545 nm).



(Figure 3.1 continued)



(Figure 3.1 continued)

The condensation of 5-methylester-2,4-dimethyl-pyrrol-3-carboxaldehyde with BODIPY **1** required more time than most other BODIPYs, stirring at 60°C for 48 hours in the presence of piperidine and *p*-TsOH to yield 19% of the mono-pyrrolylstyryl **2e** and 39% of the di-pyrrolylstyryl **3e**. The stability of these compounds was also examined as shown in Figure 3.1, i/j and j/k, and Figure 3.2 g/h and i/j. Notably, the thienylstyryl-BODIPYs **2d** and **3d** possessed similar stability to **2b/3b**, whereas the pyrrolylstyryl-BODIPYs **2e** and **3e** decomposed within 24 hours.

The structures of all compounds were confirmed by <sup>1</sup>H-NMR, <sup>13</sup>C-NMR, HRMS (ESI-TOF) or GCMS spectrometry, and UV/VIS and fluorescence spectroscopies. In the <sup>1</sup>H-NMR, the *ortho*-phenyl hydrogens for all compounds appeared as doublets at ~ 6.5 ppm, while the *para*-hydrogen presented as a triplet shifted slightly downfield at ~ 6.6 ppm. The styryl groups double bonds have a trans (*E*) configuration in all BODIPYs, as indicated by the coupling constants (*J*) of the alkene protons, between 16.2 - 17.1 Hz.

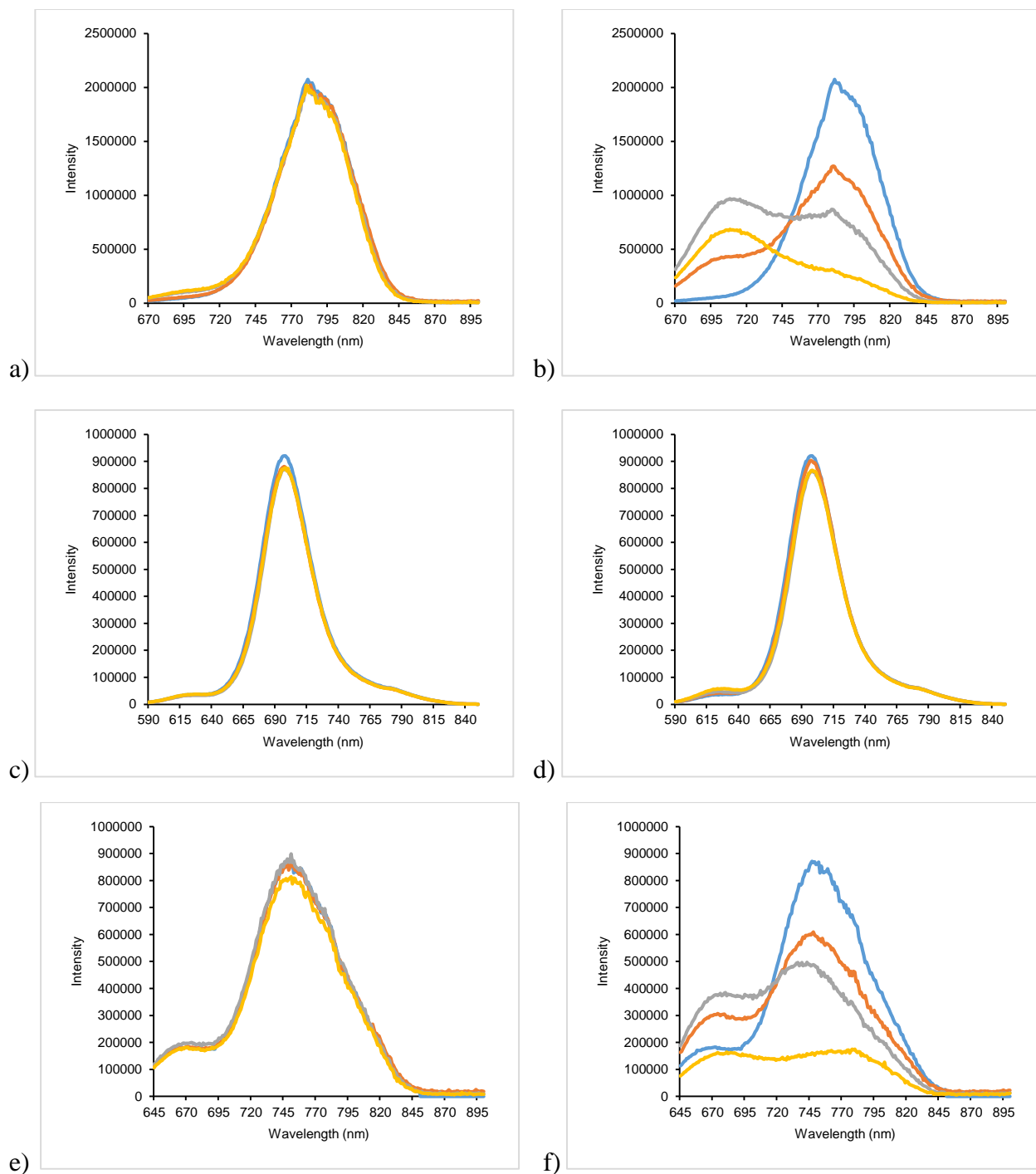
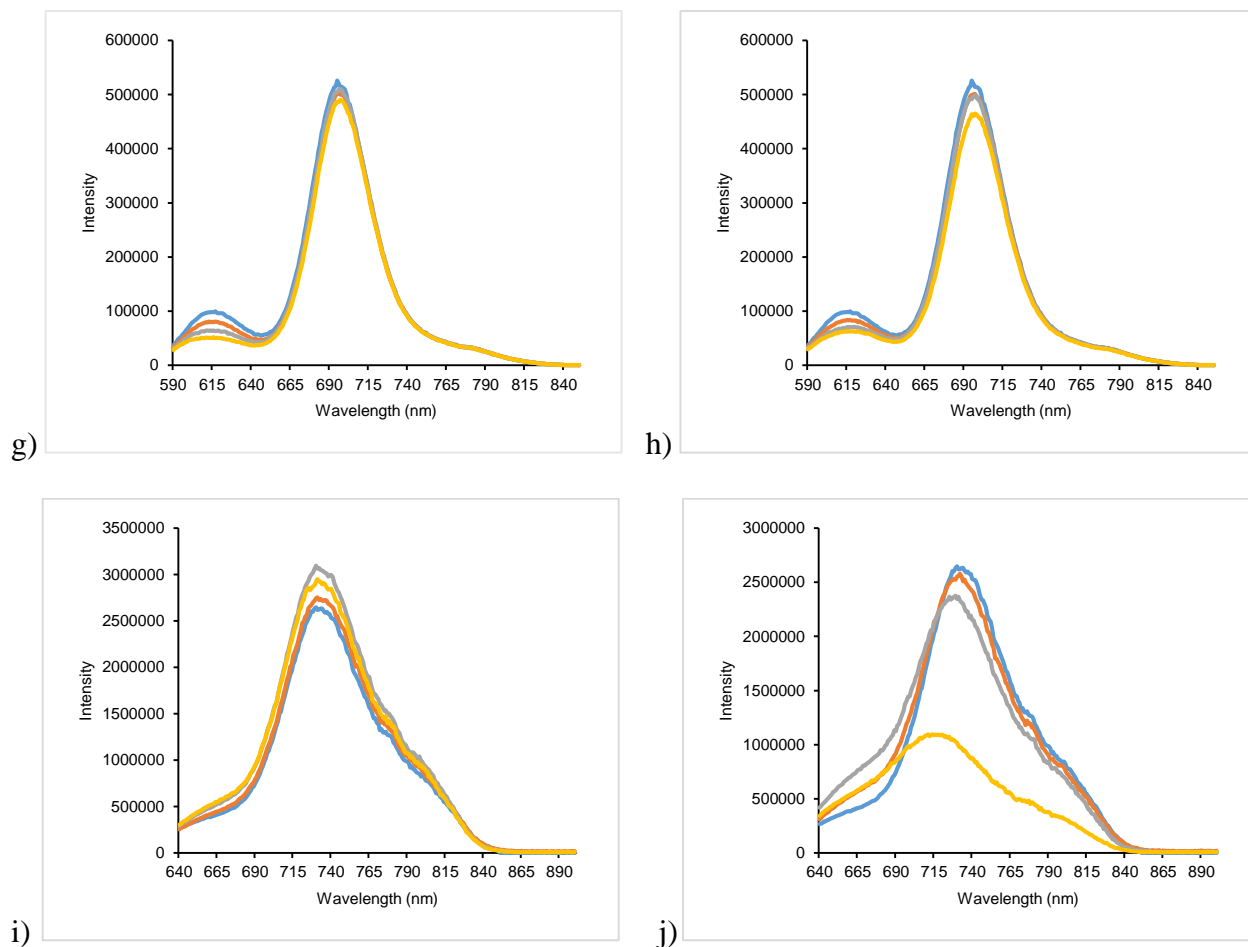


Figure 3.2: Time-dependent fluorescence spectra of 25 mM solutions of BODIPYs **3a** (a: dark, b: light), **3b** (c: dark, d: light), **3c** (e: dark, f: light), **3d** (g: dark, h: light), and **3e** (i: dark, j: light) in DMSO at 0 min (blue), 4 hours (orange), 10 hours (grey), and 24 hours (yellow) after solution preparation at room temperature. Compounds were tested in the absence of light and after exposure to ambient light. The excitation wavelengths for BODIPYs were **3a** (660 nm), **3b** (580 nm), **3c** (635 nm), **3d** (580 nm) and **3e** (630 nm).



(Figure 3.2 continued)

Significant differences were seen in chemical shifts of the 1,3,5,7-tetramethyls. Compound **1**'s tetramethyls displayed as two sets of equivalent protons, where the 1,7-dimethyls lie upfield (1.5 ppm) from the 3,5-dimethyls (2.5 ppm) due to *meso*-group shielding. Addition of one styryl group creates asymmetry in the BODIPY causing the remaining three methyls to appear as equivalent singlets at 2.7 ppm, 1.6 ppm, and 1.5 ppm. Return to symmetry through the incorporation of a second equivalent styryl group brought about a reappearance of a single signal for the 1,7-dimethyls at 1.6 ppm. Only slight changes in the chemical shifts of the styryl groups were observed in the  $^1\text{H}$ - and  $^{13}\text{C}$ -NMR spectra of the mono- versus di-styryl-BODIPYs. All

spectra were recorded in deuterated chloroform, with exception of **3c** and **3e**, which were obtained in DMSO- $d_6$  and acetone- $d_6$ , respectively, as a result of their decreased solubility in chloroform and dichloromethane.

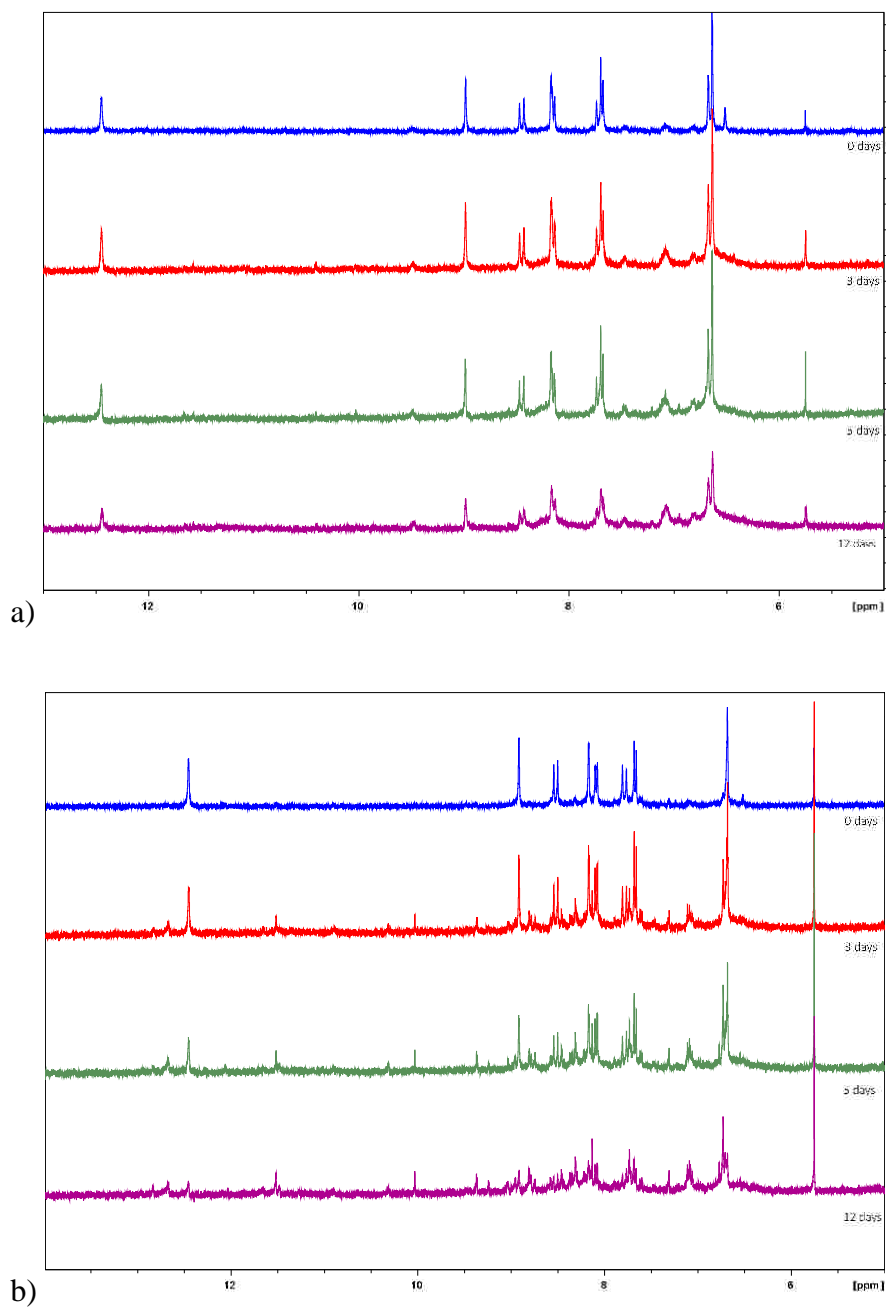


Figure 3.3: Time-dependent  $^1\text{H-NMR}$  of BODIPY **2c** (top) and **3c** (bottom) in DMSO- $d_6$ .

### 3.2.2 X-ray Crystal Structural Determinations

Single crystals of **1** and **3b** suitable for X-ray analysis, Figure 3.4, were grown from slow evaporation of acetone. Exploration of the X-ray structures of **1** and **3b** reveal the expected planarity and 2-fold symmetry of the eight carbon two nitrogen core that extended through the 2,6-diiodo groups. The C<sub>9</sub>BN<sub>2</sub> ring system exhibited mean deviation of 0.013 Å for **1** and 0.011-0.035 Å for the four independent molecules of **3b**. In both cases the iodine atoms lie less than 0.11 Å from these mean planes, and the methyl C atoms less than 0.06 Å. The *meso*-phenyl groups are roughly orthogonal to the core to reduce steric strain caused by the 1,7-dimethyls, forming dihedral angles of 79.97(2)° for **1** and 88.9(2)-90.0(2)° for the four independent molecules of **3b**. The boron atom possesses tetrahedral geometry with the BF<sub>2</sub> groups also lying perpendicular to the BODIPY core, forming dihedral angles of 89.23(4)° for **1** and 87.7(9)-89.3(10)° for **3b**. Short intermolecular B-F... $\pi$  interactions are observed between one pair of independent molecules in the crystal of **3b**. The distances between the F atoms of one molecule and the centroids of the central ring of the C<sub>9</sub>BN<sub>2</sub> ring system of another molecule are 2.750 and 2.767 Å. The polyether chains of **3b** are very flexible, and the eight independent chains exhibit a wide variation of conformations in the solid. The trans (*E*) geometry of the styryl double bonds was confirmed by the X-ray structure of **3b**.

### 3.2.3 Spectroscopic Investigations

The spectroscopic characteristics of the BODIPYs were explored in dichloromethane, tetrahydrofuran, and DMSO and the results are summarized in Figures 3.5 – 3.7 and Table 3.1. Utilization of three solvents revealed a solvent influence on the solubility and optoelectronic profiles of all BODIPYs as solvent polarity increased as follows DCM < THF < DMSO.

Incorporation of one styryl group onto the BODIPY core, as seen in **2a-e**, induced a pronounced red-shift of 59 – 98 nm in the absorption and 59 – 125 nm in emission compared to the tetramethylated BODIPY **1** in DMSO. Addition of a second styryl group created even greater red-shifts compared to **1** of 126 – 189 nm for the absorption and 129 – 220 nm in the emission profile, due to further extension of the system's  $\pi$ -conjugation. Additionally, the absorption and emission bands became broader with the increasing number of styryl substituents.

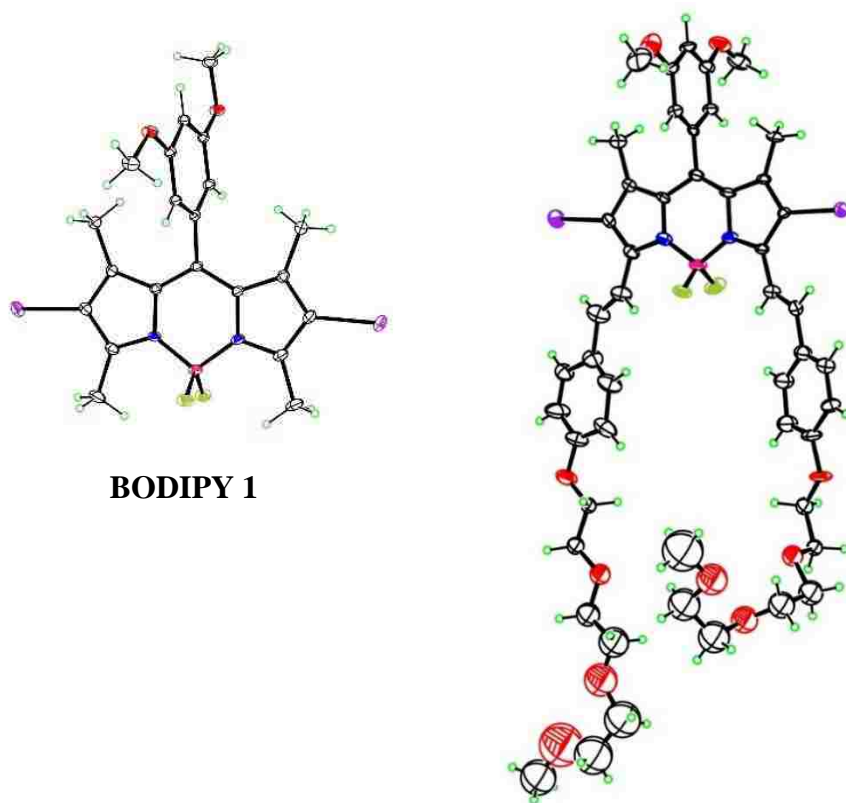


Figure 3.4: Molecular structures of BODIPYs **1** and one of the four independent molecules of **3b**, from X-ray crystal structure determinations. Ellipsoids are drawn at the 50% probability level.

A strong Q-band absorption indicating the  $S_0$ - $S_1$  ( $\pi$ - $\pi^*$ ) electronic transition is observed for all BODIPYs and is accompanied by a shoulder at slightly lower wavelength that is attributed to the vibrational transitions.<sup>37</sup> This shoulder is more pronounced for the styryl-BODIPYs and in

particular, for the distyryl-BODIPY **3a** in DMSO. Additional broader and weaker absorption bands were noted in the absorption spectra of the styryl-BODIPYs which centered at 460 nm that are likely due to the  $S_0$ - $S_2$  transition.<sup>37</sup>

All BODIPYs displayed absorption maxima within the desired PDT biological window, between ca. 600 and 770 nm in DMSO with the longest wavelength absorptions belonging to the di-styryl-BODIPYs, in particular the di-indolylstyryl- **3a** and **3c**. Interestingly, incorporation of the styryl groups and corresponding extension of  $\pi$ -conjugation, which typically creates a reduction of fluorescence quantum yields, enhanced the fluorescence quantum yields of the styryl-fluorophores **2a-c** and **3a,b** compared to **1** which lacks styryl groups.

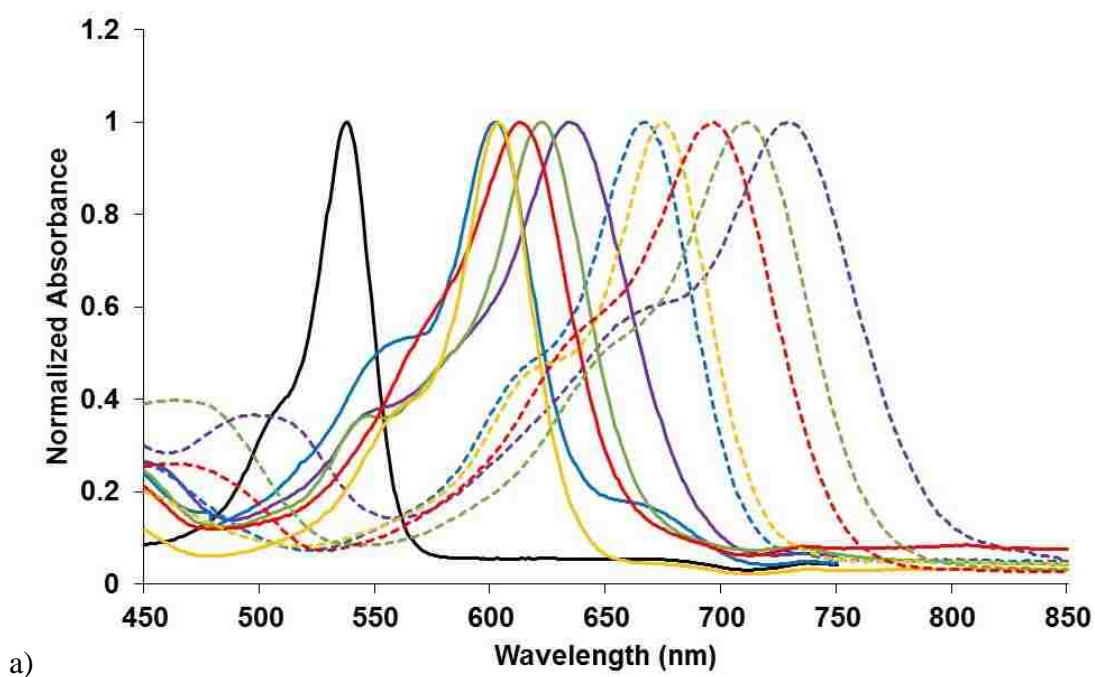
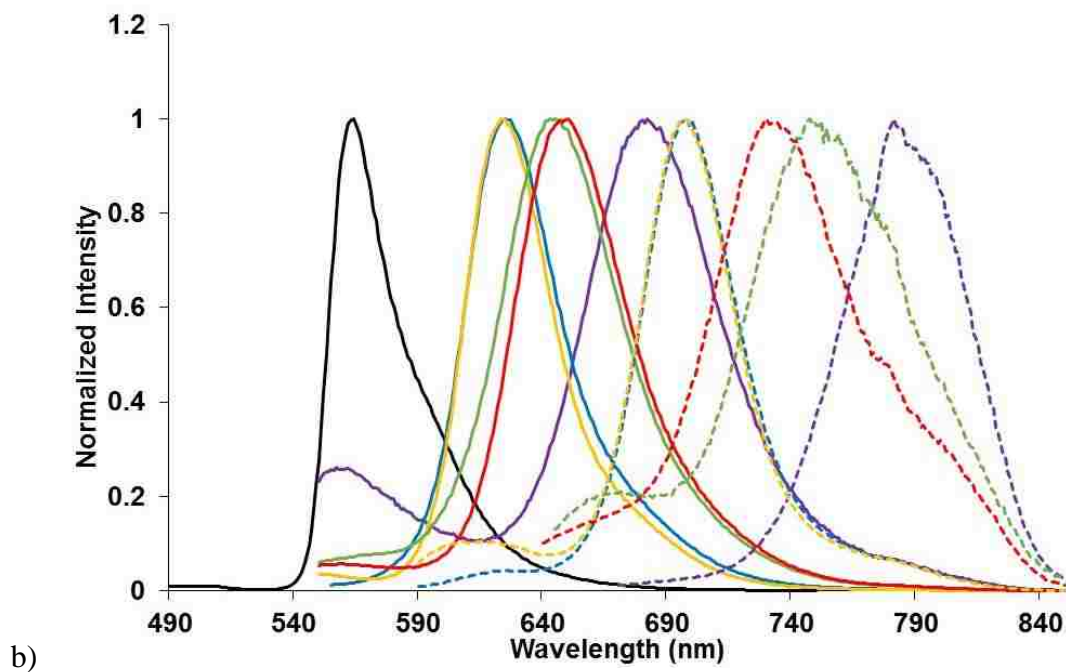


Figure 3.5: Normalized absorption spectra (a) and emission (b) of BODIPYs **1** (black solid), **2a** (purple solid), **2b** (blue solid), **2c** (green solid), **2d** (yellow solid), **2e** (red solid), **3a** (purple dash), **3b** (blue dash), **3c** (green dash), **3d** (yellow dash), and **3e** (red dash) in DMSO at room temperature.



(Figure 3.5 continued)

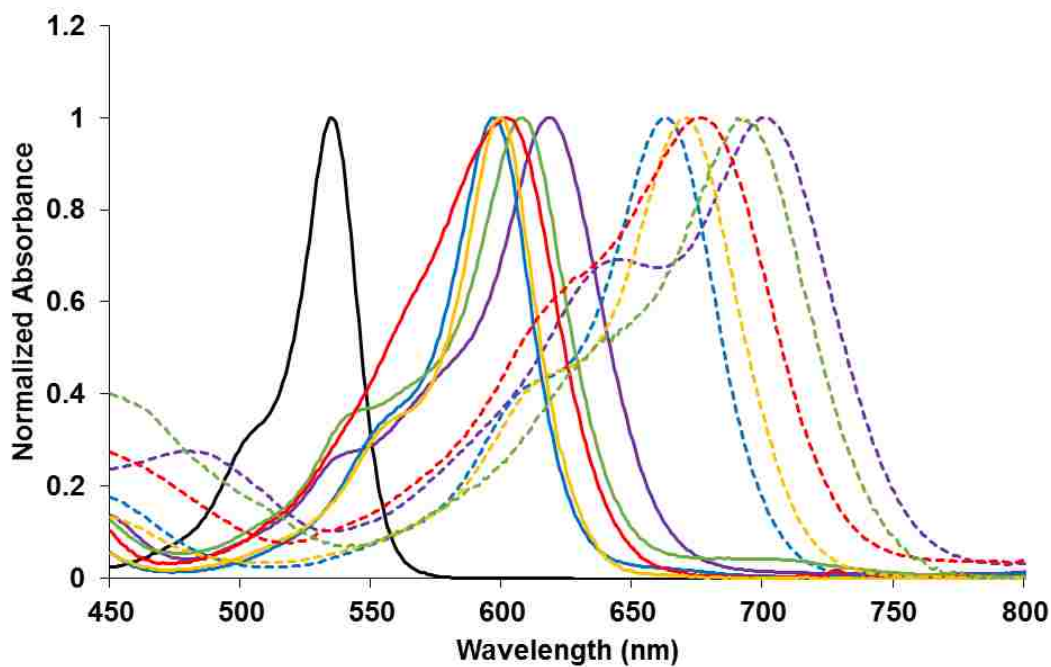


Figure 3.6: Normalized absorption spectra of BODIPYs **1** (black solid), **2a** (purple solid), **2b** (blue solid), **2c** (green solid), **2d** (yellow solid), **2e** (red solid), **3a** (purple dash), **3b** (blue dash), **3c** (green dash), **3d** (yellow dash), and **3e** (red dash) in DCM at room temperature.

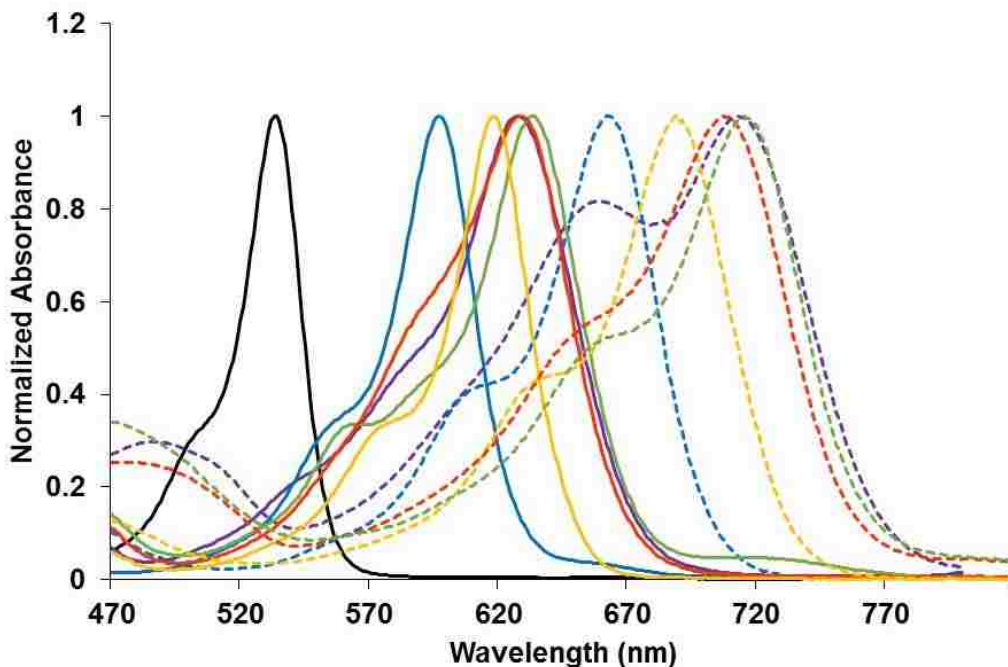


Figure 3.7: Normalized absorption spectra of BODIPYs **1** (black solid), **2a** (purple solid), **2b** (blue solid), **2c** (green solid), **2d** (yellow solid), **2e** (red solid), **3a** (purple dash), **3b** (blue dash), **3c** (green dash), **3d** (yellow dash), and **3e** (red dash) in THF at room temperature.

This effect was more pronounced in BODIPYs **2b** and **3b**, bearing the triethylene glycol groups, likely as a result of its higher solubility in the polar organic solvents.<sup>25, 44, 47</sup> Characteristic of most BODIPYs encountered in literature, the styryl-BODIPYs displayed large extinction coefficients ( $\log \epsilon = 4.1-4.9$ ) and Stokes' shifts ranging from 11 nm to 43 nm with the greater enhancement observed for the mono-styryl BODIPYs.

Concentration-dependent aggregation studies on the Q-band absorption maxima of all BODIPYs were carried out in DMSO, as shown in Figure 3.8, revealing strict correlation to the Beer-Lambert law with  $R^2$  values calculated at greater than 0.98, suggesting that aggregation did not occur with neither BODIPY **1** nor the styryl-BODIPYs aggregation in this solvent. Additionally observed were small to moderate red-shifts in  $\lambda_{\max}$  (1 - 25 nm) for the BODIPYs as solvent polarity increases from DCM (least polar) to THF to DMSO (most polar). This suggests

that the more polarized excited states of the BODIPYs find greater stabilization in the more polar solvent.<sup>37</sup>

BODIPYs bearing 2,6-diiodo groups are expected to possess red-shifted absorptions and emissions compared to their unhalogenated counterparts, likely due to a comparatively reduced HOMO – LUMO gap.<sup>24, 26</sup> Decreased fluorescent quantum yields are also observed as a result of a more favorable, competing energy release pathway from the excited S<sub>0</sub> state. Intersystem crossing induced conversion of the excited singlet state to the excited triplet state via spin-orbit coupling created by the iodine's heavy atom effect results in few excited electrons relaxing via fluorescence.

### **3.2.4 *In vitro* Studies**

**3.2.4.1 Cytotoxicity.** In order to determine the efficacy of the synthesized BODIPYs as potential PDT agents, their concentration-dependent dark and photo (light dose ~ 1.5 J/cm<sup>2</sup>) cytotoxicities were investigated using the Cell Titer Blue assay in human carcinoma HEP2 cells, the results of which are summarized in Table 3.2 and Figures 3.9 and 3.10. All of the mono- and di-styryl-BODIPYs were non-toxic in the dark (IC<sub>50</sub> > 400 μM), with exception of mono-indolylstyryl-BODIPY **2a**, which showed low cytotoxicity (IC<sub>50</sub> = 148 μM), likely as a result of its instability and suspected decomposition into toxic by-products. All the mono-styryl-BODIPYs were highly phototoxic when exposed to an approximately 1.5 J/cm<sup>2</sup> light dose, with IC<sub>50</sub> values between 2 and 15 μM. The di-styryl-BODIPY were all non-cytotoxic with determined IC<sub>50</sub> > 100 μM.

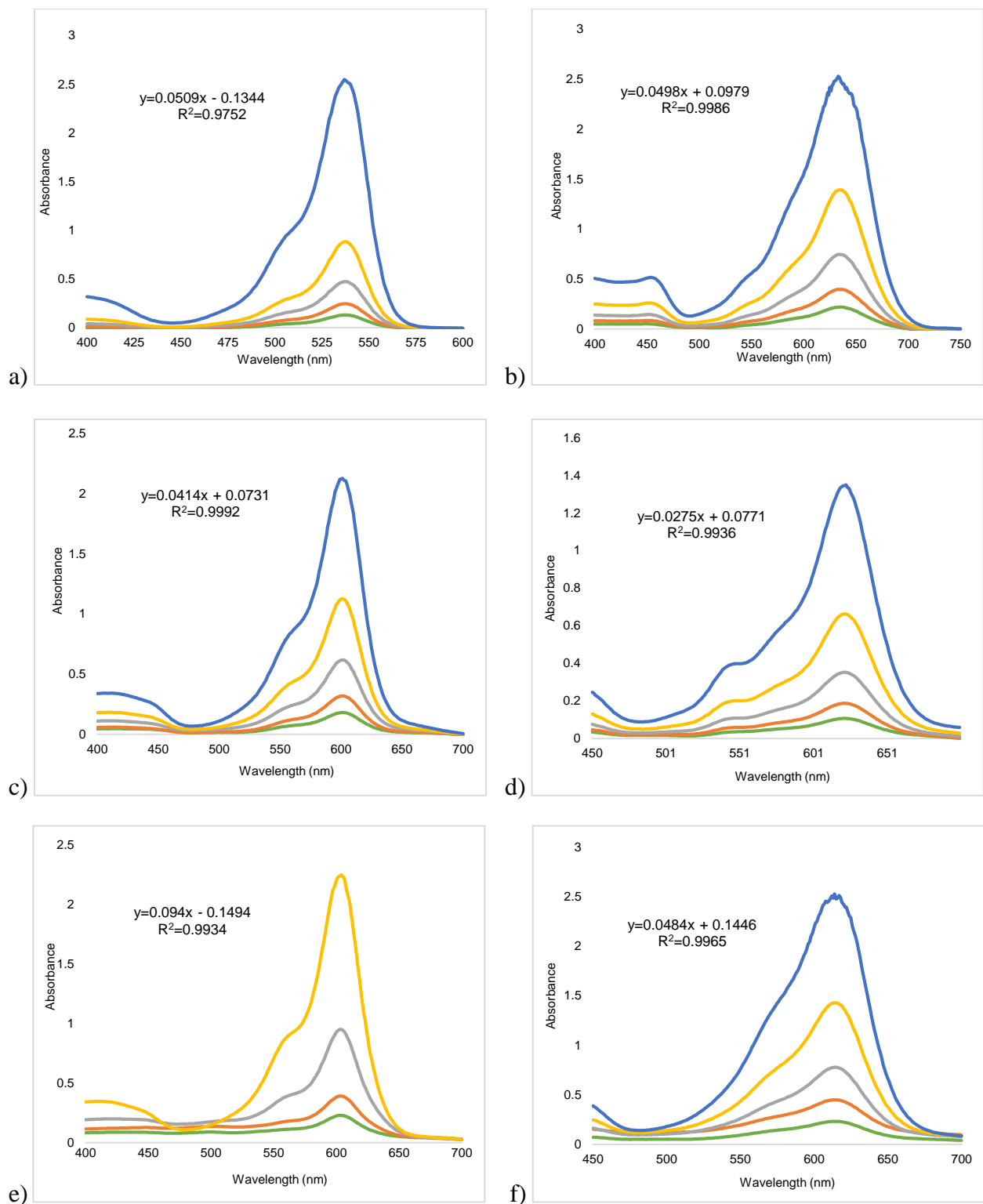
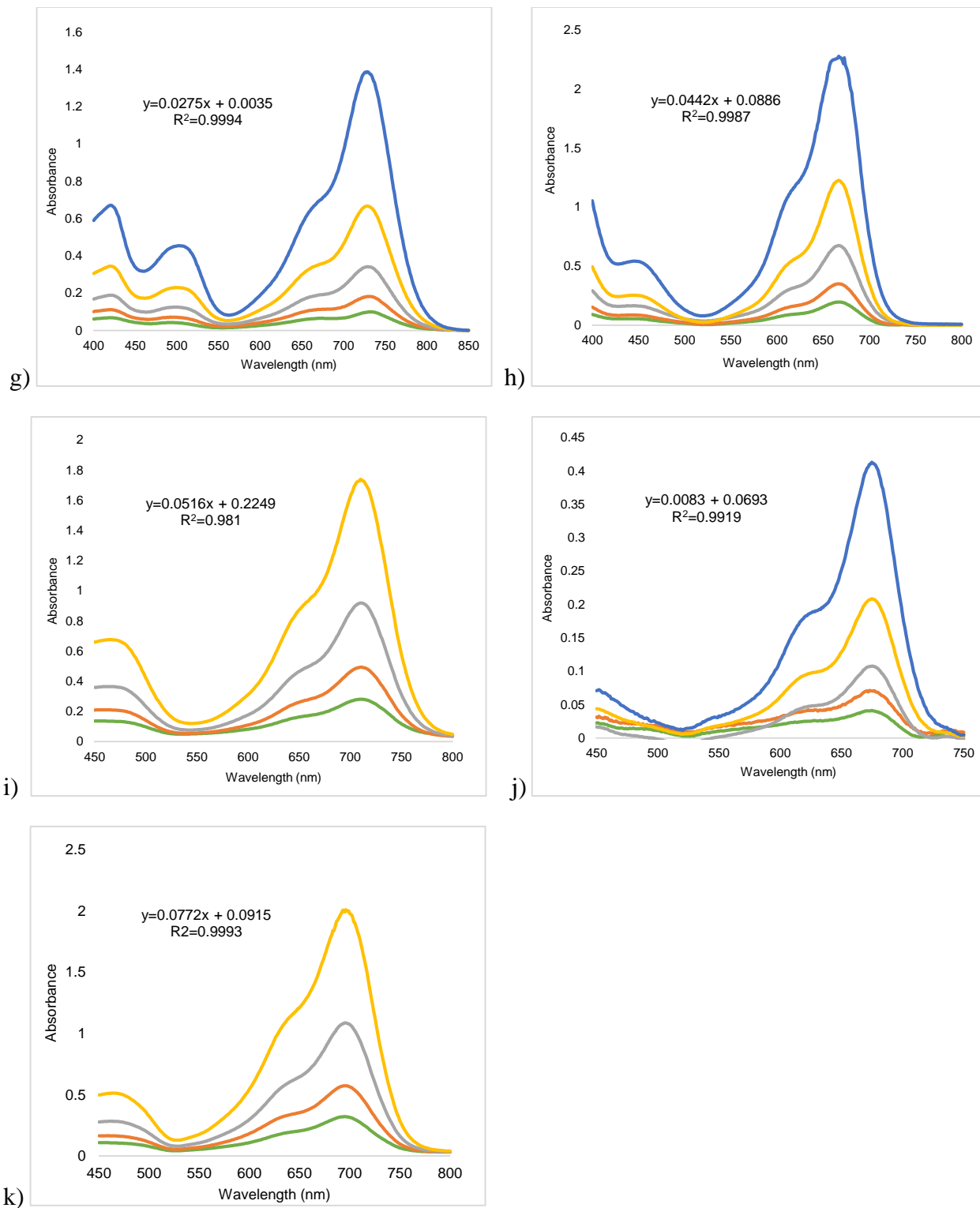


Figure 3.8: Concentration-dependent absorption of BODIPYs **1** (a), **2a** (b), **2b** (c),\* **2c** (d), **2d** (e), **2e** (f), **3a** (g), **3b** (h), **3c** (i), **3d** (j),\* and **3e** (k)\* in DMSO at 3.125 μM (green), 6.25 μM (orange), 12.5 μM (grey), 25 μM (yellow), and 50 μM (blue). \*Note: Absorbance at 50 μM extended beyond detectable limit.



(Figure 3.8 continued)

Table 3.1: Absorption and emission properties of BODIPYs in dichloromethane, THF, and DMSO relative to rhodamine 6G ( $\Phi_f = 0.95$ , EtOH for BODIPY **1**) and methylene blue ( $\Phi_f = 0.03$ , MeOH for all other BODIPYs).

BODIPY	Solvent	Abs $\lambda_{\max}$ (nm)	Log $\epsilon$ ( $M^{-1}cm^{-1}$ )	Em $\lambda_{\max}$ (nm)	$\Phi_f$	Stokes' shift (nm)
<b>1</b>	DMSO	538	3.55	551	0.03	14
	CH <sub>2</sub> Cl <sub>2</sub>	618	4.64	661	0.19	43
<b>2a</b>	THF	627	4.76	668	0.20	41
	DMSO	636	4.47	676	0.17	40
<b>2b</b>	CH <sub>2</sub> Cl <sub>2</sub>	597	4.77	611	0.30	14
	THF	598	4.70	612	0.32	14
	DMSO	601	4.17	624	0.52	23
<b>2c</b>	CH <sub>2</sub> Cl <sub>2</sub>	599	4.08	610	0.40	11
	THF	598	4.06	610	0.30	11
	DMSO	604	4.61	621	0.15	17
<b>2d</b>	CH <sub>2</sub> Cl <sub>2</sub>	606	4.41	630	0.37	24
	THF	612	4.43	635	0.32	23
	DMSO	622	4.46	651	0.19	29
<b>2e</b>	CH <sub>2</sub> Cl <sub>2</sub>	606	4.85	628	0.21	22
	THF	611	4.90	632	0.22	21
	DMSO	612	4.82	639	0.23	27
<b>3a</b>	CH <sub>2</sub> Cl <sub>2</sub>	702	4.54	735	0.15	33
	THF	715	4.62	748	0.12	33
	DMSO	727	4.39	771	0.10	44
<b>3b</b>	CH <sub>2</sub> Cl <sub>2</sub>	664	4.75	687	0.24	23
	THF	664	4.80	684	0.19	20
	DMSO	666	4.79	695	0.17	29
<b>3c</b>	CH <sub>2</sub> Cl <sub>2</sub>	690	4.45	721	0.02	31
	THF	695	4.79	720	0.03	25
	DMSO	712	4.87	748	0.02	36
<b>3d</b>	CH <sub>2</sub> Cl <sub>2</sub>	670	4.59	682	0.02	12
	THF	670	4.60	680	0.01	11
	DMSO	675	4.59	692	0.01	17
<b>3e</b>	CH <sub>2</sub> Cl <sub>2</sub>	678	4.86	710	0.10	32
	THF	685	4.80	713	0.07	28
	DMSO	693	4.96	731	0.07	38

Previous reports on similarly designed fluorophores indicate that the presence of electron-donating alkoxyphenyl substituents at the *meso*-position and two iodides or bromides at the 2,6-positions,<sup>24-26, 47</sup> as in BODIPY **1**, induces high phototoxicity with negligible dark cytotoxicity. Interestingly, despite possessing the same heavy atom bearing, 3,5-dimethoxyphenyl 8-substituted core, only the mono-styryl BODIPYs retain the phototoxic properties of BODIPY **1** whereas, the di-styryl BODIPYs lacked the phototoxicity, regardless of all being efficient singlet oxygen producers (see Table 3.2). Comparatively, the mono-styryl BODIPYs were more efficient singlet oxygen producers compared to their di-styryl analogs, with BODIPYs **2a** and **2b**, the most phototoxic of all BODIPYs, also possessing the highest singlet oxygen quantum yields. As a result of their unsymmetrical structures, the mono-styryl-BODIPYs may have more favorable cellular uptake and may bind to specific intracellular proteins, including the anti-apoptotic Bcl-2 proteins. On the other hand, the symmetric structure of the di-styryl-BODIPYs induces low or no phototoxicity, particularly for the most soluble derivatives, BODIPYs **3b**, **3c** and **3e**.

Table 3.2: Cytotoxicity (CellTiter Blue assay, 1.5 J/cm<sup>2</sup>), singlet oxygen quantum yields (relative to methylene blue) and partition coefficients in octanol-HEPES buffer (log *P*) of BODIPYs.

BODIPY	Dark toxicity (IC <sub>50</sub> , μM)	Phototoxicity (IC <sub>50</sub> , μM)	Φ <sub>Δ</sub>	Log <i>P</i>
<b>2a</b>	148	2.0	0.72	1.04
<b>2b</b>	> 400	3.8	0.78	0.72
<b>2c</b>	> 400	14.5	0.63	0.73
<b>2d</b>	> 400	5.0	0.55	1.50
<b>2e</b>	> 400	4.0	0.65	1.10
<b>3a</b>	> 400	>100	0.64	1.16
<b>3b</b>	> 400	>100	0.65	0.89
<b>3c</b>	> 400	>100	0.37	1.01
<b>3d</b>	> 400	>100	0.34	1.94
<b>3e</b>	> 400	> 100	0.43	1.88

Recent reports from Akkaya *et al.*<sup>26</sup> and Ng *et al.*<sup>47</sup> on several symmetric 3,5-distyryl-2,6-diiodo or 2,6-dibromo BODIPYs described high phototoxicity of these compounds on K562 and HT20 cells, respectively. The most phototoxic di-styryl BODIPY reported in these studies contained five triethylene glycol chains ( $IC_{50} = 7 \text{ nM}$  at  $48 \text{ J/cm}^2$ ), to which the high phototoxicity was credited to its high cellular uptake and preferential localization within the ER of the cells. Similarly, unsymmetrical distyryl-2,6-diiodo-BODIPYs bearing three ethylene glycol groups and amine functionalities were also phototoxic to HT29 cells as a result, in part, to localization within mitochondria.<sup>25</sup>

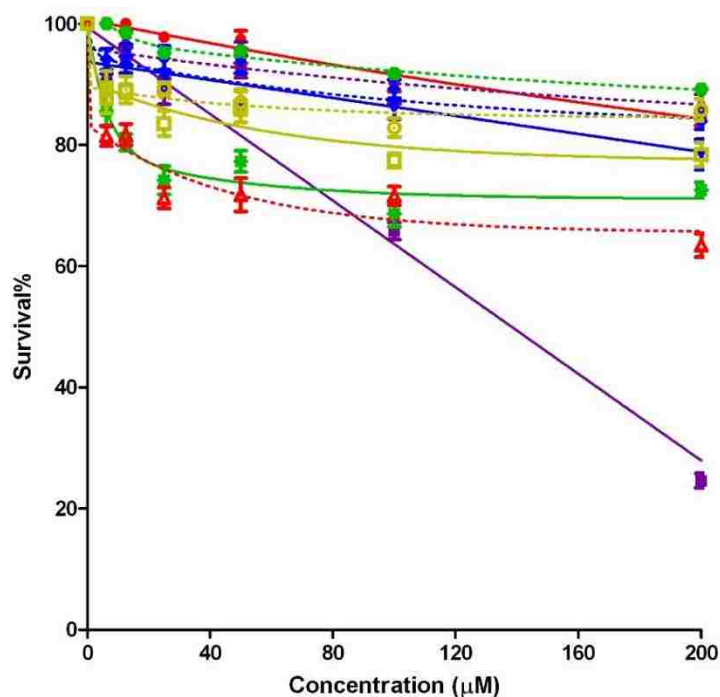


Figure 3.9: Dark toxicity of BODIPYs **2a** (purple solid), **2b** (blue solid), **2c** (yellow solid), **2d** (green solid), **2e** (red solid), **3a** (purple dash), **3b** (blue dash), **3c** (yellow dash), **3d** (green dash), and **3e** (red dash) at  $10 \mu\text{M}$  by HEP2 cells.

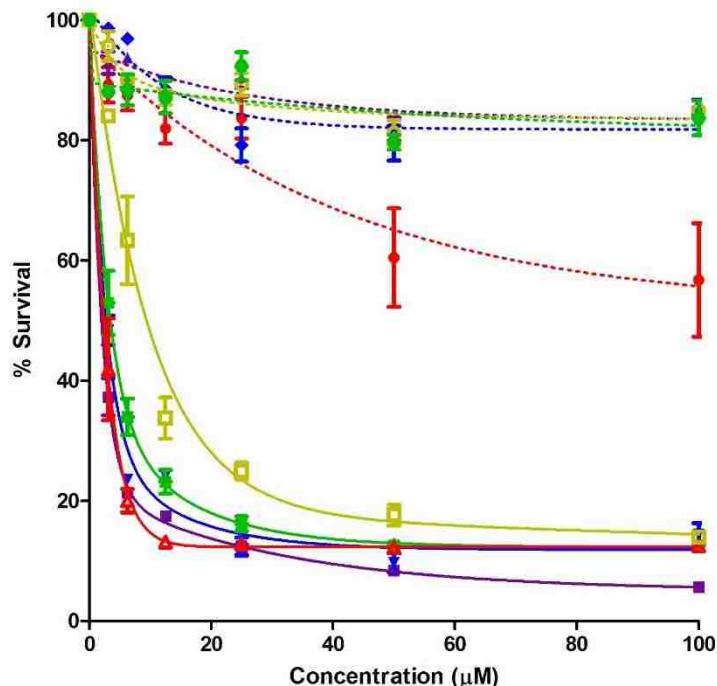


Figure 3.10: Phototoxicity ( $1.5 \text{ J/cm}^2$ ) of BODIPYs **2a** (purple solid), **2b** (blue solid), **2c** (yellow solid), **2d** (green solid), **2e** (red solid), **3a** (purple dash), **3b** (blue dash), **3c** (yellow dash), **3d** (green dash), and **3e** (red dash) at  $10 \mu\text{M}$  by HEp2 cells.

**3.2.4.2 Time-Dependent Cellular Uptake.** With toxicity results contrary to published findings on similar molecules, the cellular uptake was evaluated over a 24 hour period in an attempt to explain the cause of the observed phototoxicities, the results of which are shown in Figures 3.11 and summarized in Table 3.2. As anticipated, all BODIPYs were efficiently internalized within cells. However, no distinct trend was observed for how quickly and efficiently mono-styryl versus di-styryl BODIPYs were taken up. Additionally, the extent of their uptake failed to correlate with the calculated partition coefficients ( $\log P$ )<sup>48</sup> in octanol-HEPES buffer pH = 7.4, shown in Table 3.2, corresponding to their BODIPYs' hydrophobic character. The di-styryl BODIPYs, nonetheless, did display higher hydrophobic character when compared to their mono-styryl counterparts.

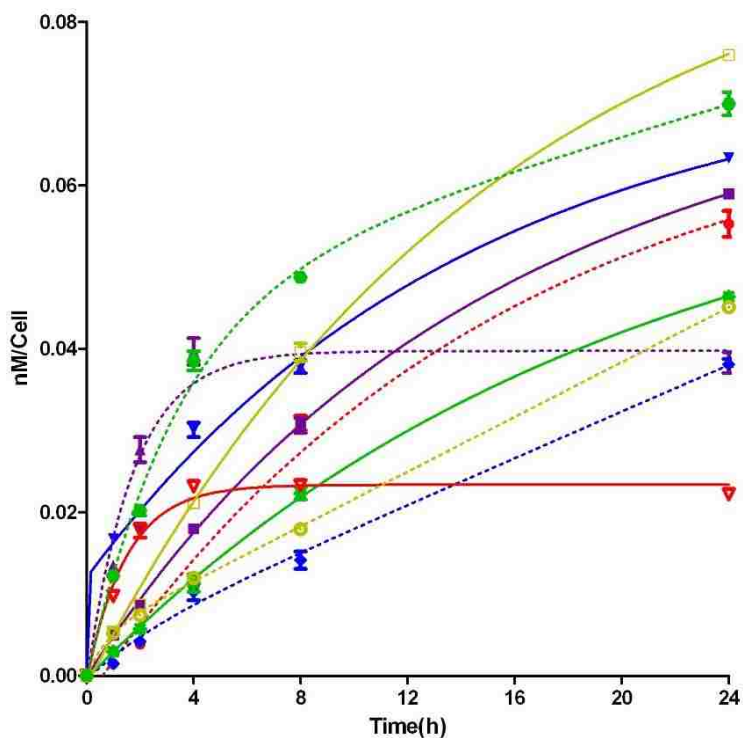


Figure 3.11: Time-dependent cellular uptake of BODIPYs **2a** (purple solid), **2b** (blue solid), **2c** (yellow solid), **2d** (green solid), **2e** (red solid), **3a** (purple dash), **3b** (blue dash), **3c** (yellow dash), **3d** (green dash), and **3e** (red dash) at 10  $\mu$ M by HEP2 cells.

In the first two hours of experimentation, BODIPYs **2b,e** and **3a,d** were taken up very quickly, however after 24 hours BODIPYs **2a-c** and **3d,e** had accumulated the greatest, while **2e** was internalized the least. From eight to 24 hours, all BODIPYs except **2e** and **3a** continued to significantly accumulate.

**3.2.4.3 Intracellular Localization.** The subcellular localization of all BODIPYs was investigated by fluorescent microscopy after six hours of uptake, Figures 3.12 – 3.19. For microscopic imaging, organelle-specific fluorophores BODIPY Ceramide (Golgi), LysoSensor Green (lysosomes), MitoTracker Green (mitochondria), and ER Tracker Blue/White (ER) were used in the overlay experiments. The purple and yellow/orange colors indicate co-localization of BODIPY and organelle tracker. All BODIPYs localized within the studied organelles. The preferential major

sites of localization for the mono-styryl-BODIPYs were the ER, lysosomes, and mitochondria, whereas the di-styryl-BODIPYs were found primarily in the Golgi and lysosomes, and in the ER and mitochondria to a lesser extent. This localization in key organelles, along with their unsymmetrical structure, may be responsible for the higher phototoxicities observed in the mono-styryl-diiodo-BODIPYs. Accumulation of photosensitizers in important PDT targets, like the cellular ER and mitochondria, can induce rapid cell death due to photodamage to anti-apoptotic Bcl-2 proteins found in the membranes of the ER and mitochondria, and/or by direct mitochondrial photodamage.<sup>49</sup> The mono-styryl-diiodo-BODIPYs may preferentially adhere better to anti-apoptotic Bcl-2 proteins compared to their di-styryl analogs, leading to cell apoptosis and/or autophagy,<sup>50</sup> and subsequent cell death. Previous studies detailing phototoxic BODIPYs that localize preferentially in the ER or mitochondria corroborate these findings.<sup>24-26, 47</sup>

### 3.2.4 Singlet Oxygen Generation Studies

Singlet oxygen generation studies were conducted on BODIPYs **2a-e** and **3a-e** by quantifying the absorbance variance of a documented singlet oxygen acceptor, 1,3-diphenylisobenzofuran (DPBF), in the presence of photosensitizer generated singlet oxygen.<sup>29, 51</sup> The decrease in DPBF's absorbance band at 410 nm (at a preliminary concentration of 50  $\mu$ M in DMSO) was determined over the course of an hour, taking measurements at 15 minute intervals. The photosensitizer and DPBF were exposed to a long-pass filtered light source of >500 nm to efficiently excite the photosensitizer. An equivalent concentration of methylene blue ( $\Phi_{\Delta} = 0.52$ ) was utilized as a reference.

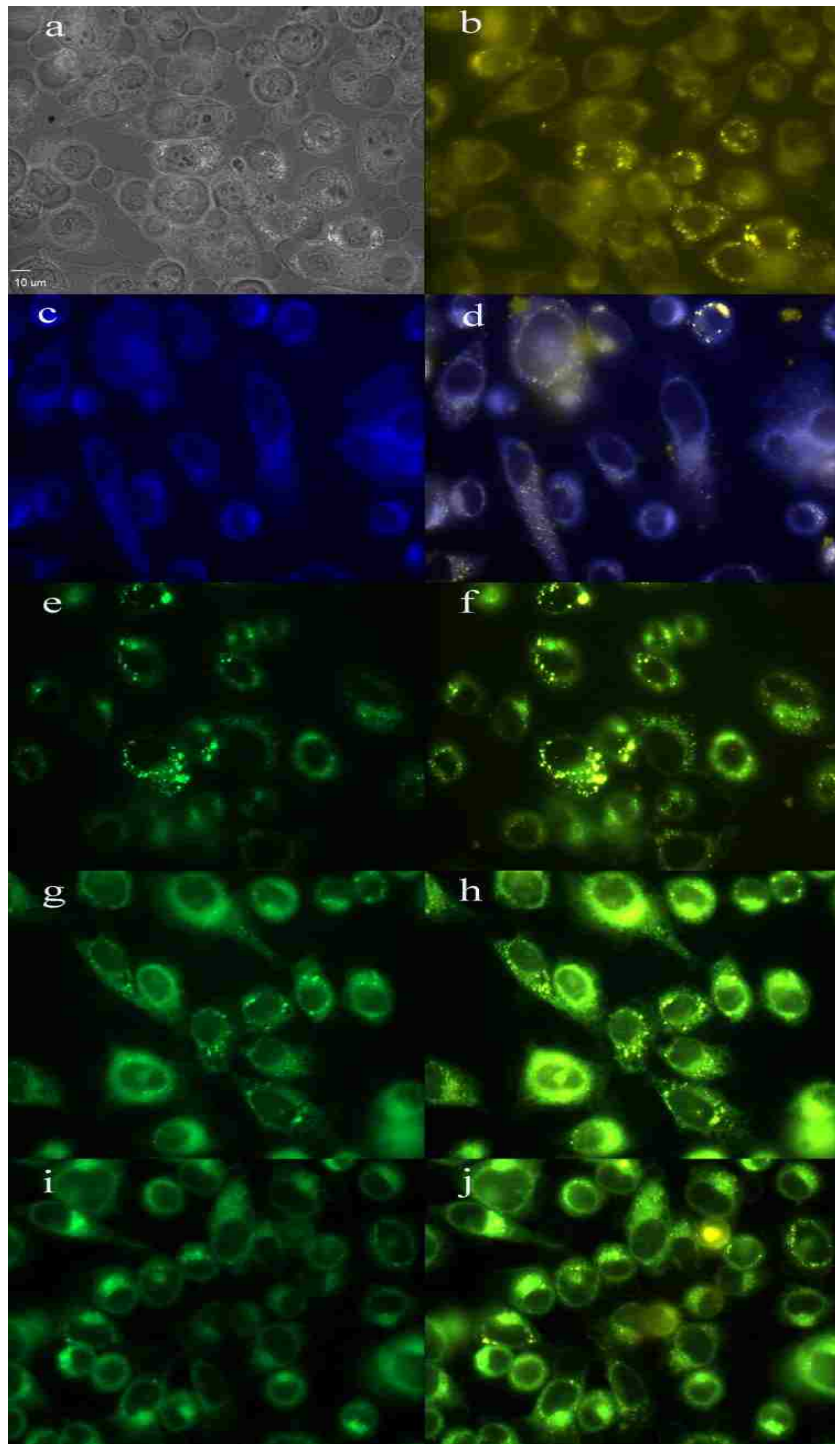


Figure 3.12: Subcellular localization of BODIPY 1 in HEp2 cells at 10 mm for 6 h. a) Phase contrast, b) overlay of the BODIPY fluorescence and phase contrast, c) ER tracker blue/white fluorescence, e) MitoTracker green fluorescence, g) BODIPY Ceramide, i) Lyso-Sensor green fluorescence, and d), f), h), and j) overlays of organelle tracers with the BODIPY fluorescence.

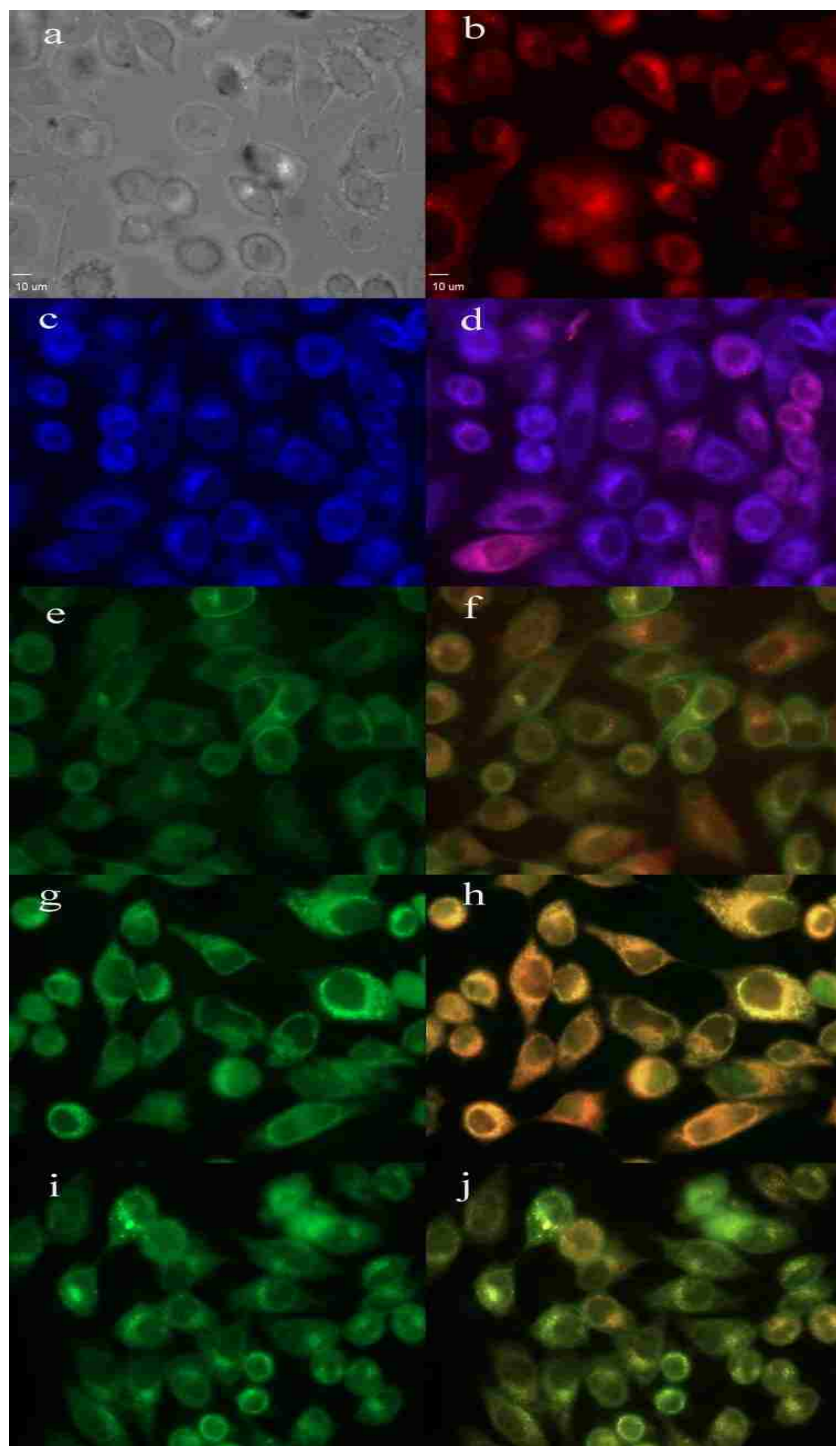


Figure 3.13: Subcellular localization of BODIPY **2a** in HEp2 cells at 10 mm for 6 h. a) Phase contrast, b) overlay of the BODIPY fluorescence and phase contrast, c) ER tracker blue/white fluorescence, e) MitoTracker green fluorescence, g) BODIPY Ceramide, i) Lyso-Sensor green fluorescence, and d), f), h), and j) overlays of organelle tracers with the BODIPY fluorescence.

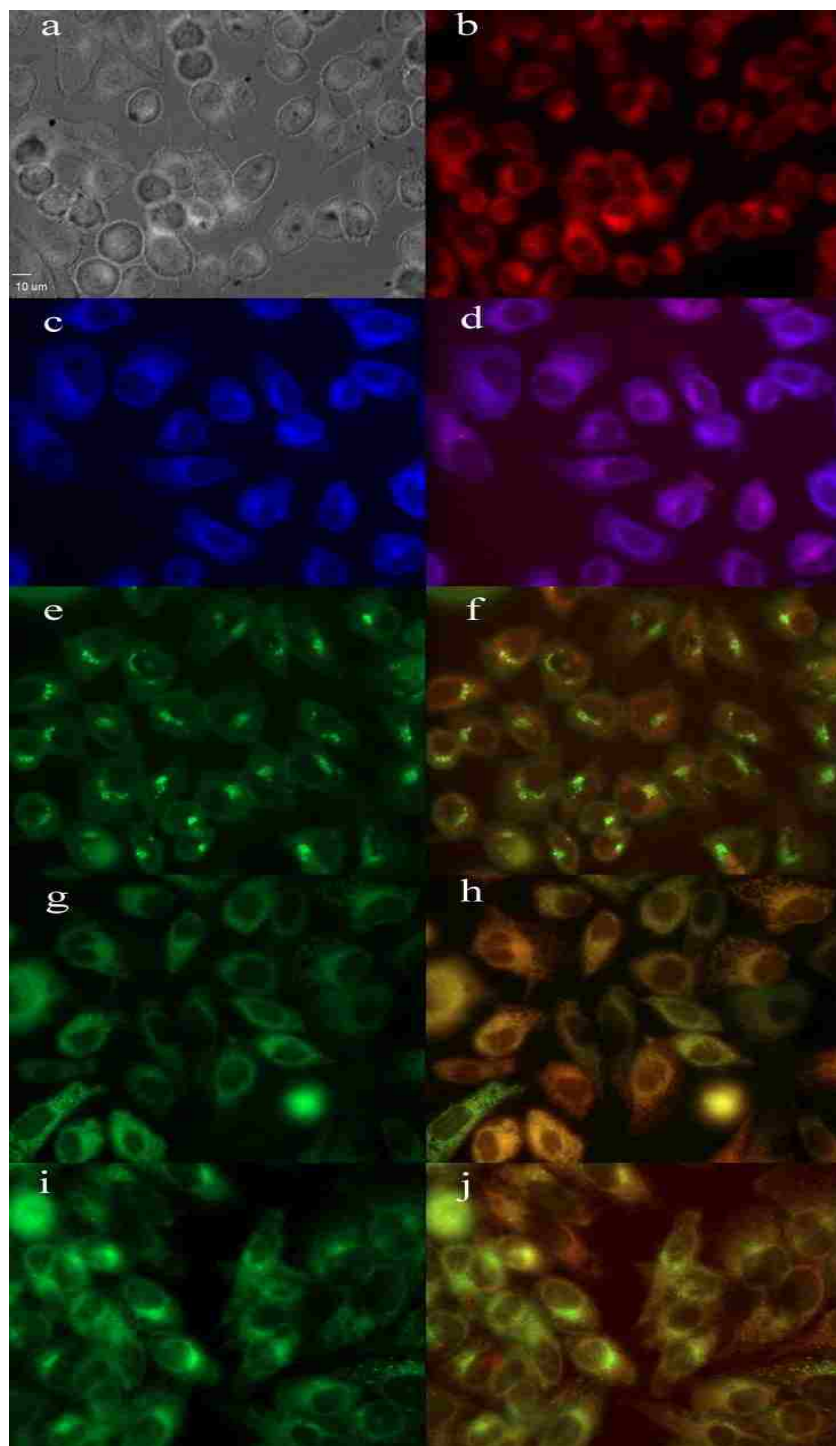


Figure 3.14: Subcellular localization of BODIPY **2b** in HEp2 cells at 10 mm for 6 h. a) Phase contrast, b) overlay of the BODIPY fluorescence and phase contrast, c) ER tracker blue/white fluorescence, e) MitoTracker green fluorescence, g) BODIPY Ceramide, i) Lyso-Sensor green fluorescence, and d), f), h), and j) overlays of organelle tracers with the BODIPY fluorescence.

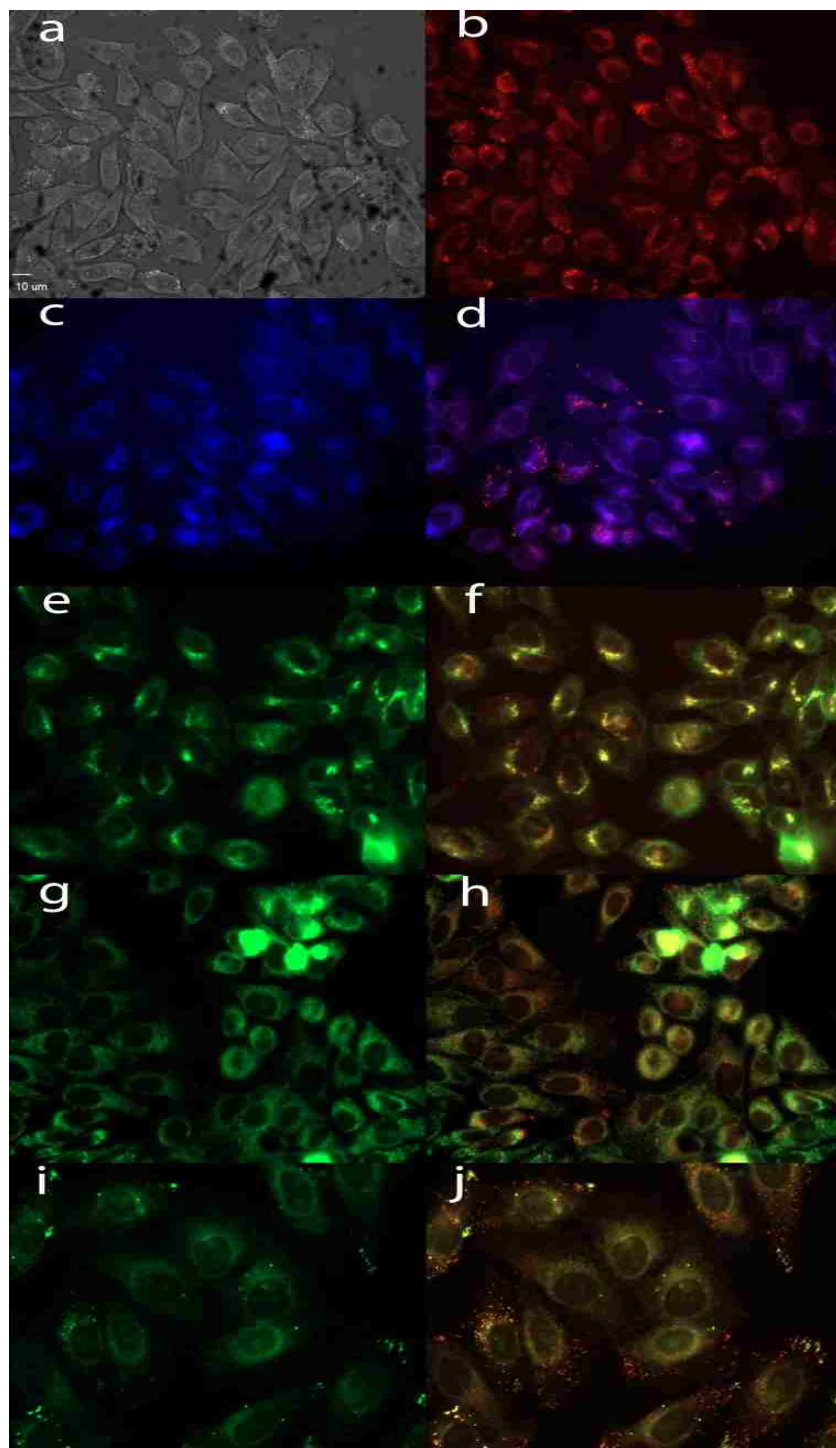


Figure 3.15: Subcellular localization of BODIPY **2c** in HEp2 cells at 10 mm for 6 h. a) Phase contrast, b) overlay of the BODIPY fluorescence and phase contrast, c) ER tracker blue/white fluorescence, e) MitoTracker green fluorescence, g) BODIPY Ceramide, i) Lyso-Sensor green fluorescence, and d), f), h), and j) overlays of organelle tracers with the BODIPY fluorescence.

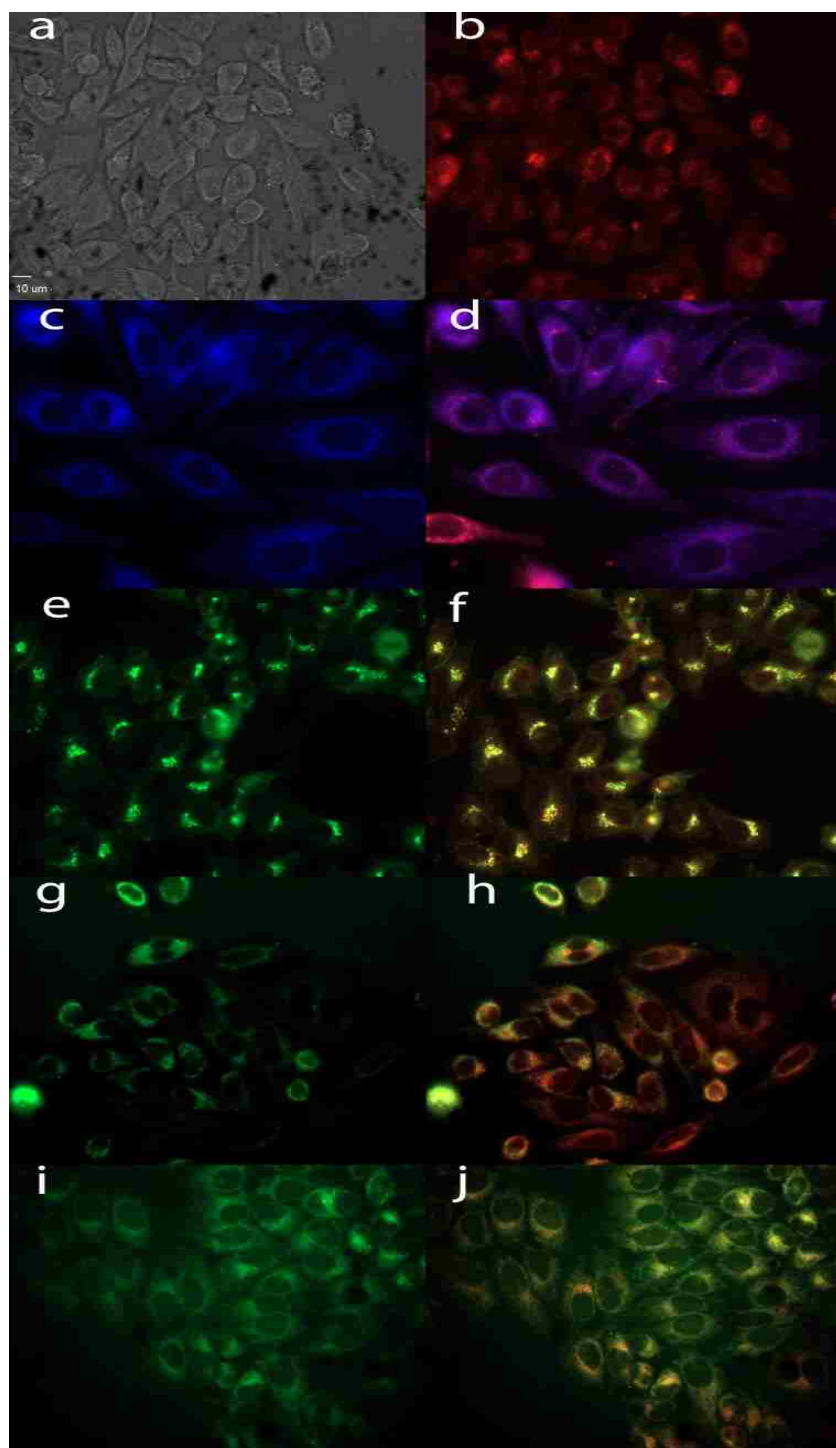


Figure 3.16: Subcellular localization of BODIPY **2d** in HEp2 cells at 10 mm for 6 h. a) Phase contrast, b) overlay of the BODIPY fluorescence and phase contrast, c) ER tracker blue/white fluorescence, e) MitoTracker green fluorescence, g) BODIPY Ceramide, i) Lyso-Sensor green fluorescence, and d), f), h), and j) overlays of organelle tracers with the BODIPY fluorescence.

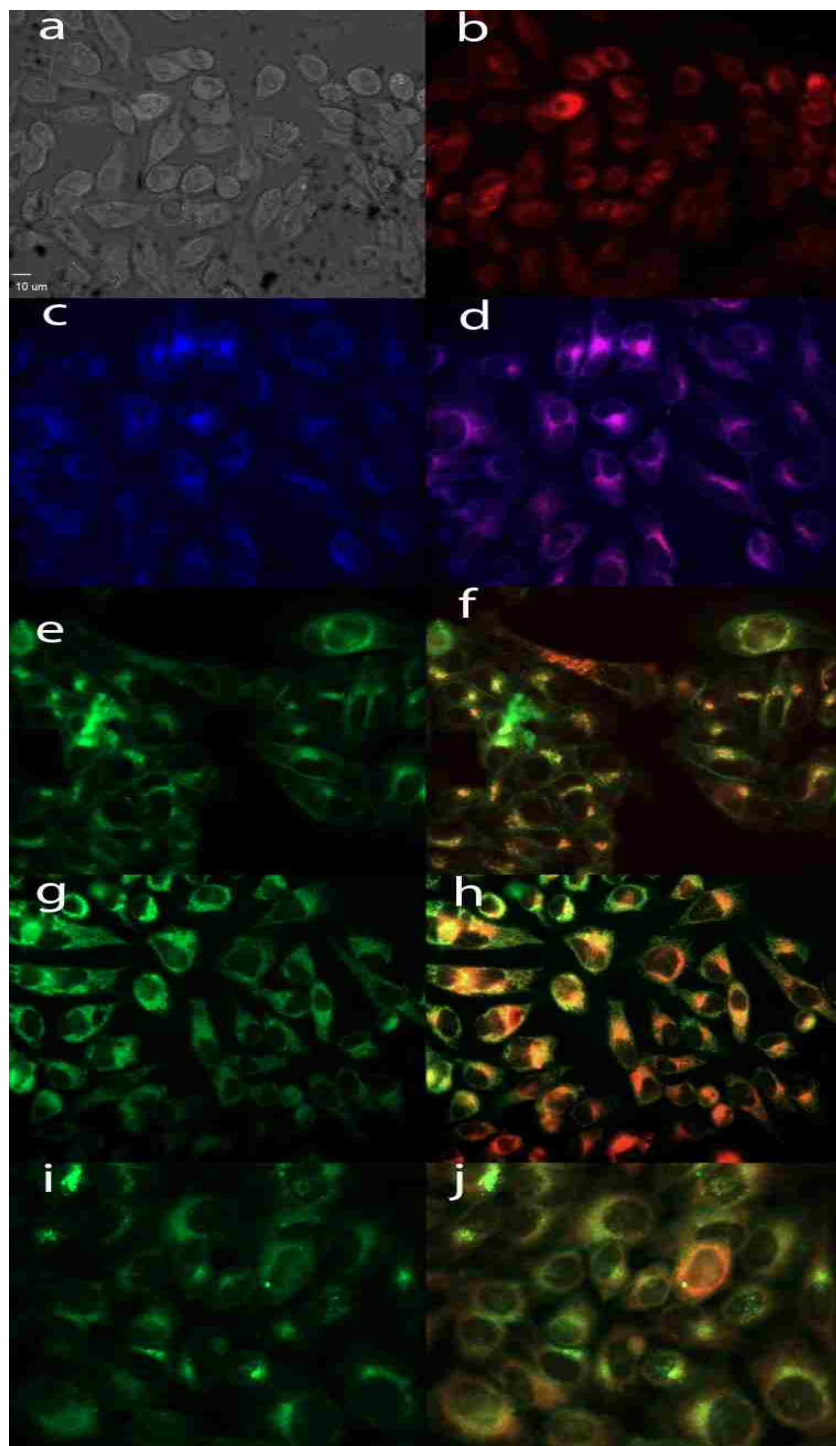


Figure 3.17: Subcellular localization of BODIPY **2e** in HEp2 cells at 10 mm for 6 h. a) Phase contrast, b) overlay of the BODIPY fluorescence and phase contrast, c) ER tracker blue/white fluorescence, e) MitoTracker green fluorescence, g) BODIPY Ceramide, i) Lyso-Sensor green fluorescence, and d), f), h), and j) overlays of organelle tracers with the BODIPY fluorescence.

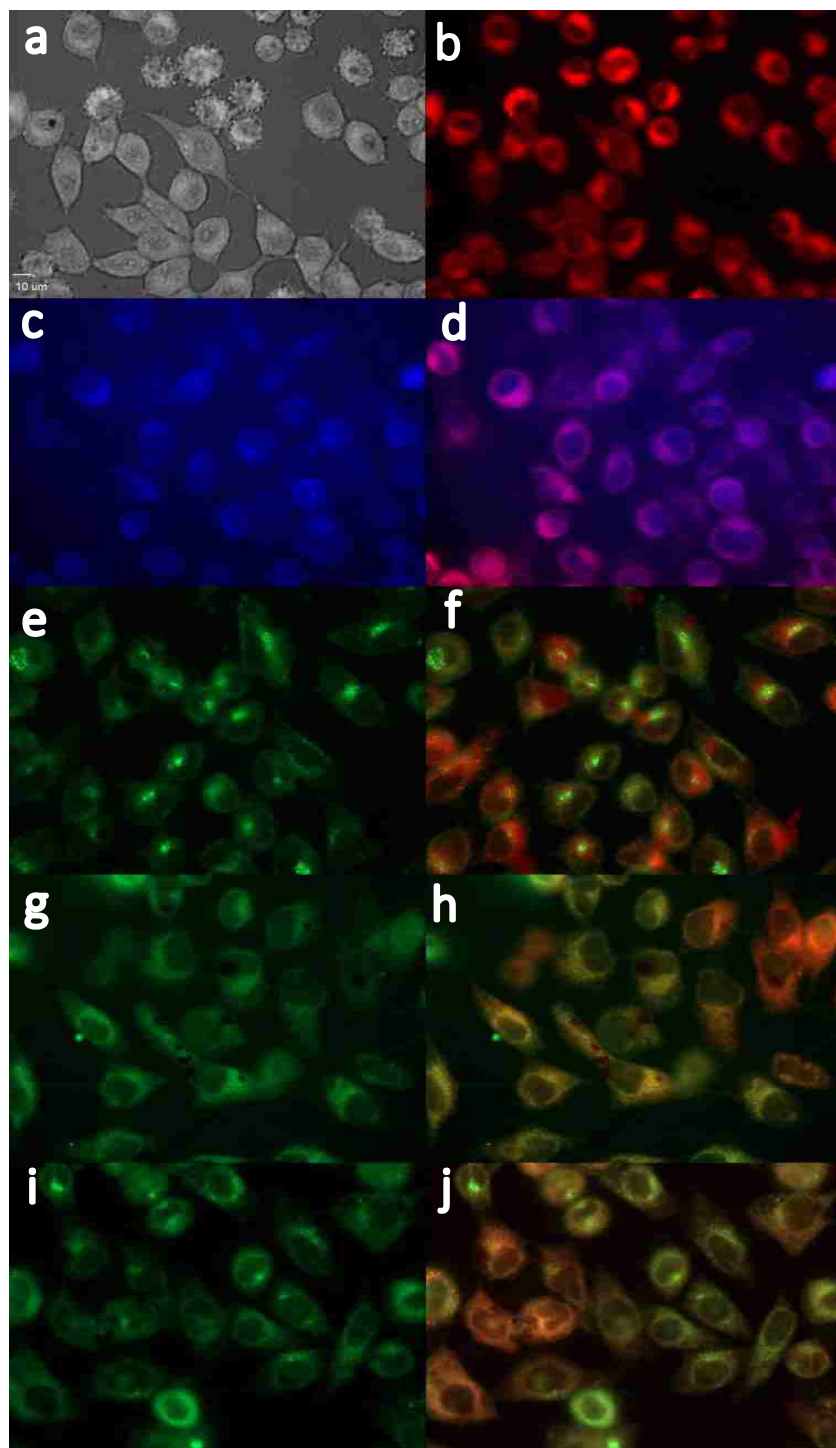


Figure 3.18: Subcellular localization of BODIPY **3a** in HEp2 cells at 10 mm for 6 h. a) Phase contrast, b) overlay of the BODIPY fluorescence and phase contrast, c) ER tracker blue/white fluorescence, e) MitoTracker green fluorescence, g) BODIPY Ceramide, i) Lyso-Sensor green fluorescence, and d), f), h), and j) overlays of organelle tracers with the BODIPY fluorescence.

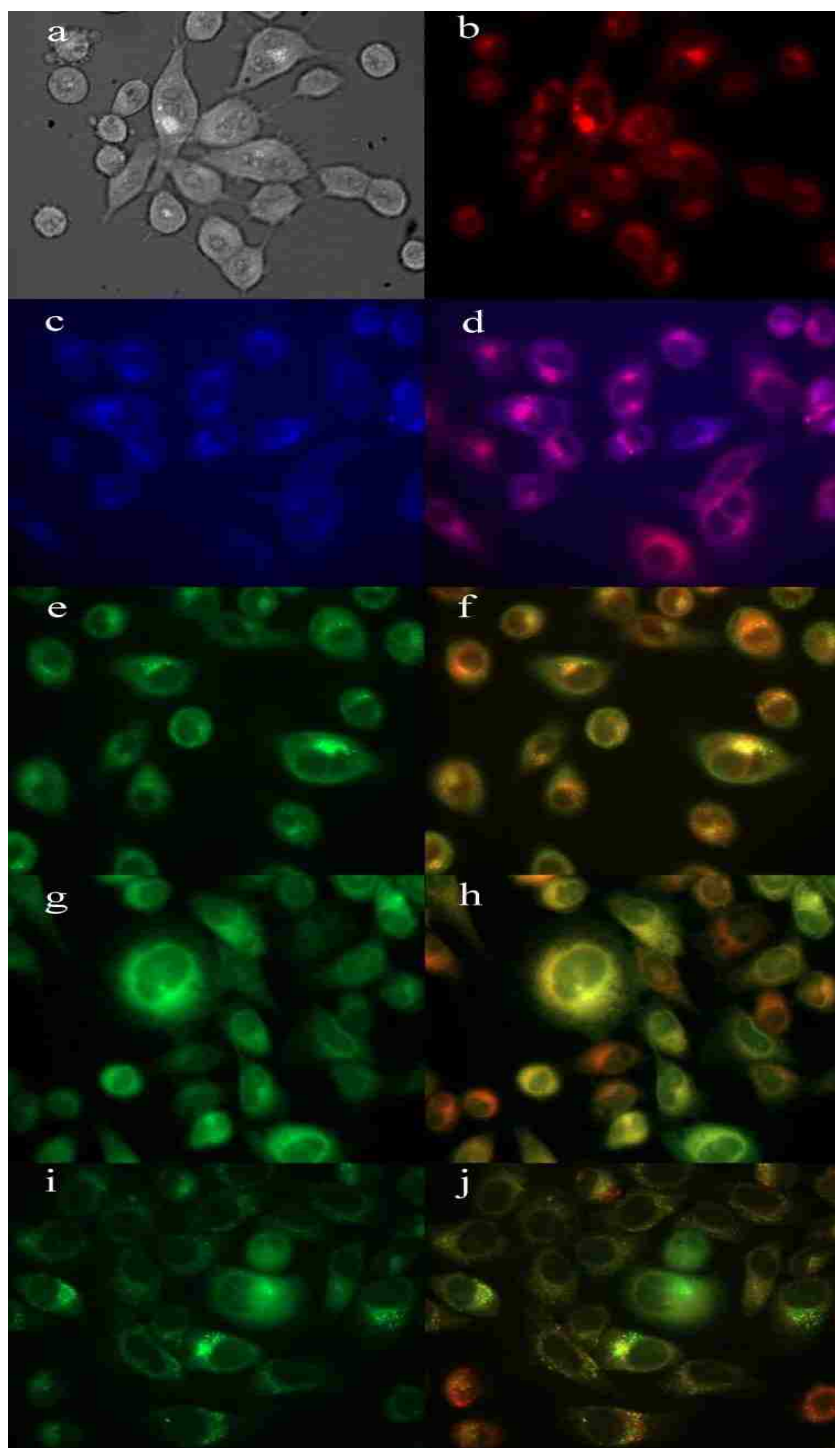


Figure 3.19: Subcellular localization of BODIPY **3b** in HEp2 cells at 10 mm for 6 h. a) Phase contrast, b) overlay of the BODIPY fluorescence and phase contrast, c) ER tracker blue/white fluorescence, e) MitoTracker green fluorescence, g) BODIPY Ceramide, i) Lyso-Sensor green fluorescence, and d), f), h), and j) overlays of organelle tracers with the BODIPY fluorescence.

As previous *in vitro* studies in Chapter 2 indicated, BODIPYs bearing 2,6-iodines are expected to enhance production of singlet oxygen, the main cytotoxic species in PDT. Yet we have shown that the *meso*-substituent plays a significant role in determining which 2,6-diiodo-BODIPYs are phototoxic to HEP2 cells.<sup>24</sup> Since BODIPY **1** was both an efficient generator of singlet oxygen ( $\Phi_{\Delta} = 0.40$ ) and showed high phototoxicity, it was expected that they styryl-derivatives of BODIPY **1** would also be good singlet oxygen generators. As anticipated, the comparative singlet oxygen quantum yields of the BODIPYs showed that all BODIPYs produced singlet oxygen ( $0.34 > \Phi_{\Delta} > 0.78$ ) but only the mono-styryl derivatives were phototoxic to HEP2 cells (*vide infra*).

### 3.3 Conclusions

A series of five mono- and five di-styryl-diiodo-BODIPYs synthesized via Knoevenagel condensations on a 2,6-diiodo-1,3,5,7-tetramethyl-BODIPY (**1**) with indolyl-, tri(ethyleneglycol)phenyl-, thienyl-, and pyrrolyl-aldehydes in yields up to 40% upon microwave irradiation (90 °C for 1h at 400 W) yield far-red to near-IR fluorophores with absorptions and emissions in the ca. 600-770 nm region. Heteroaromatic and tri(ethyleneglycol)phenyl-styryl groups were introduced with the intent in inducing a red-shift in the the absorption and emission profiles of phototoxic BODIPY **1**, as well as to increase its solubility and cellular permeability.

The X-ray structure of polyether bearing-BODIPY **3b** was obtained, which confirmed the expected planarity and symmetry of the BODIPY core and corroborated the *E* configurations of the styryl groups with <sup>1</sup>H-NMR. Incorporation of styryl groups resulted in extended  $\pi$ -conjugation of BODIPY **1**, with the mono-styryl BODIPYs **2a-e** producing 60 - 130 nm red-shifts in the absorption and emission bands, and 130 - 220 nm red-shifts were observed for the di-styryl-

BODIPYs in DMSO. The indolylstyryl- and pyrrolylstyryl-BODIPYs decomposed upon light exposure, despite an attempt to increase stability through the incorporations of electron-withdrawing groups (NO<sub>2</sub>, CO<sub>2</sub>Et). Conversely, both the mono- and di-tri(ethylene glycol)phenyl- and thienyl-styryl-BODIPYs were stable under similar light conditions.

Although all BODIPYs generate singlet oxygen, the monostyryl-diiodo-BODIPYs were found to be better generators of singlet oxygen ( $\Phi_{\Delta} = 0.55 - 0.78$ ) and displayed high phototoxicity ( $IC_{50} < 15 \mu\text{M}$  at  $1 \text{ J/cm}^2$ ) toward HEP2 cells. It is suggested that they lack of extended symmetry of the mono-styryl-BODIPYs and their preferential localization within the ER and mitochondria of cells, likely favoring their binding to intracellular proteins, such as the anti-apoptotic Bcl-2 found in these organelles. On the other hand, the distyryl-diiodo-BODIPYs were weaker generators of singlet oxygen ( $\Phi_{\Delta} = 0.34 - 0.65$ ) and had no phototoxicity ( $IC_{50} > 100 \mu\text{M}$  at  $1.5 \text{ J/cm}^2$ ). Consequently, BODIPYs **2a-e** show the most promise for application as photosensitizers in PDT, whereas **3a-e** are promising multi-mode agents for PET, SPECT, and near-IR fluorescence imaging.

Particular of interest among the phototoxic mono-styryl BODIPYs, **2a** was found to strongly absorb at  $\lambda_{\text{max}}$  636 nm in DMSO, with high extinction coefficient ( $\sim 29,000 \text{ M}^{-1} \cdot \text{cm}^{-1}$ ), to be the most phototoxic among the BODIPYs investigated ( $IC_{50} = 2 \mu\text{M}$  at  $1 \text{ J/cm}^2$  with dark to phototoxicity ratio of 74), probably as a result of efficient singlet oxygen generation ( $\Phi_{\Delta} = 0.72$ ), and is therefore particularly promising as a PDT photosensitizer. On the other hand, BODIPY **3b** shows near-IR emission at  $\lambda_{\text{max}}$  697 nm in DMSO, with high fluorescence quantum yield ( $\Phi_f = 0.44$ ) despite the 2,6-diiodides favoring intersystem crossing and singlet oxygen generation via the heavy atom effect, and is a promising dual near-IR fluorescent and PET or SPECT imaging probe upon installation of radiofluorine, via exchange of one of the fluorides in the BF<sub>2</sub>, or radioiodine at

the 2 or 6 positions. BODIPYs **2a**, the most far-red absorbing and emitting of the toxic mono-styryl BODIPYs, and **3b** and **3e**, the most efficient singlet oxygen producers of the non-toxic di-styryl-BODIPYs, will undergo *in vivo* evaluation in the near future.

### 3.4 Experimental

#### 3.4.1 General Information

Reagents and solvents were acquired from Sigma Aldrich and used without further purification. Reactions were monitored by TLC using 0.2 mm silica plates with UV indicator (UV254). Column chromatography was executed using Sorbent Technologies 60Å silica gel (230 - 400 mesh) or Merck neutral aluminum oxide (70 - 230 mesh). Merck TLC silica gel 60 glass plates were used for preparative thin layer chromatography. All  $^1\text{H}$  NMR and  $^{13}\text{C}$  NMR spectra were obtained using a Bruker AV-500, DPX-400, AV-400, or DPX-250 spectrometer (500 MHz, 400 MHz or 250 MHz for  $^1\text{H}$ , 100 MHz for  $^{13}\text{C}$ ) with samples dissolved in deuterated chloroform, acetone, or DMSO using trimethylsilane as an internal indicator. Chemical shifts ( $\delta$ ) are conveyed in ppm with  $\text{CDCl}_3$  ( $^1\text{H}$ : 7.27 ppm;  $^{13}\text{C}$ : 77.16 ppm), acetone- $\text{d}_6$  ( $^1\text{H}$ : 2.05 ppm;  $^{13}\text{C}$ : 29.84 ppm), and DMSO- $\text{d}_6$  ( $^1\text{H}$ : 2.50 ppm;  $^{13}\text{C}$ : 39.52 ppm) used as references. Coupling constants (J) are stated in Hertz (Hz). High resolution ESI mass spectra were obtained using an Agilent Technologies 6210 ESI-TOF Mass Spectrometer.

#### 3.4.2 Syntheses

**BODIPYs 2a and 3a:** BODIPY **1** (0.05 g, 0.08 mmol), indole-3-carbaldehyde (0.06 g, 0.4 mmol), and AcOH (0.4 mL) were dissolved in dry toluene over 4 Å molecular sieves (20  $\mu\text{M}$ ). To this solution was added piperidine (0.4 mL) and the mixture was stirred under 400 W microwave radiation at 90°C for 1 h. Upon cooling, the reaction was filtered to remove the sieves and the

filtrate was quenched with water and extracted with CH<sub>2</sub>Cl<sub>2</sub>. The combined organic layers were dried over Na<sub>2</sub>SO<sub>4</sub> and the solvent was removed under vacuum. The resulting residue was purified by silica column chromatography using 25% hexanes in CH<sub>2</sub>Cl<sub>2</sub> (v/v) to 100% CH<sub>2</sub>Cl<sub>2</sub> to afford 0.0225 g of a blue solid, **2a**, in 38% yield and 0.028 g of a green solid, **3a**, in 40% yield.

*Data For 2a:* mp = 175°C (decomposes); <sup>1</sup>H-NMR (400 MHz, CDCl<sub>3</sub>) δ 8.53 (s, 1H), 8.51-8.47 (d, *J* = 16.9, 1H), 8.13-8.11 (d, *J* = 7.3, 1H), 7.76-7.72 (d, *J* = 16.6, 1H), 7.56 (s, 1H), 7.41-7.39 (d, *J* = 7.1, 1H), 7.31-7.27 (m, 2H), 6.60-6.58 (t, *J* = 2, 1H), 6.46-6.45 (d, *J* = 2, 2H), 3.19 (s, 6H), 2.71 (s, 3H), 1.64 (s, 3H), 1.57 (s, 3H); <sup>13</sup>C-NMR (100 MHz, CDCl<sub>3</sub>) δ 161.82, 154.95, 152.16, 146.56, 143.39, 138.51, 137.07, 136.84, 133.86, 127.27, 125.56, 123.25, 121.56, 120.68, 116.16, 115.07, 111.61, 106.21, 101.43, 69.55, 55.63, 53.80, 31.74, 29.28, 17.42, 16.72, 16.09; MS (ESI-TOF) *m/z* Calculated for C<sub>30</sub>H<sub>26</sub>BF<sub>2</sub>I<sub>2</sub>N<sub>3</sub>O<sub>2</sub>: 763.0175; Found: [M]<sup>+</sup>: 763.0186.

*Data for 3a:* mp = 195°C (decomposes); <sup>1</sup>H-NMR (400 MHz, CDCl<sub>3</sub>) δ 8.53-8.48 (d, *J* = 16.9, 2H), 8.47 (s, 2H), 8.21-8.19 (d, *J* = 7.3, 2H), 7.89-7.84 (d, *J* = 16.6, 2H), 7.56 (s, 2H), 7.43-7.41 (d, *J* = 7.1, 2H), 7.30-7.24 (m, 4H), 6.61-6.60 (t, *J* = 2, 1H), 6.51-6.50 (d, *J* = 2, 2H), 3.83 (s, 6H), 2.64 (s, 3H), 1.65 (s, 6H); <sup>13</sup>C-NMR (100 MHz, CDCl<sub>3</sub>) 167.71, 161.75, 137.13, 132.92, 132.33, 130.91, 128.83, 127.14, 125.54, 125.03, 125.14, 121.64, 120.89, 116.45, 115.65, 111.55, 106.64, 101.45, 55.64, 17.27; MS (ESI-TOF) *m/z* Calculated for C<sub>39</sub>H<sub>31</sub>BF<sub>2</sub>I<sub>2</sub>N<sub>4</sub>O<sub>2</sub>: 890.0598; Found: [M]<sup>+</sup>: 890.0639.

**BODIPYs 2b and 3b:** BODIPY **1** (0.05 g, 0.08 mmol), aldehyde **8** (0.11 g, 0.4 mmol), and AcOH (0.4 mL) were dissolved in dry toluene over 4 Å molecular sieves (20 μM). To this solution was added piperidine (0.4 mL) and the mixture was stirred under 400 W microwave radiation at 90°C for 60 minutes. Upon cooling, the reaction was filtered to remove the sieves and the filtrate was

quenched with water and extracted with CH<sub>2</sub>Cl<sub>2</sub>. The combined organic layers were dried over Na<sub>2</sub>SO<sub>4</sub> and the solvent was removed under vacuum. The resulting residue was purified by silica column chromatography using CH<sub>2</sub>Cl<sub>2</sub> to 25% Ethyl Acetate in CH<sub>2</sub>Cl<sub>2</sub> (v/v) to afford 0.028 g of a blue solid, **2b**, in 40% yield and 0.030 g of a green solid, **3b**, in 26% yield.

*Data for 2b*: mp = 63-65°C; <sup>1</sup>H-NMR (400 MHz, CDCl<sub>3</sub>) δ 8.15-8.11 (d, *J* = 16.9, 1H), 7.60-7.57 (d, *J* = 8.6, 2H), 7.57-7.52 (d, *J* = 16.6, 1H), 6.96-6.94 (d, *J* = 8.3, 1H), 6.60-6.59 (t, *J* = 2, 1H), 6.45-6.44 (d, *J* = 2, 2H), 4.20-4.18 (t, *J* = 4.5, 2H), 3.90-3.88 (t, *J* = 4.6, 2H), 3.83-3.80 (s, 3H), 3.76-3.71 (m, 2H), 3.69-3.66 (m, 4H), 3.58-3.56 (t, *J* = 4, 2H), 3.41 (s, 3H), 2.70 (s, 3H), 1.64 (s, 3H), 1.59 (s, 3H); <sup>13</sup>C-NMR (100 MHz, CDCl<sub>3</sub>) δ 161.89, 159.96, 156.72, 150.73, 146.17, 144.86, 139.64, 139.04, 136.57, 131.97, 131.51, 129.63, 129.15, 116.59, 114.87, 106.02, 101.46, 85.98, 82.19, 71.95, 70.89, 70.67, 70.59, 69.68, 67.55, 59.06, 55.63, 17.31, 16.87, 16.17; MS (ESI-TOF) *m/z* Calculated for C<sub>35</sub>H<sub>39</sub>BF<sub>2</sub>I<sub>2</sub>NaN<sub>2</sub>O<sub>6</sub>: 909.0856; Found: [M+Na]<sup>+</sup>: 909.0847.

*Data for 3b*: mp = 131-134°C; <sup>1</sup>H-NMR (400 MHz, CDCl<sub>3</sub>) δ 8.16-8.12 (d, *J* = 16.6, 2H), 7.61-7.57 (d, *J* = 8.6, 4H), 7.59-7.57 (d, *J* = 16.6, 2H), 6.98-6.96 (d, *J* = 8.6, 4H), 6.61-6.60 (t, *J* = 2, 1H), 6.46-6.45 (d, *J* = 2, 2H), 4.21-4.18 (t, *J* = 4.5, 4H), 3.91-3.88 (t, *J* = 4.6, 4H), 3.82 (s, 6H), 3.78-7.75 (m, 4H), 3.72-3.66 (m, 8H), 3.58-3.55 (t, *J* = 4, 4H), 3.39 (s, 6H), 1.62 (s, 6H); <sup>13</sup>C-NMR (100 MHz, CDCl<sub>3</sub>) δ 161.86, 159.97, 150.53, 145.68, 139.12, 138.04, 136.86, 132.52, 129.71, 129.25, 128.82, 116.76, 114.97, 114.30, 106.31, 101.45, 71.94, 70.88, 70.67, 70.59, 69.69, 67.56, 59.07, 55.63, 17.35; MS (ESI-TOF) *m/z* Calculated for C<sub>49</sub>H<sub>57</sub>BF<sub>2</sub>I<sub>2</sub>NaN<sub>2</sub>O<sub>10</sub>: 1159.2062; Found: [M+Na]<sup>+</sup>: 1159.2065.

**BODIPYs 2c and 3c**: BODIPY **1** (0.04 g, 0.063 mmol), 5-nitroindole-3-carboxaldehyde (0.06 g, 0.315 mmol), and p-TsOH (0.005 g) were dissolved in dry toluene 20 mL. To this solution was

added piperidine (0.4 mL) and the mixture was stirred under nitrogen at 60°C for 6.5 hours. Upon cooling, the reaction was quenched with water and extracted with CH<sub>2</sub>Cl<sub>2</sub>. The combined organic layers were dried over Na<sub>2</sub>SO<sub>4</sub> and the solvent was removed under vacuum. The resulting residue was purified by silica column chromatography using CH<sub>2</sub>Cl<sub>2</sub> to 10% EtOAc/CH<sub>2</sub>Cl<sub>2</sub> (v/v) to afford 0.0095 g of a blue solid, **2c**, in 15% yield and 0.0136 g of a green solid, **3c**, in 22% yield.

*Data for 2c:* mp = 140°C (decomposes); <sup>1</sup>H-NMR (400 MHz, CDCl<sub>3</sub>) δ 9.07 (s, 1H), 8.82 (s, 1H), 8.41-8.38 (d, *J* = 16.8, 1H), 8.21-8.20 (d, *J* = 8.9, 1H), 7.80-7.77 (d, *J* = 16.8, 2H), 7.74 (s, 1H), 7.49-7.47 (d, *J* = 9.2, 1H), 6.63-6.62 (t, *J* = 2, 1H), 6.48-6.47 (d, *J* = 2, 2H), 3.84 (s, 3H), 2.76 (s, 3H), 2.20 (s, 3H), 1.67 (s, 3H); <sup>13</sup>C-NMR (100 MHz, CDCl<sub>3</sub>) δ 161.92, 157.17, 154.77, 145.03, 142.92, 139.64, 136.55, 130.26, 128.84, 127.99, 127.22, 125.22, 118.72, 118.31, 118.14, 118.02, 117.78, 117.63, 111.57, 106.05, 101.48, 55.64, 17.23, 16.89, 16.19; MS (ESI-TOF) *m/z* Calculated for C<sub>30</sub>H<sub>25</sub>BF<sub>2</sub>I<sub>2</sub>N<sub>4</sub>O<sub>4</sub>: 808.0026; Found: [M]<sup>+</sup>: 808.0020.

*Data for 3c:* mp = 170°C (decomposes); <sup>1</sup>H-NMR (500 MHz, DMSO-*d*<sub>6</sub>) δ 12.45 (s, 2H), 8.91 (s, 2H), 8.53-8.49 (d, *J* = 16.8, 2H), 8.16 (s, 2H), 8.09-8.06 (d, *J* = 8.9, 2H), 7.79-7.76 (d, *J* = 16.8, 2H), 7.67-7.65 (d, *J* = 8.9, 2H), 6.68 (s, 3H), 3.80 (s, 6H), 2.08 (s, 6H); <sup>13</sup>C-NMR (100 MHz, DMSO-*d*<sub>6</sub>) δ 161.95, 150.09, 147.42, 145.55, 142.27, 141.02, 137.51, 136.75, 133.05, 132.63, 132.15, 124.66, 118.29, 116.96, 116.49, 115.79, 113.45, 106.65, 56.09, 17.24; MS (ESI-TOF) *m/z* Calculated for C<sub>39</sub>H<sub>29</sub>BF<sub>2</sub>I<sub>2</sub>N<sub>6</sub>O<sub>6</sub>: 980.0299; Found: [M]<sup>+</sup>: 980.0327.

**BODIPYs 2d and 3d:** BODIPY **1** (0.02 g, 0.03 mmol), thiophene-2-carboxaldehyde (0.0035 g, 0.03 mmol), and *p*-TsOH (0.0025 g) were dissolved in dry toluene over 4 Å molecular sieves (5 μM). To this solution was added piperidine (0.1 mL) and the mixture was stirred at reflux for 4 hours. Upon cooling, the reaction was filtered to remove the sieves and the filtrate was quenched

with water and extracted with CH<sub>2</sub>Cl<sub>2</sub>. The combined organic layers were dried over Na<sub>2</sub>SO<sub>4</sub> and the solvent was removed under vacuum. The resulting residue was purified by careful silica preparatory plate chromatography using 1:1 DCM/Hexanes (v/v) to afford 0.0048 g of a blue solid, **2c**, in 19% yield and 0.0064 g of a green solid, **3c**, in 25% yield.

*Data for 2d:* mp = 165°C (decomposes); <sup>1</sup>H-NMR (400 MHz, CDCl<sub>3</sub>) δ 8.29-8.26 (d, *J* = 16.2, 1H), 7.47-7.44 (d, *J* = 16.2, 1H), 7.37-7.36 (d, *J* = 5.2, 1H), 7.30-7.29 (d, *J* = 3.4, 1H), 7.08-7.07 (dxd, *J* = 3.8, 1.2, 1H), 6.60-6.59 (t, *J* = 2, 1H), 6.44-6.43 (d, *J* = 2, 2H), 3.81 (s, 3H), 2.70 (s, 3H), 1.61 (s, 3H), 1.58 (s, 3H); <sup>13</sup>C-NMR (100 MHz, CDCl<sub>3</sub>) δ 161.91, 157.51, 149.64, 145.80, 145.78, 142.57, 139.77, 136.49, 131.81, 128.85, 128.06, 127.30, 117.99, 105.98, 101.47, 55.62, 17.23, 16.91, 16.23; MS (ESI-TOF) *m/z* Calculated for C<sub>26</sub>H<sub>23</sub>BF<sub>2</sub>I<sub>2</sub>N<sub>2</sub>O<sub>2</sub>S: 729.9631; Found: [M]<sup>+</sup>: 729.9656.

*Data for 3d:* mp = 170°C (decomposes); <sup>1</sup>H-NMR (500 MHz, CDCl<sub>3</sub>) δ 8.33-8.30 (d, *J* = 16.2, 2H), 7.53-7.50 (d, *J* = 16.5, 2H), 7.40-7.39 (d, *J* = 4.9, 2H), 7.33-7.32 (d, *J* = 3.4, 2H), 7.10-7.08 (dxd, *J* = 4, 2H), 6.61-6.60 (t, *J* = 2, 1H), 6.46-6.45 (d, *J* = 2, 2H), 3.82 (s, 6H), 1.62 (s, 6H); <sup>13</sup>C-NMR (100 MHz, CDCl<sub>3</sub>) δ 161.90, 149.95, 145.76, 142.66, 136.74, 132.97, 132.23, 129.01, 128.13, 127.55, 118.06, 113.93, 106.27, 101.51, 83.62, 55.64, 17.33; MS (ESI-TOF) *m/z* Calculated for C<sub>31</sub>H<sub>25</sub>BF<sub>2</sub>I<sub>2</sub>N<sub>2</sub>O<sub>2</sub>S<sub>2</sub>: 823.9508; Found: [M]<sup>+</sup>: 823.9512.

**BODIPYs 2e and 3e:** BODIPY **1** (0.04 g, 0.063 mmol), 5-methylester-2,4-dimethyl-pyrrol-3-carboxaldehyde (0.061 g, 0.315 mmol), and p-TsOH (0.005 g) were dissolved in dry toluene (20 mL) over 4 Å molecular sieves. To this solution was added piperidine (0.4 mL) and the mixture was stirred under nitrogen at 60°C for 48 hours. Upon cooling, the reaction was filtered to remove the sieves and the filtrate was quenched with water and extracted with CH<sub>2</sub>Cl<sub>2</sub>. The combined

organic layers were dried over Na<sub>2</sub>SO<sub>4</sub> and the solvent was removed under vacuum. The resulting residue was purified by silica preparatory plate chromatography using CH<sub>2</sub>Cl<sub>2</sub> to 5% EtOAc/CH<sub>2</sub>Cl<sub>2</sub> (v/v) to afford 0.0098 g of a blue solid, **2e**, in 19% yield and 0.024g of a green solid, **3e**, in 39% yield.

*Data for 2e:* mp = 160°C (decomposes); <sup>1</sup>H-NMR (500 MHz, CDCl<sub>3</sub>) δ 8.90 (br s, 1H), 8.25-8.22 (d, *J* = 16.9, 1H), 7.39-7.36 (d, *J* = 17.1, 2H), 6.59-6.58 (t, *J* = 2, 1H), 6.44-6.43 (d, *J* = 2, 2H), 4.37-4.33 (q, *J* = 6.9, 2H), 3.81 (s, 3H), 2.65 (s, 3H), 2.56 (s, 3H), 2.54 (s, 3H), 1.62 (s, 3H), 1.56 (s, 3H), 1.41-1.38 (t, *J* = 7, 3H); <sup>13</sup>C-NMR (100 MHz, CDCl<sub>3</sub>) δ 161.84, 161.58, 155.49, 151.94, 146.50, 143.81, 138.94, 136.74, 133.99, 133.28, 131.96, 131.12, 128.26, 120.25, 118.21, 116.16, 106.14, 101.40, 85.32, 81.84, 60.12, 55.61, 17.34, 16.75, 16.05, 14.52, 13.67, 11.47; MS (ESI-TOF) *m/z* Calculated for C<sub>31</sub>H<sub>32</sub>BF<sub>2</sub>I<sub>2</sub>N<sub>3</sub>O<sub>4</sub>: 813.0543; Found: [M]<sup>+</sup>: 813.0538.

*Data for 3e:* mp = 150°C (decomposes); <sup>1</sup>H-NMR (500 MHz, acetone-d<sub>6</sub>) δ 10.83 (br s, 2H), 8.38-8.34 (d, *J* = 16.9, 2H), 7.59-7.54 (d, *J* = 16.9, 2H), 6.71 (s, 3H), 4.31-4.25 (q, *J* = 6.9, 4H), 3.89 (s, 6H), 2.81 (s, 3H), 2.77 (s, 3H), 2.60 (s, 3H), 1.65 (s, 6H), 1.35-1.29 (t, *J* = 7, 3H); <sup>13</sup>C-NMR (100 MHz, acetone-d<sub>6</sub>) δ 162.13, 160.64, 134.68, 132.43, 127.58, 127.15, 119.71, 118.54, 115.85, 113.88, 106.28, 101.72, 76.34, 59.32, 55.20, 54.58, 48.21, 16.44, 13.92, 12.18, 12.13, 10.92; MS (ESI-TOF) *m/z* Calculated for C<sub>41</sub>H<sub>43</sub>BF<sub>2</sub>I<sub>2</sub>NaN<sub>4</sub>O<sub>6</sub>: 1013.1231; Found: [M+Na]<sup>+</sup>: 1013.1217.

**BODIPY 4:** General Procedure: BODIPY, aryl-aldehyde (5 equivalents), and p-TsOH (0.005 g, 0.03 mmol) were dissolved in dry toluene over 4 Å molecular sieves (20 μM). To this solution was added piperidine (0.2 mL) and the mixture was refluxed for 6.5 hours. After cooling to room temperature, the mixture was filtered to remove the molecular sieves and the filtrate was poured into water. The aqueous layer was extracted with CH<sub>2</sub>Cl<sub>2</sub> and the combined organic layers were

dried over Na<sub>2</sub>SO<sub>4</sub>. The solvent was removed under vacuum and the resulting residue was purified by silica gel column chromatography using 10% EtOAc in CH<sub>2</sub>Cl<sub>2</sub> to elute to obtain the product as a green solid.

*From BODIPY 2a:* BODIPY (0.0225 g, 0.03 mmol) and aldehyde **10** (0.0158 g, 0.06 mmol) afforded 0.0021 g of the title compound in 4% yield.

*From BODIPY 2b:* BODIPY (0.054 g, 0.06 mmol) and indole-3-carboxaldehyde (0.018 g, 0.12 mmol) provided 0.0014 g of the title compound in 2% yield.

MS (ESI-TOF) m/z Calculated for C<sub>44</sub>H<sub>44</sub>BF<sub>2</sub>I<sub>2</sub>NaN<sub>3</sub>O<sub>6</sub>: 1036.1274; Found: [M+Na]<sup>+</sup>: 1036.1300.

**Compound 5:** Triethylene glycol monomethyl ether (10.0 g, 61 mmol) and p-toluenesulfonyl chloride (12.77 g, 70 mmol) were dissolved in diethyl ether (75 mL) and cooled to 0°C. Freshly ground potassium hydroxide (13.67 g, 244 mmol) was added in small portions so that the reaction temperature never climbed above 5°C. The mixture was warmed and stirred at room temperature. After 3 hours, 10 mL of ice water was added and the mixture was transferred to a separatory funnel. The aqueous layer was extracted with diethyl ether and the combined organic layers were dried over Na<sub>2</sub>SO<sub>4</sub>. The solvent was evaporated under reduced pressure to yield a pale yellow liquid (17.5 g) in 90% yield.

<sup>1</sup>H-NMR (400 MHz, CDCl<sub>3</sub>) δ 7.69-7.66 (d, *J* = 7.8, 2H), 7.25-7.22 (d, *J* = 7.8, 2H), 4.06-4.02 (t, *J* = 4, 2H), 3.58-3.55 (t, *J* = 4, 2H), 3.47 (m, 6H), 3.42-3.41 (t, *J* = 3.3, 2H), 3.24 (s, 3H), 2.33 (s, 3H); <sup>13</sup>C-NMR (100 MHz, CDCl<sub>3</sub>) δ 145.11, 133.26, 130.16, 128.11, 72.07, 70.81, 70.65, 69.70, 68.79, 59.06, 21.75; MS (ESI-TOF) m/z Calculated for C<sub>14</sub>H<sub>23</sub>O<sub>6</sub>S: 319.1215; Found: [M+H]<sup>+</sup>:319.1206. The NMR data is in agreement with that already published.<sup>52</sup>

**Compound 6:** 4-(Hydroxymethyl) benzaldehyde dimethyl acetal (0.025 g, 0.14 mmol), sodium hydride (0.0046 g, 0.19 mmol), and compound **5** (0.0437g, 0.14 mmol) were placed in an oven dried 5 mL round bottom flask.<sup>41</sup> The flask was then evacuated and filled with Nitrogen three times. THF (2.5 mL) was added and the mixture was stirred at room temperature for 24 hours (until TLC revealed disappearance of the starting material). The reaction was quenched with water and diluted with 3 mL EtOAc. The aqueous layer was washed three times with 3 mL EtOAc. The combined organic layers were dried over Na<sub>2</sub>SO<sub>4</sub> and the solvent was evaporated under reduced pressure. The residue was purified by alumina column chromatography using 10% MeOH in dichloromethane as eluent yielding a pale yellow liquid in quantitative yield.

<sup>1</sup>H-NMR (400 MHz, CDCl<sub>3</sub>) δ 7.64 (d, *J* = 7.4, 2H), 7.24 (d, *J* = 7.4, 2H), 5.24 (s, 1H), 3.98 (m, 2H), 3.43 (m, 12H), 3.16 (s, 6H), 1.88 (s, 3H); MS (MALDI-TOF) *m/z* Calculated for C<sub>17</sub>H<sub>28</sub>NaO<sub>6</sub>: 351.178; Found: [M+Na]<sup>+</sup>: 351.189

**Compound 7:** Compound **6** (0.2 g, 0.6 mmol) was dissolved in DCM (5 mL) at room temperature in a round bottom flask equipped with magnetic stir bar. TFA (1.4 g, 12.3 mmol) was added dropwise and the solution was allowed to stir for 6 hours.<sup>42</sup> The mixture was poured into 15 mL of water. The aqueous layer was extracted with ethyl acetate (3 x 10 mL). The combined organic layers were dried over Na<sub>2</sub>SO<sub>4</sub> and the solvent was evaporated under vacuum. The residue was purified by flash chromatography using neutral alumina and 2% MeOH in dichloromethane as eluent yielding a pale yellow liquid in 67% yield.

<sup>1</sup>H-NMR (400 MHz, CDCl<sub>3</sub>) δ 9.93 (s, 1H), 7.79 (d, *J* = 7.4, 2H), 7.46 (d, *J* = 7.4, 2H), 4.10 (t, *J* = 4.7, 2H), 3.60 (m, 6H), 3.51 (m, 6H), 3.31 (s, 3H); MS (ESI-TOF) *m/z* Calculated for C<sub>15</sub>H<sub>22</sub>O<sub>5</sub>: 282.15; Found: [M+H]<sup>+</sup>: 283.16.

**Compound 8:** To a round bottom flask equipped with a magnetic stir bar was added 4-hydroxybenzaldehyde (5.0 g, 41 mmol) and 1,2-ethanedithiol (4.4 g, 47 mmol) in THF (40 mL). The flask was purged and filled with argon before being cooled to 0°C.  $\text{BF}_3 \cdot \text{OEt}_2$  (0.58 g, 4.1 mmol) was added drop-wise. The solution was stirred at room temperature for 45 minutes. The mixture was then washed once with 10% aqueous NaOH and once with saturated NaCl before being passed through a bed of  $\text{Na}_2\text{SO}_4$ . The solvent was evaporated under reduced pressure and the resulting residue was purified by silica gel column chromatography using EtOAc to afford a yellow solid (6.6 g) in 81% yield, mp = 113-117°C.

$^1\text{H-NMR}$  (400 MHz,  $\text{CDCl}_3$ )  $\delta$  7.41-7.38 (d,  $J = 7.8$ , 2H), 6.79-6.76 (d,  $J = 7.8$ , 2H), 6.09 (s, 1H), 5.62 (s, 1H), 3.53-3.43 (m, 2H), 3.39-3.29 (m, 2H);  $^{13}\text{C-NMR}$  (100 MHz,  $\text{CDCl}_3$ )  $\delta$  157.22, 130.76, 129.32, 115.09, 55.90, 39.85; GC-MS  $m/z$  Calculated for  $\text{C}_9\text{H}_{10}\text{OS}_2$ : 198.017; Found:  $[\text{M}+\text{H}]^+$ : 197.6. The NMR data is in agreement with that already published.<sup>40</sup>

**Compound 9:** Compound **8** (4.9 g, 25 mmol), potassium carbonate (3.8 g, 27 mmol) and compound **5** (7.9 g, 25 mmol) were dissolved in acetonitrile (250 mL) and the mixture was refluxed for 24 hours. Upon completion, the reaction was cooled to room temperature, then quenched with water and diluted with 75 mL EtOAc. The aqueous layer was washed three times with EtOAc and the combined organic layers were dried over  $\text{Na}_2\text{SO}_4$ . The solvent was evaporated under reduced pressure and the resulting residue was purified by alumina column chromatography using 4:1 hexanes/EtOAc as eluent to give a light brown liquid (7.96 g) in 93% yield.

$^1\text{H-NMR}$  (400 MHz,  $\text{CDCl}_3$ )  $\delta$  7.44-7.41 (d,  $J = 7.8$ , 2H), 6.86-6.82 (d,  $J = 7.8$ , 2H), 5.62 (s, 1H), 4.13-4.09 (t,  $J = 4$ , 2H), 3.85-3.81 (t,  $J = 4$ , 2H), 6.72-6.63 (m, 6H), 3.58-3.43 (m, 4H), 3.37 (s, 3H), 3.37-3.31 (m, 2H);  $^{13}\text{C-NMR}$  (100 MHz,  $\text{CDCl}_3$ )  $\delta$  158.60, 132.02, 129.11, 114.56, 71.92,

70.81, 70.63, 70.54, 69.67, 67.50, 59.00, 56.04, 40.17; MS (ESI-TOF)  $m/z$  Calculated for  $C_{16}H_{24}O_4S_2$ : 367.1014; Found:  $[M+Na]^+$ : 367.1028.

**Compound 10:** To a solution of compound **9** (8.3 g, 24 mmol) in 5% aqueous THF (40 mL) under argon was added  $Hg(ClO_4)_2 \cdot 3H_2O$  (22 g, 48.5 mmol) in THF (25 mL). The mixture was stirred at room temperature for 1 hour following which the solution was filtered and the precipitate was washed three times with diethyl ether. The combined filtrate was washed three times with saturated  $Na_2CO_3$  and twice with water before being passed through a bed of  $Na_2SO_4$ . The solvent was evaporated under reduced pressure and the resulting residue was purified by silica gel column chromatography using 4:1 EtOAc/MeOH to produce a colorless liquid (4.2 g) in 64% yield.

$^1H$ -NMR (400 MHz,  $CDCl_3$ )  $\delta$  9.81 (s, 1H), 7.74-7.72 (d,  $J = 7.8$ , 2H), 6.98-6.96 (d,  $J = 7.8$ , 2H), 5.24 (s, 1H), 4.18-4.14 (t,  $J = 4$ , 2H), 3.85-3.81 (t,  $J = 2$ , 2H), 3.63-3.44 (m, 8H), 3.30 (s, 3H);  $^{13}C$ -NMR (100 MHz,  $CDCl_3$ )  $\delta$  190.54, 163.60, 131.63, 129.71, 114.94, 71.53, 70.43, 70.19, 70.08, 69.25, 67.53, 58.49; MS (ESI-TOF)  $m/z$  Calculated for  $C_{14}H_{20}O_5$ : 291.1208; Found:  $[M+Na]^+$ : 291.1229. The NMR data is in agreement with that already published.<sup>45</sup>

### 3.4.3 X-ray Determined Molecular Structures

Diffraction data were collected at 100 K on a Bruker Kappa Apex-II DUO diffractometer equipped with  $MoK\alpha$  radiation ( $\lambda = 0.71073 \text{ \AA}$ ). Refinement was by full-matrix least squares using SHELXL, with H atoms in idealized positions. Compound **3b** has four independent molecules and large displacement parameters for its polyether chains. Isotropic atoms with heavily restrained refinement was necessary in these regions, and some disorder in the polyethers could not be modeled.

*Crystal data for 1:* C<sub>19</sub>H<sub>17</sub>BF<sub>2</sub>I<sub>2</sub>N<sub>2</sub>, M = 636.01, monoclinic space group P2<sub>1</sub>/c, a = 7.0702 (3) Å, b = 16.8644 (7) Å, c = 18.4079 (8) Å, β = 92.838 (2)°, U = 2192.17 (16) Å<sup>3</sup>, T = 100 K, Z = 4, A total of 49862 reflections were measured (R<sub>int</sub> = 0.027). R = 0.026 for 11738 data points with I > 2σ (I) of 13815 unique data points and 277 refined parameters.

*Crystal data for 3b:* C<sub>49</sub>H<sub>57</sub>BF<sub>2</sub>I<sub>2</sub>N<sub>2</sub>O<sub>10</sub>, M = 1136.57, triclinic space group P1, a = 12.2712(5), b = 19.5190(8), c = 22.4285(8) Å, α = 106.006(2)°, β = 101.516(2)°, γ = 104.576(2)°, U = 4784.1(3) Å<sup>3</sup>, T = 100 K, Z = 4. A total of 48,144 reflections were measured (R<sub>int</sub> = 0.034). R = 0.060 for 30,040 data points with I > 2σ (I) of 48,144 unique data points and 1,953 refined parameters and 2,097 restraints.

### 3.4.4 Steady-state Absorption and Fluorescence Spectroscopy

The spectroscopic properties of BODIPYs **1**, **2a-e**, and **3a-e** were determined on solutions prepared by dissolving crystalline compound in dichloromethane, THF, or DMSO. Stock solutions (5x10<sup>-5</sup> M) were prepared and diluted to appropriate concentrations for collection of absorbance and emission spectra. Absorption spectra were obtained on a Varian Cary 50 Bio UV/VIS Spectrophotometer. Measurements obtained for determining optical density were taken from solutions with concentrations between 1.2x10<sup>-5</sup> and 5x10<sup>-5</sup> M so that λ<sub>max</sub> was between 0.5 and 1.0. Fluorescence measurements were recorded on solutions with concentrations between 1.2x10<sup>-6</sup> and 2.5x10<sup>-5</sup> M to attain an optical density at the excitation wavelength between 0.04 and 0.06 to minimize intermolecular reabsorption and inner-filter effects. Compounds were excited at 485 nm for **1**, 530 nm for **2a**, **2c**, **2d**, and **2e**, 535 nm for **2b**, 660 nm for **3a**, 580 nm for **3b**, 635 nm for **3c**, 580 nm for **3d**, and 630 for **3e**. Emission spectra were acquired on a PTI QuantaMaster4/2006SE spectrofluorometer with the slit width set at 3 nm for dichloromethane and THF and 5 nm for

DMSO. Rhodamine 6G and methylene blue were used as standards in calculating the fluorescence quantum yields ( $\Phi_f = 0.95$  in ethanol and  $\Phi_f = 0.03$  in methanol, respectively). All measurements, both absorbance and emission, were acquired within 4 h of solution preparation at room temperature (23 – 25 °C), using a 10 mm path length quartz spectrophotometric cell.

### 3.4.5 Cell Studies

All reagents and tissue culture media were purchased from Invitrogen. Human carcinoma HEp2 cells used in this study were purchased from ATCC and were sustained at 37 °C and 5% CO<sub>2</sub> in a 50:50 mixture of DMEM:AMEM augmented with 10% FBS and 1% antibiotic (Penicillin-streptomycin). A working BODIPY stock solution of 32 mM BODIPY was prepared by dissolving the compound with sonication in 96% DMSO and 4% Cremophor EL.

**3.4.5.1 Time-Dependent Cellular Uptake.** The HEp2 cells were grown overnight in a Costar 96-well plate plated at 15,000 cells per well. The 32 mM stock solution was diluted to a 10  $\mu$ M BODIPY solution through the addition of medium containing 5% FBS and 1% antibiotic to a 400  $\mu$ M stock solution. The cells were exposed to the BODIPY in medium solution at 100  $\mu$ L/well at time intervals of 0, 1, 2, 4, 8, and 24 hours. At the termination of the treatment, the loading medium was removed and the cells were washed with 1X PBS, and solubilized by adding 0.25% Triton X-100 in 1X PBS. Quantification of the cells was conducted using the CyQuant Cell Proliferation Assay (Life Technologies). BODIPY concentration was determined by reading fluorescence at 355/670 nm (for **2a** and **3a**), 355/700 nm (for **2b**), and 410/700 nm (for **3b**) with a FluoStar Optima micro-plate reader (BMG LRBTEH). Cellular uptake is expressed in nM compound/cell.

**3.4.5.2 Dark Cytotoxicity.** The HEP2 cells were placed in a 96-well plate as above and allowed to incubate overnight. Following incubation, the cells were exposed to increasing concentrations of BODIPY, from 0  $\mu\text{M}$  up to 400  $\mu\text{M}$ , and then incubated at 37°C. After 24 hour incubation, the loading media containing compound was removed by washing the cells with 1X PBS. The media was replaced with media containing 20% Cell Titer Blue and the cells were incubated at 37°C for a subsequent 4 hours. Cell viability was determined by reading fluorescence at 570/615 nm with a FluoStar Optima micro-plate reader. The dark toxicity is expressed in terms of the percentage of viable cells.

**3.4.5.3 Phototoxicity.** The HEP2 cells were placed in 96-well plates as incubated as described above. Following incubation, the cells were exposed to increasing concentrations of BODIPY (0  $\mu\text{M}$ , 3.125  $\mu\text{M}$ , 6.25  $\mu\text{M}$ , 12.5  $\mu\text{M}$ , 25  $\mu\text{M}$ , 50  $\mu\text{M}$ , and 100  $\mu\text{M}$ ) and then incubated for 24 hours at 37°C. After the 24 hour treatment, the loading media was removed, the cells were washed with 1X PBS and refilled with fresh media. The cells were then exposed to a 600 W halogen lamp light filtered through a water filter (Newport) and then through a beam turning mirror (200 – 3000 nm, Newport) to generate an approximate light dose of 1.5 J/cm<sup>2</sup>. After a 20 minute exposure time, the cells were incubated for another 24 hours. Following incubation, the medium was removed and replaced with medium containing 20% of Cell Titer Blue and the cells were incubated for a subsequent 4 hours. Cell viability was determined by reading fluorescence at 570/615 nm with a FluoStar Optima micro-plate reader. The phototoxicity is expressed in terms of the percentage of viable cells.

**3.4.5.4 Microscopy.** HEP2 cells were plated in a 6-well plate and allowed to grow overnight. The cells were then exposed to 10  $\mu$ M of the compound at 37°C for more than 6 hours before adding the organelle tracer (Invitrogen). The working concentrations of organelle tracers were as following: LysoSensor Green 50 nM, MitoTracker Green 250 nM, ER Tracker Blue/white 100 nM, and BODIPY FL C5 Ceramide 50 nM. The organelle tracers were diluted in growing medium and the cells were incubated concurrently with the compound and the tracer for 30 minutes. After adding the tracer for 30 minutes, the loading medium is removed and cells were washed with 1X PBS three times. Images were acquired using a Leica DMRXA2 microscope with a water immersion objective and DAPI, GFP, YFP, Texas Red, CY5, and TRITC filter cubes (Chroma Technologies).

### **3.4.6 Comparative Singlet Oxygen Generation Studies**

To each well of a 6-well plate was added 2 mL containing 50  $\mu$ M of 1,3-diphenylisobenzofuran (DPBF) and 5  $\mu$ M of photosensitizers in DMSO. The plate was irradiated using a 71 W filtered light source of  $> 500$  nm with a Schott glass 500 nm long-pass yellow filter for 1 hour. At 15 minute intervals, 200  $\mu$ L aliquots were removed from each of the six wells and the absorbance was measured at 410 nm. The rate of singlet oxygen generation was determined by the decrease in absorbance of DPBF over time. A control solutions of DPBF/methylene blue (reference standard) was irradiated under the previous mentioned conditions. Absorption spectra were chronicled using a Varian Cary 50 Bio UV/VIS Spectrophotometer.

### 3.4.7 Time-Dependent Fluorescence Studies

The dark and photostability of all BODIPYs were assessed by measuring the change in fluorescence when excited at a compound specific wavelength (485 nm for **1**, 530 nm for **2a**, **2c**, **2d**, and **2e**, 535 nm for **2b**, 660 nm for **3a**, 580 nm for **3b**, 635 nm for **3c**, 580 nm for **3d**, and 630 nm for **3e**). Solutions of 25  $\mu$ M BODIPY were made by dissolving crystalline BODIPY in DMSO and were used immediately. For dark studies, the vials containing BODIPY solutions were covered in aluminum foil to minimize light exposure. To assess potential photo-induced decomposition, the compounds were exposed to ambient light, by keeping the BODIPYs in 20 mL scintillation vials on the bench top under 32 W fluorescent light from Sylvania OCTRON®/ECO® 4100K for a period up to 24 h. BODIPY decomposition is noted by a significant decrease in the compound's emission over time.

### 3.4.8 Octanol-HEPES buffer coefficients

The partition coefficients ( $\log P$ ) were measured at room temperature by adding 0.5 mL of a BODIPY stock solution in DMSO (50  $\mu$ M) to a 15 mL volumetric tube containing 4.0 mL of HEPES buffer (1 M, pH 7.4), followed by addition of 4.0 mL of 1-octanol. After vortexing for 5 min, the phases were allowed to separate completely. An aliquot of 0.5 mL from each layer was diluted with 0.5 mL of methanol and the absorbance was read on an Agilent Technologies 8354 UV-Vis spectrophotometer with 10 mm path length quartz cuvette.

## 3.5 References

1. Karolin, J.; Johansson, L. B. A.; Strandberg, L.; Ny, T., Fluorescence and Absorption Spectroscopic Properties of Dipyrrometheneboron Difluoride (BODIPY) Derivatives In Liquids, Lipid-Membranes, and Proteins. *Journal of the American Chemical Society* **1994**, *116*, 7801-7806.

2. Ehrenschwender, T.; Wagenknechet, H. A., 4,4-Difluoro-4-bora-3a,4a-diaza-s-indacene as a Bright Fluorescent Label for DNA. *Journal of Organic Chemistry* **2011**, *76*, 2301-2304.
3. Giessler, K.; Griesser, H.; Gohringer, D.; Sabirov, T.; Richert, C., Synthesis of 3'-BODIPY-Labeled Active Esters of Nucleotides and a Chemical Primer Extension Assay on Beads. *European Journal of Organic Chemistry* **2010**, 3611-3620.
4. Kalai, T.; Hideg, K., Synthesis of new, BODIPY-based sensors and labels. *Tetrahedron* **2006**, *62*, 10352-10360.
5. Jones, L. J.; Upson, R. H.; Haugland, R. P.; PanchukVoloshina, N.; Zhou, M. J.; Haugland, R. P., Quenched BODIPY dye-labeled casein substrates for the assay of protease activity by direct fluorescence measurement. *Analytical Biochemistry* **1997**, *251*, 144-152.
6. Bandhuvula, P.; Li, Z. G.; Bittman, R.; Saba, J. D., Sphingosine 1-phosphate lyase enzyme assay using a BODIPY-labeled substrate. *Biochemical and Biophysical Research Communications* **2009**, *380*, 366-370.
7. Ziessel, R.; Ulrich, G.; Harriman, A.; Alamiry, M. A. H.; Stewart, B.; Retailleau, P., Solid-State Gas Sensors Developed from Functional Difluoroboradiazaindacene Dyes. *Chemistry-A European Journal* **2009**, *15*, 1359-1369.
8. Baruah, M.; Qin, W. W.; Vallee, R. A. L.; Beljonne, D.; Rohand, T.; Dehaen, W.; Boens, N., A highly potassium-selective ratiometric fluorescent indicator based on BODIPY azacrown ether excitable with visible light. *Organic Letters* **2005**, *7*, 4377-4380.
9. Wu, Y. K.; Peng, X. J.; Guo, B. C.; Fan, J. L.; Zhang, Z. C.; Wang, J. Y.; Cui, A. J.; Gao, Y. L., Boron dipyrromethene fluorophore based fluorescence sensor for the selective imaging of Zn(II) in living cells. *Organic & Biomolecular Chemistry* **2005**, *3*, 1387-1392.
10. Jiao, L. J.; Li, J. L.; Zhang, S. Z.; Wei, C.; Hao, E. H.; Vicente, M. G. H., A selective fluorescent sensor for imaging Cu<sup>2+</sup> in living cells. *New Journal of Chemistry* **2009**, *33*, 1888-1893.
11. Loudet, A.; Ueno, Y.; Wu, L. X.; Jose, J.; Barhoumi, R.; Burghardt, R.; Burgess, K., Organelle-selective energy transfer: A fluorescent indicator of intracellular environment. *Bioorganic & Medicinal Chemistry Letters* **2011**, *21*, 1849-1851.
12. Dolmans, D.; Fukumura, D.; Jain, R. K., Photodynamic therapy for cancer. *Nature Reviews Cancer* **2003**, *3*, 380-387.
13. Dougherty, T. J.; Gomer, C. J.; Henderson, B. W.; Jori, G.; Kessel, D.; Korblik, M.; Moan, J.; Peng, Q., Photodynamic therapy. *Journal of the National Cancer Institute* **1998**, *90*, 889-905.
14. Brown, S. B.; Brown, E. A.; Walker, I., The present and future role of photodynamic therapy in cancer treatment. *Lancet Oncology* **2004**, *5*, 497-508.

15. Huang, Z., A review of progress in clinical photodynamic therapy. *Technology & Cancer Research Treatment* **2005**, *4*, 283-293.
16. Triesscheijn, M.; Baas, P.; Schellens, J. H. M.; Stewart, F. A., Photodynamic therapy in oncology. *Oncologist* **2006**, *11*, 1034-1044.
17. Adams, K. E.; Ke, S.; Kwon, S.; Liang, F.; Fan, Z.; Lu, Y.; Hirschi, K.; Mawad, M. E.; Barry, M. A.; Sevick-Muraca, E. M., Comparison of visible and near-infrared wavelength-excitable fluorescent dyes for molecular imaging of cancer. *Journal of Biomedical Optics* **2007**, *12*, 9.
18. Luo, S. L.; Zhang, E. L.; Su, Y. P.; Cheng, T. M.; Shi, C. M., A review of NIR dyes in cancer targeting and imaging. *Biomaterials* **2011**, *32*, 7127-7138.
19. Kadish, K. M. S., K. M.; Guillard, R., *Handbook of Porphyrin Science: with Applications to Chemistry, Physics, Materials Science, Engineering, Biology and Medicine*. World Scientific Publishing Co. Pte. Ltd.2010; Vol. 4.
20. Awuah, S. G.; You, Y., Boron dipyrromethene (BODIPY)-based photosensitizers for photodynamic therapy. *RSC Advances* **2012**, *2*, 11169-11183.
21. Kamkaew, A.; Lim, S. H.; Lee, H. B.; Kiew, L. V.; Chung, L. Y.; Burgess, K., BODIPY dyes in photodynamic therapy. *Chemical Society Reviews* **2013**, *42*, 77-88.
22. Ulrich, G.; Ziessel, R.; Harriman, A., The chemistry of fluorescent bodipy dyes: Versatility unsurpassed. *Angewandte Chemie-International Edition* **2008**, *47*, 1184-1201.
23. Loudet, A.; Burgess, K., BODIPY dyes and their derivatives: Syntheses and spectroscopic properties. *Chemistry Reviews* **2007**, *107*, 4891-4932.
24. Gibbs, J. H.; Robins, L. T.; Zhou, Z.; Bobadova-Parvanova, P.; Cottam, M.; McCandless, G. T.; Fronczek, F. R.; Vicente, M. G. H., Spectroscopic, computational modeling and cytotoxicity of a series of meso-phenyl and meso-thienyl-BODIPYs. *Bioorganic and Medicinal Chemistry* **2013**, *21*, 5770-5781.
25. He, H.; Lo, P. C.; Yeung, S. L.; Fong, W. P.; Ng, D. K. P., Preparation of unsymmetrical distyryl BODIPY derivatives and effects of the styryl substituents on their in vitro photodynamic properties. *Chemical Communications* **2011**, *47*, 4748-4750.
26. Atilgan, S.; Ekmekci, Z.; Dogan, A. L.; Guc, D.; Akkaya, E. U., Water soluble distyryl-boradiazaindacenes as efficient photosensitizers for photodynamic therapy. *Chemical Communications* **2006**, 4398-4400.
27. Ortiz, M. J.; Agarrabeitia, A. R.; Duran-Sampedro, G.; Prieto, J. B.; Lopez, T. A.; Massad, W. A.; Montejano, H. A.; Garcia, N. A.; Arbeloa, I. L., Synthesis and functionalization of new polyhalogenated BODIPY dyes. Study of their photophysical properties and singlet oxygen generation. *Tetrahedron* **2012**, *68*, 1153-1162.

28. Yogo, T.; Urano, Y.; Ishitsuka, Y.; Maniwa, F.; Nagano, T., Highly efficient and photostable photosensitizer based on BODIPY chromophore. *Journal of the American Chemical Society* **2005**, *127*, 12162-12163.
29. Lim, S. H.; Thivierge, C.; Nowak-Sliwinska, P.; Han, J. Y.; van den Bergh, H.; Wagnieres, G.; Burgess, K.; Lee, H. B., In Vitro and In Vivo Photocytotoxicity of Boron Dipyrromethene Derivatives for Photodynamic Therapy. *Journal of Medicinal Chemistry* **2010**, *53*, 2865-2874.
30. Jiao, L. J.; Yu, C. J.; Uppal, T.; Liu, M. M.; Li, Y.; Zhou, Y. Y.; Hao, E. H.; Hu, X. K.; Vicente, M. G. H., Long wavelength red fluorescent dyes from 3,5-diiodo-BODIPYs. *Organic & Biomolecular Chemistry* **2010**, *8*, 2517-2519.
31. Li, Z. B.; Lin, T. P.; Liu, S. L.; Huang, C. W.; Hudnall, T. W.; Gabbai, F. P.; Conti, P. S., Rapid aqueous F-18 -labeling of a bodipy dye for positron emission tomography/fluorescence dual modality imaging. *Chemical Communications* **2011**, *47*, 9324-9326.
32. Liu, S. L.; Lin, T. P.; Li, D.; Leamer, L.; Shan, H.; Li, Z. B.; Gabbai, F. P.; Conti, P. S., Lewis Acid-Assisted Isotopic F-18-F-19 Exchange in BODIPY Dyes: Facile Generation of Positron Emission Tomography/Fluorescence Dual Modality Agents for Tumor Imaging. *Theranostics* **2013**, *3*, 181-189.
33. Hendricks, J. A.; Keliher, E. J.; Wan, D. P.; Hilderbrand, S. A.; Weissleder, R.; Mazitschek, R., Synthesis of F-18 BODIPY: Bifunctional Reporter for Hybrid Optical/Positron Emission Tomography Imaging. *Angewandte Chemie-International Edition* **2012**, *51*, 4603-4606.
34. Uppal, T.; Bhupathiraju, N.; Vicente, M. G. H., Synthesis and cellular properties of Near-IR BODIPY-PEG and carbohydrate conjugates. *Tetrahedron* **2013**, *69*, 4687-4693.
35. Rohand, T.; Qin, W.; Boens, N.; Dehaen, W., Palladium-catalyzed coupling reactions for the functionalization of BODIPY dyes with fluorescence spanning the visible spectrum. *European Journal of Organic Chemistry* **2006**, 4658-4663.
36. Kajiwara, Y.; Nagai, A.; Chujo, Y., Microwave-assisted preparation of intense luminescent BODIPY-containing hybrids with high photostability and low leachability. *Journal of Materials Chemistry* **2010**, *20*, 2985-2992.
37. Baruah, M.; Qin, W. W.; Flors, C.; Hofkens, J.; Vallee, R. A. L.; Beljonne, D.; Van der Auweraer, M.; De Borggraeve, W. M.; Boens, N., Solvent and pH dependent fluorescent properties of a dimethylaminostyryl borondipyrromethene dye in solution. *Journal of Physical Chemistry A* **2006**, *110*, 5998-6009.
38. Sharma, V.; Kumar, P.; Pathak, D., Biological Importance of the Indole Nucleus in Recent Years: A Comprehensive Review. *Journal of Heterocycle Chemistry* **2010**, *47*, 491-502.

39. Greenwald, R. B., PEG drugs: an overview. *Journal of Controlled Release* **2001**, *74*, 159-171.
40. Kamitori, Y.; Hojo, M.; Masuda, R.; Kimura, T.; Yoshida, T., Selective Protection of Carbonyl-Compounds- Silica-Gel Treated with Thionyl-Chloride as an Effective Catalyst for Thioacetalization. *Journal of Organic Chemistry* **1986**, *51*, 1427-1431.
41. Rihn, S.; Retailleau, P.; Bugsaliewicz, N.; De Nicola, A.; Ziessel, R., Versatile synthetic methods for the engineering of thiophene-substituted Bodipy dyes. *Tetrahedron Letters* **2009**, *50*, 7008-7013.
42. Li, W.; Li, J.; Wu, Y.; Fuller, N.; Markus, M. A., Mechanistic Pathways in CF<sub>3</sub>COOH-Mediated Deacetalization Reactions. *Journal of Organic Chemistry* **2010**, *75*, 1077-1086.
43. Vicente, M. G. H.; Nurco, D. J.; Shetty, S. J.; Osterloh, J.; Ventre, E.; Hegde, V.; Deutsch, W. A., Synthesis, dark toxicity and induction of in vitro DNA photodamage by a tetra(4-nido-carboranylphenyl)porphyrin. *Journal of Photochemistry & Photobiology B-Biology* **2002**, *68*, 123-132.
44. Zhu, S. L.; Zhang, J. T.; Vegesna, G.; Luo, F. T.; Green, S. A.; Liu, H. Y., Highly Water-Soluble Neutral BODIPY Dyes with Controllable Fluorescence Quantum Yields. *Organic Letters* **2011**, *13*, 438-441.
45. McFarland, J. M.; Francis, M. B., Reductive alkylation of proteins using iridium catalyzed transfer hydrogenation. *Journal of the American Chemical Society* **2005**, *127*, 13490-13491.
46. Nishimura, T.; Yamada, K.; Takebe, T.; Yokoshima, S.; Fukuyama, T., (1-nosyl-5-nitroindol-3-yl)methyl ester: A novel protective group for carboxylic acids. *Organic Letters* **2008**, *10*, 2601-2604.
47. He, H.; Lo, P. C.; Yeung, S. L.; Fong, W. P.; Ng, D. K. P., Synthesis and in Vitro Photodynamic Activities of Pegylated Distyryl Boron Dipyrromethene Derivatives. *Journal of Medicinal Chemistry* **2011**, *54*, 3097-3102.
48. Sangster, J., Octanol-Water Partition Coefficients of Simple Organic Compounds. *Journal of Physical and Chemical Reference Data* **1989**, *18*, 1111-1229.
49. Kessel, D., Correlation between subcellular localization and photodynamic efficacy. *Journal of Porphyrins and Phthalocyanines* **2004**, *8*, 1009-1014.
50. Kessel, D.; Oteinick, N. L., Initiations of Autophagy by Photodynamic Therapy. In *Methods in Enzymology Vol 453: Autophagy in Disease and Clinical Applications, Pt C*, Klionsky, D. J., Ed.2009; Vol. 453, pp 1-16.
51. Kochevar, I. E.; Redmond, R. W., Photosensitized production of singlet oxygen. *Methods in Enzymology* **2000**, *319*, 20-28.

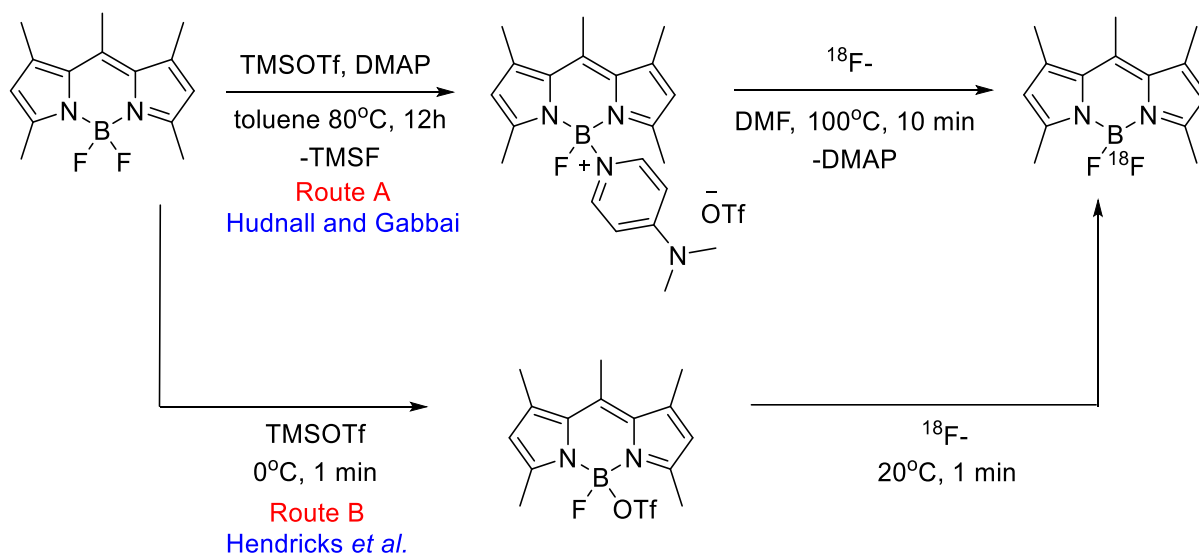
52. Rosso, M.; Nguyen, A. T.; de Jong, E.; Baggerman, J.; Paulusse, J. M. J.; Giesbers, M.; Fokkink, R. G.; Norde, W.; Schroen, K.; van Rijn, C. J. M.; Zuilhof, H., Protein-Repellent Silicon Nitride Surfaces: UV-Induced Formation of Oligoethylene Oxide Mono layers. *ACS Applied Materials Interfaces* **2011**, *3*, 697-704.

## CHAPTER 4: SYNTHESIS, SPECTROSCOPIC, AND IN VITRO EVALUATION OF NEAR-IR BODIPYS WITH MULTI-MODE IMAGING APPLICATIONS

### 4.1 Introduction

Fluorophores that allow for imaging using various modalities with minimal modification to the chemical structure are useful for imaging and three dimensional mapping of cancerous tissues and masses. Specifically, radioisotopic driven imaging techniques, including PET and SPECT, offer significant benefits to tumor mapping over other imaging techniques. BODIPYs hold substantial potential to serve as multi-modal imaging agents, due to their characteristic tunable fluorescence and their ability to undergo facile modifications via a variety of well-established synthetic methodology to install desired radioisotopes, specifically radiofluorine and radioiodine. However, while optical imaging via fluorescence does allow for *in vivo* visualization over a broad scope from subcellular to whole body anatomical imaging, the limited optical transparency of tissues hinders its widespread application.<sup>1,2</sup> On the other hand, PET and SPECT are used clinically but are limited to macroscopic spatial and temporal imaging. Therefore, imaging agents that allow for seamless switching between fluorescence and radioimaging would be highly beneficial for multidimensional imaging. Improvements in the realm of PET agents that are capable of being visualized at the microscopic level, as well as the development of hybrid imaging probes that allow for the superimposition of signal maps to visualize the macro- and microscopic physiological events of cancers and other diseases,<sup>3</sup> would fulfill many necessary improvements in clinical imaging and diagnosis. The development of hybrid optical/radioimaging probes has been hindered as a result of methodological limitations, proving the need for a synthetic strategy that enables generic access to these type of compounds.

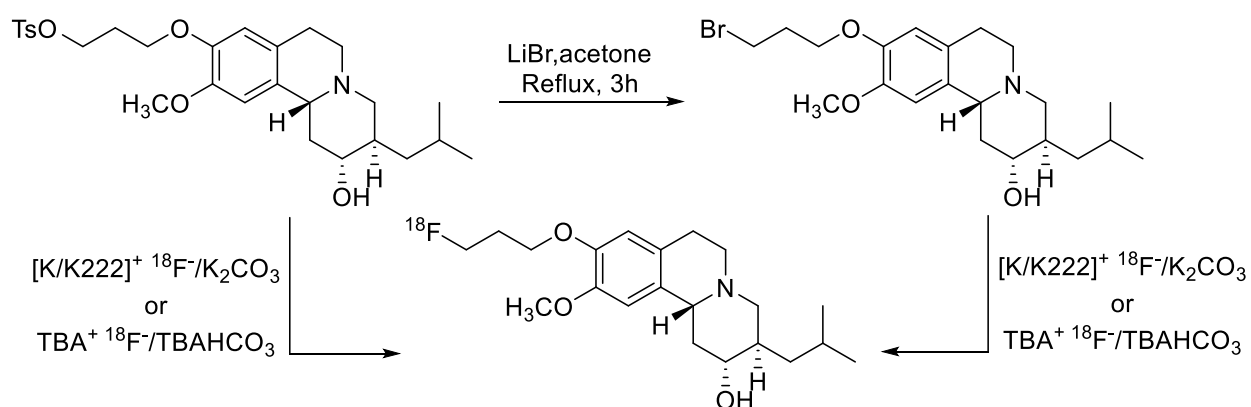
To date, several reports have detailed methodology to install  $^{18}\text{F}$  on BODIPY via substitution of the boron chelate as shown in Scheme 4.1. Hudnall and Gabbai<sup>4</sup> developed the first protocol, Route A, in which 1,3,5,7,8-pentamethyl BODIPY was first treated with TMSOTf and DMAP at elevated temperatures for an extended period of time to facilitate substitution of fluorine with DMAP. This reasonably stable, yet reactive intermediate was then treated with fluorine-18 (half-life of 110 minutes) anions in DMF at 100°C to afford the radiofluorine labeled BODIPY. Despite the success of this method, the conditions required for this approach are likely to be incompatible with many functional groups. As a result, a few years later Hendricks and co-workers<sup>5</sup> noted that treatment of the same BODIPY with TMSOTf at 0°C afforded the triflyl-substituted BODIPY almost instantaneously, Route B. This intermediate could be stabilized by adding a small amount of mild, non-nucleophilic base, such as diisopropylethylamine or 2,6-lutidine, and would remain as the triflyl-BODIPY in solution at room temperature for a prolonged period of time. When desired, fluorine-18 anions could be introduced with rapid and complete conversion to the radiolabeled BODIPY.



Scheme 4.1: Fluoride exchange of BODIPY.<sup>4,5</sup>

Hendricks *et al.* went on to investigate the *in vivo* stability and found that the non-targeting <sup>18</sup>F-BODIPY did not display tissue-specific labeling and was eliminated from the system within 1 hour. Additionally, their protocol was applied to BODIPYs bearing *N*-hydroxysuccinimide-ester moieties which demonstrated high stability under these conditions and allowed for clean TMSOTf activation and re-fluorination.

Alternatively, simple nucleophilic substitution of a sufficiently labile leaving group at the terminal end of an appended spacer moiety, as shown in Scheme 4.2, would enable the streamlined production of a multitude of radioimaging agents. Kung *et al.*<sup>6</sup> made use of a tosylated-alcohol terminated spacer or a bromine terminated spacer attached to dihydrotetrabenazine which underwent <sup>18</sup>F-substitution via two radiofluorinating agents, [<sup>18</sup>F]KF/K22 and [<sup>18</sup>F]TBAF, to obtain the desired <sup>18</sup>F-dihydrotetrabenazine. It was noted that the reaction showed little preference in achieving the desired fluorinated product in terms of precursor (-OTs vs -Br), with both offering efficient production. Optimization of reaction time, temperature, and solvent were necessary to establish an effective protocol for fluorination, and may produce challenges if the same strategy is applied to BODIPY fluorophores with similar appendages.

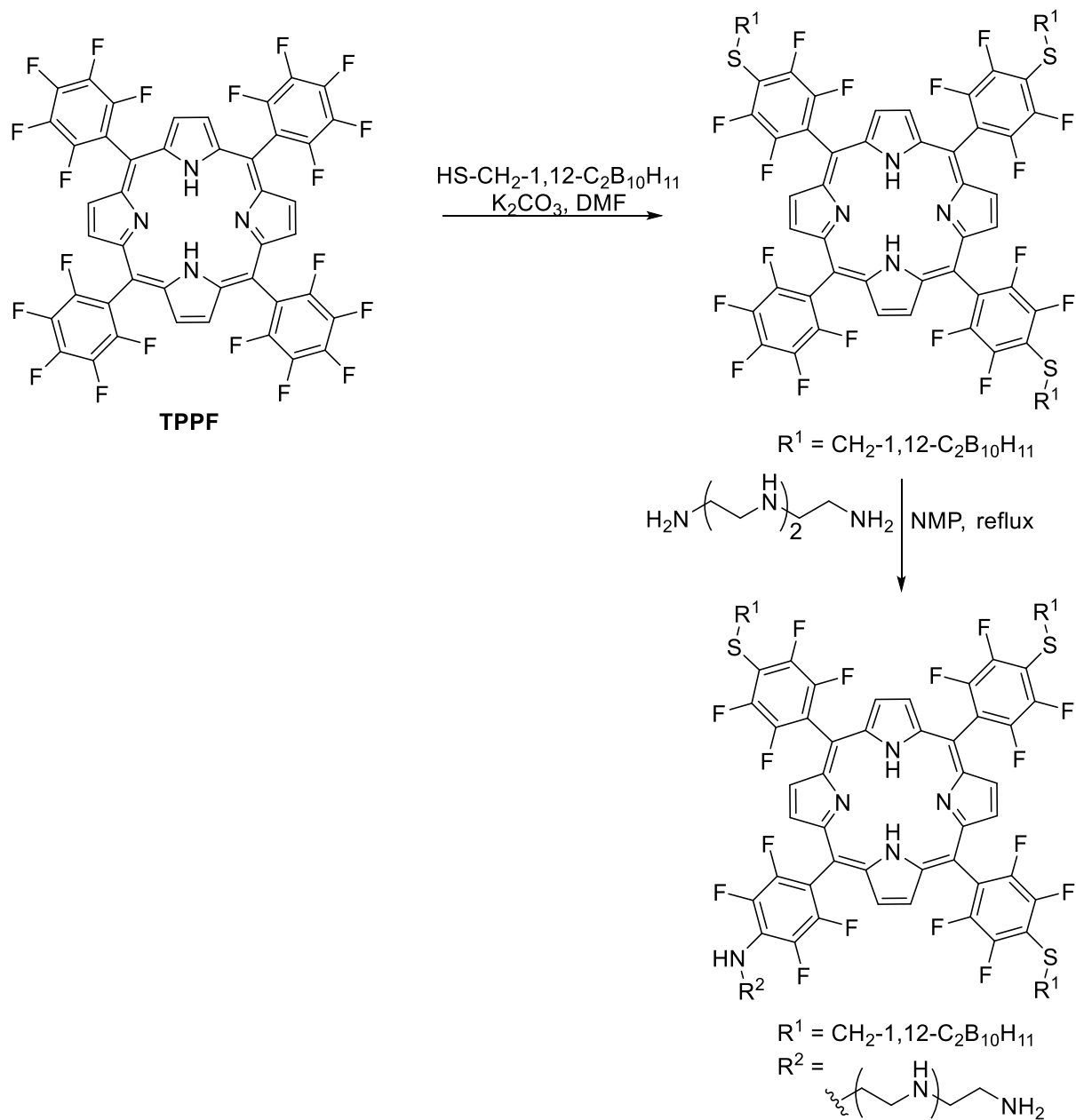


#### Scheme 4.2: Fluorination via nucleophilic substitution.<sup>6</sup>

In another approach, BODIPYs bearing highly electron deficient pentafluorophenyl moieties<sup>7</sup> may undergo nucleophilic substitution of the *para*-fluoride to directly yield radiolabeled BODIPYs through the addition of radiofluorine or radioiodine containing salts, such as [<sup>18</sup>F]TBAF or Na<sup>124</sup> I, or through substitution of a previously installed spacer moiety bearing a labile terminal leaving group as described previously. Several reports are available that detail the nucleophilic substitution of the *p*-fluoro phenyl moieties of porphyrins and porphyrin derivatives.<sup>8-10</sup> Bhupathiraju and Vicente<sup>11</sup> have recently reported a tetrakis(pentafluorophenyl)porphyrin (TPPF) that underwent facile nucleophilic substitution of the *para*-fluorines with both sulfur and nitrogen nucleophiles, Scheme 4.3. With BODIPY possessing similar behavior to porphyrins in terms of reactivity, these substitutions could lead to facile attachment of radiolabeling moieties. Direct fluorination of the 2,6-positions of the BODIPY aromatic system may also be accomplished using *N*-fluorophyridinium triflate, a mild fluorinating agent, that has shown success in the *meso*-perfluorination of porphyrins.<sup>12</sup>

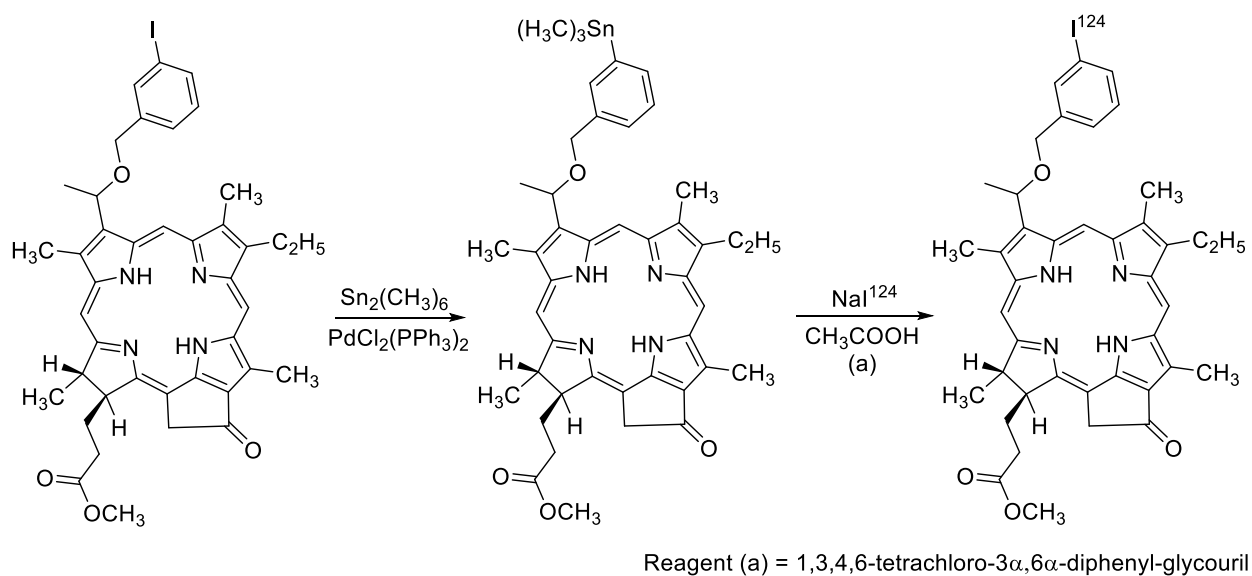
On the other hand, radioisotopes can possibly be installed via substitution of a trimethylstannyl derivative, as shown in Scheme 4.4. Pandey *et al.*<sup>13, 14</sup> successfully installed iodine-124 onto 3-(1'-*m*-iodobenzyloxyethyl)pyropheophorbide-*a* methyl ester by first reacting the pheophorbide derivative with hexamethylditin and bis(triphenylphosphine)palladium(II) dichloride, to give the trimethyltin derivative. This intermediate was then reacted with Na<sup>124</sup>I in acetic acid in the presence of 1,2,4,6-tetrachloro-3 $\alpha$ ,6 $\alpha$ -diphenylglucouril to yield the desired radioiodine labeled pheophorbide derivative. The glucose and galactose conjugates of the pheophorbide derivative withstood the Na<sup>124</sup>I substitution of the trimethylstannyl-substituent,

displaying the mild nature of these reaction conditions in the presence of biomolecules and its future applicability to biomolecules conjugated to various radioisotope-ready fluorophores.



Scheme 4.3: Nucleophilic aromatic substitution of pentafluoroporphyrin (TPPF).<sup>11</sup>

Nevertheless, to date, only a handful of BODIPY-based PET agents have been synthesized and there are no reports of radiolabeled BODIPY for SPECT. Through the combination of known protocols, including Knoevenagel condensation, which successfully extends  $\pi$ -conjugation to produce long wavelength BODIPYs with absorptions and emissions that extend into the far red and near-IR regions of the visible spectrum, with the previously discussed methods for introducing radioisotopes for PET and SPECT, a new strategy for the development of dual-modal imaging - agents based on BODIPY will be explored herein.



Scheme 4.4: Trimethylstannyl-mediated radiolabeling.<sup>13</sup>

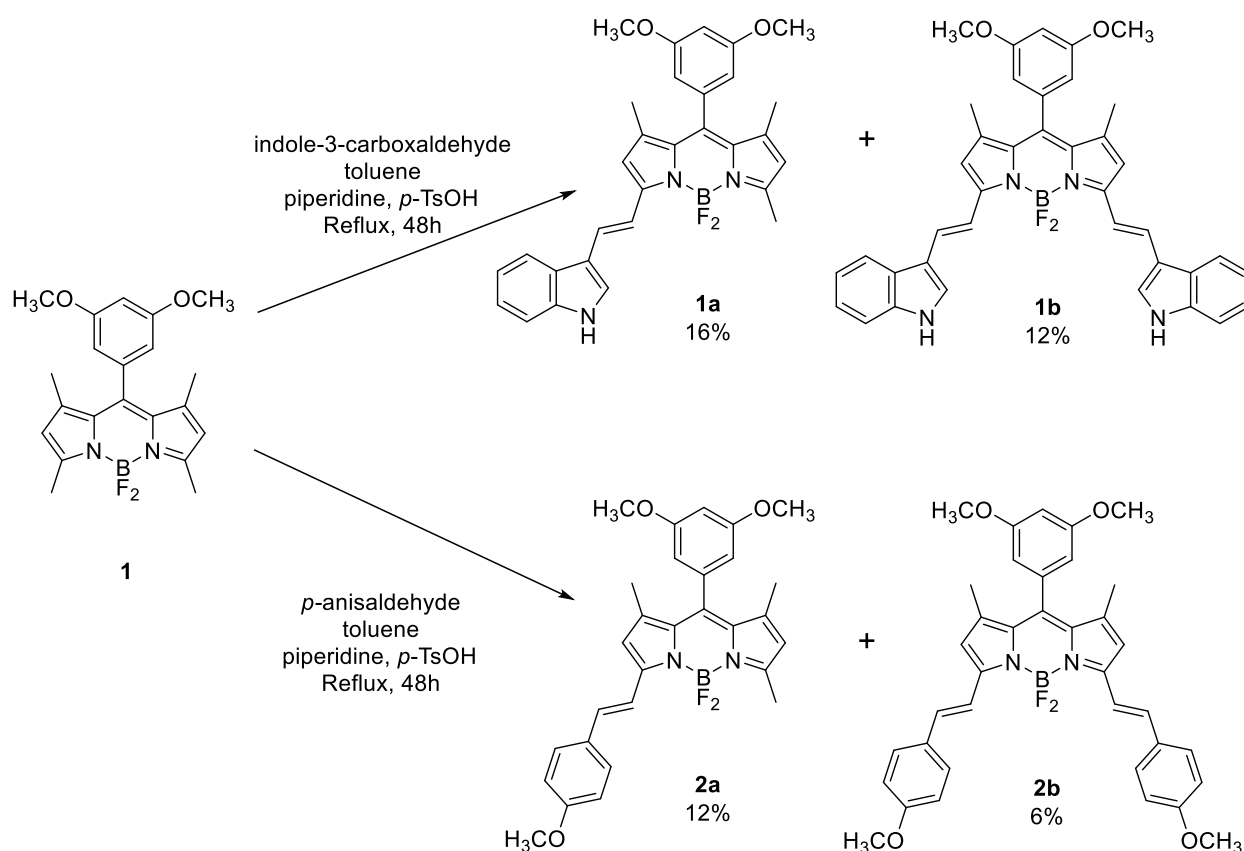
## 4.2 Results and Discussion

### 4.2.1 Syntheses

The synthesis of far red and near-IR mono- and di-styryl 2,6-diiodo-BODIPYs explored in Chapter 3 with varying cytotoxicities prompted the need to explore the potential of the non-toxic fluorophores as dual-modal fluorescence/radioimaging agents. None of the di-styryl-diiodo-

BODIPYs (**3a-e**, Chapter 3) showed phototoxicity,  $IC_{50} > 100$ , when exposed to a light dose of  $1.5 \text{ J/cm}^2$ , however, the presence of iodines made these compound more susceptible to oxidation and tended to decompose when left in the presence of light for too long. As a result, near-IR dyes that lack iodines at the 2,6-positions of the BODIPY core were synthesized using the well-established Knoevenagel condensation protocol.

For direct comparison to the previously synthesized compounds with the most red-shifted absorption and emission profiles (**2a**, **3a**, Chapter 3), and with the greatest stability (**2b**, **3b**, Chapter 3), mono- and di-indolylstyryl and *para*-methoxyphenylstyryl were synthesized from BODIPY **1**, Scheme 4.5. Condensation of **1** with excess indole-3-carboxyaldehyde in refluxing toluene in the presence of piperidine and *p*-TsOH yielded mono-indolylstyryl-BODIPY **1a** as a purple solid in 16% yield and di-indolylstyryl-BODIPY **1b** as a blue solid in 12% yield.<sup>15</sup>



Scheme 4.5: Knoevenagel condensation of BODIPY **1** with formyl-indole and *p*-anisaldehyde.

Similarly, the mono- and di-*p*-methoxyphenylstyryl-BODIPYs **2a** and **3a** were synthesized via condensation with excess *p*-anisaldehyde to afford the desired compounds as purple and blue solids in 12% and 6%, respectively. The low yields of these condensations are likely a result of the presence of water in the reaction mixture, both from water containing solvent and as a by-product of the condensation. Even with the addition of 3Å molecular sieves, yields remained low. In order to improve yields, the reaction flask should be fitted with a Soxhlet extractor filled with calcium chloride, as described by Hao *et al.*,<sup>16</sup> for the toluene to be dried over the course of the reaction. Removal of water from the starting solvents, by first drying over molecular sieves, would also improve the yield of both the mono and distyryl-BODIPYs. With such an excess of aldehyde

being employed, the reaction should favor formation of the more favorable greater red-shifted distyryl-BODIPYs.

BODIPY **1a**, **1b**, **2a**, and **2b** were characterized by  $^1\text{H-NMR}$ ,  $^{13}\text{C-NMR}$ , and high resolution ESI-MS. Comparison with the  $^1\text{H-NMR}$  data obtained from the diiodo-analogs revealed the same profile of peaks for the indolylstyryl- and *p*-methoxyphenylstyryl- aromatic protons, as well as the signals for the remaining 1,5,7- and 1,7-methyls found in the mono- and di-derivatives, respectively. Seven signals were visible in both **1a** and **1b** corresponding to the indolylstyryl substituent, observed at 8.4 (NH), 8.17/8.07 (di/mono), 7.87/7.75 (di/mono), 7.54, 7.53, 7.42, and 7.30 ppm. The only notable difference between the diiodo- and iodine-free dyes was the presence of peaks corresponding to the  $\beta$ -hydrogens. The spectra of the mono-indolyl **1a** revealed two equivalent peaks for these hydrogens at 6.6 and 6.0 ppm. These were identified through comparison to the starting BODIPY **1** and di-indolylstyryl-BODIPY **1b** as the  $\beta$ -hydrogen on the styryl-bearing hemisphere (6.6 ppm) and the  $\beta$ -hydrogen on the methyl-bearing hemisphere (6.0 ppm). With the return to symmetry in **1b** the two  $\beta$ -hydrogen signals merged into one at 6.6 ppm.

The geometry of the styryl-alkene were confirmed as the suspected *trans* (E) configuration through determination of the coupling constants (J) at 16.1 and 16.5 Hz. The division of the two equivalent tetramethyl peaks at 2.5 and 1.6 ppm in the starting material into three signals at 2.6, 1.6, and 1.2 ppm confirmed the identity of the mono-indolylstyryl-BODIPY **1a**. Condensation with the remaining 3/5-methyl to yield the di-indolylstyryl **1b** was observed by loss of the signal at 2.6 ppm and a doubling of the integration of the peak at 1.6 ppm, as expected. Finally, HR-MS via ESI-TOF confirmed the desired products with *m/z* found at 511.2253 (**1a**) and 638.2677 (**1b**).

Likewise,  $^1\text{H-NMR}$  of BODIPYs **2a** and **2b** exhibited four aromatic signal in two equivalent sets corresponding to the styryl phenyl at 7.6/7.56 ppm (di/mono) and 6.98/6.92 ppm

(di/mono) and to the styryl alkene at 7.64/7.57 ppm (di/mono) and 7.24 ppm. Again, the *trans* (E) configuration of the styryl-alkene were confirmed with coupling constants (J) calculated at 16.3 Hz. The  $\beta$ -hydrogen followed an identical pattern to that described for **1a,b** with signals visible at 6.6 and 6.0 ppm in **2a** and 6.6 ppm in **2b**. The three equivalent methyl groups of **2a** were observed at 2.6, 1.6, and 1.5 ppm indicating loss of symmetry, and a return to symmetry in **2b** with only a single signal visible at 1.6 ppm corresponding to the 1,7-dimethyls. The most noticeable difference between the starting BODIPY **1**, **2a**, and **2b** was the appearance of a second methoxy peak at ~3.8 ppm and its increase in integration from three to six with the addition of the second styryl arm. Confirmation of both BODIPYs was also achieved via high resolution ESI-TOF MS through identification of m/z peaks for **2a** at 503.2320 and **2b** at 621.2725.

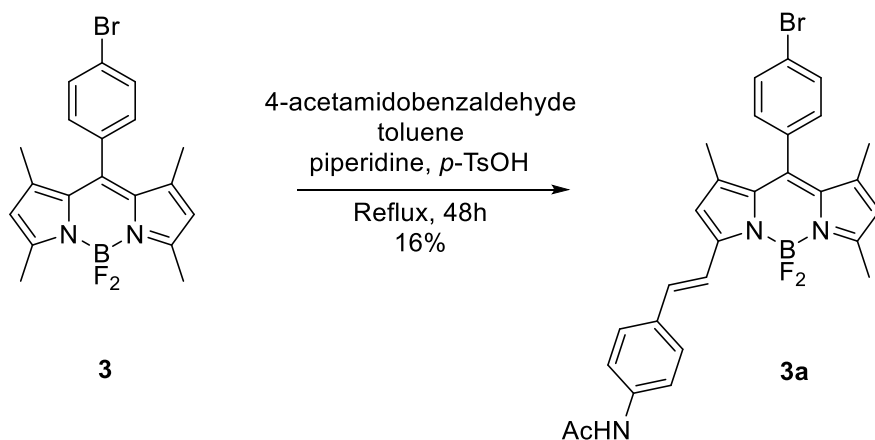
Attempts to iodinate the styryl-BODIPYs using the same protocol used to iodinate the tetramethyl-BODIPY derivatives with iodine and iodic acid in a 1:1 mixture of ethanol and DCM lead to decomposition, suggesting that the styryl arm alkenes are more nucleophilic than the 2,6-positions of the BODIPY core. This demonstrates that radioiodine cannot be added to the styrylated BODIPY via electrophilic aromatic substitution. Additionally, there have been no reports to date of nucleophilic aromatic substitution of the 2,6-positions, the only remaining active sites, and efforts of this lab to accomplish this task have proved unsuccessful. Thus, another method for radiolabeling must be explored. The previously described fluoride substitution with fluorine-18 may be employed to convert **1a**, **1b**, **2a**, and **2b** into PET radiotracers and will be discussed in the following pages.

In order to employ another tactic in hopes of securing a suitable route for labeling long wavelength absorbing and emitting BODIPYs, bromine-containing BODIPY **3a** was synthesized, Scheme 4.6. BODIPY **3**, bearing a *meso*-4-bromophenyl substituent, was condensed with excess

4-acetamidobenzaldehyde in refluxing toluene in the presence of piperidine and *p*-TsOH. It was hoped that the acyl-protected amine would mimic a conjugated biomolecule for the purpose of exploring the compound's photophysical properties. Free amines located on both the *meso*-substituent and conjugated through functionalized styryl groups are known to be highly basic and readily protonate to yield non-fluorescent dyes.<sup>17</sup> The mono-styryl BODIPY **3a** was the only isolated product from this reaction obtained in 16% yield. Trace amounts of the di product were visible by TLC but were not isolated. A large amount of the starting BODIPY **3** was returned unreacted even after exposure to excess aldehyde for 48 hours. This could be a result of low reactivity of the less electron-rich BODIPY, because of the electron-deficient aldehyde, the presence of water in the reaction mixture, or a combination of these effects. Future attempts to remove water from the reaction mixture using a calcium chloride filled Soxhlet extractor as described previously may effectively improve the yields of both the mono and di products. As a result of the low yields, only the mono-acetamidophenyl-BODIPY **3a** was evaluated.

Proton NMR characterization of **3a** strongly resembled that of BODIPY **2a** in the aromatic region and in regards to the 1,5,7-trimethyls. Two equivalent sets of two doublets corresponding to the equivalent the *meso*- and styryl-phenyl protons were identified at 7.66-7.65 and 7.21-7.19, as well as 7.38-7.36 and 7.12-7.11, respectively. The alkene protons were identified at 7.57-7.55 and 7.21-7.18, with a coupling constant calculated at 16.3 ppm indicating *trans* (E) geometry, as with all styryl BODIPYs. The  $\beta$ -hydrogens were split into two singlets of identical integration with the hydrogen on the same side as the styryl arm lying downfield at 6.6 ppm compared to the hydrogen on the same side as the 3/5-methyl located 6.02 ppm. The alkane region of the spectra indicated four signals relating to the three core methyl groups at 2.6, 1.47, and 1.43 ppm and the

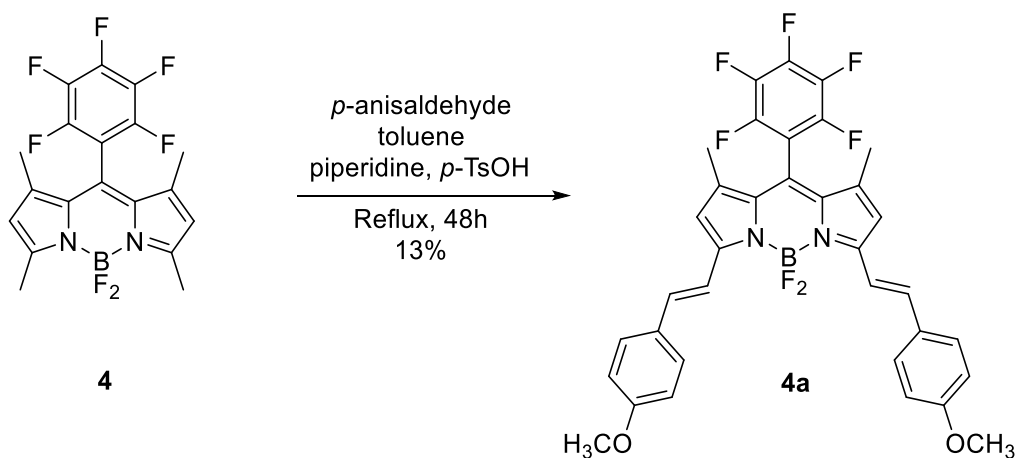
acetyl-methyl found downfield at 3.3 ppm. The molecular weight of BODIPY **3a** was confirmed as the  $[M+H]^+$  by high resolution ESI-MS with an  $m/z$  identified at 548.1372.



Scheme 4.6: Synthesis of BODIPY **3a**.

Additionally, a long wavelength BODIPY bearing the electron-deficient pentafluorophenyl substituent was synthesized with the hopes of later substitution of the *para*-fluorine with either radionuclei directly, via nucleophilic aromatic substitution, or through attachment of a pendent spacer with a terminal labile leaving group that could be subsequently substituted to yield the radiolabeled BODIPY. BODIPY **4** was synthesized from the condensation of 2,4-dimethylpyrrole and pentafluorobenzaldehyde as detailed in Chapter 2. The electron-deficient *meso*-pentafluorophenyl substituent of BODIPY **4** decreases the electron density in the BODIPY core and, as a result enhances the acidity of the 3,5-dimethyl protons. Consequently, the di-*p*-methoxyphenylstyryl-BODIPY **4a** was isolated as a green solid as the major product in 13% yield from the condensation of **4** with excess *p*-anisaldehyde in refluxing toluene in the presence of piperidine and *p*-TsOH, Scheme 4.7. The mono-*p*-methoxyphenylstyryl BODIPY was observed

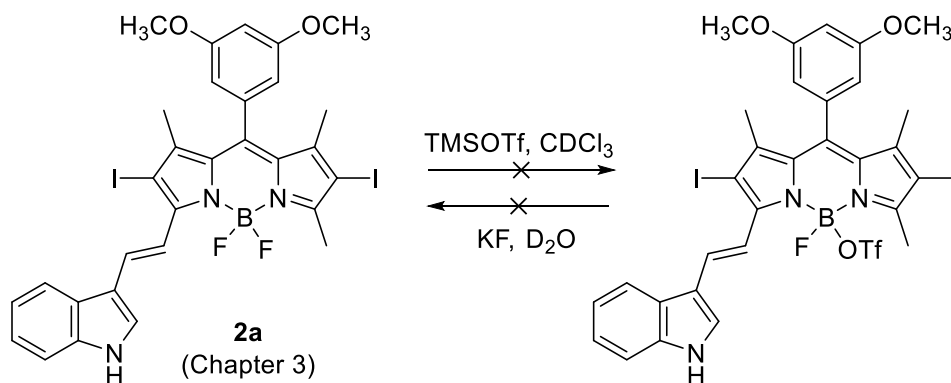
as a faint blue spot with red fluorescence when exposed to long wavelength UV light by TLC but was not isolated by column chromatography.



Scheme 4.7: Synthesis of BODIPY **4a** from pentafluorophenyl-BODIPY **4**.

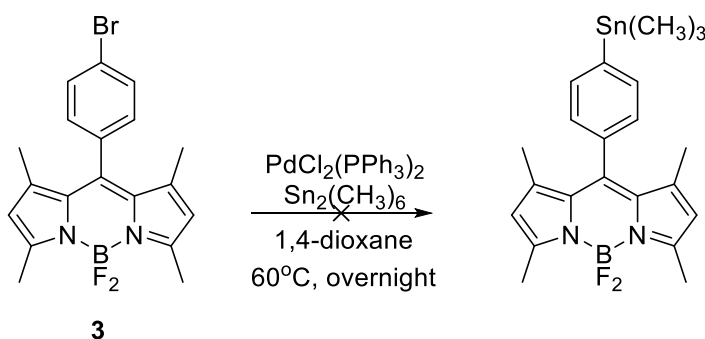
BODIPY **4a** displayed a similar, yet simplified  $^1\text{H-NMR}$  spectra in terms of the number of signals in comparison to the previously synthesized fluorophores. Because **4a** lacks *meso*-phenyl hydrogens, the aromatic region contains fewer peaks than **2a** and **3a**, which are similarly decorated. However, despite fewer signals being present, there is a greater degree of overlap between the signals that are present. A multiplet found at 7.67-7.58 ppm contains a singlet corresponding to the two  $\beta$ -hydrogens, a doublet representing one set of four equivalent styrylphenyl-hydrogens, and a second doublet belonging to two styryl-alkene protons. The remaining set of four equivalent styrylphenyl-hydrogens is seen as a doublet at 7.08-7.06 ppm, whereas the remaining two alkene protons show up as a doublet at 6.99-6.98 ppm with a coupling constant of 16.1 Hz indicating *trans* (E) geometry. An  $m/z$  peak at 673.1859 from HR-MS matching the calculated value for the  $[\text{M}+\text{Na}]^+$  ion further confirmed the identity of **4a**.

Several attempts were made to apply the previously mentioned protocols for substituting the fluorine bound to the boron center, to install trimethyltin to the halogen bearing *meso*-phenyl, and to substitute the *p*-fluorine of *meso*-pentafluorophenyl BODIPY. The procedure for F-substitution dictated by Hendricks *et al.*<sup>5</sup> was modified with the intent of allowing for facile monitoring of the boron substitution via <sup>11</sup>B-NMR, Scheme 4.8. Initial attempts were made on BODIPY **2a** from Chapter 3 by dissolving the BODIPY in deuterated chloroform and acquiring the NMR spectrum of the –BF<sub>2</sub> chelated structure.



deuterium oxide, was added in hopes that the addition of free fluoride ions would restore the structure, solubility, and fluorescence of the BODIPY. Regretfully, upon addition of KF, the solution remained non-fluorescent and the insoluble particles did not dissolve.

Next, Pandey *et al.*'s<sup>13, 14</sup> procedure for substituting an aromatic halide with trimethyltin with attempted on BODIPY **3** as a model system before subjecting the protocol to the more valuable **3a** as shown in Scheme 4.9. BODIPY **3** and bis(triphenylphosphine)palladium(II) chloride were dissolved in 1,4-dioxane, the solution was degassed, and the flask was fitted with an Argon balloon. To this solution was added hexamethyldistannane and the mixture was stirred at 60°C overnight. The solvent was then removed and the residue was purified by a short silica column using 50:50 DCM/hexanes as eluent to separate the single fluorescent band from the non-fluorescent bi-products residing at the baseline. NMR of the fluorescent band showed unreacted starting material.



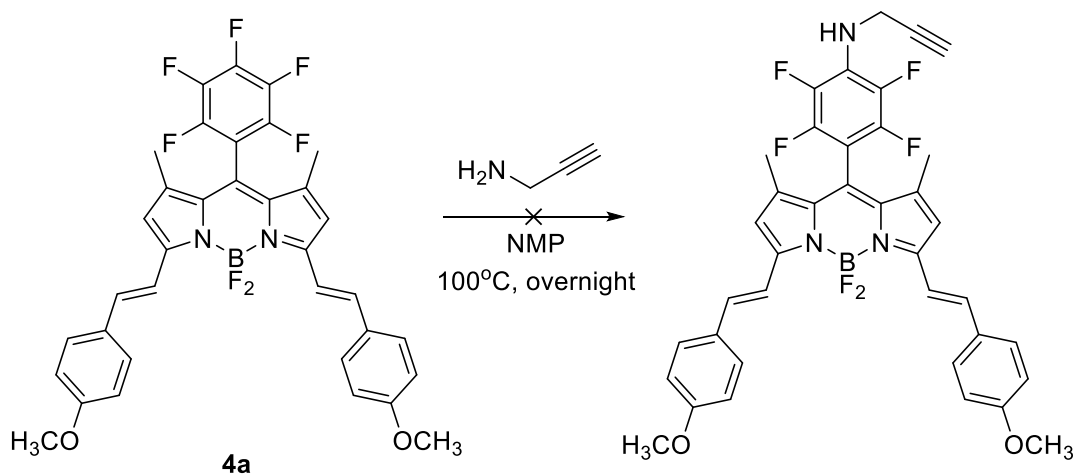
Scheme 4.9: Attempted substitution of **3** with hexamethyldistannane.

The primary differences between the halogenated BODIPY **3** and Pandey's iodo-phorphorbide derivative are the halogen being substituted, bromine versus iodine, the connectivity of the halogen on the halogen-bearing phenyl, and the conjugation of the system. First, iodine is a

more labile leaving group than bromine with its weaker carbon-halogen bond and may undergo the necessary oxidative insertion onto palladium more readily. Next, the phenyl ring containing the iodine that underwent substitution of the pheophorbide derivative was not conjugated with the pheophorbide macrocycle, whereas the bromine-bearing phenyl of the BODIPY is connected to the conjugated core. Although the *meso*-aryl substituent is known to lie perpendicular to the BODIPY core, direct connection of the two aromatic systems may make the carbon-bromine bond stronger than expected. Additionally, the bromine resides at the *para*-position of the phenyl on BODIPY, which imparts a greater effect on the electronics of the phenyl ring compared to the *meta*-iodine of the pheophorbide. Nevertheless, the simplest explanation may be that the palladium used to install the trimethyltin was not reduced to palladium(0) *in situ* as is required for the oxidative insertion to occur. Addition of a reducing agent, such as copper(I) iodide may facilitate this conversion.

The final attempt to synthesize a near-IR BODIPY suitable for radioimaging involved the substitution of the *para*-fluorine of BODIPY **4a**, Scheme 4.10. Assuming that the electron-deficient *meso*-pentafluorophenyl would behave similarly to porphyrins bearing the same substituent,<sup>11</sup> BODIPY **4a** was subjected to nucleophilic substitution by an amine. The BODIPY and propargyl amine were dissolved in *N*-methyl-pyrrolidinone and the mixture was allowed to stir at 100°C. Propargyl amine was selected for its capacity to only undergo nucleophilic substitution at the amine and for possible subsequent “click” couplings with azides, if successful. After two hours, TLC showed a new, more polar blue spot below the green spot of starting material. The product was expected to be of similar polarity to the starting material and display no change in the fluorescence intensity. The new spot showed much brighter fluorescence under long

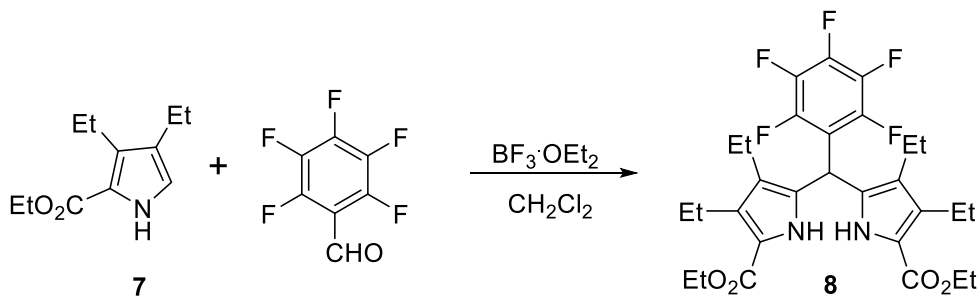
wavelength UV light, which suggests that the product was likely being converted to the mono-styryl product.



Scheme 4.10: Attempted nucleophilic substitution of BODIPY **4a**.

Future work to furnish an efficient protocol for installing radioisotopes for PET and SPECT imaging is planned. The substitution of bromine with trimethyltin of BODIPY **3** with the addition of copper iodine to induce *in situ* reduction of palladium(II) will be attempted. Since the double bonds of the styryl arms of the long wavelength BODIPYs are reactive towards nucleophiles and electrophiles, as seen through failed attempts at nucleophilic substitution on the *meso*-phenyl and preliminary attempts to iodinate  $\beta$ -free styryl-BODIPYs resulting in decomposition, design of long wavelength BODIPYs via other routes is necessary. Preliminary work to synthesize a *meso*-pentafluorophenyl BODIPY from a conjugated pyrrole has begun. The successful Suzuki coupling of benzyl 4-chloro-5-iodo-3-methyl-1H-pyrrole-2-carboxylate **5** with 4-methoxyphenyl boronic acid yielded pyrrole **6a** or **6b** after refluxing in toluene in the presence of tetrakis(triphenylphosphine)palladium(0) and 1M sodium carbonate, Scheme 4.11. NMR shows





Scheme 4.12: Synthesis of dipyrromethane **8**.

### 4.2.2 Spectroscopic Investigations

The spectroscopic properties of BODIPYs **1a,b**, **2a,b**, **3a**, and **4a** were carried out in DMSO using methylene blue in methanol ( $\Phi_F = 0.03$ ) as the standard and are summarized in Figures 4.1 - 4.2 and Table 4.1. DMSO was chosen as the sole solvent since it most closely resembles how BODIPYs behave in the polar environment of the body. Incorporation of the styryl groups produces a pronounced red shift in the absorbance and emission profiles compared to the 1,3,5,7-tetramethyl BODIPYs, which absorb around 500 nm and emit around 510 nm. Addition of a single styryl arm produces approximately 70 - 100 nm red-shift as seen in BODIPYs **1a**, **2a**, and **3a**. Among the mono-styryl BODIPYs, the indolylstyryl BODIPY **1a** produces the greatest red-shift as a result of the extended  $\pi$ -conjugation compared to the phenylstyryl **2a** and **3a**. Phenylstyryl-BODIPYs bearing electron withdrawing groups on the styryl arm, as in the amide of **3a**, induce a slightly greater red shift (6 nm) than phenylstyryl-BODIPY **2a** bearing an electron donating substituent. The emission spectra also show the same trend, displaying 70 – 120 nm red-shifts compared to the simple tetramethyl BODIPY. Incorporation of a second styryl group, BODIPYs **1b**, **2b**, and **4a**, created an even greater red shift of 150 – 190 nm in the absorption and 140 – 210 nm in the emission profile, due to greater extension of the fluorophore's  $\pi$ -conjugation. The absorption bands also became broader with the addition of multiple styryl substituents.

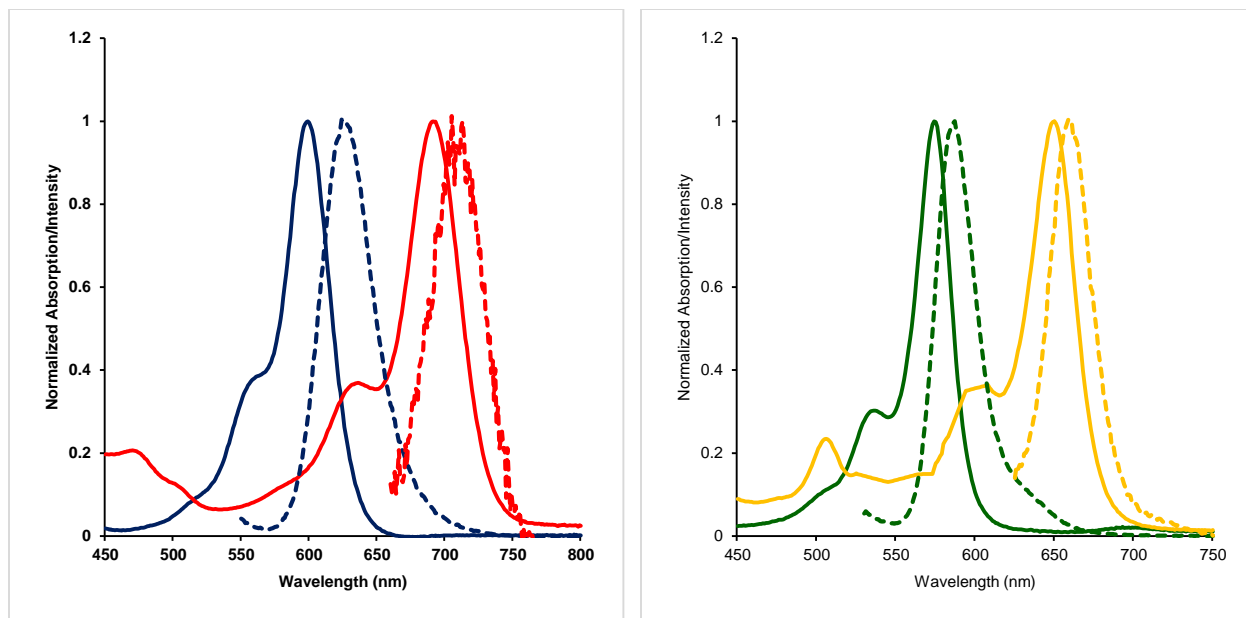


Figure 4.1: Absorption (solid line) and emission (dashed line) of BODIPYs **1a** (blue) and **1b** (red) on the left and BODIPYs **2a** (green) and **2b** (yellow) on the right in DMSO.

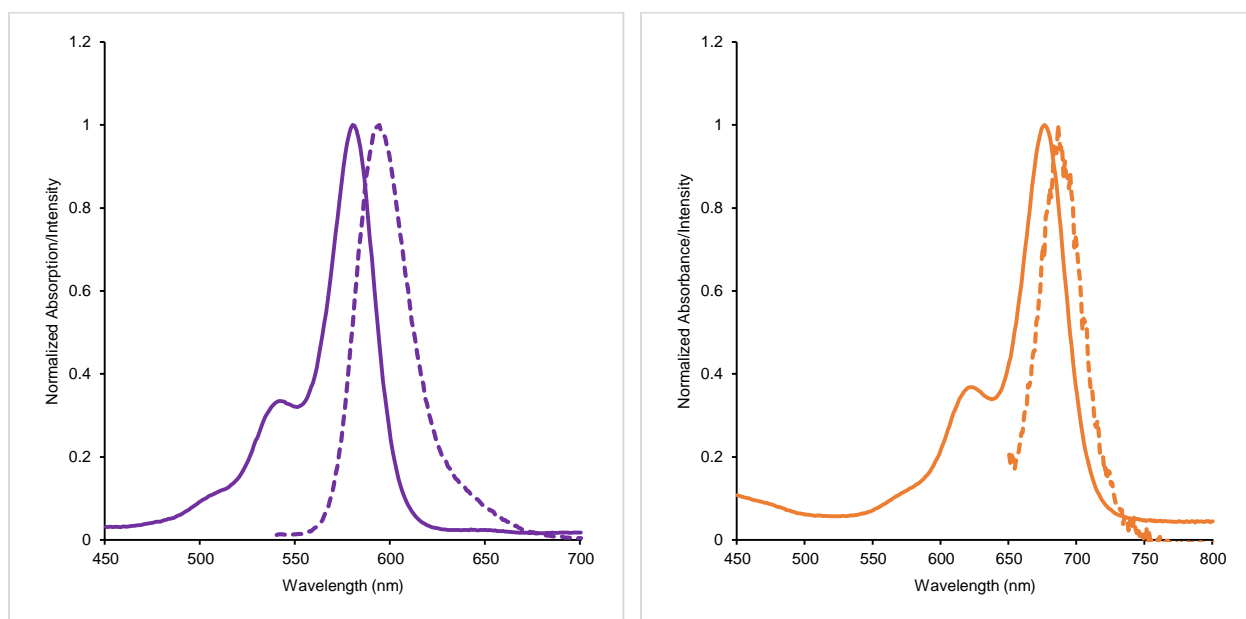


Figure 4.2: Absorption (solid line) and emission (dashed line) of BODIPY **3a** (purple) on the left and BODIPY **4a** (orange) on the right in DMSO.

Table 4.1: Absorption and emission properties of BODIPYs in DMSO relative to methylene blue ( $\Phi_f = 0.03$ , MeOH).

Compound	$\lambda_{\max}$ abs (nm)	$\lambda_{\max}$ em (nm)	log $\epsilon$	$\Phi_f$	Stokes' Shift (nm)
<b>1a</b>	599	637	4.60	0.46	38
<b>1b</b>	691	724	4.62	0.06	33
<b>2a</b>	574	587	4.29	0.73	13
<b>2b</b>	650	667	4.55	0.18	17
<b>3a</b>	580	597	4.12	0.54	17
<b>4a</b>	676	697	4.60	0.16	21

All BODIPYs displayed the characteristic Q-band absorption for the  $S_0$ - $S_1$  ( $\pi$ - $\pi^*$ ) electronic transition with a shoulder at slightly lower wavelength corresponding to the vibrational translations.<sup>19</sup> Additionally, the styryl-BODIPYs displayed large extinction coefficients (log  $\epsilon = 4.12 - 4.62$ ) and Stokes' shifts of 13 - 38 nm, with the largest shift seen in the indolylstyryl-BODIPYs **1a,b**. Compared to the diiodo-styryl-BODIPYs discussed in Chapter 3, the  $\beta$ -free BODIPYs possessed larger fluorescence quantum yields of 0.46 - 0.73 for the mono-styryl-BODIPYs and 0.06 - 0.18 for the di-styryl-BODIPYs. Quantum yields greater than 0.2 are desirable for fluorescence imaging to better distinguish the fluorophore from endogenous chromophores.

### 4.2.3 *In vitro* Studies

**4.2.3.1 Cytotoxicity.** In order to determine the efficacy of the synthesized BODIPYs as potential imaging agents, their concentration-dependent dark and photo (light dose  $\sim 1.5$  J/cm<sup>2</sup>) cytotoxicities were investigated using the Cell Titer Blue assay in human carcinoma HEP2 cells,

the results of which are summarized in Figure 4.3. All of the BODIPYs were non-toxic in the dark ( $IC_{50} > 400 \mu\text{M}$ ) with the exception of di-methoxyphenylstyryl-BODIPY **2b** which was slightly toxic ( $IC_{50} \sim 150 \mu\text{M}$ ). Furthermore, none of the BODIPYs were phototoxic when exposed to an approximately  $1.5 \text{ J/cm}^2$  light dose, with  $IC_{50}$  values greater than  $100 \mu\text{M}$ . These results were as expected, in comparison to similar di-iodo-styryl-BODIPYs discussed in Chapter 3.

**4.2.3.2 Time-Dependent Cellular Uptake.** The time-dependent cellular uptake of all BODIPYs at a  $10 \mu\text{M}$  concentration were evaluated in HEP2 cells over a 24 hour period, and are shown in Figure 4.4. The mono-styryl BODIPYs **1a** and **2a** displayed similar uptake and were more internalized by cells than the di-styryl-BODIPYs **1b** and **4a**. The di-methoxyphenylstyryl-BODIPY **2b** was internalized the greatest, likely as a result of its more hydrophilic character from the four methoxy-substituents it contains. The cellular uptake of **3a** produced interesting results, surpassing the standard used in concentration determining calculations. Consequently, the uptake of this compound bears repeating to accurately quantify this compound's internalization.

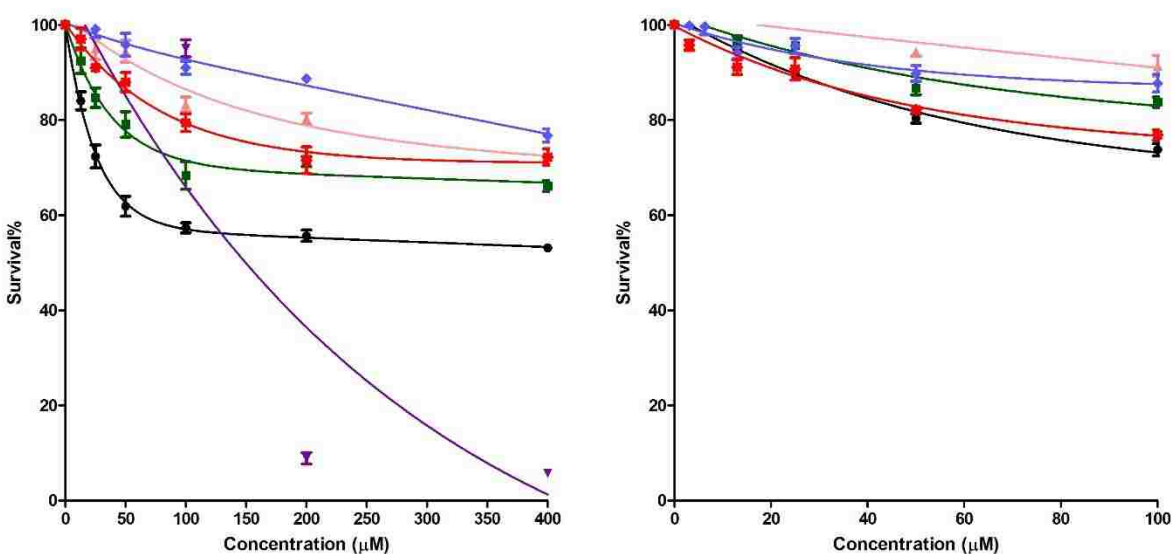


Figure 4.3: Dark toxicity (left) and phototoxicity (right, 1.5 J/cm<sup>2</sup>) of BODIPYs **1a** (black), **1b** (green), **2a** (pink), **2b** (purple), **3a** (blue), and **4a** (red) at 10  $\mu$ M by HEp2 cells.

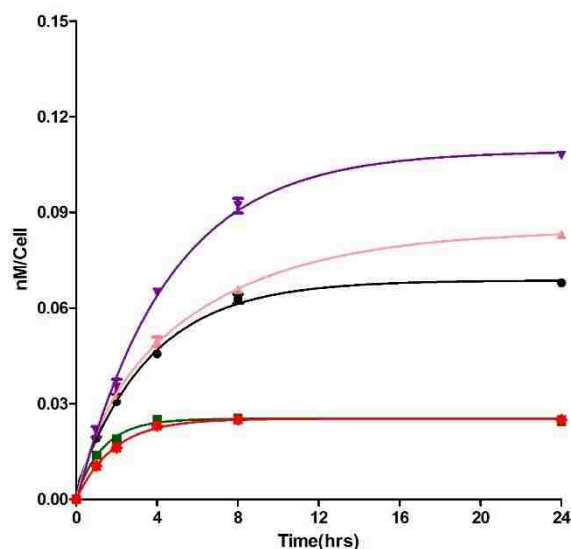


Figure 4.4: Time-dependent cellular uptake of BODIPYs **1a** (black), **1b** (green), **2a** (pink), **2b** (purple), and **4a** (red) at 10  $\mu$ M by HEp2 cells.

### 4.3 Conclusions

A series of six styryl-BODIPYs were synthesized from  $\beta$ -free BODIPYs with the intent of producing long wavelength absorbing and emitting dyes of sufficient fluorescence quantum yield, that would readily undergo modification to include radioisotopes of fluorine and/or iodine for multi-modal near-IR fluorescence/PET/SPECT imaging. All of the BODIPYs displayed significantly red-shifted spectral profiles compared to their starting materials, with absorbances ranging from 570 nm to 690 nm. Although the di-styryl BODIPYs **1b**, **2b**, and **4a** possessed the most long wavelength absorbances ( $> 650$  nm), they were significantly less fluorescent than the mono-styryl BODIPYs **1a**, **2a**, and **3a**, with  $\Phi_F$  of 0.06 – 0.18 and 0.46 - 0.73, respectively. Favorably, all BODIPYs were non-toxic in the dark ( $IC_{50} > 400 \mu$ M) with the exception of the mildly toxic **3a** with an  $IC_{50} \sim 150 \mu$ M, and non-phototoxic ( $IC_{50} > 100 \mu$ M), making all

compounds potentially suitable as imaging agents. However, despite several attempts to modify the variously decorated BODIPYs to bearing potential radioisotopes, none suitable for multi-modal imaging were acquired. Future endeavors are necessary to produce long wavelength absorbing and emitting dyes with high fluorescence quantum yields capable of undergoing late state modification to incorporate radioisotopes of fluorine and iodine.

## 4.4 Experimental

### 4.4.1 General Information

Reagents and solvents were acquired from Sigma Aldrich and used without further purification. Reactions were monitored by TLC using 0.2 mm silica plates with UV indicator (UV254). Column chromatography was executed using Sorbent Technologies 60Å silica gel (230 - 400 mesh). Merck TLC silica gel 60 glass plates were used for preparative thin layer chromatography. All  $^1\text{H}$  NMR and  $^{13}\text{C}$  NMR spectra were obtained using a Bruker AV-500 or AV-400 (500 MHz or 400 MHz for  $^1\text{H}$ , 100 MHz for  $^{13}\text{C}$ ) with samples dissolved in deuterated chloroform or acetone using trimethylsilane as an internal indicator. Chemical shifts ( $\delta$ ) are conveyed in ppm with  $\text{CDCl}_3$  ( $^1\text{H}$ : 7.27 ppm;  $^{13}\text{C}$ : 77.16 ppm) and acetone- $\text{d}_6$  ( $^1\text{H}$ : 2.05 ppm;  $^{13}\text{C}$ : 29.84 ppm) used as references. Coupling constants (J) are stated in Hertz (Hz). High resolution ESI mass spectra were obtained using an Agilent Technologies 6210 ESI-TOF Mass Spectrometer.

### 4.4.2 Syntheses

**BODIPYs 1a and 1b:** BODIPY **1** (0.1 g, 0.26 mmol), indole-3-carbaldehyde (0.11 g, 0.78 mmol), and p-TsOH (0.01 g) were dissolved in dry toluene (60 mL) over 3 Å molecular sieves. To this solution was added piperidine (0.4 mL) and the mixture was at reflux for 48 hours. Upon cooling,

the reaction was filtered to remove the sieves and the filtrate was quenched with water and extracted with CH<sub>2</sub>Cl<sub>2</sub>. The combined organic layers were dried over Na<sub>2</sub>SO<sub>4</sub> and the solvent was removed under vacuum. The resulting residue was purified by silica column chromatography using 50:50 hexanes/CH<sub>2</sub>Cl<sub>2</sub> (v/v) to afford 0.021 g of a purple solid, **1a**, in 16% yield and 0.019 g of a blue solid, **1b**, in 12% yield.

*Data For 1a:* <sup>1</sup>H-NMR (400 MHz, CDCl<sub>3</sub>) δ 8.41 (s, 1H), 8.07-8.05 (d, *J* = 7.3, 1H), 7.75-7.70 (d, *J* = 16.1, 1H), 7.54 (s, 1H), 7.54-7.50 (d, *J* = 16.1, 1H), 7.42-7.39 (d, *J* = 6.2, 1H), 7.30-7.29 (m, 2H), 6.66 (s, 1H), 6.56 (s, 1H), 6.51-6.50 (d, *J* = 2.2, 2H), 6.00 (s, 1H), 3.81 (s, 6H), 2.62 (s, 3H), 1.62 (s, 3H), 1.26 (s, 3H); <sup>13</sup>C-NMR (100 MHz, CDCl<sub>3</sub>) δ 161.50 153.13, 142.98, 140.96, 138.72, 137.04, 136.89, 136.34, 130.88, 130.23, 126.24, 125.57, 123.21, 121.43, 120.50, 120.39, 117.23, 115.93, 115.63, 111.49, 106.35, 105.42, 100.93, 55.58, 14.67, 14.57, 14.14; MS (ESI-TOF) *m/z* Calculated for C<sub>30</sub>H<sub>28</sub>BF<sub>2</sub>N<sub>3</sub>O<sub>2</sub>: 511.2243; Found: [M]<sup>+</sup>: 511.2253.

*Data for 1b:* <sup>1</sup>H-NMR (400 MHz, CDCl<sub>3</sub>) δ 8.39 (s, 2H), 8.17-8.16 (d, *J* = 7, 2H), 7.87-7.83 (d, *J* = 16.5, 2H), 7.54 (s, 2H), 7.53-7.48 (d, *J* = 16.5, 2H), 7.43-7.42 (d, *J* = 7, 2H), 7.31-7.29 (m, 4H), 6.67 (s, 2H), 6.56-6.55 (m, 3H), 3.83 (s, 6H), 1.63 (s, 6H); <sup>13</sup>C-NMR (100 MHz, CDCl<sub>3</sub>) 161.40, 153.28, 141.24, 136.98, 128.99, 126.11, 125.60, 124.57, 123.10, 122.08, 121.24, 120.66, 116.76, 116.23, 116.11, 111.52, 106.74, 100.97, 55.06, 53.75, 14.48, 14.15; MS (ESI-TOF) *m/z* Calculated for C<sub>39</sub>H<sub>33</sub>BF<sub>2</sub>N<sub>4</sub>O<sub>2</sub>: 638.2665; Found: [M]<sup>+</sup>: 638.2677.

**BODIPYs 2a and 2b:** BODIPY **1** (0.15 g, 0.39 mmol), *p*-anisaldehyde (0.53 g, 3.9 mmol), and *p*-TsOH (0.01 g) were dissolved in dry toluene (50 mL) over 3 Å molecular sieves. To this solution was added piperidine (0.4 mL) and the mixture was at reflux for 48 hours. Upon cooling, the reaction was filtered to remove the sieves and the filtrate was quenched with water and extracted

with CH<sub>2</sub>Cl<sub>2</sub>. The combined organic layers were dried over Na<sub>2</sub>SO<sub>4</sub> and the solvent was removed under vacuum. The resulting residue was purified by silica column chromatography using 20% EtOAc in hexanes (v/v) to afford 0.024 g of a purple solid, **2a**, in 12% yield and 0.015 g of a blue solid, **2b**, in 6% yield.

*Data for 2a:* <sup>1</sup>H-NMR (400 MHz, CDCl<sub>3</sub>) δ 7.57-7.55 (d, *J* = 16.3, 1H) 7.56-7.54 (d, *J* = 8.7, 2H), 7.23-7.19 (d, *J* = 16.3, 1H), 6.92-6.89 (d, *J* = 8.7, 2H), 6.60 (s, 1H), 6.56-6.55 (t, *J* = 2.1, 1H), 6.49-6.48 (d, *J* = 2.3, 2H), 6.01 (s, 1H), 3.84 (s, 3H), 3.80 (s, 6H), 2.60 (s, 3H), 1.60 (s, 3H), 1.56 (s, 3H); <sup>13</sup>C-NMR (100 MHz, CDCl<sub>3</sub>) δ 161.57, 160.44, 154.68, 153.47, 142.63, 142.26, 139.64, 136.78, 136.12, 129.35, 129.04, 121.00, 117.41, 116.99, 114.24, 106.19, 100.95, 69.53, 55.58, 55.38, 53.75, 14.72, 14.49, 14.23; MS (ESI-TOF) *m/z* Calculated for C<sub>29</sub>H<sub>30</sub>BF<sub>2</sub>N<sub>2</sub>O<sub>3</sub>: 503.2318; Found: [M+H]<sup>+</sup>: 503.2320.

*Data for 2b:* <sup>1</sup>H-NMR (400 MHz, CDCl<sub>3</sub>) δ 7.64-7.61 (d, *J* = 16.3, 2H) 7.60-7.58 (d, *J* = 8.7, 4H), 7.24-7.20 (d, *J* = 16.3, 2H), 6.98-6.93 (d, *J* = 8.7, 4H), 6.63 (s, 2H), 6.57-6.56 (t, *J* = 2.2, 1H), 6.52-6.51 (d, *J* = 2.1, 2H), 3.86 (s, 6H), 3.81 (s, 6H), 1.61 (s, 6H); <sup>13</sup>C-NMR (100 MHz, CDCl<sub>3</sub>) δ 161.52, 160.38, 152.74, 141.77, 137.73, 136.93, 135.74, 132.84, 129.84, 129.77, 129.55, 129.06, 128.67, 117.42, 117.23, 114.26, 114.08, 114.03, 113.95, 106.49, 100.96, 55.60, 55.39, 14.48; MS (ESI-TOF) *m/z* Calculated for C<sub>37</sub>H<sub>36</sub>BF<sub>2</sub>N<sub>2</sub>O<sub>4</sub>: 621.2736; Found: [M+H]<sup>+</sup>: 621.2725.

**BODIPYs 3a:** BODIPY **3** (0.1 g, 0.25 mmol), 4-acetamidobenzaldehyde (0.4 g, 2.5 mmol), and *p*-TsOH (0.01 g) were dissolved in dry (50 mL) over 3 Å molecular sieves. To this solution was added piperidine (0.4 mL) and the mixture was at reflux for 48 hours. Upon cooling, the reaction was filtered to remove the sieves and the filtrate was quenched with water and extracted with CH<sub>2</sub>Cl<sub>2</sub>. The combined organic layers were dried over Na<sub>2</sub>SO<sub>4</sub> and the solvent was removed under

vacuum. The resulting residue was purified by silica column chromatography using 1:1:1 acetone/hexanes/CH<sub>2</sub>Cl<sub>2</sub> (v/v) to afford 0.01 g of a purple solid, **3a**, in 10% yield.

*Data for 3a:* <sup>1</sup>H-NMR (500 MHz, CDCl<sub>3</sub>) δ 7.66-7.65 (d, *J* = 8.2, 2H) 7.57-7.54 (d, *J* = 16.3, 1H), 7.38-7.36 (d, *J* = 8.2, 2H), 7.21-7.19 (d, *J* = 8.2, 2H), 7.21-7.18 (d, *J* = 16.3, 1H), 7.12-7.11 (d, *J* = 8.2, 2H) 6.61 (s, 1H), 6.02 (s, 1H), 3.35 (s, 3H), 2.59 (s, 3H), 1.47 (s, 3H), 1.43 (s, 1H); <sup>13</sup>C-NMR (100 MHz, CDCl<sub>3</sub>) δ 168.24, 155.57, 153.20, 142.32, 138.66, 135.95, 135.91, 135.24, 133.94, 132.40, 130.92, 130.02, 128.56, 128.32, 128.24, 123.26, 121.50, 119.99, 119.63, 117.77, 46.20, 14.89, 14.73, 14.66; MS (ESI-TOF) *m/z* Calculated for C<sub>28</sub>H<sub>26</sub>BBrF<sub>2</sub>N<sub>3</sub>O: 548.1320; Found: [M+H]<sup>+</sup>: 548.1372.

**BODIPYs 4a:** BODIPY **4** (0.1 g, 0.24 mmol), *p*-anisaldehyde (0.33 g, 2.4 mmol), and *p*-TsOH (0.01 g) were dissolved in dry toluene (50 mL) over 3 Å molecular sieves. To this solution was added piperidine (0.4 mL) and the mixture was at reflux for 48 hours. Upon cooling, the reaction was filtered to remove the sieves and the filtrate was quenched with water and extracted with CH<sub>2</sub>Cl<sub>2</sub>. The combined organic layers were dried over Na<sub>2</sub>SO<sub>4</sub> and the solvent was removed under vacuum. The resulting residue was purified by silica column chromatography using 50:50 hexanes/CH<sub>2</sub>Cl<sub>2</sub> (v/v) to afford 0.021 g of a green solid, **4a**, in 13% yield.

*Data for 4a:* <sup>1</sup>H-NMR (400 MHz, acetone-d<sub>6</sub>) δ 7.67-7.58 (m, 8H), 7.08-7.06 (d, *J* = 8.1, 4H), 6.99-6.96 (d, *J* = 16.1, 2H), 3.89 (s, 6H), 1.79 (s, 6H); <sup>13</sup>C-NMR (100 MHz, acetone-d<sub>6</sub>) δ 161.23, 161.13, 137.92, 137.45, 129.26, 129.20, 129.16, 129.07, 128.75, 118.83, 118.51, 116.39, 116.27, 114.60, 114.57, 54.91, 13.09; MS (ESI-TOF) *m/z* Calculated for C<sub>35</sub>H<sub>26</sub>BF<sub>7</sub>NaN<sub>2</sub>O<sub>2</sub>: 673.1873; Found: [M+Na]<sup>+</sup>: 673.1859.

#### 4.4.3 Steady-state Absorption and Fluorescence Spectroscopy

The spectroscopic properties of BODIPYs **1a,b**, **2a,b**, **3a**, and **4a** were determined on solutions prepared by dissolving crystalline compound in dimethylsulfoxide. Stock solutions ( $5 \times 10^{-5}$  M) were prepared and diluted to appropriate concentrations for collection of absorbance and emission spectra. Absorption spectra were obtained on a Varian Cary 50 Bio UV/VIS Spectrophotometer. Measurements obtained for determining optical density were taken from solutions with concentrations between  $1.2 \times 10^{-5}$  and  $5 \times 10^{-5}$  M so that  $\lambda_{\text{max}}$  was between 0.5 and 1.0. Fluorescence measurements were recorded on solutions with concentrations of  $5 \times 10^{-6}$  M to attain an optical density at the excitation wavelength between 0.04 and 0.06 to minimize intermolecular reabsorption and inner-filter effects. Compounds were excited at 540 nm for **1a**, 650 nm for **1b**, 520 nm for **2a**, 615 nm for **2b**, 530 nm for **3a**, and 600 nm for **4a**. Emission spectra were acquired on a PTI QuantaMaster4/2006SE spectrofluorometer with the slit width set at 3 nm for dichloromethane and THF and 5 nm for DMSO. Methylene blue was used as a standard in calculating the fluorescence quantum yields ( $\Phi_f = 0.03$  in methanol). All measurements, both absorbance and emission, were acquired within 4 h of solution preparation at room temperature (23 – 25 °C), using a 10 mm path length quartz spectrophotometric cell.

#### 4.4.4 Cell Studies

All reagents and tissue culture media were purchased from Invitrogen. Human carcinoma HEp2 cells used in this study were purchased from ATCC and were sustained at 37°C and 5% CO<sub>2</sub> in a 50:50 mixture of DMEM:AMEM augmented with 10% FBS and 1% antibiotic (Penicillin-streptomycin). A working BODIPY stock solution of 32 mM BODIPY was prepared by dissolving the compound with sonication in 96% DMSO and 4% Cremophor EL.

**4.4.4.1 Time-Dependent Cellular Uptake.** The HEP2 cells were grown overnight in a Costar 96-well plate plated at 15,000 cells per well. The 32 mM stock solution was diluted to a 10  $\mu$ M BODIPY solution through the addition of medium containing 5% FBS and 1% antibiotic to a 400  $\mu$ M stock solution. The cells were exposed to the BODIPY in medium solution at 100  $\mu$ L/well at time intervals of 0, 1, 2, 4, 8, and 24 hours. At the termination of the treatment, the loading medium was removed and the cells were washed with 1X PBS, and solubilized by adding 0.25% Triton X-100 in 1X PBS. Quantification of the cells was conducted using the CyQuant Cell Proliferation Assay (Life Technologies). BODIPY concentration was determined by reading fluorescence at 355/700 nm with a FluoStar Optima micro-plate reader (BMG LRBTEH). Cellular uptake is expressed in nM compound/cell.

**4.4.4.2 Dark Cytotoxicity.** The HEP2 cells were placed in a 96-well plate as above and allowed to incubate overnight. Following incubation, the cells were exposed to increasing concentrations of BODIPY, from 0  $\mu$ M up to 400  $\mu$ M, and then incubated at 37°C. After 24 hour incubation, the loading media containing compound was removed by washing the cells with 1X PBS. The media was replaced with media containing 20% Cell Titer Blue and the cells were incubated at 37°C for a subsequent 4 hours. Cell viability was determined by reading fluorescence at 570/615 nm with a FluoStar Optima micro-plate reader. The dark toxicity is expressed in terms of the percentage of viable cells.

**4.4.4.3 Phototoxicity.** The HEP2 cells were placed in 96-well plates as incubated as described above. Following incubation, the cells were exposed to increasing concentrations of BODIPY (0

$\mu\text{M}$ , 3.125  $\mu\text{M}$ , 6.25  $\mu\text{M}$ , 12.5  $\mu\text{M}$ , 25  $\mu\text{M}$ , 50  $\mu\text{M}$ , and 100  $\mu\text{M}$ ) and then incubated for 24 hours at 37°C. After the 24 hour treatment, the loading media was removed, the cells were washed with 1X PBS and refilled with fresh media. The cells were then exposed to a 600 W halogen lamp light filtered through a water filter (Newport) and then through a beam turning mirror (200 – 3000 nm, Newport) to generate an approximate light dose of 1.5 J/cm<sup>2</sup>. After a 20 minute exposure time, the cells were incubated for another 24 hours. Following incubation, the medium was removed and replaced with medium containing 20% of Cell Titer Blue and the cells were incubated for a subsequent 4 hours. Cell viability was determined by reading fluorescence at 570/615 nm with a FluoStar Optima micro-plate reader. The phototoxicity is expressed in terms of the percentage of viable cells.

#### 4.4.5 Octanol-HEPES buffer coefficients

The partition coefficients ( $\log P$ ) were measured at room temperature by adding 0.5 mL of a BODIPY stock solution in DMSO (50  $\mu\text{M}$ ) to a 15 mL volumetric tube containing 4.0 mL of HEPES buffer (1 M, pH 7.4), followed by addition of 4.0 mL of 1-octanol. After vortexing for 5 min, the phases were allowed to separate completely. An aliquot of 0.5 mL from each layer was diluted with 0.5 mL of methanol and the absorbance was read on an Varian Cary 50 Bio UV/VIS Spectrophotometer with 10 mm path length quartz cuvette.

#### 4.5 References

1. Orth, J. D.; Kohler, R. H.; Fojjer, F.; Sorger, P. K.; Weissleder, R.; Mitchison, T. J., Analysis of Mitosis and Antimitotic Drug Responses in Tumors by In Vivo Microscopy and Single-Cell Pharmacodynamics. *Cancer Research* **2011**, *71*, 4608-4616.
2. Reiner, T.; Thurber, G.; Gaglia, J.; Vinegoni, C.; Liew, C. W.; Upadhyay, R.; Kohler, R. H.; Li, L.; Kulkarni, R. N.; Benoist, C.; Mathis, D.; Weissleder, R., Accurate measurement

- of pancreatic islet beta-cell mass using a second-generation fluorescent exendin-4 analog. *Proceedings from the National Academy of Science U. S. A.* **2011**, *108*, 12815-12820.
- Nahrendorf, M.; Keliher, E.; Marinelli, B.; Waterman, P.; Feruglio, P. F.; Fexon, L.; Pivovarov, M.; Swirski, F. K.; Pittet, M. J.; Vinegoni, C.; Weissleder, R., Hybrid PET-optical imaging using targeted probes. *Proceedings from the National Academy of Science U. S. A.* **2010**, *107*, 7910-7915.
  - Hudnall, T. W.; Gabbai, F. P., A BODIPY boronium cation for the sensing of fluoride ions. *Chemical Communications* **2008**, 4596-4597.
  - Hendricks, J. A.; Keliher, E. J.; Wan, D. P.; Hilderbrand, S. A.; Weissleder, R.; Mazitschek, R., Synthesis of F-18 BODIPY: Bifunctional Reporter for Hybrid Optical/Positron Emission Tomography Imaging. *Angewandte Chemie-International Edition* **2012**, *51*, 4603-4606.
  - Zhu, L.; Liu, Y. J.; Plossl, K.; Lieberman, B.; Liu, J. Y.; Kung, H. F., An improved radiosynthesis of F-18 AV-133: a PET imaging agent for vesicular monoamine transporter 2. *Nuclear Medicine and Biology* **2010**, *37*, 133-141.
  - Gibbs, J. H.; Robins, L. T.; Zhou, Z.; Bobadova-Parvanova, P.; Cottam, M.; McCandless, G. T.; Fronczek, F. R.; Vicente, M. G. H., Spectroscopic, computational modeling and cytotoxicity of a series of meso-phenyl and meso-thienyl-BODIPYs. *Bioorganic and Medicinal Chemistry* **2013**, *21*, 5770-5781.
  - Shaw, S. J.; Elgie, K. J.; Edwards, C.; Boyle, R. W., Mono-(pentafluorophenyl)porphyrins - Useful intermediates in the regioselective synthesis of multifunctionalised porphyrins. *Tetrahedron Letters* **1999**, *40*, 1595-1596.
  - Suzuki, M.; Shimizu, S.; Shin, J. Y.; Osuka, A., Regioselective nucleophilic substitution reaction of meso-hexakis(pentafluorophenyl) substituted 26 hexaphyrin. *Tetrahedron Letters* **2003**, *44*, 4597-4601.
  - Samaroo, D.; Vinodu, M.; Chen, X.; Drain, C. M., meso-Tetra(pentafluorophenyl)porphyrin as an efficient platform for combinatorial synthesis and the selection of new photodynamic therapeutics using a cancer cell line. *Journal of Combinatorial Chemistry* **2007**, *9*, 998-1011.
  - Bhupathiraju, N.; Graca, M.; Vicente, H., Synthesis and cellular studies of polyamine conjugates of a mercaptomethyl-carboranylporphyrin. *Bioorganic & Medicinal Chemistry* **2013**, *21*, 485-495.
  - Naruta, Y.; Tani, F.; Maruyama, K., Meso-Perfluorination of Porphyrins with N-Fluoropyridinium Triflate. *Tetrahedron Letters* **1992**, *33*, 1069-1072.
  - Pandey, S. K.; Saijad, M.; Chen, Y.; Zheng, X.; Yao, R.; Missert, J. R.; Batt, C.; Nabi, H. A.; Oseroff, A. R.; Pandey, R. K., Comparative Positron-Emission Tomography (PET) Imaging and Phototherapeutic Potential of I-124- Labeled Methyl-3-(1 '-

- iodobenzoyloxyethyl)pyropheophorbide-a vs the Corresponding Glucose and Galactose Conjugates. *Journal of Medicinal Chemistry* **2009**, *52*, 445-455.
14. Pandey, S. K.; Gryshuk, A. L.; Sajjad, M.; Zheng, X.; Chen, Y. H.; Abouzeid, M. M.; Morgan, J.; Charamisinau, I.; Nabi, H. A.; Oseroff, A.; Pandey, R. K., Multimodality agents for tumor imaging (PET, fluorescence) and photodynamic therapy. A possible "see and treat" approach. *Journal of Medicinal Chemistry* **2005**, *48*, 6286-6295.
  15. Uppal, T.; Bhupathiraju, N.; Vicente, M. G. H., Synthesis and cellular properties of Near-IR BODIPY-PEG and carbohydrate conjugates. *Tetrahedron* **2013**, *69*, 4687-4693.
  16. Yu, C. J.; Xu, Y. J.; Jiao, L. J.; Zhou, J. Y.; Wang, Z. Y.; Hao, E. H., Isoindole-BODIPY Dyes as Red to Near-Infrared Fluorophores. *Chemistry-A European Journal* **2012**, *18*, 6437-6442.
  17. Baruah, M.; Qin, W. W.; Basaric, N.; De Borggraeve, W. M.; Boens, N., BODIPY-based hydroxyaryl derivatives as fluorescent pH probes. *Journal of Organic Chemistry* **2005**, *70*, 4152-4157.
  18. Brizet, B.; Bernhard, C.; Volkova, Y.; Rousselin, Y.; Harvey, P. D.; Goze, C.; Denat, F., Boron functionalization of BODIPY by various alcohols and phenols. *Organic & Biomolecular Chemistry* **2013**, *11*, 7729-7737.
  19. Baruah, M.; Qin, W. W.; Flors, C.; Hofkens, J.; Vallee, R. A. L.; Beljonne, D.; Van der Auweraer, M.; De Borggraeve, W. M.; Boens, N., Solvent and pH dependent fluorescent properties of a dimethylaminostyryl borondipyrromethene dye in solution. *Journal of Physical Chemistry A* **2006**, *110*, 5998-6009.

## CHAPTER 5: SYNTHESIS, SPECTROSCOPIC, AND IN VITRO EVALUATION OF CARBORANYL-BODIPY DYES AS BNCT ANTI-CANCER AGENTS

### 5.1 Introduction

The treatment of late stage cancers of the brain is inundated by a multitude of challenges. The conventional approaches of cancer treatment, chemotherapy, radiation therapy, and surgery, all are plagued by drawbacks corresponding to the unique environment of the brain.<sup>1</sup> Although, surgery to remove the bulk of a tumorous mass is often the most efficacious treatment method, it has its limitations in that not even the most skilled surgeons are able to remove every cancer cell. Currently, this “debulking” surgery is accompanied by chemotherapy and radiation treatments in an attempt to remove any persistent cells.<sup>1,2</sup> However, current chemotherapy drugs are unable to efficiently cross the blood brain barrier (BBB), thus limiting their effective doses of anticancer agents to the cancerous brain tissues while at the same time destroying normal cells as a result of unspecific cellular targeting. Additionally, radiation therapy is limited to tumors on the outermost parts of the brain due to limited penetration depth of radiation sources.<sup>3</sup> As a result, the tumor often returns and becomes malignant, or spreads to other areas of the body. In response to the demand for brain-specific therapies, a multitude of anti-brain cancer agents have been developed. Several clinical trials are currently underway using various targeting therapies including PDT and boron neutron capture therapy (BNCT).<sup>4-8</sup>

Current molecules used in the treatment of brain tumors have drawbacks which prevent them from being effective, including challenges with delivering the necessary concentration of their therapeutic component to tumor cells. Despite being under extensive clinical trials across the globe in the recent decade, the small molecules currently used in BNCT, sodium borocaptate (BSH) and boronophenylalanine (BPA), Figure 5.1, are flawed preventing them from being highly

therapeutic.<sup>2,3</sup> These small molecules, and many others that have been explored *in vivo*, tend to have low accumulation in tumor cells and lack selectivity of tumor cells over normal cells, as seen by low target-to-background ratios.

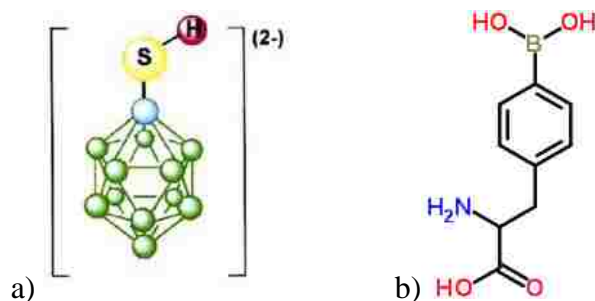


Figure 5.1: Chemical structures of a) BSH and b) BPA.

On the other hand, some large molecules also under investigation, including porphyrins, tend to have high background signals, making them indistinguishable from normal tissues. Additionally, they tend to have high retention rates and clear from the body slowly. A proposed solution to these challenges is through the design of an activatable boron-containing fluorescent probe that will allow for visualization and quantification of the compound within the body so that the anti-cancer agent may be activated when the ideal systemic localization is achieved.<sup>3,9</sup>

### 5.1.1 Brain Tumors

A brain tumor is an abnormal mass of tissues caused by a dysregulation in the normal brain stem cell differentiation pathway, Figure 5.2 which causes uncontrolled growth and multiplication of brain cells. To be considered a cancerous brain tumor, the abnormal mass must be rapidly growing and invasive toward normal brain tissue. They are named from the cell type of origin and

the location in the brain, and are graded on a scale of I to IV, with grade IV being the most aggressive.<sup>1</sup> The most common brain cancer is metastatic glioblastoma multiforme (GBM).

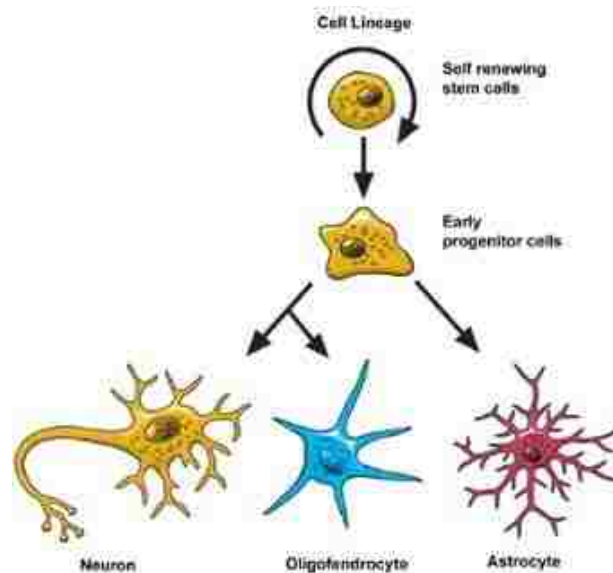


Figure 5.2: The normal cell differentiation pathway of brain stem cells.<sup>10</sup>

GBM is a grade IV astrocytoma, a type of brain tumor. Astrocytomas develop from the star-shaped glial cells, called astrocytes, which support nerve cells (Figure 5.3).<sup>1</sup> GBM is the final stage of astrocytoma formation and is the most invasive, readily spreading to near-by tissues. Once the tumor has spread to surrounding tissues it is no longer made up of solely glial cells. It may be composed of many different types of cells, which makes treatment increasingly difficult. GBM is found in both men and women, typically affecting those ages 50 to 70, and is more prevalent in men. According to the National Brain Tumor Society, GBM accounts for 17 percent of all primary brain tumors.<sup>1</sup> In 2014, approximately 23,380 new cases of primary malignant brain tumors will be diagnosed in the United States, 12,820 in men and 10,560 in women. More than 14,000 individuals are estimated to perish due to a lack to effective treatment.<sup>11</sup>

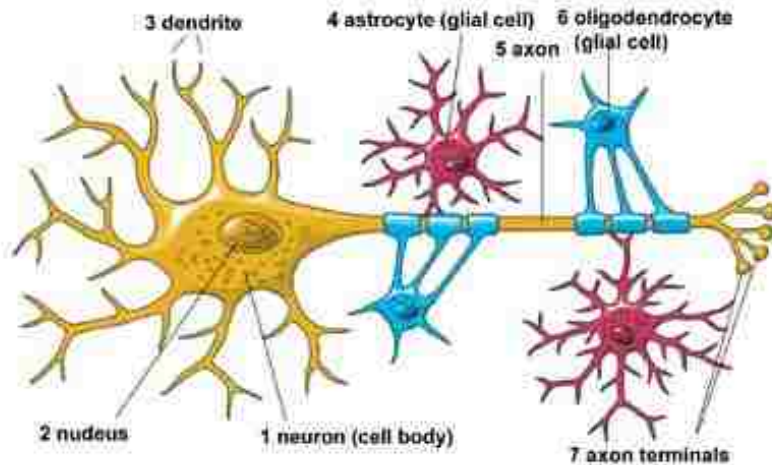


Figure 5.3: Structure and cellular support of a neuron.<sup>10</sup>

Because brain tumors occupy space within the confines of the skull, their presence can interfere with normal brain activity. Depending upon the location of the tumor, damage can occur to healthy nerves and tissues either through cellular infiltration or through deformation of the brain caused by increased intracranial pressure resulting from the compression of the brain against the skull. The areas typically affected by astrocytomas are the cerebrum, cerebellum, brain stem, and optic nerve.<sup>1</sup> Symptoms caused by large astrocytomas are typically dependent upon the location of the tumor. Diagnosis of brain tumor involves a neurological examination, brain scan, and analysis of the brain tissue via biopsy. After the composition of the tumor is identified a strategic therapeutic approach may be determined.

### 5.1.2 Boron Neutron Capture Therapy (BNCT)

BNCT is under-utilized as a cancer treatment option greatly due to the lack of efficient therapeutic agents. BNCT is a binary radiation therapy involving irradiation of boron-10 containing molecules that have the possibility of being selectively delivered to tumor cells with

low-energy thermal neutrons.<sup>12</sup> Upon neutron-capture by a stable boron-10 atom, the nucleus splits, releasing highly charged, high linear energy transferring  $\alpha$ -particles ( $^4\text{He}$ ), recoiling lithium-7 ( $^7\text{Li}$ ) nuclei and kinetic energy which destroys the boron containing cell, Figure 5.4.<sup>3, 13-16</sup> The amount of kinetic energy released during this process is only enough to cause expulsion of poisonous ions one cell diameter in length, thus containing destruction to only boron bearing cells and possibly to close proximity adjacent cells within the radiation path.<sup>12</sup>

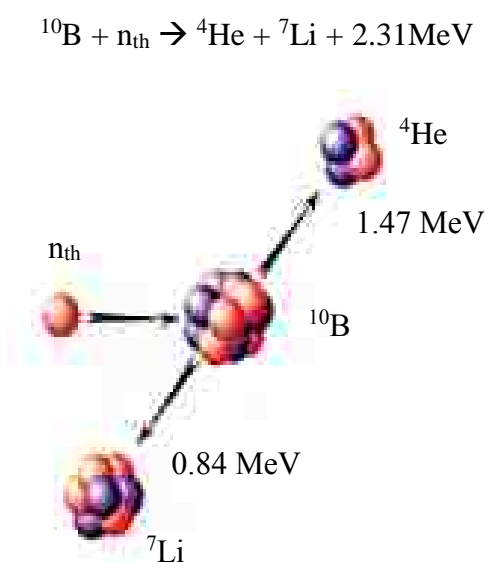


Figure 5.4: Nuclear fission of a boron atom upon impact with a thermal neutron.<sup>17</sup>

As of 2007, several carborane containing BNCT agents have been synthesized including nucleosides, nucleoside-sugar derivatives and porphyrins which show promising results including tumor targeting ability and low cytotoxicity, Figure 5.5.<sup>3, 13-15, 18</sup> However, despite their promising preliminary studies, many of these boron delivery agents have yet to be subjected to preclinical and clinical studies to prove their effectiveness at delivering the necessary quantities of boron-10 with great enough selectivity.<sup>19</sup>

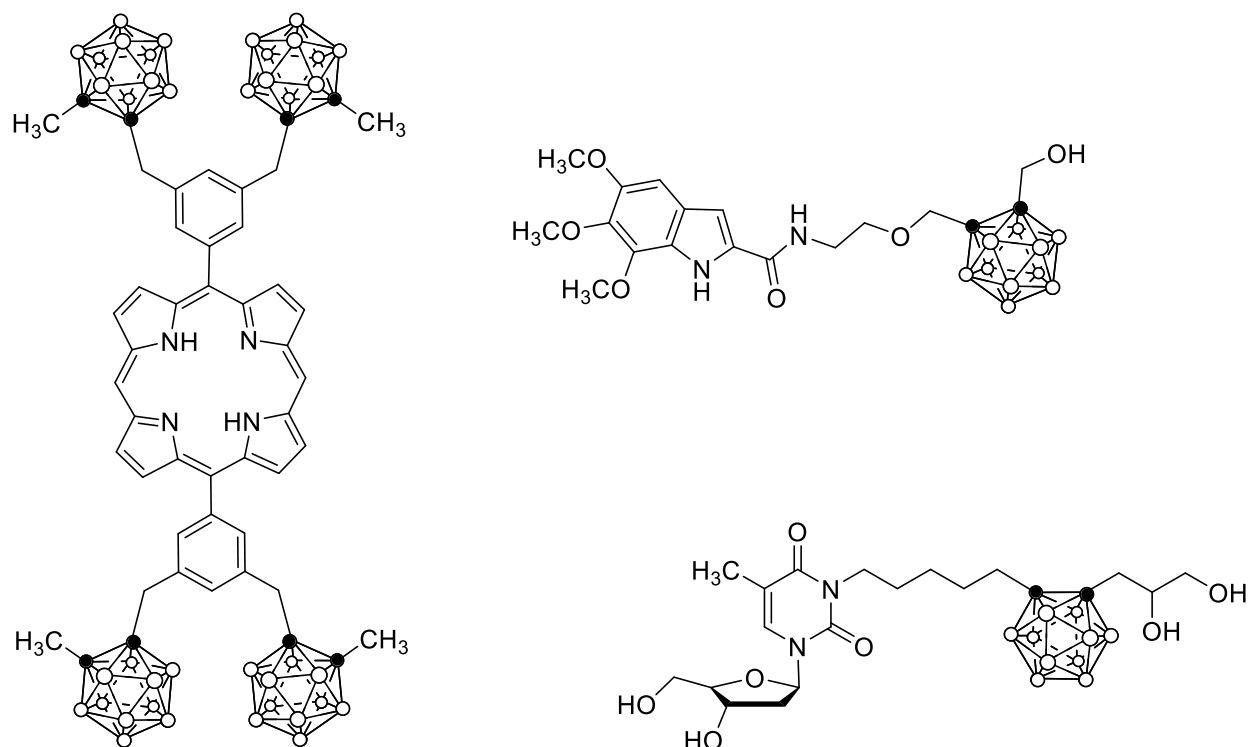


Figure 5.5: Boron containing potential BNCT agents.<sup>18</sup>

### 5.1.3 Blood Brain Barrier

The greatest challenge with chemically treating diseases of the brain is getting drug molecules through the BBB. The BBB is a protective barrier surrounding the blood vessels that feed the brain. The BBB is formed when astrocytes, a type of nerve support cell, extend their foot processes to attach to and surround the blood vessels (Figure 5.6). Where these processes meet the astrocytes secrete enzymes, called paracrines, which causes their edges to seal forming tight junctions.<sup>20,21</sup> Tight junctions prevent the passage of ions and large molecules through the spaces between the endothelial cells comprising the outer layer of blood vessels. Many of the drug molecules that are used in chemotherapy treatment of cancer are incapable of permeating the BBB, thus reducing their efficacy.<sup>20</sup>

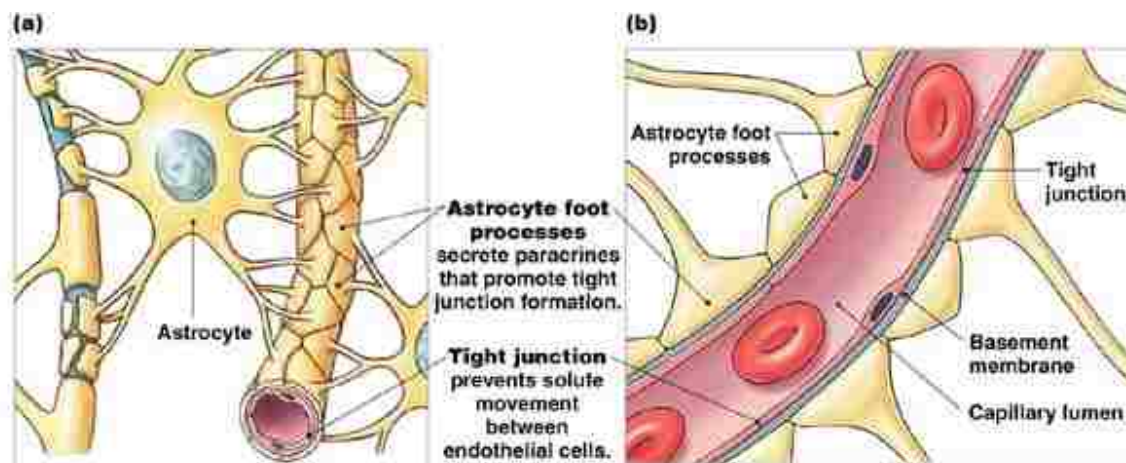


Figure 5.6: Formation of tight junctions by astrocyte foot processes.<sup>22</sup>

Various channels lie on the surface of the BBB allowing for the transport of water, nutrients, and specially designed drugs into and out of the brain.<sup>21</sup> Water and ions necessary for normal cellular function pass through the membrane via passive diffusion and ion channels. Larger, more complex molecules must be brought across the BBB by way of transport proteins which lie at the surface of and traverse the cell membrane. Receptor mediated endocytosis and absorptive-mediated transport are two ways in which these large molecules may cross the BBB.<sup>21,</sup>  
<sup>23</sup> The lipophilic nature of these receptor proteins may be employed through strategically designed amphiphilic drugs that are capable of intravenously delivering therapeutic amounts of boron-10 to cancerous brain cells.

#### 5.1.4 Carboranes

Icosahedral carboranes have become a popular delivery agent for boron-10 in regards to BNCT.<sup>3</sup> Carboranes are electron deficient boron and carbon containing cages most commonly used in the neutral  $C_2B_{10}H_{12}$  form. This series of carboranes exists in three closed icosahedral stereoisomeric forms: *ortho* ( $1,2-C_2B_{10}H_{12}$ ), in which the two carbons are oriented adjacent to one

another, *meta* (1,7-C<sub>2</sub>B<sub>10</sub>H<sub>12</sub>), where a boron atom separates the two carbons, and *para* (1,12-C<sub>2</sub>B<sub>10</sub>H<sub>12</sub>), the most stable form, in which the carbon atoms lie at opposite apices of the icosahedron (Figure 5.7).<sup>24</sup>

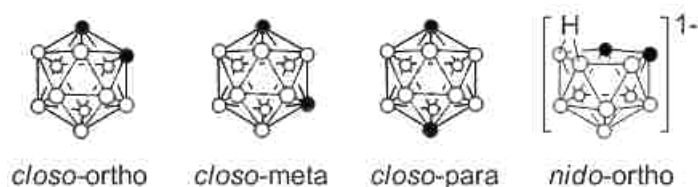


Figure 5.7: Stereoisomers of C<sub>2</sub>B<sub>10</sub>H<sub>12</sub> *closo*-carboranes and [C<sub>2</sub>B<sub>9</sub>H<sub>12</sub>]<sup>-1</sup> *nido*-carborane (closed circle: CH, open circle: BH).

Thermodynamic rearrangement at elevated temperatures allows for conversion of *ortho* to *meta* (400 - 500°C) and *meta* to *para* (>620°C). *Ortho* and *meta* carboranes are sensitive to basic environments and effectively lose one boron atom to form negatively charged open *nido*-carboranes.<sup>24</sup>

Carboranes are electron deficient and possess special bonding in which the molecular orbitals (MOs) that participate in bonding extend over the entire cage creating a highly electron delocalized structure. The extreme delocalization of electron density creates substantial stability.<sup>24</sup> These highly thermal and chemically stable compounds possess aromatic characteristics similar to benzene and as such, have been studied for their abilities to increase  $\pi$ -conjugation and enhance fluorescence of a conjugated fluorophore.<sup>24, 25</sup>

The icosahedron can be split into equatorial and polar-regions in order to better explain bonding. The equatorial region houses boron atoms that lie in a planar ring and are sp<sup>2</sup> hybridized similar to aromatic structures. The remaining p-orbitals not involved in cyclic formation are perpendicular to the ring and combine to form five delocalized MOs which can bond to apex boron

or carbon atoms.<sup>24</sup> Bonds between carbon or boron and hydrogen are localized, forming sigma bonds. The cage has electrophilic nature that decreases with addition of substituents and readily undergoes substitution reactions without harming the integrity of the carborane cage.<sup>24, 25</sup>

Incorporation of carboranes into the  $\pi$ -system of a fluorophore increases conjugation and structural rigidity resulting in a red-shift in absorption and emission wavelengths. *Ortho*-carboranes have shown to cause the greatest red-shift with *meta* and *para* falling similarly in second. Thermal and chemical stability is enhanced with multiple carborane clusters, with *ortho*-carborane appended structures owning the greatest thermal stability.<sup>25</sup>

Carborane appended compounds have also shown to possess larger extinction coefficients than their structurally equivalent counterparts with *meta*-carboranes increasing emission intensity the greatest. The 3D structure of the cage prevents  $\pi$ - $\pi$  stacking which also enhances fluorescence quantum yield, however carboranes tend to enhance aggregation which causes fluorescence quenching.<sup>25</sup> In addition to their enhancement of a fluorophore's photophysical properties, studies indicate carboranes show promise as boron-10 drug delivery agents due to their high stability and low cellular toxicity.<sup>3</sup>

### **5.1.5 Research Prospective**

The objective of this work is to design a low molecular weight fluorescent molecule capable of delivering a therapeutic component for the treatment of late stage brain tumors via Boron Neutron Capture Therapy (BNCT).<sup>3</sup> The compounds herein were designed to deliver boron-10, which has been shown to cause cell death upon irradiation with low energy thermal neutrons.<sup>3, 13-15</sup> Carbon-boron cages, or carboranes, were attached to a fluorescent core in order to achieve a greater concentration of boron-10 delivered to tumor cells over current drug molecules.

Carboranes present an acceptable avenue for delivering the necessary quantity of boron-10 of 20  $\mu\text{g/g}$  tumor to the target cells.<sup>3, 13-15</sup> The greatest challenge presents itself in getting the drug molecule across the BBB. Molecules must be lipophilic in nature in order to enter the protective covering of the brain, yet must be hydrophilic in order to be administered intravenously.<sup>3</sup> BODIPY serves as the fluorescent core to which the therapeutic components are attached. BODIPY is hydrophobic by nature and provides a reasonable platform on which to build our drug molecule. In order to achieve amphiphilicity, water solubilizing groups must be added. The use of polyethylene glycols, polyamines, or charged amino acids may increase water solubility while at the same time enhancing BBB permeability.

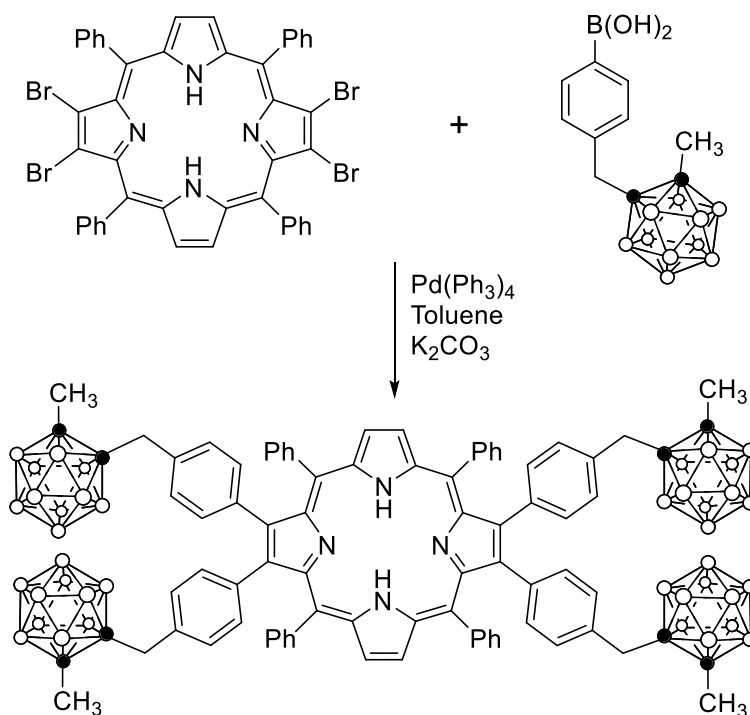
## 5.2 Results and Discussion

### 5.2.1 Syntheses

With iodines already installed at the 2,6-positions of several BODIPY platforms as detailed in Chapter 2,<sup>26</sup> subsequent work was attempted to mount carborane moieties onto the core through various palladium-catalyzed coupling reactions. Previous endeavors by the Vicente group have shown that carboranes could be attached to a halogenated or boronic ester/acid derivatized benzyl moiety and subsequently subjected to a Suzuki-type coupling to readily incorporate boron-dense carboranes onto a fluorescent scaffold, Scheme 5.1.<sup>27</sup> Under such mild basic conditions, the carborane maintained its structural integrity and the product of the coupling reactions retained the neutral charge of the *closo-ortho*-carborane.

Halogenated BODIPYs have also been reported to readily undergo Sonogashira couplings with terminal alkynes in the presence of palladium (II) and copper iodide, as discussed in Chapter

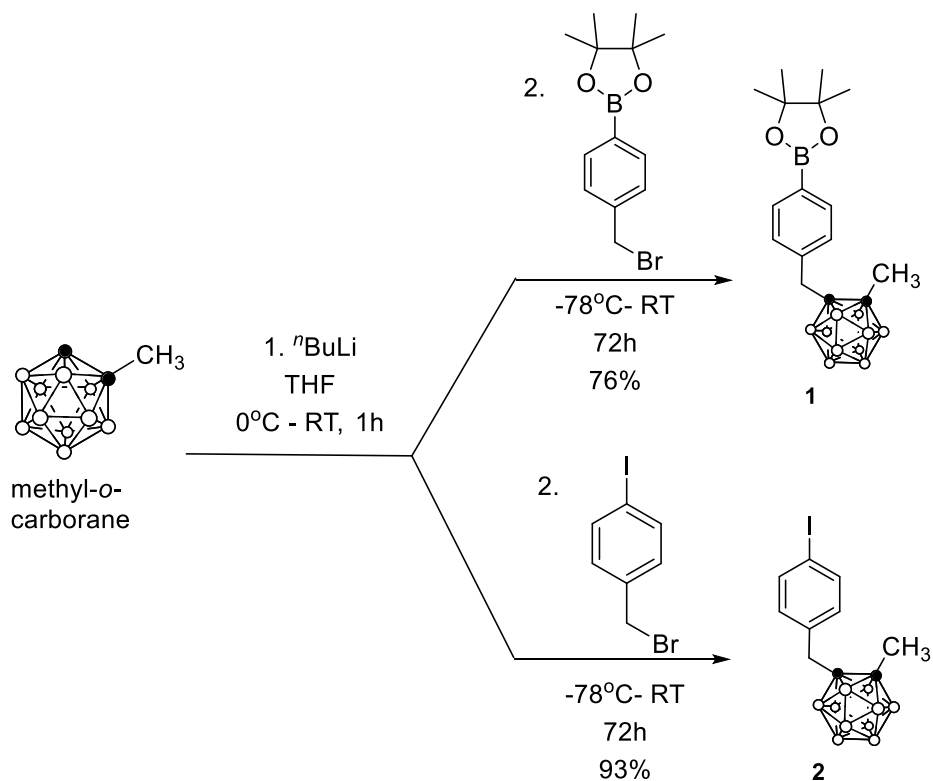
1. Such facile and typically high yielding palladium couplings seemed desirable avenues to pursue to install the carboranes.



Scheme 5.1: Suzuki couplings of porphyrin with functionalized carborane moieties.<sup>27</sup>

In order to attempt cross-couplings between the 2,6-diiodo-BODIPYs and a properly embellished carborane moiety, the boronic ester/acid and alkynyl reagents had to be synthesized. The synthesis of compounds **1** and **2** began with the deprotonation of methyl-*o*-carborane using *n*-butyl lithium in dry tetrahydrofuran according to literature, Scheme 5.2.<sup>28</sup> To the resulting carborane anion was added either 4-(bromomethyl)benzeneboronic acid pinacol ester or 4-iodobenzyl bromide to yield 76% and 93% of compounds **1** and **2**, respectively. Compound **1**, bearing the boronic ester, was suitable to attempt a Suzuki coupling to the diiodo-BODIPY compounds, whereas the iodo-benzyl-methyl-*o*-carborane, compound **2**, could potentially undergo

a Sonogashira coupling with 2,6-diethynyl-BODIPY compounds after first installing an alkyne via Sonogashira coupling with the 2,6-diiodo-BODIPYs. The structure of compound **2** was confirmed by X-ray analysis of a single crystal grown from the slow evaporation of acetone (Figure 5.8).<sup>29</sup>



Scheme 5.2: Synthesis of carborane moieties **1** and **2**.

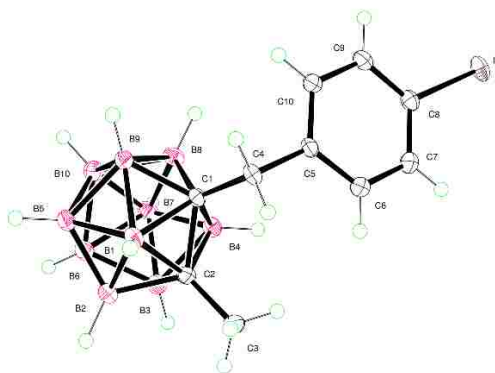
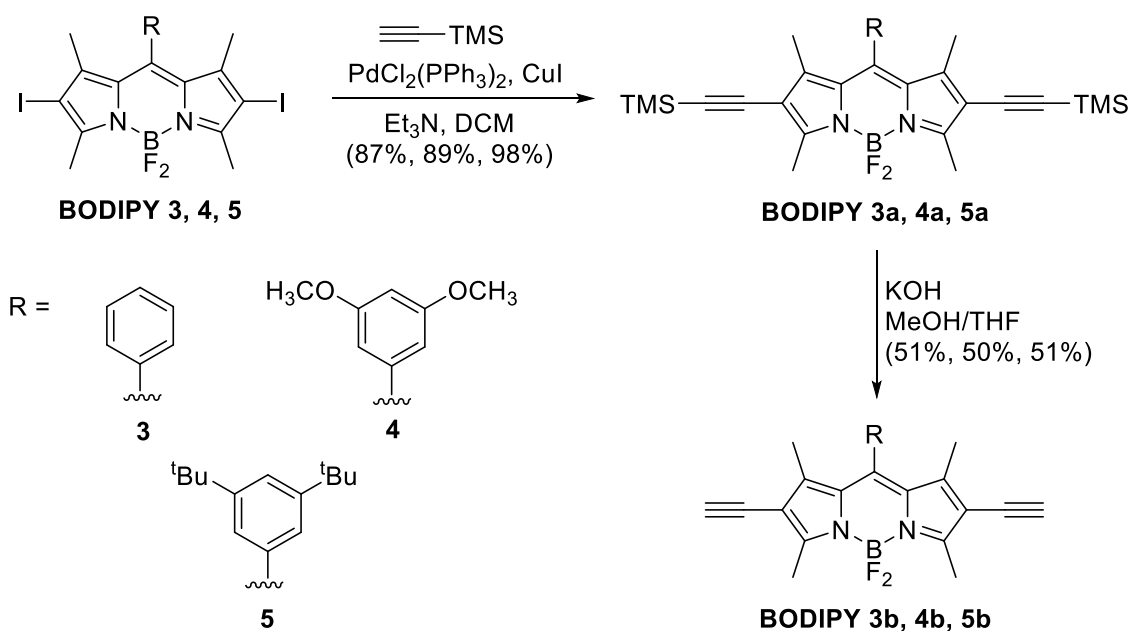


Figure 5.8: Molecular structure of compound **2** from X-ray crystal structure determinations. Ellipsoids are drawn at the 50% probability level.

Trimethylsilyl (TMS)-protected terminal alkynes were installed at the 2,6-positions of BODIPYs **3a**, **4a**, and **5a** via palladium-catalyzed cross-couplings of the 2,6-diiodides of **3**, **4**, and **5** with ethynyltrimethylsilane to produce BODIPYs **3a** (87%), **4a** (89%), and **5a** (98%) as red crystalline solids, Scheme 5.3.<sup>30</sup> Removal of the TMS protecting group was achieved through reaction with excess potassium hydroxide in MeOH/THF and provided BODIPYs **3b**, **4b**, and **5b** as red crystalline solids (51%, 50%, and 51% yield, correspondingly).<sup>31</sup>



Scheme 5.3: Functional modification of BODIPYs **3**, **4**, and **5**.

All BODIPYs were confirmed by <sup>1</sup>H-NMR, <sup>13</sup>C-NMR, HRMS (ESI-TOF), and, in the case of **3b**, X-ray crystallography. The <sup>1</sup>H-NMR displayed two equivalent signals corresponding to the 1,3,5,7-tetramethyls. The 3,5-dimethyls were visible as singlets between 1.36 and 1.63 ppm, while the 1,7-dimethyls appeared as singlets between 2.56 and 2.66 ppm. Singlets corresponding to the equivalent *tert*-butyl groups found in the **5** series was identified at 1.3 ppm, whereas the methoxy

groups seen in the **4** series could be found at 3.8 ppm. Signals corresponding to the phenyl-hydrogens were identified as the only peaks that lie between 6.40 and 7.53 ppm. Installation of the TMS-protected ethynyl groups was accompanied by the appearance of a signal at 0.2 ppm (Figure 5.9) and 0.08-0.09 ppm in the  $^{13}\text{C}$ -NMR.

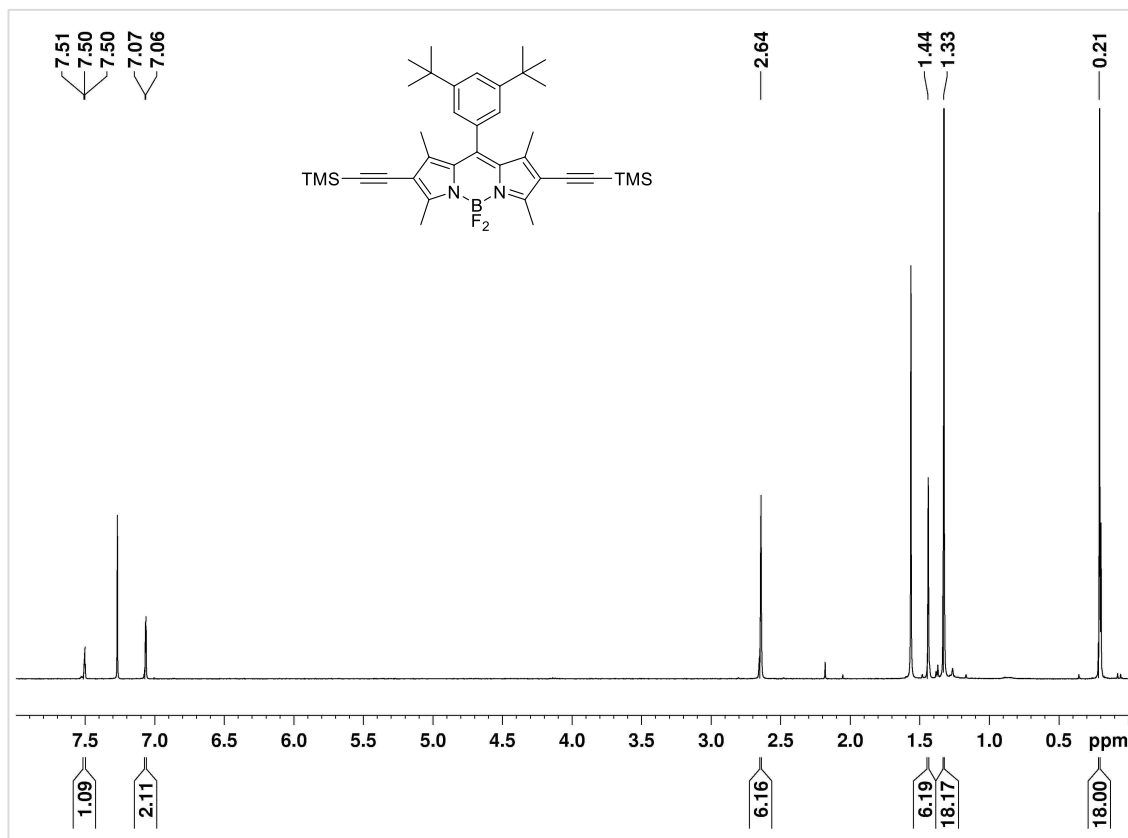


Figure 5.9:  $^1\text{H}$  NMR of BODIPY **5a** at 400 MHz in deuterated chloroform.

Subsequent removal of the TMS-group leaving the ethynyl unprotected was observed by the disappearance of the signal at 0.2 ppm and an appearance of the acetylene hydrogen peak at 3.3 ppm, Figure 5.10. Identification by ESI-TOF or MALDI-TOF MS yielded corresponding  $m/z$  peaks: **3b**, 517.253; **4b**, 576.294; **5b**, 628.403; **3c**, 372.279; **4c**, 433.189; **5c**, 485.286.

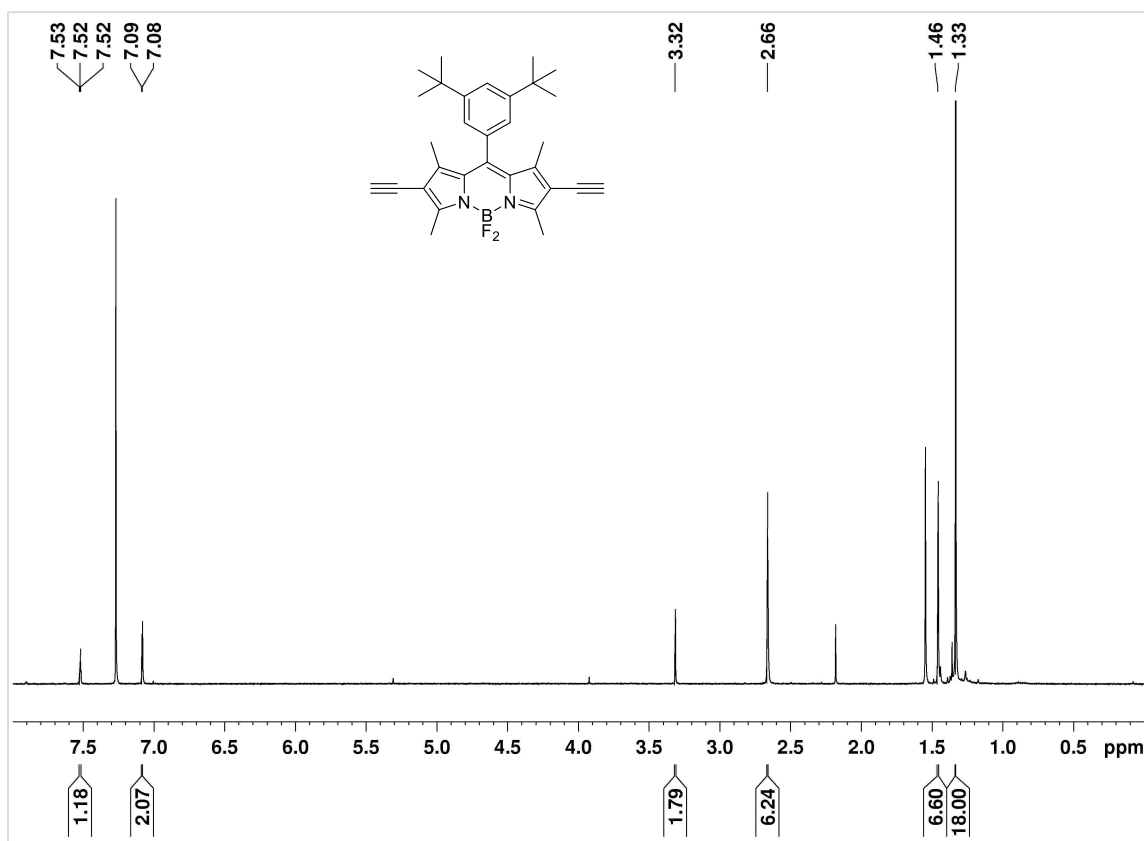


Figure 5.10:  $^1\text{H}$  NMR of BODIPY **5b** at 400 MHz in deuterated chloroform.

A single crystal suitable for X-ray analysis was grown from the slow evaporation of acetone from a pure sample of BODIPY **3b** (Figure 5.11). In comparison to previously reported boron-dipyrromethene compounds, and BODIPY **1a** from Chapter 2, the BODIPY core of **3b** adopts expected symmetry, bond lengths, planarity, and orthogonal dihedral angles of the F atoms relative to the  $\text{C}_9\text{N}_2\text{B}$  aromatic framework.<sup>32, 33</sup> The dihedral angle of the *meso*-substituent are also nearly  $90^\circ$  out-of-plane of the BODIPY core in the crystal structure at  $88.01(5)^\circ$ . The refinement details and cell parameters are reported in the experimental details Section 5.4.3.

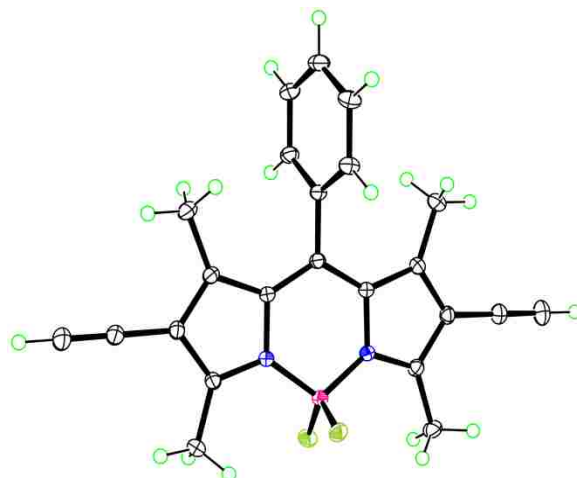
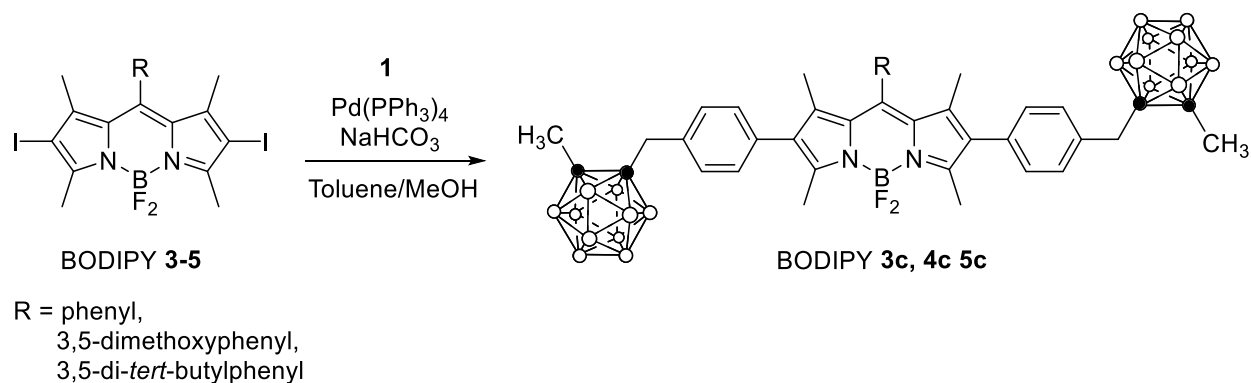


Figure 5.11: Molecular structure of BODIPY **3b** from X-ray crystal structure determinations. Ellipsoids are drawn at the 50% probability level.

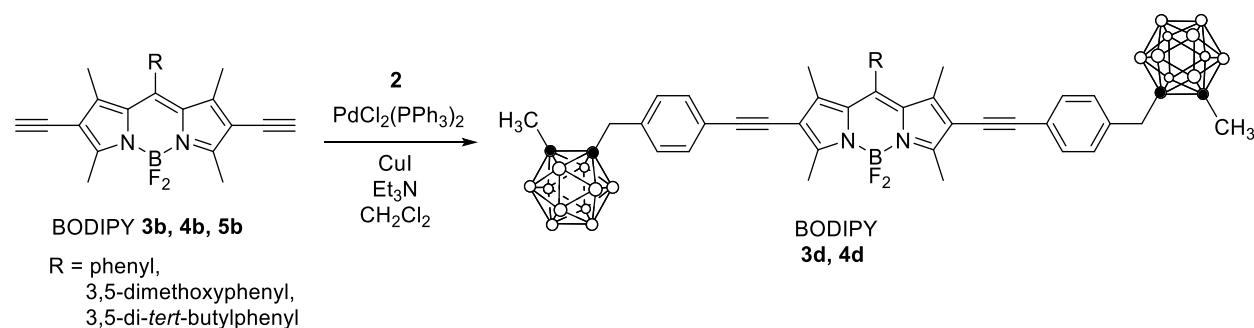
Attaching the carboranyl-compounds **1** and **2** to BODIPYs **3 - 5** and **3b - 5b**, respectively, was attempted via two synthetic routes, Suzuki and Sonogashira palladium-catalyzed couplings. In the first, the carborane functionality **1** was successfully added to the diiodo-BODIPY compounds **3b - 5b** via a Suzuki coupling, Scheme 5.4, facilitated by refluxing palladium tetrakis(triphenylphosphine) in the presence of a mild inorganic base, sodium bicarbonate, in a solution of toluene and methanol under Argon atmosphere.<sup>28</sup>



Scheme 5.4: Synthesis of BODIPYs **3c**, **4c**, and **5c** via Suzuki couplings.



Alternatively, an attempt was made to add the therapeutic carborane moiety to the 2,6-diethynyl-BODIPY compounds **3b**, **4b**, and **5b** via a Sonogashira coupling with compound **2**, as shown in Scheme 5.5. The additional alkyne subunit was anticipated to allow for facile addition of the *para*-iodo-phenyl-carborane **2** as well as to extend the  $\pi$ -conjugation of the system to yield more red-shifted absorption and emission profiles compared to that of both the starting alkynes and of the products of the previously described Suzuki couplings. BODIPY **3b**, **4b**, and **5b** were stirred under argon at room temperature in a mixture of DCM and triethylamine in the presence of bis(triphenylphosphine) palladium dichloride and a copper iodide reducing agent. However, despite numerous attempts in which the palladium source, reaction time, and temperature were varied, the Sonogashira coupling produced limited amounts of the desired products **3d** and **4d** and none of **5d**, as well as a multitude of inseparable bi-products as indicated by TLC.



Scheme 5.5: Attempted syntheses of BODIPY **3d**, **4d**, and **5d** via Sonogashira coupling.

Analysis of the crude mixture obtained from the attempted Sonogashira couplings by MALDI-TOF mass spectrometry revealed successful coupling to a limited extent, yielding both mono and di-coupled products, and the loss of one or two boron atoms from the carborane to yield the anion *nido*-carboranes. Corresponding  $m/z$  peaks for the mono coupling products of **3b** and **4b**

were found as  $[M-B]^+$  at 711.13 and 771.15, whereas the di coupling product of **3b** was found as  $[M+1]^+$  at 855.47, and the di coupling product of **4d** was identified as  $[M-B]^+$  at 916.50. Despite innumerable attempts, pure forms of neither the mono nor di products could be isolated, even after careful preparative thin layer chromatography (TLC), and spectrometric results varied between runs.

At this point it was realized that the triethylamine used to facilitate the conversion of the alkyne into the organocuprate was likely the tyrant preventing successful coupling, Figure 5.13.

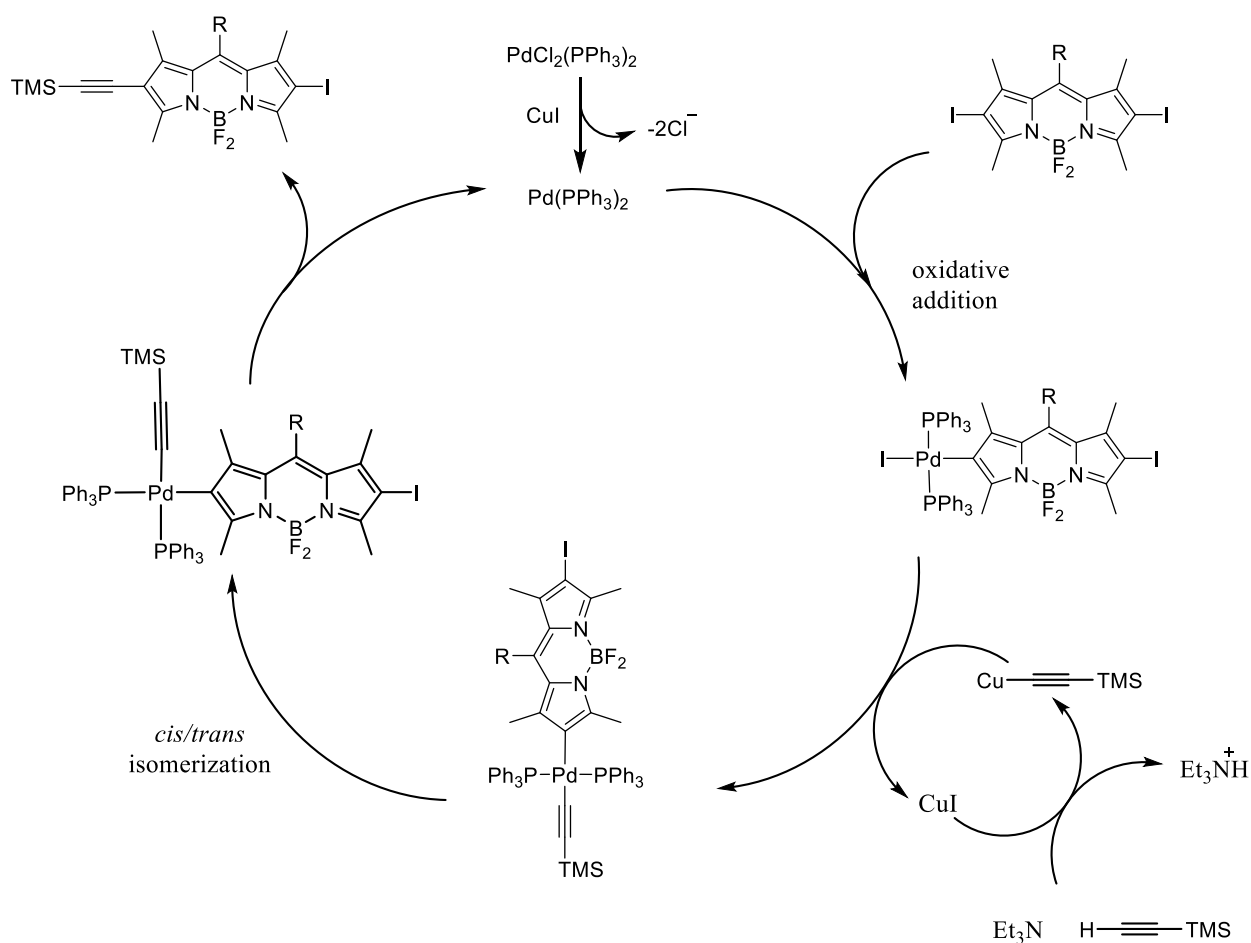
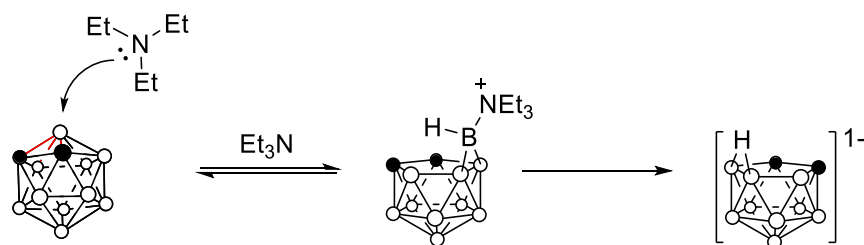


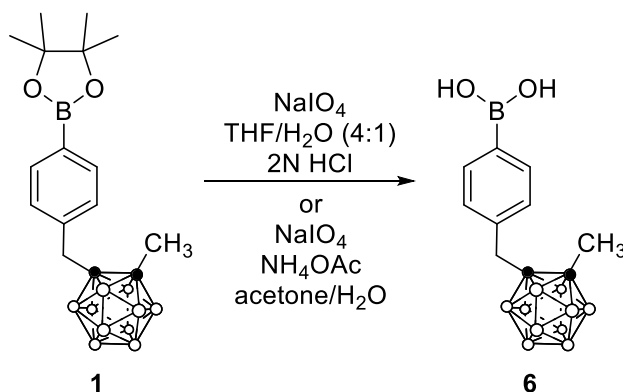
Figure 5.13: Proposed catalytic cycle for palladium-mediated Sonogashira couplings of BODIPYs.

The methyl-*ortho*-carborane which makes up compound **2**, despite the added stability of the methyl substituent on the second carbon, was highly sensitive to organic base and would readily convert to the *nido*-carborane form, as shown in Scheme 5.6. Once in this form, extended exposure to base in the presence of palladium led to further decomposition and a multitude of side reactions.



Scheme 5.6. Proposed mechanism for conversion of closo-*o*-carborane to nido-*o*-carborane.<sup>34</sup>

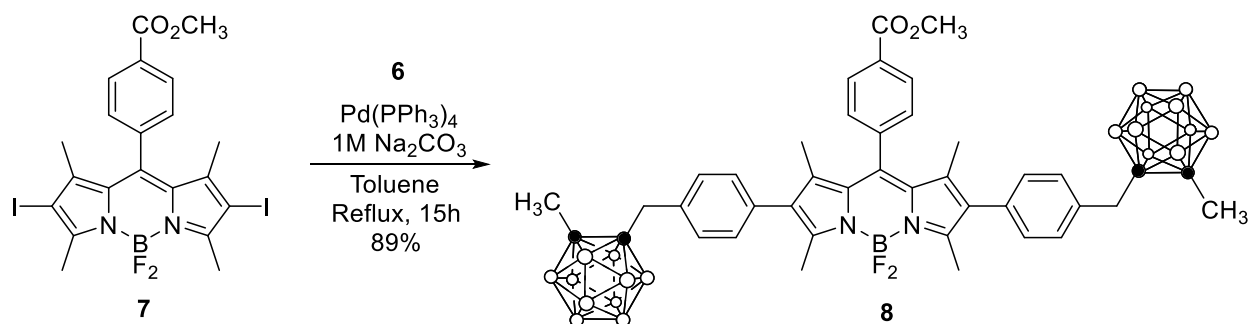
Reevaluation of the Suzuki coupling attempts led to the thought to convert the boronic acid pinacol ester into the boronic acid to reduce potential steric repulsion. Several attempts were made to convert **1** into **6**, following a published procedure using sodium periodate followed by overnight exposure to aqueous hydrochloric acid,<sup>27</sup> Scheme 5.7.



Scheme 5.7: Conversion of boronic acid pinacol ester **1** to boronic acid **6**.

This reaction produced inconsistent conversion, and afforded the desired boronic acid **6** in 82% yield following 30 minute exposure to sodium periodate in THF/H<sub>2</sub>O (4:1) followed by the addition of 2N HCl and overnight stirring on only one occasion. Alternatively, the acid work-up was replaced by reaction of the ester/periodate mixture in acetone/H<sub>2</sub>O with ammonium acetate to afford **6** in 50% yield.

With the boronic acid in hand, the Suzuki coupling could be attempted with a 2,6-diiodo-BODIPY. Anticipating that the boronic acid would successfully yield the desired long wavelength absorbing and emitting, carborane-bearing BODIPY, a diiodo-BODIPY bearing a suitable appendage for further conjugation to targeting functionalities, such as biomolecules, was selected. BODIPY **7** which bears a methyl ester at the *para*-position of the *meso*-phenyl substituent, the synthesis of which was previously described in Chapter 2, underwent successful coupling with compound **6** after refluxing in toluene in the presence of Pd(PPh<sub>3</sub>)<sub>4</sub> and 1M Na<sub>2</sub>CO<sub>3</sub> for 15 hours to produce compound **8** in 89% yield after work up and column chromatography, Scheme 5.8, Figures 5.14 and 5.15.



Scheme 5.8: Suzuki coupling of BODIPY **7** and compound **6**.

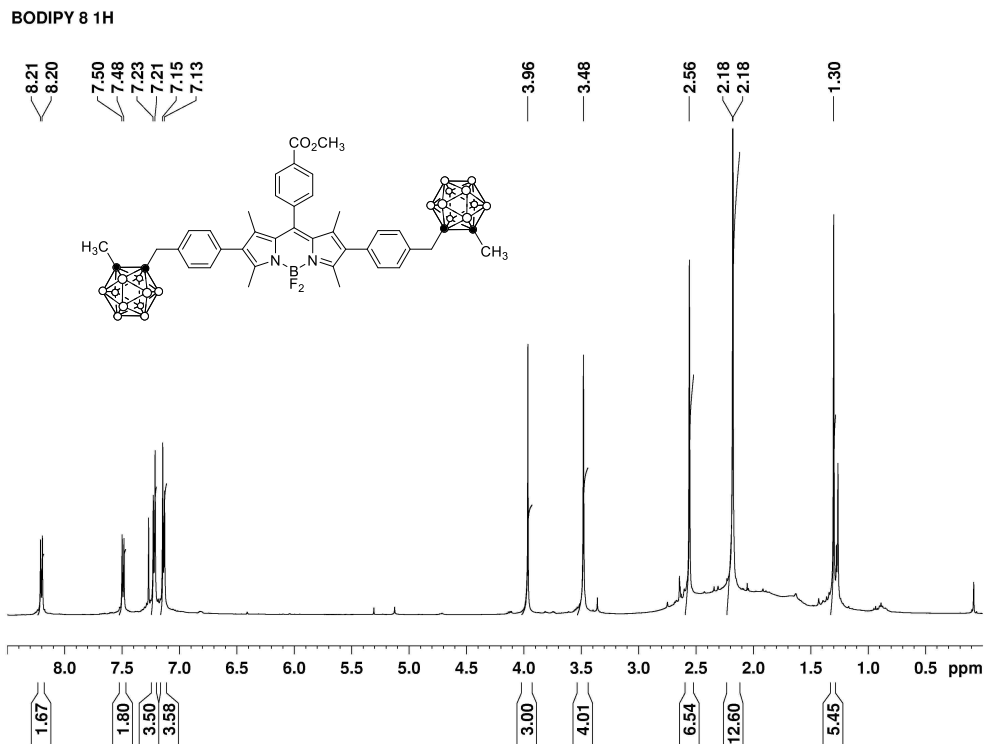


Figure 5.14: <sup>1</sup>H NMR spectrum of BODIPY 8 in deuterated chloroform at 400MHz.

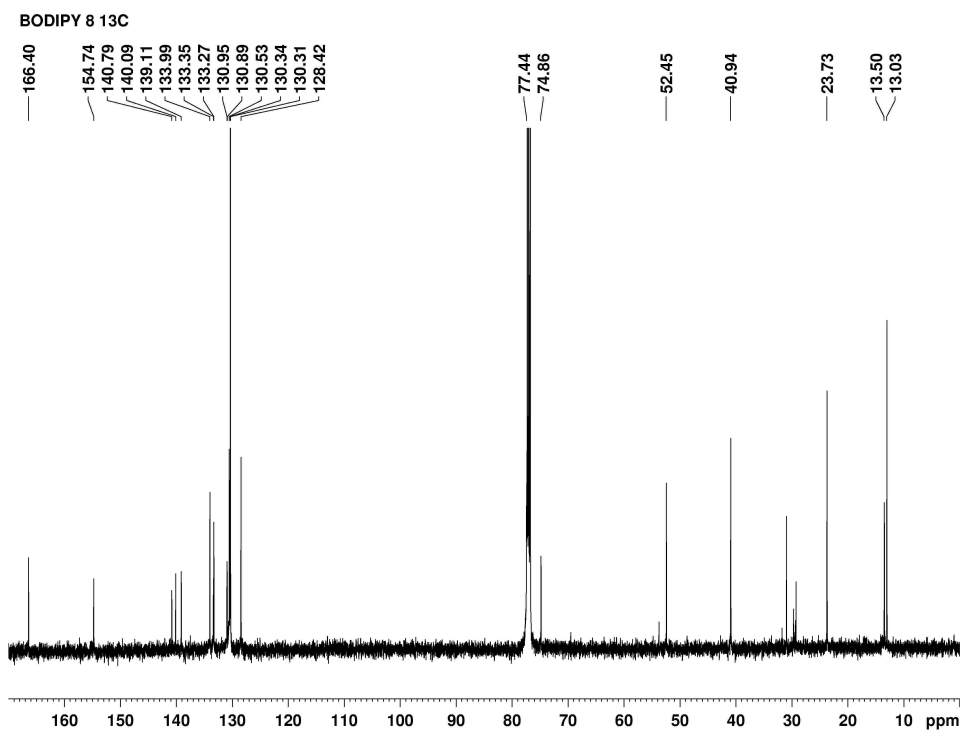
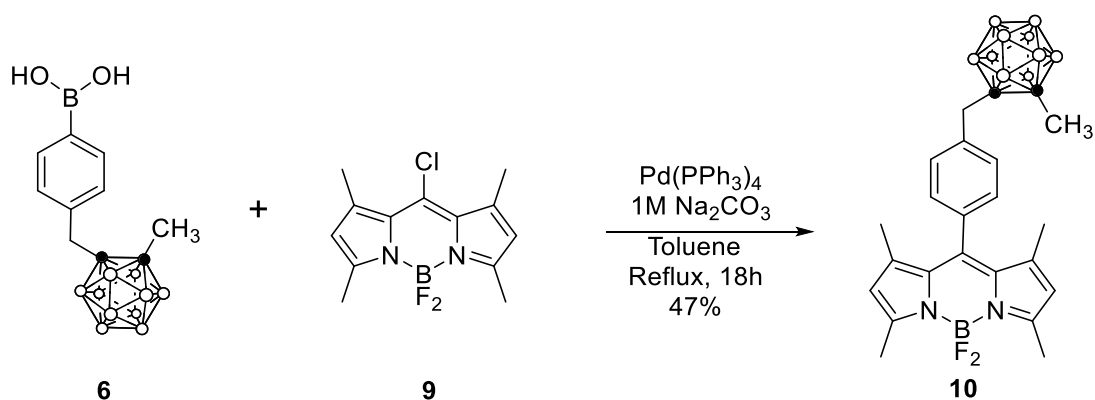


Figure 5.15: <sup>13</sup>C NMR spectrum of BODIPY 8 in deuterated chloroform at 100MHz.

In order to explore the scope of the Suzuki cross-coupling of halogenated BODIPYs with the carboranyl-phenyl boronic acid, *meso*-chloro-1,3,5,7-tetramethyl BODIPY **9** was obtained from fellow group-mate Dr. Haijun Wang.<sup>35</sup> Although many reports can be found in literature detailing the palladium-catalyzed cross-couplings of halogens located at the pyrrolic positions of the BODIPY core, Misra *et al.*<sup>36</sup> described the only palladium-catalyzed couplings of *meso*-chloro-BODIPY via Sonogashira protocol with alkynes. Compound **6** and BODIPY **9** were refluxed in toluene with Pd(PPh<sub>3</sub>)<sub>4</sub> and 1M Na<sub>2</sub>CO<sub>3</sub> for 18 hours to produce BODIPY **10** in 47% yield, as shown in Scheme 5.9.



Scheme 5.9: Suzuki coupling of **6** with *meso*-chloro-BODIPY **9**.

The coupling at the *meso*-position of BODIPY was achieved in lower yields than that accomplished at the 2,6-positions, likely as a result of reduced reactivity of this position compared to the relatively more electron rich 2,6-positions, as well as the less favorable oxidative insertion of palladium between C8 and chlorine versus C2/6 and iodine. BODIPYs **8** and **10** along with two additional *meso*-carboranyl-BODIPYs, **11** and **12** synthesized by Dr. Haijun Wang (Figure 5.16),<sup>37</sup> were subjected to *in vitro* BBB permeability studies.

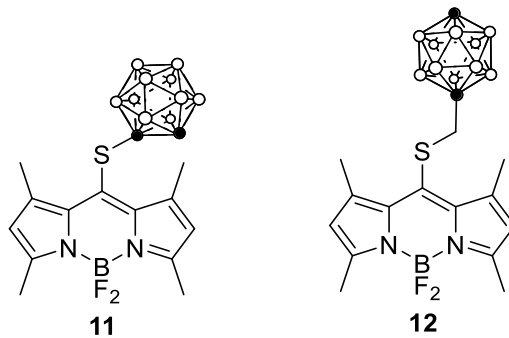


Figure 5.16: Chemical structures of BODIPYs **11** and **12**.

With the development of an efficient route to synthesizing carborane bearing BODIPYs, subsequent work was initiated to improve the water-solubility of BODIPY **8** and to enhance its cellular uptake and BBB permeability. Conjugation of polyamines, charged amino acids, such as arginine, lysine, and glutamate, and the biomolecule folate, through the carbonyl functionality on the *meso*-phenyl of BODIPY **8** may allow for the development of more effective BBB permeable BNCT agents. Polyamines have been shown to increase uptake into cancer cells due to up-regulated polyamine transports on cancer cells,<sup>38-41</sup> and folate, whose receptors are overexpressed on epithelial cells, has recently been shown by Ng *et al.* to favor greater internalization of BODIPYs in MCF-7 cells.<sup>42-45</sup>

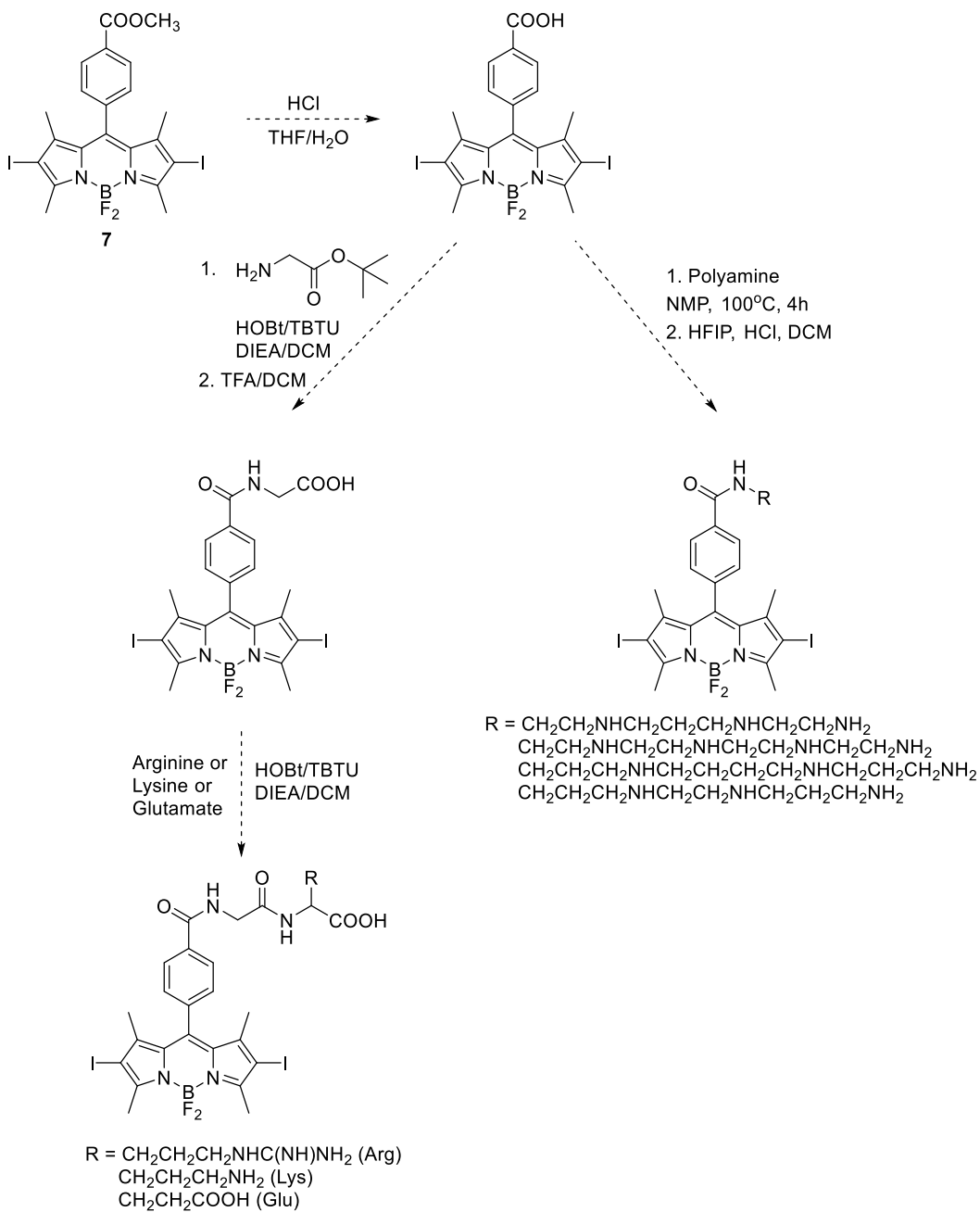
The initial strategy for incorporating these potential directing groups involved first installing the polyamine, folate, and amino acids to the *meso*-phenyl of BODIPY **7** followed by the previously described cross-coupling reaction with compound **6**, as shown in Scheme 5.10. It was believed that the polyamines could be directly conjugated to the free acid, due to the limited steric strain they would encounter. On the other hand, the amino acids and folate were thought to be too sterically congested at the amino terminus desired for conjugation, and thus were expected to undergo more facile conjugation with a spacer between the BODIPY and the biomolecule. A

glycine spacer was selected for conjugation to the amino acids. Conversely, the folate would first be modified by conjugation with *N*-Boc-ethylenediamine through either of the free carboxylic acids. Following removal of the Boc-protecting group, the folate moiety could be conjugated to the BODIPY.

Nonetheless, cleavage of the methyl ester from **7** to obtain the free carboxylic acid proved futile. Attempted hydrolysis following a procedure reported by Giessler *et al.*<sup>46</sup> with dilute and concentrated HCl returned unreacted starting material even when heat was applied. Basic hydrolysis with NaOH, LiOH, and NaCN/DBU all resulted in immediate decomposition of starting material. Presence of iodines at the 2,6-positions was assumed to be the cause of rapid decomposition, therefore, the synthetic scheme was reevaluated to first cleave the methyl ester from unhalogenated BODIPY **13**, conjugate the desired biomolecule, and complete with late stage iodination and Suzuki coupling to produce the desired conjugates.

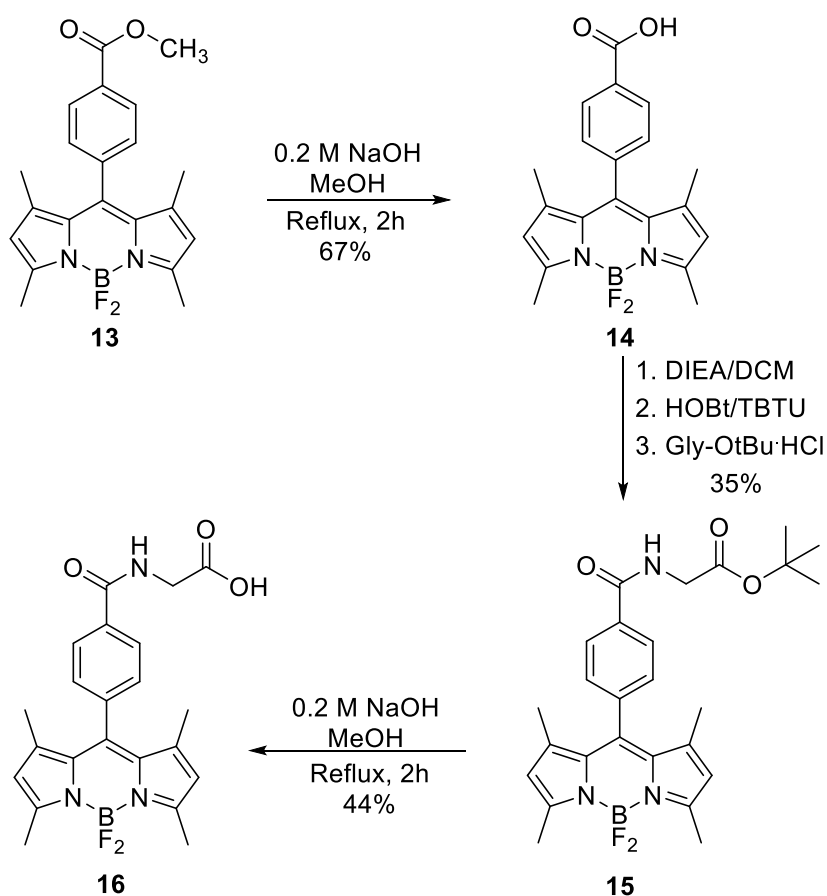
This latter approach proved successful in the early stages. BODIPY **13** underwent facile hydrolysis of the methyl ester, as indicated by loss of the methoxy signal at 6.96 ppm in the <sup>1</sup>H-NMR, by refluxing in methanol doped with 0.2 M sodium hydroxide for two hours to yield 67% of the free carboxylic acid BODIPY **14** as an orange solid following acidification of the condensed residue with 2N HCl and filtration, Scheme 5.11.<sup>47</sup> Glycine *tert*-butyl ester hydrochloride (Gly-OtBu·HCl) was then reacted with the free carboxylic acid of **14**. BODIPY **14** was first treated with diisopropylethylamine in DCM for one hour followed by activation of the carboxylic acid with peptide coupling reagents HOBt and TBTU for an additional hour. Finally, Gly-OtBu was added and the resulting solution was allowed to stir overnight. The reaction was transferred to a separatory flask and quenched with 5% citric acid. The organic layer was subsequently washed with brine and water and dried over Na<sub>2</sub>SO<sub>4</sub>. Following removal of the solvent, the resulting

residue was purified by silica gel column chromatography using DCM as eluent to obtain the desired conjugate **15** in 35% yield. The  $^1\text{H-NMR}$ , shown in Figure 5.17, displays new signals at 6.78, 4.19-4.17, and 1.52 ppm corresponding to the newly added NH-,  $\text{CH}_2$ , and *tert*-butyl group of the glycine.



Scheme 5.10: Proposed synthetic pathway of BODIPY-biomolecule conjugates.

Typically, *tert*-butyl esters are readily cleaved with trifluoroacetic acid in high yields. Although this route would have been the easiest way to free the carboxylic acid, attempts to remove acid labile protecting groups from BODIPYs often results in the loss of the BF<sub>2</sub> chelate and product decomposition as observed by countless failed experiments in the Vicente lab. As a result, the same procedure for removal of the methyl ester was employed to remove the *tert*-butyl ester to produce BODIPY **16** in 44% yield following purification, and was confirmed by the disappearance of the nine equivalent proton signal corresponding to the *tert*-butyl group at 1.52 ppm in the <sup>1</sup>H-NMR.



Scheme 5.11: Synthesis of BODIPY **16**.

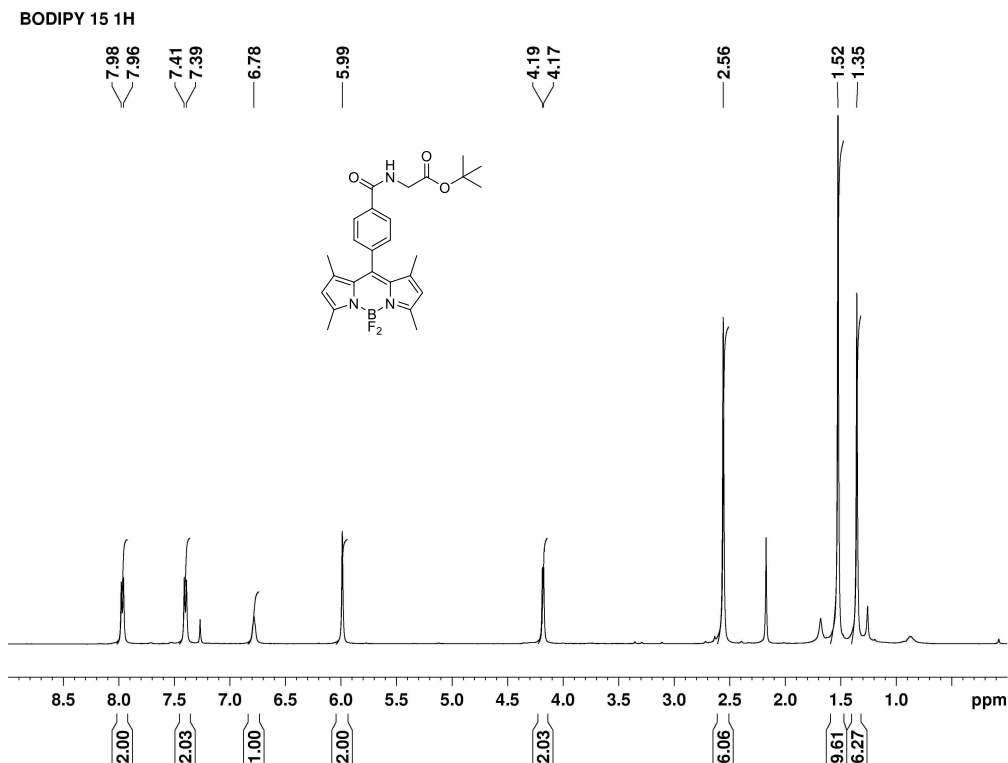
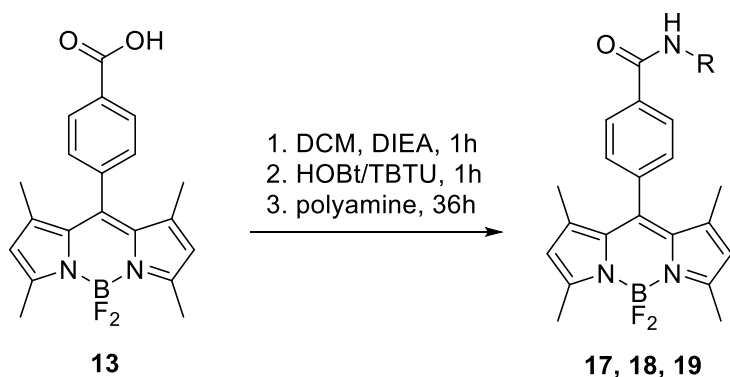


Figure 5.17:  $^1\text{H}$  NMR spectrum of BODIPY **15** in deuterated chloroform at 400MHz.

Preliminary attempts to synthesize the polyamine and amino acid conjugates from BODIPY **13** and BODIPY **16**, respectively, produced a small amount of each conjugate from ~10 mg of starting material, Schemes 5.12 and 5.13. The BODIPYs were dissolved in 5 mL of DCM to which six equivalents of diisopropylethylamine (DIEA) were added and the mixture was allowed to stir for one hour. The starting BODIPYs were poorly soluble in DCM prior to addition of base, but quickly solubilized once DIEA was added. Next, 1.25 equivalents of both HOBt and TBTU were added to activate the terminal carboxylic acid and stirred for an additional hour. Finally, polyamines PA2, PA3, and PA 7 (synthesized by Dr. Dinesh Bhupathiraju) were added to the solutions containing BODIPY **13**, for BODIPYs **17** – **19**, and L-glutamic acid diethyl ester was

added to the solution of BODIPY **16**, for BODIPY **20**. The resulting solutions were left to stir overnight.



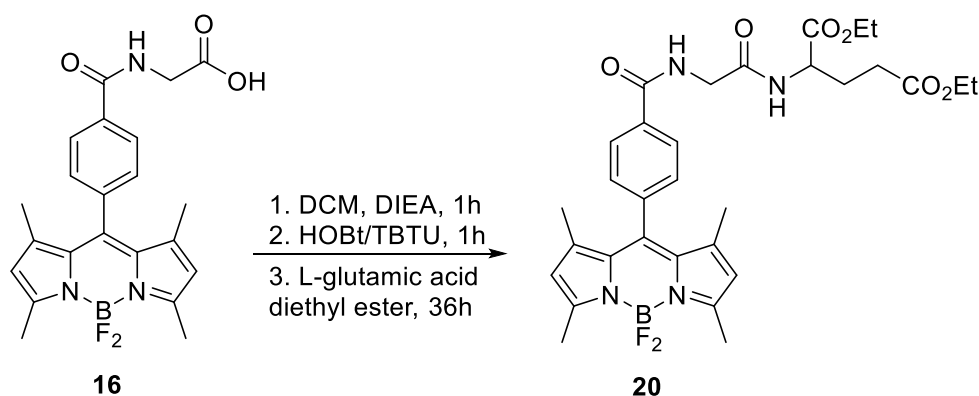
**17** R = CH<sub>2</sub>CH<sub>2</sub>NBocCH<sub>2</sub>CH<sub>2</sub>CH<sub>2</sub>NBocCH<sub>2</sub>CH<sub>2</sub>NHBoc (PA2)  
**18** R = CH<sub>2</sub>CH<sub>2</sub>NBocCH<sub>2</sub>CH<sub>2</sub>NBocCH<sub>2</sub>CH<sub>2</sub>NBocCH<sub>2</sub>CH<sub>2</sub>NHBoc (PA3)  
**19** R = CH<sub>2</sub>CH<sub>2</sub>CH<sub>2</sub>NBocCH<sub>2</sub>CH<sub>2</sub>NBocCH<sub>2</sub>CH<sub>2</sub>CH<sub>2</sub>NHBoc (PA7)

Scheme 5.12: Conjugation of polyamines to BODIPY **13**.

After 36 hours, samples of the crude mixtures were submitted to high resolution ESI-MS. The desired products were identified by their [M+H]<sup>+</sup> peaks of 811.4724, 940.5516, and 611.2848 for BODIPYs **17**, **18**, and **20**, respectively, and by the [M+Na]<sup>+</sup> peak of 847.4724 for BODIPY **19**. The reactions were quenched with 5% citric acid and the organic layer was separated and washed with brine and water. The combined organic layers were dried over Na<sub>2</sub>SO<sub>4</sub> and the solvent was removed under vacuum. TLC of the resulting residues revealed several fluorescent spots. Further purification to obtain pure products for further characterization will be achieved by HPLC.

Further optimization is required to synthesize the glycine-BODIPY conjugate **15** in greater yields, possibly through a change in solvent from DCM to DMF, the solvent of choice for most bench-top peptide coupling reactions. The coupling reagents HOBt/TBTU could also be exchanged for similar reagents, including DCC/DMAP, which may provide greater activation of

the carboxylic acid prior to the attempted conjugation. With conditions that return more efficient conversion of **14** to **15** deduced, attention can be turned to applying that protocol to the conjugation of the targeting biomolecules. Once conjugated, iodination and ensuing Suzuki coupling with **6** will complete the synthesis and the carboranyl-BODIPYs can undergo *in vitro* uptake, cytotoxicity, and BBB permeability evaluations, as proposed in Scheme 5.14.

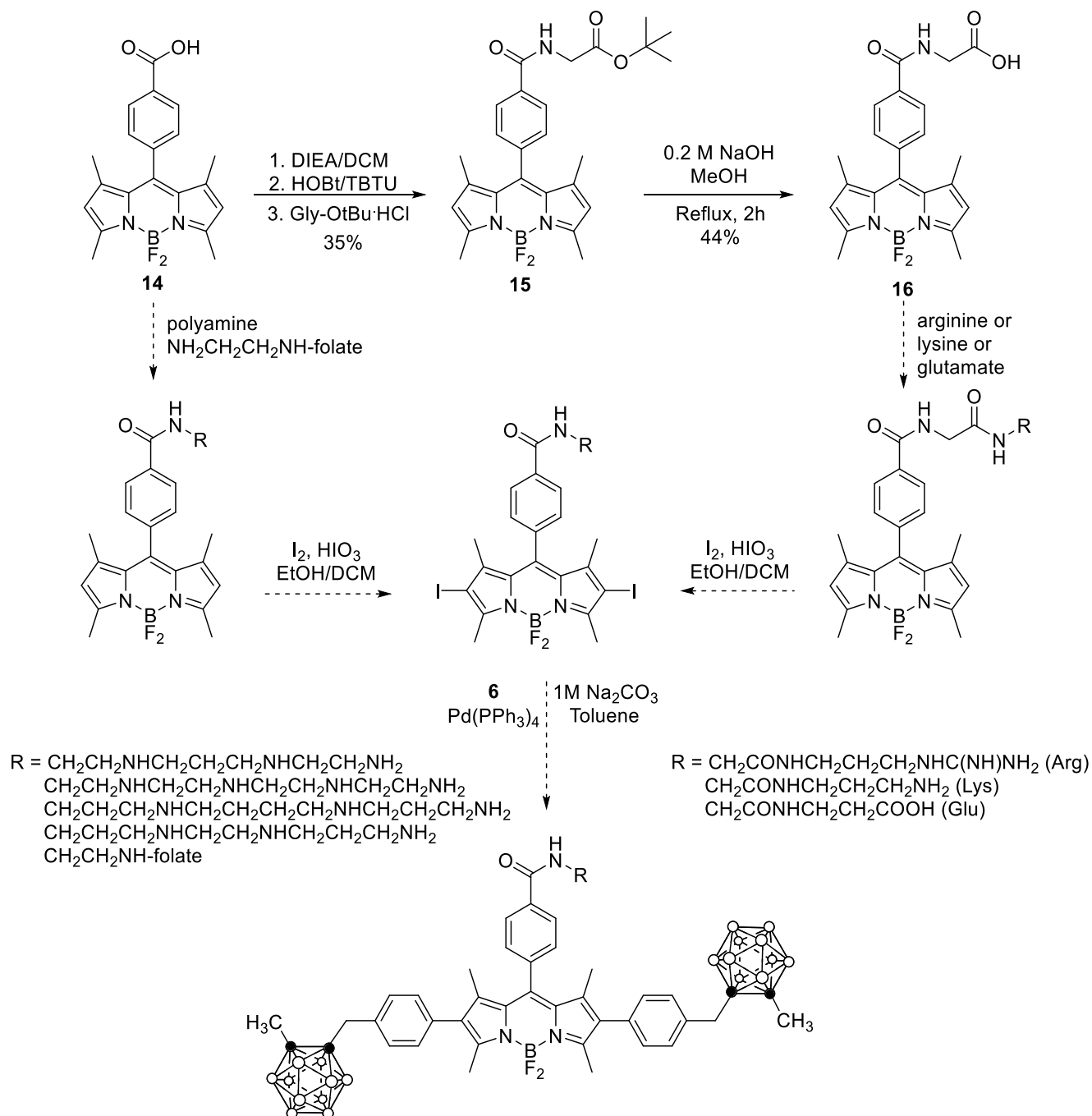


Scheme 5.13: Conjugation of amino acid to BODIPY **16**.

### 5.2.2 Spectroscopic Investigations

Preliminary photophysical evaluations were carried out on BODIPY **3a,b**, **4a,b**, and **5a,5b** in dichloromethane and tetrahydrofuran, while evaluation of BODIPYs **8**, **11**, and **12** were conducted in dimethyl sulfoxide. The fluorescent quantum yields were calculated using Rhodamine 6G in ethanol ( $\Phi_F = 0.95$ ) as the standard, the results of which are shown in Figures 5.18 – 20 and summarized in Table 5.1.

As expected, BODIPYs **3a,b**, **4a,b**, and **5a,b** displayed greater red-shifted absorption and emission profiles than their unsubstituted counterparts (abs/em 499-502 nm/507-511 nm). BODIPYs **3a**, **4a**, and **5a**, bearing ethynyltrimethylsilane functionalities at the  $\beta$ -position displayed a Stokes' shift of 52-56 nm for **3a** and **4a**, and 33 nm for **5a**.



Scheme 5.14: Proposed synthetic completion of targeting carboranyl-BODIPYs.

It has been reported that addition of ethynyltrimethylsilane groups at the  $\beta$ -position induces a shift of approximately 50 nm in absorption accompanied by a 20 nm Stokes' shift due to the extension of  $\pi$ -conjugation.<sup>48</sup> The electron withdrawing effect of the silicon might play a role in decreasing the HOMO/LUMO gap thus increasing the  $\lambda_{\text{abs,max}}$ .<sup>49, 50</sup> Removal of the TMS-group causes the energy of the LUMO to increase and creates a decrease in the  $\lambda_{\text{abs,max}}$ , as observed in BODIPYs **3b**, **4b**, and **5b**.

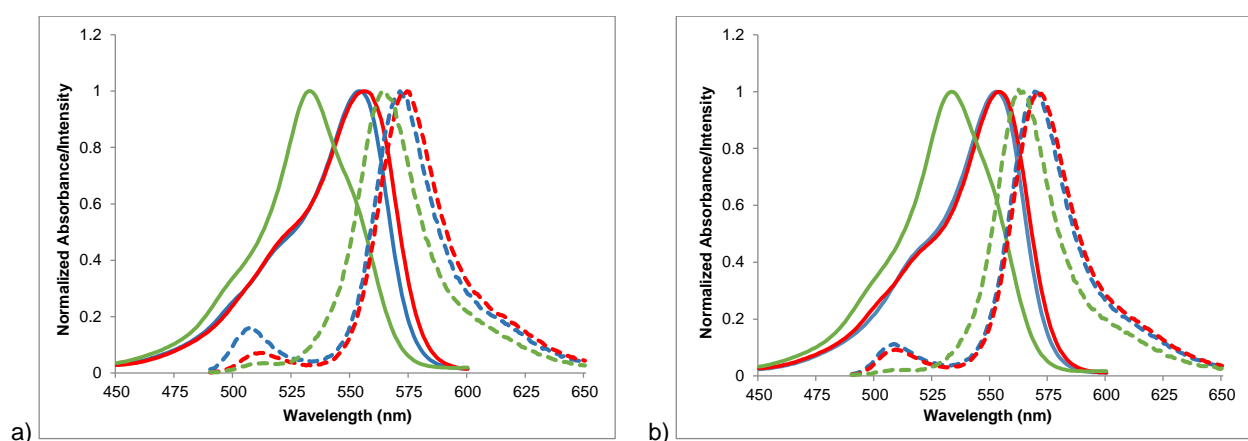


Figure 5.18: Normalized absorption (solid line) and emission (dashed line) spectrum of BODIPYs **3a** (blue), **4a** (red), and **5a** (green) in DCM (a) and THF (b).

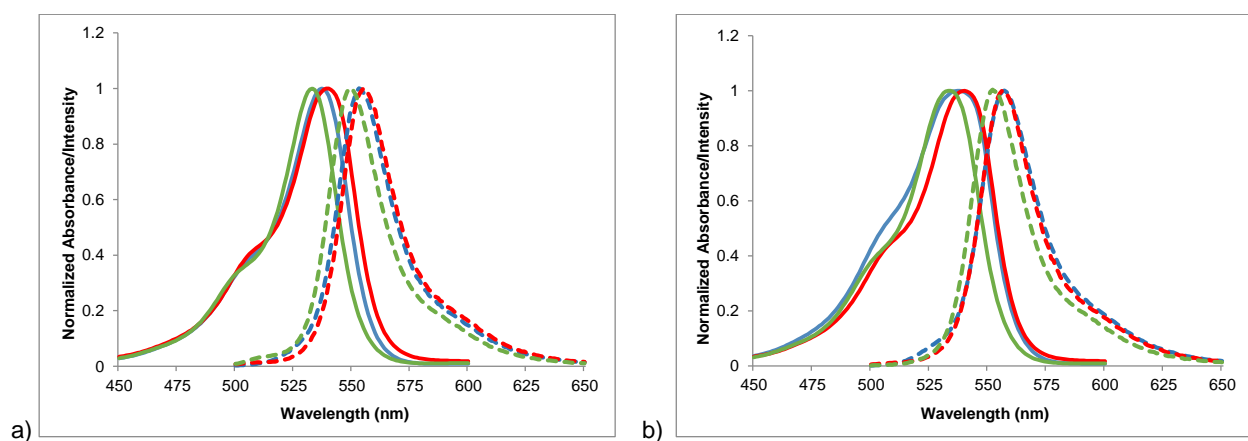


Figure 5.19 Normalized absorption (solid line) and emission (dashed line) spectrum of BODIPYs **3b** (blue), **4b** (red), and **5b** (green) in DCM (a) and THF (b).

The carboranyl-BODIPYs **8**, **11**, and **12** displayed similar absorption and emission shifts to the diiodo-BODIPYs (detailed in Chapter 2) in DMSO. All BODIPYs displayed the characteristic Q-band absorption around 530 nm with a shoulder at slightly lower wavelength. Additionally, large extinction coefficients were calculated ( $\log \epsilon = 4.68 - 4.37$ ) as anticipated and Stokes' shifts of 14 – 27 nm were observed. The extended  $\pi$ -conjugation through the 2,6-positions of BODIPY **8** produced an approximately 30 nm red-shift in absorption and a 45 nm red-shift in the emission profile in agreement with previously reports of similarly decorated BODIPYs.<sup>51</sup> On the other hand, the electron-donating effect of the lone pairs on sulfur in BODIPYs **11** and **12** increase the  $\pi$ -conjugation of the core. This stabilizes the LUMO via greater delocalization of electron density compared to the *meso*-aryl BODIPYs whose *meso*-substituents do not participate in the conjugation of the BODIPY core.<sup>50</sup> The resultant decreased HOMO – LUMO gap corresponds to a red-shift in the photophysical profiles of **11** and **12**.

When excited at 500 nm, BODIPY **11**'s emission profile overlapped with the long wavelength end of another fluorescence producing energy transition, preventing the visualization of the expected peak around 550 nm. When excited at a shorter wavelength, 490 nm, a sharp emission peak was produced centered around 509 nm. This product impurity or more fluorescent transition results in a blue shift compared to the absorption maximum at 538 nm.

Due to an insufficient amount of BODIPY **10**, its photophysical properties could not be evaluated. However, to the naked eye, **10** appears as an orange solid, a yellow solution, and emits green fluorescence, much like the *meso*-aryl tetramethyl-BODIPYs of Chapter 2.

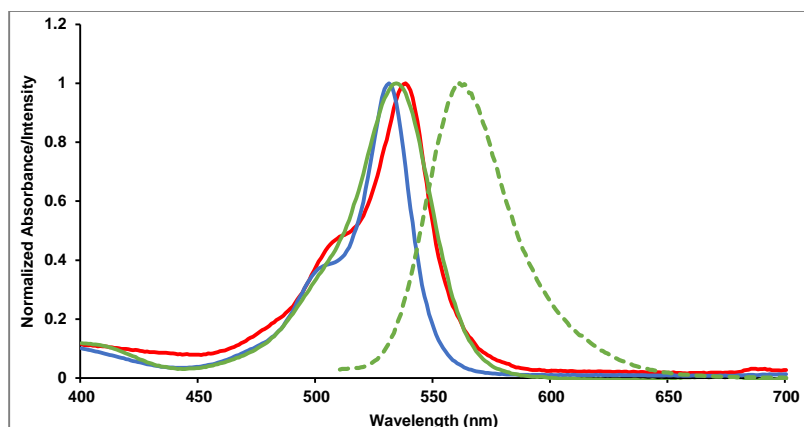


Figure 5.20: Normalized absorption (solid line) spectra of BODIPYs **8** (green), **11** (red), and **12** (blue) and emission (dashed line) spectra of **8** in DMSO.

Table 5.1: Photophysical properties of BODIPY **3a** - **5a** and **3b** - **5b** in dichloromethane and tetrahydrofuran, and BODIPY **8** and **10-12** in dimethyl sulfoxide.

Compound	Solvent	$\lambda_{\max}$ abs (nm)	$\lambda_{\max}$ em (nm)	log $\epsilon$	$\Phi_F$	Stokes' Shift (nm)
<b>3a</b>	DCM	554	571	4.77	0.09	17
	THF	552	569	4.80	0.15	17
<b>4a</b>	DCM	556	574	4.73	0.20	18
	THF	554	570	4.75	0.50	16
<b>5a</b>	DCM	533	564	4.70	0.19	31
	THF	533	562	4.68	0.08	29
<b>3b</b>	DCM	537	553	4.88	0.13	16
	THF	537	557	5.05	0.27	20
<b>4b</b>	DCM	540	555	5.02	0.13	15
	THF	540	556	5.05	0.14	16
<b>5b</b>	DCM	533	550	4.83	0.33	17
	THF	533	552	5.04	0.11	19
<b>8</b>	DMSO	534	561	4.38	0.99	27
<b>10</b>	DMSO	n/a	n/a	n/a	n/a	n/a
<b>11</b>	DMSO	538	n/a	4.37	n/a	n/a
<b>12</b>	DMSO	531	545	4.68	0.03	14

### 5.2.3 *In vitro* BBB Permeability

The BBB permeability of BODIPYs **8** and **10 - 12** was investigated by Dr. Dinesh Bhupathiraju using the human brain endothelial cell line hCMEC/D3. The hCME/D3 cell line was determined to be the ideal model for *in vitro* studies on the human BBB. Previous *in vitro* BBB studies have been successfully conducted to study the drug transportation across the BBB.<sup>52-54</sup> Therefore, the carboranyl-BODIPYs' BBB permeability on hCMEC/D3 cells were investigated and were compared to a fluorescent molecule known to bypass the BBB, Lucifer yellow FTIC40K.<sup>52</sup> Prior to being exposed to the compounds under investigation, the *in vitro* BBB model composed of basolateral and apical chambers as shown in Figure 5.21, was prepared from a known protocol.<sup>55</sup>

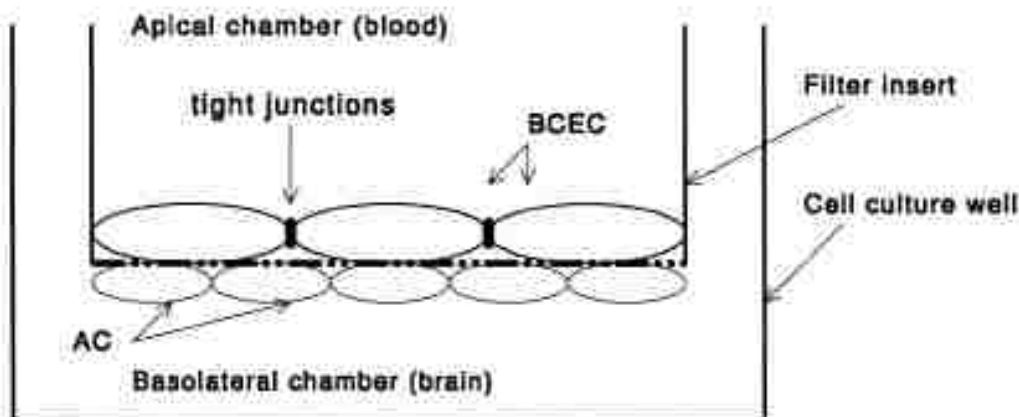


Figure 5.21: Blood brain barrier model used *in vitro*.<sup>55</sup>

Once prepared, the carboranyl-BODIPYs were added to the apical chamber containing a monolayered cell membrane. Then, at time intervals of 0, 30, and 60 minutes, the concentration of compounds in the basolateral layer was measured using a fluorescence plate reader. This

measurement was then applied to the equation for the permeability coefficient ( $P$ ) (found in Section 5.4.4.4),<sup>55</sup> the results of which are summarized in Table 5.3.

Only one carboranyl-BODIPY, **11**, showed high permeability, and was more efficiently able to migrate to the basolateral layer than the standard. BODIPYs **8** and **10** in which the carborane moiety was conjugated to the BODIPY with a phenyl spacer, showed decreased solubility in the cellular media as a result of their highly hydrophobic character, noted by their  $\text{Log } P$  values of 1.41, respectively compared to 0.85 and 0.89 of BODIPYs **11** and **12**. *In vitro* investigations of the cellular uptake, cytotoxicity, and subcellular localization in T98G cells are planned in the near future. Subsequent work to promote water solubility and uptake potential of BODIPY **8** has been initiated, as detailed in Section 5.2.1, and will be completed in the near future.

Table 5.3: *In vitro* permeability coefficient values for carboranyl-BODIPYs **8**, **10** - **12**.

Compound	Permeability coefficient (Pc) cm/s at 30 min	Permeability coefficient (Pc) cm/s at 60 min	Log $P$
Lucifer Yellow	$2.9351 \times 10^{-5}$	$2.03585 \times 10^{-5}$	
<b>8</b>	$4.76443 \times 10^{-8}$	$2.80537 \times 10^{-8}$	1.41
<b>10</b>	$6.58966 \times 10^{-8}$	$3.98496 \times 10^{-8}$	n/a
<b>11</b>	$2.75514 \times 10^{-5}$	$3.40739 \times 10^{-5}$	0.85
<b>12</b>	$3.23795 \times 10^{-7}$	$2.79189 \times 10^{-7}$	0.89

### 5.3 Conclusions

The synthesis, spectroscopic properties and BBB permeability toward the human brain endothelial cell line hCMEC/D3 of four BODIPYs were investigated. Two different synthetic

routes, Suzuki and Sonogashira cross coupling reactions, were explored to provide a facile approach to attaching carborane-bearing moieties to the BODIPY scaffold. Attempts at utilizing the Sonogashira protocol led to decomposition of the carborane after prolonged exposure to organic, non-nucleophilic base. The Suzuki method with a boronic ester functionalized carborane moiety **6** proved successful, allowing for the synthesis of two carboranyl-BODIPYs **8** and **10** of different connectivity. Studies of the spectroscopic profile of BODIPY **8** revealed an absorption around 534 nm and emission of 561 nm. Along with two additional *meso*-carboranyl BODIPYs **11** and **12** synthesized by Dr. Haijun Wang, the BBB permeability assessment of four carboranyl-BODIPYs revealed only one, BODIPY **10**, to efficiently penetrate the BBB. Subsequent work was initiated to install polyamines, amino acids, and a folate moiety to BODIPY **8** to aid in the water solubility, BBB permeability, and tumor selectivity of the carborane-containing BODIPY.

## 5.4 Experimental

### 5.4.1 General Information

Reagents and solvents were acquired from Sigma Aldrich and used without further purification. Reactions were monitored by TLC using 0.2 mm silica plates with UV indicator (UV254). Column chromatography was executed using Sorbent Technologies 60Å silica gel (230 - 400 mesh). Merck TLC silica gel 60 glass plates were used for preparative thin layer chromatography. All  $^1\text{H}$  NMR and  $^{13}\text{C}$  NMR spectra were obtained using a Bruker AV-500, DPX-400, AV-400, or DPX-250 spectrometer (500 MHz, 400 MHz or 250 MHz for  $^1\text{H}$ , 100 MHz for  $^{13}\text{C}$ ) with samples dissolved in deuterated chloroform or acetone using trimethylsilane as an internal indicator. Chemical shifts ( $\delta$ ) are conveyed in ppm with  $\text{CDCl}_3$  ( $^1\text{H}$ : 7.27 ppm;  $^{13}\text{C}$ : 77.16 ppm) and acetone- $\text{d}_6$  ( $^1\text{H}$ : 2.05 ppm;  $^{13}\text{C}$ : 29.84 ppm) used as references. Coupling constants (J)

are stated in Hertz (Hz). High resolution ESI mass spectra were obtained using an Agilent Technologies 6210 ESI-TOF Mass Spectrometer. MALDI mass spectra were acquired using a Bruker UltrafleXtreme MALDI-TOF/TOF Mass Spectrometer.

#### 5.4.2 Syntheses

**Compound 1:** In a round bottom flask equipped with magnetic stir bar, methyl-o-carborane (0.11 g 0.67 mmol) was dissolved in 10 mL of dry THF. The flask was purged of air and filled with argon three times before being cooled to 0°C. nBuLi solution (0.5 mL, 0.74 mmol; 1.6 M in hexanes) was added drop-wise to the cooled mixture. The mixture was brought to room temperature and stirred for 1 hour. The mixture was then cooled to -78°C. 4-(bromomethyl)benzeneboronic acid pinacol ester (0.2 g, 0.67 mmol) was dissolved in 5 mL THF and added drop-wise to the chilled solution. The mixture was warmed to room temperature and stirred until TLC indicated no starting materials remained. The reaction mixture was poured into 25 mL of brine and extracted with ethyl acetate (3 x 25 mL), dried over Na<sub>2</sub>SO<sub>4</sub> and purified by silica gel column chromatography using 50:50 hexanes/dichloromethane yielding a white solid (0.185 g) in 76% yield.

<sup>1</sup>H-NMR (400 MHz, CDCl<sub>3</sub>) δ 7.80-7.78 (d, *J* = 7.8, 2H), 7.39-7.37 (d, *J* = 7.8, 2H), 4.48 (s, 2H), 1.99 (s, 3H), 3.2-1.2 (br m, 10H), 1.35 (s, 12H); <sup>13</sup>C-NMR (100 MHz, CDCl<sub>3</sub>) δ 137.81, 134.93, 129.62, 128.23, 83.84, 74.86, 41.16, 33.25, 24.85, 23.57; MS (ESI-TOF) *m/z* Calculated for C<sub>16</sub>H<sub>28</sub>B<sub>11</sub>O<sub>2</sub>: 373.3112; Found: negative ion [M-H]<sup>-</sup>: 373.3349. The NMR data is in agreement with that already published.<sup>27</sup>

**Compound 2:** In a round bottom flask equipped with magnetic stir bar, methyl-o-carborane (0.11 g 0.67 mmol) was dissolved in 10 mL of dry THF. The flask was purged of air and filled with argon three times before being cooled to 0°C. nBuLi solution (0.5 mL, 0.74 mmol; 1.6 M in hexanes) was added drop-wise to the cooled mixture. The mixture was brought to room temperature and stirred for 1 hour. The mixture was then cooled to -78°C. 4-iodobenzyl bromide (0.2 g, 0.67 mmol) was dissolved in 5 mL THF and added drop-wise to the chilled solution. The mixture was warmed to room temperature and stirred until TLC indicated no starting materials remained. The reaction mixture was poured into 25 mL of brine and extracted with ethyl acetate (3 x 25mL), dried over Na<sub>2</sub>SO<sub>4</sub> and purified by silica gel column chromatography using 50:50 hexanes/dichloromethane yielding a white solid (0.235 g) in 93% yield.

<sup>1</sup>H-NMR (400 MHz, CDCl<sub>3</sub>) δ 7.69-7.67 (d, *J* = 8.2, 2H), 7.15-7.13 (d, *J* = 8.2, 2H), 4.43 (s, 2H), 3.2-1.2 (br m, 10H), 2.04 (s, 3H); <sup>13</sup>C-NMR (100 MHz, CDCl<sub>3</sub>) δ 137.97, 137.47, 130.83, 94.09, 80.09, 61.52, 32.43, 25.91; MS (ESI-TOF, negative ion) *m/z* Calculated for C<sub>10</sub>H<sub>16</sub>B<sub>10</sub>I: 373.1227; Found: [M-H]<sup>+</sup>: 373.1449. The NMR data is in agreement with that already published.<sup>29</sup>

**BODIPY 3a:** To a mixture of BODIPY **3** (0.16 g, 0.27 mmol), bis(triphenylphosphine) palladium (II) dichloride (0.009 g, 0.01 mmol), and copper iodide (0.002 g, 0.01 mmol) in triethylamine (10 mL) and DCM (10 mL), ethynyl trimethylsilane (0.12 g, 0.74 mmol) was added drop-wise under Argon. The resulting solution was stirred at room temperature for 12 hours. The mixture was quenched with water washed three times with water. The combined aqueous layers were extracted three times with ethyl acetate and passed through a bed of Na<sub>2</sub>SO<sub>4</sub>. The solvent was removed under vacuum and the resulting residue was purified using silica gel column chromatography with 50:50 Hexanes/DCM as eluent yielding a red solid (0.122 g) in 87% yield.

$^1\text{H-NMR}$  (400 MHz,  $\text{CDCl}_3$ )  $\delta$  7.51-7.50 (m, 3H), 7.25-7.23 (m, 2H), 2.64 (s, 6H), 1.45 (s, 6H), 0.20 (s, 18H);  $^{13}\text{C-NMR}$  (100 MHz,  $\text{CDCl}_3$ )  $\delta$  158.41, 157.09, 152.16, 145.53, 133.14, 130.97, 122.30, 121.58, 83.91, 75.87, 35.00, 31.23, 13.36, 13.87; MS (ESI-TOF)  $m/z$  Calculated for  $\text{C}_{29}\text{H}_{35}\text{BF}_2\text{N}_2\text{Si}_2$ : 516.2399; Found:  $[\text{M}+\text{H}]^+$ : 517.2530.

**BODIPY 3b:** BODIPY **3a** (0.006 g, 0.01 mmol) and freshly ground potassium hydroxide (0.005 g, 0.08 mmol) were dissolved in 1:1 THF/MeOH (1 mL) at room temperature. The reaction was stirred for 2 hours. The mixture was poured into water and the aqueous layer was extracted twice with DCM. The combined organic layers were washed with water and dried over  $\text{Na}_2\text{SO}_4$ . The solvent was evaporated under reduced pressure and resulting residue was purified by silica gel column chromatography using dichloromethane as eluent yielding a red solid (0.030 g) in 51% yield.

$^1\text{H-NMR}$  (400 MHz,  $\text{CDCl}_3$ )  $\delta$  7.53-7.52 (m, 3H), 7.27-7.25 (m, 2H), 3.22 (s, 2H), 2.66 (s, 6H), 1.47 (s, 6H);  $^{13}\text{C-NMR}$  (100 MHz,  $\text{CDCl}_3$ )  $\delta$  129.47, 129.45, 129.42, 129.40, 127.80, 127.76, 127.71, 84.09, 75.91, 16.93, 16.03, 13.50, 13.22; MS (MALDI-TOF-TOF)  $m/z$  Calculated for  $\text{C}_{23}\text{H}_{19}\text{BF}_2\text{N}_2$ : 372.1609; Found:  $[\text{M}]^+$ : 372.297.

**BODIPY 4a:** To a mixture of BODIPY **4** (0.096 g, 0.15 mmol), bis(triphenylphosphine) palladium (II) dichloride (0.005 g, 0.008 mmol), and copper iodide (0.001 g, 0.008 mmol) in triethylamine (10 mL) and DCM (10 mL), ethynyl trimethylsilane (0.075 g, 0.45 mmol) was added drop-wise under Argon. The resulting solution was stirred at room temperature for 12 hours. The mixture was poured into water. The aqueous layer was washed three times with water. The combined aqueous layers were extracted three times with ethyl acetate and passed through a bed of  $\text{Na}_2\text{SO}_4$ .

The solvent was removed under vacuum and the resulting residue was purified using silica gel column chromatography with 50:50 hexanes/DCM as eluent yielding a red solid (0.077 g) in 89% yield.

$^1\text{H-NMR}$  (400 MHz,  $\text{CDCl}_3$ )  $\delta$  6.58-6.57 (t,  $J = 2.3$ , 1H), 6.41-6.40 (d,  $J = 2$ , 2H), 3.80 (s, 6H), 2.64 (s, 6H), 1.63 (s, 6H), 0.22 (s, 18H);  $^{13}\text{C-NMR}$  (100 MHz,  $\text{CDCl}_3$ )  $\delta$  161.98, 158.91, 144.98, 142.47, 135.94, 111.18, 105.72, 101.73, 101.44, 97.11, 55.58, 29.69, 13.56, 13.52, 0.08; MS (ESI-TOF)  $m/z$  Calculated for  $\text{C}_{31}\text{H}_{39}\text{BF}_2\text{N}_2\text{O}_2\text{Si}_2$ : 576.2611; Found:  $[\text{M}]^+$ : 576.279.

**BODIPY 4b:** BODIPY **4a** (0.05 g, 0.1 mmol) and freshly ground potassium hydroxide (0.046 g, 0.8 mmol) were dissolved in 1:1 THF/MeOH (25 mL) at room temperature. The reaction was stirred for 2 hours. The mixture was poured into water and the aqueous layer was extracted twice with DCM. The combined organic layers were washed with water and dried over  $\text{Na}_2\text{SO}_4$ . The solvent was evaporated under reduced pressure and resulting residue was purified by silica gel column chromatography using dichloromethane as eluent yielding a red solid (0.043 g) in 50% yield.

$^1\text{H-NMR}$  (400 MHz,  $\text{CDCl}_3$ )  $\delta$  6.58-6.57 (t,  $J = 2.3$ , 1H), 6.41-6.40 (d,  $J = 2$ , 2H), 3.80 (s, 6H), 3.32 (s, 2H), 2.64 (s, 6H), 1.63 (s, 6H);  $^{13}\text{C-NMR}$  (100 MHz,  $\text{CDCl}_3$ )  $\delta$  161.98, 158.91, 144.98, 142.47, 135.94, 111.18, 105.72, 101.73, 101.44, 97.11, 55.58, 29.69, 13.56, 13.52; MS (ESI-TOF)  $m/z$  Calculated for  $\text{C}_{25}\text{H}_{24}\text{BF}_2\text{N}_2\text{O}_2$ : 433.1898; Found:  $[\text{M}+\text{H}]^+$ : 433.1896.

**BODIPY 5a:** To a mixture of BODIPY **5** (0.11 g, 0.16 mmol), bis(triphenylphosphine) palladium (II) dichloride (0.006 g, 0.008 mmol), and copper iodide (0.002 g, 0.008 mmol) in triethylamine (10 mL) and DCM (10 mL), ethynyl trimethylsilane (0.08 g, 0.48 mmol) was added drop-wise

under Argon. The resulting solution was stirred at room temperature for 12 hours. The mixture was poured into water. The aqueous layer was washed three times with water. The combined aqueous layers were extracted three times with ethyl acetate and passed through a bed of Na<sub>2</sub>SO<sub>4</sub>. The solvent was removed under vacuum and the resulting residue was purified using silica gel column chromatography with 50:50 hexanes/DCM as eluent yielding a red solid (0.189 g) in 93% yield.

<sup>1</sup>H-NMR (400 MHz, CDCl<sub>3</sub>) δ 7.51-7.50 (t, *J* = 1.7, 1H), 7.07-7.06 (d, *J* = 1.2, 2H), 2.64 (s, 6H), 1.44 (s, 6H), 1.32 (s, 18H), 0.20 (s, 18H); <sup>13</sup>C-NMR (100 MHz, CDCl<sub>3</sub>) δ 156.49, 152.23, 145.41, 133.82, 122.47, 122.27, 121.88, 121.80, 101.52, 97.22, 85.44, 35.14, 31.37, 16.67, 15.96, 0.09; MS (ESI-TOF) *m/z* Calculated for C<sub>37</sub>H<sub>52</sub>BF<sub>2</sub>N<sub>2</sub>Si<sub>2</sub>: 629.3730; Found: [M+H]<sup>+</sup>: 629.3648.

**BODIPY 5b:** BODIPY **5a** (0.11 g, 0.18 mmol) and freshly ground potassium hydroxide (0.08 g, 1.4 mmol) were dissolved in 1:1 THF/MeOH (25 mL) at room temperature. The reaction was stirred for 2 hours. The mixture was poured into water and the aqueous layer was extracted twice with DCM. The combined organic layers were washed with water and dried over Na<sub>2</sub>SO<sub>4</sub>. The solvent was evaporated under reduced pressure and resulting residue was purified by silica gel column chromatography using dichloromethane as eluent yielding a red solid (0.044 g) in 51% yield.

<sup>1</sup>H-NMR (400 MHz, CDCl<sub>3</sub>) δ 7.53-7.52 (t, *J* = 1.7, 1H), 7.09-7.08 (d, *J* = 1.2, 2H), 3.31 (s, 2H), 2.66 (s, 6H), 1.45 (s, 6H), 1.33 (s, 18H); <sup>13</sup>C-NMR (100 MHz, CDCl<sub>3</sub>) δ 158.32, 152.42, 145.44, 133.62, 122.59, 121.66, 114.81, 94.23, 83.82, 75.91, 35.01, 31.24, 13.39, 12.93; MS (ESI-TOF) *m/z* Calculated for C<sub>31</sub>H<sub>36</sub>BF<sub>2</sub>N<sub>2</sub>: 485.2939; Found: [M+H]<sup>+</sup>: 485.2868.

**Compound 6:** In a round bottom flask equipped with a stir bar, compound **1** (0.1 g, 0.27 mmol) and sodium periodate (0.18 g, 0.83 mmol) were dissolved in a 4:1 mixture of THF/H<sub>2</sub>O (4 mL) and stirred at room temperature for 30 minutes. To this mixture was added 2N HCl (0.5 mL) and the reaction was allowed to stir overnight. The mixture was poured into water and extracted with EtOAc. The combined organic layers were dried over Na<sub>2</sub>SO<sub>4</sub> and the solvent was removed under reduced pressure. The resulting residue was purified by silica gel column chromatography using EtOAc as eluent to obtain a white solid (0.064 g) in 82% yield.

<sup>1</sup>H-NMR (400 MHz, CDCl<sub>3</sub>) δ 7.14-7.12 (d, *J* = 7.8, 2H), 7.00-6.97 (d, *J* = 7.8, 2H), 3.41 (s, 2H), 2.75-1.50 (br m, 10H), 2.14 (s, 3H). The <sup>1</sup>H-NMR was in agreement with that already published.<sup>27</sup>

**Compound 8:** BODIPY **7** (0.02 g, 0.03 mmol), compound **6** (0.04 g, 0.13 mmol), and Pd(PPh<sub>3</sub>)<sub>4</sub> (0.004 g, 0.003 mmol) were dissolved in dry toluene (2 mL) over 3Å molecular sieves. A solution of 1M Na<sub>2</sub>CO<sub>3</sub> (0.5 mL) was added and the mixture was stirred at reflux for 15 hours. The reaction was quenched with water and extracted with DCM. The combined organic layers were dried over Na<sub>2</sub>SO<sub>4</sub> and the solvent was evaporated. The resulting residue was purified by silica gel column chromatography using a gradient from hexanes to 50:50 hexanes/DCM as eluent to obtain a red crystalline solid (0.025 g) in 89% yield.

<sup>1</sup>H-NMR (400 MHz, CDCl<sub>3</sub>) δ 8.21-8.20 (d, *J* = 8, 2H), 7.50-7.48 (d, *J* = 8, 2H), 7.23-7.21 (d, *J* = 7.8, 4H), 7.15-7.13 (d, *J* = 7.8, 4H) 3.96 (s, 3H), 3.48 (s, 4H), 2.8-1.5 (br m, 22H), 2.56 (s, 6H), 2.18 (s, 6H), 1.30 (s, 6H); <sup>13</sup>C-NMR (100 MHz, CDCl<sub>3</sub>) δ 166.40, 157.74, 140.79, 140.09, 139.11, 133.99, 133.35, 133.27, 130.95, 130.89, 130.53, 130.34, 130.31, 128.42, 77.44, 74.86, 52.45, 40.94, 23.73, 13.50, 13.03; MS (ESI-TOF) *m/z* Calculated for C<sub>41</sub>H<sub>57</sub>B<sub>21</sub>F<sub>2</sub>N<sub>2</sub>O<sub>2</sub>: 874.6488; Found: [M]<sup>+</sup>: 874.6523.

**Compound 10:** BODIPY **9** (0.01 g, 0.035 mmol), compound **6** (0.022 g, 0.074 mmol), and Pd(PPh<sub>3</sub>)<sub>4</sub> (0.004 g, 0.0035 mmol) were dissolved in dry toluene (2 mL) over 3Å molecular sieves. A solution of 1M Na<sub>2</sub>CO<sub>3</sub> (0.5 mL) was added and the mixture was stirred at reflux for 15 hours. The reaction was quenched with water and extracted with DCM. The combined organic layers were dried over Na<sub>2</sub>SO<sub>4</sub> and the solvent was evaporated. The resulting residue was purified by preparative thin layer chromatography using 5:1 hexanes/EtOAc as eluent to obtain an orange solid (0.008 g) in 47% yield.

<sup>1</sup>H-NMR (400 MHz, CDCl<sub>3</sub>) δ 7.35-7.33 (d, *J* = 7.8, 2H), 7.31-7.30 (d, *J* = 7.8, 2H), 5.99 (s, 2H), 3.55 (s, 2H), 3.0-1.0 (br m, 10H), 2.56 (s, 6H), 2.20 (s, 3H), 1.40 (s, 6H); <sup>13</sup>C-NMR (100 MHz, CDCl<sub>3</sub>) δ 155.75, 142.98, 140.73, 135.84, 131.27, 128.41, 123.20, 121.38, 95.34, 82.90, 71.40, 41.07, 37.50, 14.57, 13.93; MS (ESI-TOF) *m/z* Calculated for C<sub>23</sub>H<sub>34</sub>B<sub>11</sub>F<sub>2</sub>N<sub>2</sub>: 495.3786; Found: [M+H]<sup>+</sup>: 495.3772.

**Compound 14:** In a round bottom flask equipped with a stir bar, BODIPY **13** (0.25 g, 0.65 mmol) was dissolved in MeOH (150 mL). A solution of 0.2 M NaOH (20 mL) was added and the resulting mixture was refluxed for two hours. After allowing the mixture to cool, the solvent was evaporated under reduced pressure. The resulting residue was acidified with 2 M HCl and the resulting precipitate was removed by filtration. The dry orange solid (0.160 g) yielded the target compound in 67% yield.

<sup>1</sup>H-NMR (400 MHz, CDCl<sub>3</sub>) δ 8.25-8.23 (d, *J* = 7.8, 2H), 7.47-7.45 (d, *J* = 7.8, 2H), 6.00 (s, 2H), 2.57 (s, 6H), 1.38 (s, 6H); MS (ESI-TOF) *m/z* Calculated for C<sub>20</sub>H<sub>21</sub>BF<sub>2</sub>N<sub>2</sub>O<sub>2</sub>: 369.1586; Found: [M+H]<sup>+</sup>: 369.1576. The NMR data was in agreement with that already published.<sup>47</sup>

**Compound 15:** BODIPY **14** (0.01 g, 0.016 mmol) was dissolved in dry DCM (5 mL). Diisopropylethylamine (0.0125 g, 0.98 mmol) was added and the mixture was allowed to stir for one hour. HOBt (0.003 g, 0.02 mmol) and TBTU (0.007 g, 0.02 mmol) were added consecutively and the resulting solution stirred for an additional hour. Finally, glycine *tert*-butyl ester hydrochloride (0.003 g, 0.019 mmol) was added and the mixture stirred overnight. The solution was transferred into a separatory funnel and quenched with 5% citric acid. The organic layer was then washed with brine and water and dried over Na<sub>2</sub>SO<sub>4</sub>. The solvent was evaporated under reduced pressure and the resulting solid was purified by silica column chromatography using DCM as eluent to obtain a red-orange solid (0.0046 g) in 37% yield.

<sup>1</sup>H-NMR (400 MHz, CDCl<sub>3</sub>) δ 7.97-7.95 (d, *J* = 7.8, 2H), 7.41-7.39 (d, *J* = 7.8, 2H), 6.78 (s, 1H), 5.98 (s, 2H), 4.18-4.17 (d, *J*=4.6, 2H), 2.55 (s, 6H), 1.52 (s, 9H), 1.35 (s, 6H); MS (ESI-TOF) *m/z* Calculated for C<sub>26</sub>H<sub>30</sub>BF<sub>2</sub>N<sub>3</sub>O<sub>3</sub>: 482.2427; Found: [M+H]<sup>+</sup>: 482.2419.

**Compound 16:** In a round bottom flask equipped with a stir bar, BODIPY **15** (0.018 g, 0.037 mmol) was dissolved in MeOH (15 mL). A solution of 0.2 M NaOH (0.5 mL) was added and the resulting mixture was refluxed for two hours. After allowing the mixture to cool, the solvent was evaporated under reduced pressure. The resulting residue was acidified with 2 M HCl and the resulting precipitate was removed by filtration. The dry orange solid (0.007 g) yielded the target compound in 44% yield.

<sup>1</sup>H-NMR (400 MHz, CDCl<sub>3</sub>) δ 7.98-7.96 (s, *J* = 7.8, 2H), 7.42-7.40 (d, *J* = 7.8, 2H), 6.75 (s, 1H), 6.00 (s, 2H), 4.20-4.18 (d, *J* = 4.6, 2H), 2.56 (s, 6H), 1.36 (s, 6H); <sup>13</sup>C-NMR (100 MHz, CDCl<sub>3</sub>) δ 206.41, 206.03, 171.39, 167.06, 156.51, 143.96, 142.25, 138.92, 136.02, 129.37, 129.20, 122.32,

41.97, 14.76; MS (ESI-TOF) m/z Calculated for C<sub>22</sub>H<sub>23</sub>BF<sub>2</sub>N<sub>3</sub>O<sub>3</sub>: 426.1801; Found: [M+H]<sup>+</sup>: 426.1796.

### 5.4.3 X-ray Determined Molecular Structures

Diffraction data were collected at 95 K on a Bruker Kappa Apex-II DUO diffractometer equipped with MoK $\alpha$  radiation ( $\lambda = 0.71073$  Å). Refinement was by full-matrix least squares using SHELXL, with H atoms in idealized positions.

*Crystal data for 3b*: C<sub>23</sub>H<sub>19</sub>BF<sub>2</sub>N<sub>2</sub>, M = 372.21, triclinic space group *P*1, a = 10.1333 (10) Å, b = 10.5938 (10) Å, c = 10.9775 (10) Å,  $\beta = 113.773$  (4)°, U = 942.87 (17) Å<sup>3</sup>, T = 95 K, Z = 2, A total of 8,560 reflections were measured ( $R_{\text{int}} = 0.0000$ ). R = 0.044 for 8,560 data points with  $I > 2\sigma(I)$  of 7,042 unique data points and 257 refined parameters.

### 5.4.4 Steady-state Absorption and Fluorescence Spectroscopy

The spectroscopic properties of BODIPYs **3a,b**, **4a,b**, **5a,b**, **8**, **11**, and **12** were determined on solutions prepared by dissolving crystalline compound in dichloromethane, THF, or DMSO. Stock solutions ( $5 \times 10^{-5}$  M) were prepared and diluted to appropriate concentrations for collection of absorbance and emission spectra. Absorption spectra were obtained on a PerkinElmer Lambda 35 UV/VIS Spectrometer for BODIPYs **3a,b**, **4a,b**, and **5a,b** and on a Varian Cary 50 Bio UV/VIS Spectrophotometer for BODIPYs **8**, **11**, and **12**. Measurements obtained for determining optical density were taken from solutions with concentrations between  $1.2 \times 10^{-5}$  and  $5 \times 10^{-5}$  M so that  $\lambda_{\text{max}}$  was between 0.5 and 1.0. Fluorescence measurements were recorded on solutions with concentrations between  $1.2 \times 10^{-6}$  and  $2.5 \times 10^{-5}$  M to attain an optical density at the excitation wavelength between 0.04 and 0.06 to minimize intermolecular reabsorption and inner-filter

effects. Compounds were excited at 500 nm for **3a,b**, **4a,b**, and **5a, b**, 500 nm for **8**, 480 nm for **11**, and 490 nm for **12**. Emission spectra were acquired on a Fluorolog3 Fluorometer with the slit width set at 5 nm for BODIPYs **3a**, **4a**, and **5a** and 2 nm BODIPYs **3b**, **4b**, and **5b** and on a PTI QuantaMaster4/2006SE spectrofluorometer with the slit width set at 3 nm for **8**, **11**, and **12**. Rhodamine 6G was used as a standard in calculating the fluorescence quantum yields ( $\Phi_f = 0.95$  in ethanol). All measurements, both absorbance and emission, were acquired within 4 h of solution preparation at room temperature (23 – 25 °C), using a 10 mm path length quartz spectrophotometric cell.

## 5.4.5 Cell Studies

### 5.4.5.1 BBB Permeability

The hCMEC/D3 cells were incubated in a 6-well, 0.4  $\mu\text{m}$  porosity PET transwell plate (Corning) and allowed to grow for 48 h. EBM-2 medium containing 5% FBS (Fetal Bovine Serum), 1% Penicillin-Streptomycin, hydrocortisone, ascorbic acid, chemically defined lipid concentrate (1/100), HEPES, and bFGF was used as growth medium. A 0.5 ml sample of each carboranyl-BODIPY at 1 mg/ml concentration was added to the upper chamber and 1.5 ml HBSS buffer was added to the lower chamber. The cells were incubated for 0, 30, and 60 minutes, and at the end of each incubation time five aliquots of 100  $\mu\text{L}$  of solution from the lower chamber is pipetted and fresh 500  $\mu\text{L}$  HBSS buffer is added back to the lower chamber. The five 100  $\mu\text{L}$  (five replicates) solutions that were collected from the lower chamber were pipetted in a 96 well plate. To determine the BODIPY concentration, fluorescence emission was read at 520/590 using a BMG FLUOstar plate reader. The permeability coefficients ( $P$ , expressed in  $\text{cm s}^{-1}$ ) were calculated using the following equation:

$$P = \frac{(C_f - C_0)}{(t_f - t_0)} \times \frac{1}{60A \cdot C_0}$$

Where  $C_f$  is the final concentration of the compound (ng/ml),  $C_0$  is the initial concentration of compound (ng/ml),  $t_f$  is the final time (minutes),  $t_0$  is the initial time (minutes) and  $A$  is the surface area of the filter (cm<sup>2</sup>).

#### 5.4.6 Octanol-HEPES buffer partition coefficients

The partition coefficients ( $\log P$ ) were measured at room temperature by adding 0.5 mL of a BODIPY stock solution in DMSO (50  $\mu$ M) to a 15 mL volumetric tube containing 4.0 mL of HEPES buffer (1 M, pH 7.4), followed by addition of 4.0 mL of 1-octanol. After vortexing for 5 min, the phases were allowed to separate completely. An aliquot of 0.5 mL from each layer was diluted with 0.5 mL of methanol and the absorbance was read on an Varian Cary 50 Bio UV/VIS Spectrophotometer with 10 mm path length quartz cuvette.

#### 5.5 References

1. Lund, F. W.; Lomholt, M. A.; Solanko, L. M.; Bittman, R.; Wustner, D., Two-photon time-lapse microscopy of BODIPY-cholesterol reveals anomalous sterol diffusion in chinese hamster ovary cells. *BMC Biophysics* **2012**, *5*, 15.
2. Barth, R. F.; Coderre, J. A.; Vicente, M. G. H.; Blue, T. E., Boron neutron capture therapy of cancer: Current status and future prospects. *Clinical Cancer Research* **2005**, *11*, 3987-4002.
3. Barth, R. F., Coderre, J. A., Vicente, M. G. H., Blue, T. E., and Miyatake, S.-I., In *Current Clinical Oncology: High-Grade Gliomas: Diagnosis and Treatment*, Barnett, G. H., Ed. Humana Press Inc.: Totowa, NJ, 2007; pp 431-459.
4. Nakagawa, Y.; Pooh, K.; Kobayashi, T.; Kageji, T.; Uyama, S.; Matsumura, A.; Kumada, H., Clinical review of the Japanese experience with boron neutron capture therapy and a

- proposed strategy using epithermal neutron beams. *Journal of Neuro-Oncology* **2003**, *62*, 87-99.
5. Diaz, A. Z., Assessment of the results from the phase I/II boron neutron capture therapy trials at the Brookhaven National Laboratory from a clinician's point of view. *Journal of Neuro-Oncology* **2003**, *62*, 101-109.
  6. Busse, P. M.; Harling, O. K.; Palmer, M. R.; Kiger, W. S.; Kaplan, J.; Kaplan, I.; Chuang, C. F.; Goorley, J. T.; Riley, K. J.; Newton, T. H.; Santa Cruz, G. A.; Lu, X.; Zamenhof, R. G., A critical examination of the results from the Harvard-MIT NCT program phase I clinical trial of neutron capture therapy for intracranial disease. *Journal of Neuro-Oncology* **2003**, *62*, 111-121.
  7. Joensuu, H.; Kankaanranta, L.; Seppala, T.; Auterinen, I.; Kallio, M.; Kulvik, M.; Laakso, J.; Vahatalo, J.; Kortesianiemi, M.; Kotiluoto, P.; Seren, T.; Karila, J.; Brander, A.; Jarviluoma, E.; Ryyanen, P.; Paetau, A.; Ruokonen, I.; Minn, H.; Tenhunen, M.; Jaakelainen, J.; Farkkila, M.; Savolainen, S., Boron neutron capture therapy of brain tumors: clinical trials at the Finnish facility using boronophenylalanine. *Journal of Neuro-Oncology* **2003**, *62*, 123-134.
  8. Capala, J.; Stenstam, B. H.; Skold, K. S.; af Rosenschold, P. M.; Giusti, V.; Persson, C.; Wallin, E.; Brun, A.; Franzen, L.; Carlsson, J. O.; Salford, L.; Ceberg, C.; Persson, B.; Pellettieri, L.; Henriksson, R., Boron neutron capture therapy for glioblastoma multiforme: clinical studies in Sweden. *Journal of Neuro-Oncology* **2003**, *62*, 135-144.
  9. Urano, Y., Asanuma, D., Hama, Y., Koyama, Y., Barrett, T., Kamiya, M., Nagano, T., Watanabe, T., Hasegawa, A., Choyke, P. L., and Kobayashi, H., *Nature Medicine* **2009**, *15*, 104-109.
  10. The Life and Death of a Neuron. [http://www.ninds.nih.gov/disorders/brain\\_basics/ninds\\_neuron.htm](http://www.ninds.nih.gov/disorders/brain_basics/ninds_neuron.htm)
  11. Siegel, R.; Ma, J. M.; Zou, Z. H.; Jemal, A., Cancer Statistics, 2014. *Ca-a Cancer Journal for Clinicians* **2014**, *64*, 9-29.
  12. BNCT <http://nanomed.missouri.edu/institute/research/BNCT.html>
  13. Barth, R. F.; Soloway, A. H.; Goodman, J. H.; Gahbauer, R. A.; Gupta, N.; Blue, T. E.; Yang, W. L.; Tjarks, W., Boron neutron capture therapy of brain tumors: An emerging therapeutic modality. *Neurosurgery* **1999**, *44*, 433-450.
  14. Easson, M. W.; Fronczek, F. R.; Jensen, T. J.; Vicente, M. G. H., Synthesis and in vitro properties of trimethylamine- and phosphonate-substituted carboranylporphyrins for application in BNCT. *Bioorganic & Medicinal Chemistry* **2008**, *16*, 3191-3208.
  15. Soloway, A. H.; Tjarks, W.; Barnum, B. A.; Rong, F. G.; Barth, R. F.; Codogni, I. M.; Wilson, J. G., The chemistry of neutron capture therapy. *Chemical Reviews* **1998**, *98*, 1515-1562.

16. Barth, R. F., A critical assessment of boron neutron capture therapy: an overview. *Journal of Neuro-Oncology* **2003**, *62*, 1-5.
17. Ziessel, R.; Ulrich, G.; Harriman, A., The chemistry of Bodipy: a new El Dorado for fluorescence tools. *New Journal of Chemistry* **2007**, *31*, 496-501.
18. Barth, R. F.; Coderre, J. A.; Vicente, M. G. H.; Blue, T. E., Boron neutron capture therapy of cancer: Current status and future prospects. *Clinical Cancer Research* **2005**, *11*, 3987-4002.
19. Bhupathiraju, N. V. S. D. K.; Gottumukkala, V.; Hao, E.; Hu, X.; Fronczek, F. R.; Baker, D. G.; Wakamatsu, N.; Vicente, M. G. H., Synthesis and toxicity of cobaltabisdicarbollide-containing porphyrins of high boron content. *Journal of Porphyrins and Phthalocyanines* **2011**, *15*, 973-983.
20. Pham, W.; Zhao, B. Q.; Lo, E. H.; Medarova, Z.; Rosen, B.; Moore, A., Crossing the blood-brain barrier: A potential application of myristoylated polyarginine for in vivo neuroimaging. *Neuroimage* **2005**, *28*, 287-292.
21. Davis, T. P. Transport at the Blood Brain Barrier (BBB). <http://davislab.med.arizona.edu/content/transport-blood-brain-barrier-bbb>
22. Human Physiology (IPHY 3430), University of Colorado at Boulder. <http://www.colorado.edu/intphys/Class/IPHY3430-200/007cns.htm>
23. Deguchi, Y.; Miyakawa, Y.; Sakurada, S.; Naito, Y.; Morimoto, K.; Ohtsuki, S.; Hosoya, K.; Terasaki, T., Blood-brain barrier transport of a novel mu(1)-specific opioid peptide, H-Tyr-D-Arg-Phe-beta-Ala-OH (TAPA). *Journal of Neurochemistry* **2003**, *84*, 1154-1161.
24. Grimes, R. N., Carboranes. In *Organometallic Chemistry: A Series of Monographs*, Maitlis, P. M. e. a., Ed. Academic Press: New York, NY, 1970.
25. Dash, B. P.; Satapathy, R.; Gaillard, E. R.; Norton, K. M.; Maguire, J. A.; Chug, N.; Hosmane, N. S., Enhanced pi-Conjugation and Emission via Icosahedral Carboranes: Synthetic and Spectroscopic Investigation. *Inorganic Chemistry* **2011**, *50*, 5485-5493.
26. Gibbs, J. H.; Robins, L. T.; Zhou, Z.; Bobadova-Parvanova, P.; Cottam, M.; McCandless, G. T.; Fronczek, F. R.; Vicente, M. G. H., Spectroscopic, computational modeling and cytotoxicity of a series of meso-phenyl and meso-thienyl-BODIPYs. *Bioorganic and Medicinal Chemistry* **2013**, *21*, 5770-5781.
27. Hao, E. H.; Fronczek, F. R.; Vicente, M. G. H., Carborane functionalized pyrroles and porphyrins via the Suzuki cross-coupling reaction. *Chemical Communications* **2006**, 4900-4902.
28. Hao, E. H. Ph. D. Dissertation. Louisiana State University, 2007.

29. Hao, E.; Fabre, B.; Fronczek, F. R.; Vicente, M. G. H., Syntheses and electropolymerization of carboranyl-functionalized pyrroles and thiophenes. *Chemistry of Materials* **2007**, *19*, 6195-6205.
30. Rao, M. R.; Mobin, S. M.; Ravikanth, M., Boron-dipyrromethene based specific chemodosimeter for fluoride ion. *Tetrahedron* **2010**, *66*, 1728-1734.
31. Anthony, J.; Diederich, F., Biphenyldialkylsilyl Chlorides-Reagents for the Formation of Crystalline Derivatives of Small Terminal Alkynes. *Tetrahedron Letters* **1991**, *32*, 3787-3790.
32. Shen, Z.; Rohr, H.; Rurack, K.; Uno, H.; Spieles, M.; Schulz, B.; Reck, G.; Ono, N., Boron-diindomethene (BDI) dyes and their tetrahydrobicyclo precursors - en route to a new class of highly emissive fluorophores for the red spectral range. *Chemistry-A European Journal* **2004**, *10*, 4853-4871.
33. Zheng, Q. D.; Xu, G. X.; Prasad, P. N., Conformationally restricted dipyrromethene boron difluoride (BODIPY) dyes: Highly fluorescent, multicolored probes for cellular imaging. *Chemistry-A European Journal* **2008**, *14*, 5812-5819.
34. Zhang, J.; Zheng, F. R.; Chan, H. S.; Xie, Z. W., Reaction of a 14-Vertex Carborane with Nucleophiles: Formation of nido-C2B12, nido-C2B11, and closo-CB11 Carborane Anions. *Inorganic Chemistry* **2009**, *48*, 9786-9791.
35. Wang, H.; Vicente, M. G. H.; Fronczek, F. R.; Smith, K. M., Synthesis and Transformations of 5-Chloro-2,2'-Dipyrins and Their Boron Complexes, 8-Chloro-BODIPYs. *Chemistry-A European Journal* **2014**, *20*, 5064-5074.
36. Misra, R.; Dhokale, B.; Jadhav, T.; Mobin, S. M., Donor-acceptor meso-alkynylated ferrocenyl BODIPYs: synthesis, structure, and properties. *Dalton Transactions* **2013**, *42*, 13658-13666.
37. Wu, L.; Burgess, K., A new synthesis of symmetric boraindacene (BODIPY) dyes. *Chemical Communications* **2008**, 4933-4935.
38. Bhupathiraju, N.; Graca, M.; Vicente, H., Synthesis and cellular studies of polyamine conjugates of a mercaptomethyl-carboranylporphyrin. *Bioorganic & Medicinal Chemistry* **2013**, *21*, 485-495.
39. Niemand, J.; Burger, P.; Verlinden, B. K.; Reader, J.; Joubert, A. M.; Kaiser, A.; Louw, A. I.; Kirk, K.; Phanstiel, O.; Birkholtz, L. M., Anthracene-Polyamine Conjugates Inhibit In Vitro Proliferation of Intraerythrocytic Plasmodium falciparum Parasites. *Antimicrobial Agents and Chemotherapy* **2013**, *57*, 2874-2877.
40. Cullis, P. M.; Green, R. E.; Merson-Davies, L.; Travis, N., Probing the mechanism of transport and compartmentalisation of polyamines in mammalian cells. *Chemistry & Biology* **1999**, *6*, 717-729.

41. Carlisle, D. L.; Devereux, W. L.; Hacker, A.; Woster, P. M.; Casero, R. A., Growth status significantly affects the response of human lung cancer cells to antitumor polyamine-analogue exposure. *Clinical Cancer Research* **2002**, *8*, 2684-2689.
42. Ke, M. R.; Yeung, S. L.; Ng, D. K. P.; Fong, W. P.; Lo, P. C., Preparation and in Vitro Photodynamic Activities of Folate-Conjugated Distyryl Boron Dipyrromethene Based Photosensitizers. *Journal of Medicinal Chemistry* **2013**, *56*, 8475-8483.
43. Sharman, W. M.; van Lier, J. E.; Allen, C. M., Targeted photodynamic therapy via receptor mediated delivery systems. *Advanced Drug Delivery Reviews* **2004**, *56*, 53-76.
44. Verma, S.; Watt, G. M.; Mal, Z.; Hasan, T., Strategies for enhanced photodynamic therapy effects. *Photochemistry and Photobiology* **2007**, *83*, 996-1005.
45. Schmitt, F.; Juillerat-Jeanneret, L., Drug Targeting Strategies for Photodynamic Therapy. *Anti-Cancer Agents in Medicinal Chemistry* **2012**, *12*, 500-525.
46. Giessler, K.; Griesser, H.; Gohringer, D.; Sabirov, T.; Richert, C., Synthesis of 3'-BODIPY-Labeled Active Esters of Nucleotides and a Chemical Primer Extension Assay on Beads. *European Journal of Organic Chemistry* **2010**, 3611-3620.
47. Kondo, M.; Furukawa, S.; Hirai, K.; Kitagawa, S., Coordinatively Immobilized Monolayers on Porous Coordination Polymer Crystals. *Angewandte Chemie-International Edition* **2010**, *49*, 5327-5330.
48. Bonardi, L.; Ulrich, G.; Ziessel, R., Tailoring the properties of boron-dipyrromethene dyes with acetylenic functions at the 2,6,8 and 4-B substitution positions. *Organic Letters* **2008**, *10*, 2183-2186.
49. Kim, K.; Jo, C.; Easwaramoorthi, S.; Sung, J.; Kim, D. H.; Churchill, D. G., Crystallographic, Photophysical, NMR Spectroscopic and Reactivity Manifestations of the "8-Heteroaryl Effect" in 4,4-Difluoro-8-(C<sub>4</sub>H<sub>3</sub>X)-4-bora-3a,4a-diaza-s-indacene (X=O, S, Se) (BODIPY) Systems. *Inorganic Chemistry* **2010**, *49*, 4881-4894.
50. Kim, K.; Jo, C.; Easwaramoorthi, S.; Sung, J.; Kim, D. H.; Churchill, D. G., Crystallographic, Photophysical, NMR Spectroscopic and Reactivity Manifestations of the "8-Heteroaryl Effect" in 4,4-Difluoro-8-(C<sub>4</sub>H<sub>3</sub>X)-4-bora-3a,4a-diaza-s-indacene (X=O, S, Se) (BODIPY) Systems. *Inorganic Chemistry* **2010**, *49*, 4881-4894.
51. Jiao, L. J.; Pang, W. D.; Zhou, J. Y.; Wei, Y.; Mu, X. L.; Bai, G. F.; Hao, E. H., Regioselective Stepwise Bromination of Boron Dipyrromethene (BODIPY) Dyes. *Journal of Organic Chemistry* **2011**, *76*, 9988-9996.
52. Poller, B.; Gutmann, H.; Krahenbuhl, S.; Weksler, B.; Romero, I.; Couraud, P. O.; Tuffin, G.; Drewe, J.; Huwyler, J., The human brain endothelial cell line hCMEC/D3 as a human blood-brain barrier model for drug transport studies. *Journal of Neurochemistry* **2008**, *107*, 1358-1368.

53. Vu, K.; Weksler, B.; Romero, I.; Couraud, P. O.; Gelli, A., Immortalized Human Brain Endothelial Cell Line HCMEC/D3 as a Model of the Blood-Brain Barrier Facilitates In Vitro Studies of Central Nervous System Infection by *Cryptococcus neoformans*. *Eukaryotic Cell* **2009**, *8*, 1803-1807.
54. Weksler, B. B.; Subileau, E. A.; Perriere, N.; Charneau, P.; Holloway, K.; Leveque, M.; Tricoire-Leignel, H.; Nicotra, A.; Bourdoulous, S.; Turowski, P.; Male, D. K.; Roux, F.; Greenwood, J.; Romero, I. A.; Couraud, P. O., Blood-brain barrier-specific properties of a human adult brain endothelial cell line. *Faseb Journal* **2005**, *19*, 1872-1874.
55. Gaillard, P. J.; Voorwinden, L. H.; Nielsen, J. L.; Ivanov, A.; Atsumi, R.; Engman, H.; Ringbom, C.; de Boer, A. G.; Breimer, D. D., Establishment and functional characterization of an in vitro model of the blood-brain barrier, comprising a co-culture of brain capillary endothelial cells and astrocytes. *European Journal of Pharmaceutical Sciences* **2001**, *12*, 215-222.

## APPENDIX A: NMR SPECTRA OF COMPOUNDS FOUND IN CHAPTER 2

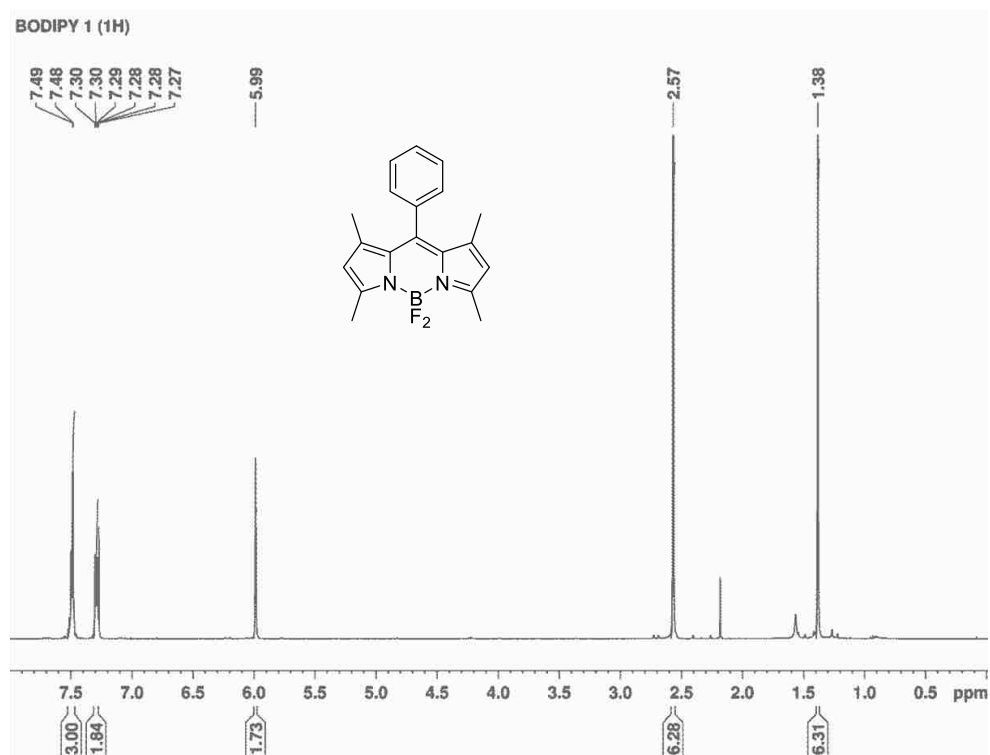


Figure A.1: <sup>1</sup>H NMR spectrum of BODIPY 1 in deuterated chloroform at 400MHz.

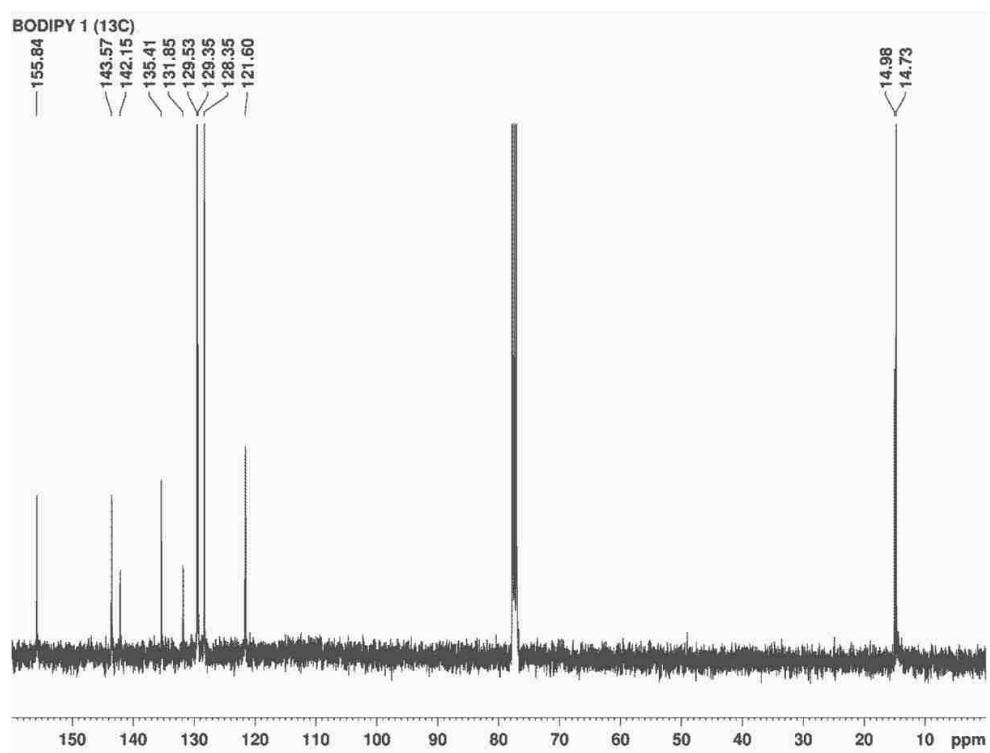


Figure A.2: <sup>13</sup>C NMR spectrum of BODIPY 1 in deuterated chloroform at 100MHz.

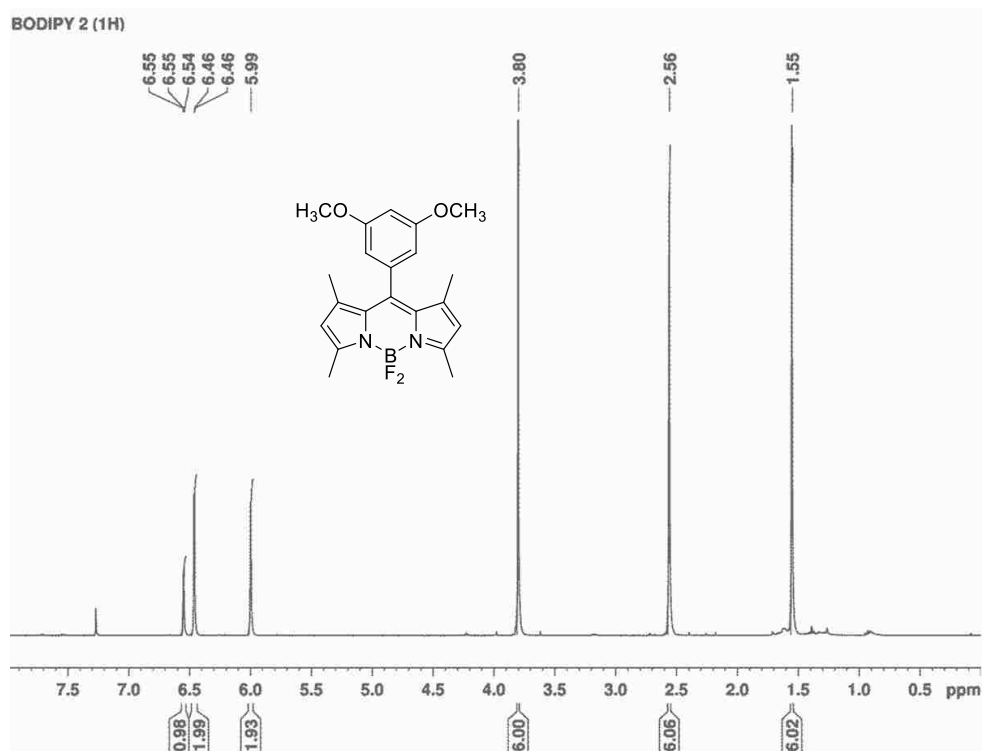


Figure A.3:  $^1\text{H}$  NMR spectrum of BODIPY 2 in deuterated chloroform at 400MHz.

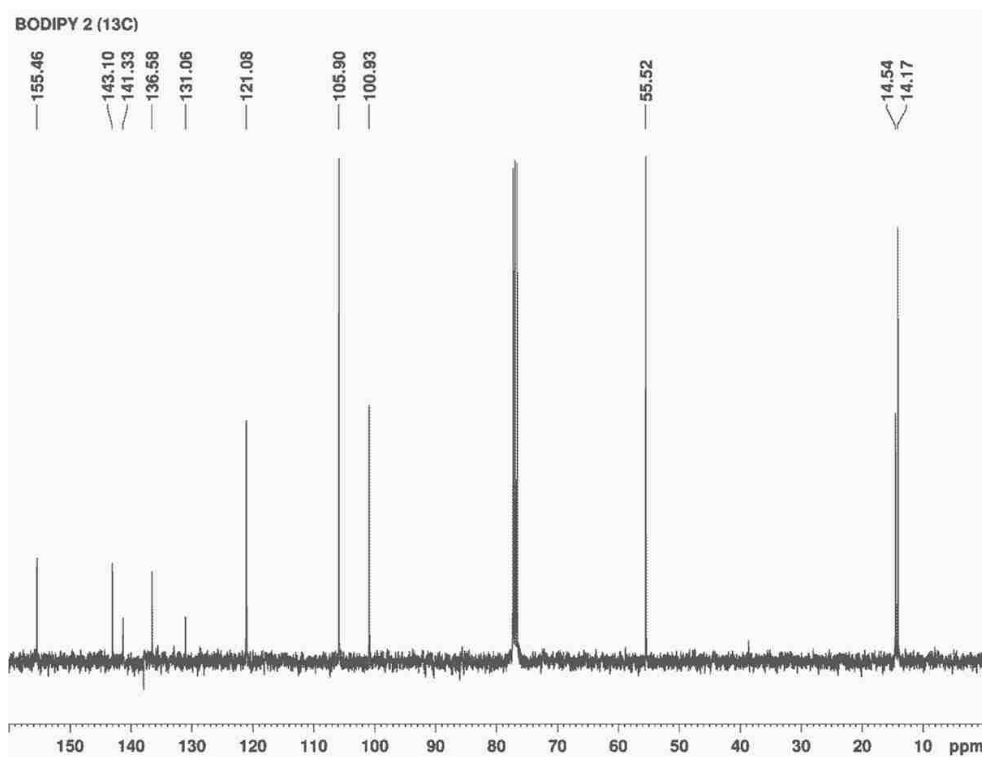


Figure A.4:  $^{13}\text{C}$  NMR spectrum of BODIPY 2 in deuterated chloroform at 100MHz.

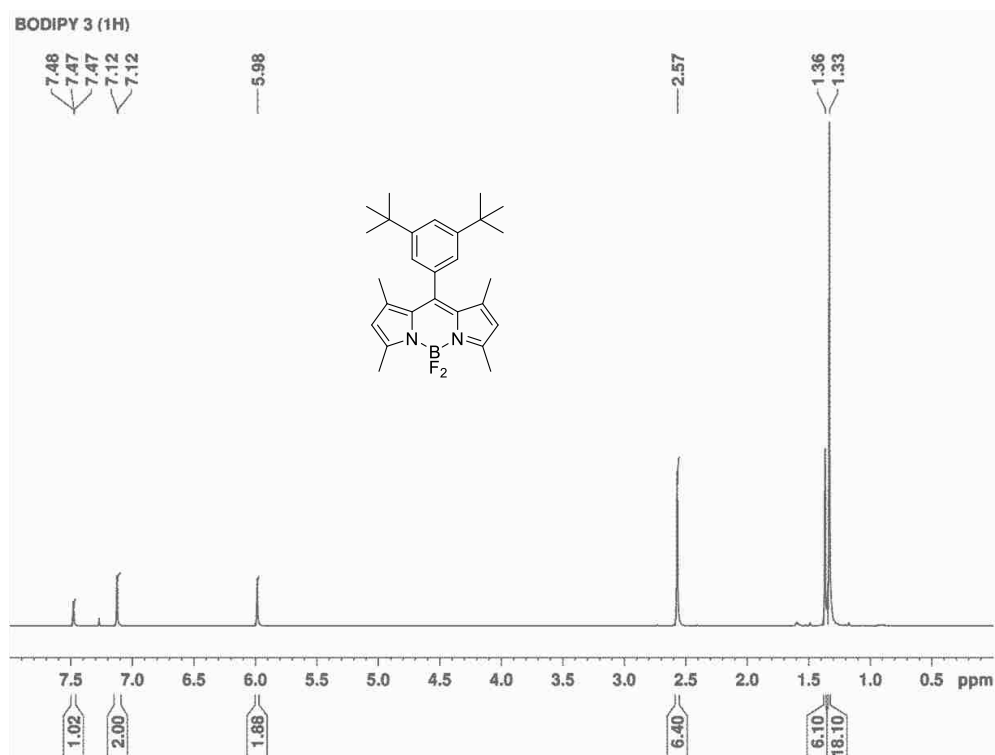


Figure A.5:  $^1\text{H}$  NMR spectrum of BODIPY 3 in deuterated chloroform at 400MHz.

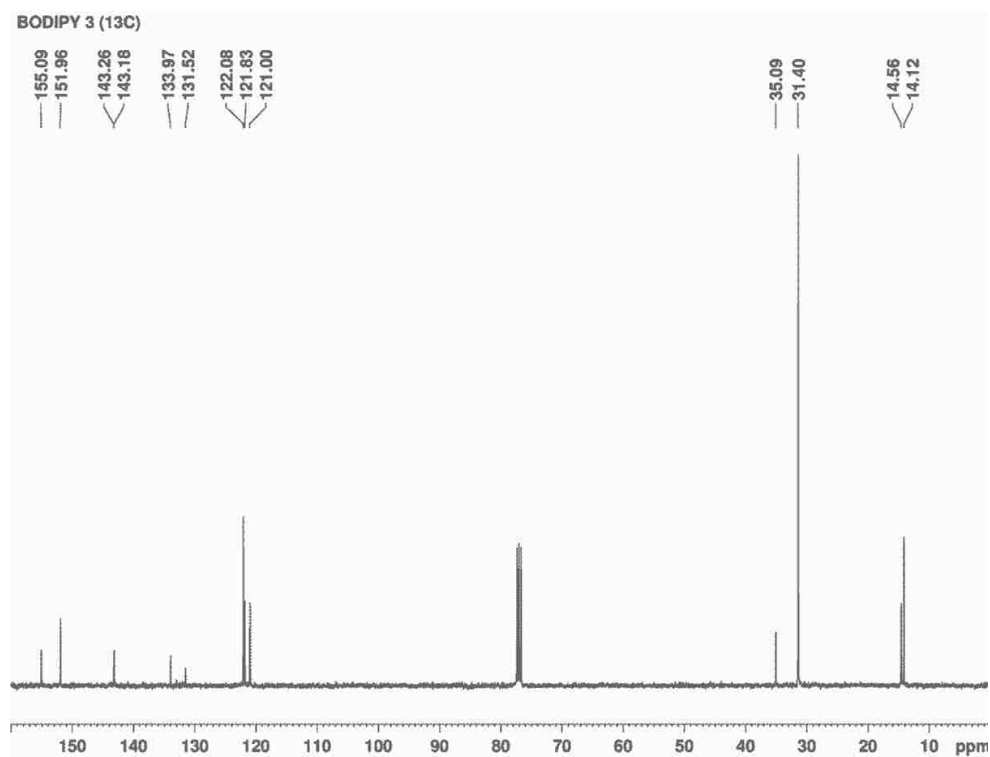


Figure A.6:  $^{13}\text{C}$  NMR spectrum of BODIPY 3 in deuterated chloroform at 100MHz.

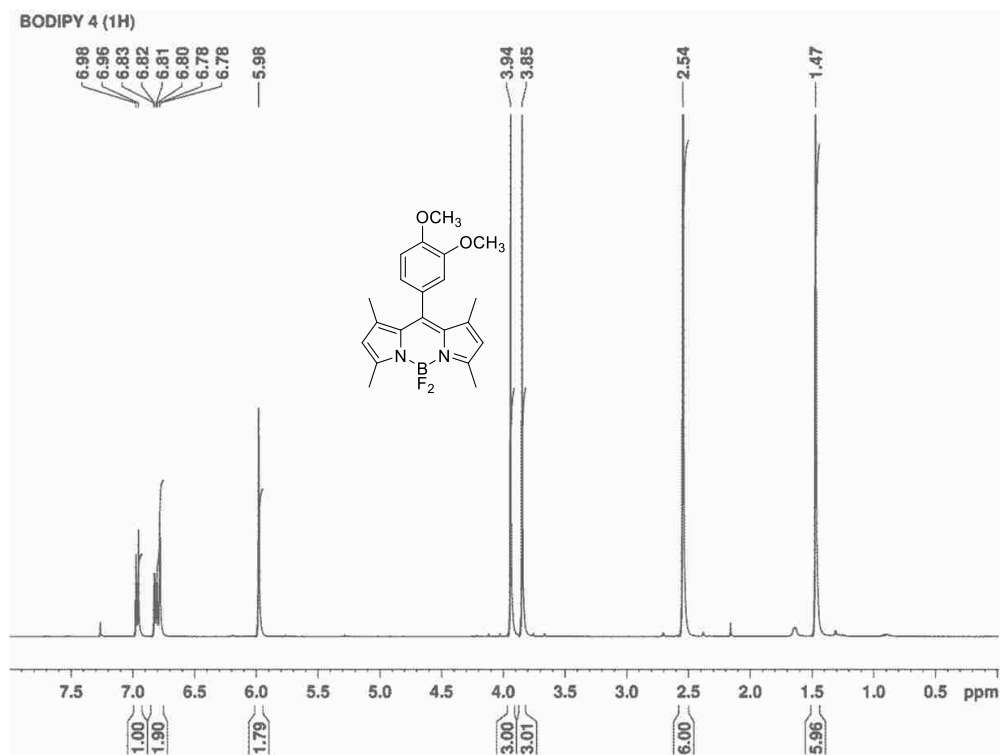


Figure A.7:  $^1\text{H}$  NMR spectrum of BODIPY 4 in deuterated chloroform at 400MHz.

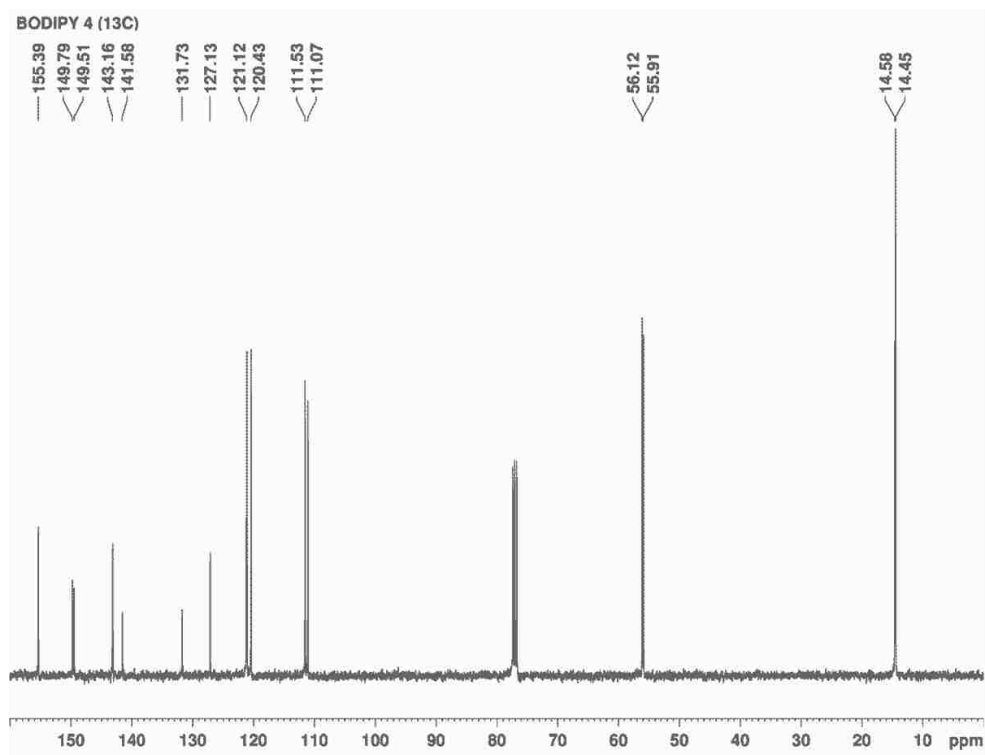


Figure A.8:  $^{13}\text{C}$  NMR spectrum of BODIPY 4 in deuterated chloroform at 100MHz.

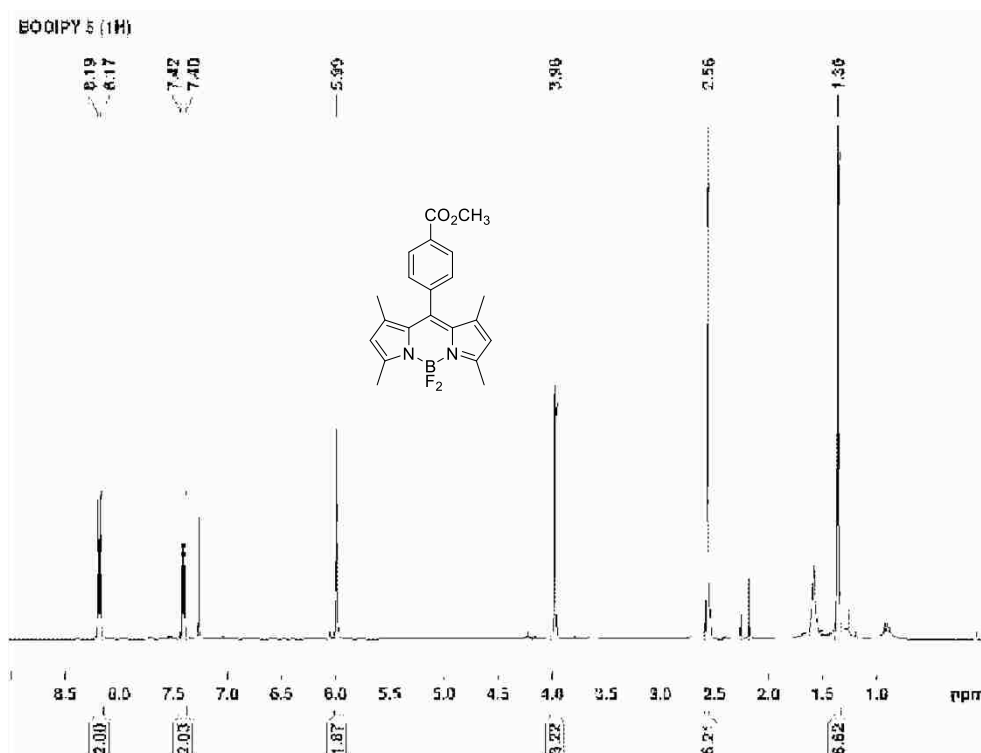


Figure A.9:  $^1\text{H}$  NMR spectrum of BODIPY **5** in deuterated chloroform at 400MHz.

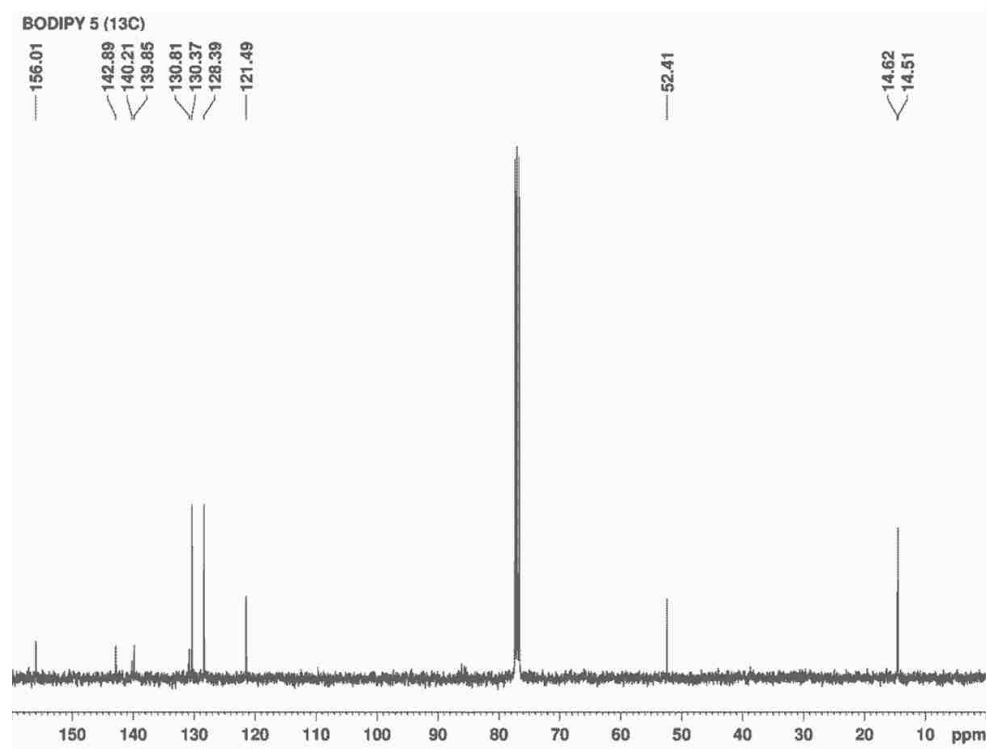


Figure A.10:  $^{13}\text{C}$  NMR spectrum of BODIPY **5** in deuterated chloroform at 100MHz.

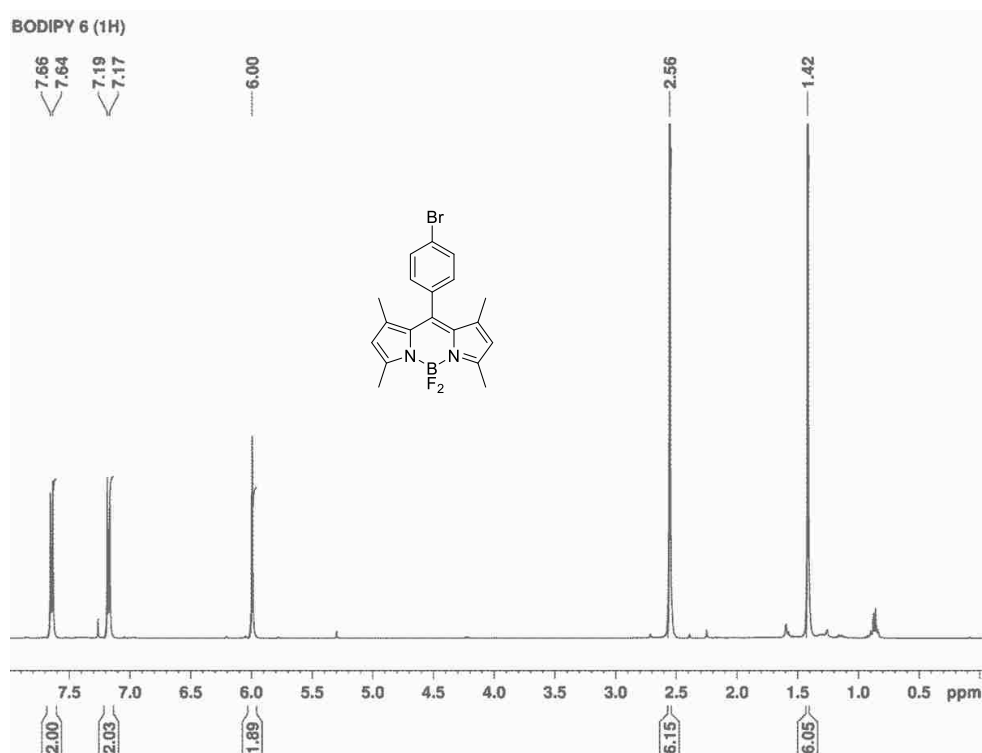


Figure A.11:  $^1\text{H}$  NMR spectrum of BODIPY **6** in deuterated chloroform at 400MHz.

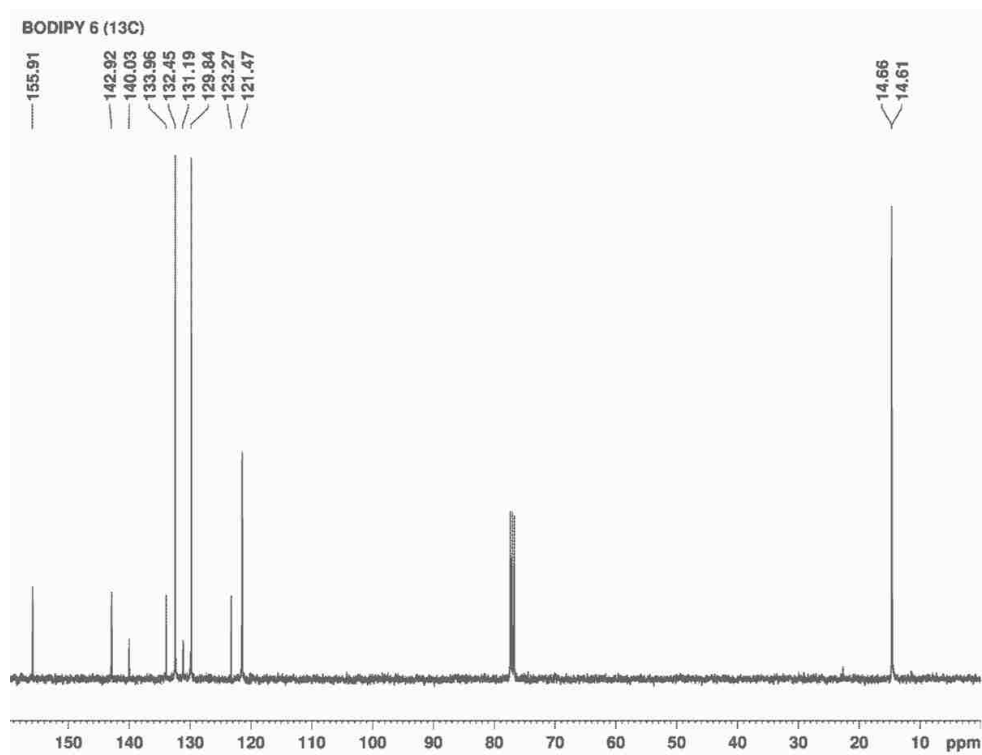


Figure A.12:  $^{13}\text{C}$  NMR spectrum of BODIPY **6** in deuterated chloroform at 100MHz.

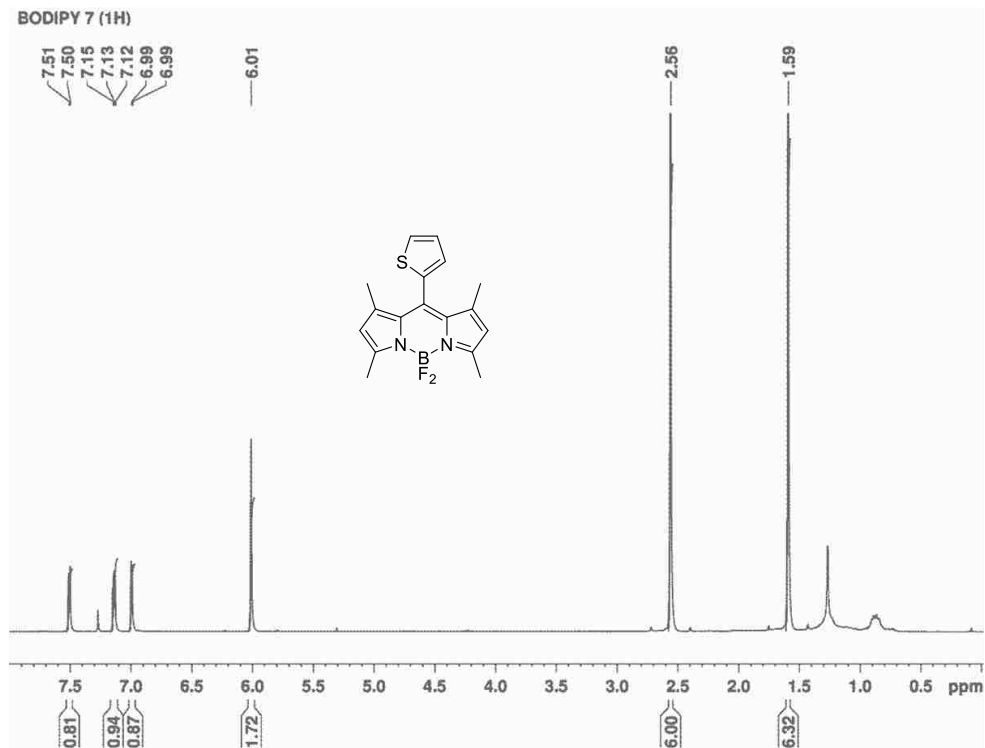


Figure A.13:  $^1\text{H}$  NMR spectrum of BODIPY 7 in deuterated chloroform at 400MHz.

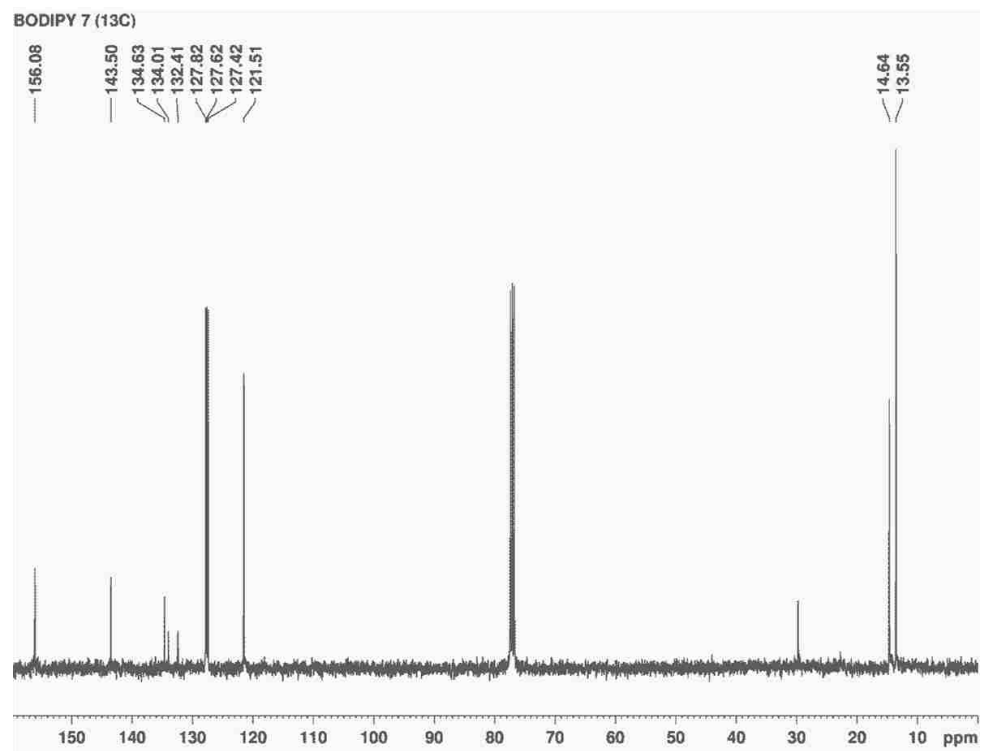


Figure A.14:  $^{13}\text{C}$  NMR spectrum of BODIPY 7 in deuterated chloroform at 100MHz.

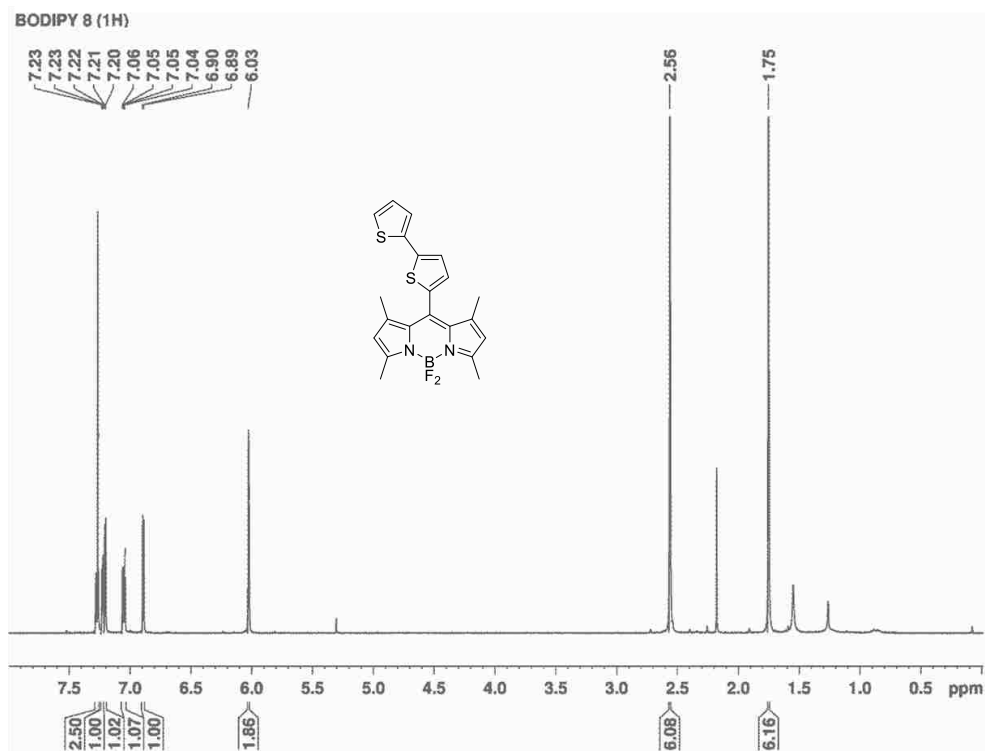


Figure A.15:  $^1\text{H}$  NMR spectrum of BODIPY **8** in deuterated chloroform at 400MHz.

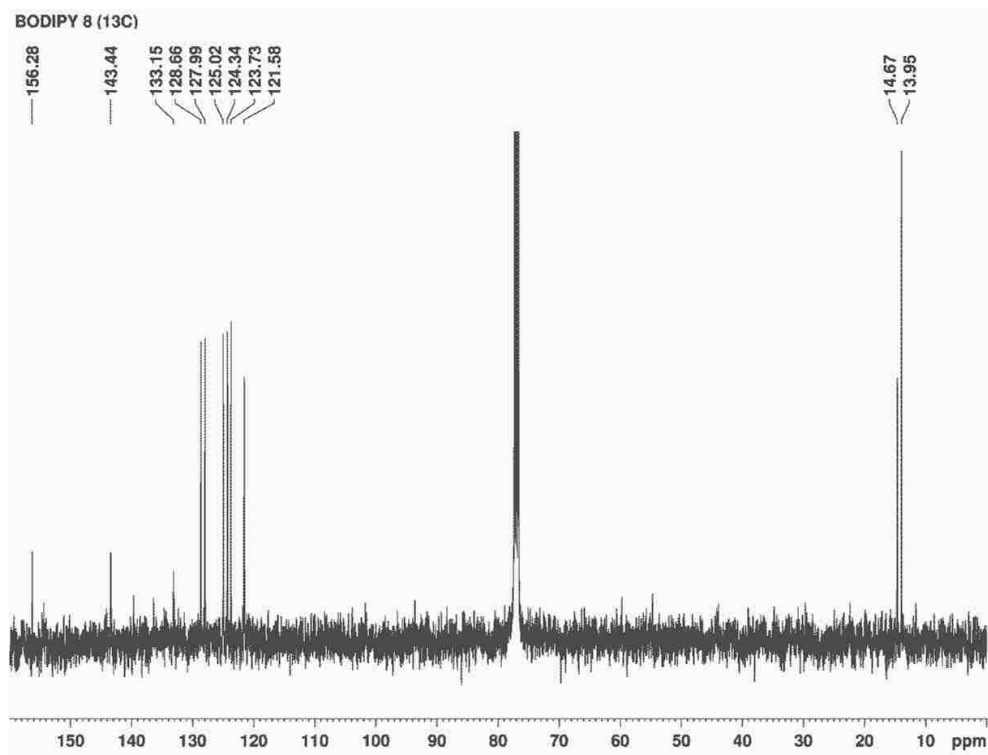


Figure A.16:  $^{13}\text{C}$  NMR spectrum of BODIPY **8** in deuterated chloroform at 100MHz.

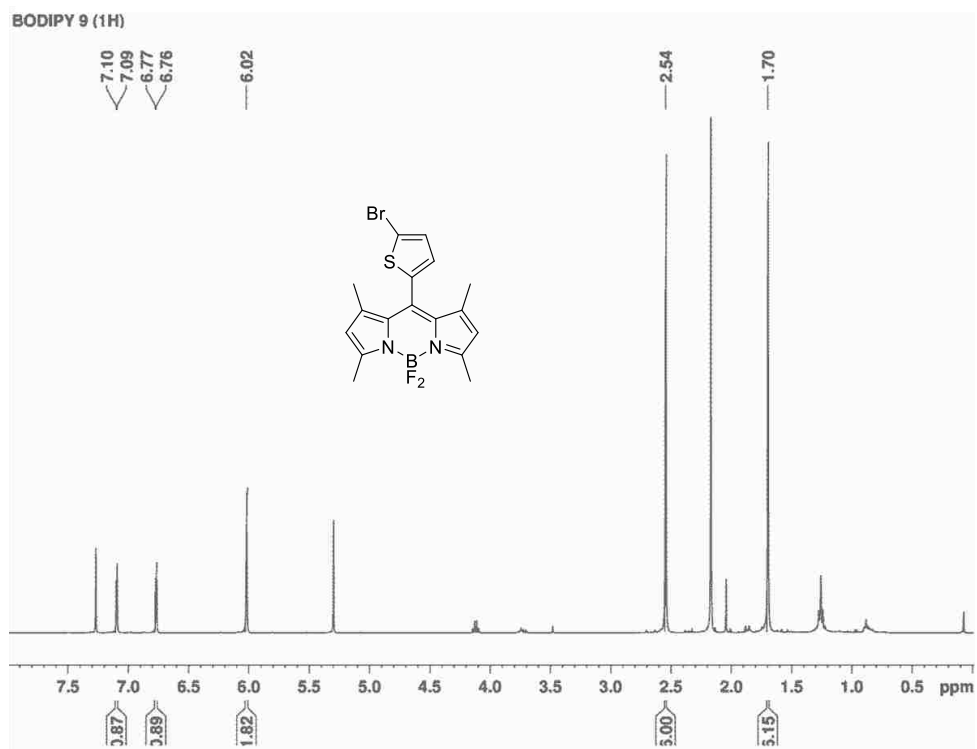


Figure A.17:  $^1\text{H}$  NMR spectrum of BODIPY **9** in deuterated chloroform at 400MHz.

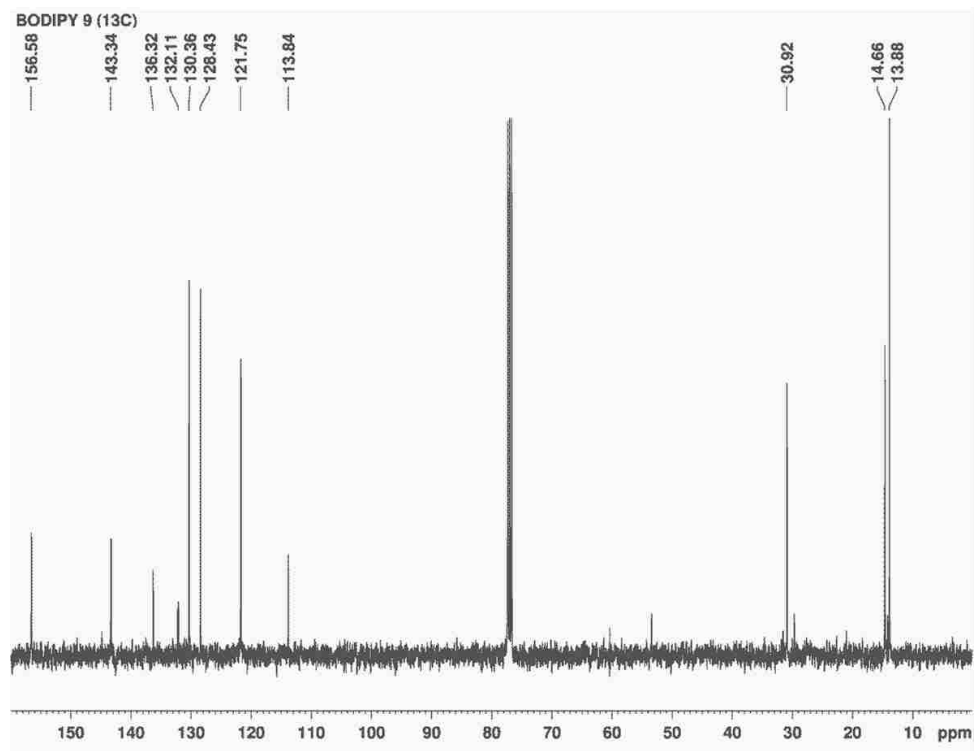


Figure A.18:  $^{13}\text{C}$  NMR spectrum of BODIPY **9** in deuterated chloroform at 100MHz.

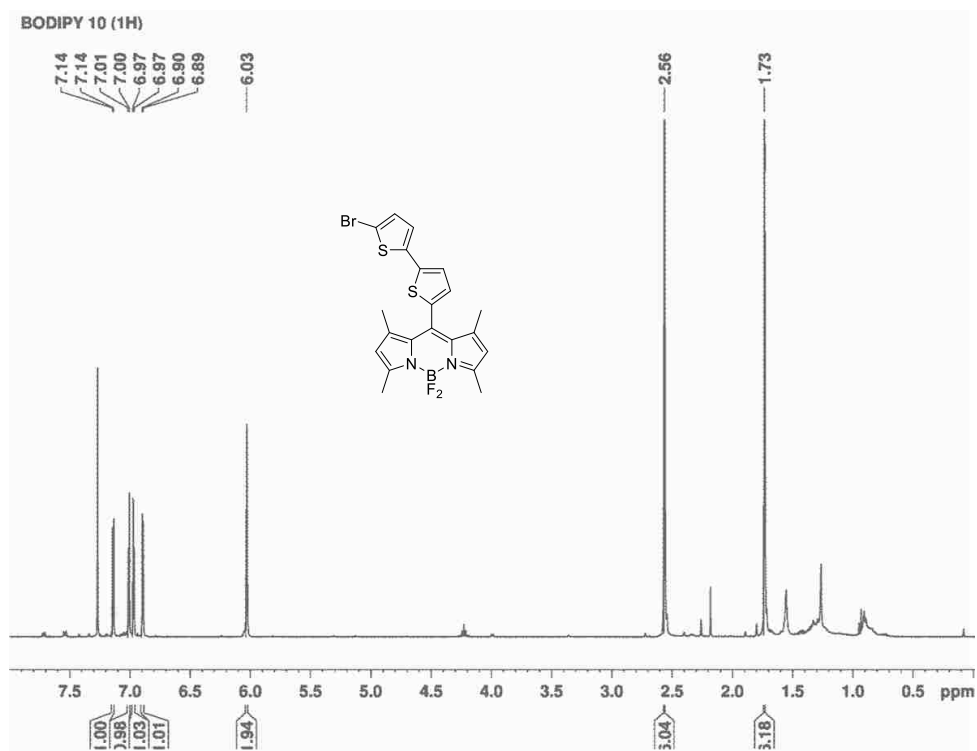


Figure A.19:  $^1\text{H}$  NMR spectrum of BODIPY **10** in deuterated chloroform at 400MHz.

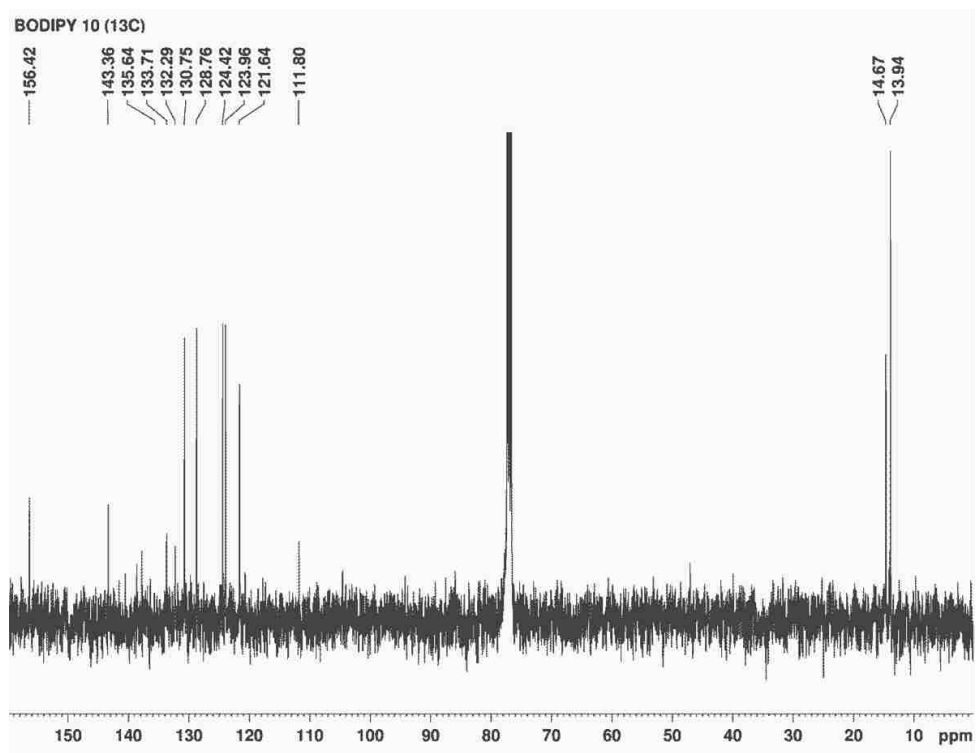


Figure A.20:  $^{13}\text{C}$  NMR spectrum of BODIPY **10** in deuterated chloroform at 100MHz.

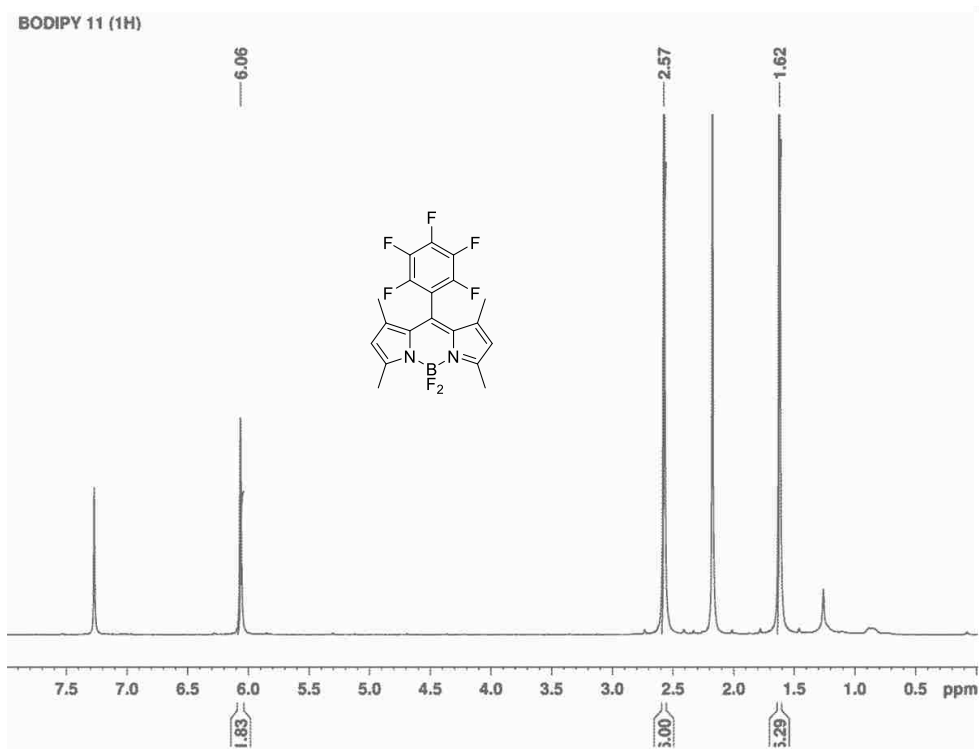


Figure A.21:  $^1\text{H}$  NMR spectrum of BODIPY **11** in deuterated chloroform at 400MHz.

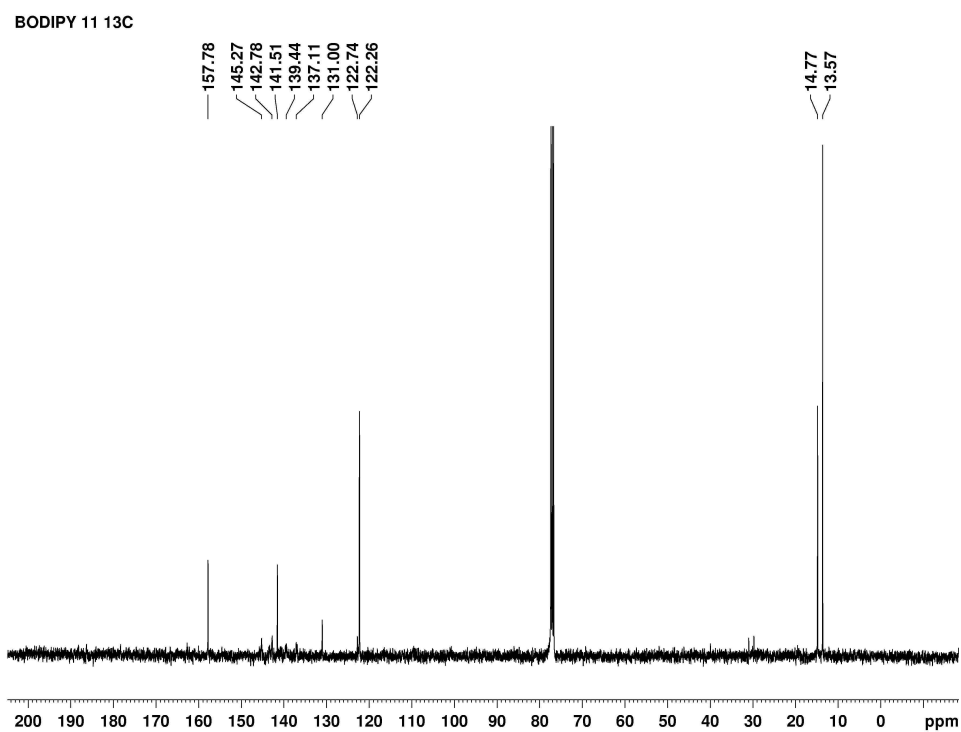


Figure A.22:  $^{13}\text{C}$  NMR spectrum of BODIPY **11** in deuterated chloroform at 100MHz.

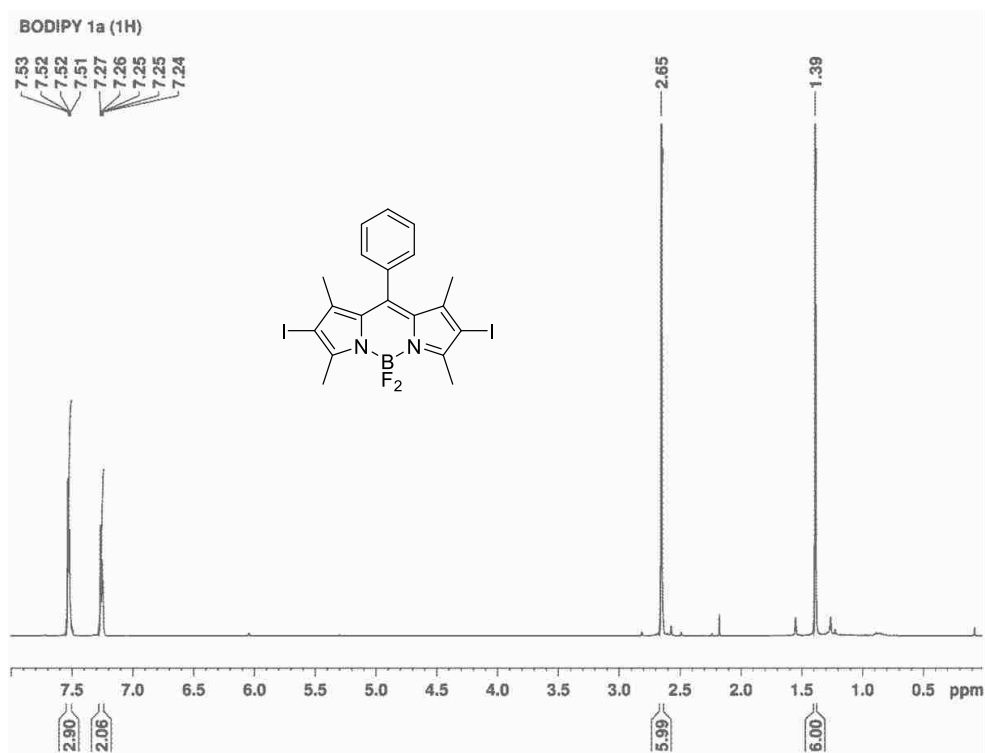


Figure A.23:  $^1\text{H}$  NMR spectrum of BODIPY **1a** in deuterated chloroform at 400MHz.

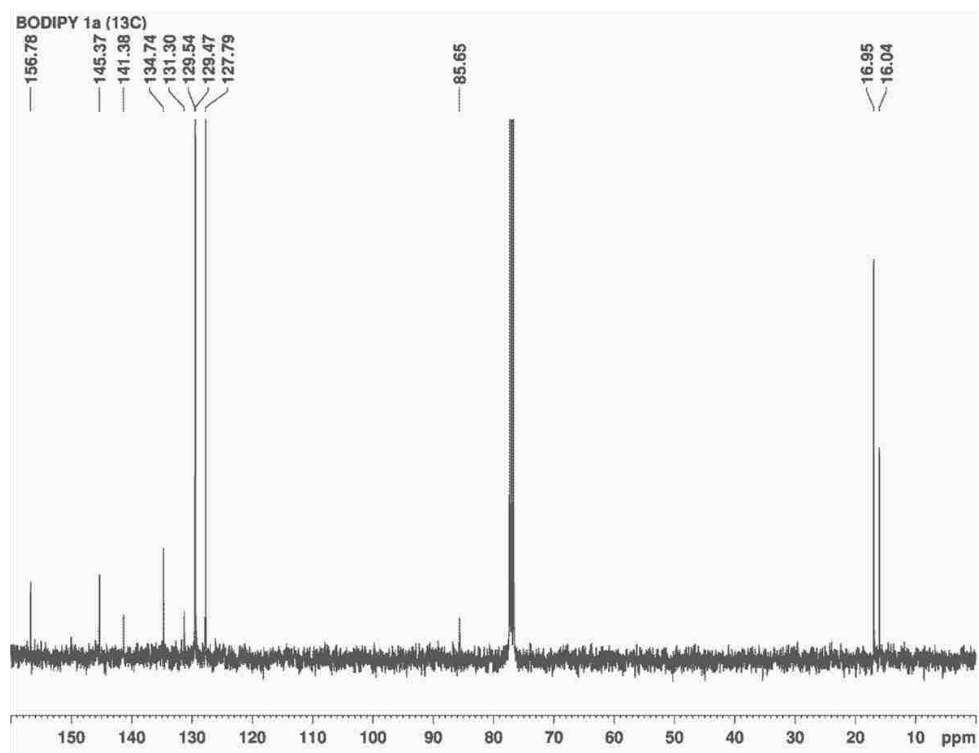


Figure A.24:  $^{13}\text{C}$  NMR spectrum of BODIPY **1a** in deuterated chloroform at 100MHz.

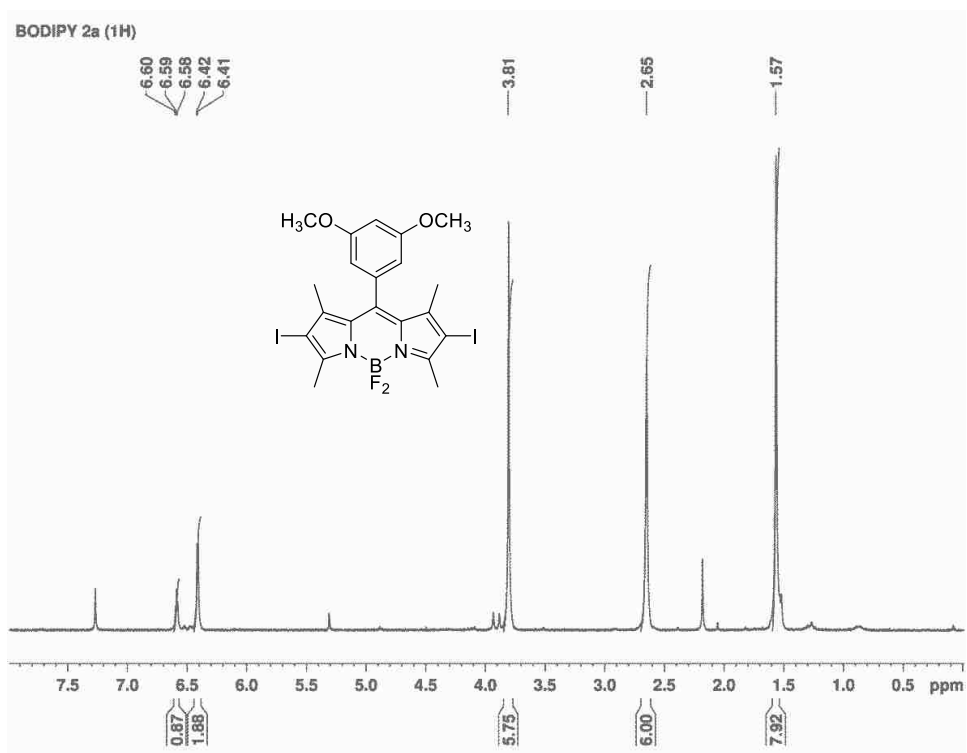


Figure A.25:  $^1\text{H}$  NMR spectrum of BODIPY **2a** in deuterated chloroform at 400MHz.

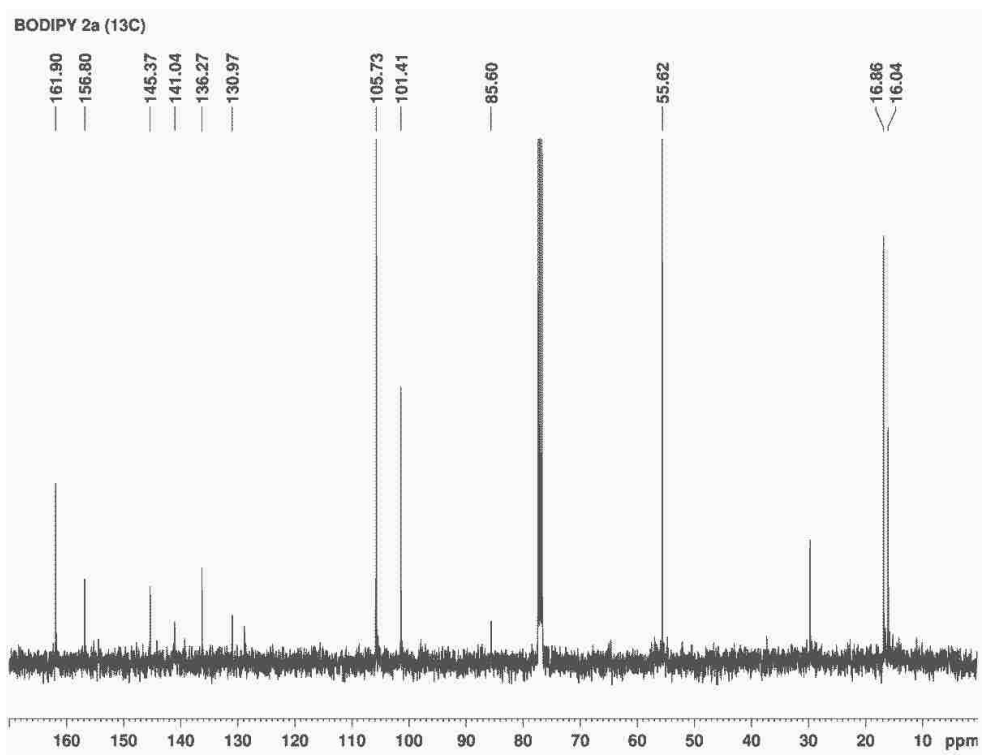


Figure A.26:  $^{13}\text{C}$  NMR spectrum of BODIPY **2a** in deuterated chloroform at 100MHz.

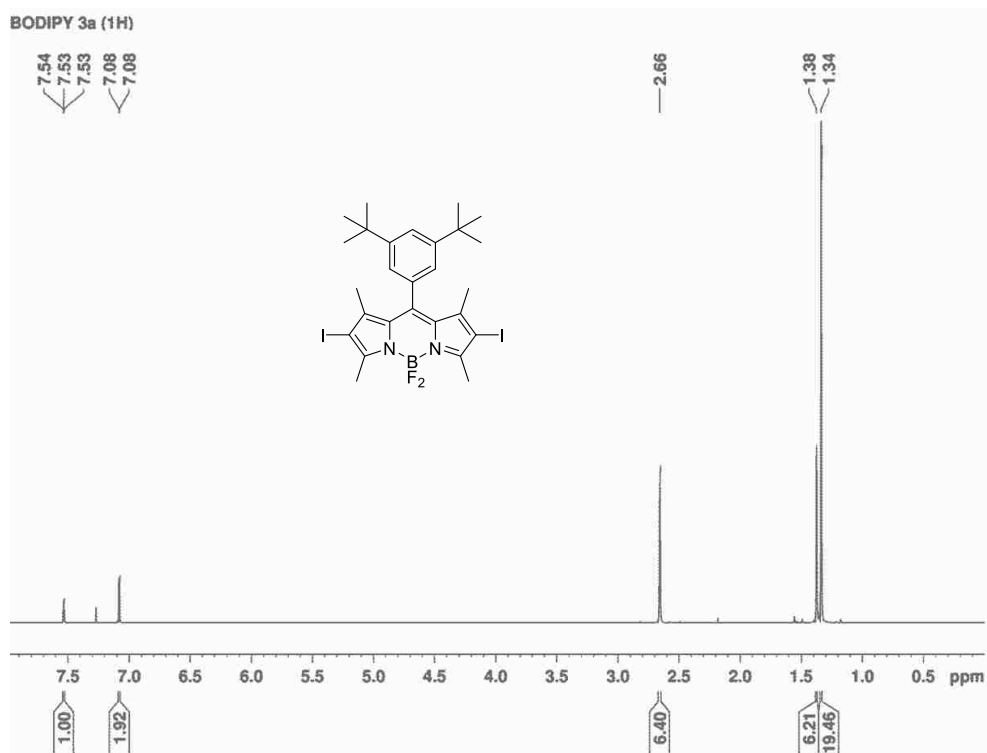


Figure A.27:  $^1\text{H}$  NMR spectrum of BODIPY **3a** in deuterated chloroform at 400MHz.

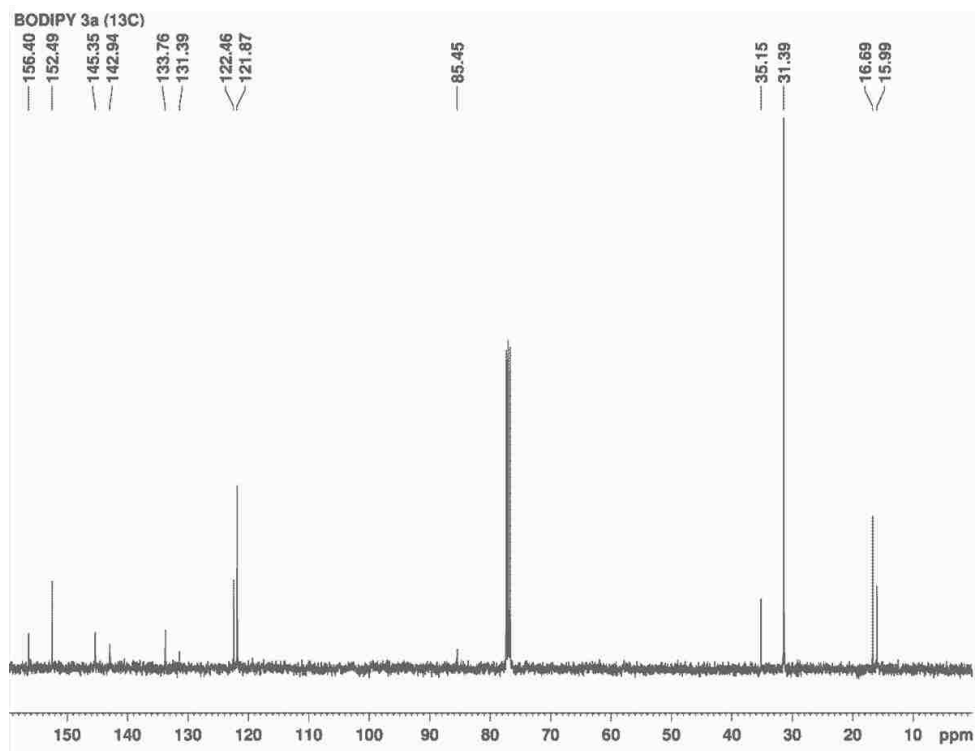


Figure A.28:  $^{13}\text{C}$  NMR spectrum of BODIPY **3a** in deuterated chloroform at 100MHz.

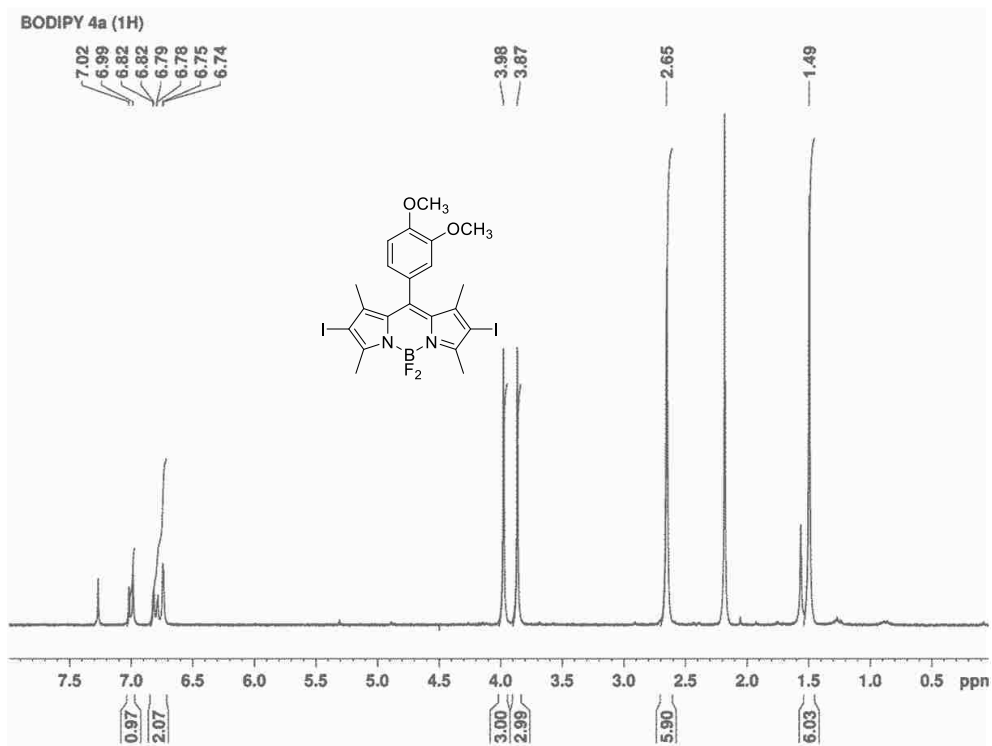


Figure A.29:  $^1\text{H}$  NMR spectrum of BODIPY **4a** in deuterated chloroform at 400MHz.

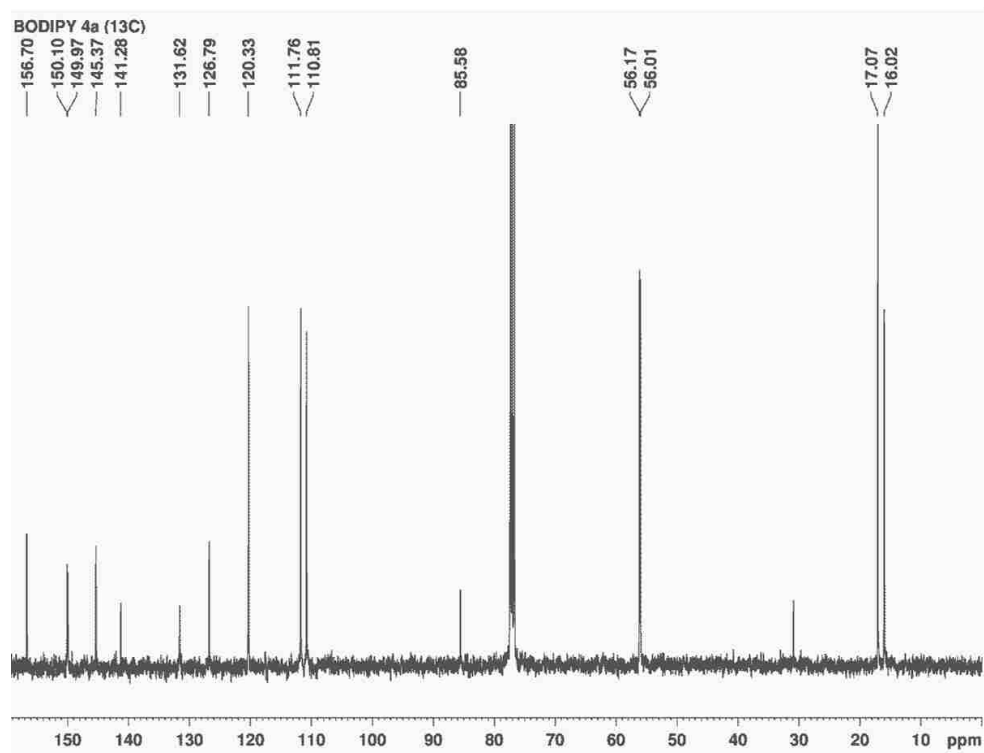


Figure A.30:  $^{13}\text{C}$  NMR spectrum of BODIPY **4a** in deuterated chloroform at 100MHz.

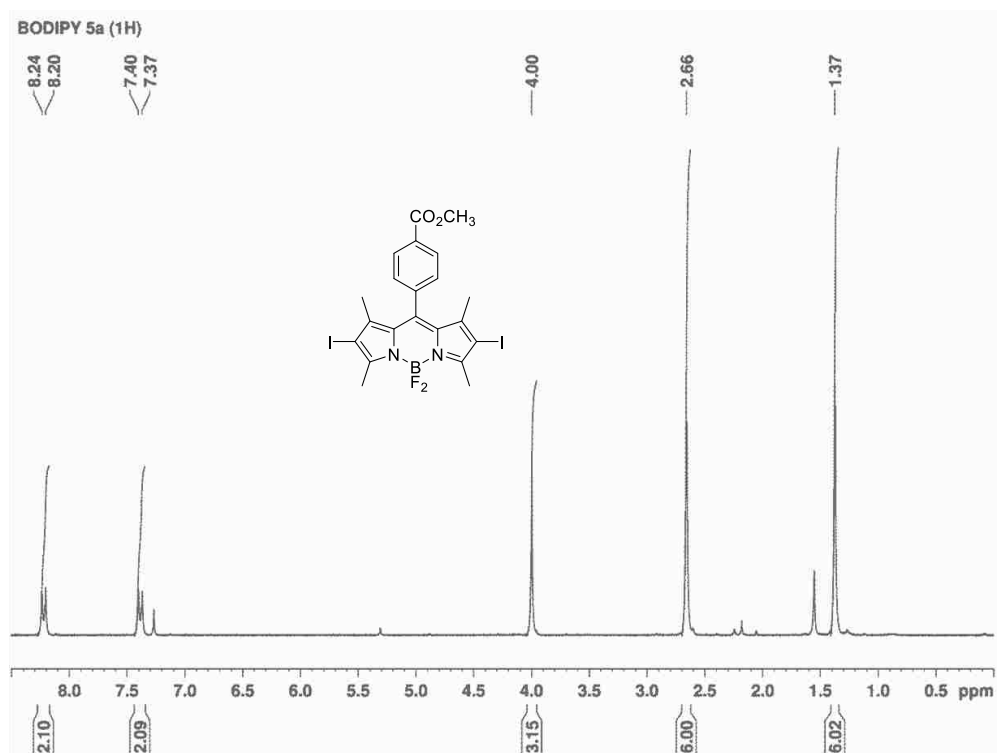


Figure A.31:  $^1\text{H}$  NMR spectrum of BODIPY **5a** in deuterated chloroform at 400MHz.

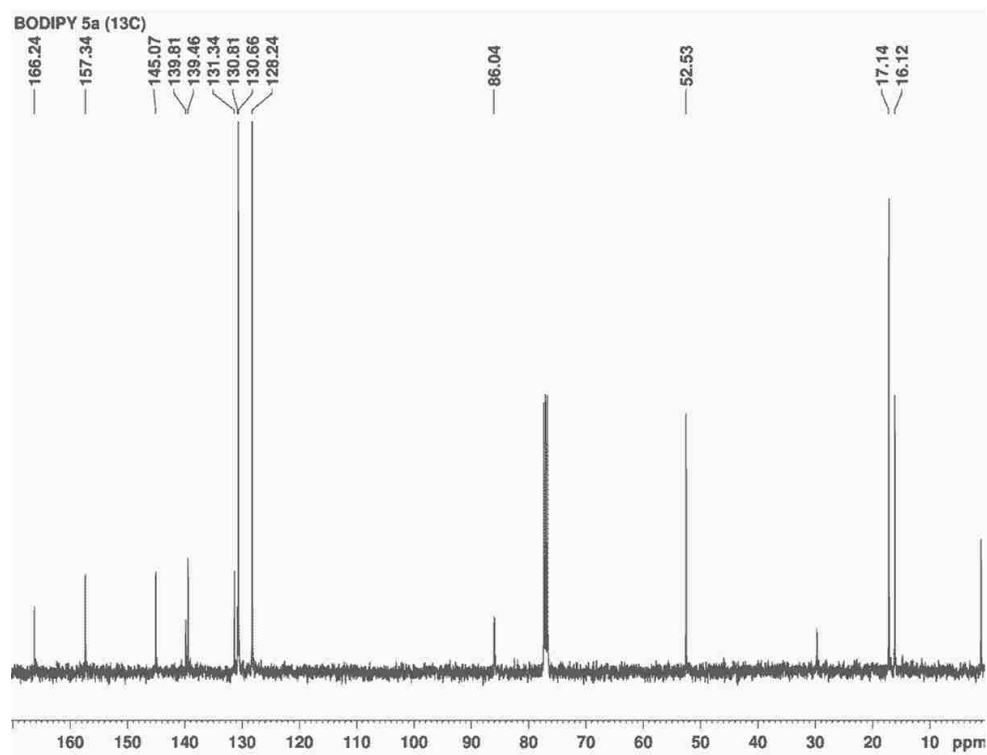


Figure A.32:  $^{13}\text{C}$  NMR spectrum of BODIPY **5a** in deuterated chloroform at 100MHz.

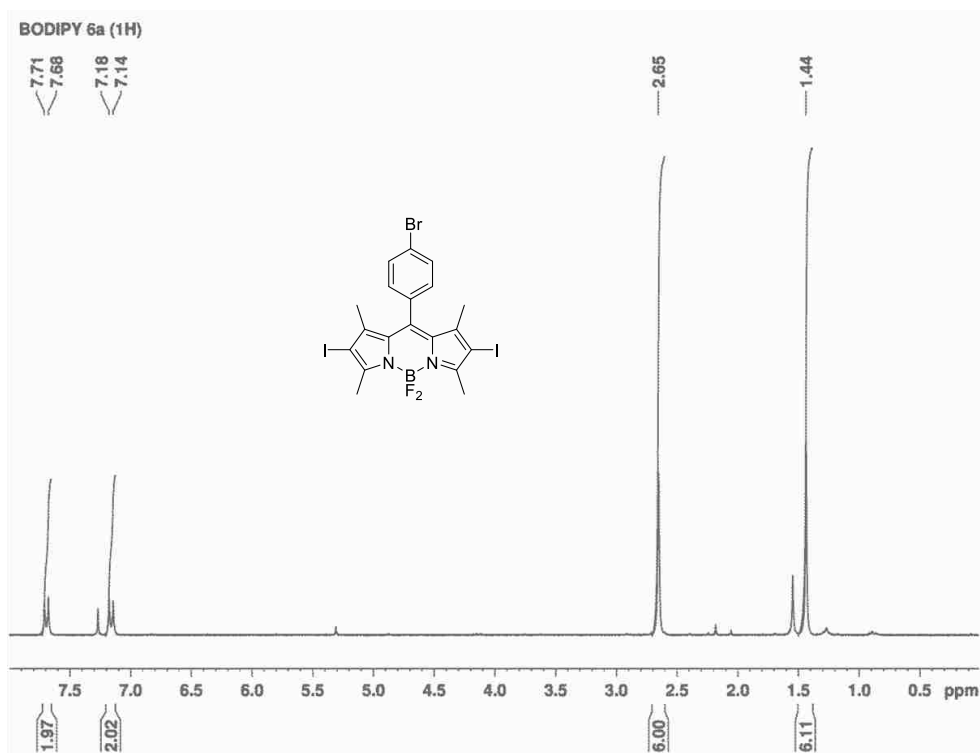


Figure A.33:  $^1\text{H}$  NMR spectrum of BODIPY **6a** in deuterated chloroform at 400MHz.

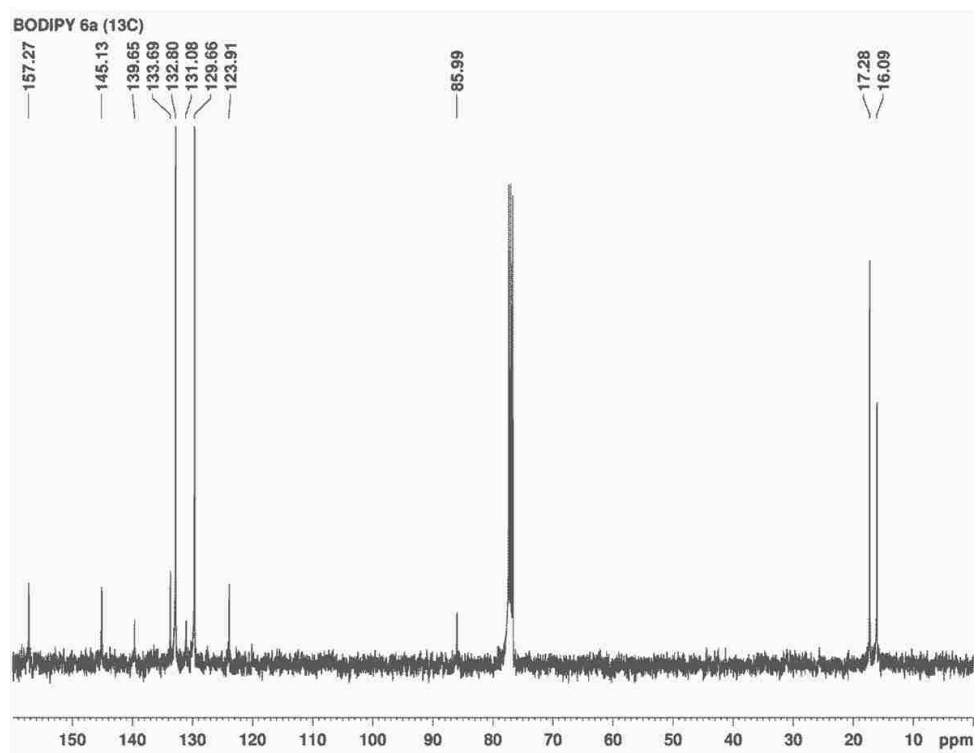


Figure A.34:  $^{13}\text{C}$  NMR spectrum of BODIPY **6a** in deuterated chloroform at 100MHz.

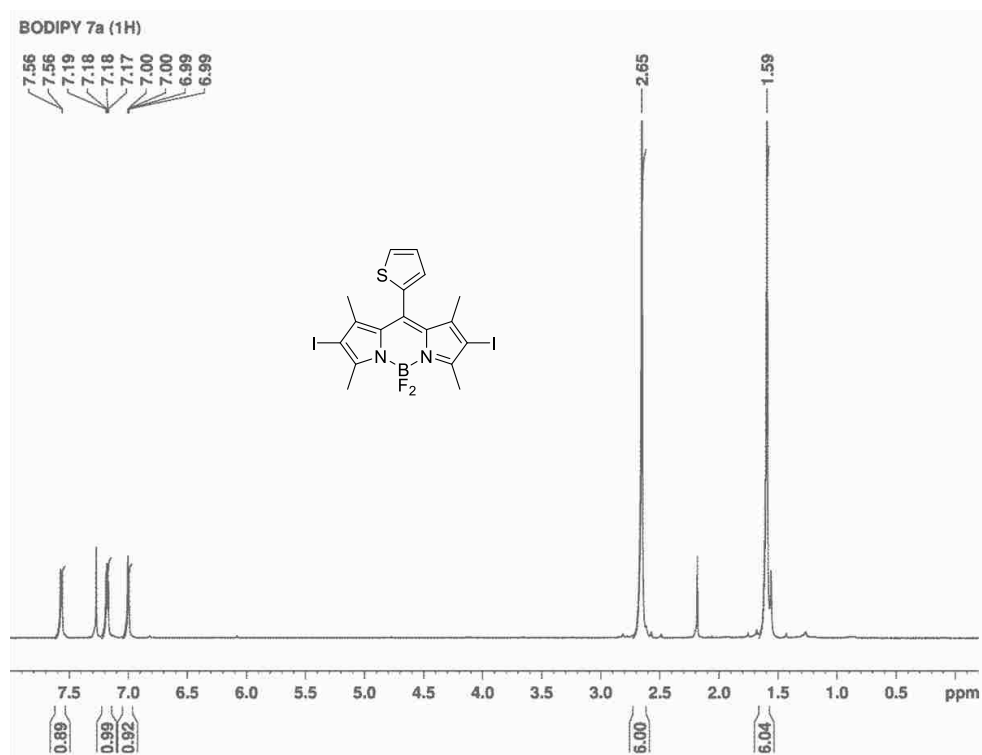


Figure A.35:  $^1\text{H}$  NMR spectrum of BODIPY **7a** in deuterated chloroform at 400MHz.

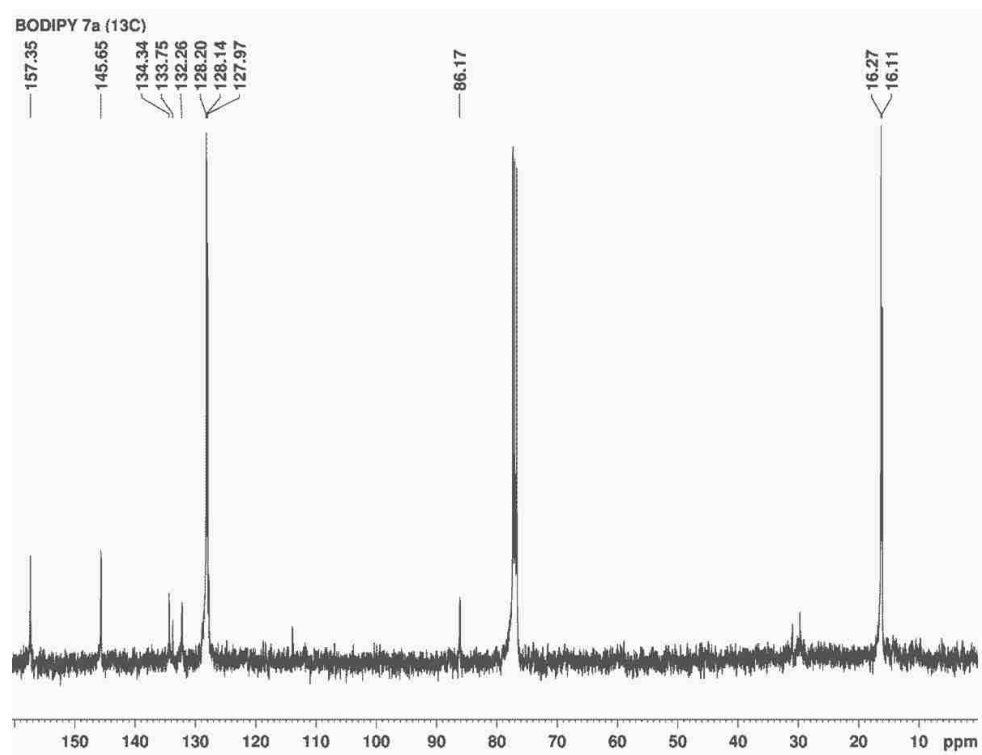


Figure A.36:  $^{13}\text{C}$  NMR spectrum of BODIPY **7a** in deuterated chloroform at 100MHz.

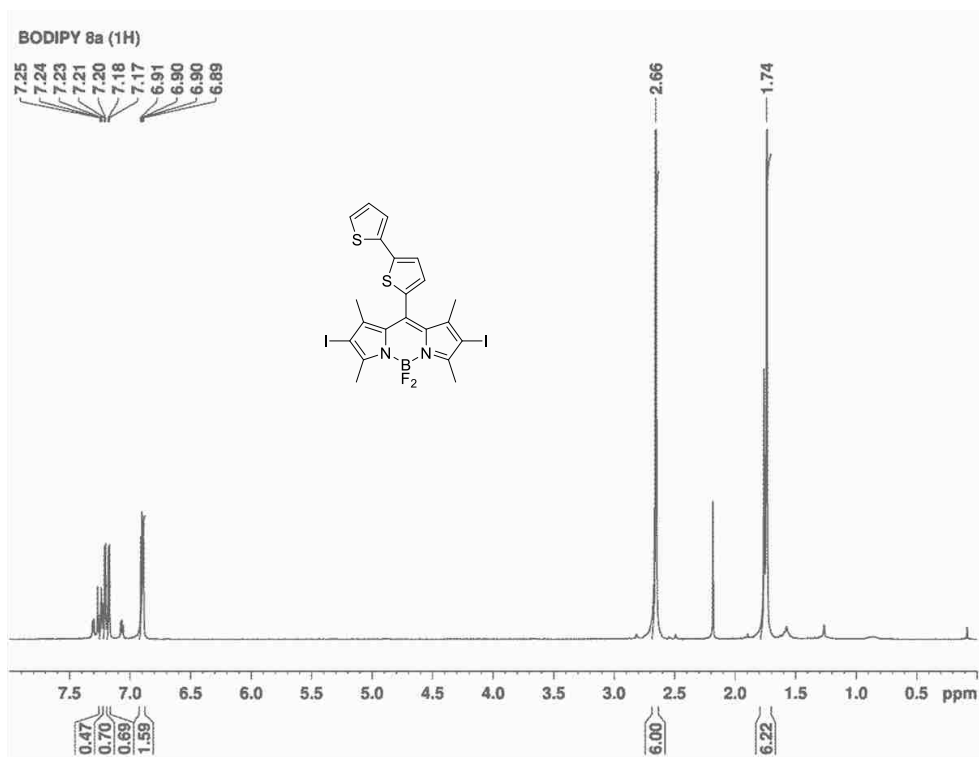


Figure A.37: <sup>1</sup>H NMR spectrum of BODIPY **8a** in deuterated chloroform at 400MHz.

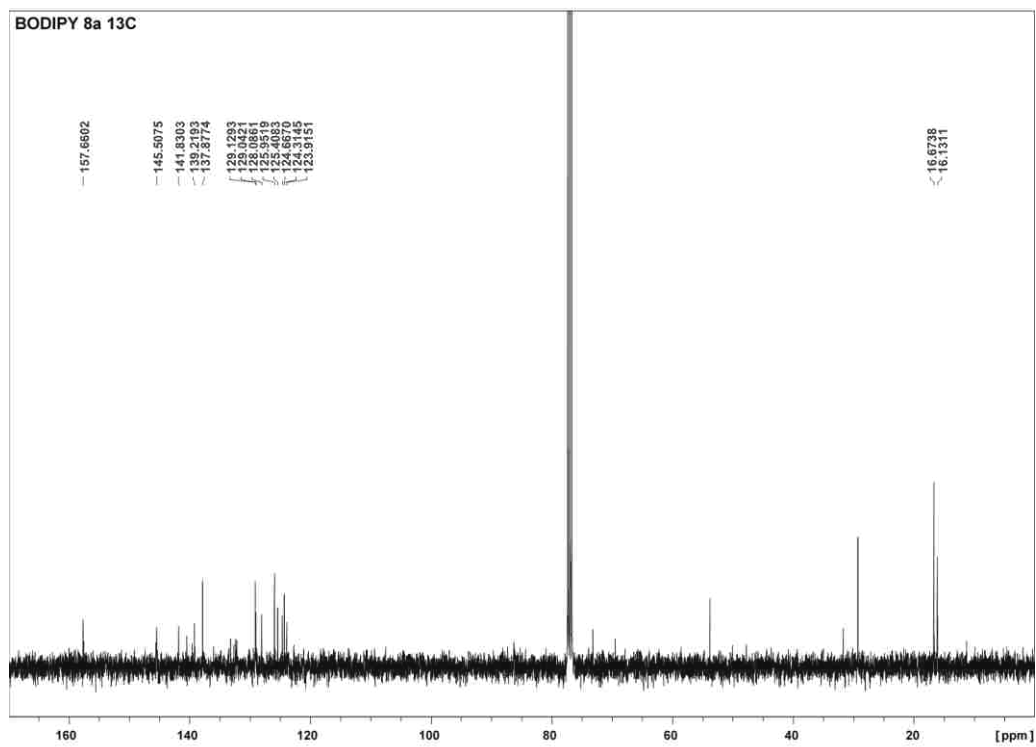


Figure A.38: <sup>13</sup>C NMR spectrum of BODIPY **8a** in deuterated chloroform at 100MHz.

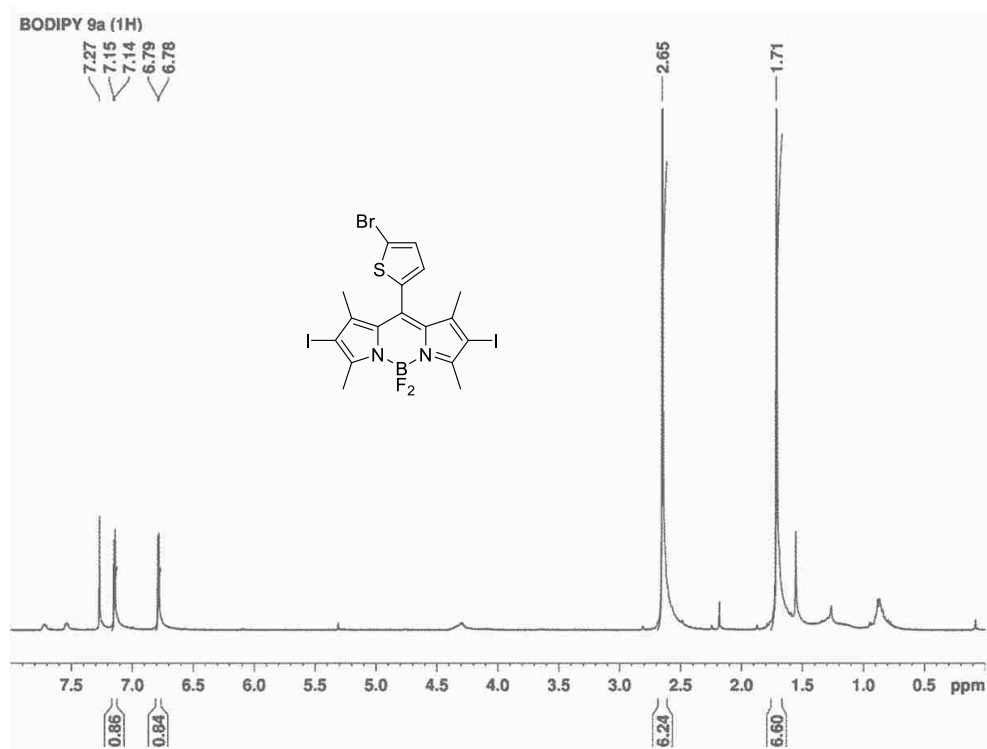


Figure A.39:  $^1\text{H}$  NMR spectrum of BODIPY **9a** in deuterated chloroform at 400MHz.

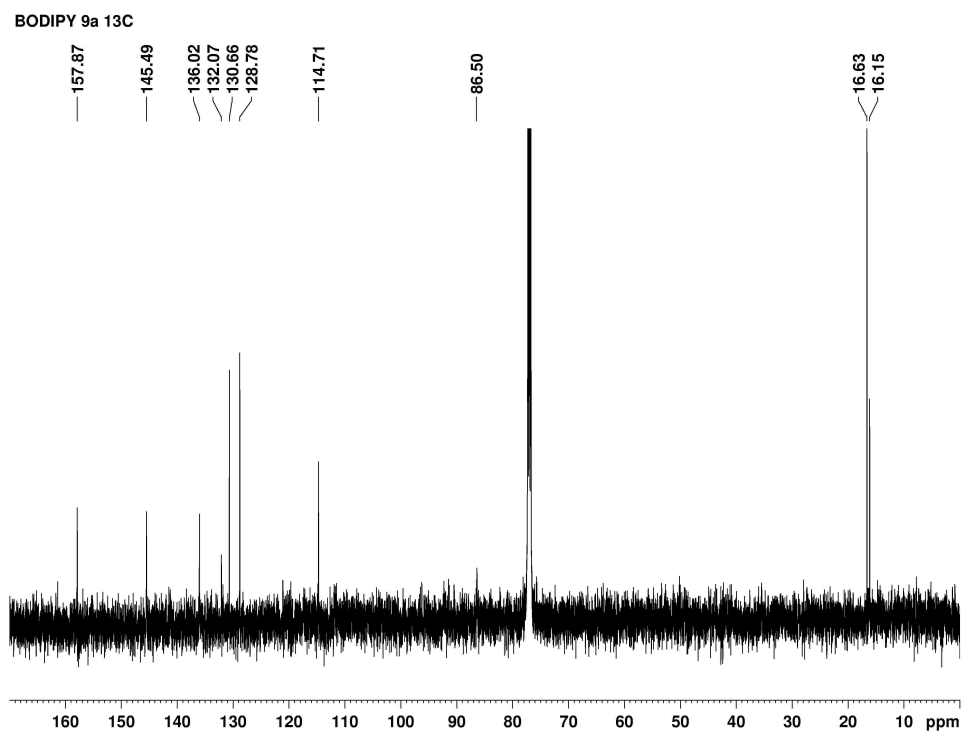


Figure A.40:  $^{13}\text{C}$  NMR spectrum of BODIPY **9a** in deuterated chloroform at 100MHz.

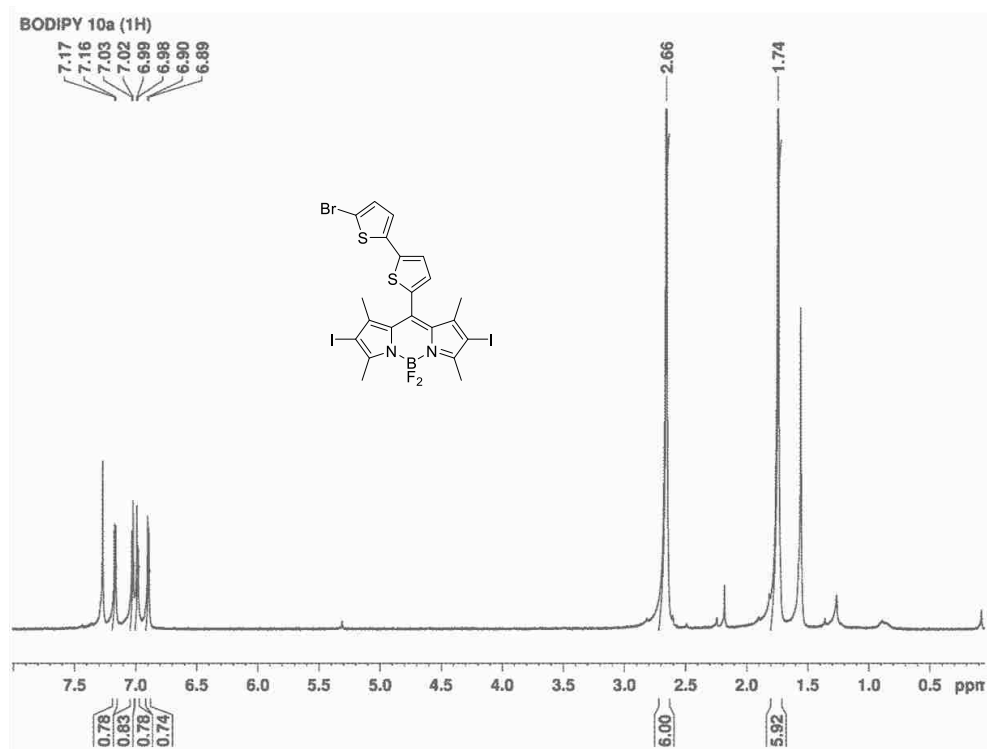


Figure A.41:  $^1\text{H}$  NMR spectrum of BODIPY **10a** in deuterated chloroform at 400MHz.

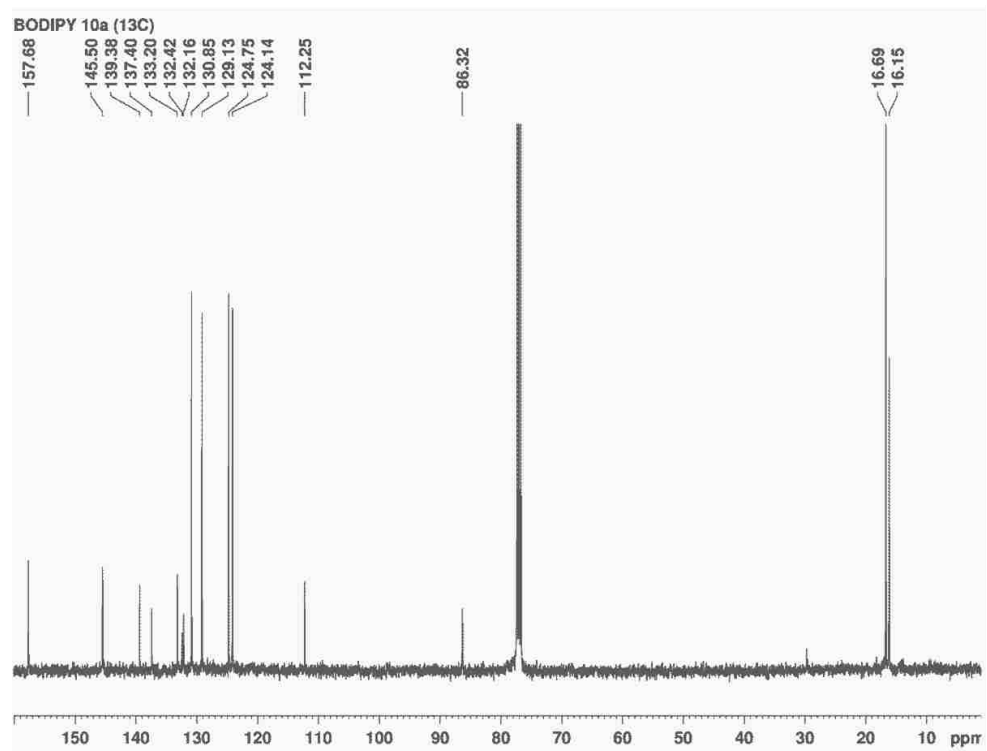


Figure A.42:  $^{13}\text{C}$  NMR spectrum of BODIPY **10a** in deuterated chloroform at 100MHz.

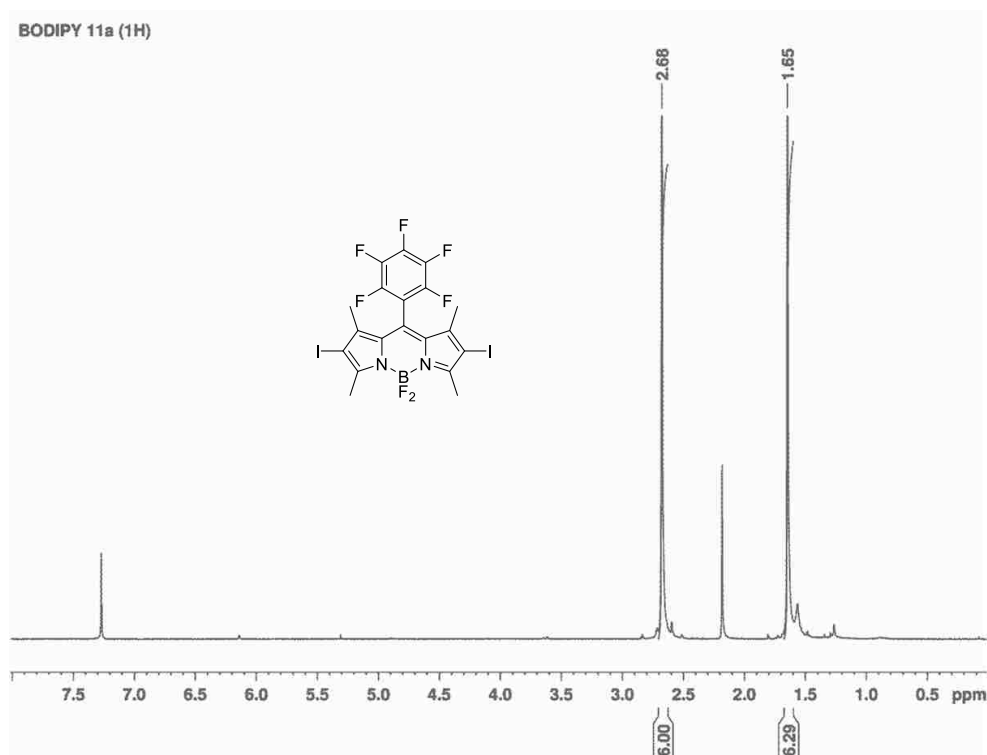


Figure A.43:  $^1\text{H}$  NMR spectrum of BODIPY **11a** in deuterated chloroform at 400MHz.

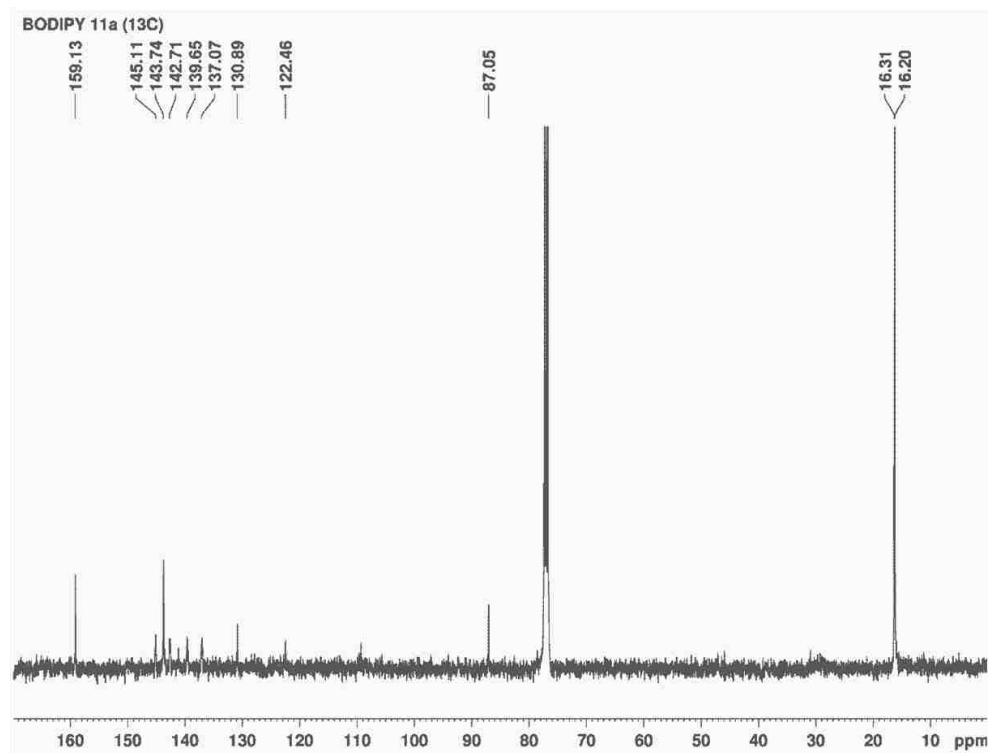


Figure A.44:  $^{13}\text{C}$  NMR spectrum of BODIPY **11a** in deuterated chloroform at 100MHz.

## APPENDIX B: NMR SPECTRA OF COMPOUNDS FOUND IN CHAPTER 3

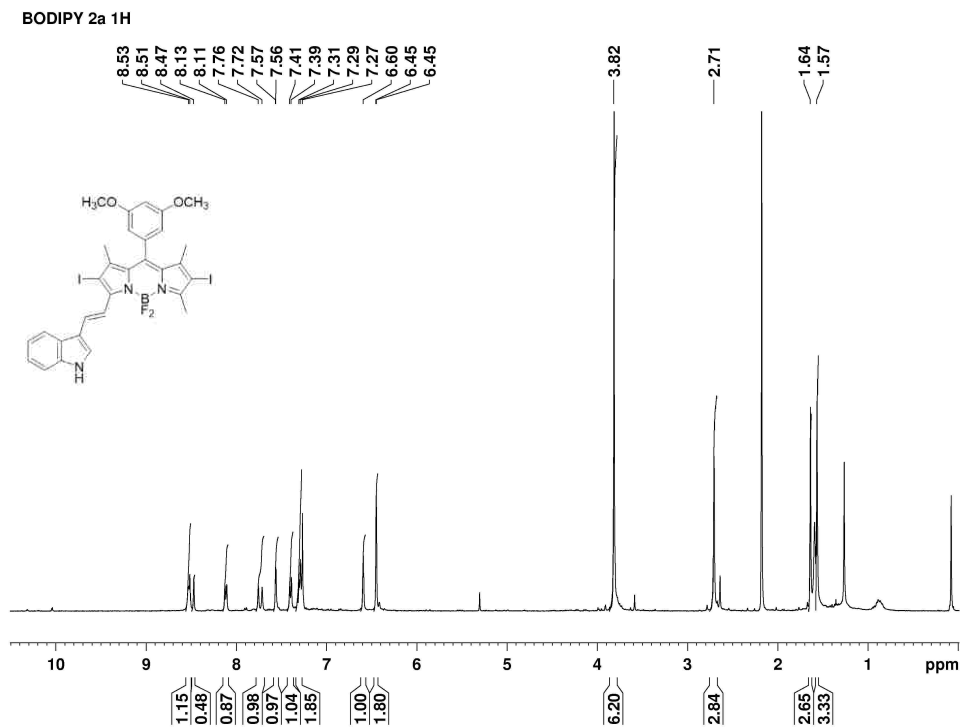


Figure B.1:  $^1\text{H}$  NMR spectrum of BODIPY **2a** in deuterated chloroform at 400MHz.

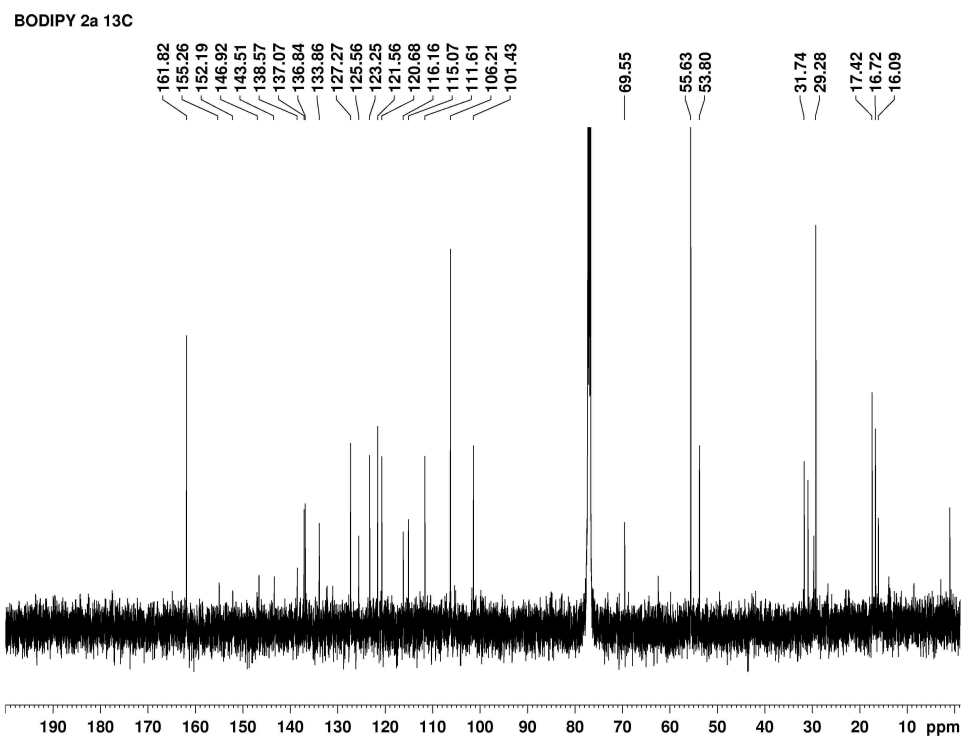


Figure B.2:  $^{13}\text{C}$  NMR spectrum of BODIPY **2a** in deuterated chloroform at 100MHz.

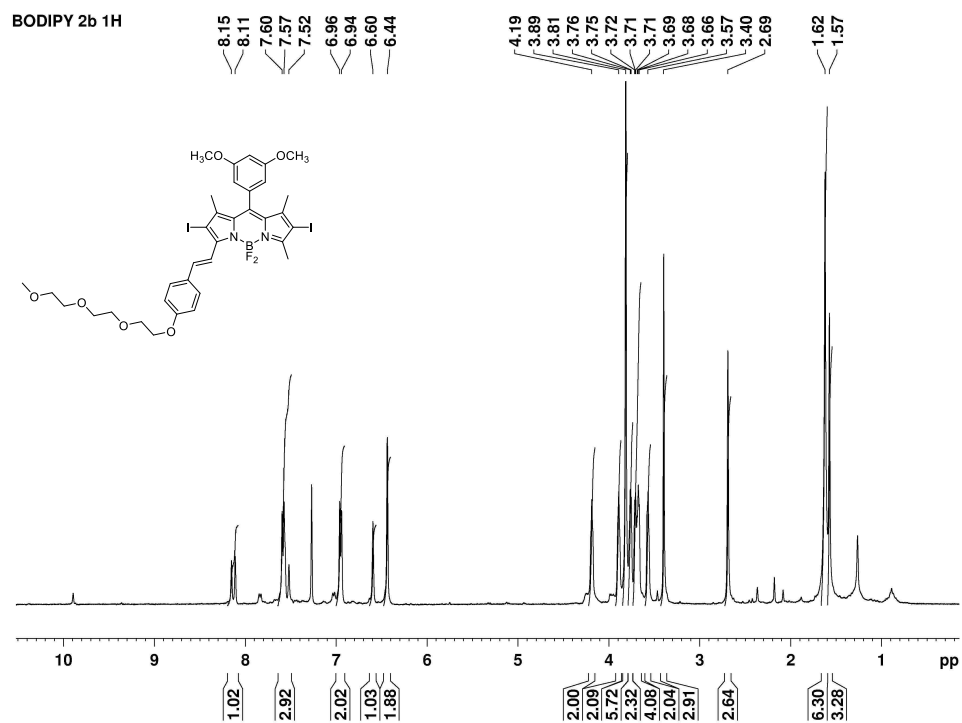


Figure B.3:  $^1\text{H}$  NMR spectrum of BODIPY **2b** in deuterated chloroform at 400MHz.

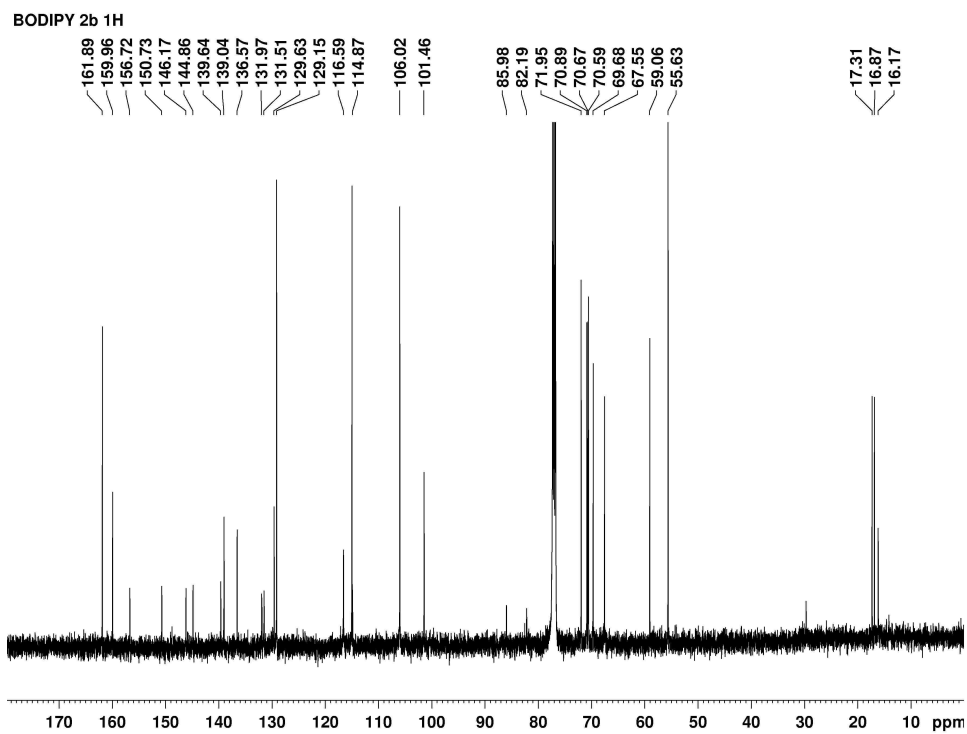


Figure B.4  $^{13}\text{C}$  NMR spectrum of BODIPY **2b** in deuterated chloroform at 100MHz.

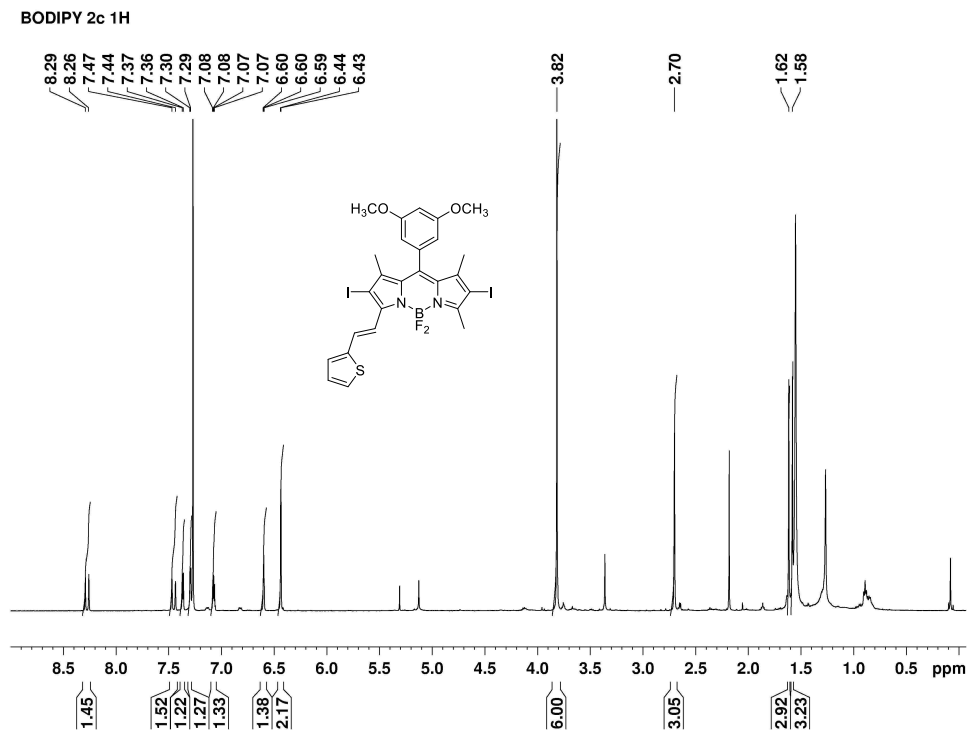


Figure B.5:  $^1\text{H}$  NMR spectrum of BODIPY **2c** in deuterated chloroform at 400MHz.

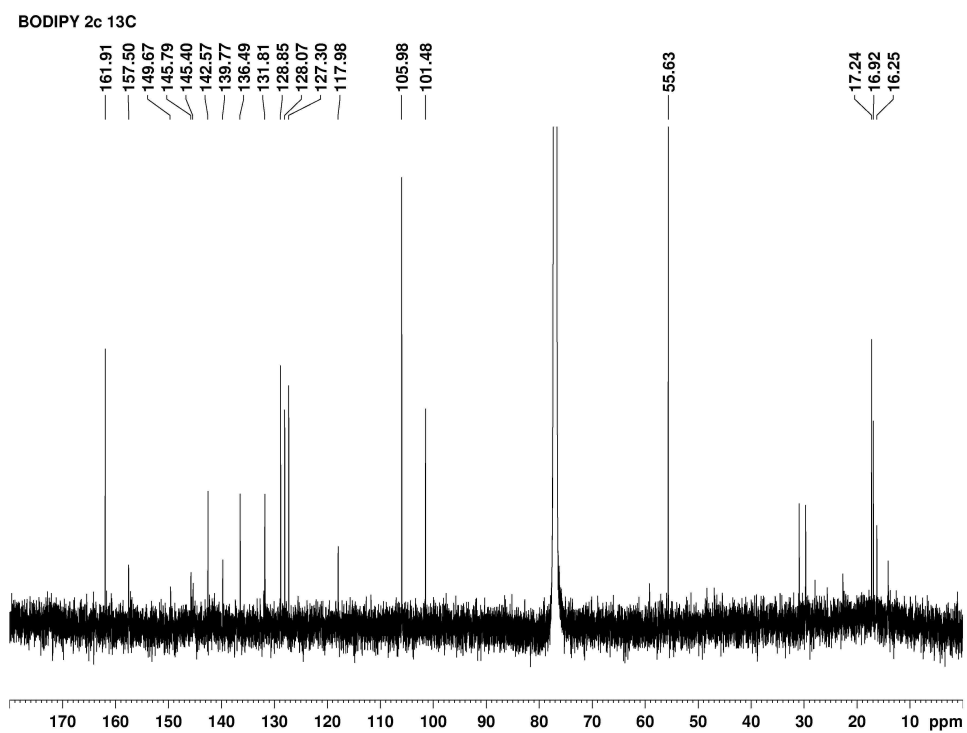


Figure B.6:  $^{13}\text{C}$  NMR spectrum of BODIPY **2c** in deuterated chloroform at 100MHz.

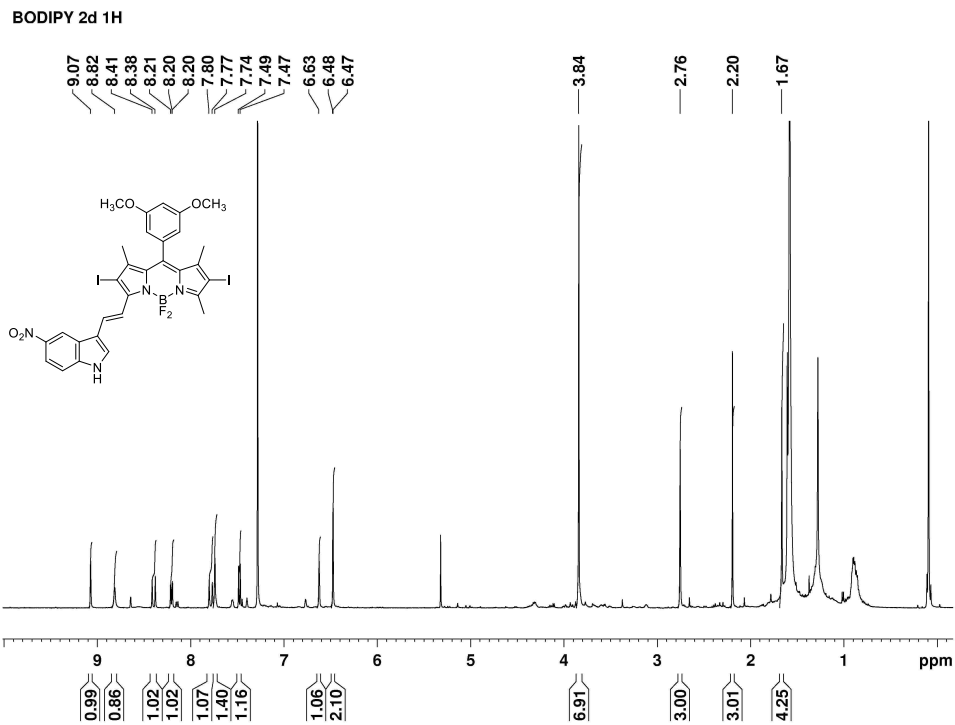


Figure B.7:  $^1\text{H}$  NMR spectrum of BODIPY **2d** in deuterated chloroform at 400MHz.

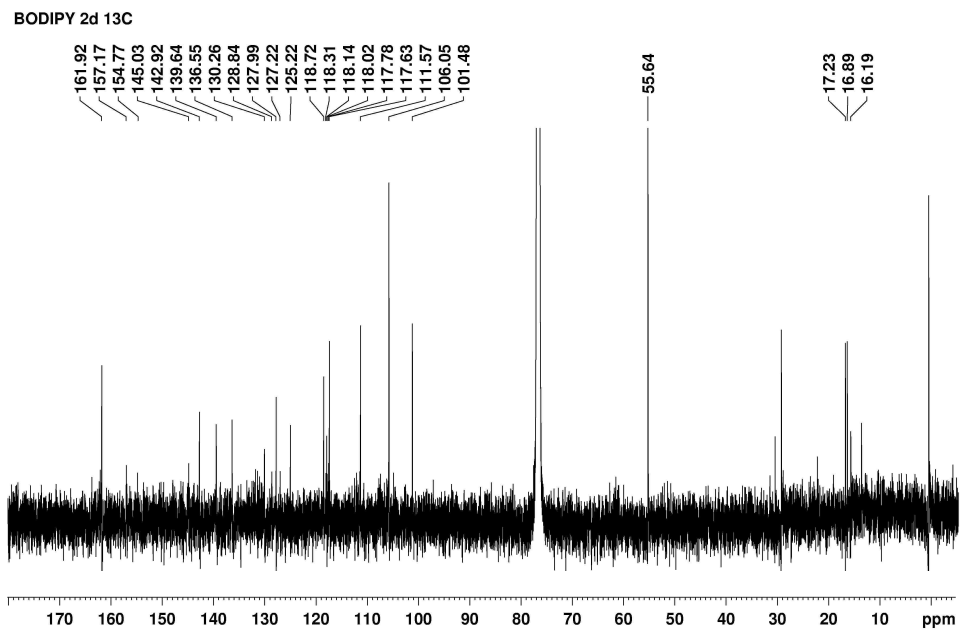


Figure B.8:  $^{13}\text{C}$  NMR spectrum of BODIPY **2d** in deuterated chloroform at 100MHz.

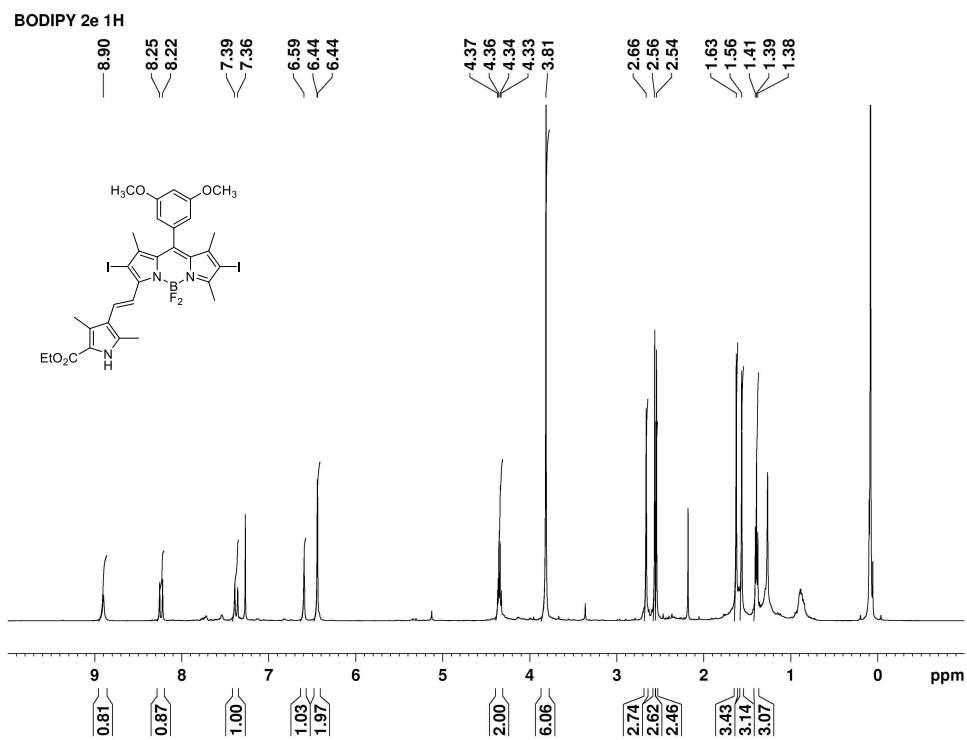


Figure B.9:  $^1\text{H}$  NMR spectrum of BODIPY **2e** in deuterated chloroform at 500MHz.

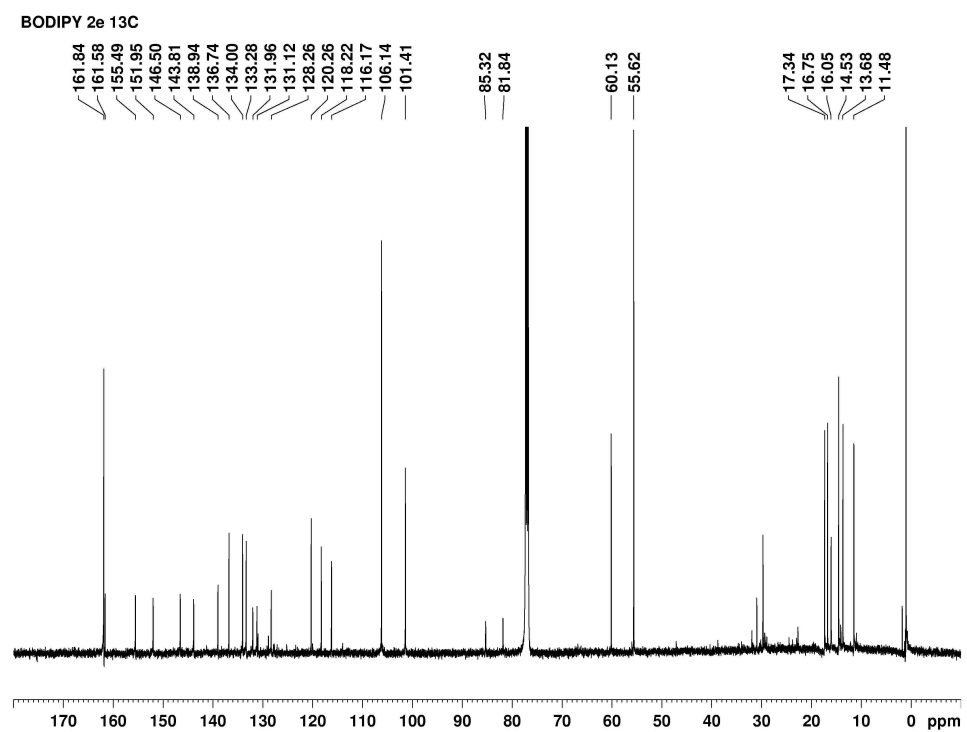


Figure B.10:  $^{13}\text{C}$  NMR spectrum of BODIPY **2e** in deuterated chloroform at 100MHz.

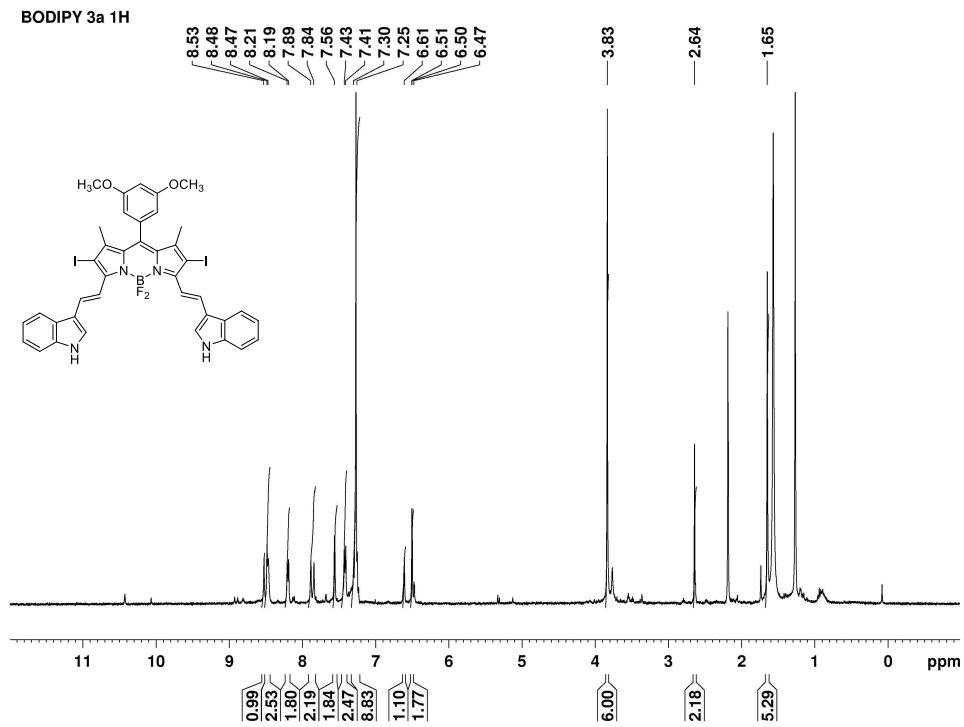


Figure B.11:  $^1\text{H}$  NMR spectrum of BODIPY **3a** in deuterated chloroform at 400MHz.

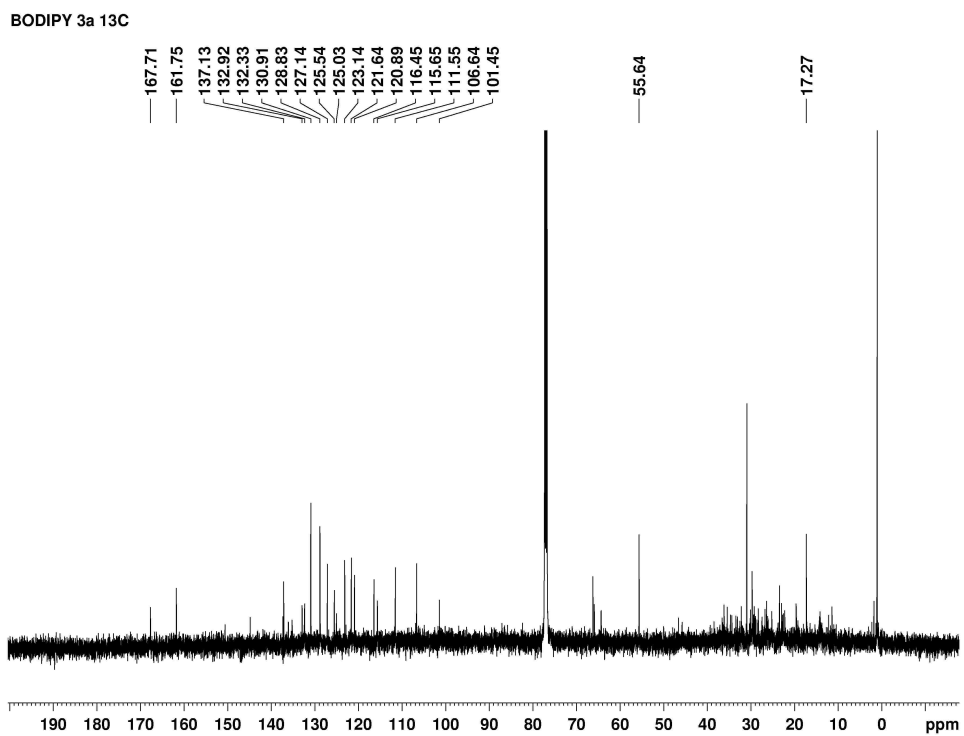


Figure B.12:  $^{13}\text{C}$  NMR spectrum of BODIPY **3a** in deuterated chloroform at 100MHz.

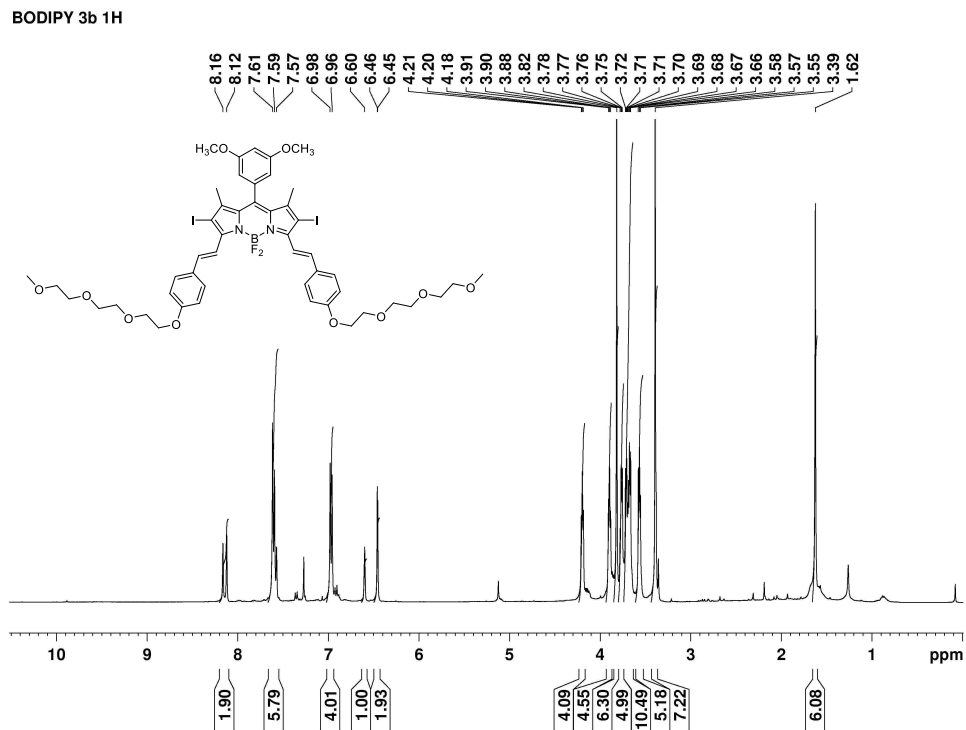


Figure B.13:  $^1\text{H}$  NMR spectrum of BODIPY **3b** in deuterated chloroform at 400MHz.

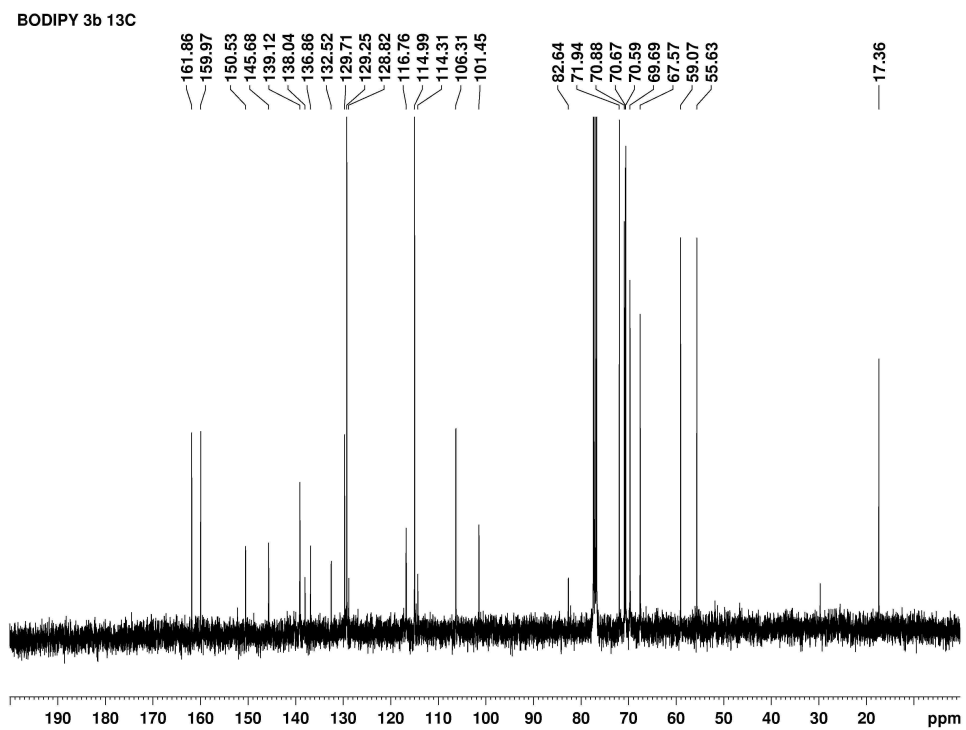


Figure B.14:  $^{13}\text{C}$  NMR spectrum of BODIPY **3b** in deuterated chloroform at 100MHz.

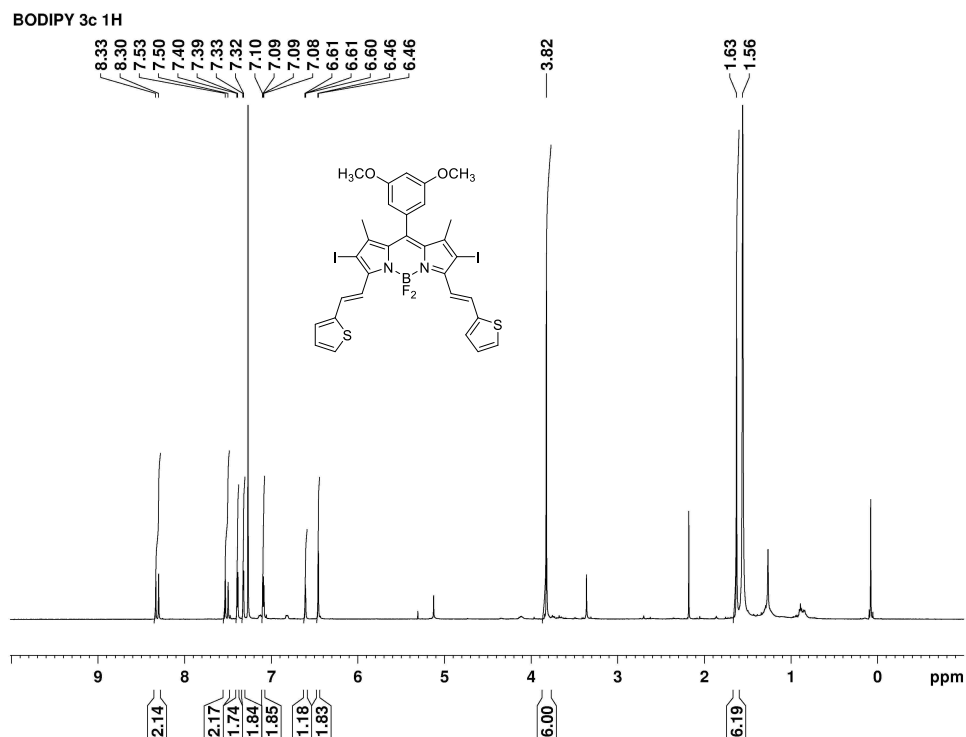


Figure B.15: <sup>1</sup>H NMR spectrum of BODIPY 3c in deuterated chloroform at 500MHz.

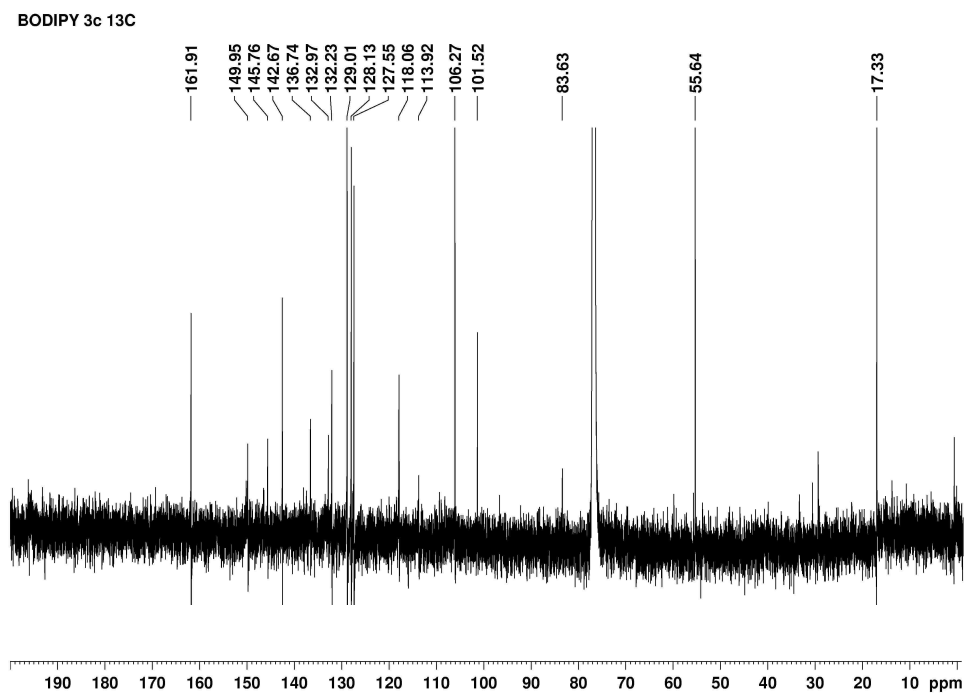


Figure B.16: <sup>13</sup>C NMR spectrum of BODIPY 3c in deuterated chloroform at 100MHz.

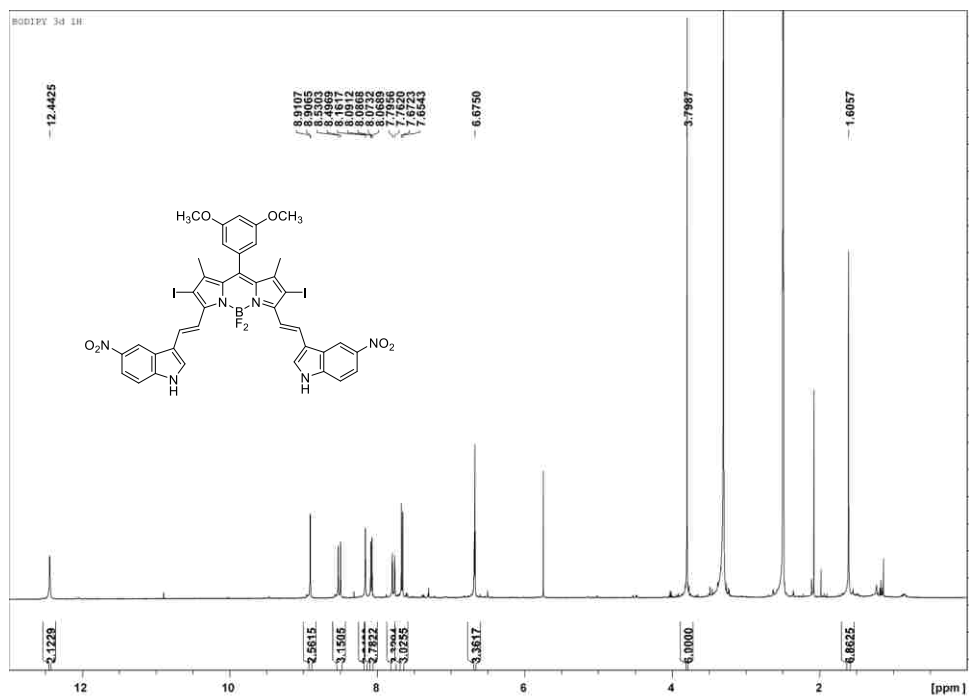


Figure B.17: <sup>1</sup>H NMR spectrum of BODIPY **3d** in deuterated DMSO at 500MHz.

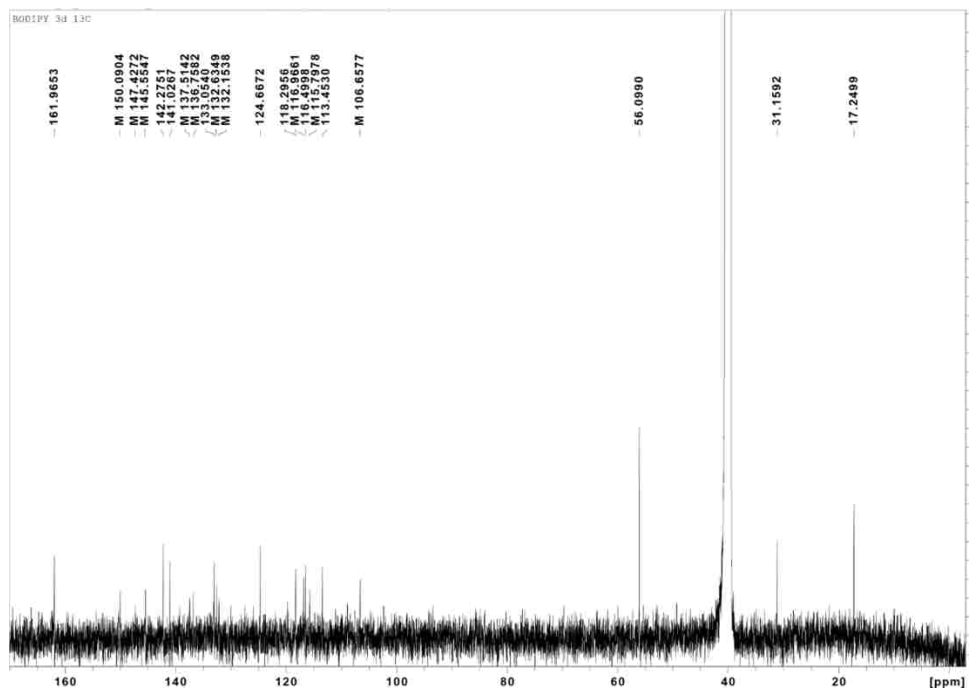


Figure B.18: <sup>13</sup>C NMR spectrum of BODIPY **3d** in deuterated DMSO at 100MHz.

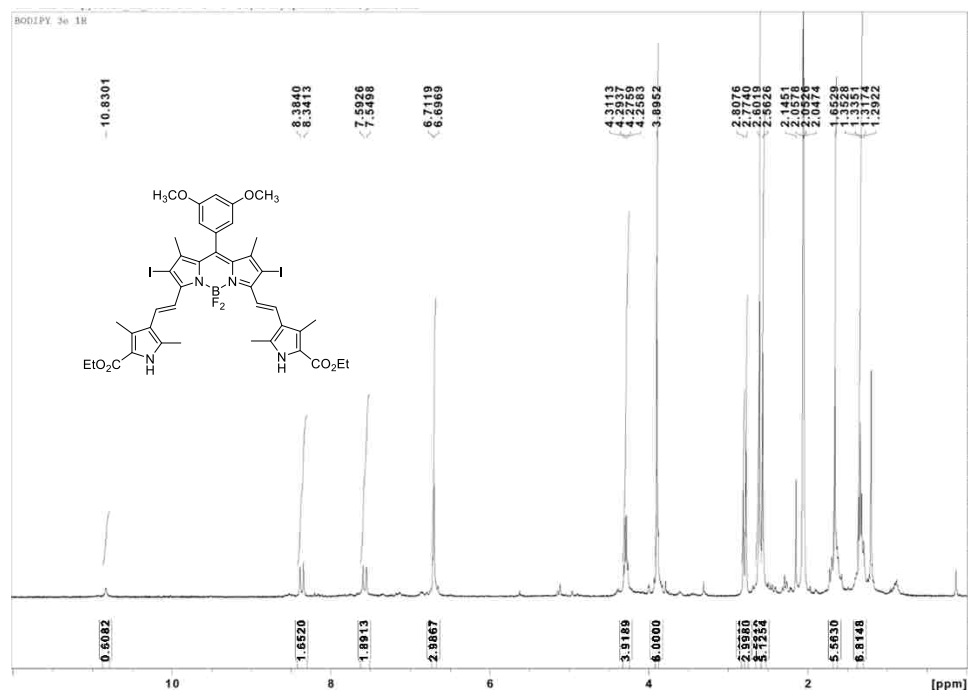


Figure B.19:  $^1\text{H}$  NMR spectrum of BODIPY **3e** in deuterated acetone at 500MHz.

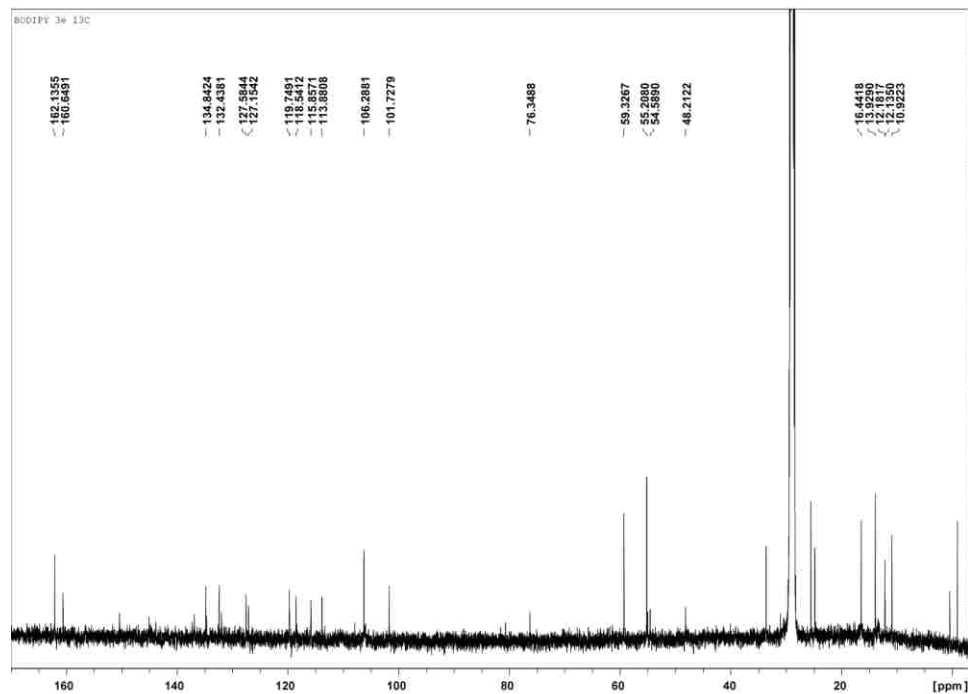


Figure B.20:  $^{13}\text{C}$  NMR spectrum of BODIPY **3e** in deuterated acetone at 500MHz.

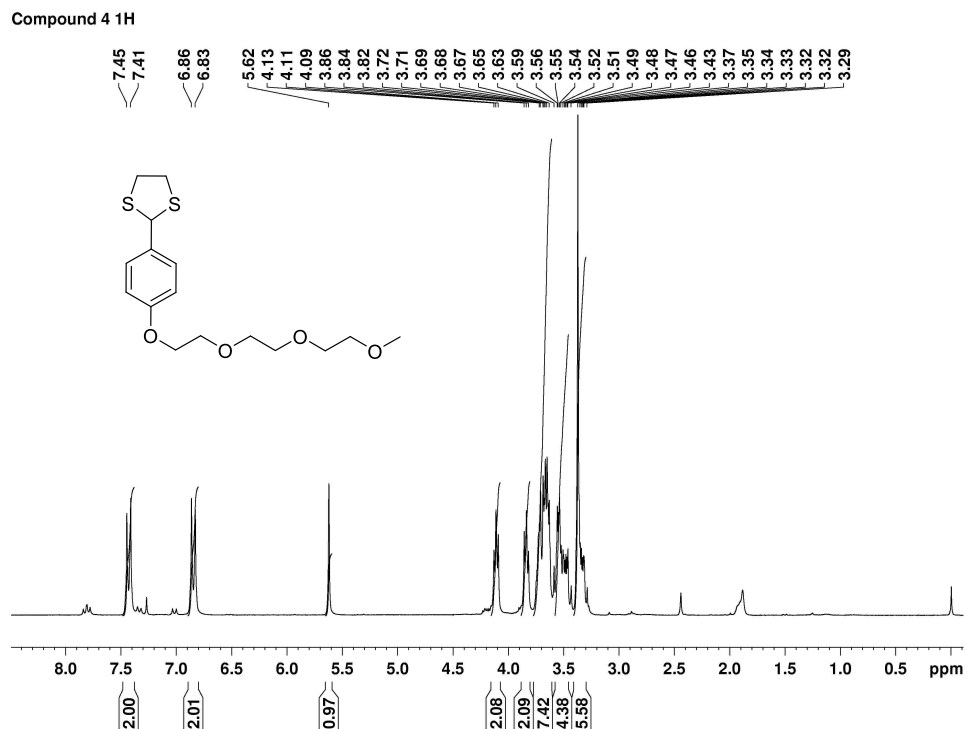


Figure B.21: <sup>1</sup>H NMR spectrum of Compound **4** in deuterated chloroform at 400MHz.

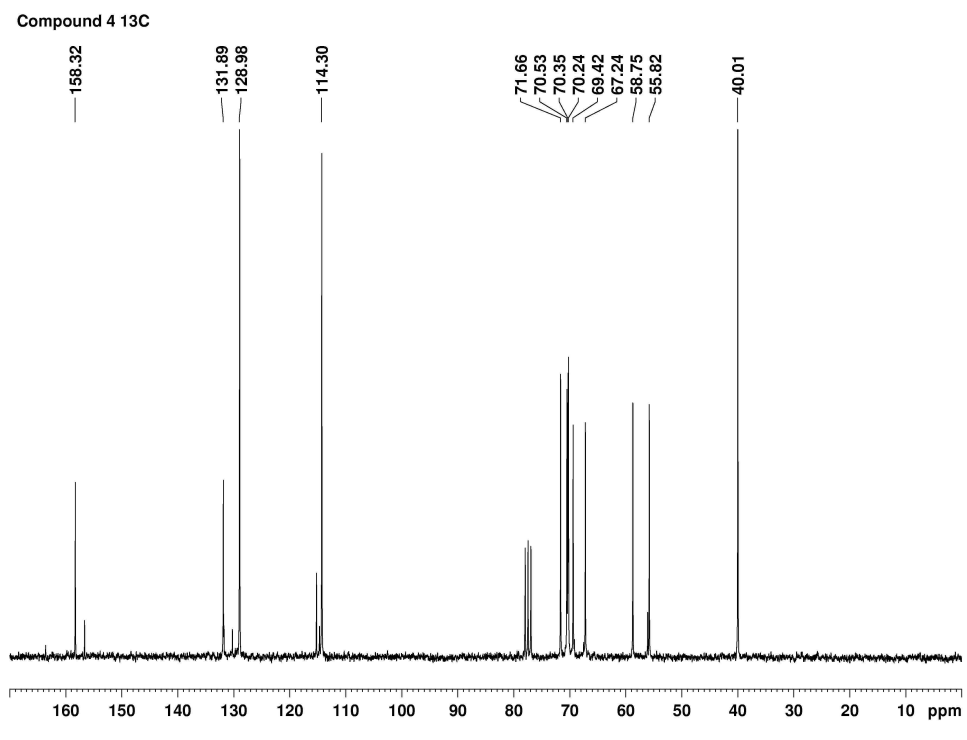


Figure B.22: <sup>13</sup>C NMR spectrum of Compound **4** in deuterated chloroform at 100MHz.

## APPENDIX C: NMR SPECTRA OF COMPOUNDS FOUND IN CHAPTER 4

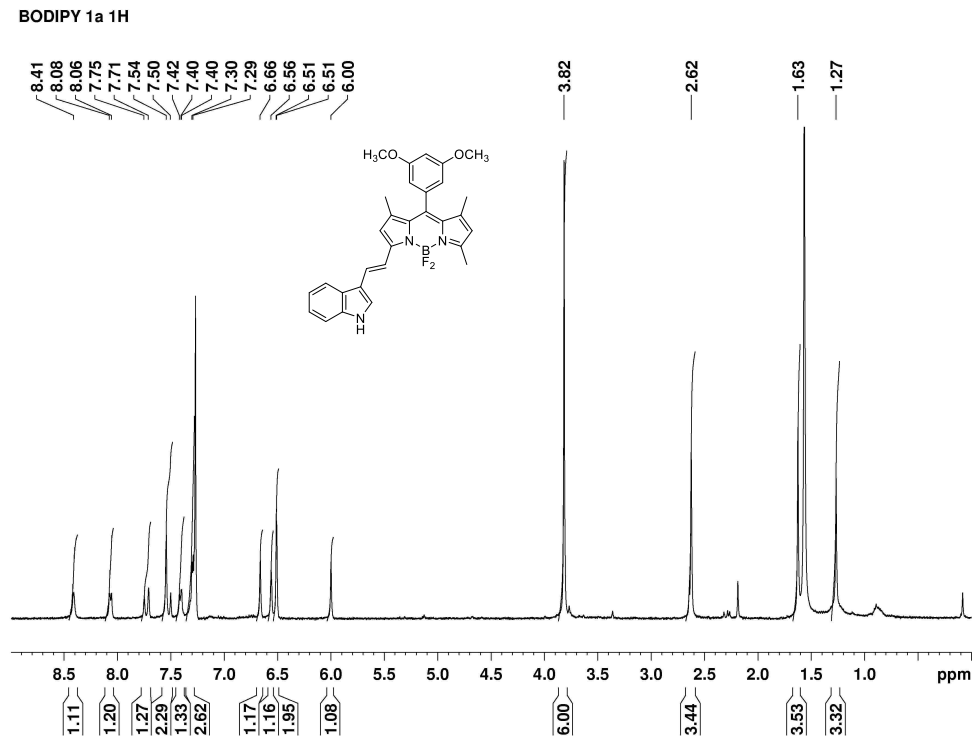


Figure C.1:  $^1\text{H}$  NMR spectrum of BODIPY **1a** in deuterated chloroform at 400MHz.

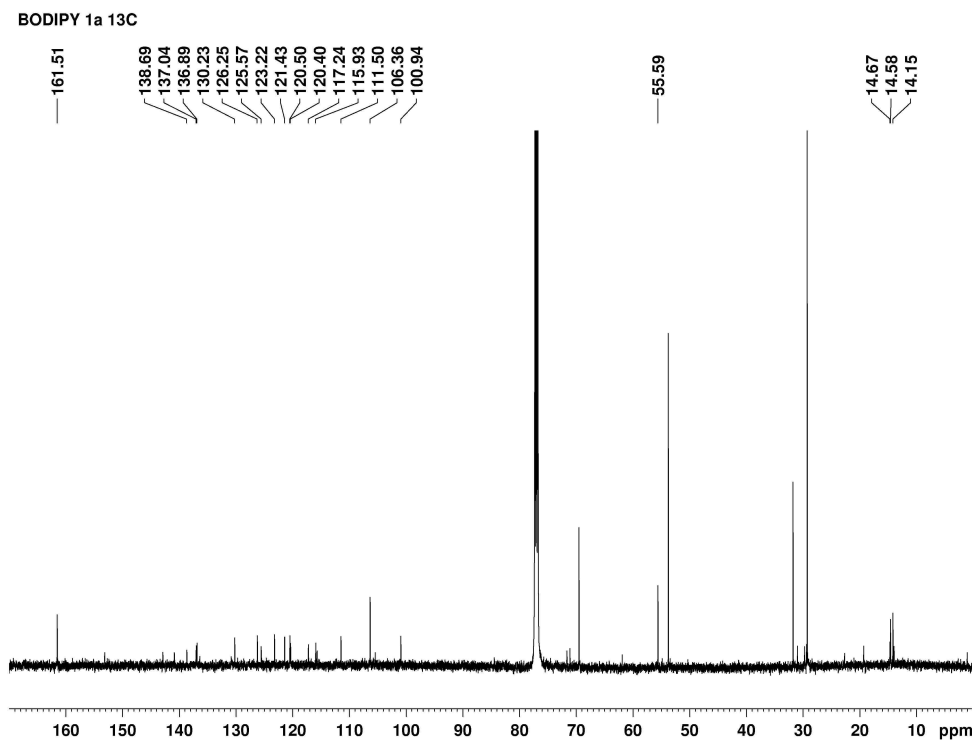


Figure C.2:  $^{13}\text{C}$  NMR spectrum of BODIPY **1a** in deuterated chloroform at 100MHz.

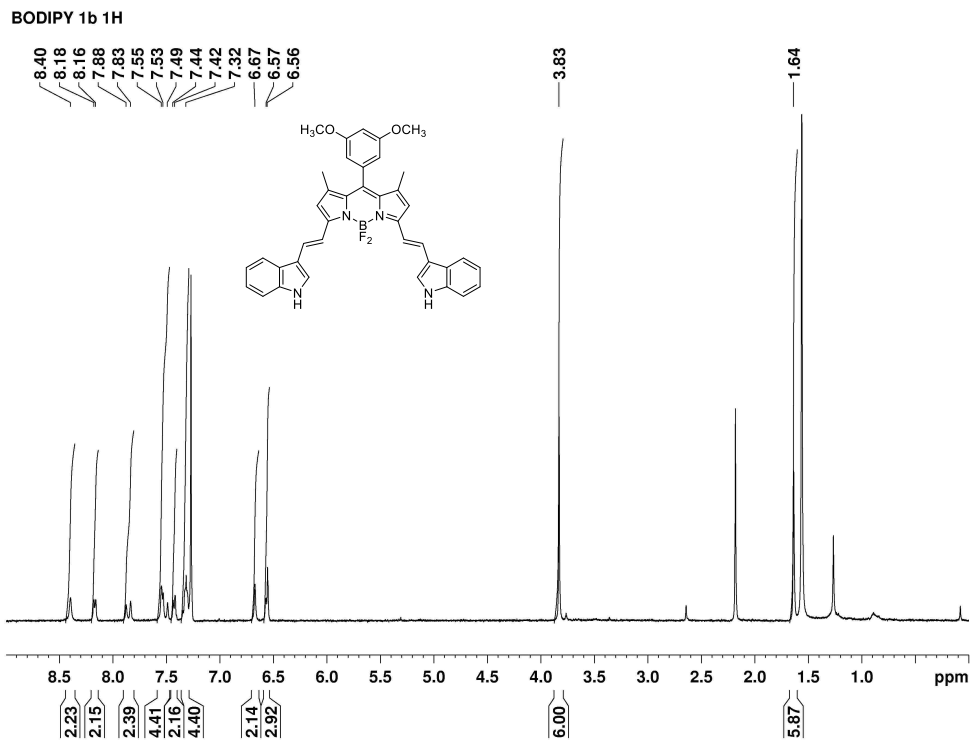


Figure C.3:  $^1\text{H}$  NMR spectrum of BODIPY **1b** in deuterated chloroform at 400MHz.

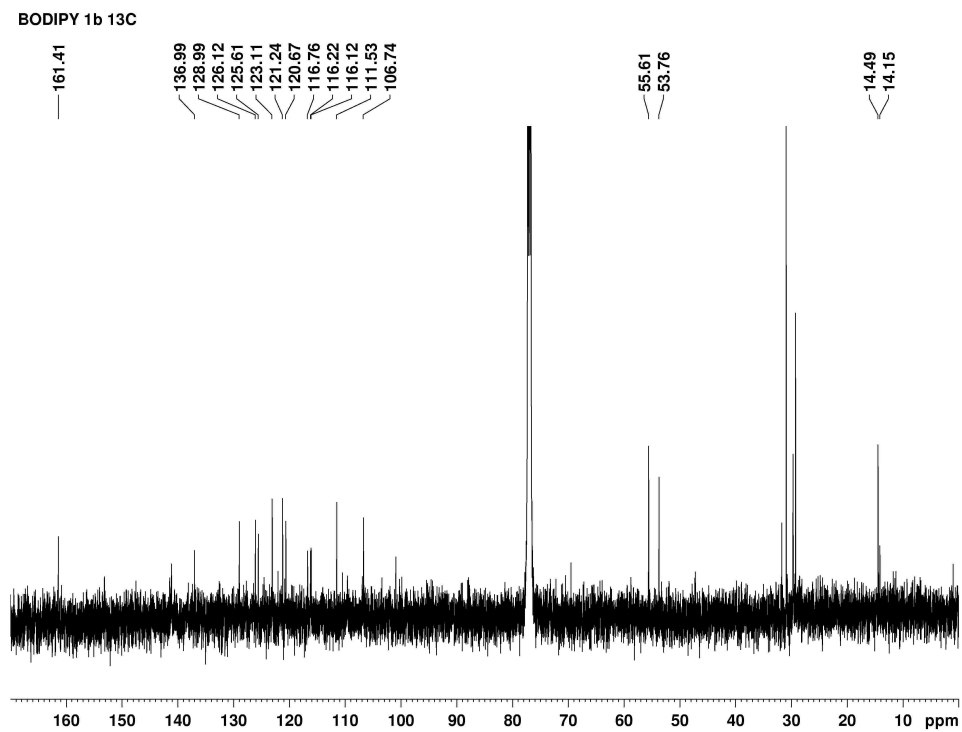


Figure C.4:  $^{13}\text{C}$  NMR spectrum of BODIPY **1b** in deuterated chloroform at 100MHz.

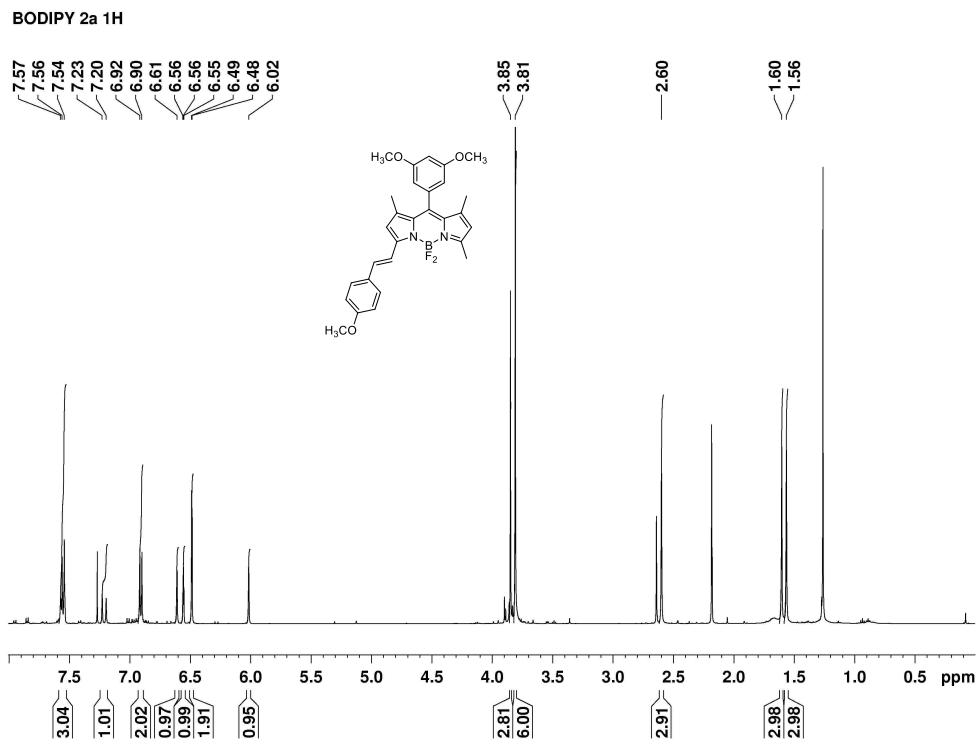


Figure C.5:  $^1\text{H}$  NMR spectrum of BODIPY **2a** in deuterated chloroform at 400MHz.

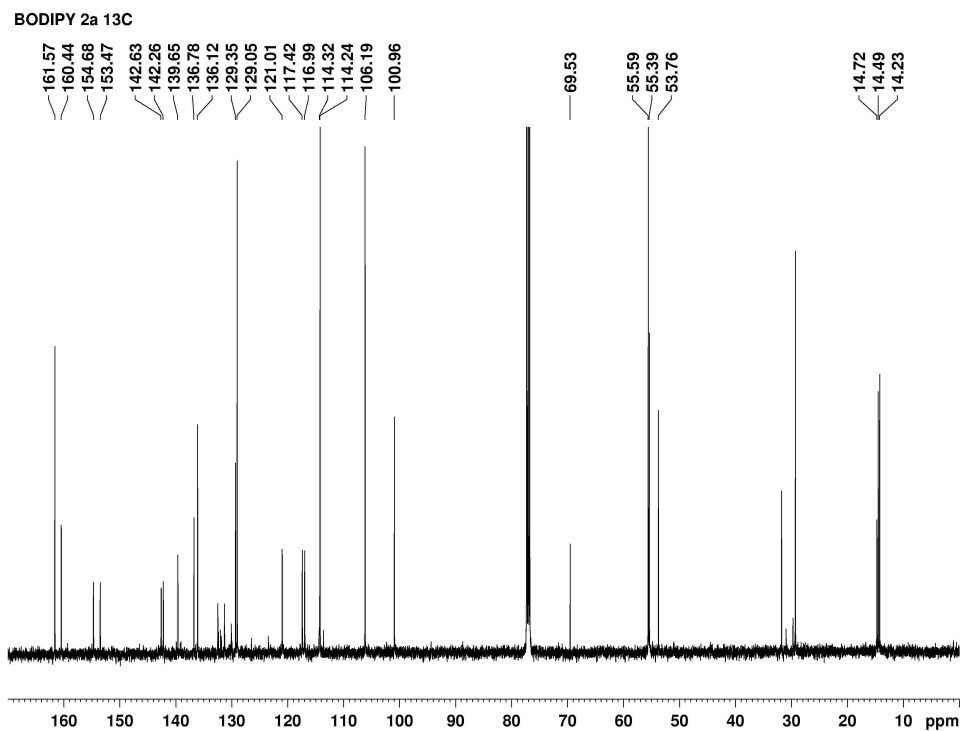


Figure C.6:  $^{13}\text{C}$  NMR spectrum of BODIPY **2a** in deuterated chloroform at 100MHz.

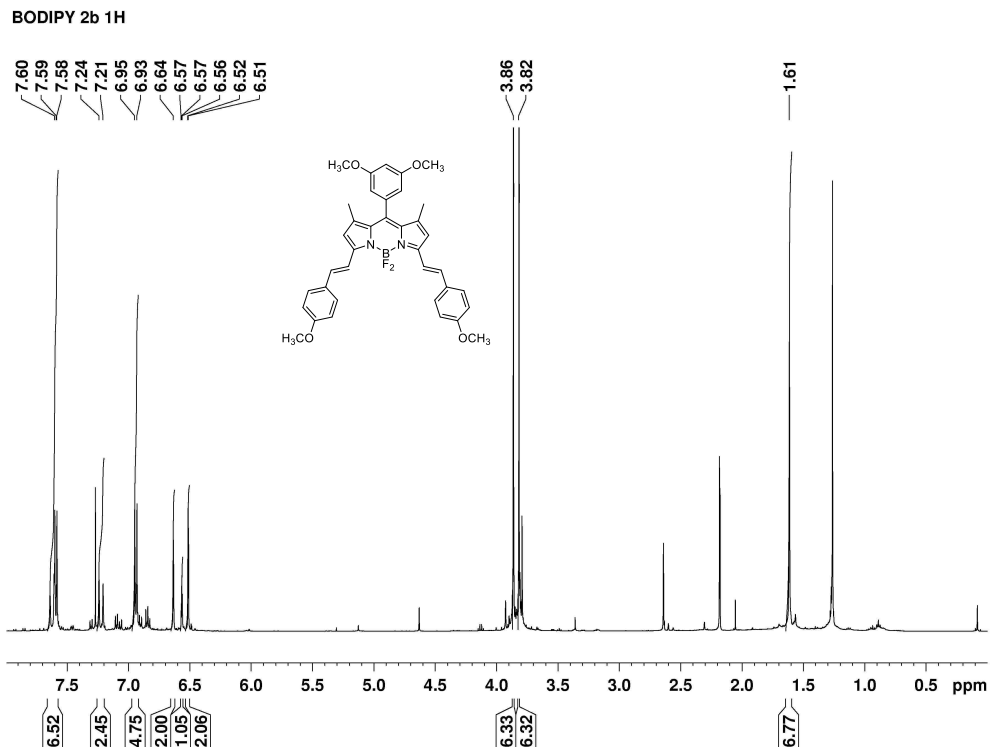


Figure C.7:  $^1\text{H}$  NMR spectrum of BODIPY **2b** in deuterated chloroform at 400MHz.

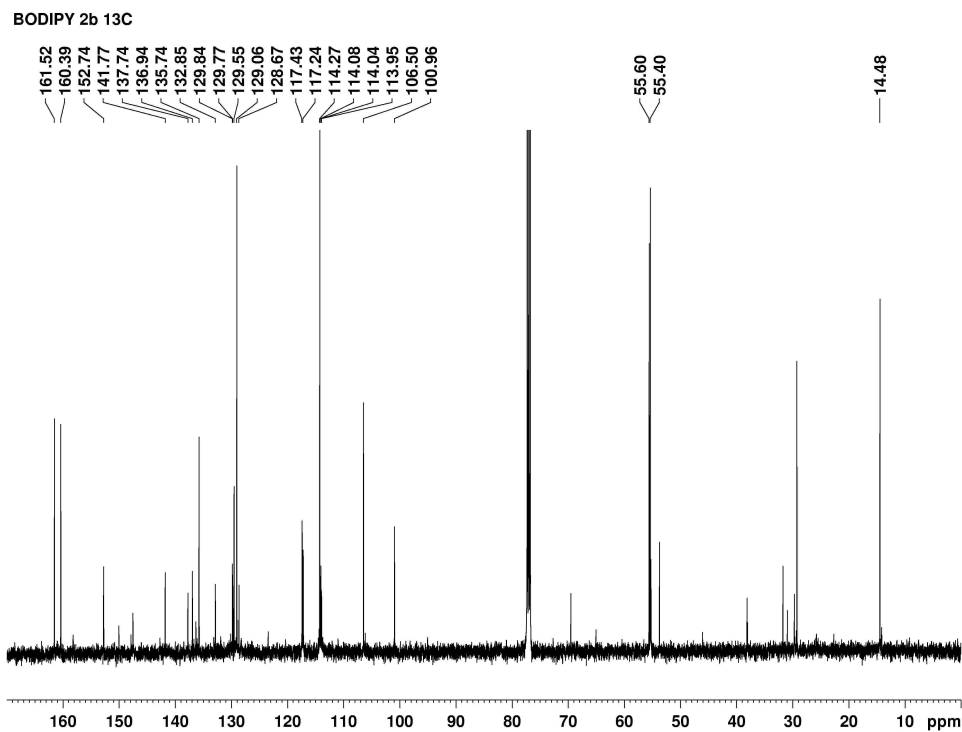


Figure C.8:  $^{13}\text{C}$  NMR spectrum of BODIPY **2b** in deuterated chloroform at 100MHz.



## APPENDIX D: COPYRIGHT RELEASES

### ELSEVIER LICENSE TERMS AND CONDITIONS

May 06, 2014

This is a License Agreement between Jaime H Gibbs ("You") and Elsevier ("Elsevier") provided by Copyright Clearance Center ("CCC"). The license consists of your order details, the terms and conditions provided by Elsevier, and the payment terms and conditions.

**All payments must be made in full to CCC. For payment instructions, please see information listed at the bottom of this form.**

Supplier	Elsevier Limited The Boulevard, Langford Lane Kidlington, Oxford, OX5 1GB, UK
Registered Company Number	1982084
Customer name	Jaime H Gibbs
Customer address	1144 Parlange Drive BATON ROUGE, LA 70806
License number	3383231065817
License date	May 06, 2014
Licensed content publisher	Elsevier
Licensed content publication	Current Opinion in Chemical Biology
Licensed content title	<i>In vivo</i> near-infrared fluorescence imaging
Licensed content author	John V Frangioni
Licensed content date	October 2003
Licensed content volume number	7
Licensed content issue number	5
Number of pages	9
Start Page	626
End Page	634
Type of Use	reuse in a thesis/dissertation
Intended publisher of new work	other
Portion	figures/tables/illustrations
Number of figures/tables/illustrations	1
Format	electronic
Are you the author of this Elsevier article?	No
Will you be translating?	No
Title of your thesis/dissertation	Synthesis, Characterization, and Evaluation of Novel BODIPY Dyes with Theranostic Applications
Expected completion date	May 2014
Estimated size (number of pages)	300
Elsevier VAT number	GB 494 6272 12
Permissions price	0.00 USD
VAT/Local Sales Tax	0.00 USD / 0.00 GBP
Total	0.00 USD
Terms and Conditions	

ELSEVIER LICENSE  
TERMS AND CONDITIONS

May 06, 2014

This is a License Agreement between Jaime H Gibbs ("You") and Elsevier ("Elsevier") provided by Copyright Clearance Center ("CCC"). The license consists of your order details, the terms and conditions provided by Elsevier, and the payment terms and conditions.

**All payments must be made in full to CCC. For payment instructions, please see information listed at the bottom of this form.**

Supplier:	Elsevier Limited The Boulevard, Langford Lane Kidlington, Oxford, OX5 1GB, UK
Registered Company Number	1982084
Customer name	Jaime H Gibbs
Customer address	1144 Parlange Drive BATON ROUGE, LA 70806
License number	3383230683468
License date	May 06, 2014
Licensed content publisher	Elsevier
Licensed content publication	Bioorganic & Medicinal Chemistry
Licensed content title	Spectroscopic, computational modeling and cytotoxicity of a series of <i>meso</i> -phenyl and <i>meso</i> -thienyl-BODIPYs
Licensed content author	Jaime H. Gibbs, Larry T. Robins, Zehua Zhou, Petia Bobadova-Parvanova, Michael Cottam, Gregory T. McCandless, Frank R. Fronczek, M. Graça H. Vicente
Licensed content date	15 September 2013
Licensed content volume number	21
Licensed content issue number	18
Number of pages	12
Start Page	5770
End Page	5781
Type of Use	reuse in a thesis/dissertation
Portion	full article
Format	electronic
Are you the author of this Elsevier article?	Yes
Will you be translating?	No
Title of your thesis/dissertation	Synthesis, Characterization, and Evaluation of Novel BODIPY Dyes with Theranostic Applications
Expected completion date	May 2014
Estimated size (number of pages)	300
Elsevier VAT number	GB 494 6272 12
Permissions price	0.00 USD
VAT/Local Sales Tax	0.00 USD / 0.00 GBP
Total	0.00 USD
Terms and Conditions:	

## VITA

Jaime S. Hayes (Jaime H. Gibbs) was born to Thomas M. Hayes and Teri B. Hayes in Minneapolis, Minnesota and is married to David J. Gibbs. Following completion of her primary studies in 2006, she enrolled at St. Andrews Presbyterian College in Laurinburg, North Carolina where she earned dual Bachelors of Science degrees in Chemistry and Biology in May of 2010. The following August, she entered the Doctoral Program in the Department of Chemistry at Louisiana State University, Baton Rouge, Louisiana. She joined the research group of Dr. M. Graça H. Vicente shortly thereafter. Jaime is currently a candidate for the Doctor of Philosophy degree in organic chemistry, which will be awarded at the August 2014 commencement.